R-06-38

Site descriptive modelling Forsmark stage 2.1

Feedback for completion of the site investigation including input from safety assessment and repository engineering

Svensk Kärnbränslehantering AB

May 2006

Svensk Kärnbränslehantering AB
Swedish Nuclear Fuel
and Waste Management Co
Box 5864
SE-102 40 Stockholm Sweden
Tel 08-459 84 00
+46 8 459 84 00
Fax 08-661 57 19
+46 8 661 57 19

ISSN 1402-3091
SKB Rapport R-06-38

Site descriptive modelling Forsmark stage 2.1

Feedback for completion of the site investigation including input from safety assessment and repository engineering

Svensk Kärnbränslehantering AB

May 2006

Preface

The Swedish Nuclear Fuel and Waste Management Company (SKB) is undertaking site characterisation at two different locations, the Forsmark and Simpevarp/Laxemar areas, with the objective of siting a geological repository for spent nuclear fuel. An integrated component in the characterisation work is the development of a Site Descriptive Model (SDM) that constitutes a description of the site and its regional setting. The model addresses the current state of the geosphere and the biosphere as well as the ongoing natural processes that affect their long-term evolution.

Since the start of site characterisation in 2002, two complete site descriptions (versions 1.1 and 1.2) have been produced for the Forsmark area. Version 1.2 concluded the Initial Site Investigation (ISI) stage. In 2005, SKB decided for a slightly modified working mode for site modelling during the remaining Complete Site Investigation (CSI) stage. Three modelling stages will be carried out, where the scope of the first two, stages 2.1 and 2.2, is limited, whereas the third and final, stage 2.3, will result in a complete site description.

The present report documents the site modelling activities for the Forsmark area during modelling stage 2.1. The primary objective of the work is to give a feedback to the investigations at Forsmark, in order to ensure that sufficient information is obtained during the remainder of the site investigation phase. In order to focus on uncertainties of importance for repository layout and long-term safety, it was also essential to include a feedback from the work with repository layout D1 and from the Preliminary Safety Evaluation (PSE) in the identification of remaining site data needs.

As before, the work has been conducted by a multi-disciplinary project group and associated discipline-specific working groups. Data available in data freeze 2.1 have been analysed with the purpose to assess the implications of the new data for the understanding of the site and the validity of previous model versions. In addition, updated versions of the geological model of rock domains and deformation zones as well as of some aspects of the rock mechanics model, version 2.1, have been developed. However, no complete integrated site description based on data compiled in data freeze 2.1 is provided within the framework of modelling stage 2.1.

The following individuals and expert groups contributed to the project and/or to the report:

- *Kristina Skagius – project leader and editor.*
- *Michael Stephens, Assen Simeonov, Hans Isaksson, Christopher Juhlin, Calin Cosma, Ola Forssberg and Isabelle Olofsson – geology.*
- *Flavio Lanaro, Rolf Christiansson, Isabelle Olofsson, Anders Fredriksson and Hossein Hakami – rock mechanics.*
- *Jan Sundberg, John Wrafter and co-workers – thermal properties.*
- *Sven Follin, Jakob Levén, Per-Olof Johansson, Sten Berglund, Bengt Gentzschein, Magnus Odén – hydrogeology and hydrology.*
- *Marcus Laaksoharju, Ann-Chatrin Nilsson and the members of the ChemNet group – hydrogeochemistry.*
- *James Crawford, Martin Löfgren, Johan Byegård and co-workers – transport properties.*
- *Björn Söderbäck, Mats Tröjbom – chemical properties of the surface system.*
- *Johan Andersson – remaining site-specific uncertainties and their handling.*
- *Kaj Ahlbom, Lennart Ekman and the site investigation team at Forsmark – implications of remaining uncertainties for the site investigation programme.*
- *Anders Lindblom – production of maps and figures.*

Anders Ström

Site Investigations – Analysis

Summary

The candidate area for site investigations at Forsmark is situated within the north-western part of a major tectonic lens. The lens is approximately 25 km long and it extends along the Uppland coast from north-west of the Forsmark nuclear power plant south-eastwards to Öregrund. The candidate area is approximately 6 km long and the north-western part of the candidate area has been selected as the target area for continued site investigations during the Complete Site Investigation (CSI) stage.

This report documents the work conducted during stage 2.1 of the site descriptive modelling for the Forsmark site. The primary objective of this work is to provide feedback to the site investigations at Forsmark, in order to ensure that sufficient information is attained during the remainder of the site investigation stage. The work has been conducted in cooperation with the site investigation team at Forsmark and representatives from repository engineering and safety assessment, with focus on the assembly of data that are required to resolve remaining uncertainties of importance for repository layout and long-term safety. The results of the work are compiled in this report as recommended additions and modifications to the CSI programme published in 2005.

Compared with the CSI programme, four new telescope- or core-drilled boreholes (KFM01C, KFM01D, KFM02B and KFM07C) in the target area are suggested, whereas one of the boreholes previously planned for investigating the bedrock at the border of the current repository layout (KFM09C) is now judged to be less justified. The purpose of the new boreholes is to provide more data from the repository target volume, in order to resolve remaining uncertainties concerning rock stresses, the occurrence and characteristics of deformation zones, the occurrence and geometry of subdomains with different fracture characteristics and hydraulic properties as well as the hydrogeochemical character of groundwaters in low-conductive zones and in the rock matrix.

The plans outlined in the CSI programme for drilling outside the target area have been further developed in terms of specification of the locations of boreholes south of Bolundsfjärden, through the Singö deformation zone and through the Forsmark deformation zone. Investigations that need to be carried out in these boreholes are also specified. Further work along the Eckarfjärden deformation zone, as outlined in the CSI programme, is judged to be less judtified. In addition to telescope- and core-drilling activities, the need for a number of additional percussion-drilled boreholes, various surface investigations, and in situ and laboratory tests have been identified. These are necessary in order to resolve remaining uncertainties related to geological, thermal, rock mechanics, hydrogeological and bedrock transport properties of importance for repository engineering and safety assessment. They include, for example, an extensive study of lineaments at the site.

In order to meet the primary objective of the stage 2.1 work, data available in data freeze 2.1 have been analysed and updated versions of the geological models for rock domains and deterministic deformation zones have been developed. However, no completely integrated site description based on data compiled in data freeze 2.1 is provided within the framework of modelling stage 2.1.

Local models for the geometry of rock domains and deterministic deformation zones, with a higher resolution, are presented for the first time. The version 2.1 local model volume covers the north-western part of the candidate area, which is the target area for a repository at the site. Compared with version 1.2 of the rock domain model, new borehole data as well as the higher resolution in the local model volume have resulted in the inclusion of two new, minor rock domains. Only one of these domains occurs in the central part of the local model volume, where the target area for a repository at the site is located. The current regional rock domain model strongly resembles earlier model versions. Minor modifications have been carried out in the geometry of rock domains RFM029 and RFM032, in the north-western part of the candidate volume. Furthermore, two new domains have been added and one domain from model version 1.1 has been restored.

The regional model for deterministic deformation zones has several similarities to the base model in version 1.2 of the Forsmark site descriptive model, but there are significant changes in the cut-off length of especially the gently dipping deformation zones. In addition, all steeply dipping deformation zones that are inferred to be longer than 3,000 m at the surface are included in the regional model as well as all gently dipping deformation zones, even those that are geologically minor struc-

tures. Steeply dipping zones with trace lengths shorter than 3,000 m are included in the local model. Most of these zones are inferred solely from the interpretation of geophysical lineaments and, since direct data from boreholes or surface outcrops are lacking, they are assigned a low confidence of occurrence. The few gently dipping zones that are present in the north-western part of the candidate volume are also included in the local model. The only significant changes in the repository target area concern the presence of a high confidence deformation zone longer than 3,000 m close to the south-western margin of the area and the occurrence of shorter, high confidence deformation zones with NS strike, partly or entirely within the target area.

On the basis of the observed three-dimensional spatial variability of fracturing, which was recognised already in model version 1.2, and an inferred relationship between the occurrence of gently dipping deformation zones and the in situ stress magnitudes in the bedrock, a working conceptual model for division of rock domain RFM029 into separate fracture domains has been developed. This concept will be further developed and tested during stage 2.2 of the modelling work, as an integrated issue between geology, rock mechanics, hydrogeology and hydrogeochemistry.

Interpretations of new rock mechanics and thermal properties data have, in general, confirmed the version 1.2 results, although the potential impact of subordinate rock types, such as amphibolite and pegmatite, on properties at a domain level has been recognised. This will be further analysed during stage 2.2 of the modelling work when more data on these subordinate rock types become available. Effects of microcracking due to large rock stresses are observed in the results from laboratory tests of rock mechanics properties of samples from depths larger than 550 m. Furthermore, there are indications that the rock mechanics properties of the uppermost part of the bedrock are different from those at depth. This will be further analysed in the light of possible correlations with geology and rock stresses and the working conceptual model for division of the bedrock into separate fracture domains.

Analyses of the strength and deformability properties of some minor deformation zones by both empirical and theoretical methods have provided consistent results showing, for example, that both the strength and deformability properties of these minor deformation zones are dependent on confining stress and thus also depth dependent. These results can be used for design applications and for numerical modelling of the rock stress field.

No new data on rock stresses were available in data freeze 2.1. However, rock stress modelling has been initiated, with the purpose to seek support for the current conceptual models for the formation and evolution of deformation zones and fracture domains at the site. This includes large-scale regional modelling to support the hypothesis of a strike-slip regime for the formation of the regional deformation zones and to study the local variation and gradient of the stresses induced by the deformation zones in the target area.

New hydrogeological data have confirmed the version 1.2 results that the north-western part of the candidate volume is characterised by highly transmissive structures in the uppermost part of the bedrock, which are in good hydraulic contact over large distances, and very few flow anomalies at depth, beneath the gently dipping deformation zone ZFMNE00A2. This gives support to the concept of a division of rock domain RFM029 into separate fracture domains. The data also suggests that the highly transmissive structures in the uppermost part of the bedrock may be important by acting as main conductors for both recharging surface water and discharging deep groundwater.

Evaluation of the new hydrogeochemical data has confirmed the results from version 1.2 and has also provided support for the predictions made in this earlier version. This has increased the confidence in the description of the three-dimensional variability in processes and hydrogeochemical properties. However, the hydrogeochemical evaluation still provides a biased picture, since it is based on data from the most conductive part of the bedrock. In this respect, it is expected that the results of the matrix fluid characterisation programme will make it possible to arrive at a more unbiased conceptualisation of the hydrogeochemical system.

New data on bedrock transport properties have implied only minor changes to the version 1.2 properties, although noting that the evaluation still suffers from a lack of site-specific data. Despite this, there is good data support for the diffusive properties of the dominant rock type metagranite, and there does not appear to be large differences between the diffusive properties of the various

unaltered rock types. There are currently no sorption data available. However, measurements of the relative surface areas indicate that the different rock types should have substantially similar sorption properties with only minor differences between rock types that are typically less than the spatial variability and measurement uncertainty inherent in the data itself. The available data also indicate that altered bedrock most likely exhibits significantly stronger solute sorption than the unaltered matrix rock and that crushing of the rock material results in the formation of new surfaces that are not representative for the intact rock. This introduces considerable uncertainty concerning the use of crushed rock material for the determination of sorption coefficients.

In summary it can be concluded that interpretations of site data and the modelling undertaken have, in general, confirmed the version 1.2 results and that no new important site-specific issues have been identified. The larger database available has allowed for further development of concepts that will be tested in the forthcoming modelling stages. In addition, more focus on interdisciplinary feedback and consistency in the results of the data interpretation and modelling have improved our understanding of the Forsmark site.

Sammanfattning

Kandidatområdet där platsundersökningarna i Forsmark genomförs är beläget i den nordvästliga delen av en tektonisk lins. Denna lins är ca 25 km lång och sträcker sig längs Upplandskusten från ett område nordväst om Forsmarks kärnkraftverk i sydöstlig riktning till Öregrund. Kandidatområdet är ca 6 km långt och den nordvästra delen har valts ut som fokuserat område för fortsatta undersökningar under det kompletta platsundersökningsskedet.

Denna rapport redovisar arbetet som utförts under etapp 2.1 av den platsbeskrivande modelleringen för Forsmark. Huvudsakliga syftet med detta arbete är att ge återkoppling till platsundersökningarna i Forsmark för att säkerställa tillräcklig insamling av information under återstoden av platsundersökningsskedet. Detta arbete har utförts i samarbete med platsundersökningsgruppen i Forsmark och representanter från projektering och säkerhetsanalys. Fokus för arbetet har varit att identifiera data som behövs för att lösa kvarvarande osäkerheter som är av betydelse för förvarets layout och långsiktiga säkerhet. Resultatet av detta arbete är sammanställt i denna rapport som rekommenderade förändringar och tillägg till det program för kompletta platsundersökningar (KPLU) i Forsmark som publicerades 2005.

Jämfört med KPLU programmet föreslås borrning av fyra nya teleskop- eller kärnborrhål (KFM01C, KFM01D, KFM02B och KFM07C) i det fokuserade området. Ett av de tidigare planerade borrhålen för undersökning av berget vid gränsen till nuvarande förvarslayout (KFM09C) bedöms nu ha lägre prioritet. Syftet med de nya borrhålen är att samla mer data från bergvolymen i det tilltänkta förvarsområdet för att lösa kvarvarande osäkerheter avseende bergspänningar, förekomsten av deformationszoner och deras egenskaper, förekomsten och geometrier av delområden med olika sprickkaraktäristik och hydrauliska egenskaper samt kvarvarande osäkerheter i den hydrogeokemiska beskrivningen av grundvattnet i såväl zoner med låg konduktivitet som i bergmatrisen.

Planerna i KPLU programmet för borrning utanför det fokuserade området har vidareutvecklats vad det gäller lokalisering av borrhålen söder om Bolundsfjärden, i Singözonen och i Forsmarkzonen samt specificering av de undersökningar som ska göras i dessa borrhål. Vidare undersökningar av Eckarfjärdszonen, som indikerades i KPLU programmet, bedöms nu vara av lägre prioritet. Utöver teleskop- och kärnborrning, finns ett behov av ett antal ytterligare hammarborrhål, olika ytundersökningar samt in-situ och laboratorietester. Detta för att komma till rätta med kvarvarande osäkerheter kopplade till geologiska, termiska, bergmekaniska hydrogeologiska och bergets transportegenskaper som är av betydelse för projektering och säkerhetsanalys. Ett exempel på sådana undersökningar är en omfattande studie av lineament i området.

För att uppnå syftet med arbetet i etapp 2.1 har data tillgängliga vid datafrys 2.1 analyserats och uppdaterade versioner av de geologiska modellerna för bergdomäner och deformationszoner har tagits fram. Ingen fullständig integrerad platsbeskrivning baserad på data i datafrys 2.1 levereras dock inom ramen för arbetet i etapp 2.1.

För första gången presenteras en lokal modell med högre upplösning i beskrivningen av bergdomäners och deterministiska deformationszoners geometri. Den lokala modellvolymen för version 2.1 inkluderar den nordvästliga delen av kandidatområdet med det tilltänkta förvarsområdet. Nya borrhålsdata och den högre upplösningen i den lokala modellvolymen har motiverat införandet av två nya, mindre domäner i bergdomänmodellen jämfört med version 1.2. Endast en av dessa förekommer i den centrala delen av den lokala modellvolymen där det tilltänkta förvarsområdet är beläget. Den nuvarande regionala bergdomänmodellen är snarlik tidigare versioner. Mindre förändringar har gjorts i geometrin av bergdomänerna RFM029 och RFM032 i den nordvästra delen av kandidatområdet. Dessutom har två nya domäner lagts till och en domän från version 1.1 har åter införts.

Den regionala modellen för deterministiska deformationszoner har många likheter med basmodellen i version 1.2 av den platsbeskrivande modellen för Forsmark, men det finns signifikanta skillnader i framför allt längden av de flacka deformationszonerna. Dessutom har alla brant stående deformationszoner som härletts vara längre än 3 000 m vid markytan tagits med i modellen liksom alla flacka deformationszoner, även de som geologiskt sett är mindre strukturer. Brant stående zoner med

spårlängder på ytan kortare än 3 000 m har gått in i den lokala modellen. De flesta av dessa zoner är härledda enbart från tolkningen av geofysiska lineament. Förekomsten av dessa zoner är tilldelade en låg tilltro eftersom direkta data från borrhål och berghällar på ytan saknas. De få flacka zoner som identifierats i den nordvästra delen av kandidatområdet är också medtagna i den lokala modellen. De enda signifikanta ändringarna i det tilltänkta förvarsområdet rör några zoner med hög tilltro till deras förekomst. En av dessa är längre än 3 000 m och belägen nära den sydvästra kanten av området. De övriga är kortare deformationszoner med nordsydlig strykning som helt eller delvis återfinns inom området.

En konceptuell arbetsmodell för uppdelning av bergdomän RFM029 i olika sprickdomäner har tagits fram. Denna modell baseras på den, redan i modellversion 1.2, observerade tredimensionella rumsliga variationen i bergets sprickighet och antagandet att det finns ett samband mellan förekomsten av flacka deformationszoner och bergspänningarnas storlek. Detta koncept kommer att utvecklas vidare och testas under etapp 2.2 av modelleringsarbetet som en integrerad fråga mellan geologi, bergmekanik, hydrogeologi och hydrogeokemi.

Generellt sett har tolkningar av nya data för bergmekaniska och termiska egenskaper bekräftat resultaten i modellversion 1.2. En möjlig inverkan av underordnade bergarter, såsom amfibolit och pegmatit, på egenskaperna i domänskala har dock identifierats. Detta kommer att analyseras vidare under etapp 2.2 av modelleringsarbetet när mer data för dessa underordnade bergarter blir tillgängliga. Effekter av mikrosprickning på grund av höga bergspänningar har observerats i resultaten från laboratorietester av bergmekaniska egenskaper för prover tagna på större djup än 550 m. Dessutom finns det indikationer på att den övre delen av berget har bergmekaniska egenskaper som skiljer sig från de på djupet i berget. Detta kommer att analyseras vidare i skenet av möjliga kopplingar med geologi och bergspänningar och den konceptuella arbetsmodellen för uppdelning av berget i olika sprickdomäner.

Analyser av hållfasthet och deformationsegenskaper hos bergmassan i mindre deformationszoner har utförts med både empiriska och teoretiska metoder. Dessa metoder ger sinsemellan samstämmiga resultat som visar t ex att både hållfasthet och deformationsegenskaper hos bergmassan i dessa mindre deformationszoner beror av den inneslutna bergspänningen och därför också av djupet. Dessa resultat kan användas i designtillämpningar och för numerisk modellering av bergets spänningsfält.

Inga nya bergspänningsdata fanns tillgängliga i datafrys 2.1. Modellering av bergspänningar har dock påbörjats med syftet att söka stöd för den nuvarande konceptuella modellen för hur deformationszonerna och sprickdomänerna i berget har bildats och förändrats över tiden. Detta omfattar storskalig regional modellering för att testa hypotesen att de regionala zonerna har bildats i en regim med horisontell rörelse samt studier av lokala variationer och gradienter i bergspänningar orsakade av deformationszonerna i det fokuserade området i den nordvästra delen av kandidatområdet.

Nya hydrogeologiska data har styrkt resultaten från version 1.2. Dessa visar att den nordvästra delen av kandidatområdet karaktäriseras av strukturer med hög transmissivitet i den övre delen av berget, som också är hydrauliskt förbundna med varandra över långa sträckor, medan berget på djupet under den flacka deformationszonen ZFMNE00A2 har väldigt få flödesanomalier. Detta ger stöd för konceptet att dela upp berget i olika sprickdomäner. Data antyder också att strukturerna med hög transmissivitet i den övre delen av berget kan vara betydelsefulla genom att agera som huvudsakliga ledare för både inströmmande ytvatten och utströmmande djupt grundvatten.

Utvärderingen av nya hydrogeokemiska data har konfirmerat resultaten från version 1.2 och har också allmänt gett stöd för det arbete som gjordes i denna tidigare version. Detta har ökat tilltron till beskrivningen av den tredimensionella variabiliteten i processer och hydrogeokemiska egenskaper. Den hydrogeokemiska beskrivningen är dock fortfarande påverkad av att den enbart bygger på data från den mest konduktiva delen av berget. I detta avseende förväntas resultaten från karaktärisering av vatten i bergmatrisen göra det möjligt att ta fram en mer balanserad konceptuell beskrivning av det hydrogeokemiska systemet.

Nya data har föranlett enbart små förändringar i bergets transportegenskaper jämfört med de egenskaper som redovisades i version 1.2. Tillgången på platsspecifika data är dock fortfarande bristfällig, vilket har påverkat utvärderingen av data. Trots detta ger tillgängliga data gott stöd för diffusionsegenskaperna i den dominanta bergarten metagranit och det verkar inte vara stora skillna-

der i diffusionsegenskaper mellan olika bergarter som inte är omvandlade. För närvarande finns inga sorptionsdata tillgängliga, men mätningar av de olika bergarternas specifika yta antyder liknande sorptionsegenskaper för de olika bergarterna. De skillnaderna som finns mellan bergarterna är små och typiskt mindre än den rumsliga variabiliteten inom varje bergart och osäkerheten i själva data. Tillgängliga data indikerar också att omvandlat berg sannolikt har avsevärt högre sorptionskapacitet än bergmatrisen som inte är omvandlad och att krossning av bergmaterial skapar nya sprickytor i materialet som inte är representativa för det intakta berget. Detta innebär att det är stora osäkerheter kopplade till användandet av krossat bergmaterial för bestämning av sorptionskoefficienter.

Sammanfattningsvis kan det konstateras att de datatolkningar och modelleringar som utförts överlag har bekräftat resultaten i modellversion 1.2 och att inga nya betydelsefulla platsspecifika frågor har identifierats. Den större mängden tillgängliga data har gjort det möjligt att vidareutveckla koncept som kommer att testas i kommande modellarbeten. Dessutom har mer fokus på återkoppling mellan disciplinerna och samstämmighet i resultaten från datatolkningar och modellring förbättrat vår förståelse av platsen.

Contents

1 Introduction

1.1 Background

The Swedish Nuclear Fuel and Waste Management Company (SKB) is undertaking site characterisation at two different locations, the Forsmark and Simpevarp/Laxemar areas, with the objective of siting a geological repository for spent nuclear fuel. The investigations are conducted in campaigns, data freezes. After each data freeze, the site data are analysed and site descriptive modelling is carried out with the purpose to develop a Site Descriptive Model (SDM) of the site. A Site Descriptive Model is a synthesis of geology, rock mechanics, thermal properties, hydrogeology, hydrogeochemistry and a surface system description.

So far, three versions of SDM (versions 0, 1.1 and 1.2) have been developed for the Forsmark area. Version 0 /SKB 2002/ established the state of knowledge prior to the site investigation. Version 1.1 /SKB 2004/ was completed during 2004 and version 1.2 in June 2005 /SKB 2005a/. Version 1.2 of the SDM concluded the Initial Site Investigation stage (ISI). It formed the basis for a preliminary repository layout (layout D1) as well as for a preliminary safety evaluation (PSE) of the Forsmark site /SKB 2005b/ and a Safety Assessment (SR-Can) of repository layout D1 at Forsmark.

According to present plans, three modelling stages will be carried out during the Complete Site Investigation stage. The scope of the two first modelling stages, 2.1 and 2.2, is limited, whereas the third and final stage, 2.3, will result in a complete site description. However, an important component of all three stages is to address and continuously try to resolve uncertainties of importance for repository engineering and safety assessment. The working mode and the results of the work in modelling stage 2.1 for the Forsmark site is compiled in this report.

1.2 Scope and objective

The primary objective of the version 2.1 work is to provide feedback to the site investigations at Forsmark in order to ensure sufficient information gathering during the remainder of the site investigation stage. This should be done in terms of specifying investigations/modelling actions that are needed to resolve remaining important uncertainties, in addition to those already in the current plans for the CSI and modelling stages 2.1–2.3. Furthermore, investigations included in the current CSI programme, but not necessary for resolving critical issues, should be pointed out. The preliminary site description (SDM version 1.2) provided feedback to the forthcoming Complete Site Investigation stage (CSI) in terms of additional data needs to aid in reducing SDM uncertainty. However, in order to capture and focus on uncertainties of importance for repository layout and long-term safety it is essential to include also feedback from the work with repository layout D1 and from the PSE in the identification of remaining site data needs.

A secondary objective is to evaluate the analysis and modelling work carried out so far and to resolve remaining modelling issues identified during previous modelling stages.

In order to meet the objective of the version 2.1 work, data available in data freeze 2.1 have been analysed with the purpose to assess the implications of the new data for the understanding of the site and the validity of previous model versions. In addition, updated versions of the geological model of rock domains (lithology) and deformation zones as well as of some aspects of the rock mechanics model, versions 2.1, have been developed. However, no complete integrated site description based on data compiled in data freeze 2.1 is provided within the framework of modelling stage 2.1.

1.3 Setting

The Forsmark site is located in northern Uppland within the municipality of Östhammar, about 170 km north of Stockholm. The candidate area is located along the shoreline of Öregrundsgrepen and it extends from the Forsmark nuclear power plant and the access road to the SFR-facility in the northwest to Kallrigafjärden in the southeast (Figure 1-1). The candidate area is approximately 6 km long and 2 km wide, and the north-western part of the candidate area has been selected as the target area for the Complete Site Investigation stage /SKB 2005c/.

The bedrock was formed between 1,900 and 1,850 million years ago and it has been affected by both ductile and brittle deformation. The ductile deformation has resulted in large-scale ductile high-strain zones and the brittle deformation has given rise to large-scale fracture zones. Tectonic lenses, in which the bedrock is much less affected by ductile deformation, are enclosed between the ductile high-strain zones. The candidate area is located in the north-westernmost part of one of these tectonic lenses that extends from north-west of the nuclear power plant south-eastwards to Öregrund (Figure 1-1).

1.4 Methodology and organisation of work

The site descriptive modelling comprises the iterative steps of primary data evaluation, descriptive and quantitative modelling in 3-D and an overall confidence assessment. Methodologies for developing discipline-specific models and for integrated evaluation are available and documented in methodology reports or strategy reports, as described in the preliminary site description for the Forsmark area /SKB 2005a/. The development of version 2.1 of the geological models of rock domains (lithology) and deformation zones has followed the guidelines given in the methodology report for geological site descriptive modelling /Munier et al. 2003/, but considering also experience gained during previous site descriptive modelling work, as reported in Chapter 13 of the SDM

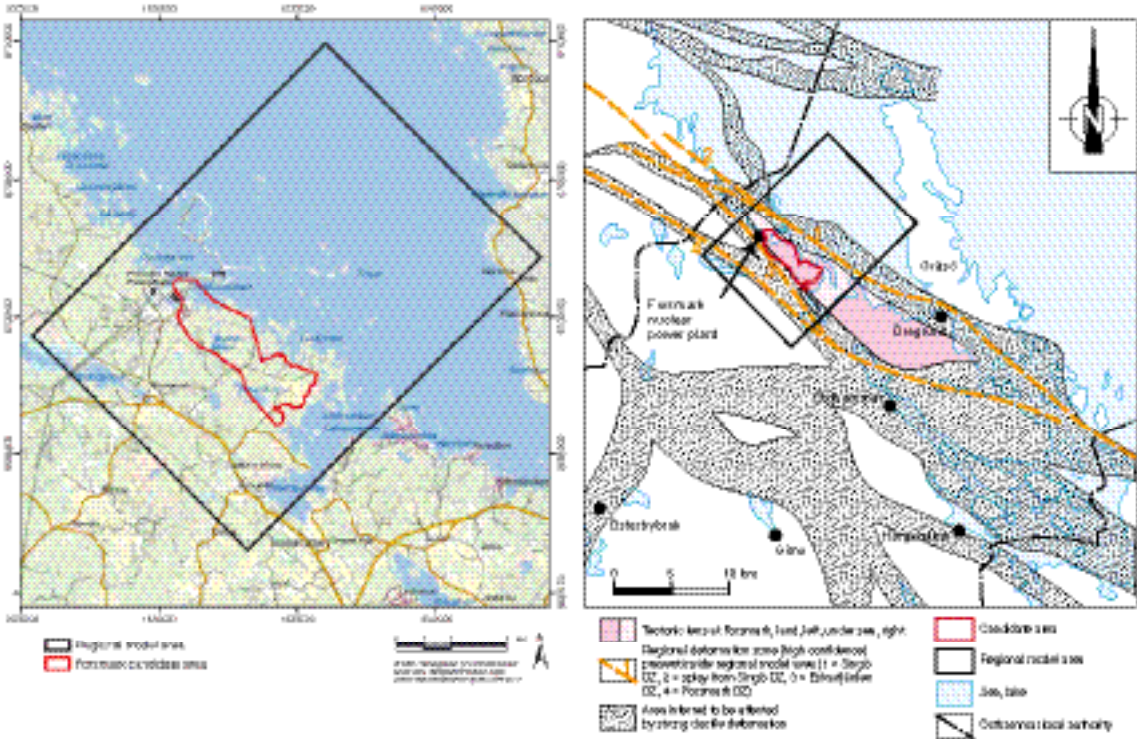

Figure 1-1. *The Forsmark candidate area (red) and the regional model area (black) in the preliminary site descriptive model /SKB 2005a/ (left). The extension of the tectonic lens within which the candidate area at Forsmark is situated /SKB 2005a/ (right).*

version 1.2 /SKB 2005a/. Similarly, the methodology report for rock mechanics site descriptive modelling /Andersson et al. 2002/ and experience gained during previous site descriptive modelling work have guided the development of the version 2.1 rock mechanics model.

The focus of the remaining disciplines has been on the interpretation of new preliminary site data in order to assess whether these data confirm the current concepts and understanding of the site or if they raise new questions or uncertainties that need to be resolved. The procedures for the data interpretations are the same as those adopted in previous modelling work, i.e. builds on guidelines in the methodology reports and improvements made during the site modelling work /SKB 2005a/.

The procedure adopted for an integrated evaluation of uncertainties in the current site description and identification of data and modelling activities to resolve these uncertainties builds on the format for uncertainty and confidence assessment applied in model version 1.2 /SKB 2005a/. By the use of protocols, critical issues and uncertainties have been compiled and evaluated in terms of data requirements and implications for the site investigation programme. The work was conducted in a series of seminars and workshops with joint participation from the Forsmark modelling team, the Forsmark site investigation team, Repository Engineering and Safety Assessment. Important input to this work has been, in addition to the preliminary site description (version 1.2) /SKB 2005a/ and the new analyses conducted within modelling stage 2.1, the preliminary safety evaluation (PSE) /SKB 2005b/ and conclusions from the work with repository layout D1 /Brantberger et al. 2006/.

The analysis and modelling work conducted within modelling stage 2.1 has been organised in the same manner as for the previous modelling version, with a project group acting as the core and with discipline-specific working groups, Net-groups, or persons acting as conductors for specified tasks /SKB 2005a/. As a preparation for coming modelling stages, the analysis of a number of remaining critical discipline-specific issues has begun already during modelling stage 2.1.

1.5 This report

The first part of this report contains accounts of the data interpretation and modelling undertaken in stage 2.1 of the site descriptive modelling for Forsmark, whereas the results of the identification of critical remaining issues and their implications for the remainder of the site investigation programme are provided in the second part of the report.

Chapter 2 gives an overview of the data available in data freeze 2.1 together with descriptions of the discipline-specific interpretations of data that have been undertaken as part of modelling stage 2.1. In Chapter 3, updated versions of the geological models for rock domains and deterministic deformation zones are provided together with accounts of the assessed implications of the different discipline-specific new data for the understanding of the site and the validity of previous model version. The current understanding of the Forsmark site are then summarised in Chapter 4.

Chapter 5 describes the results of the integrated evaluation of uncertainties in the current site description as well as the data and modelling activities identified as necessary to resolve these uncertainties. The implications of the identified data requirements for the remainder of the site investigation programme are given in Chapter 6 as recommended additions and modifications to the Complete Site Investigation programme published in 2005.

2 Available primary data and data interpretation

2.1 Overview of investigations

This section gives a short overview of the investigations that provided primary data to the previous data freeze 1.2, used in model version 1.2 /SKB 2005a/, and of the new investigations made between data freezes 1.2 (July 31st 2004) and 2.1 (July 29th 2005), and used for the first time in model version 2.1. The new data contained in data freeze 2.1 are described in more detail in the discipline-specific sub-sections in this Chapter.

2.1.1 Investigations and primary data acquired up to data freeze 1.2

The investigations leading up to data freeze 1.2 comprised geoscientific and ecological surface investigations, airborne geophysical measurements, drilling and borehole investigations during and after drilling.

The surface investigations comprised airborne photography, airborne and surface geophysical investigations, lithological mapping of the rock surface, mapping of structural characteristics and investigations of Quaternary deposits including marine and lacustrine sediments in the Baltic and in lakes. Furthermore, data from meteorological and hydrological monitoring and measurements, hydrochemical sampling and analyses of precipitation, surface waters and shallow groundwater and various ecological inventory compilation and investigations were included in data freeze 1.2.

The drilling activities comprised five, approximately 1,000 m long cored-drilled boreholes (KFM01A, 02A, 03A, 04A, 05A) at drill sites 1–5 and two shallower cored boreholes, KFM01B approximately 500 m long and KFM03B approximately 100 m long. In addition, drilling of 19 percussion holes (HFM01 to HFM19 c. 200 m deep) and c. 65 boreholes through the Quaternary deposits provided data to data freeze 1.2 (see Figure 2-1).

The borehole investigations performed following the drilling of the boreholes comprised geophysical logging, radar measurements, boremap mapping and single-hole interpretation, rock stress measurements, hydraulic measurements (flow logging, pumping tests, interference tests), hydrogeochemical logging and sampling of groundwater for chemical characterization, and electrical resistivity logging. In addition, sampling of intact rock and fractures for determination of density, porosity, susceptibility, mineralogy, geochemistry, diffusivity, sorption properties, rock strength and thermal properties, was undertaken.

The investigations conducted up to data freeze 1.2 are described in more detail in version 1.2 of the Forsmark site descriptive model (SDM) /SKB 2005a/ and in the associated P-reports[1]. A compilation of P-reports is also given in Appendix 1.

2.1.2 Data freeze 2.1 – investigations performed and data acquired

The data included in data freeze 2.1 are those that were available for model version 1.2 and new data acquired between data freezes 1.2 and 2.1. The investigations associated with data collection during the period between the two data freezes comprised both surface and borehole investigations.

The ecological surface investigations during the period have been focussed on characterising the aquatic system. New surface geological data have been obtained from mapping of excavations across two lineaments and from seismic reflection studies to the south-west and north-west of the candidate area. New seismic refraction data are also available from a limited number of profiles.

Hydrological surface investigations have involved the establishment of two meteorological stations and collection of another year of meteorological data and registration of snow depth. Three additional surface discharge gauging stations have been established in addition to the station established

[1] The P-series report the results of the on-going site investigations at Forsmark and Oskarshamn (Simpevarp and Laxemar subareas). These reports are available on the SKB web page (www.skb.se).

prior to data freeze 1.2. These four stations have provided data on discharge, water temperature and electrical conductivity. In addition, surface water level monitoring in six lakes and at two locations in the Baltic Sea as well as monitoring of groundwater levels in 38 of the groundwater observation wells have been undertaken, adding another year of data to the time series of surface- and groundwater levels. Hydrochemical sampling and analysis of precipitation, surface waters and shallow groundwaters have continued and have extended the time-series of these data.

New drilling activities that have provided information to data freeze 2.1 comprise five core-drilled boreholes (KFM06A, 06B, 07A, 08A and KFM08B) and three percussion-drilled boreholes (HFM20, 21 and HFM22) (Figure 2-1). Data from these holes include standard geological and geophysical data and single hole interpretations. In addition, complementary mineralogical, geochemical and petrophysical data from KFM04A, KFM05A and KFM06A, and fracture mineralogical data from these boreholes and borehole KFM01B are new in the 2.1 data freeze. Vertical seismic profile (VSP) measurements have been conducted in the cored boreholes KFM01A and KFM02A, and these data are included in the 2.1 data freeze.

Hydraulic tests carried out comprise flow logging and double-packer injection tests in the new cored boreholes, but also in the cored boreholes KFM03B, KFM04A and KFM05A. Pumping tests and flow logging have been conducted in the new percussion-drilled holes and a number of short-term

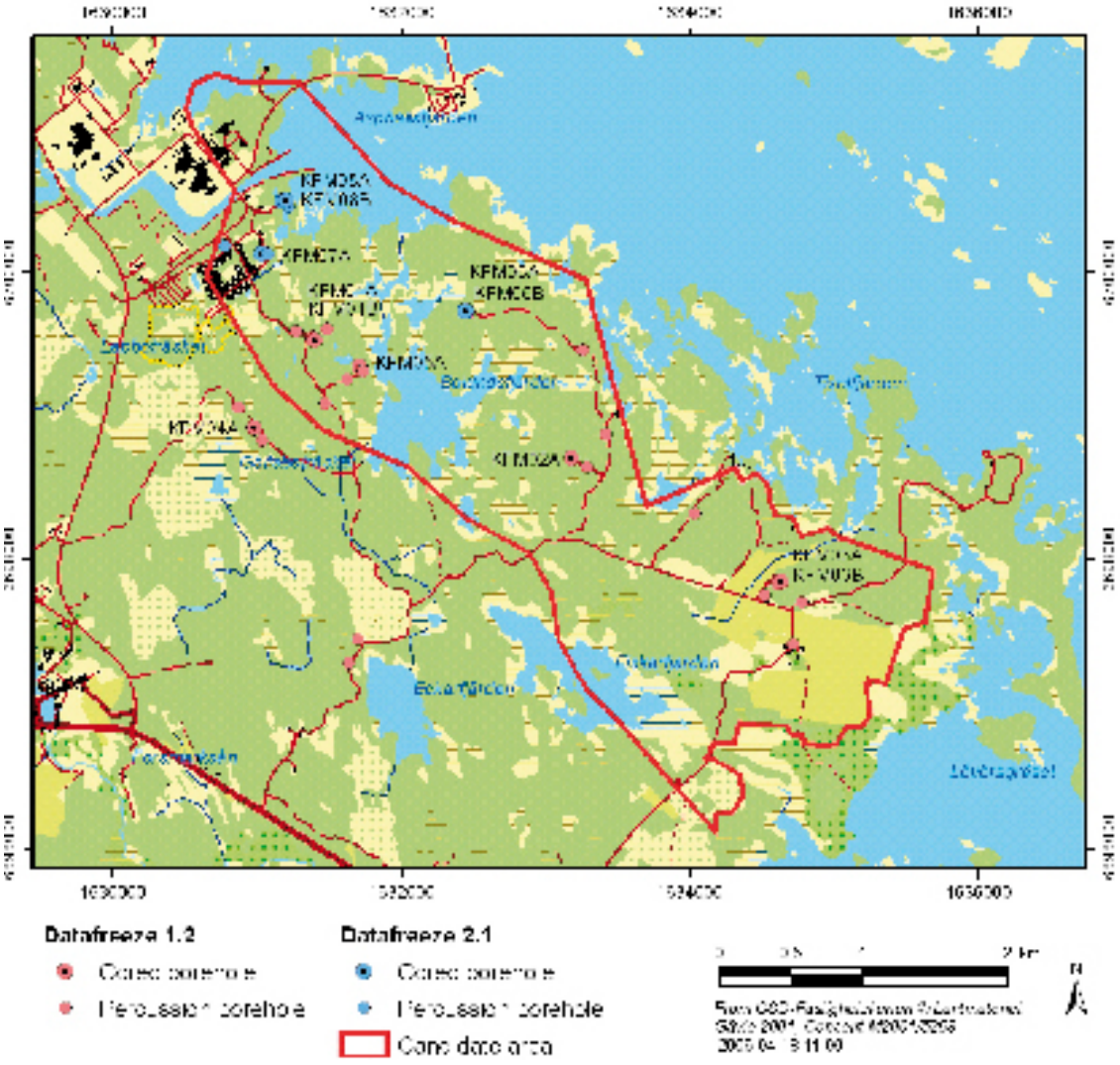

Figure 2-1. *Boreholes included in data freeze 1.2 (pink) and new boreholes included in data freeze 2.1 (blue).*

cross-hole interference tests have been performed between percussion-drilled boreholes and cored boreholes and between various percussion holes. In addition, monitoring in percussion-drilled and core-drilled boreholes has provided additional data to the time series of hydrogeological data.

Hydrogeochemical logging and characterisation as well as microbial investigations have provided new data from the cored boreholes KFM05A, 06A, 07A and KFM08A and from the percussion-drilled holes HFM20, 21 and HFM22. In addition, core samples have been collected from KFM06A for determination of the composition of the rock matrix pore water.

Sampling for testing of rock mechanics properties and thermal properties has been conducted and new data derive mainly from the cored boreholes KFM04A, 05A and KFM06A. Sampling and testing for bedrock transport properties have provided new data from the cored boreholes KFM01A–KFM08A.

2.2 Databases

The basis for the work conducted in modelling stage 2.1 are quality assured field data from Forsmark that were available in the SKB database Sicada and the SKB Geographic Information System (GIS) at the time of data freeze 2.1. These data are compiled in tables in Appendix 1. The purpose of these tables is to give a reference and account of which data were available and were considered in the interpretation and modelling work conducted during stage 2.1 of the site descriptive modelling. Data per se are not given in these tables, but a specification and a reference to the data source, i.e. the relevant P-report. Primary data used in the analysis and modelling work are described in more detail in the discipline-specific subsections in this Chapter.

2.3 Model volumes

The site descriptive modelling is performed using two different scales of model volume, the *regional* and the *local* model volumes. Generally, the local model is required to cover the volume within which the repository is expected to be placed, including accesses and the immediate environs. In addition to the description on the local scale, a description is also devised for a much larger volume, the regional model, in order to place the local model in a larger context and to allow for a sensitivity analysis of, mainly, hydrogeological boundary conditions.

In selecting the model volumes for version 1.2 /SKB 2005a/, some rules of thumb, taken from the SKB strategy document for integrated evaluation /Andersson 2003/ were applied. These rules also apply for version 2.1. It needs also to be understood that the distinct model sizes primarily concern the development of the geological model in the SKB Rock Visualisation System, RVS. This is also the reason why the model areas and volumes have a rectangular shape.

2.3.1 Regional model volume

The regional model area selected for version 2.1 is shown in Figure 2-2. It is the same as the regional model area/volume in version 1.2 /SKB 2005a/ and the arguments of selecting this area/volume remain.

- It includes the candidate area and it is not prohibitively large as it has a surface area of 165 km^2.
- It captures relevant portions of the extensive regional deformation zones, which strike in a north-westerly direction and surround the candidate area. Any expansion of the regional model area to the northwest or southeast would not provide any significant changes in the regional geological picture. It should also be noted that the geological evolution was assessed in version 1.2 over a much larger area than the regional model area. Based on this, as far as geological aspects are concerned, the size of the regional model area is sufficient.
- It adequately covers the variations in rock type in the candidate area and its immediate surroundings.

- It captures the main hydrogeological features of the region, as the boundaries perpendicular to the shoreline are judged to be sufficiently far away from each other so that they do not influence the groundwater flow in the candidate area. The boundary to the southwest lies on the south-western side of a local topographic divide and the boundary to the northeast lies northeast of a major bathymetric break in Öregrundsgrepen. Sensitivity analyses undertaken in version 1.2 of the site descriptive modelling have addressed the proper locations of the boundaries in the regional hydrogeological model and the results confirm that the selected regional volume is appropriate also from a hydrogeological point of view.
- A depth of 2,100 m below sea-level is considered to provide a reasonable vertical extent for description and is the maximum depth down to which any meaningful extrapolations of deformation zones could be made. To represent this depth in RVS, the vertical dimension is set to 2,200 m since the upper boundary is set to +100 m above mean sea level.

The coordinates defining the regional model volume are (in metres):

RT90 (RAK) system; (Easting, Northing): (1625400, 6699300), (1636007, 6709907), (1643785, 6702129), (1633178, 6691522)

RHB 70; elevation: +100, –2,100

2.3.2 Local model volume

The local model area selected for version 2.1 is reduced in size compared to the version 1.2 local model area, but still contained within its boundaries, as shown in Figure 2-2. The need for a reduction in size of the local domain was recognised in the version 1.2 modelling work and has now been implemented by selecting a smaller area covering the north-western part of the candidate area. The main argument for selecting this part is that it covers the target area selected for the location of a potential repository where on-going field work is now largely focused. Other arguments for selecting this local model volume, of which some are the same as for model version 1.2, are:

- Both to the north-east and south-west, it includes the boundaries to more inhomogeneous and banded bedrock outside the candidate area.
- It includes key rock boundaries within and immediately adjacent to the candidate area which help to define the structural framework within the tectonic lens.
- The north-western and south-eastern model boundaries are located well outside the outer borders of the repository area according to the current layout D1 /Brantberger et al. 2006/. Furthermore, the north-western boundary is positioned so that the parts of the tectonic lens below the current reactor site as well as potential access ramps from the SFR peninsula are included in the model.
- The surface area is c. 12 km^2, i.e. comparable to the size of 5–10 km^2 recommended in the general execution programme /SKB 2001/.
- A depth of 1,100 m beneath sea level permits inclusion of all information from the existing and future deep boreholes at the site. To represent this depth in RVS, the vertical dimension is set to 1,200 m since the upper boundary is set to +100 m above mean sea level.

The coordinates defining the local model volume are (in metres):

RT90 (RAK) system; (Easting, Northing): (1629171, 6700562), (1631434, 6702824), (1634099, 6700159), (1631841, 6697892)

RHB 70; elevation: +100, –1,100

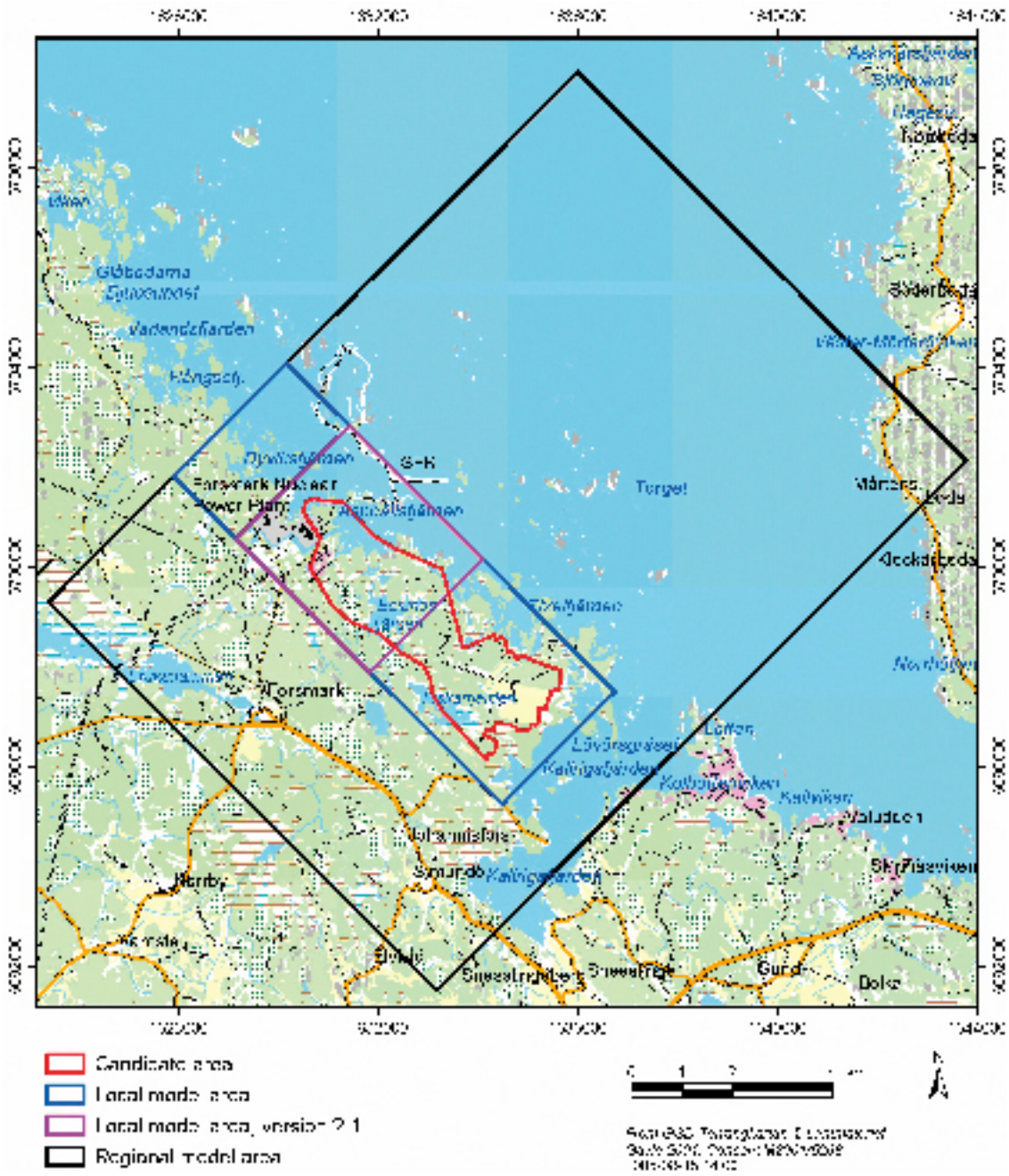

Figure 2-2. *Version 2.1 regional (black) and local (purple) model area. The regional model area is the same as in model versions 0, 1.1 and 1.2. The local model area is smaller than in version 1.2 (blue line) and covers the north-western part of the candidate area selected as target area for a potential repository.*

2.4 Interpretation of primary geological data

2.4.1 Additional data acquisition and nomenclature

New surface geological data that have been used during model version 2.1 include field data, attained during the mapping of excavations across two lineaments, and stage 2 seismic reflection data to the south-west and north-west of the candidate area. New seismic refraction data are also available from a limited number of profiles. However, since an extended programme to acquire seismic refraction data is presently in progress, all the seismic refraction data will be evaluated together during model version 2.2.

New borehole data include geological and geophysical data as well as single-hole interpretations from the cored boreholes KFM06A, KFM06B, KFM07A, KFM08A and KFM08B, and from the percussion boreholes HFM20, HFM21 and HFM22. Complementary mineralogical, geochemical and petrophysical data are available from KFM04A, KFM05A and KFM06A, and fracture mineralogical data from these boreholes and borehole KFM01B. Since the limited amount of new data is judged to have only marginal affects on the estimates presented in SDM version 1.2, no updating of the properties of the different rock types at the site has been carried out. However, an update is planned in model version 2.2.

An evaluation of the new vertical seismic profiling (VSP) data from KFM01A and KFM02A showed that a closer integration with the geological and other geophysical data from these two boreholes was necessary before a confident understanding of the geological significance of the data can be carried out. This work is now in progress and, for this reason, the VSP data also awaits an assessment during modelling stage 2.2.

In the text that follows, the term deformation zone is used according to the definition in /Munier et al. 2003/. The term refers, in a general manner, to any zone in the crust where strain has been concentrated. More specific information on the character of a particular zone can be obtained from the property tables for deformation zones. In these tables, composite zones that show both ductile and brittle deformation are distinguished from zones that only show deformation in the brittle regime. Many of the zones at the Forsmark site and all the zones that have been recognised on the basis of the new borehole data are brittle structures. For purposes of linguistic simplicity, the term fracture zone is used for these structures, according to the definition in /Stråhle 2001/. Fracture zones defined by an increased frequency of extensional fractures (joints) or shear fractures (faults) are not distinguished. An ongoing study that aims to shed more light on this question, as well as the kinematics of faults, is in progress at the site. The results of this study will be available in model version 2.2.

2.4.2 Surface data − excavations and stage 2 reflection seismic data

Identification of lineaments along excavations AFM001243 and AFM001244

Excavations AFM001243 and AFM001244 have been carried out across the linked lineaments XFM0062A0 and XFM0126A0, respectively (Figure 2-3a). These lineaments trend across the candidate area in a NE and NS direction, respectively, and are strongly based on the occurrence of magnetic minima /Isaksson et al. 2004, Isaksson and Keisu 2005/. Lineament 62 is also based on a minor topographic depression along a major part of its length.

Since slope stability conditions were not considered to fulfil safety requirements, only generalised mapping was possible along excavation AFM001243 that transects lineament 62 /Cronquist et al. 2005/. Inspection of the bedrock along this excavation shows that it is affected by alteration in the form of hematization (Figure 2-3b). Magnetic susceptibility values for all rock types are low. There is also a high frequency of steeply dipping fractures that strike in a NE direction (Figure 2-3b) and that are sealed with adularia and quartz. Gently dipping fractures coated with calcite, chlorite and, less frequently, asphaltite are also present. Scan line mapping was not carried out along this excavation, since it was not possible to recognise a sufficiently large area with a rock mass quality high enough to fulfil the criteria for such mapping.

Although a minor, steeply dipping fracture zone that strikes NE is present along the northern part of excavation AFM001244, the magnetic minimum that defines this lineament corresponds to a swarm of Group D granite dykes (Figure 2-3c). These dykes (SKB code 111058) are locally associated with pegmatite and show low magnetic susceptibility values /Cronquist et al. 2005/.

The two excavations confirm that the magnetic data are a reliable source of information to detect geological features in the bedrock. Lineament XFM0062A0 with NE trend is interpreted to represent a fracture zone, while lineament XFM0126A0 with NS trend is inferred to be related to a lithological contrast and not specifically to a deformation zone.

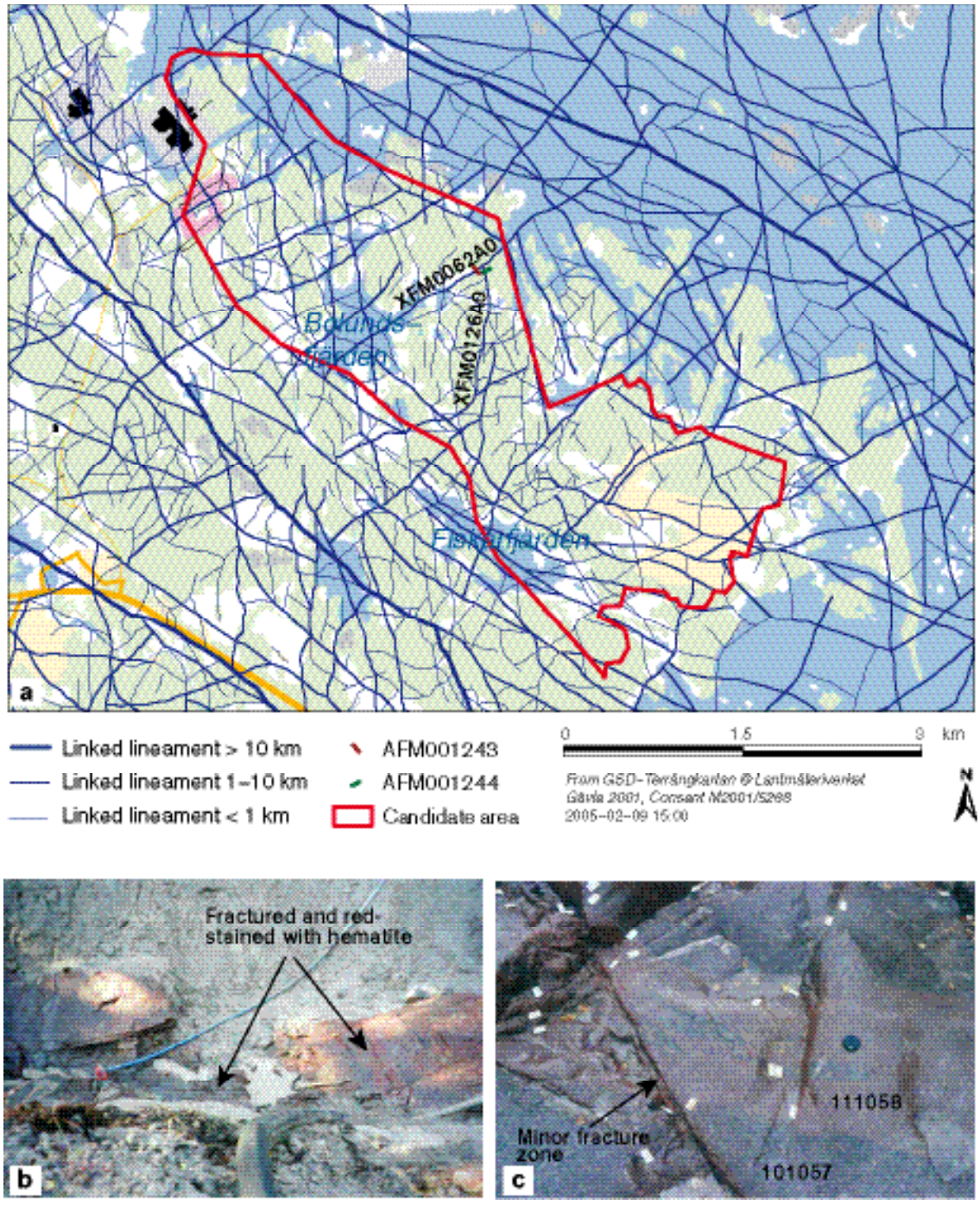

Figure 2-3. *a) Location of excavations AFM001243 and AFM001244. b) Altered (red-stained with fine-grained hematite dissemination) and highly fractured bedrock along excavation AFM001243. Most of the fractures strike NE and dip steeply. View approximately to the SW. c) Granite dyke (SKB code 111058) with low magnetic susceptibility that strikes NS and intrudes medium-grained metagranite (101057) along excavation AFM001244. A minor fracture zone with NE strike and steep dip is present to the left in the picture. View approximately to the east.*

High resolution reflection seismic data, stage 2

Integration of stage 1 seismic reflection data /Juhlin et al. 2002, Juhlin and Bergman 2004/ and cored borehole data from boreholes KFM02A, KFM03A and KFM03B have shown that the prominent, gently dipping reflectors in the south-eastern part of the candidate area correspond to hydraulically conductive fracture zones /SKB 2005a/. Further assessment of the data from KFM03A and KFM03B indicates that small lenses of amphibolite within the fracture zones serve to enhance the reflectivity

/Juhlin and Stephens, in press/. It is apparent that seismic reflection data from the surface is of major significance for the modelling of water-bearing fracture zones at the Forsmark site.

Stage 2 data from high resolution seismic reflection measurements have been acquired at the surface, in the areas to the south-west and north-west of the candidate area /Juhlin and Palm 2005/. A source and receiver spacing at a maximum distance of 10 m and a minimum of 160 active channels have been used in the assembly of these data. They complement the stage 1 data /Juhlin et al. 2002, Juhlin and Bergman 2004/ that were attained more or less entirely inside the candidate area (Figure 2-4). Approximately 80% of the 2,100 source points were activated using the VIBSIST mechanical source that consists of an industrial hammer mounted on a tractor /Park et al. 1996, Cosma and Enescu 2001/. Data were collected along ten profiles that vary in length from 1–4.3 km (total survey length, 24.6 km). Crustal images down to a few kilometres have been presented /Juhlin and Palm 2005/. Due to noise conditions, the quality of the data close to the nuclear power plant and along the coastal profiles 5b and 8 is poorer relative to that acquired along the other profiles.

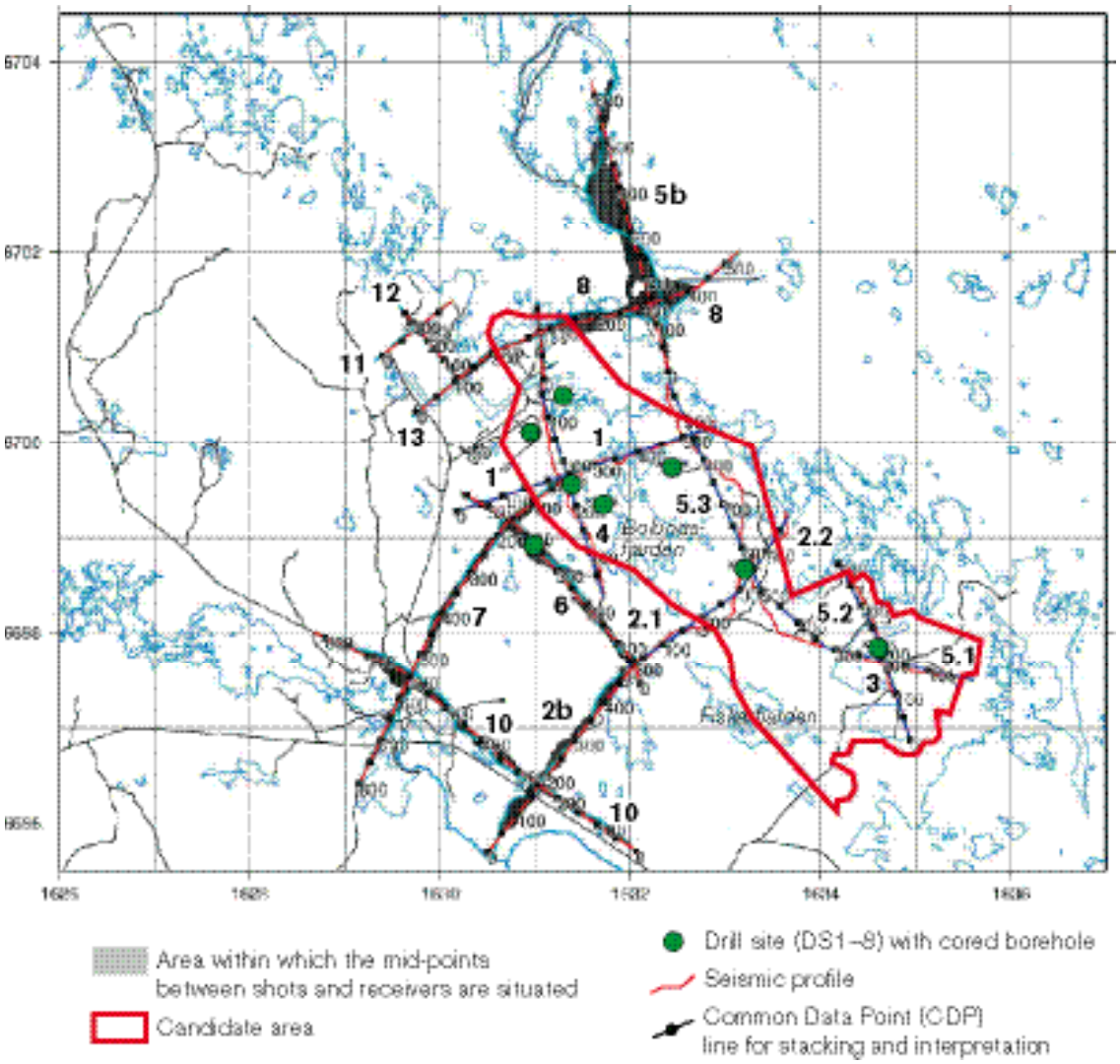

Figure 2-4. *Common Data Point (CDP) lines along which the surface reflection seismic data (stages 1 and 2) have been projected for stacking and interpretation (after /Juhlin et al. 2002, Cosma et al. 2003, Juhlin and Palm 2005/). The area within which the mid-points between shots and receivers are situated are only shown for the stage 2 data to the south-west and north-west of the candidate area. Coordinates are provided using the RT90 (RAK) system.*

Stacked sections from the new profiles are generally consistent with the results from the stage 1 work. The prominent sub-horizontal C1 and C2 reflectors, at approximately 3 km depth, are present on nearly all the profiles. The A2 reflector has been recognised in the northern parts of profiles 6 and 7, confirming that this reflector should be intersected by borehole KFM04A /SKB 2005a/. However, this reflector can only be traced a short distance to the south-east of drill site 2. The stage 2 data also show that the significant A1 reflector is not visible beneath the nuclear power plant, along profiles 11, 12 and 13. There are also difficulties to trace this reflector up to the surface. No pronounced set of reflectors that correspond to the groups A and B in the south-eastern part of the candidate area /Juhlin et al. 2002, Juhlin and Bergman 2004/ have been observed in the stage 2 data. The structures related to these reflectors are restricted more or less to the south-eastern part of the candidate area.

Four new reflectors have been recognised with a high level of confidence during stage 2. Reflectors J1, J2 and K1 are confined to the bedrock that lies south-west of the candidate area, while reflector B8 is situated beneath the nuclear power plant, north-west of the candidate area. The orientations of the J1, J2 and K1 reflectors (Table 2-1) are somewhat different from the orientations observed for the reflectors identified with a high degree of confidence inside the candidate area. All dip more steeply and reflectors J1 and J2 strike in an ESE direction. The prominent reflector B8 (Figure 2-5) strikes NNE and dips gently to the ESE (Table 2-1). Following the same procedure as that used in

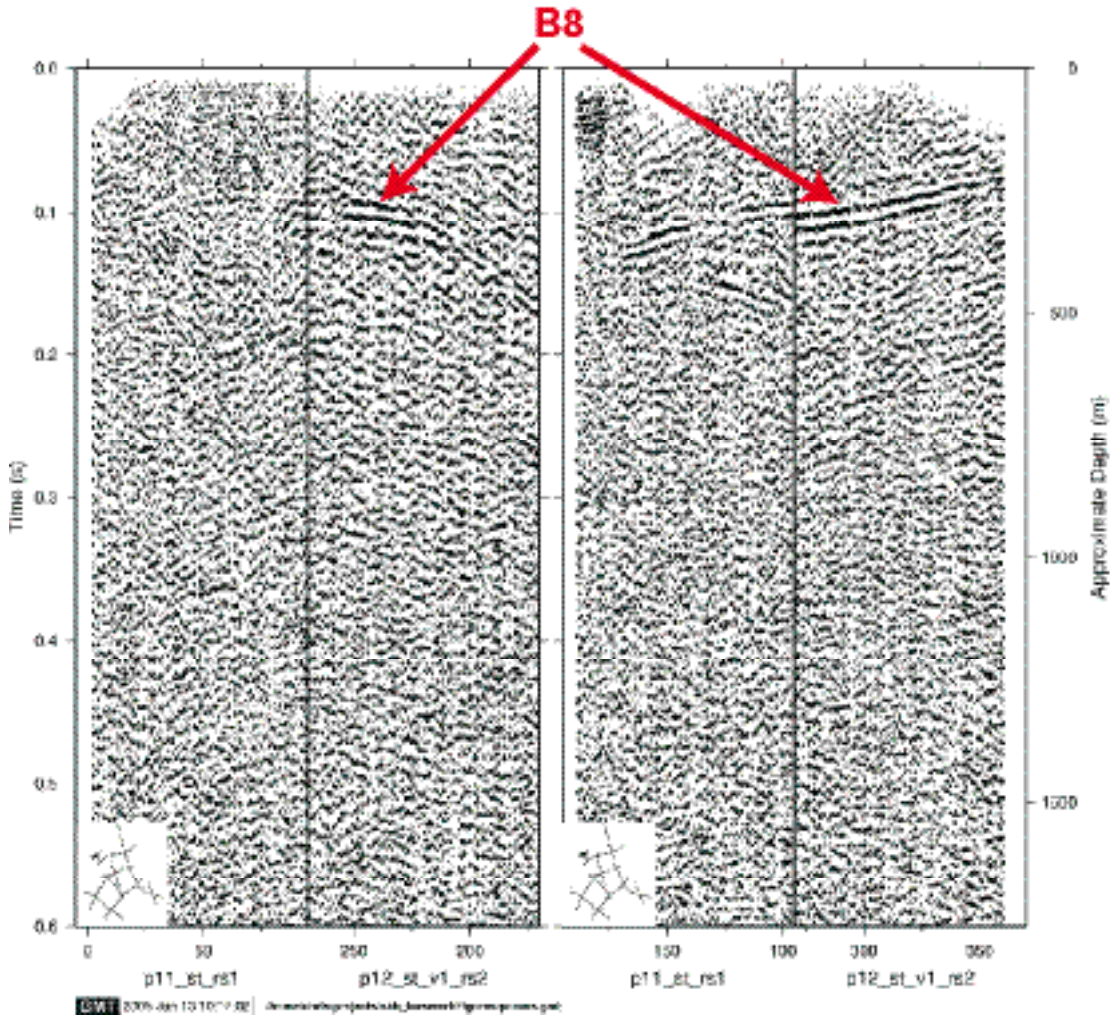

Figure 2-5. *Correlation of stacks from profiles 11 and 12 at their crossing points, north-west of the candidate area. The location of each section is shown in the lower left-hand part of the two figures. The depth scale along the vertical axis is only valid for sub-horizontal reflectors. The numbers along the horizontal axis refer to the CDP line along which the data have been projected for stacking and interpretation (after /Juhlin and Palm 2005/). Note the pronounced B8 reflector.*

Table 2-1. Estimates of the orientation of the new reflectors recognised with high confidence in the stage 2 data (based on /Juhlin and Palm 2005/).

Reflector ID	Profile	Strike	Dip
B8	11, 12, 13	015	22
J1	2b, 10	115	48
J2	7, 10	100	37
K1	7, 10	050	40

SDM versions 1.1 and 1.2 /Cosma et al. 2003, Balu and Cosma 2005/, the reflectors J1, J2, K1 and B8 have been placed in three-dimensional space, in order to permit their use in the modelling work /Cosma et al. 2006/.

Reflections from the regionally important Forsmark, Eckarfjärden and Singö deformation zones, which strike WNW and NW, are not directly conspicuous along the profiles that cut across these zones (profiles 2b, 5b, 7 and 8 in Figure 2-4). This is consistent with their inferred sub-vertical dip /e.g. SKB 2005a/. An attempt to identify sub-vertical zones or corridors in the Forsmark area, which constrain the along-strike extension of the gently and moderately dipping reflectors, is presented in connection with the geological modelling work in Appendix 2. The sub-horizontal C1 and C2 reflectors are conspicuous, since they can be traced over most of the area, in particular across the Singö deformation zone. They are only restricted to the south-west against the Forsmark zone.

2.4.3 Borehole data − geological mapping, borehole radar and geophysical logs, rock types, ductile structures and fracture mineral sets

Boreholes and geological mapping

The geological mapping and geophysical logging programmes for the boreholes generate subsurface data that bear on the character of rock type (including alteration), ductile deformation, and brittle deformation including fractures. These programmes are of vital importance for the geological modelling work.

Data from approximately 8,100 m of cored boreholes, which were drilled at eight separate sites (Figure 2-6), have been used in model version 2.1. Data from boreholes KFM06A, KFM06B, KFM07A, KFM08A and KFM08B complement the data used in SDM version 1.2. All boreholes except the short borehole KFM06B (angle 85°) entered the bedrock at an angle of 60°. Complementary data from the percussion boreholes HFM20, HFM21 and HFM22, which were drilled close to drill sites 7 and 8 (Figure 2-6) and vary in length from 202–301 m, are also available. The length and orientation of all the boreholes, and a description of the drilling activities have been presented in a series of reports (Appendix 1).

All the cored and percussion boreholes have been mapped using the Boremap methodology adopted by SKB and the relevant data acquisition reports are listed in Appendix 1. A key input in the mapping procedure is the oriented image of the borehole walls that is obtained with the help of the *B*orehole *I*mage *P*rocessing *S*ystem (BIPS). The terminology and procedures used in the acquisition of fracture data follow those summarised in /SKB 2005a/. It needs to be noted that significant changes in the documentation of data bearing on fractures occurred after the mapping of boreholes KFM01A, KFM02A and KFM03A/KFM03B. Furthermore, the term “sealed fracture network” was not employed during the mapping of these first four boreholes. As in SDM version 1.2 /SKB 2005a/, linear grain fabric data from the boreholes are lacking.

The inherent, restricted quality of the data from the percussion boreholes remains (see /SKB 2005a/). For this reason, focus is addressed in the present model version, as in SDM version 1.2, on the cored borehole data. Data from the percussion boreholes have primarily been used as a help in the recognition of rock units and possible deformation zones in the single hole interpretation (see Section 2.4.5).

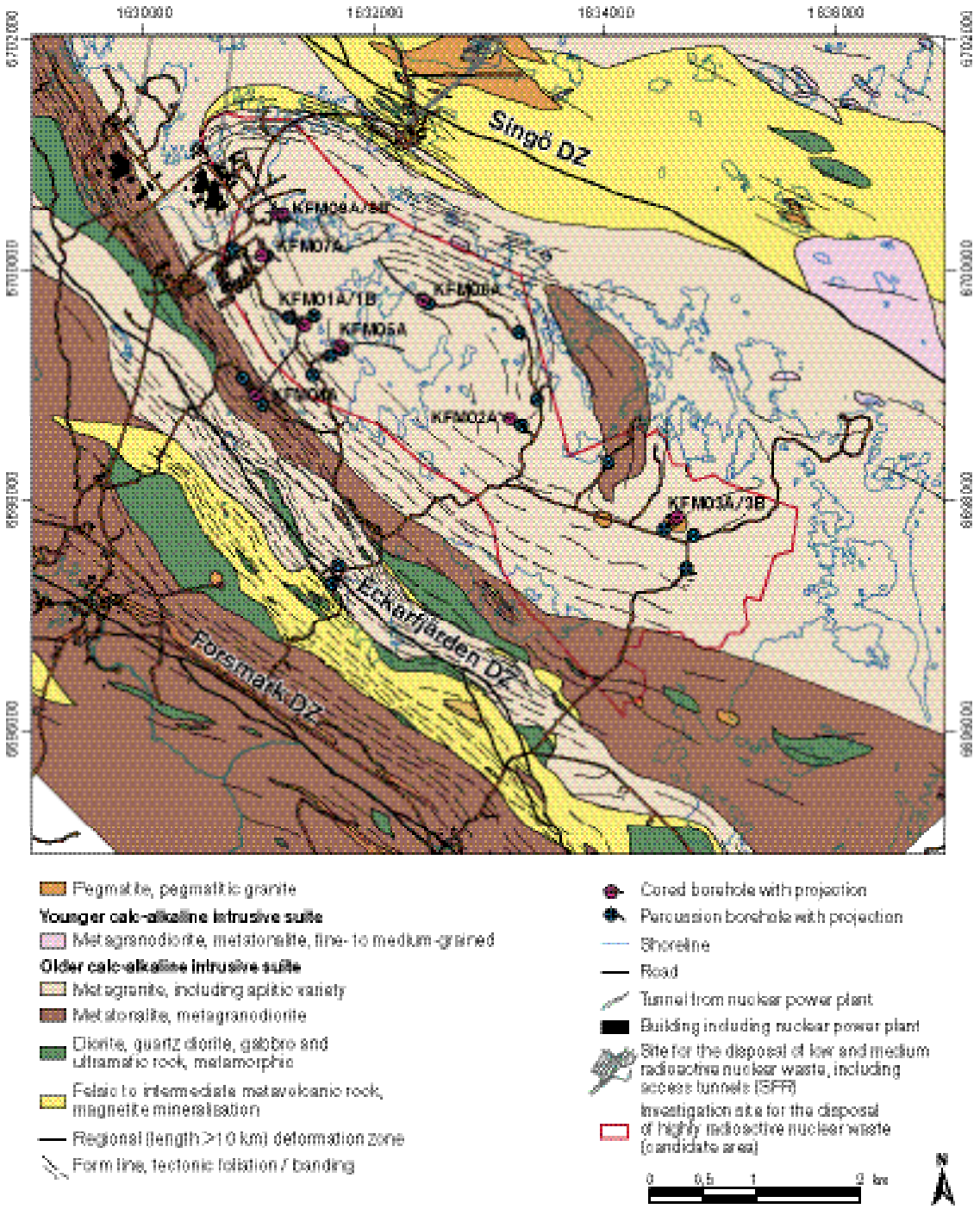

Figure 2-6. *Location of boreholes, from which data were available for model version 2.1, shown on a simplified bedrock map of the candidate area and its surroundings (Bedrock geological map, Forsmark, version 1.2). Coordinates are provided using the RT90 (RAK) system.*

Borehole radar and geophysical logs

Borehole radar and geophysical logs, and their interpretation, have been completed for cored boreholes KFM06A, KFM07A, KFM08A and KFM08B, and for the percussion boreholes HFM20, HFM21 and HFM22 (see reference list in Appendix 1). Radar data are also available from cored borehole KFM06B. As described in SDM version 1.2 /SKB 2005a/, these data have played an important function in both the geological mapping and, particularly, the single hole interpretation of the boreholes.

In SDM version 1.2, it was noted that attempts had been made to document the orientation of the inferred radar reflectors. However, the results proved to be inconsistent and difficult to use in the interpretation of the orientation of structures in the bedrock. For this reason, it was decided in the 1.2 modelling work that the orientation of, for example, deformation zones could not be determined from these data. Data quality assessment at the Oskarshamn site has subsequently established some problems in the presentation of the radar anomaly orientation data. At the present time, revised deliveries of orientation data are in progress and an attempt to make more use of these data is planned in modelling stage 2.2.

Rock types in cored boreholes

A summary of the different rock types at the Forsmark site, that is based on the compilations from the abundant surface data carried out in previous modelling versions /SKB 2004, 2005a/, is shown in Table 2-2. In the present work, both the dominant rock type and the rock occurrences that are less than 1 m in borehole length have been included in the analysis of the proportions of different rock types in the boreholes (cf. SDM version 1.2). This evaluation (Figure 2-7) shows that medium-grained metagranite (101057) dominates (c. 80%) in boreholes KFM07A (Figure 2-7b, mapped borehole length 915 m) and KFM08B (199 m). Subordinate amounts of pegmatitic granite (101061) and amphibolite (102017) are also present (10–15% and c. 5%, respectively). The proportion of fine-to medium-grained metagranitoid (101051) is distinctly less compared to that documented in all the other boreholes at the site.

As expected, boreholes KFM06A (914 m) and KFM08A (871 m), which partly intersect the bedrock outside rock domain RFM029 (see Section 3.1), contain significant quantities of rock types other than the medium-grained metagranite. Aplitic metagranite (101058), which is commonly altered and pale grey or white in colour, comprises c. 20% of borehole KFM06A (Figure 2-7a). Aplitic metagranite, felsic metavolcanic rock and amphibolite (101058, 103076 and 102017, respectively) comprise c. 20% of the rock types in borehole KFM08A (Figure 2-7c). The amphibolites in all the boreholes are oriented parallel to the planar grain-shape fabric in the host rocks (see Boremap references in Appendix 1).

Table 2-2. Major groups of rock types recognised during outcrop mapping at the Forsmark site (based on /Stephens et al. 2003/). SKB rock codes are shown in brackets after each lithology.

Rock types	
All rocks are affected by brittle deformation. The fractures generally cut the boundaries between the different rock types. The boundaries are predominantly not fractured.	
Rocks in Group D are affected only partly by ductile deformation and metamorphism.	
Group D (c. 1,851 million years)	• Fine- to medium-grained granite and aplite (111058). Pegmatitic granite and pegmatite (101061). Variable age relationships with respect to Group C. Occur as dykes and minor bodies that are commonly discordant and, locally, strongly discordant to ductile deformation in older rocks.
Rocks in Group C are affected by penetrative ductile deformation under lower amphibolite-facies metamorphic conditions.	
Group C (c. 1,864 million years)	• Fine- to medium-grained granodiorite, tonalite and subordinate granite (101051). Occur as lenses and dykes in Groups A and B. Intruded after some ductile deformation in the rocks belonging to Groups A and B with weakly discordant contacts to ductile deformation in these older rocks.
Rocks in Groups A and B are affected by penetrative ductile deformation under amphibolite-facies metamorphic conditions.	
Group B (c. 1,886–1,865 million years)	• Biotite-bearing granite (to granodiorite) (101057) and aplitic granite (101058), both with amphibolite (102017) as dykes and irregular inclusions. • Tonalite to granodiorite (101054) with amphibolite (102017) enclaves. Granodiorite (101056). • Ultramafic rock (101004). Gabbro, diorite and quartz diorite (101033).
Group A (supracrustal rocks older than 1,885 million years)	• Sulphide mineralisation, possibly epigenetic (109010). • Volcanic rock (103076), calc-silicate rock (108019) and iron oxide mineralisation (109014). Subordinate sedimentary rocks (106001).

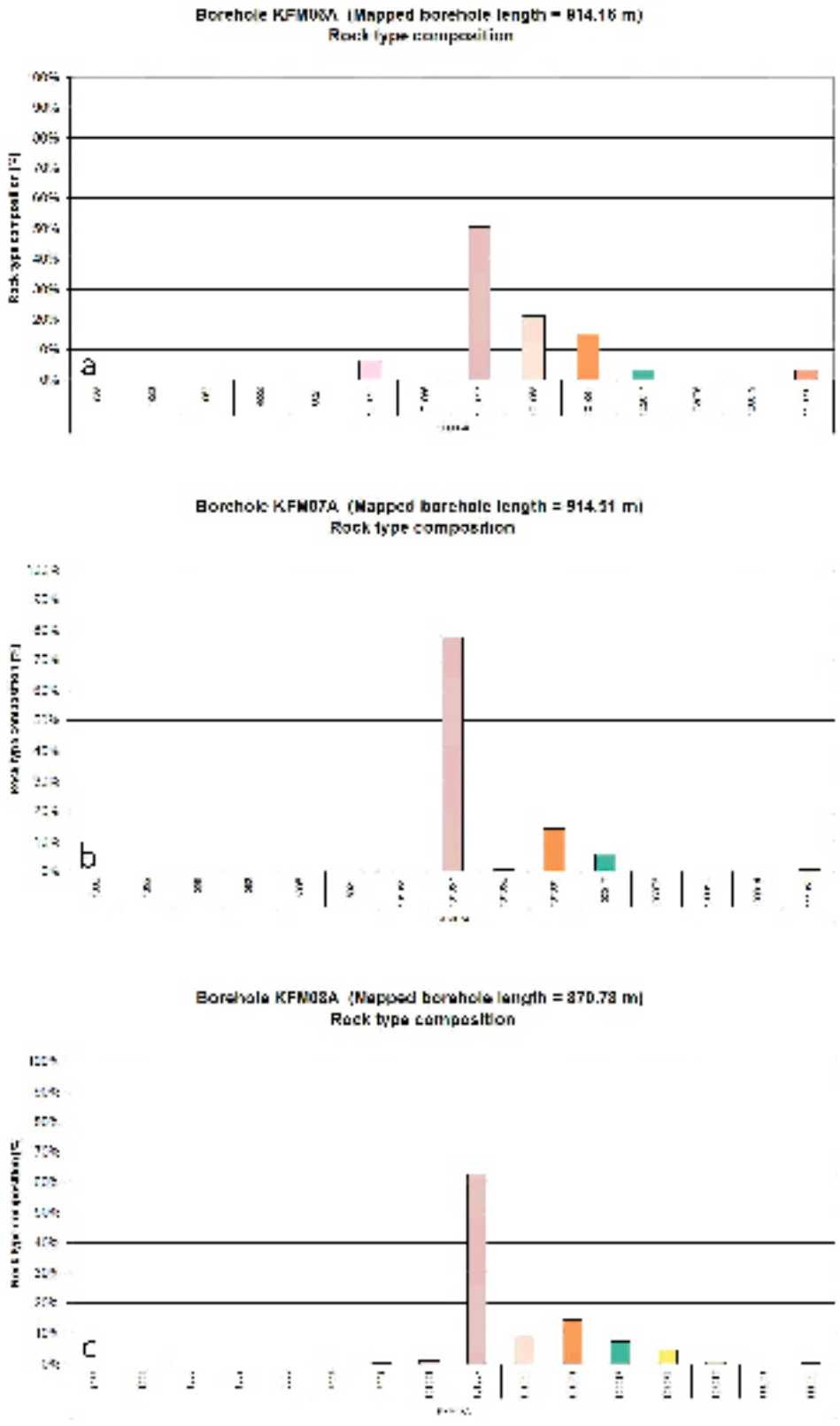

Figure 2-7. *Quantitative estimates of the proportions of different rock types in the cored boreholes KFM06A (a), KFM07A (b) and KFM08A (c). The translation of rock codes to rock type is provided in Appendix 2.1.*

As in SDM version 1.2, the standard borehole mapping has been complemented with analytical data, in order to establish, with higher confidence, the character of the rock types. Rock samples in KFM04A, KFM05A and KFM06A have been studied. New petrographic data have been acquired from 19 rock samples, including 15 modal analyses /Petersson et al. 2005/. Furthermore, geochemical data from 15 rock samples, which were collected adjacent to the samples analysed modally, are also available /Petersson et al. 2005/. In accordance with the complete site investigation programme (see p. 72 in /SKB 2005c/), special attention has been focused on the altered rocks in KFM06A. This type of alteration was initially recognised during the geological mapping at the surface /Stephens et al. 2003, 2005/ and five surface samples have also been included in the alteration study. The latter involved modal analyses, determination of feldspar composition using energy-dispersive spectrometer (EDS) analyses, and standard whole-rock geochemical analyses. New petrophysical data from boreholes KFM04A, KFM05A and KFM06A /Mattsson et al. 2005/ have not been evaluated during modelling stage 2.1.

There is a good consistency between the modal and whole-rock geochemical analyses for samples taken at the surface and at depth at the Forsmark site. This is illustrated, for example, by the similar trends in modal analyses for both sets of samples from the whole study area (Figure 2-8), as well as by the compositional variation in the samples from the candidate volume in rock domains RFM029 and RFM045 (Figure 2-9. See also Section 3.1). It is clear that the character of rocks at the surface is a good guide to judge the character of the rocks at depth. The content of quartz in the metagranite

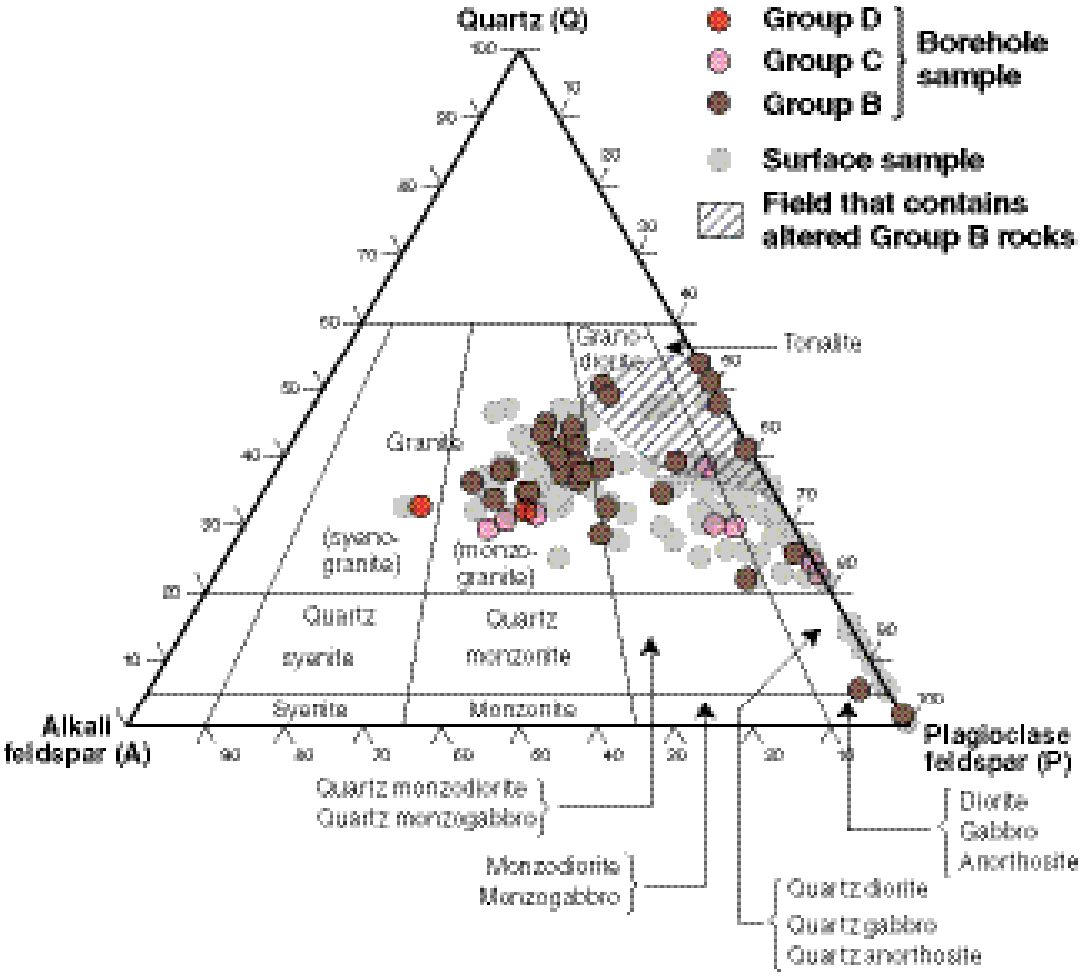

Figure 2-8. *QAP(F = 0) modal classification of the analysed intrusive rock samples at the Forsmark site. Surface samples after /Stephens et al. 2003, 2005/ and borehole samples after /Petersson et al. 2004, 2005/. The classification is based on /Streckeisen 1976/. Groups B, C and D are defined in Table 2-2.*

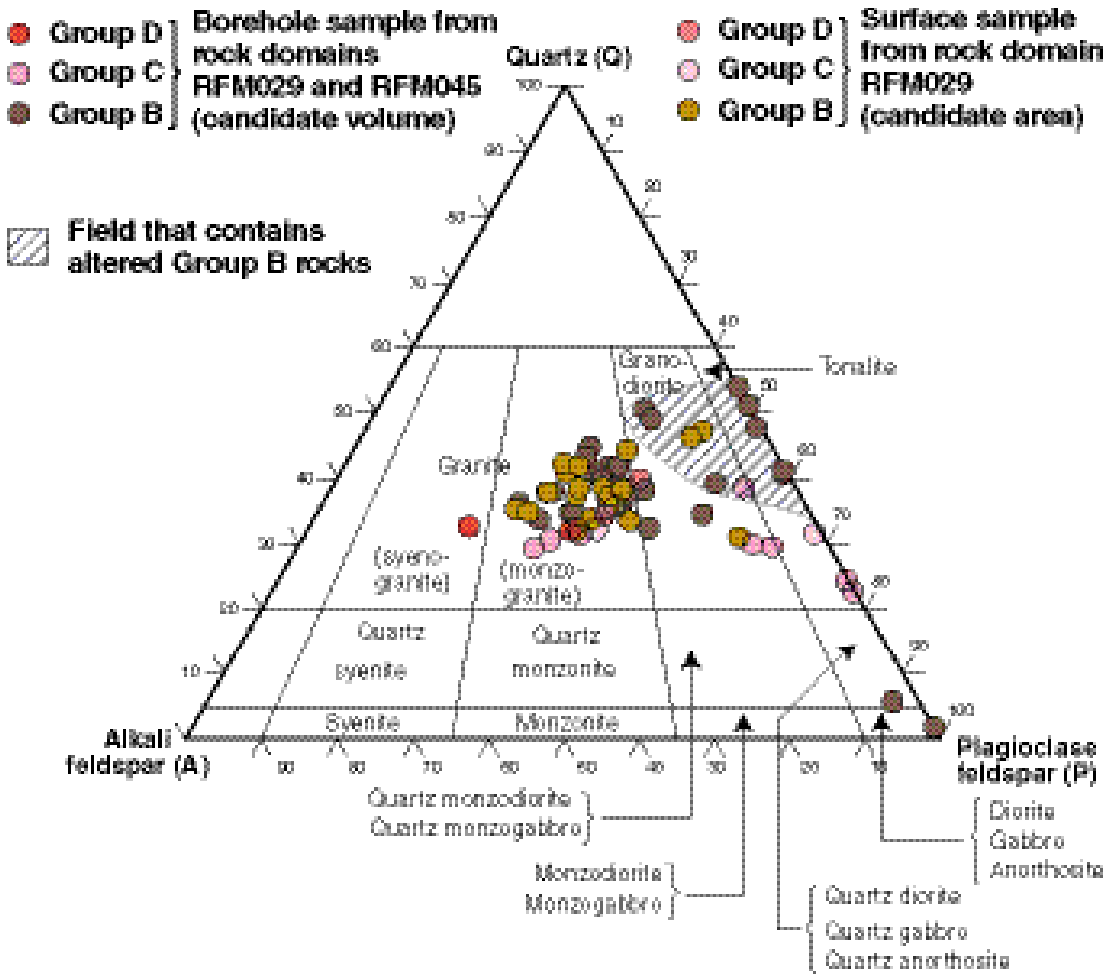

Figure 2-9. *QAP(F = 0) modal classification of the analysed intrusive rock samples inside the candidate volume in rock domains RFM029 and RFM045 (see Section 3.1). Surface samples after /Stephens et al. 2003, 2005/ and borehole samples after /Petersson et al. 2004, 2005/. The classification is based on /Streckeisen 1976/. Groups B, C and D are defined in /Table 2-2/.*

(101057) samples from the new boreholes falls inside the range reported in SDM version 1.2, i.e. 28−46%. The low-to medium-grained metagranitoid (101051) sample has a quartz content that also falls inside the range for these rocks, which was established during SDM version 1.2, i.e. 15−35%. As expected, the amphibolite samples contain little quartz (< 5%). Duplicate modal analysis of a sample of aplitic metagranite (101058) yielded a difference in quartz content of 0.5%.

The altered granitic rocks, which were affected by a strong redistribution of alkalis prior to the regional metamorphism /Stephens et al. 2003, 2005, Petersson et al. 2005/, show pseudotonalitic compositions on the QAP(F=0) diagram (Figure 2-8). Slightly higher contents of quartz are present in the borehole samples from KFM06A relative to the surface samples. An alteration in the form of albitisation is inferred from the feldspar analyses /Petersson et al. 2005/. A similar type of alteration has been observed along the contacts to amphibolites in both surface outcrops /Stephens et al. 2005/ and in the boreholes /Petersson et al. 2005/, suggesting that this alteration may have been triggered by the heat supply provided by the intrusion of the amphibolites.

Ductile structures in cored boreholes

As noted in SDM version 1.2, the bedrock in all the boreholes shows ductile mineral fabrics that were formed under amphibolite facies metamorphic conditions, at mid-crustal depths. These fabrics are defined by oriented mineral grains and mineral grain aggregates.

A composite linear and planar grain-shape fabric, with a slight predominance of the linear structural element, is present in boreholes KFM06A, KFM06B, KFM08A and KFM08B. However, the altered, fine-grained rocks in the lower part of KFM06A show a more planar grain-shape fabric. The intensity of fabric development varies from faint to medium. By contrast, the fabric in KFM07A is generally more planar in character, consistent with the location of this borehole closer to the margin of the tectonic lens at Forsmark (Figure 2-6 and /SKB 2005a/). Beneath a depth of 657 m in borehole KFM07A, the rocks show more intense ductile strain. Over 75% of the discrete ductile and ductile-brittle deformation zones in the borehole are concentrated beneath this depth. Mica enrichment is also conspicuous in this strongly deformed bedrock.

The orientations of both the planar grain-shape fabric and the discrete, ductile and ductile-brittle zones in each borehole are presented in the borehole mapping reports (see references in Appendix 1). In KFM06A, both sets of planar structures strike E to ESE and dip moderately to steeply to the south. By contrast, in borehole KFM07A, which intersects the bedrock on the south-western flank of a major synformal structure /Stephens et al. 2003, SKB 2005a/, the planar grain-shape fabric as well as the ductile and ductile-brittle zones strike N-S and are vertical or sub-vertical. Boreholes KFM08A and KFM08B intersect the bedrock in the hinge of the fold structure. An overall great circle distribution for these structures on an equal area stereographic plot (see Figure 5-1 in Petersson et al. 2005) confirms the influence of folding in this area. The folding is also manifested in the change in orientation of the planar fabric from NNW and steeply dipping in KFM08B and the uppermost part of KFM08A to more E-W and moderately dipping in the deeper part of KFM08A.

Growth of mineral sets along fractures in cored boreholes − evidence for a long geological history

On the basis of the growth relationships between different minerals along fractures in boreholes KFM01B, KFM04A, KFM05A and KFM06A, six generations of mineral sets along fractures have been identified /Sandström and Tullborg 2005/. This analysis confirms, with some modifications, the results presented earlier for boreholes KFM01A, KFM02A, KFM03A and KFM03B /Sandström et al. 2004/ that were used in SDM version 1.2 /SKB 2005a/. The different mineral generations are summarised below, from oldest (1) to youngest (6):

1. Epidote, quartz and chlorite.
2. Adularia/hematite, quartz and albite followed by prehnite, laumontite (Ca-rich zeolite), calcite and chlorite/corrensite.
3. Formation of cavities and voids along fractures followed by precipitation of euhedral quartz as well as adularia, chlorite/corrensite and calcite.
4. Pyrite, calcite, corrensite and analcime (Na-rich zeolite).
5. Asphaltite with subordinate sulphides and baryte.
6. Calcite and clay minerals.

An important phase of fracture formation occurred in connection with the precipitation of the minerals in generation 1. Epidote, in particular, is conspicuous along steeply dipping fractures that strike NW and also along gently dipping or sub-horizontal fractures (Figure 2-10a). The mineral paragenesis in generation 1 formed under greenschist facies metamorphic conditions, i.e. at temperatures > 350°C. Assuming that the temperature in the hydrothermal fluids is similar to that in the surrounding wall rock, the $^{40}Ar/^{39}Ar$ biotite cooling ages at the site /Page et al. 2004/ indicate that generation 1 formed prior to 1,700 million years ago, i.e. during the later part of the Svecokarelian orogeny (see also /SKB 2005a/).

Laumontite commonly fills or coats steeply dipping fractures with NE strike /SKB 2005a, Sandström and Tullborg 2005/. However, laumontite and, especially, prehnite in generation 2 are also present along steeply dipping fractures that strike NW, and along fractures that are gently dipping or are sub-horizontal /SKB 2005a/. Reactivation of fractures with these orientations is apparent. Isotopic data for calcite in generation 2 indicate a hydrothermal origin /Sandström and Tullborg 2005/. Furthermore, the occurrence of hematite, both as a staining in fracture minerals (e.g. adularia) and as wall rock alteration adjacent to fractures, indicates oxidising redox conditions for both generations 1 and 2 /Sandström and Tullborg 2005/.

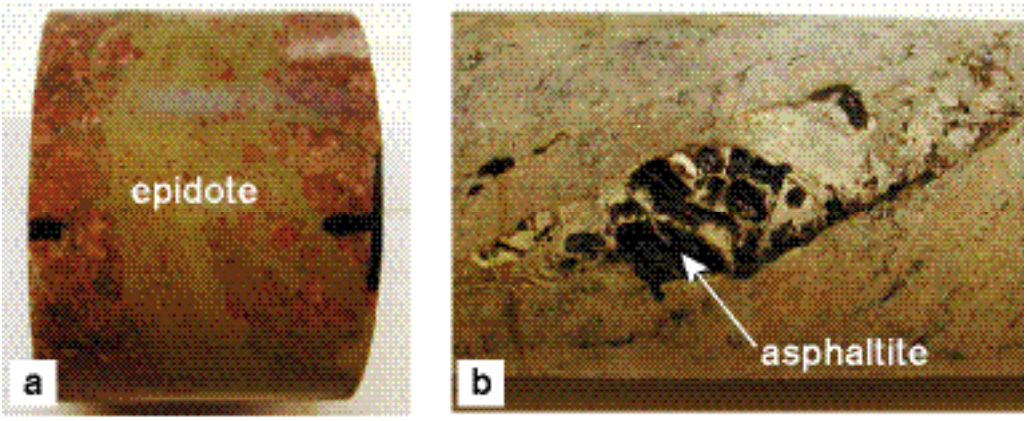

Figure 2-10. *a) Epidote-bearing cataclasite that dips gently towards the NW. The diameter of the drill core (KFM06A) is c. 5 cm (after /Sandström and Tullborg 2005/). b) Asphaltite in voids in older, partly dissolved calcite along a steeply dipping fracture. The diameter of the drill core (KFM06A) is c. 5 cm (after /Sandström and Tullborg 2005/).*

The minerals prehnite and laumontite in generation 2 formed under prehnite-pumpellyite and upper zeolite facies metamorphic conditions, respectively, i.e. at temperatures < 350°C and between 250–150°C. The biotite cooling ages at the site define a maximum age of 1,700 million years, at least for the growth of laumontite in generation 2. Bearing in mind the tectonic development of the Fennoscandian Shield /SKB 2004, 2005a/, laumontite-bearing fractures formed or reactivated in a different tectonic regime, relative to that indicated by the fractures in generation 1. Since laumontite forms the oldest mineral coating along several fractures, it is possible that generation 2 developed in connection with an important phase of new fracture development /Sandström and Tullborg 2005/. However, fluid movement during a reactivation event may have destroyed the mineral traces that formed during older events. For this reason, the relative importance of new fracture formation and reactivation of older fractures for generation 2 remains an open question.

The formation or reactivation of fractures with generation 2 minerals may be related to Gothian tectonic reworking during the time period 1,700–1,560 million years /SKB 2004, 2005a/. Furthermore, the disturbance of the U-Pb system for titanite after 1,100 million years ago /Page et al. 2004/ is consistent with a tectonic reworking of the Forsmark area during the Sveconorwegian orogeny. For this reason, this important tectonic event is also considered to be a possible candidate for the development of the minerals in generation 2. The development of cavities and voids along fractures during generation 3 confirms the inferences made in /Möller et al. 2004/ that the conspicuous vuggy metagranite in borehole KFM02A formed in the brittle regime, following the completion of ductile deformation in the bedrock.

The isotopic composition of calcite and the occurrence of pyrite in mineral generation 4 indicate a marked change in the character of the fluids relative to generations 1 and 2. There appears to be both an influence of biogenic carbon in the calcite and a changeover to reducing redox conditions /Sandström and Tullborg 2005/. The character of the minerals in generation 5, including the occurrence of asphaltite (Figure 2-10b), which is restricted to fractures at shallow crustal levels (< 170 m), confirms the significance of organic material in the fluids and the occurrence of a reducing environment. Late Cambrian and Early Ordovician oil shales, which covered the old crystalline bedrock at Forsmark during the earlier part of the Phanerozoic /SKB 2004, 2005a/, has been proposed as a source for the hydrocarbons in the asphaltite /Sandström and Tullborg 2005, Sandström et al. 2006/. The depth dependence for this mineral indicates downward migration of hydrocarbon-bearing fluids into the crystalline bedrock during the Phanerozoic /Sandström et al. 2006/.

The calcite and clay minerals in the youngest group of minerals (generation 6) commonly occur along hydraulically conductive fractures. Furthermore, downward migration of fluids and the filling of reactivated ancient fractures or newly formed, sub-horizontal sheet joints with glacial sediment is apparent in the uppermost (< few tens of metres) part of the crystalline bedrock. This process occurred during the Quaternary, in connection with the removal of one or more ice sheets /Carlsson 1979, Leijon 2005/, and is discussed further in Section 3.2.

In summary, the fracture mineralogy /Sandström et al. 2004, Sandström and Tullborg 2005/, in combination with the $^{40}Ar/^{39}Ar$ biotite cooling ages /Page et al. 2004/ and an assessment of the tectonic development in the Fennoscandian Shield /SKB 2004, 2005a/, indicate a long geological history for the development of fractures at Forsmark. Some significant events are listed below:

1. Formation of epidote-bearing fractures (steeply dipping NW and gently dipping) in connection with tectonic activity during the later part of the Svecokarelian orogeny.
2. Significant reactivation and/or formation of steeply dipping fractures with NE strike in connection with tectonic activity during the Gothian and/or Sveconorwegian orogenies.
3. Downward migration of hydrocarbon-bearing fluids along fractures in the crystalline bedrock during the Phanerozoic.
4. Downward migration of fluids containing glacial sediment along fractures in the uppermost part of the crystalline bedrock during the Quaternary.

2.4.4 Fracture frequency in cored borehole data

Data that bear on the occurrence, orientation and character of fractures in the bedrock have been generated in connection with the mapping of the boreholes KFM06A, KFM06B, KFM07A, KFM08A, KFM08B and HFM20–22 (see reference list in Appendix 1). Since model version 2.1 has not involved any discrete fracture network (DFN) modelling work, only fracture frequency data, which are highly relevant for the identification of fracture zones (see Section 2.4.5), are addressed in this section. The analysis of these data has also proved to be of importance for the conceptual understanding of the structural geology of the site (see Section 3.2). On account of data quality considerations (see above), only cored borehole data are discussed here. The orientation and mineralogy of fractures within the zones that have been recognised in connection with the version 2.1 work are addressed in Sections 2.4.5 and 3.2.

The quantity of different categories of fractures that have been documented during the mapping of the boreholes used in model version 2.1 are shown in Table 2-3. The same parameters for fractures outside modelled deformation zones are listed in Table 2-4. Bearing in mind the uncertainty in the calculation of the number of fractures in so-called crush zones and sealed fracture networks, the values in both tables do not include the fractures that have been estimated in these structures. The deformation zones in Table 2-4 have been identified with the help of the single hole interpretations of the boreholes (see Section 2.4.5), but correspond to the zones actually modelled in version 2.1 (see Section 3.2). For this reason, the fractures in the potential zones that have been identified in the single hole interpretation, but that have not been modelled, are also included in Table 2-4.

Table 2-3. Fractures in cored boreholes analysed in modelling stage 2.1. Crush zones and sealed fracture networks are not included.

Cored borehole	Total number of fractures	Open fractures	Partly open fractures	Sealed fractures	Percent of open fractures	Fracture frequency per metre (all)	Fracture frequency per metre (open)
KFM01A	1,638	775	41	822	47%	1.69	0.80
KFM01B	1,753	571	89	1,093	33%	3.59	1.17
KFM02A	2,354	343	138	1,873	15%	2.38	0.35
KFM03A–B	2,019	297	114	1,608	15%	2.03	0.30
KFM04A	4,426	1,226	232	2,968	28%	4.48	1.24
KFM05A	2,835	591	42	2,202	21%	3.16	0.66
KFM06A–B	4,239	970	136	3,133	23%	4.29	0.98
KFM07A	3,173	561	56	2,556	18%	3.54	0.63
KFM08A	4,265	663	50	3,552	16%	5.03	0.78
KFM08B	743	176	23	544	24%	3.82	0.91

Table 2-4. Fractures in cored boreholes analysed in modelling stage 2.1 and situated outside the modelled deformation zones. Crush zones and sealed fracture networks are not included.

Cored borehole	Total number of fractures	Percent of fractures outside DZ	Open fractures		Partly open fractures	Sealed fractures	Percent of open fractures	Fracture frequency per metre (all)	Fracture frequency per metre (open)	
			All	Certain					All	Certain
KFM01A	1,157	71%	612	128	37	508	53%	1.19	0.63	0.13
KFM01B	863	49%	222	34	17	624	26%	1.77	0.45	0.07
KFM02A	1,264	54%	91	15	44	1,129	7%	1.28	0.09	0.02
KFM03A–B	1,578	78%	182	43	83	1,313	12%	1.59	0.18	0.04
KFM04A	2,485	56%	605	53	65	1,815	24%	2.51	0.61	0.05
KFM05A	1,602	57%	347	32	27	1,228	22%	1.78	0.39	0.04
KFM06A–B	1,397	33%	284	37	22	1,091	20%	1.41	0.29	0.04
KFM07A	2,475	78%	339	27	32	2,104	14%	2.76	0.38	0.03
KFM08A	3,547	83%	504	87	34	3,009	14%	4.19	0.59	0.10
KFM08B	600	81%	150	18	22	428	25%	3.09	0.77	0.09

Compared to all the boreholes except KFM04A, which were analysed in SDM version 1.2 /SKB 2005a/, boreholes KFM06A/KFM06B, KFM08A and KFM08B contain a high, overall frequency of fractures (4–5 fractures/metre, see Table 2-3). This value is comparable to that in borehole KFM04A, where the majority of fractures are concentrated in the upper half of the borehole, i.e. in the bedrock that lies outside the candidate volume. However, the frequency of inferred open fractures in boreholes KFM06A/KFM06B, KFM08A and KFM08B is less than that in KFM04A and similar to that, for example, in the cored boreholes at drill site 1. Indeed, the maximum number of sealed fractures in all the boreholes at the Forsmark site occurs in borehole KFM08A. The overall fracture frequency in borehole KFM07A is lower than that in the other new boreholes (3–4 fractures/metre, see Table 2-3). Once again, the frequency of inferred open fractures is comparable to several of the boreholes used in SDM version 1.2.

In boreholes KFM06A/KFM06B, it has been possible to model all the deformation zones recognised in the single hole interpretation (Figure 2-11). For this reason, the frequency of fractures outside deformation zones is low and comparable to that in the boreholes used for SDM version 1.2 (excluding KFM04A), i.e. 1–2 fractures/metre (Table 2-4). Since modelled zones and zones recognised in the single hole interpretation differ somewhat from each other in boreholes KFM07A (Figure 2-12) and KFM08A (Figure 2-13), the frequency of fractures outside modelled deformation zones is, as a consequence, higher (2–3 and over 4 fractures/metre, respectively, see Table 2-4). Once again it needs to be emphasised that the anomaly is caused by the high frequency of sealed fractures.

The mode of variation of different types of fractures with depth in boreholes KFM06A/KFM06B (Figure 2-11), KFM07A (Figure 2-12) and KFM08A (Figure 2-13) resembles the pattern recognised in boreholes KFM01A, KFM01B and KFM05A in SDM version 1.2. All these boreholes are situated in the north-western part of the candidate area. This pattern is characterised by a concentration of open and partly open fractures in the upper part of each borehole. For example, approximately 50% of the inferred open fractures occur in the upper 300–350 m in these boreholes. However, there is a significant increase in the occurrence of open and partly open fractures in the deformation zone at the base of KFM07A. Excluding the restricted, flatter intervals associated with deformation zones, the sealed fractures appear to be more evenly distributed with depth in all three boreholes. This contrast in behaviour between the open and sealed fractures suggests a relationship between the development of aperture in the fractures and the present topographic surface. This point is addressed again later in Section 3.2, in the context of a conceptual understanding of the Forsmark site.

A second feature concerns the marked contrast in the variation of fractures with depth between the data from the boreholes in the north-western part of the candidate area (e.g. Figure 2-11 and Figure 2-12) and the data from boreholes KFM03A/KFM03B in the south-eastern part of the area (Figure 2-14). Excluding once again the restricted, flatter intervals associated with deformation zones, there is a far more even distribution of both open and sealed fractures with depth in boreholes KFM03A/KFM03B (Figure 2-14). This contrast between the two parts of the candidate area was recognised in SDM version 1.2 /SKB 2005a/ and is confirmed here. The results of the inspection of the cumulative fracture frequency plots are discussed further in Section 3.2.

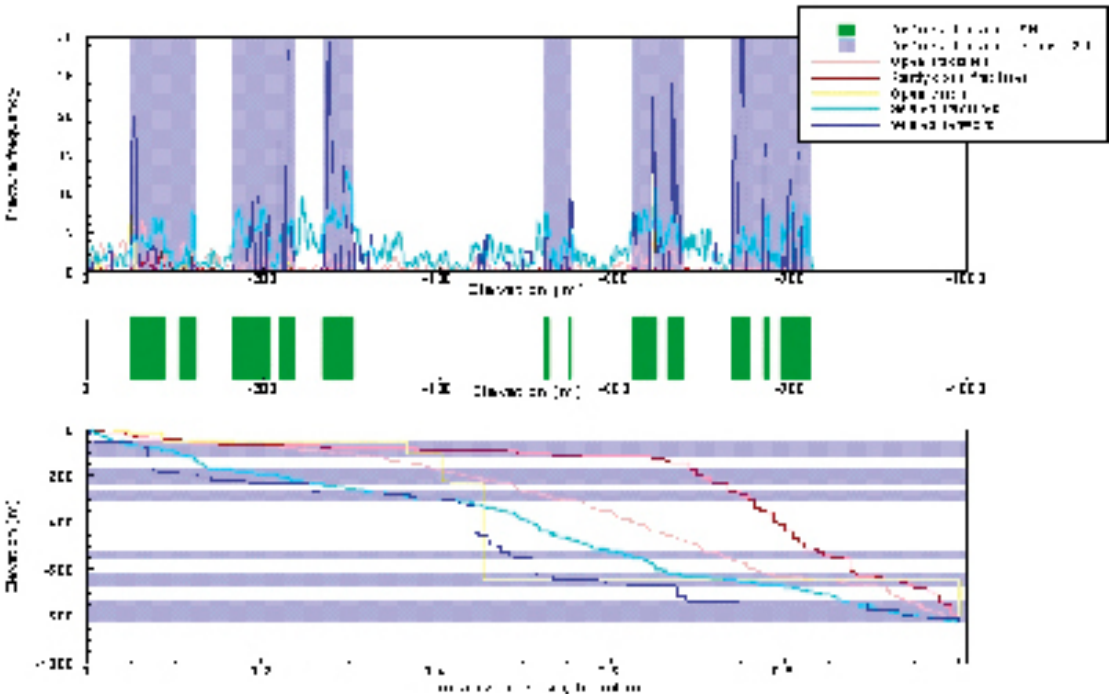

Figure 2-11. *Fracture frequency plots for the cored boreholes KFM06A and KFM06B. The upper diagram is a moving average plot with a 5 m window and 1 m steps, and the lower diagram is a cumulative frequency plot. Fracture zones, as defined in the single hole interpretation (see Section 2.4.5) and in the modelling procedure (see Section 3.2), are also marked. Elevation is provided using the RHB 70 system.*

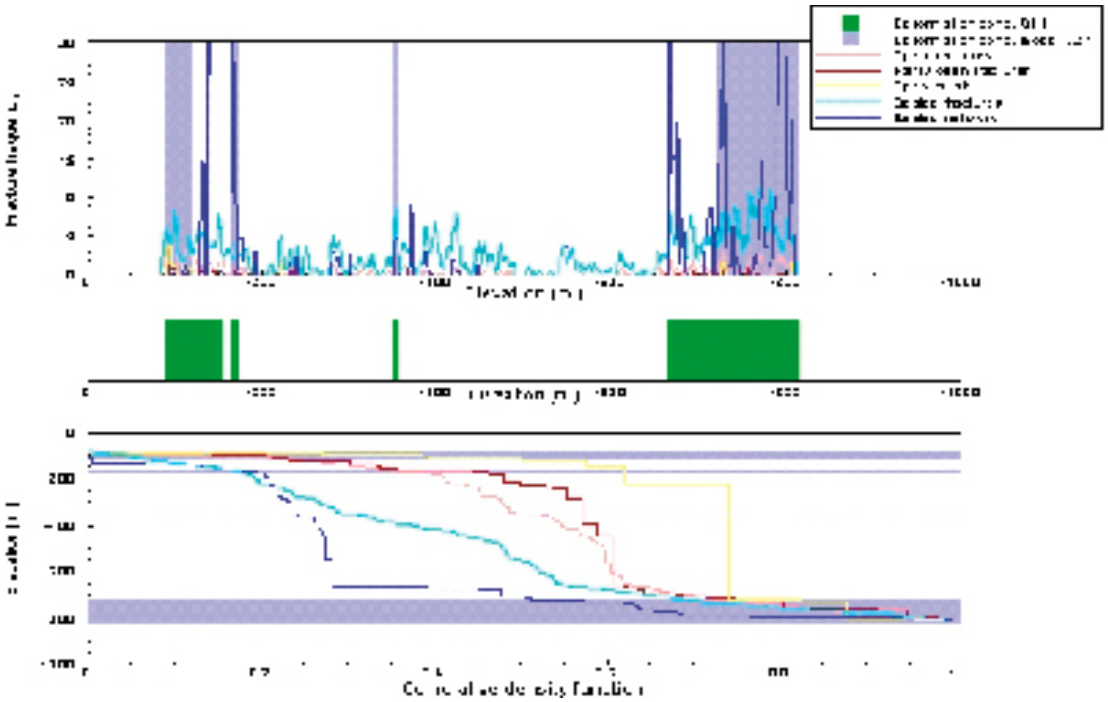

Figure 2-12. *Fracture frequency plots for the cored borehole KFM07A. The upper diagram is a moving average plot with a 5 m window and 1 m steps, and the lower diagram is a cumulative frequency plot. Fracture zones, as defined in the single hole interpretation (see Section 2.4.5) and in the modelling procedure (see Section 3.2), are also marked. Elevation is provided using the RHB 70 system.*

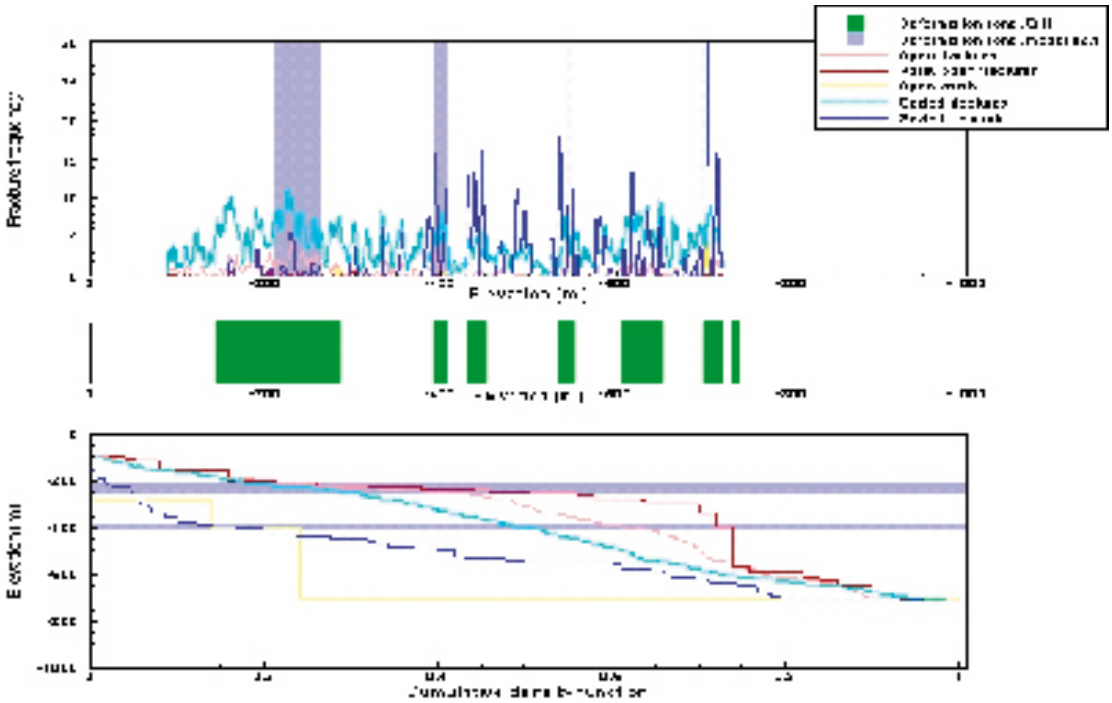

Figure 2-13. *Fracture frequency plots for the cored borehole KFM08A. The upper diagram is a moving average plot with a 5 m window and 1 m steps, and the lower diagram is a cumulative frequency plot. Fracture zones, as defined in the single hole interpretation (see Section 2.4.5) and in the modelling procedure (see Section 3.2), are also marked. Elevation is provided using the RHB 70 system.*

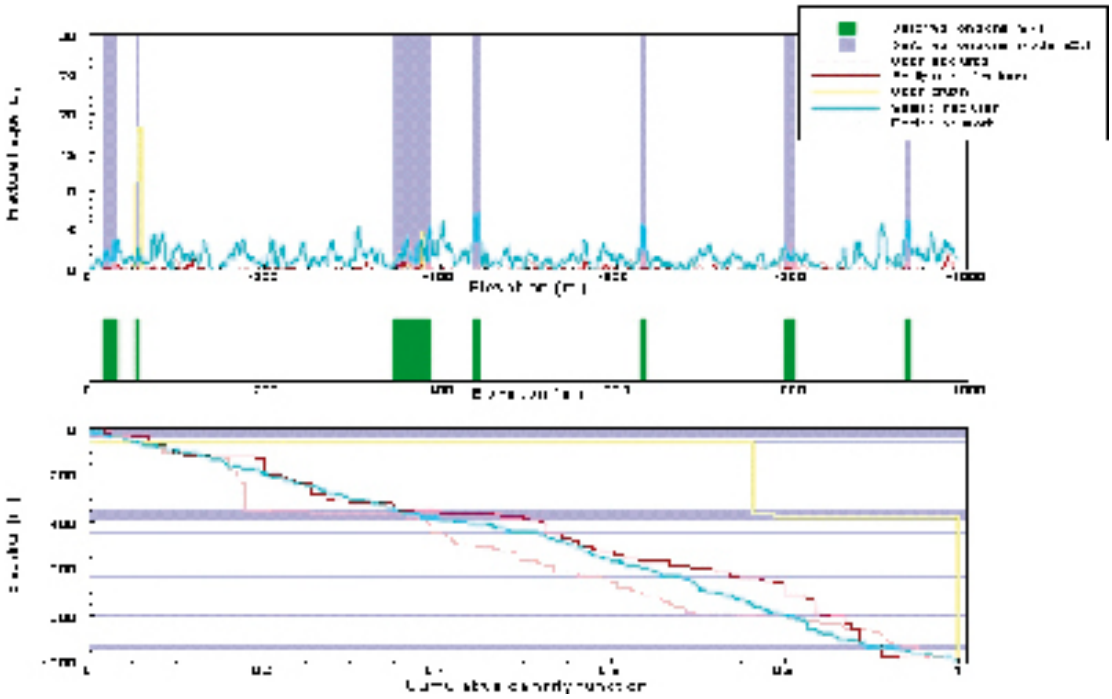

Figure 2-14. *Fracture frequency plots for the cored boreholes KFM03A/KFM03B. The upper diagram is a moving average plot with a 5 m window and 1 m steps, and the lower diagram is a cumulative frequency plot. Fracture zones, as defined in the single hole interpretation (see Section 2.4.5) and in the modelling procedure (see Section 3.2), are also marked. Elevation is provided using the RHB 70 system.*

2.4.5 Single hole interpretation

Aims and methodology

A single hole interpretation provides a synthesis of all the geological and geophysical information in a borehole. It aims to document the rock units that show a minimum length of 5–10 m along the borehole as well as the possible deformation zones that are intersected in the borehole, i.e. fixed data points for these zones at depth. The identification of these geological features is made independently for each borehole. Correlation of these features between boreholes and with surface data forms a key part of the modelling work (see Section 3.1).

The following input data have been used in all the single hole interpretations:

- Geological mapping data using BIPS and the Boremap system.
- Borehole radar data and their interpretation. The orientation of radar reflectors has not been used in the modelling work (see above).
- Geophysical logs and their interpretation.

Short descriptions of each rock unit and deformation zone in the boreholes, which have been assessed for the first time in connection with model version 2.1 (KFM06A/KFM06B, KFM07A and HFM20–21, KFM08A/KFM08B and HFM22), are provided in /Carlsten et al. 2005abc/, respectively. The confidence in the interpretation of the different geological components has been assessed on the following basis: 3 = certain, 2 = probable, 1 = possible. The rock units and deformation zones that have been identified in the boreholes analysed for the first time in connection with model version 2.1 are shown in Figure 2-15.

Rock units

According to the recommendations in the revised method description for single hole interpretation (March 2006), rock units that are similar in composition, but occur at different depths along a borehole, share the same general identification code (e.g. RU1). However, they are distinguished with the use of different letters (e.g. RU1a, RU1b, RU1c etc). Even rock units that are compositionally identical but show some other difference (e.g. frequency of fractures) have been distinguished in the same manner. This procedure permits a unique identity for each borehole interval.

Throughout the cored boreholes KFM06B, KFM07A and KFM08B, and the percussion boreholes HFM20, HFM21 and HFM22, rock units dominated by medium-grained metagranite are present (Figure 2-15). Subordinate occurrences of pegmatitic granite and amphibolite as well as only minor occurrences of fine- to medium-grained metagranitoid occur within these units. Between c. 500 and 657 m depth in KFM07A, metamorphosed and altered (bleached) varieties of the granite are present (Figure 2-15). Similar alteration of the medium-grained granitic rock has been observed in shallow boreholes beneath the nuclear reactor sites 1 and 2. Beneath 657 m, borehole KFM07A consists of rock units that are compositionally similar to the remainder of the borehole (RU2a, RU2b) or are dominated by pegmatitic granite (RU3). However, the rocks in these units are affected by more intense ductile deformation, grain-size reduction and enrichment in mica (Figure 2-15).

Gently dipping or sub-horizontal fractures with wide apertures, some crush zones, and both caliper and resistivity anomalies have been noted in the rock units dominated by medium-grained metagranite in the upper parts of boreholes KFM06B, KFM08B, HFM20 and HFM22. These features have not been coupled with deformation zones. However, they illustrate the “open” character of the bedrock at the shallowest crustal levels. A rock unit (RU1b) dominated by medium-grained metagranite, but characterised by a somewhat higher frequency of sealed fractures, relative to that observed outside the deformation zones, occurs between 353 and 425 m depth in borehole KFM07A (Figure 2-15). In the same manner, RU1, throughout the whole borehole length in KFM08B, is characterised by a high frequency of sealed fractures (Figure 2-15).

Rock units (RU1a, RU1b) that are composed of medium-grained metagranite, with subordinate amounts of pegmatitic granite, amphibolite, fine-to medium-grained metagranitoid and leucocratic granite, dominate down to 629 m depth in borehole KFM06A (Figure 2-15). Bleached and strongly albitised rocks (RU4) are present along more or less the remainder of this borehole (Figure 2-15).

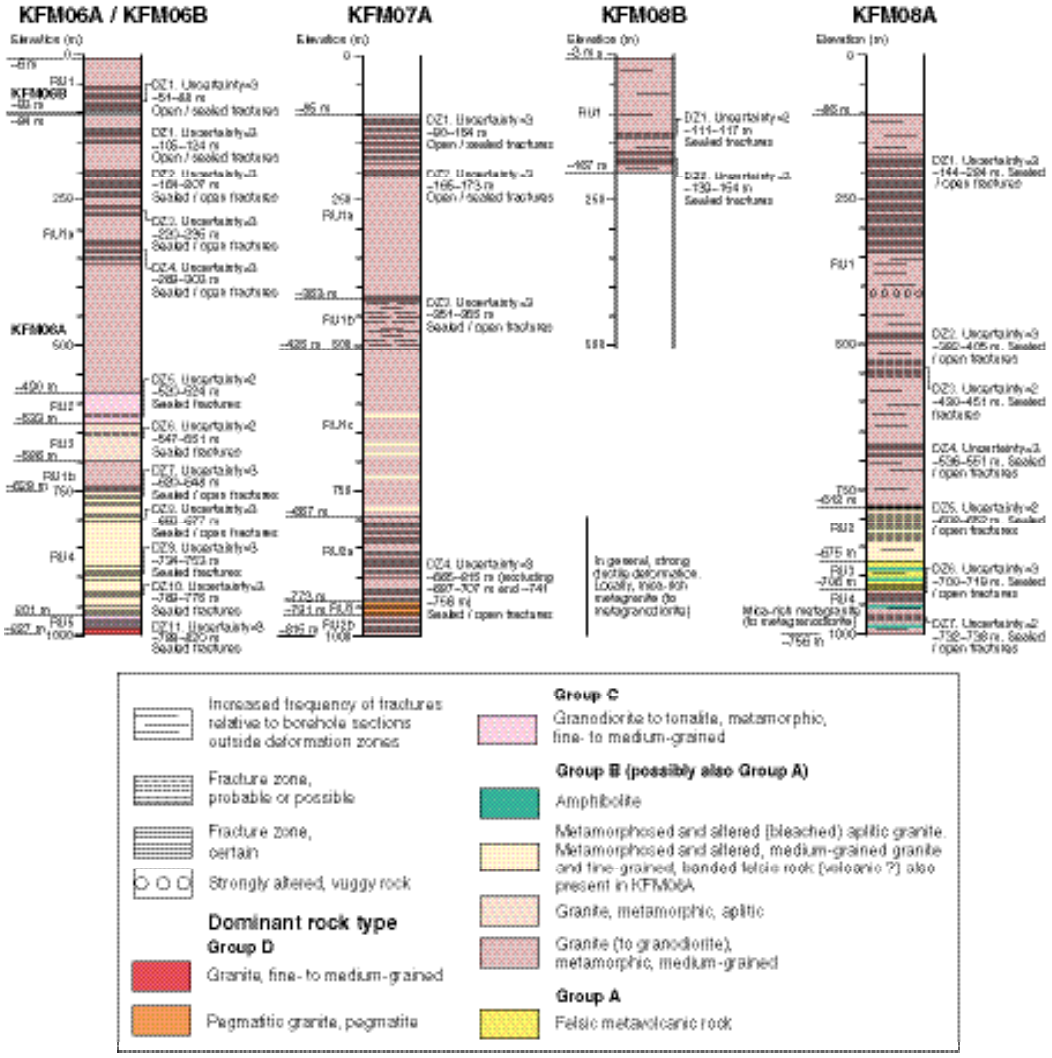

Figure 2-15. *Rock units and possible deformation zones based on the single hole interpretations of the cored boreholes analysed for the first time during modelling stage 2.1. Both elevation and borehole interval values are shown for each borehole. Elevation is provided using the RHB 70 system.*

The precursor to these metamorphosed and altered rocks is predominantly an aplitic granite. Medium-grained granite and a banded, fine-grained rock, that is possibly volcanic in origin, form subordinate precursors.

Down to 612 m and beneath 706 m depth, borehole KFM08A intersects rock units (RU1, RU4) that are also composed of medium-grained metagranite, with subordinate amounts of pegmatitic granite and amphibolite (Figure 2-15). A conspicuous feature of these units is the high frequency of sealed fractures, relative to that observed along borehole sections outside deformation zones in, for example, boreholes KFM06A and KFM07A. At depths between 612 and 706 m, aplitic metagranite, which is affected by faint to medium albitisation, lies structurally above an inhomogeneous mixture of felsic metavolcanic rock, amphibolite, pegmatitic granite and aplitic metagranite (Figure 2-15). Both these rock units (RU2, RU3) also show the same, increased frequency of sealed fractures.

Possible deformation zones

Only brittle, deformational structures, which are referred to here as possible fracture zones, have been recognised in the single hole interpretations that have been completed as a prequisite to model version 2.1. The geological and geophysical features used for the identification of such zones and the terminological considerations for these brittle structures are summarised in /SKB 2005a, p. 205–208/.

High fracture frequency (Figure 2-11, Figure 2-12 and Figure 2-13) in association with wall rock alteration and decreased rock resistivity have so far proven to be the prime criteria in the identification of these zones. The alteration involves a red-staining that is associated with the development of a fine-grained dissemination of hematite. It can be expected that such an alteration will correspond to low magnetic anomalies in a bedrock that shows normal, background magnetic susceptibility values. Zones defined by a high frequency of sealed fractures, open fractures or both are present. The occurrence of groundwater-bearing fractures has not played any role in the identification of fracture zones. A detailed description of all deformation zones recognised in the single hole interpretations at Forsmark is in progress. This study complements the short descriptions in the present data reports (Appendix 1) and the results will be used in model version 2.2.

An analysis of the orientation of the fractures in each zone has been completed (see also /Carlsten et al. 2005abc/). Only fractures that are visible in BIPS have been included in this analysis. Furthermore, sealed fractures are distinguished from open and partly open fractures in the orientation plots. An analysis of the orientation of fractures along which a particular mineral filling or coating is present has also been completed. Plots for the minerals calcite, chlorite, clay minerals, epidote, adularia-hematite, laumontite, prehnite and quartz are present. The orientation of fractures that show red-staining along their walls or that are devoid of any mineral coatings have also been documented. Some figures that illustrate the results of these analyses are presented below.

The boundaries of deformation zones, where the transitional part of the zone gradually fades out into the background fracture signature in the host rock, are often difficult to recognise. In order to gain a more confident assessment of these boundaries, a critical reappraisal of the moving average diagrams for fracture frequency (see, for example, Figure 2-11 to Figure 2-14) in all the cored boreholes at the Forsmark site has been completed during modelling stage 2.1. This inspection has resulted in a few modifications of the borehole intervals that define the deformation zones (see, for example, Figure 2-11 to Figure 2-13). A full listing of these modifications is provided in tabular format in Section 3.2. This exercise has also resulted in a structural classification of each borehole interval. Borehole sections that have been modelled as a deformation zone in model version 2.1 are distinguished from borehole sections that belong to different fracture domains. The latter are discussed further in the conceptual understanding of the structures at the Forsmark site in Section 3.2.

Steeply dipping, possible fracture zones

Fracture zones beneath 150 m and 200 m depth in boreholes KFM06A and KFM07A, respectively, as well as throughout boreholes KFM08A and KFM08B (Figure 2-15) are dominated by steeply dipping, sealed fractures and sealed fracture networks, i.e. steeply dipping, cohesive structures. More than one orientation set of fractures is present along many of these zones, commonly a steeply dipping set and a subordinate gently dipping set (Figure 2-16). Zones DZ2−DZ4 and DZ5−DZ11 in borehole KFM06A and DZ1 in KFM08A are dominated by fractures that strike NE (or ENE) and dip steeply (Figure 2-16a). Calcite, chlorite, adularia-hematite and quartz form mineral fillings or coatings along the fractures in these zones (Figure 2-17). Laumontite is also present along both steeply and gently dipping fractures in zones DZ9, DZ10 and DZ11, close to the base of KFM06A, and along DZ1 in KFM08A.

Zone DZ4 in the lower part of KFM07A and the more subordinate zones DZ2 in KFM08A and DZ2 in KFM08B share several features. Sealed fractures that strike NNW and dip steeply are conspicuous (Figure 2-16b, c). However, steeply dipping sealed fractures that strike NE as well as gently dipping fractures are also present. The subordinate open and partly open fractures along these zones belong to the steeply dipping NNW set or are gently dipping (Figure 2-16b, c), and clay minerals are present along the former in DZ4 in KFM07A (Figure 2-18). As in several of the other fracture zones at the Forsmark site, calcite, chlorite and adularia-hematite are common fracture minerals. Laumontite and quartz are also present along the fractures in DZ4 in KFM07A. It is inferred that these zones represent geologically old, steeply dipping NNW structures that opened up during one or more later events in the geological development. DZ4 in borehole KFM07A shows a similar orientation and occurs more or less at the same depth as the strong ductile deformation in the borehole (see above and Figure 2-15).

Gently dipping, possible fracture zones

Fracture zones that are characterised by a relatively high proportion of gently dipping, open and partly open fractures (Figure 2-16d), as well as some crush zones, are conspicuous in the upper part of boreholes KFM06A (DZ1) and KFM07A (DZ1 and DZ2), and in borehole KFM06B (DZ1). Open or partly open fractures are prominent in the upper parts of all these zones. Calcite, chlorite and adularia-hematite are conspicuous mineral fillings or coatings along the fractures. By contrast, clay minerals are present in predominantly gently dipping, open fractures, and quartz in both sealed and open, steeply dipping fractures (Figure 2-19). Asphaltite and pyrite have also been observed along DZ1 in KFM6B. The higher-temperature mineral epidote is present along fractures that dip gently towards the north-west along DZ1 in KFM07A. Laumontite is also conspicuous along the fractures in this zone. It is once again inferred that all these fracture zones are geologically old structures that opened up during one or more later events in the geological history.

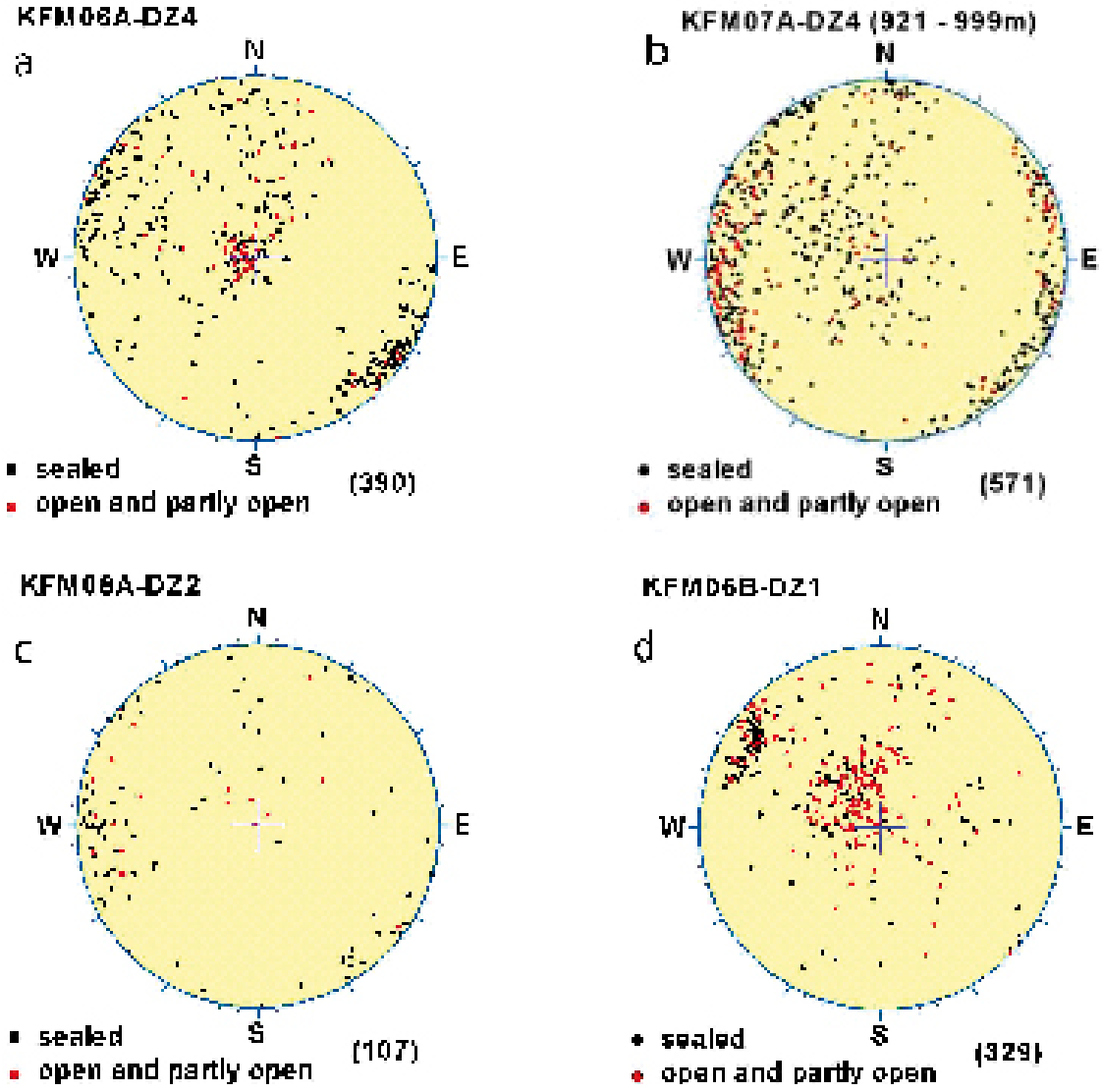

Figure 2-16. *Orientation of fractures within (a) the steeply dipping fracture zone DZ4 with NE strike in KFM06A, (b) the steeply dipping fracture zone DZ4 with NNW strike in KFM07A, (c) the steeply dipping fracture zone DZ2 with NNW strike in KFM08A, (d) the gently dipping fracture zone DZ1 in KFM06B. Fractures along a part of DZ4 in KFM07A (borehole interval 921–999 m) are shown in (b). The pole to each fracture plane is plotted on the lower hemisphere of an equal-area stereographic plot.*

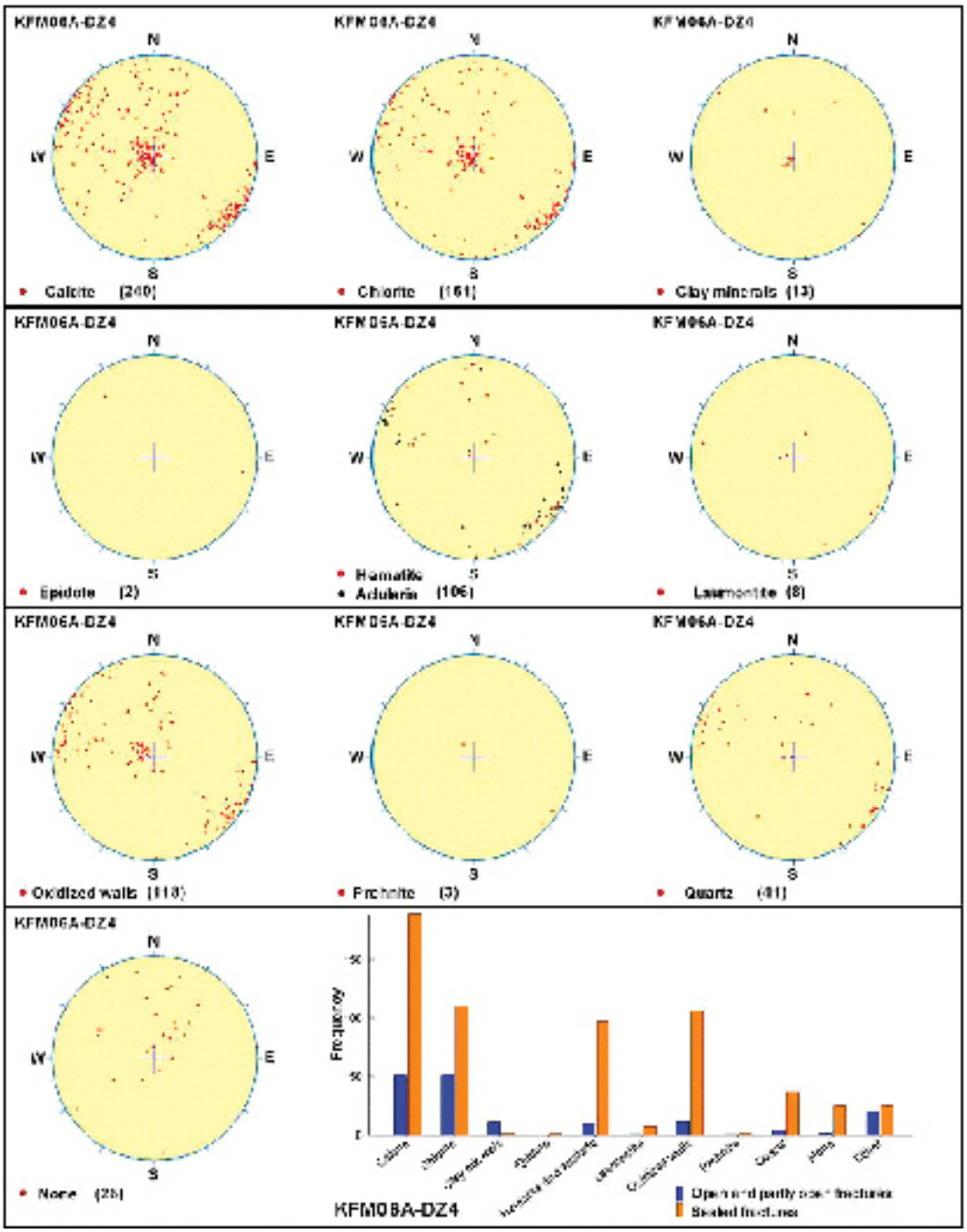

Figure 2-17. *Orientation of fractures, along which a particular mineral filling or coating has been documented, within the steeply dipping fracture zone DZ4 with NE strike in KFM06A. The frequency histogram for the minerals along this zone is also shown. The pole to each fracture plane is plotted on the lower hemisphere of an equal-area stereographic plot.*

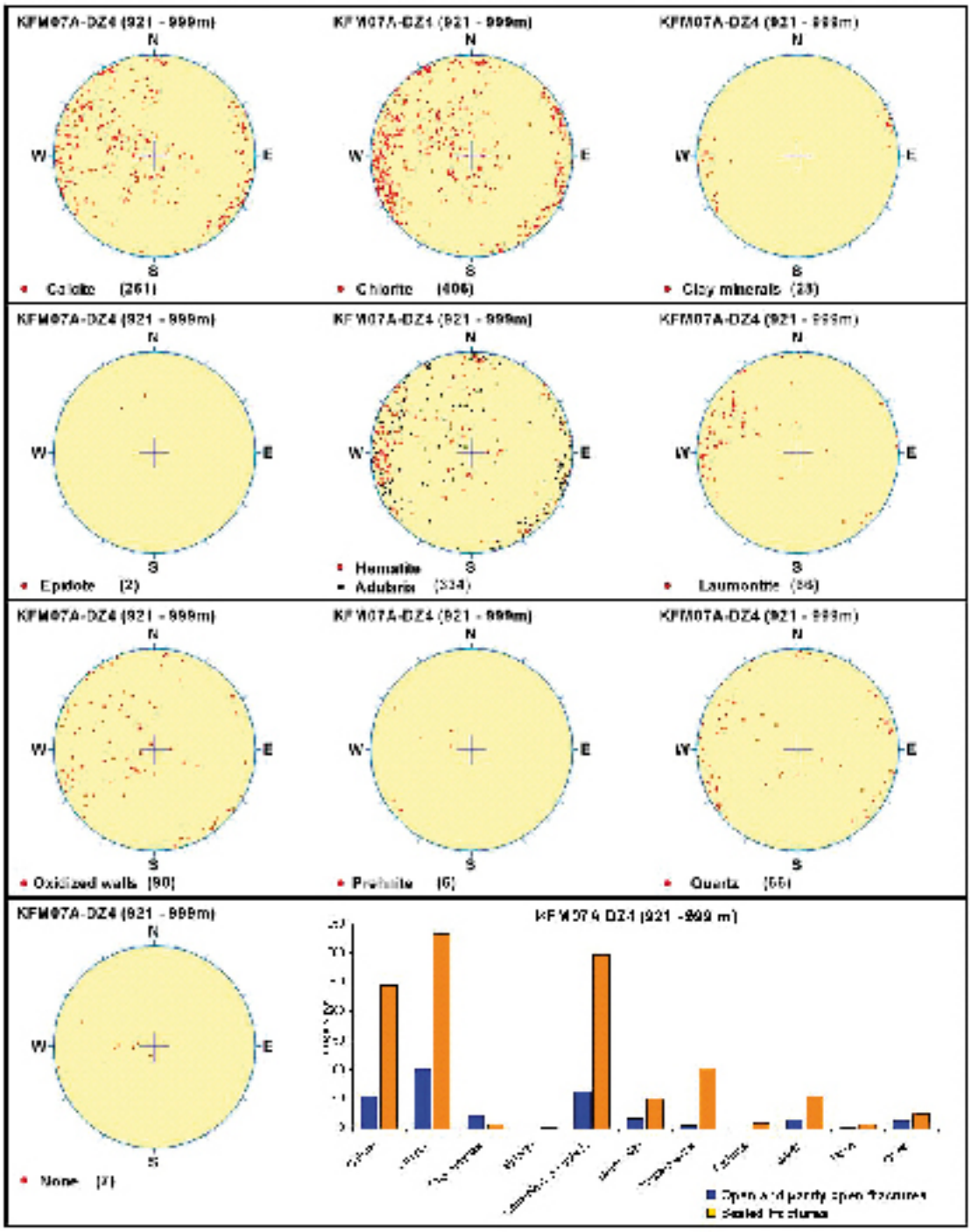

Figure 2-18. *Orientation of fractures, along which a particular mineral filling or coating has been documented, within the steeply dipping fracture zone DZ4 (720–811 m depth) with NNW strike in KFM07A. The frequency histogram for the minerals along this zone is also shown. The pole to each fracture plane is plotted on the lower hemisphere of an equal-area stereographic plot.*

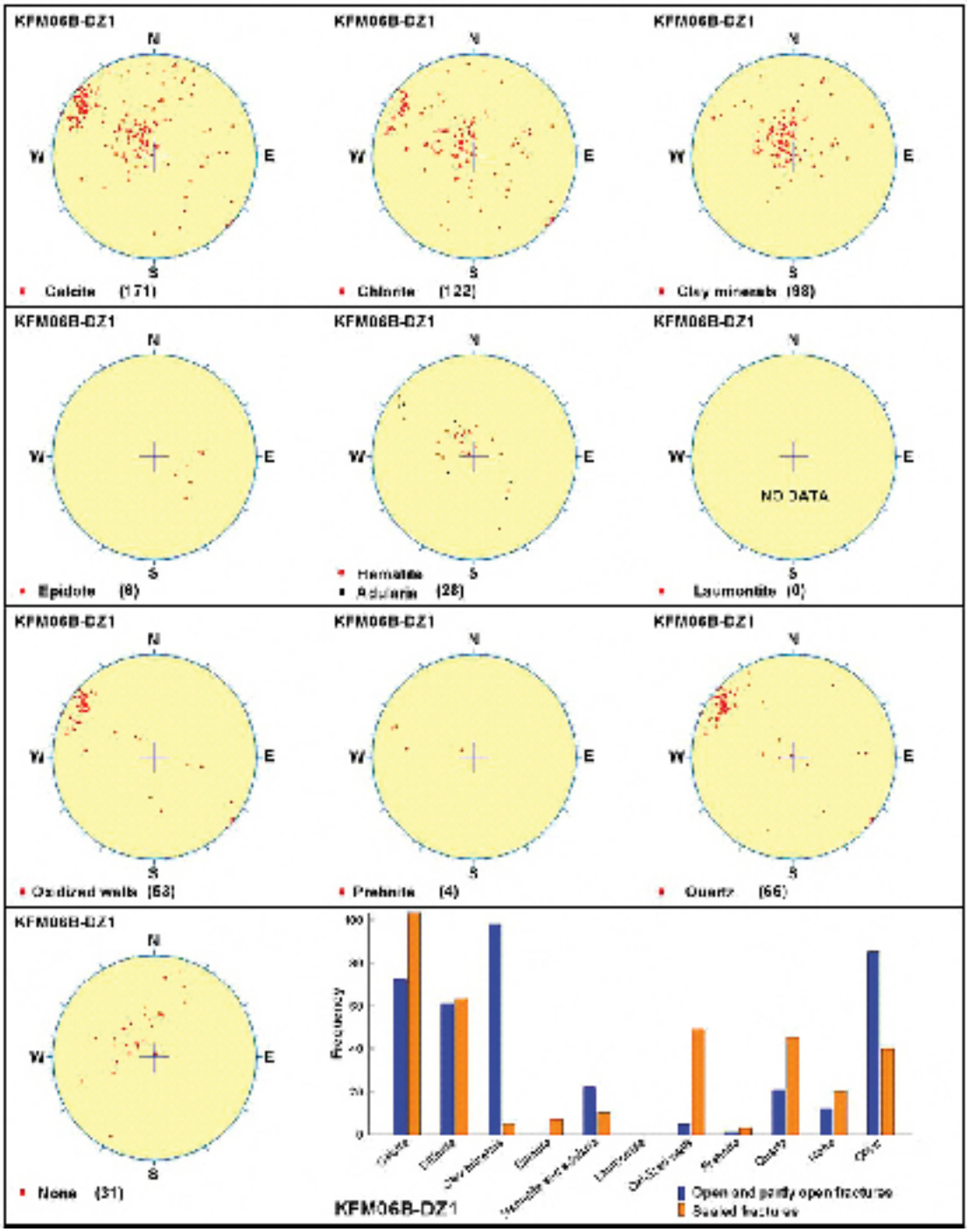

Figure 2-19. *Orientation of fractures, along which a particular mineral filling or coating has been documented, within the gently dipping fracture zone DZ1 in KFM06B. The frequency histogram for the minerals along this zone is also shown. The pole to each fracture plane is plotted on the lower hemisphere of an equal-area stereographic plot.*

2.5 Interpretation of primary rock mechanics data

Analyses of the laboratory results from testing of the intact rock (matrix) and fracture samples are presented in the following sections. More details about the statistical treatment of the data and the evaluation of the uncertainties can be found in Appendix 3.

2.5.1 Mechanical properties of intact rock

Compared to the data set available for version 1.2, new data from testing of several samples of intact rock from boreholes KFM05A and KFM06A were available in data freeze 2.1. The new samples all come from boreholes in the target area (Figure 2-2). These samples were tested in the laboratory and comprise: i) 44 additional samples of granite to granodiorite (code 101057), of which 8 are tested in triaxial and 20 in indirect tensile conditions, ii) 7 samples of aplitic granite (code 101058), all tested in uniaxial conditions, and iii) 7 samples of pegmatitic granite/pegmatite (code 101061), of which 2 are tested in uniaxial and 5 in tensile conditions. The aplitic granite and pegmatite are considered as secondary rock types in rock domain RFM029. Aplitic granite also occurs as the dominant rock type in a minor rock domain (RFM045) in the north-western part of the candidate area.

An updated list of the material properties of the tested rock types, as compared to model version 1.2, is given in Table 2-5. Due to the scarcity of the available data for the secondary rock types, the range of variation and standard deviation of the parameters are determined based on engineering judgement and on the analysis of old laboratory test data from the construction of the SFR Facility, reported in version 1.1 of the Forsmark SDM /SKB 2004/.

The uncertainties given in Table 2-5, based on the 95% confidence interval of the mean values, are evaluated in the following way.

1. Compared to version 1.2, the mechanical properties of the granite to granodiorite are either unchanged or have lower uncertainty.
2. For the aplitic granite, the evaluation is made based on about 8 uniaxial test results only. Thus, the uncertainties are considered to be comparable with those of the tonalite to granodiorite reported in version 1.2 /SKB 2005a/.
3. For the pegmatite (pegmatitic granite), results from 2 uniaxial compressive tests could certainly be attributed to this rock type. The uncertainties in the mechanical parameters are estimated to be twice as large as those reported in version 1.2 /SKB 2005a/ for the rock type granite to granodiorite.

Table 2-5. Updated mechanical properties of intact rock for some of the rock types in the Forsmark local model area version 2.1. The mean value and the standard deviation of the properties are given together with the truncation intervals for the normal distribution. The samples were collected from boreholes KFM01A–KFM06A. The uncertainties are quantified by the confidence interval of the mean value as a percentage of the mean value.

	Granite to granodiorite		Aplitic granite		Pegmatitic granite	
Parameter for intact rock (drillcore scale)	**Mean/ Std. dev. *Uncertainty of the mean***	**Truncation interaval: Min and Max**	**Mean/ Std. dev. *Uncertainty of the mean***	**Truncation interaval: Min and Max**	**Mean/ Std. dev. *Uncertainty of the mean***	**Truncation interaval: Min and Max**
Uniaxial compressive strength, UCS	227/24 MPa ± *1%*	165–290 MPa	275/80 MPa ± *3%*	150–370 MPa	223/60[3] MPa ± *6%*	80[3]–240[3] MPa
Young's modulus, E	76/3 GPa ± *1%*	70–85 GPa	81/4 GPa ± *1%*	73–85 GPa	72/13[3] GPa ± *2%*	40[3]–85[3] GPa
Poisson's ratio, ν	0.23/0.04 ± *4%*	0.15–0.32	0.26/0.04 ± *9%*	0.18–0.34	0.29/0.04[3] ± *18%*	0.20[3]–0.35[3]
Indirect tensile strength, TS	13.5/2 MPa ± *4%*	10–17 MPa			14/2 MPa ± *18%*	10–18 MPa
Coulomb's cohesion, c' [1, 2]	27.6/3 MPa ± *5%*	22–34 MPa				
Coulomb's friction angle, ϕ' [1, 2]	60.5°/0.3° ± *2%*	59.5°–61.0°				
Crack initiation stress, σ_{ci}	116/21 MPa ± *3%*	60–190 MPa	149/42 MPa ± *3%*	65–200 MPa	120/30 MPa ± *6%*	60–180 MPa

[1] The cohesion and friction angle according to the Coulomb's Criterion are assumed non-correlated.
[2] The cohesion and friction angle are determined for a confinement stress between 0 and 15 MPa.
[3] These values are based on new test results and results from Forsmark 1.1 /SKB 2004/.

The reason for the uncertainty in the mechanical parameters for the pegmatite is the limited number of samples tested. Furthermore, Boremap logging indicates another rock type for some of the samples. This suggests some uncertainties in the rock type determination. The use of old data for pegmatite from the SFR facility /SKB 2004/ also contributes to the uncertainties, due to the assumption that the mechanical properties of the pegmatite at the two adjacent sites are comparable.

The average mechanical properties of the granite to granodiorite within the target area are slightly higher than those determined for the whole rock domain RFM029. This can be explained with a larger homogeneity of the samples from a smaller rock mass volume (Figure 2-20). The rather large amount of test results for the granite to granodiorite also allows for an analysis of the depth dependence of the intact rock properties. Three depth intervals were chosen to correspond to pseudo-superficial (200–400 m), repository depth (400–550 m) and deep sample conditions (550–700 m). Table 2-6 shows the results for the main mechanical parameters at these depth intervals. For depths between 400 and 550 m, the values often show higher mean and smaller range of variation, although the number of samples is larger than from the other depth intervals. This can be explained in the following way.

a) Pseudo-superficial samples show a larger variability of mechanical properties than samples from depth. This is quantified by the large standard deviation.

b) The samples at repository depth show almost the same range of the properties and standard deviation as the samples from larger depth.

c) The samples from depth systematically show lower mean values of the properties than those from repository depth. This can be explained by microcracking of the samples during drilling in high rock stress conditions. The uniaxial compressive strength and crack initiation stress diminish about 10% for samples from depths between 550 and 700 m, whereas the deterioration of the Young's modulus and Poisson's ratio is only about 3% (Figure 2-21).

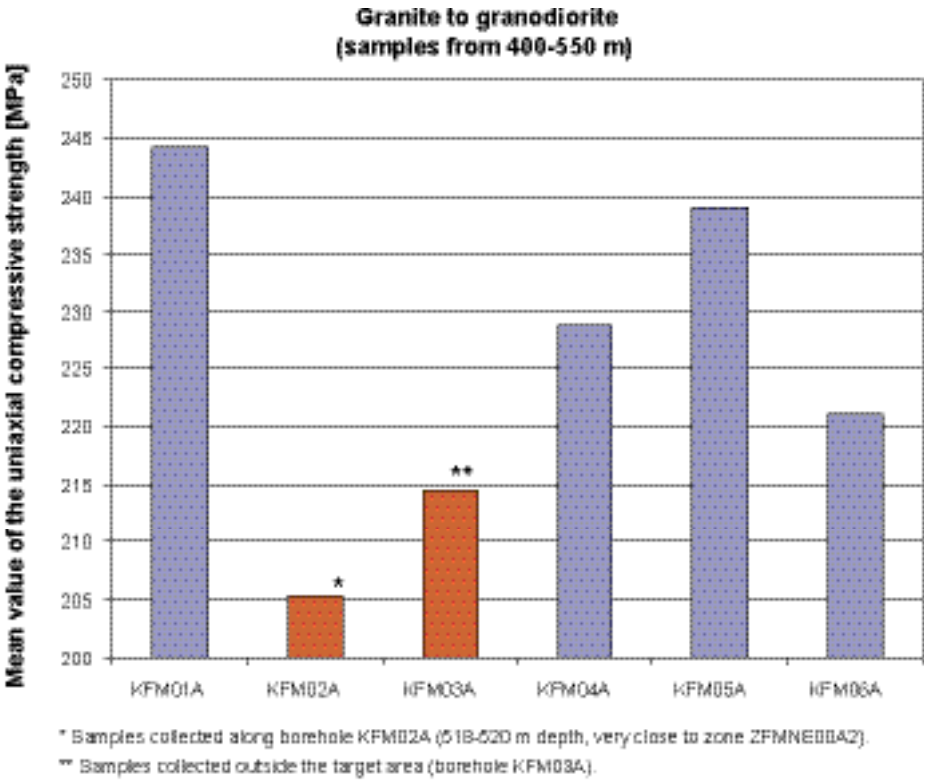

Figure 2-20. *Mean value of the uniaxial compressive strength of the intact rock samples of granite to granodiorite (code 101057) collected from depths between 400 and 550 m. The results considered as being representative for the target area are shown in blue.*

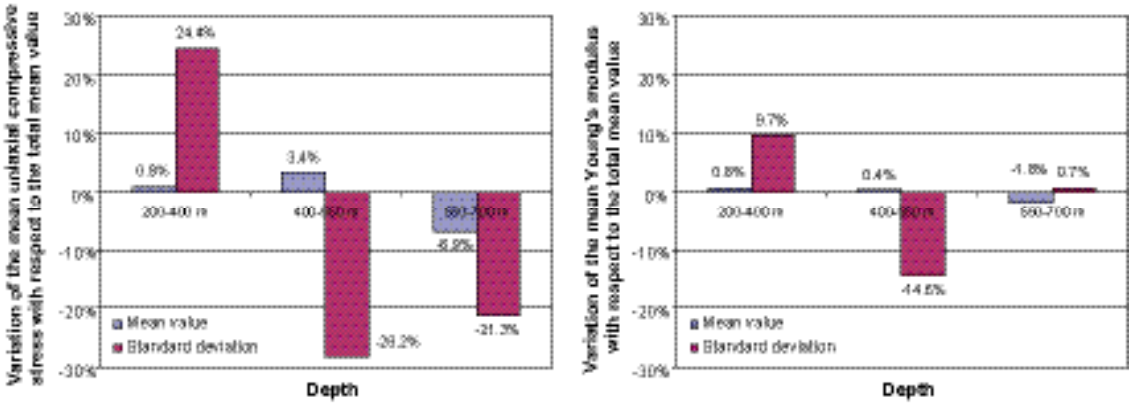

Figure 2-21. *Variation of the mean value and standard deviation of the uniaxial compressive strength (left) and Young's modulus (right) with depth for the granite to granodiorite samples (code 101057) samples from the target area.*

Table 2-6. Observed mechanical properties of the granite to granodiorite (code 101057) in rock domain RFM029 at different depths within the target volume. The mean value and the standard deviation of the properties are given.

Granite to granodiorite in target area in RFM029	Depth			
	200–400 m	400–550 m	550–700 m	All depths
Uniaxial compressive strength, UCS	231/30 MPa	237/17 MPa	214/19 MPa	229/24 MPa
Young's modulus, E	76.5/3 GPa	76/2.5 GPa	74.5/2.7 GPa	76/2.7 MPa
Poisson's ratio, ν	0.23/0.04	0.26/0.04	0.23/0.04	0.24/0.04
Tensile strength, TS	14.3/1.8 MPa	13.5/1.4 MPa	12.8/1.6 MPa	13.6/1.6 MPa
Crack initiation stress, σ_{ci}	116/34 MPa	121/13 MPa	110/10 MPa	116/22 MPa

* Samples collected along borehole KFM02A (518–520 m depth, very close to zone ZFMNE00A2).

** Samples collected outside the target area (borehole KFM03A).

Since the Young's modulus and Poisson's ratio of the rock are related to the P-wave velocity, results from P-wave measurements give an indication of the mechanical properties of the rock. The P-wave velocities measured on cores in the laboratory also indicate microcracking of the core due to the stress-path during drilling in high in situ stress conditions. Although natural fractures can sometimes influence the measured values, the in situ P-wave velocity is higher than the laboratory P-wave velocity measured on the cores. Measurements of in situ P-wave velocity do not indicate any decrease in mechanical properties with depth. This is illustrated in Figure 2-22, where the in situ and laboratory P-wave velocities are shown as a function of depth (elevation). The velocity measured in the laboratory clearly decreases with depth in cores from the vertical boreholes KFM01A and KFM02A located within the target area. No clear deterioration of the P-wave velocity is shown in the core from borehole KFM04A. This is probably due to the presence of other rock domains than RFM029 along the core and because of the inclination of this borehole with respect to the major principal stress that mitigates the stress-path effects during drilling. For the vertical borehole KFM03A, the laboratory-measured P-wave velocity in the core does not decrease with depth, probably because of lower stresses in that part of rock domain RFM029 /SKB 2005a/. It should be noted that samples from borehole KFM03A, which is located outside the target area, were not considered in the analyses summarised in Table 2-6.

Some other aspects concerning the strength and deformability of the intact rock that have been addressed in modelling stage 2.1 are summarised below.

Indirect tensile strength (Brazil) tests were carried out for different rock types parallel and perpendicular to the foliation. The frequency distribution of the tensile strength for granite to granodiorite (code 101057) is shown in Figure 2-23. The difference in average tensile strength parallel and

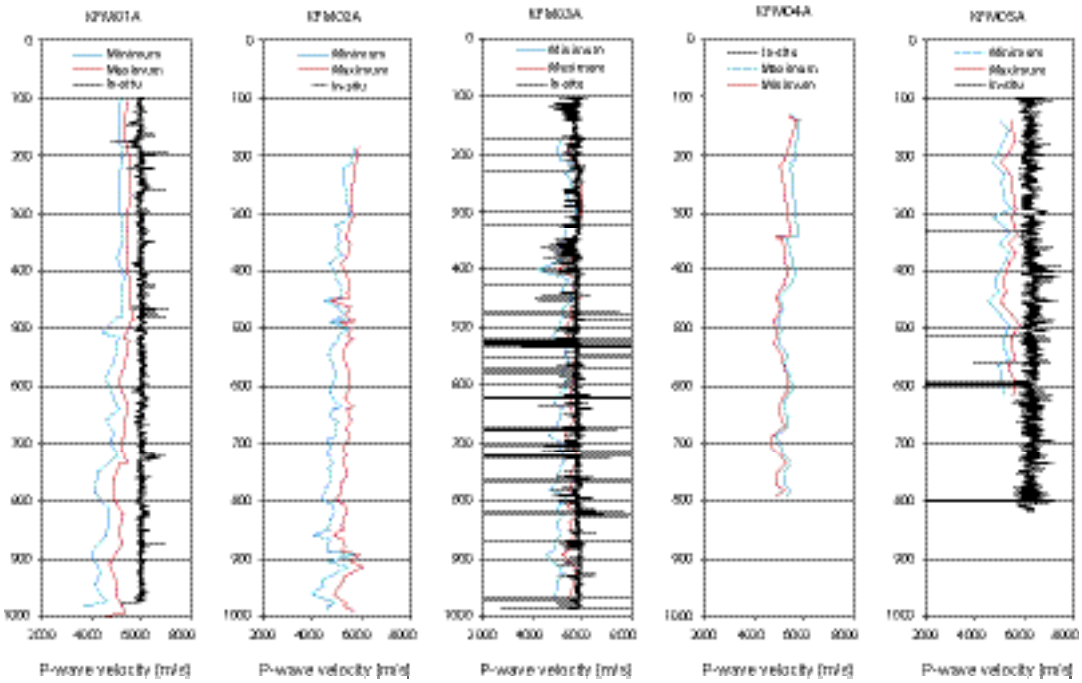

Figure 2-22. *Plot of the P-wave velocity measured in situ and on the borehole cores (maximum and minimum) versus depth for all the boreholes included in version 1.2.*

perpendicular to foliation is about 4.5%, whereas the standard deviation is approximately the same (between 1.6 and 1.8 MPa). These differences are judged to be small enough to be negligible for engineering applications. Consequently, it was decided to report the indirect tensile strength of all samples disregarding the direction of loading with respect to the foliation. In analogy, isotropy of all the other material properties of the intact rock material is assumed here, such as uniaxial strength, triaxial strength and deformability.

Based on the results of the uniaxial and triaxial laboratory tests, the strength envelope for the most common rock types was determined. Two criteria were used to approximate the experimental results in the maximum versus minimum principal stress space: the Hoek and Brown's Criterion and the Coulomb's Criterion /Hoek et al. 2002/. The approximation is rather good for the uniaxial and triaxial experimental results, but does not match the results from indirect tensile testing very well. For example, the tensile strength of the granite to granodiorite (code 101057), estimated from the Hoek and Brown's Criterion, is on average 8 MPa, whereas the results from the laboratory tests indicate an average indirect tensile strength of 13.5 MPa (Figure 2-24). To overcome this mismatch, it is suggested to use the Coulomb's Criterion with truncation equal to the tensile strength of the samples tested in laboratory.

The representativity of the laboratory samples with respect to the variability in rock types occurring in rock domain RFM029 was also of concern. It was concluded that among all rock types, the size of the sample population for granodiorite (code 101056) and pegmatitic granite/pegmatite (code 101061) was still too small to allow robust statistical analyses of the results (less than 5 samples for uniaxial and triaxial tests). Moreover, amphibolite (code 102017), present in about 5% of the volume of RFM029, was not sampled at all. Sampling of these rock types is planned for the remaining stage of the site investigation.

Besides representing all dominant rock types, the choice of the samples to be tested in the laboratory should reflect the alteration conditions of the intact rock in the rock domains. In the boreholes, about 3–20% of the rock shows alteration, particularly faint to strong oxidation. Some bias in sampling can have occurred because the selected core samples seem to be taken prevalently from unaltered or non-oxidised rock. However, the mechanical properties of the altered or oxidised samples tested in the laboratory (e.g. 4 samples out of 14 in KFM02A) do not seem to be affected. On the contrary, most of these samples show higher uniaxial and tensile strength compared to the unaltered samples.

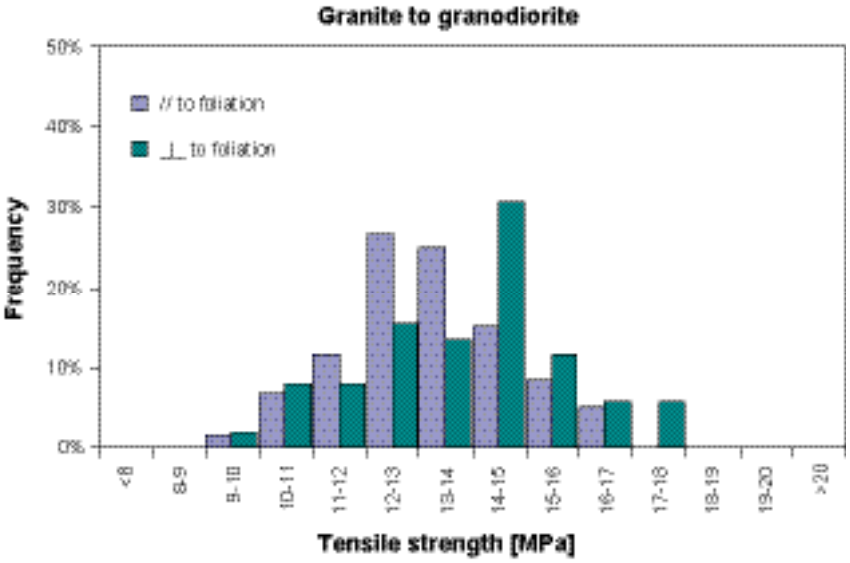

Figure 2-23. *Comparison of the frequency distribution of the indirect tensile strength for the samples of granite to granodiorite (101057) measured parallel and perpendicular to the foliation.*

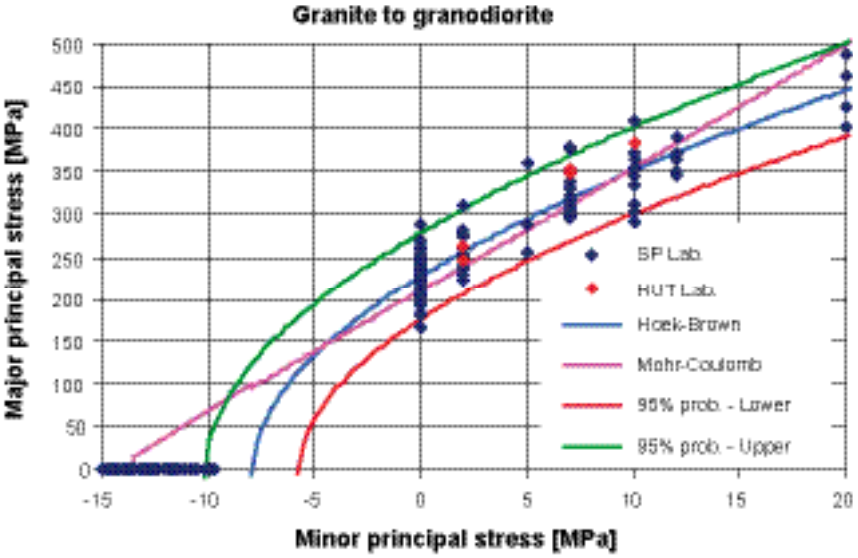

Figure 2-24. *Hoek and Brown's and Coulomb's failure criteria for the samples of granite to granodiorite (101057) from the uniaxial and triaxial tests contained in version 2.1. The indirect tensile test results are also shown with the suggested truncation of the Coulomb's failure criterion.*

It should be mentioned that the tested samples were at most "medium" oxidised according to SKB's nomenclature. A more comprehensive study about intact rock sampling bias is currently ongoing /Hakami and Johansson 2006/.

Most of the rock types at Forsmark fail in brittle mode when loaded in uniaxial conditions. Figure 2-25 shows the typical behaviour of a sample of granite to granodiorite (code 101057). The shape of the stress-strain curve indicates "class II" behaviour /Fairhurst and Hudson 1999/ where the strains almost monotonically decrease after failure at peak stress. On the other hand, a couple of samples of granodiorite (code 101056) showed very clear "class I" behaviour with post-peak strains monotonically increasing (Figure 2-26).

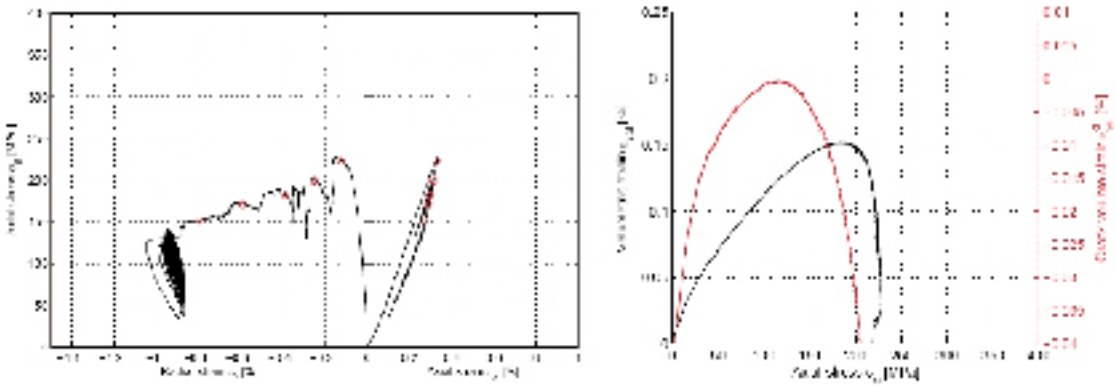

Figure 2-25. *Stress-strain (left) and strain-strain (right) curves for sample KFM07A-113-01 of medium grained granite to granodiorite (code 101057) tested under uniaxial loading conditions /Jacobsson 2005/. The sample exhibits "class II" behaviour because the post failure axial strain diminishes after the peak stress.*

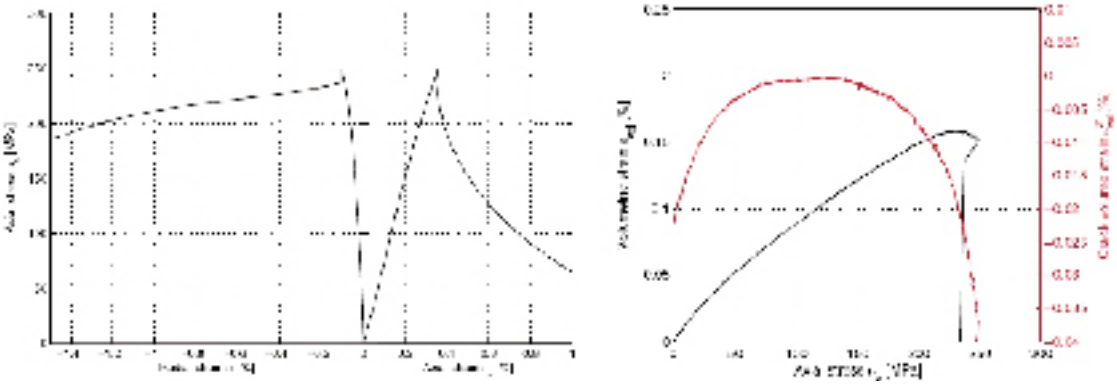

Figure 2-26. *Stress-strain (left) and strain-strain (right) curves for sample KFM07A-113-01 of granodiorite (code 101056) tested under uniaxial loading conditions /Jacobsson 2005/. The sample exhibits "class I" behaviour because the post failure axial strain increases after failure.*

2.5.2 Mechanical properties of the fractures

For version 1.2, 28 results from direct shear test on rock fracture samples were available /SKB 2005a/. For modelling stage 2.1, 14 additional fracture samples from boreholes KFM05A and KFM06A have been tested in the laboratory. These samples were prepared with new materials according to an updated preparation procedure in order to reduce the influence of the deformation of the mould on the total deformations. Furthermore, the available 113 tilt tests analysed in version 1.2 were integrated with 38 new tests on samples from KFM05A. Tilt tests easily provide a large amount of data for statistical analyses.

The laboratory results from direct shear and tilt test have been divided according to the fracture sets observed in the local model area in Forsmark SDM version 1.2, as presented in Figure 2-27. The mechanical properties of each fracture set have also been determined and compared. For some of the fracture sets, there are too few samples to allow for a comparison. For fracture sets NS, NW and NE, the comparison can be made but the differences in mechanical properties are not significant. The average properties of all samples can then represent well the properties of each fracture set, as shown for the peak friction angle in Figure 2-28 (left).

The new laboratory results for samples from KFM05A and KFM06A show significantly higher values of the normal stiffness of the fracture samples (up to a factor 8). Since the new sample preparation technique is claimed to be more reliable than the old technique, the normal stiffness of the samples is determined only on the basis of the 10 new test results. On the other hand, the values

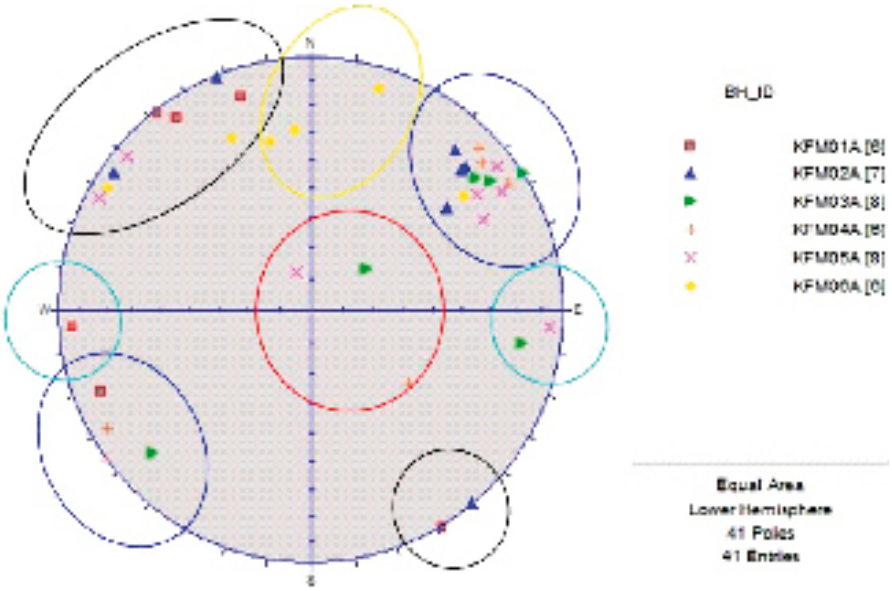

Figure 2-27. *Plot of fracture poles of the fractures tested in direct shear with identification of the fracture sets.*

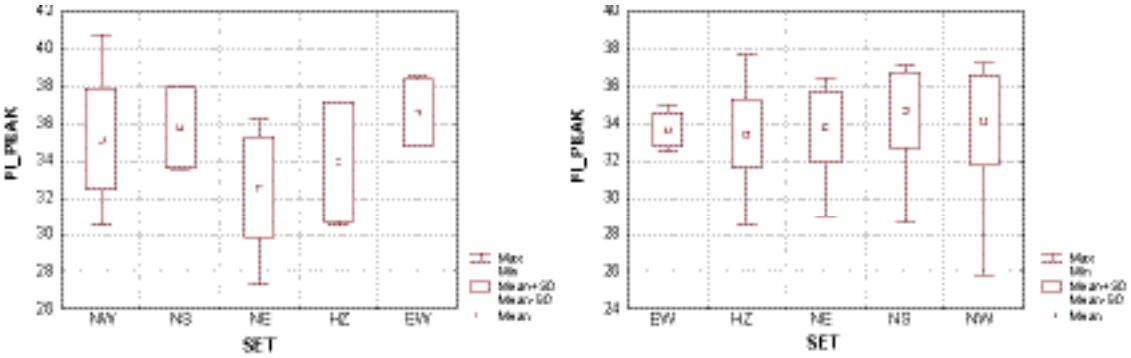

Figure 2-28. *Box plot of the peak friction angle obtained from direct shear tests (left) and from tilt tests (right) of the fracture samples sorted according to fracture orientation sets (see Appendix 3).*

of the shear stiffness, cohesion, friction angle and dilation seem to be faintly affected by the new sample preparation. For this reason, all 42 test results obtained by means of both the old and new sample preparation technique are used for the fracture characterisation.

The tilt test results have also been analysed considering the fracture orientation of the samples. Because of the rather large amount of tilt test results, more results from samples belonging to the sub-horizontal set are available from this type of test compared to the direct shear tests. The sub-horizontal fracture samples seem to show slightly lower cohesion than the samples from the vertical sets. Despite this difference, the friction angle of all fracture sets appears to be insensitive to the fracture orientation (Figure 2-28, right) as was also observed in the direct shear test results.

Tilt test results have also been grouped according to the depth from which the samples were taken. Even this comparison shows that fractures in samples from the depth interval 200–700 m exhibit almost exactly the same strength properties. Slightly different properties are observed for samples outside this depth range. Samples from the upper 200 m show lower friction angles compared with the other samples.

The mechanical properties of the rock fractures in the target area are summarised in Table 2-7 and Table 2-8. These tables show that the parameter values do not differ from those determined for the whole version 2.1 local model area (Appendix 3).

Compared to the results of the Forsmark version 1.2, the differences are small except for the fracture normal stiffness. The values of the other mechanical parameters obtained by the new and the old techniques are comparable and, therefore, have been used to determine the statistics of the fracture parameters for the target area. This choice is supported by the fact that the cohesion and friction angle determined from shear tests and tilt tests are of the same order of magnitude and the differences are not statistically significant.

Some of the fractures for direct shear (3 samples) and tilt (36 samples) testing are taken within deformation zones that are included in the deterministic deformation zone model. Since the experimental results for all these samples differ very little from the results for samples taken outside these deterministic deformation zones, the hypothesis that they belong to the same parent population cannot be rejected (Appendix 3). Thus, also these results have been considered when defining the set of parameters for the target area.

In addition to uncertainties due to measuring errors related to the methods of recording loads and deformations in the laboratory, some other sources of uncertainty have been analysed.

- The coupling between the fracture samples collected from the core and the fracture mapped in Boremap is uncertain. Due to the time shift between the collection of the samples and the mapping of the cores, the identification of some of the samples in Boremap was uncertain or even impossible. For example, the coupling was uncertain for about 25% of the samples collected for direct shear tests.

Table 2-7. Summary of the results obtained from shear tests on fracture samples from the target area (boreholes KFM01A, KFM02A, KFM04A, KFM05A and KFM06A). Strength and stiffness parameters apply for normal stresses between 0 and 20 MPa. The uncertainty in the mean values is given in italic as a percentage of the mean value.

	Mean value	Std. dev.	Minimum value	Maximum value
Normal stiffness, Kn (MPa/mm)[1)]	937.4 ± *31%*	462.1	319.1	1,527.6
Shear stiffness, Ks (MPa/mm)	30.5 ± *14%*	12.5	9.5	51.7
Peak cohesion. C_p (MPa)	0.7 ± *14%*	0.4	0.0	1.3
Peak friction angle, ϕ_p (°)	34.3 ± *3%*	3.1	27.3	40.8
Residual cohesion, C_r (MPa)	0.4 ± *25%*	0.3	0.0	1.3
Residual friction angle, ϕ_r (°)	32.0 ± *4%*	4.1	19.8	39.2
Dilation angle, i (°) at normal stress 0.5 MPa	18.9 ± *13%*	7.0	3.9	32.1
Dilation angle, i (°) at normal stress 5 MPa	6.9 ± *20%*	4.2	1.1	15.3
Dilation angle, i (°) at normal stress 20 MPa	3.5 ± *23%*	2.4	0.0	10.4

[1)] The normal stiffness is evaluated only from samples tested with the new modified methodology.

Table 2-8. Summary of the results from tilt tests on samples from the target area (rock fracture samples from boreholes KFM01A, KFM02A, KFM04A and KFM05A). The strength parameters apply for low normal stresses. The uncertainty in the mean values is given in italic as a percentage of the mean value.

	Mean value	Std. dev.	Minimum value	Maximum value
Peak cohesion. C_p (MPa)	0.5 ± *20%*	0.1	0.2	0.8
Peak friction angle, ϕ_p (°)	33.6 ± *1%*	2.1	25.8	37.2
Residual cohesion, C_r (MPa)	0.4 ± *25%*	0.1	0.2	0.7
Residual friction angle, ϕ_r (°)	29.5 ± *2%*	3.2	20.3	37.9

- The chosen laboratory testing technique affects the magnitude of the normal stiffness of the fractures.
- The representativity of the samples cannot be guaranteed for some fracture orientations, fracture conditions and depths. Some bias might have been introduced when collecting the samples to be tested in the laboratory by choosing preferentially some fracture orientations, mineralisation, roughness, alteration, rock types, etc, instead of others. For example, 40–80% of the fractures in the cores are rough, planar, fresh and unaltered, while among the tested fractures, about 30% of the samples are rough and 60% planar. A study to quantify the influence of such sampling biases is currently ongoing /Hakami and Johansson 2006/.

The possible sources of uncertainty described above have been considered in the evaluation of the expected intervals for the variation in the the mean values that quantifies the uncertainties reported in Table 2-7. This interval is defined as the 95% confidence interval of the mean value of the distributions of the different mechanical properties of the fractures.

While the uncertainty intervals of the mean for the friction angle from direct shear and that from tilt tests are in rather good agreement, the tilt tests provide much narrower uncertainty intervals for the cohesion in peak and residual conditions. The values in Table 2-7 have, therefore, been adjusted so that the uncertainty interval of the mean value obtained from one method to some extent overlapped the uncertainty interval of the mean obtained by the other method.

2.6 Interpretation of primary data on thermal properties

The rock volume for which thermal properties have been investigated in model version 2.1 is enclosed by the local model volume version 2.1, see Figure 2-2 and Figure 3-2. This bedrock volume is dominated by granite to granodiorite, metamorphic, medium grained (101057). Other locally important rock types are tonalite to granodiorite (101054) and aplitic granite (101058). Several subordinate rock types occur within the bedrock volume, the most important being granite, granodiorite and tonalite, metamorphic, fine to medium grained (101051), amphibolite (102017) and pegmatite (101061). For illustration of the surface geology and the location of boreholes see Figure 2-6.

Subsequently, in the description of the thermal properties, rock types will generally be identified and described by their rock code. Table 2-9 lists the rock codes for the rock types referred to in the thermal section of this report.

Table 2-9. Translation between rock codes and rock types.

Rock code	Rock type
101057	Granite to granodiorite, metamorphic, medium grained
101056	Granodiorite, metamorphic
101054	Tonalite to granodiorite, metamorphic
101051	Granite, granodiorite and tonalite, metamorphic, fine- to medium grained
101061	Pegmatite, pegmatitic granite
103076	Felsic to intermediate volcanic rock, metamorphic
101058	Granite, metamorphic, aplitic
111058	Granite, fine- to medium-grained
101033	Diorite, quartz diorite and gabbro, metamorphic
101004	Ultramafic rock, metamorphic
102017	Amphibolite
108019	Calc-silicate rock (skarn)

Data from nine cored boreholes (see Figure 2-6 for locations) within the Forsmark area have been used for the purpose of describing thermal properties. Much of this data was described and evaluated in model version 1.2. New data produced for data freeze 2.1 derives primarily from boreholes KFM04A, KFM05A and KFM06A. Boremap mapping of boreholes KFM07A and KFM08A is also considered.

2.6.1 Thermal conductivity from measurements

Measurement results

Thermal conductivity has been measured using the TPS (Transient Plane Source) method on an additional 16 rock samples /Adl-Zarrabi 2004b, 2005/. Previously produced data are described in /Sundberg et al. 2005/. Summary statistics of thermal conductivity and thermal diffusivity for each rock type are presented in Table 2-10 and Table 2-11, respectively.

The results of all thermal conductivity measurements are presented graphically in Figure 2-29. A comparison of data for rock type granite to granodiorite (101057) from different boreholes and different depths indicates little spatial variation in thermal conductivity.

Table 2-10. Measured thermal conductivity (W/(m·K)) of different rock types using the TPS method. Samples are from boreholes KFM01A, KFM02A, KFM03A, KFM04A and KFM06A together with 5 surface samples.

Rock code	Rock name	Sample location	Mean	St. dev.	Max	Min	No. of samples	Comment
101057	Granite to granodiorite metamorphic, medium grained	Boreholes KFM01A, KFM02A, KFM03A, KFM04A and surface	3.70	0.17	4.01	3.42	59	10 new samples from KFM04A. No significant change in statistics relative to version 1.2.
101056	Granodiorite metamorphic	Borehole KFM04A	3.04	0.09	3.20	2.98	5	
101054	Tonalite to granodiorite metamorphic	Borehole KFM03A, and surface	2.73	0.19	2.94	2.45	5	
101051	Granite, granodiorite and tonalite metamorphic, fine- to medium grained	Borehole KFM03A	2.51	0.08	2.60	2.46	3	
101058	Granite, metamorphic, aplitic	Borehole KFM06A	3.89	0.14	4.06	3.70	6 (albitized)	All new samples
101033	Diorite, quartz diorite and gabbro, metamorphic	Surface	2.28		2.28	2.28	1	

Table 2-11. Measured thermal diffusivity (mm²/s) of different rock types using the TPS method. Samples are from boreholes KFM01A, KFM02A, KFM03A, KFM04A and KFM06A together with 5 surface samples.

Rock code	Rock name	Sample location	Mean	St. dev.	Max	Min	No. of samples
101057	Granite to granodiorite, metamorphic, medium grained	Boreholes KFM01A, KFM02A, KFM03A, KFM04A and surface	1.71	0.11	2.05	1.47	59
101056	Granodiorite, metamorphic	Borehole KFM04A	1.35	0.05	1.42	1.29	5
101054	Tonalite to granodiorite, metamorphic	Borehole KFM03A and surface	1.30	0.13	1.51	1.18	5
101051	Granite, granodiorite and tonalite, metamorphic, fine- to medium grained	Borehole KFM03A	1.16	0.02	1.17	1.14	3
101058	Granite, metamorphic, aplitic	Borehole KFM06A	1.84	0.09	1.97	1.68	6
101033	Diorite, quartz diorite and gabbro, metamorphic	Surface	0.98				1

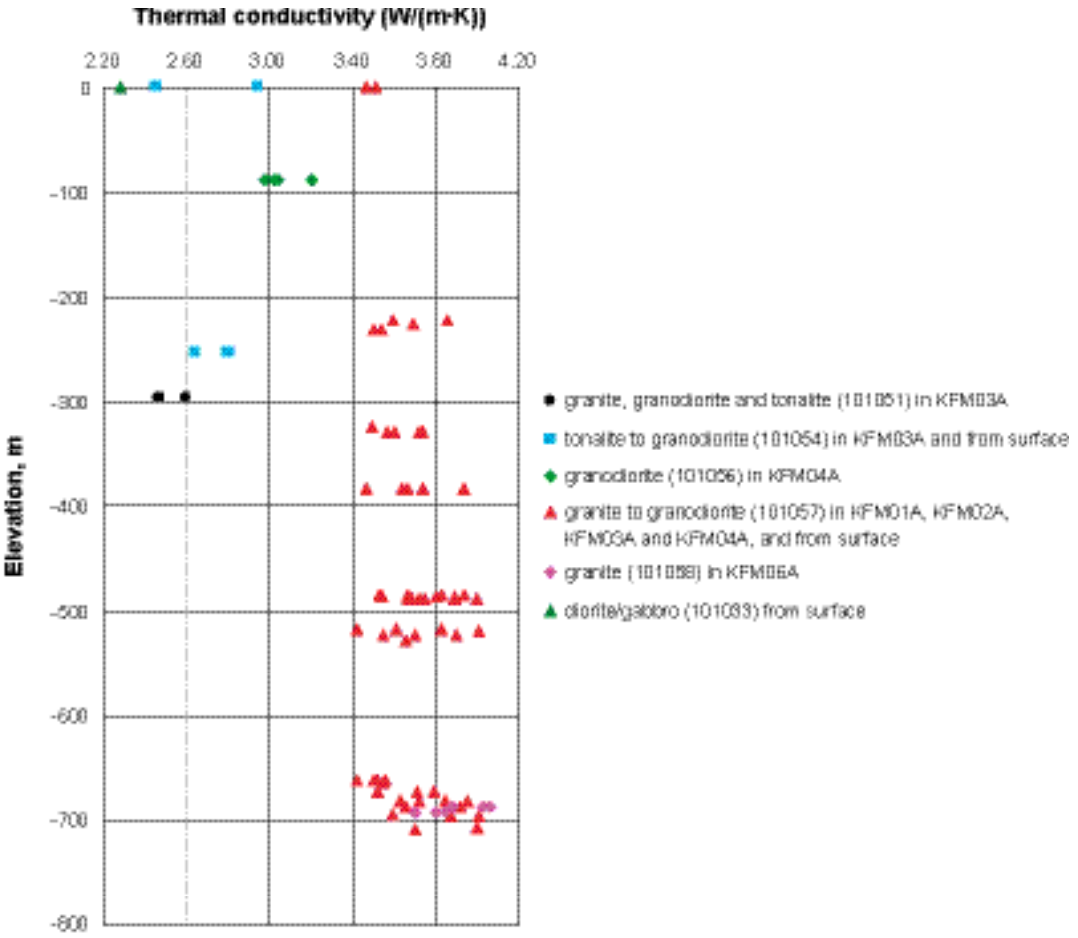

Figure 2-29. *Thermal conductivity and location in boreholes for samples measured using the TPS method, divided according to rock type.*

For aplitic granite (101058), a rock type for which data have not been previously available, it should be noted that the data derive from samples that are considered to be altered. This alteration has been observed in the lower part of KFM06A and in outcrops along the north-eastern margin of the candidate area. Alteration has produced a whitened rock, a result of the process of albitization, which produces plagioclase having a lower anorthite content than in the unaltered rocks /Petersson et al. 2005/. The six samples indicate a high thermal conductivity. No measurements from unaltered equivalents are available.

Declustering of thermal conductivity data for granite to granodiorite (101057)

Since several samples have been taken in groups from short, c. 1 m, sections of a borehole core, the data distributions for the dominant rock type granite to granodiorite (101057), is not necessarily representative. This spatial clustering of sample data may produce bias in both the mean and the standard deviation. The effect of non-representative sampling can be analysed by using different declustering methods. The cell declustering approach is used to obtain an estimate of the mean. Using this method, each spatially related group of samples (< 1 m) receives the same weight as a single isolated sample. Another method can be employed to obtain a representative estimate of the standard deviation. This is achieved by randomly selecting one sample from each group, and then calculating the standard deviation from these values. The results of de-clustering are presented in Table 2-12.

A comparison of the different methods reveals that declustering has little impact on the mean and standard deviation of thermal conductivity obtained using the complete data set. This probably reflects the low degree of spatial variation present within this rock type. In conclusion, it is proposed that the mean and standard deviation estimated from the complete data set appear to be representative for the rock type, granite to granodiorite.

Table 2-12. Thermal conductivity TPS of rock type granite to granodiorite (101057). Comparison of summary statistics calculated by different methods.

	No declustering	Cell declustering	Random declustering
Mean	3.695	3.691	3.698
St. dev.	0.165	0.143	0.167
Variance	0.027	0.020	0.028
No. of samples	59	24	24

Spatial variability of thermal conductivity within granite to granodiorite (101057)

When modelling thermal conductivity at domain level according to the approaches used in previous model versions, knowledge of the spatial variability of thermal conductivity within the dominant rock types, at scales larger than measurement scale, is required. The variance at the 1 m scale for granite to granodiorite (101057) has been evaluated here. Figure 2-30 illustrates the variability within groups comprising four or more samples from a length of borehole core less than 1 m. The red box in Figure 2-30 represents variability at the 1 m scale, which can be compared with the much larger variability present at the sample scale (green box). It is clear that the variability at the 1 m scale is considerably smaller than at the cm scale. Analysis of variability for different scales has shown that approximately 50% of the variability present at the cm scale is evened out at the 1 m scale.

2.6.2 Thermal conductivity from mineral composition

Method

The thermal conductivity of rock samples has been calculated by the SCA method (Self Consistent Approximation) using mineral compositions from modal analyses and reference values of the thermal conductivity of different minerals, as described in /Sundberg 1988, 2003/.

New data comprise a total of 73 new modal analyses on samples both from the surface and from boreholes KFM04A, KFM05A, and KFM06A, where some samples were taken adjacent to samples for laboratory measurement of thermal properties /Petersson et al. 2005, Adl-Zarrabi 2004b/. Results of previous data for 119 samples are reported in model version 1.2 /Sundberg et al. 2005/.

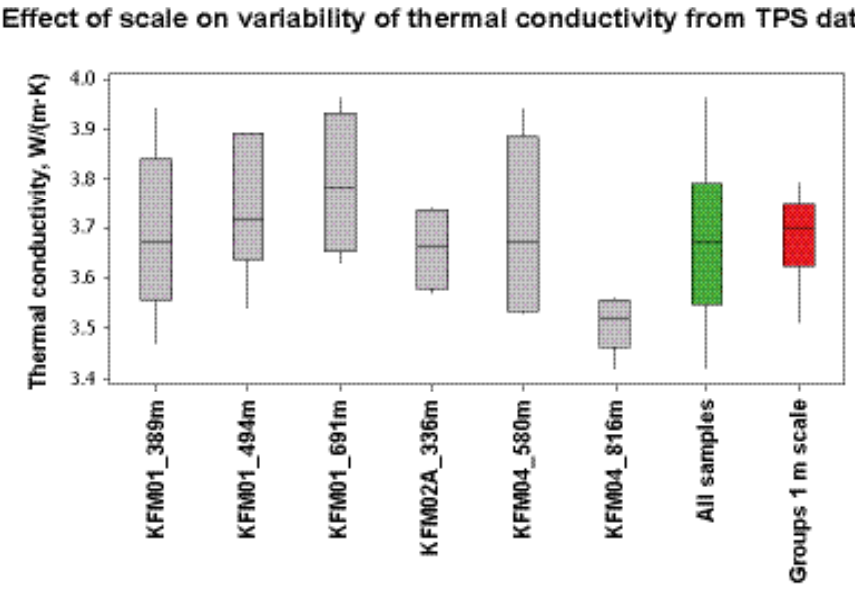

Figure 2-30. *Up-scaling of TPS measurements from cm scale to 1 m scale for rock type 101057. Six groups of TPS measurements (grey boxes), each representing approximately 1 m, are used to estimate variability in thermal conductivity at the 1 m scale (red box). This can be compared with the total variability at the sample scale (green box).*

Results

The results of the SCA calculations based on all available modal analyses arranged according to rock type are presented in Table 2-13.

Table 2-14 shows SCA calculations for granite to granodiorite (101057), the dominating rock type in the local model area, divided according to location (per borehole and surface samples). Similar to that shown by the TPS data, little spatial variation in thermal conductivity is indicated, although it should be noted that statistical tests were not performed.

With the exception of aplitic granite (101058), the various rock types show broadly similar means and standard deviations to those presented in model version 1.2. However, for some rock types, data were very limited in model version 1.2; in the case of some rock types represented by one or two samples only. The new data is particularly important for amphibolite (102017), which is now represented by four samples as compared to only one previously. The calculated values for this rock type indicate a relatively low thermal conductivity and a low degree of variability; all four samples fall in the range 2.3–2.5 W/(m·K). This rock type was not considered in domain modelling in model version 1.2 because of lack of data.

With the inclusion of the new data, aplitic granite (101058) has yielded a noticeably higher mean thermal conductivity; 3.74 W/(m·K) compared to the previous 3.47 W/(m·K) based on only two samples. The samples can be divided into two groups according to whether or not they have been affected by alteration (albitization) /Petersson et al. 2005/. Albitized samples show generally higher SCA values than unaltered samples (Table 2-15), perhaps due to their enriched quartz content relative to unaltered equivalents /Petersson et al. 2005/. Furthermore, the albitized variety is K-feldspar deficient, and have plagioclase with lower anorthite contents /Petersson et al. 2005/. The aplitic granite (101058) is not the only rock affected by albitization. This feature is also noted in some samples of granite to granodiorite (101057) /Petersson et al. 2005/. However, SCA values for a limited number of albitized samples of rock type 101057 are not significantly different to non-albitized equivalents. Common to all rocks subjected to albitization is bleaching or whitening.

Table 2-13. Thermal conductivity (W/(m·K)) calculated from the mineralogical composition using the SCA method.

Rock code	Rock type	Arithmetic mean	St. dev.	Max	Min	No. of samples
101057	Granite to granodiorite, metamorphic, medium grained	3.55	0.23	4.05	3.08	77
101056	Granodiorite, metamorphic	3.11	0.21	3.52	2.83	11
101054	Tonalite to granodiorite, metamorphic	3.00	0.35	3.97	2.28	26
101051	Granite, granodiorite and tonalite, metamorphic, fine- to medium grained	3.09	0.24	3.42	2.61	25
101061	Pegmatite, pegmatitic granite	3.49	0.16	3.65	3.27	5
103076	Felsic to intermediate volcanic rock, metamorphic	3.06	0.39	3.63	2.44	15
101058	Granite, metamorphic, aplitic	3.74	0.31	4.21	3.38	12
111058	Granite, fine- to medium-grained	3.44	0.43	4.04	3.02	4
101033	Diorite, quartz diorite and gabbro, metamorphic	2.51	0.23	3.00	2.20	11
101004	Ultramafic rock, metamorphic	3.61	0.14	3.71	3.50	2
102017	Amphibolite	2.41	0.08	2.50	2.31	4

Table 2-14. Calculated (SCA method) thermal conductivity of rock type 101057 for samples from individual boreholes and from the surface.

	KFM01A	KFM02A	KFM03A	KFM04A	KFM05A	KFM06A	Surface
Mean	3.65	3.51	3.61	3.48	3.68	3.60	3.50
St. dev.	0.25	0.28	0.21	0.19	0.19		0.20
No. of samples	14	13	11	6	3	1	29

Table 2-15. Calculated (SCA method) thermal conductivity of altered (albitized) and unaltered varieties of aplitic granite (101058).

Rock type	Alteration	Mean	No. of samples	Comment
Granite, metamorphic, aplitic	Unaltered	3.63	8	KFM06A and surface
Granite, metamorphic, aplitic	Albitized	3.96	4	KFM06A and surface

Comparison with measurements

For several of the borehole core samples taken for laboratory determination of thermal conductivity (TPS method), sampling for modal analysis and SCA calculations have also been carried out /Sundberg et al. 2005/. The objective is to compare determinations from the different methods so as to evaluate the accuracy of the SCA calculations. Six new data pairs are available, four for granite to granodiorite (101057) and two for granodiorite (101056). In Table 2-16, a comparison of TPS and SCA data is presented. For granite to granodiorite (101057) a good agreement was found between measured thermal conductivity (TPS) and calculated thermal conductivity (SCA), although there is a considerable amount of dispersion (Figure 2-31). For the other rock types there are too few samples on which to base any firm conclusions.

In model version 1.2 /Sundberg et al. 2005/, a significant difference in the means determined by the TPS and the SCA methods was found for tonalite to granodiorite (101054) and granite, granodiorite and tonalite (101051), when all available data were considered. These differences remain after the incorporation of the new SCA data, see Table 2-17. No new TPS data are available for these rock types. For the rock types tonalite to granodiorite (101054) and granite, granodiorite and tonalite (101051), the mean thermal conductivity from TPS measurements is lower than the mean value from SCA calculations. This does not necessarily mean that the SCA method overestimates the thermal conductivity, since the data, especially the TPS measurements, suffer from a lack of representativity, i.e. few samples from only one or two locations.

Table 2-16. Comparison of thermal conductivity (W/(m·K)) calculated by different methods for two rock types. SCA values are calculated from mineralogical composition and the TPS values are from laboratory measurement. Samples are from boreholes KFM01A, KFM02A, KFM03A and KFM04A and from the outcrops. Mean refers to arithmetic mean.

Method	Granite to granodiorite (101057) 24 samples	Granodiorite (101056) 2 samples
Calculated (SCA) Mean	3.60	2.99
Measured (TPS) Mean	3.67	3.00
Diff. (SCA-TPS)/TPS	–1.6%	–0.3%

For rock types 101054 and 101051, see /Sundberg et al. 2005/.

Table 2-17. Thermal conductivity (W/(m·K)) calculated from the SCA and TPS methods.

Rock code	Rock type	SCA mean	No. of samples	TPS mean	No. of samples
101057	Granite to granodiorite, metamorphic, medium grained	3.55	77	3.70	59
101056	Granodiorite, metamorphic	3.11	11	3.04	5
101054	Tonalite to granodiorite, metamorphic	3.00	26	2.73	5
101051	Granite, granodiorite and tonalite, metamorphic, fine- to medium grained	3.09	25	2.51	3
101058	Granite, metamorphic, aplitic	3.74	12	3.89	6
101033	Diorite, quartz diorite and gabbro, metamorphic	2.51	11	2.28	1

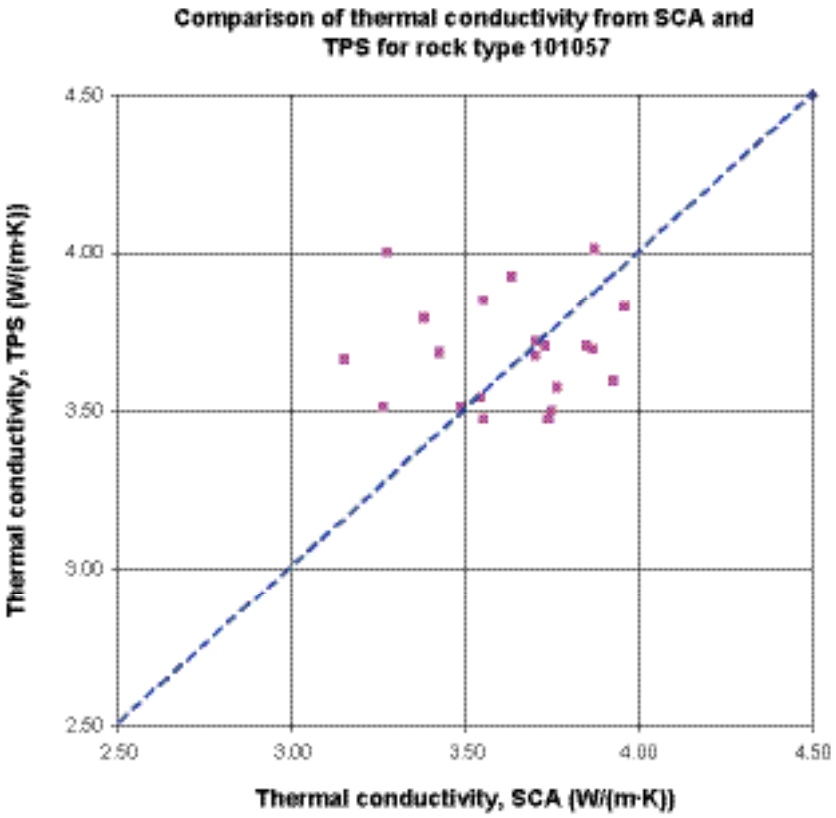

Figure 2-31. *Comparison between thermal conductivity calculated from SCA and measured according to the TPS-method for granite to granodiorite (101057).*

2.6.3 Alteration

Alteration observed in the cores includes oxidation, albitization, sericitization, saussuritization, epidotization, chloritization and argillization. With the exception of albitization, which is restricted to certain parts of the candidate volume, rock affected by alteration comprises approximately 13% of the mapped boreholes.

With the exception of the six samples of albitized aplitic granite from KFM06A, the samples on which TPS measurements were performed were taken from borehole cores showing little (“faint”) or no alteration. One sample of rock type granite to granodiorite (101057) from KFM02A (secup 528 m), described in Boremap mapping as having “faint” oxidation and illustrated in Figure 2-32, yielded a thermal conductivity of 4.01 W/(m·K), which is at the higher end of the range of thermal conductivity values for this rock type.

The situation as regards SCA calculations is similar. Although thin section analysis indicates that alteration is ubiquitous, virtually all of the modal analyses used in SCA calculations are taken from sections of cores for which no alteration has been recorded in the boremap mapping. An exception to this are samples of rock types 101058 and 101057 from borehole sections which have been mapped as albitized, primarily in borehole KFM06A.

The main alteration phenomena reported from thin-section analyses /Petersson et al. 2004, 2005/ are sericitisation and saussuritization of plagioclase, and chloritization of biotite. Other alteration products include calcite, prehnite and hematite.

Summing up, it can be stated that samples for which thermal properties have been determined either by measurement or from mineral composition are, with some exceptions, taken from cores that are considered to be unaltered. Therefore, a relatively large part of the rock mass is not represented by the available TPS or SCA data.

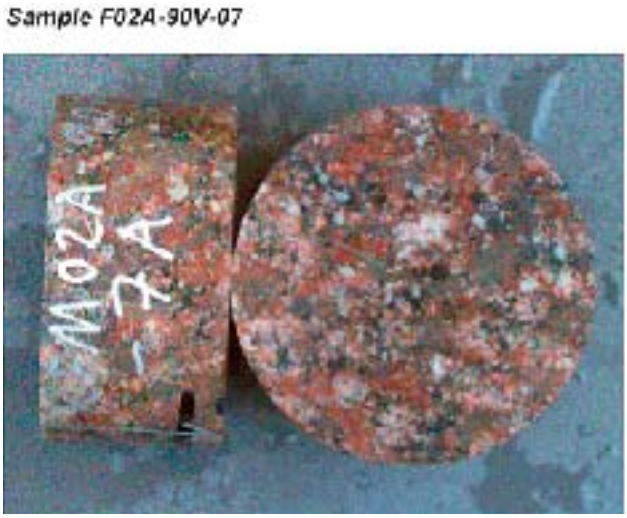

Figure 2-32. *Core sample of granite to granodiorite from KFM02A (secup: 528 m) used for measuring thermal properties using the TPS method /Adl-Zarrabi 2004a/. Note the red colouration indicative of oxidation.*

According to the boremap data, oxidation is the most common form of alteration, making up about 12% of the rock mass in boreholes KFM01A–08A. Characterised by red colouration, oxidation is generally, but not always, associated with fractures and fracture zones /Sandström and Tullborg 2005/. Zones of intense fracturing are defined as deformation zones /SKB 2005a/. The rock mass in at least the larger deformation zones will not be exploited for the nuclear waste repository.

Generally speaking, there is a lack of knowledge regarding the mineralogy of rock described in the boremap as oxidised. Studies of wall-rock alteration adjacent to fractures have shown that the growth of hematite under oxidising conditions has imparted a red colouration to the rock /SKB 2005a/. Other common forms of wall-rock alteration are saussuritization of plagioclase, chloritization of biotite and sericitisation of K-feldspar /Sandström and Tullborg 2005/. The extent of the alteration in association with fractures varies from < 1 cm to tens of centimetres.

Albitization is locally important, especially in the lower part of borehole KFM06A, where it affects the rock type aplitic granite (101058). About 80% of this rock type in the borehole interval 751–966 m is albitized. Even substantial sections (5–10%) of KFM07A and KFM08A have been subjected to albitization. Evidence from SCA calculations as well as mineralogical changes associated with albitization suggests that this form of alteration leads to an increase in thermal conductivity.

Other forms of alteration have been mapped in less than 1% of the total borehole length in the eight boreholes investigated, namely KFM01A–08A. Many of the minerals associated with these forms of alteration, such as sericite, epidote, chlorite, prehnite, calcite etc, have thermal conductivities that are similar to or higher than their parent minerals, for example, feldspars, biotite, etc /Sundberg et al. 2005/. Theoretically, these mineralogical changes should then produce higher rock thermal conductivities.

In KFM02A, an anomalous, strongly reddened and vuggy metagranite occurs. These so-called episyenites are characterised by dissolution of quartz, resorbtion of K-feldspar and intense alteration of plagioclase, biotite and hornblende /Möller et al. 2004/. From a thermal properties perspective, the fact that these granites are highly porous (2–13%) would affect the thermal properties negatively.

2.6.4 Small-scale anisotropy

A rock is isotropic if it has the same properties in all directions. A distinct structural anisotropy is present in the rocks at the Forsmark site, which is evidenced by both a foliation and a lineation. The planar fabrics vary both as regards orientation and degree of development (see Section 2.4.3 and Boremap reports for boreholes referred to in Appendix 2).

Laboratory results, reported in model version 1.2 /Sundberg et al. 2005/, from measurements on cores indicate a distinct anisotropy of thermal conductivity, with the higher conductivities being found in directions parallel to the foliation. However, the heat capacity values determined from TPS measurements, and used as input for the calculations, resulted in uncertainties. Preliminary results (not delivered to Sicada as of February 2006) using direct measurements of heat capacity as input indicate a somewhat lower level of anisotropy than reported in model version 1.2 /Sundberg et al. 2005/. The analysed samples were of granite to granodiorite (101057) and were considered to have a stronger foliation than is usual for this rock type in the candidate volume. The anisotropy effect of the lineation has not been investigated.

Field experiments to investigate thermal conductivity anisotropy, again in granite to granodiorite (101057), are ongoing.

2.6.5 Large-scale anisotropy

Large-scale anisotropy may be present as a result of the preferential orientation of subordinate rock types occurring, for example, as dykes of significant extension, and having thermal properties significantly different to the dominant rock type. At the Forsmark site, amphibolite dykes are a common feature throughout the local model volume making up about 5% of the rock mass (see Table 3-2). As indicated in Section 2.6.2, the thermal conductivity of amphibolites is significantly lower from that of granitoid rocks into which the amphibolites intrude. Their occurrences in the boreholes rarely exceed a few metres in length. Amphibolites are oriented consistently parallel to the tectonic foliation in the host rocks (see Boremap references in Appendix 2). Normally the dykes dip steeply, either to the E or to the W, although occurrences in KFM06A show considerable variation in strike and dip.

Other common subordinate rock types occurring as dykes are pegmatite and pegmatitic granite (101061). These and most other subordinate rock types are generally felsic in composition and have been shown or can be assumed to have similar thermal properties to the dominant granitoid rocks, for example, granite to granodiorite (101057). For this reason they should not contribute to anisotropy in thermal properties. One other rock type which may also contribute to large-scale anisotropy is granite, granodiorite and tonalite (101051). However, analysis of the 3D distribution of this rock type has not been carried out.

Modelling of large-scale anisotropy has not been performed. It is envisaged that the distribution of thermal conductivity values will be in directions parallel to the dykes compared to perpendicular to the dykes. However, the nature and degree of thermal conductivity anisotropy is largely a factor of the scale considered. For example, the anisotropic effects caused by thin dykes may be essentially evened out at larger scales.

2.6.6 Heat capacity – measurement results

Heat capacity has been measured using the TPS (Transient Plane Source) method. In Table 2-18 the results from all conducted measurements of heat capacity are summarised /Adl-Zarrabi 2004b, 2005/. Previously produced data are described in /Sundberg et al. 2005/. The data includes 16 new measurements, ten for rock type 101057 and six for rock type 101058. Observe that samples of rock types tonalite to granodiorite (101054), granite, granodiorite and tonalite (101051), granodiorite (101056) and aplitic granite (101058) were sampled in groups from short sections of cores, 0.2–1 m, from boreholes KFM03, KFM04 and KFM06A. The summary statistics for the latter rock types cannot, therefore, be considered to be representative.

Table 2-18. Measured heat capacity (MJ/(m³·K)) of samples (all TPS measurements) with different rock types, using the TPS method. Samples are from boreholes KFM01A, KFM02A, KFM03A, KFM04A and KFM06A together with 5 surface samples.

Rock code	Rock name	Sample location	Mean	St. dev.	Max	Min	No of samples	Comment
101057	Granite to granodiorite, metamorphic, medium grained	Borehole KFM01A, KFM02A, KFM03A, KFM04A and surface	2.18	0.17	2.55	1.76	59	10 new samples from KFM04A. No significant change in statistics relative to version 1.2.
101056	Granodiorite, metamorphic	Borehole KFM04A	2.25	0.07	2.34	2.16	5	
101054	Tonalite to granodiorite, metamorphic	Borehole KFM03A, PFM001157 and surface	2.12	0.20	2.39	1.93	5	
101051	Granite, granodiorite and tonalite, metamorphic, fine- to medium grained	Borehole KFM03A	2.17	0.05	2.22	2.13	3	
101058	Granite, metamorphic, aplitic	Borehole KFM06A	2.12	0.11	2.29	1.97	6	All new samples.
101033	Diorite, quartz diorite and gabbro	Surface	2.33		2.33	2.33	1	

In model version 1.2, rock type models of heat capacity were produced from the results of the TPS measurements. The data distributions were shown to be normal. The new data for rock type 101057 does not change the model parameters significantly. A model for rock type 101058 can now be constructed based on the new data.

2.6.7 Thermal expansion – measurement results

The coefficient of thermal expansion has been measured on 12 additional samples of rock type 101057 and six samples of rock type 101056 /Åkesson 2004/. These, as well as previously performed measurements /Sundberg et al. 2005/ divided according to rock type, are summarised in Table 2-19. The mean value of measured thermal expansion varies for the different rock types between $7.2 \cdot 10^{-6}$ and $8.1 \cdot 10^{-6}$ m/(m·K). For the dominant rock type, 101057, the mean thermal expansion coefficient is $7.7 \cdot 10^{-6}$ m/(m·K).

Table 2-19. Measured thermal expansion (m/(m·K)) on samples with different rock types from boreholes KFM01A, KFM02A, KFM03A and KFM04A (interval of temperature: 20–80°C).

Rock code	Rock name	Sample location	Mean	St. dev.	Max	Min	No of samples	Comment
101057	Granite to granodiorite, metamorphic, medium grained	Borehole KFM01A, KFM02A, KFM03A, KFM04A	$7.7 \cdot 10^{-6}$	$2.2 \cdot 10^{-6}$	$2.1 \cdot 10^{-6}$	$1.5 \cdot 10^{-5}$	56	12 new samples from KFM04A. No significant change in statistics.
101056	Granodiorite, metamorphic	Borehole KFM04A	$8.1 \cdot 10^{-6}$	$3.4 \cdot 10^{-6}$	$5.2 \cdot 10^{-6}$	$1.4 \cdot 10^{-5}$	6	All new samples.
101054	Tonalite to granodiorite, metamorphic	Borehole KFM03A	$7.2 \cdot 10^{-6}$	$1.6 \cdot 10^{-6}$	$5.3 \cdot 10^{-6}$	$8.2 \cdot 10^{-6}$	3	
101051	Granite, granodiorite and tonalite, metamorphic, fine- to medium grained	Borehole KFM03A	$8.0 \cdot 10^{-6}$	$1.8 \cdot 10^{-6}$	$6.5 \cdot 10^{-6}$	$1.0 \cdot 10^{-5}$	3	

2.6.8 In situ temperature

Temperature was measured by fluid temperature loggings in boreholes KFM05A, KFM06A, KFM07A, and KFM08A. Figure 2-33 illustrates the results for the four investigated boreholes.

In Table 2-20, the temperature for boreholes KFM05A, KFM06A, KFM07A and KFM08A are presented at the depths 400 m, 500 m and 600 m. The inclinations for the boreholes are given as mean values.

For several of the boreholes, for example KFM03A /Pöllänen and Sokolnicki 2004/, temperature was measured in association with difference flow loggings (PFL). For the same borehole and the same depth, differences of up to 2°C occur between the different logging methods. This, together with the large differences in temperature at the same depth in different boreholes, indicates large errors associated with the temperature logging data. An important factor with regard to the quality of the temperature logging data is the period of time between termination of drilling activity and temperature logging. This period varies from borehole to borehole, being approximately 2 weeks for KFM05A, 6 weeks for KFM06A, 9 weeks for KFM07A and 4 weeks for KFM08A. For KFM05A in particular, the relatively short interval might result in a disturbance of the logging results due to the borehole not being stabilised.

A quality assessment of the data was performed in May 2005 (Nissen 2006, personal communication). This revision identified errors in the temperature loggings for some boreholes, KFM05A and KFM06A included. These boreholes have been re-logged, but the data was not produced in time for the version 2.1 data freeze. A preliminary review of the temperature curves indicates that recent loggings have produced better quality data showing a smaller range in temperature between boreholes at a specific depth.

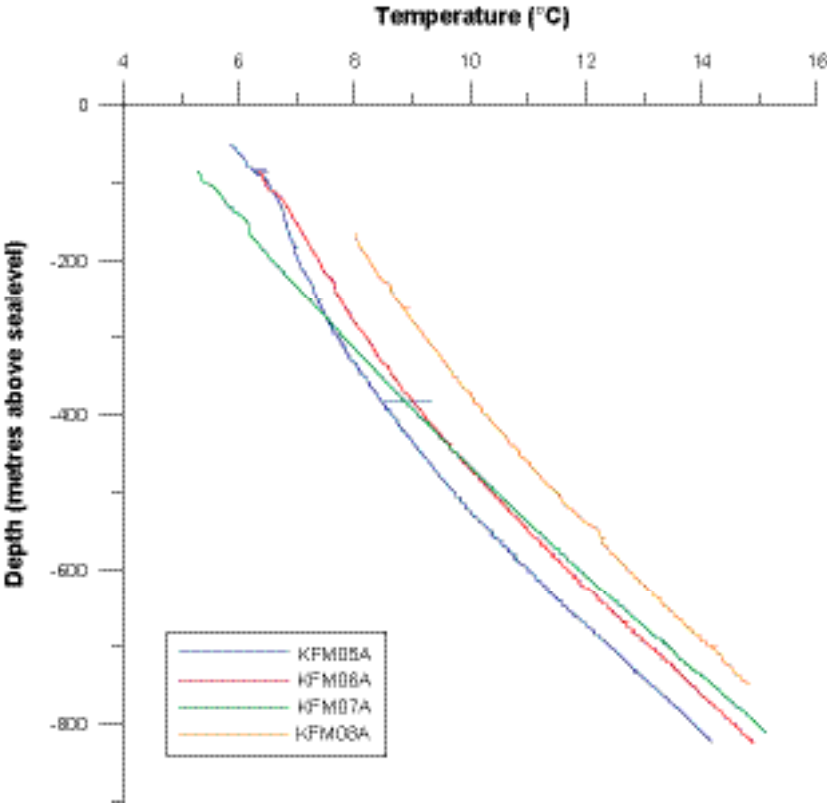

Figure 2-33. *Temperature loggings for four boreholes at Forsmark.*

Table 2-20. Temperature (°C) for the four investigated boreholes at the Forsmark site, at different levels. Borehole inclinations are also included for the boreholes, given as a mean value for each borehole. Elevation (metres above sea level) refers to the start point for each investigated borehole.

Borehole	Temperature at 400 m depth	Temperature at 500 m depth	Temperature at 600 m depth	Inclination (°)	Elevation (metres above sea level)
KFM05A	8.6	9.6	10.9	55.4	4.9
KFM06A	9.1	10.3	11.6	56.4	4.1
KFM07A	9.1	10.4	11.8	54.7	2.8
KFM08A	10.3	11.5	12.7	47.4	0.4
Arithmetic mean	**9.3**	**10.5**	**11.8**		

2.7 Interpretation of primary hydrogeological data

The updated geological deformation zone model presented in Section 3.2 will be integrated with the hydrogeological data acquired up to the 2.1 data freeze during the 2.2 modelling stage. This integration will also make use of a planned, new geological DFN model. Hence, the interpretation of hydrogeological data acquired up to the 2.1 data freeze is based on the 1.2 geological deformation zone and DFN models. It should also be noted that no numerical groundwater flow simulations were conducted in the 2.1 modelling stage. This strategy permitted more time to be spent on issues such as conceptual understanding, data quality assurance, and integrated data interpretation. The subsections below treat in order:

- Overview of available hydrological and hydrogeological data.
- Summary of the version 1.2 bedrock hydrogeological model and database.
- Bedrock hydrogeological data acquired up to the 2.1 data freeze.
- Hydraulic properties of the rock mass in the RFM029 rock domain.
- Quaternary hydrogeology and bedrock hydrogeology.

2.7.1 Overview of available hydrological and hydrogeological data

The investigations performed and the data acquired up to the 1.2 data freeze encompass 12 activities related to surface hydrology (including meteorology), 11 activities related to Quaternary hydrogeology, and 21 activities related to bedrock hydrogeology. Appendix 1 lists the associated P-reports. Among the activities treated in the 1.2 modelling stage, the following are noted in particular:

- Establishment of two meteorological stations and collection of meteorological data (starting May 2003), and registration of snow depth (winters 2002/03 and 2003/04).
- Identification of lake catchments and determination of lake morphological data, and measurements of brook gradients and lake thresholds.
- Establishment of one surface discharge gauging station and collection of discharge, and water temperature and electrical conductivity data.
- Installation of surface water level gauges in six lakes and at two locations in the Baltic Sea and level monitoring (first measurements starting in May 2003).
- Installation of 50 groundwater observation wells and six BAT-filter tips in the Quaternary deposits, and monitoring of groundwater levels in 38 of the wells (first measurements starting in September 2002).
- Slug tests in 48 monitoring wells in the Quaternary deposits and pumping tests in two wells (one in till/bedrock and one in glaciofluvial material).
- HTHB tests (flow logging during pumping) in the short percussion-drilled boreholes HFM01–19 (except HFM07 (dry) and HFM14).
- PSS tests (double-packer injection) in the long core-drilled boreholes KFM01A, KFM02A and KFM03A.

- PFL-f tests (flow logging with 1 m section length and 0.1 m overlap between sections) in the long core-drilled boreholes KFM01A, 02A, 03A, 04A and KFM05A.
- Short term reciprocal cross-hole interference tests between HFM01 and HFM02.
- Short term cross-hole interference tests between HFM11 (observation well) and HFM12 (pump well).

The investigations performed and the data acquired between data freezes 1.2 and 2.1 encompass 5 activities related to surface hydrology (including meteorology), 3 activities related to Quaternary hydrogeology, and 15 activities related to bedrock hydrogeology. Appendix 1 lists the associated P-reports. Among the activities that will be addressed in the 2.2 and 2.3 modelling stages, the following are noted (references to specific SKB P-reports are given when applicable):

- Establishment of two meteorological stations and collection of meteorological data, and registration of snow depth /Wern and Jones 2006/.
- Establishment of three additional surface discharge gauging stations and collection of discharge, and water temperature and electrical conductivity data at four stations.
- Surface water level monitoring in six lakes and at two locations in the Baltic Sea.
- Installation of three additional groundwater observation wells and monitoring of groundwater levels in 38 of the wells.
- Soil core sampling in till for analyses of water retention properties and hydraulic conductivity in three profiles (6–7 depths) /Lundin et al. 2005/.
- Bedrock hydrogeology monitoring data measured in percussion-drilled and core-drilled boreholes between June 2002 and July 2005 /Nyberg et al. 2005, Nyberg and Wass 2005/.
- Single-hole HTHB tests (pumping and flow logging) in the short percussion-drilled boreholes HFM20–22 /Jönsson et al. 2005/.
- Single-hole PSS tests (double-packer injection) in the short core-drilled borehole KFM03B /Hjerne et al. 2004/.
- Single-hole PSS tests (double-packer injection) in the long core-drilled boreholes KFM04A and KFM05A /Hjerne and Ludvigson 2005, Gokall-Norman et al. 2005a/. These boreholes were previously hydraulically tested with the PFL-f method only (see above)
- Single-hole PFL-f tests (flow logging with 1 m section length and 0.1 m overlap between sections) of the long core-drilled boreholes KFM06A and KFM07A /Rouhiainen and Sokolnicki 2005a, Sokolnicki and Rouhiainen 2005/.
- Single-hole PSS tests (double-packer injection) in the short core-drilled borehole KFM06B and the long core-drilled boreholes KFM06A /Hjerne et al. 2005/ and KFM07A /Gokall-Norman et al. 2005c/.
- Short term cross-hole interference test between HFM16 (pump well) and KFM02A (observation well) using the PFL method in KFM02A /Rouhiainen and Sokolnicki 2005b/.
- Short term cross-hole interference test between HFM18 (pump well) and KFM03A (observation well) /Gokall-Norman et al. 2004/.
- Short term cross-hole interference test between HFM16 (pump well) and KFM02A and HFM19 (observation wells) /Gokall-Norman and Ludvigson 2005/.
- Short term cross-hole interference test between KFM04A (pump well) and HFM10, HFM13, HFM19 and HFK252 (observation wells) /Gokall-Norman et al. 2005b/.

2.7.2 Summary of the 1.2 bedrock hydrogeological model and database

Figure 2-34 presents a schematic NW-SE cross-section through the central part of the tectonic lens within the candidate area in Forsmark. A similar cross-section was reported in SDM version 1.2 /SKB 2005a/. The cross-section highlights the following components of importance for the bedrock hydrogeological description.

- The uppermost c. 200 m of bedrock. This subvolume is probably intersected by horizontal sheet joints covering more or less the entire candidate area, though more irregularly distributed, both laterally and vertically, than indicated in Figure 2-34. Possibly, there is a structural difference with regard to the foot wall and hanging wall of the gently dipping ZFMNE00A2 deformation zone affecting also the hydraulic properties.
- The bedrock below c. 200 m depth. The rock mass on either side of the deformation zone ZFMNE00A2 is very sparsely fractured by open fractures at depth. It is noted that the thickness of zone ZFMNE00A2 varies in space. The maximum thickness observed in the boreholes drilled so far is c. 60 m (KFM02A).
- The rock mass above zone ZFMNE00A2 is cross cut by at least five, hydraulically significant, gently dipping deformation zones, many of which have geometrical properties (strike, dip) similar to the ZFMNE00A2 zone, but are generally much thinner (an order of magnitude less).

Up to the 1.2 data freeze, hydraulic tests with the Posiva Flow Log (PFL) equipment were conducted in the cored boreholes KFM01A–KFM05A and with the Pipe String System (PSS) equipment in the boreholes KFM01A–KFM03A. Hydraulic tests (HTHB) were also conducted in the percussion boreholes HFM01–HFM19 (except HFM07 (dry) and HFM14). The hydraulic data gathered in all of these boreholes are presented in /Follin et al. 2005/.

2.7.3 Bedrock hydrogeological data acquired up to the 2.1 data freeze

Between the 1.2 and the 2.1 data freezes additional hydraulic tests with the Posiva Flow Log equipment were conducted in the cored boreholes KFM06A–KFM07A and with the Pipe String System equipment in boreholes KFM04A–KFM07A. Hydraulic tests were also conducted in the percussion boreholes HFM20–HFM22. Figure 2-35 shows the penetration elevations of the percussion boreholes HFM01–HFM22.

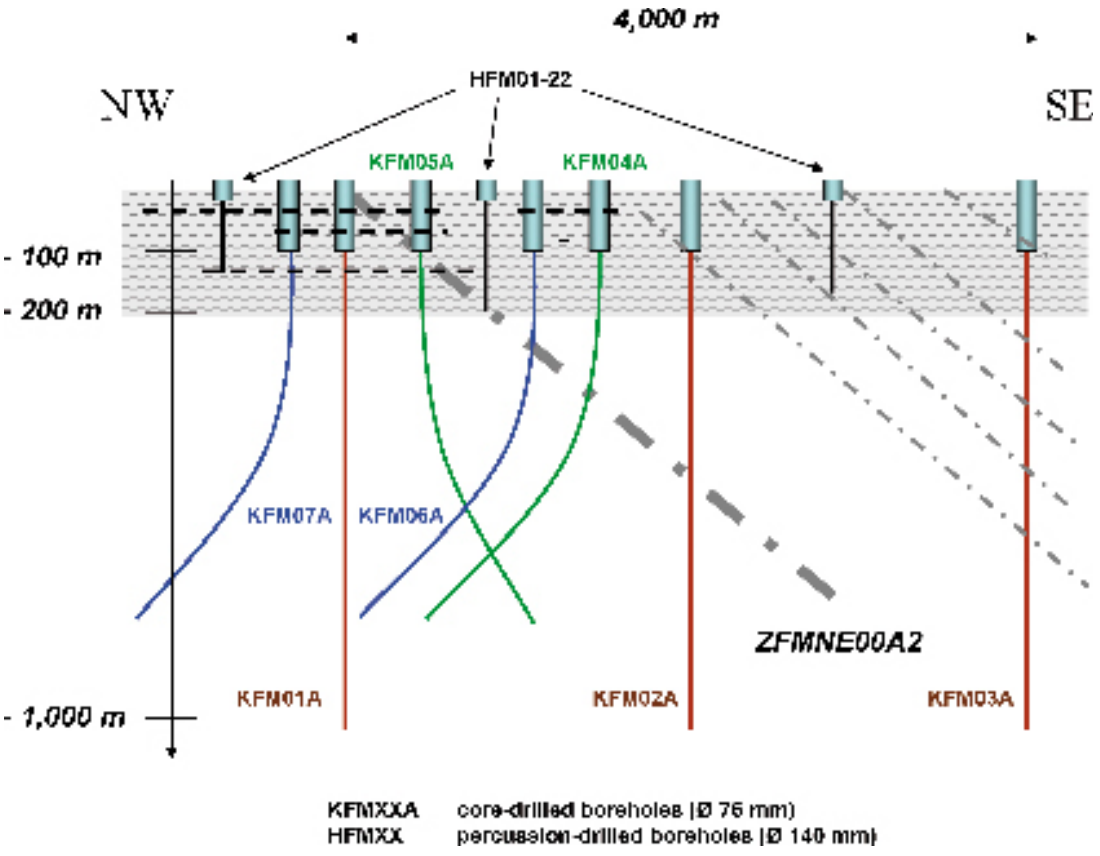

Figure 2-34. *Schematic cross-section through the central part of the tectonic lens. The cored boreholes are c. 1,000 m long; KFM01A–KFM03A are close to vertical (c. 85°), whereas KFM04A–KFM07A are drilled with an inclination (c. 60°).*

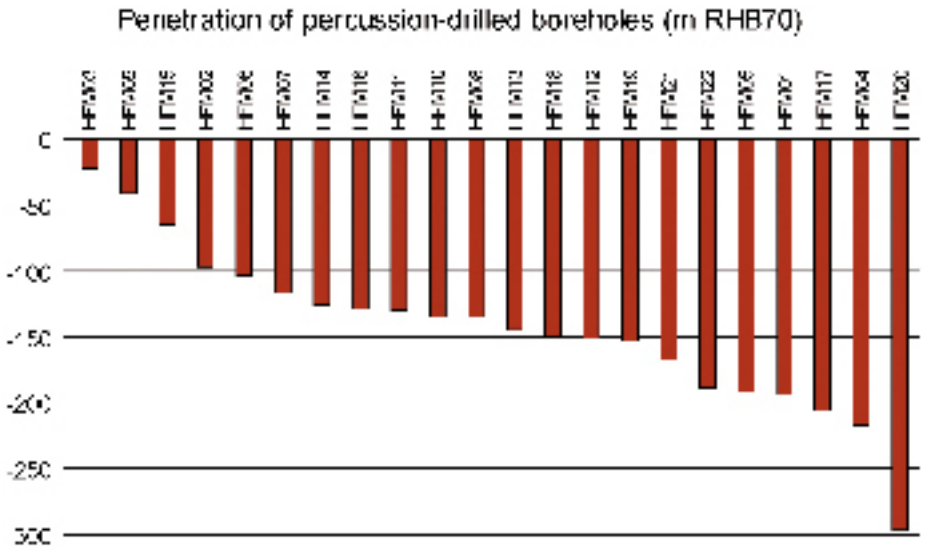

Figure 2-35. *Penetration elevations of the percussion boreholes HFM01–HFM22. The median penetration elevation is c. –140 m above sea level. The borehole lengths vary between 26 and 301 m and the borehole inclinations vary between 49 and 88°.*

Figure 2-36 and Figure 2-37 show the single-hole hydraulic test data acquired in the KFM01A–KFM07A boreholes. The double-packer injection test (PSS) data are given as the transmissivity of contiguous 5 m, 20 m and 100 m test sections. The difference flow logging (PFL) data are available as the transmissivity of contiguous 5 m intervals (PFL-s) and as the transmissivity of individual fractures (flow anomalies, PFL-f). The window for detecting individual facture flow anomalies has a resolution of 0.1 m.

The RFM029 rock domain spans the tectonic lens and is by far the most abundant rock domain within the candidate area. The single-hole hydraulic test transmissivities associated with the flowing fractures in the rock mass outside the deterministically modelled deformation zones as acquired by the PFL-f data in the KFM01A–KFM07A boreholes are commented on in Section 2.7.4. Comparisons between PFL data and PSS data are presented in the associated P-reports. The single-hole transmissivity data acquired in the HFM01–HFM22 boreholes are commented on in Section 2.7.5.

2.7.4 Hydraulic properties of the rock mass in rock domain RFM029

Red circles in Figure 2-36 and Figure 2-37 indicate PFL-f data in the rock masses of the RFM029 rock domain, i.e. the rock outside the large, deterministically modelled deformation zones. Table 2-21 presents some primary PFL-f statistics.

The orientations of the fractures poles associated with the PFL-f transmissivities are shown in Figure 2-38. The stereo net plots are based on the data screening provided by /Forssman et al. 2004, 2006/, cf. Appendix 4 and the correlation method used by /Follin et al. 2005/ in the 1.2 modelling stage. The data screening lists the possible positions of mapped fractures with regard to the positions of the PFL-f anomalies. The correlation method accredits the aperture confidence of Open fractures as well as the hydraulic confidence of the PFL-f anomalies. The 25%, 50% and 75% density contours of the fracture poles to the five fracture sets deduced in the 1.2 geological DFN modelling by /LaPointe et al. 2005/ are inserted into the stereo nets to improve the structural interpretation. Figure 2-39 shows a normal probability plot of the common logarithm of all PFL-f transmissivity data in Table 2-21. Figure 2-40 shows a log-log plot of the complementary cumulative density function of the same data set. The number of data points in the lower end is censored by the practical lower measurement limit of the PFL method. It is difficult to discriminate between the two distribution models.

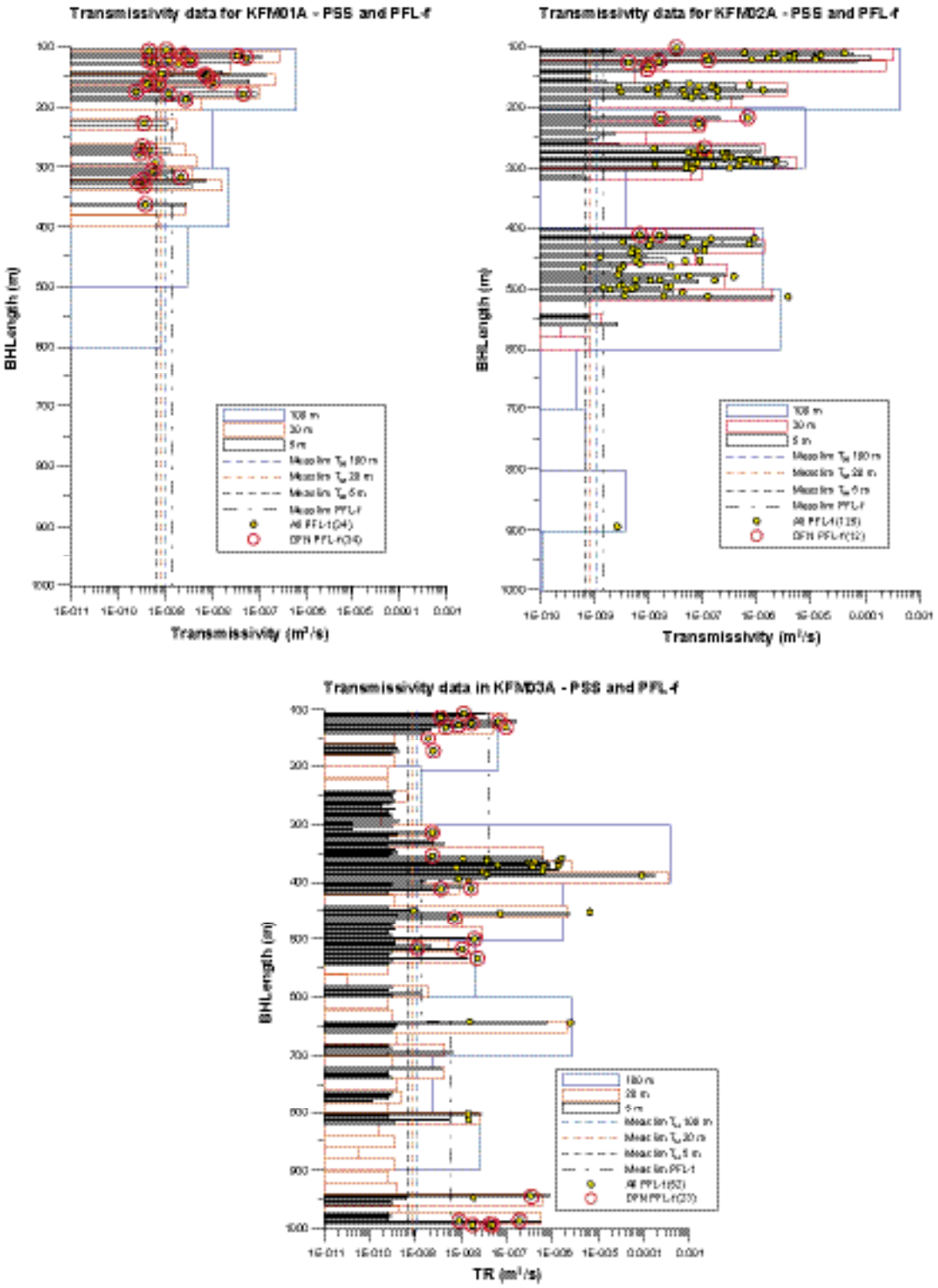

Figure 2-36. *Data from the PFL-f fracture flow measurements (yellow dots) and the PSS double-packer injection tests (blue, red and black bars) in the sub-vertical KFM01A–KFM03A boreholes. Red circles indicate PFL-f data in the rock mass of rock domain RFM029 outside the deterministically modelled deformation zones.*

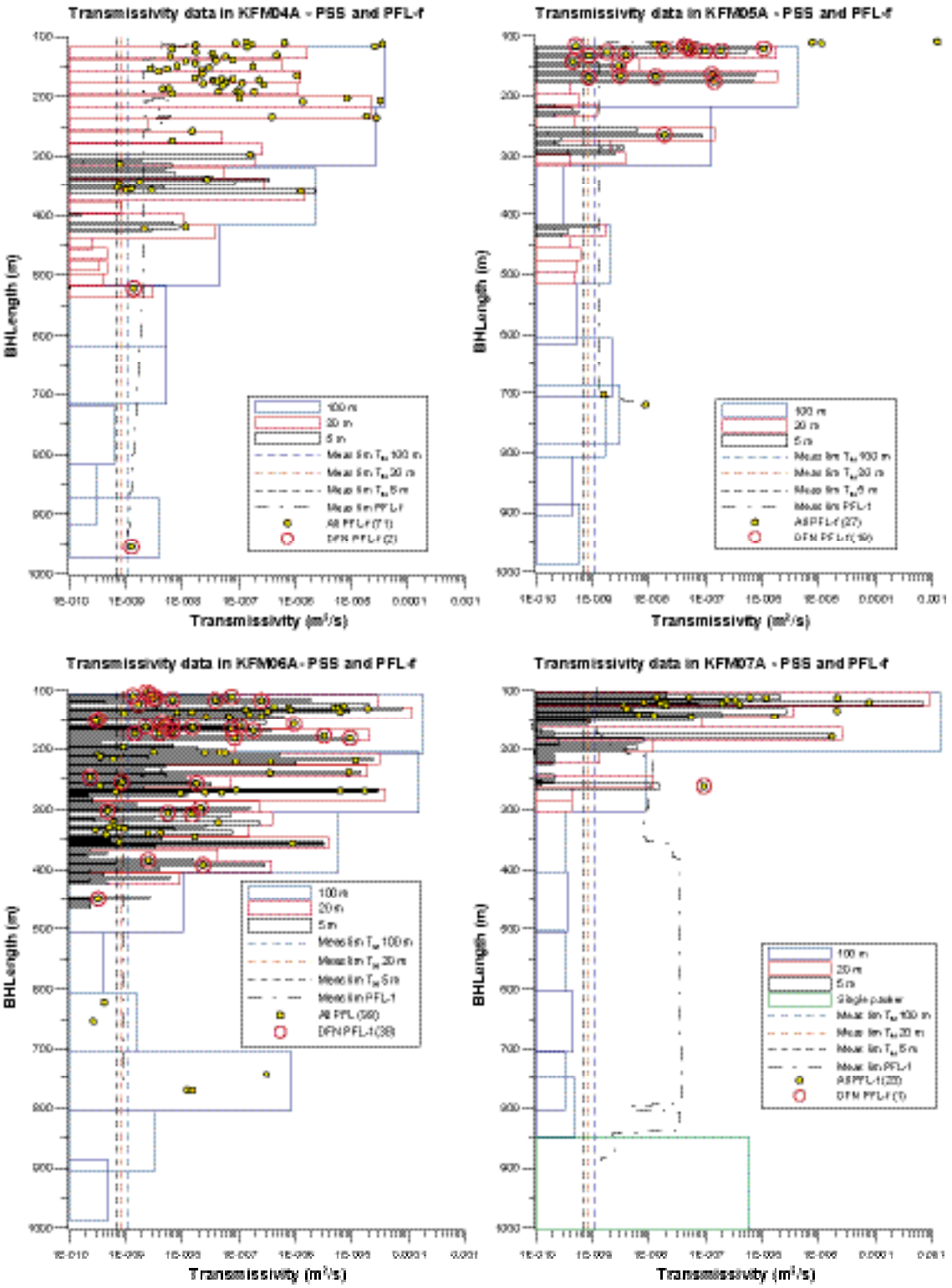

Figure 2-37. *Data from the PFL-f fracture flow measurements (yellow dots) and the PSS double-packer injection tests (blue, red and black bars) in the inclined KFM04A–KFM07A boreholes. Red circles indicate PFL-f data in the rock mass of rock domain RFM029 outside the deterministically modelled deformation zones.*

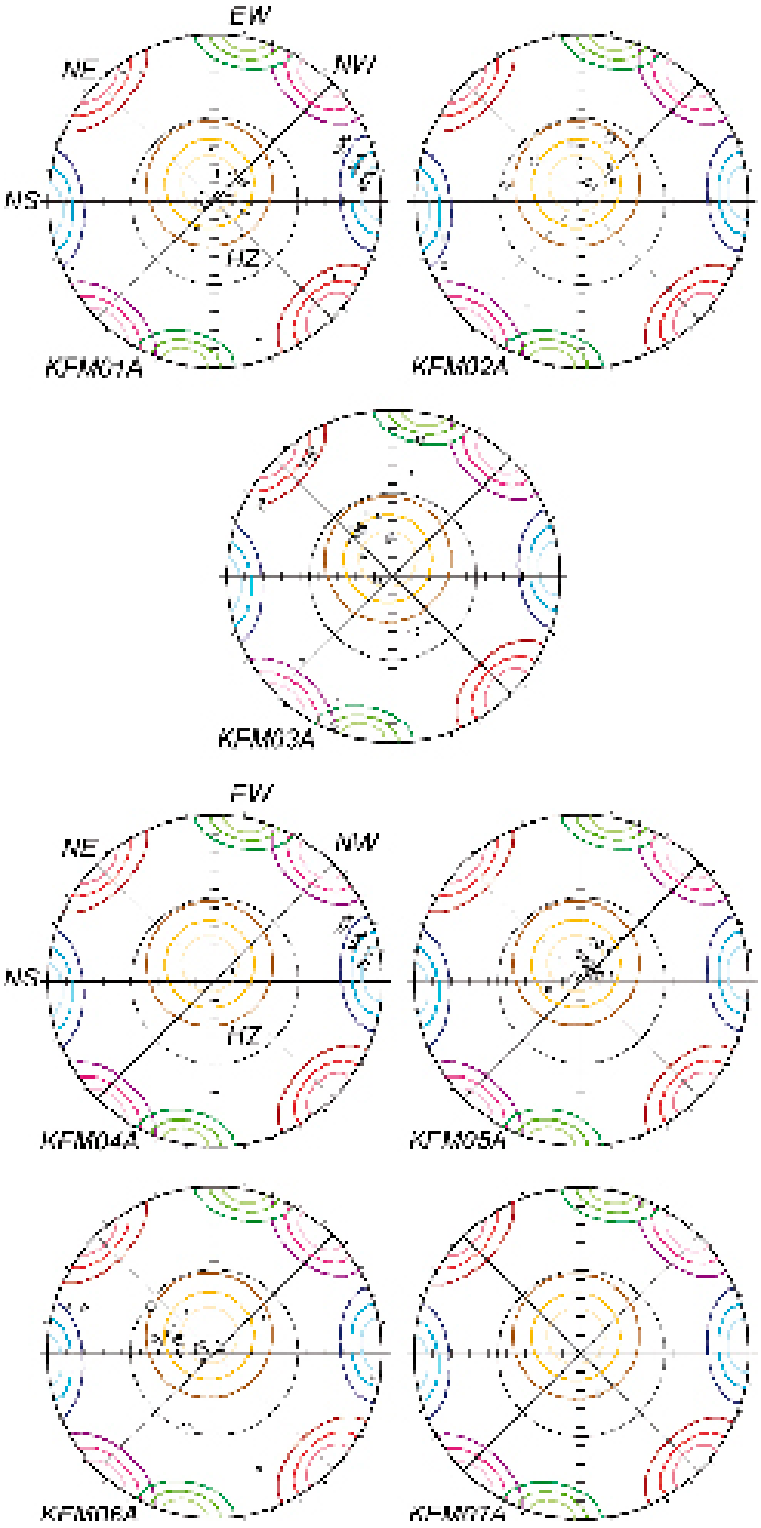

Figure 2-38. *Orientations of fractures associated with the PFL-f transmissivities in the rock mass of rock domain RFM029 outside the deterministically modelled deformation zones. Data are shown for the sub-vertical KFM01A–KFM03A boreholes (top) and the inclined KFM04A–KFM07A boreholes (bottom). The coloured circles represent the 25%, 50% and 75% density contours of the five fracture sets (NS, NE, NW, EW and HZ) deduced in the 1.2 geological DFN model by /La Pointe et al. 2005/.*

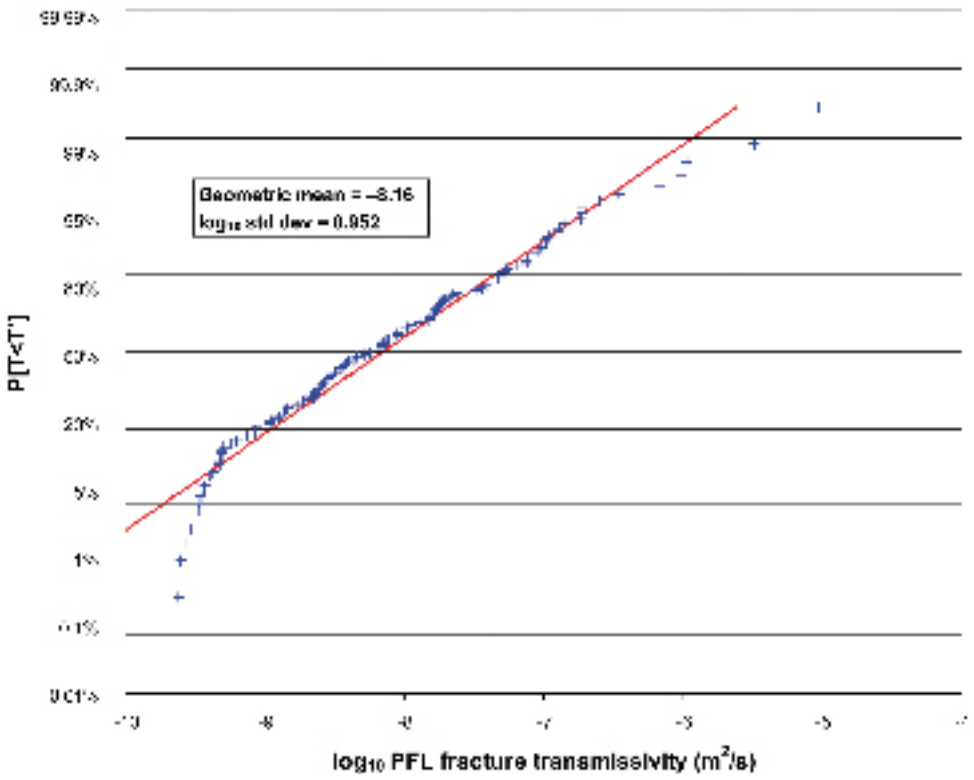

Figure 2-39. *Normal probability plot of the common logarithm of all PFL-f transmissivities in the rock mass of rock domain RFM029 outside the deterministically modelled deformation zones.*

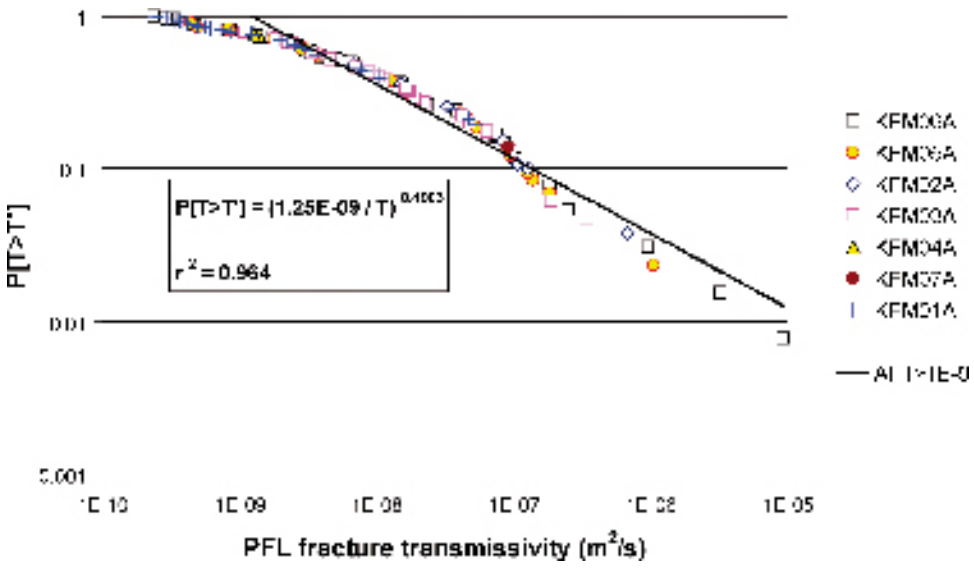

Figure 2-40. *Log-log plot of the complementary cumulative density function of all PFL-f transmissivities in the rock mass of rock domain RFM029 outside the deterministically modelled deformation zones.*

Table 2-21. Primary PFL fracture transmissivity data in the rock mass of rock domain RFM029, i.e. outside the deterministically treated deformation zones.

Borehole	Above/Below relative to DZ ZFMNE00A2	Upper/Lower elevations of PFL fracture flow data (m)	No. of N_{PFL} (–)	T_{PFLmin} (m^2/s)	T_{PFLmax} (m^2/s)
KFM01A	Below	–101/–357	34	2.47E–10	5.35E–08
KFM02A	Both	–94/–403	12	4.26E–09	6.77E–07
KFM03A	Above	–97/–980	23	1.09E–09	3.46E–07
KFM04A	Below	–436/–790	2	1.29E–09	1.41E–09
KFM05A	Both	–95/–222	19	4.45E–10	1.06E–06
KFM06A	Both	–92/–380	38	2.40E–10	9.43E–06
KFM07A	Below	–195/–195	1	9.27E–08	9.27E–08

2.7.5 Quaternary hydrogeology and bedrock hydrogeology

The hydrogeological analyses conducted during the 2.1 modelling stage involved a substantial amount of data screening, which called for a close co-operation between the site investigation and modelling teams at Forsmark. Below follows a brief presentation of the hydrogeological studies conducted by /Gentzschein et al. 2006, Juston et al. 2006, Follin et al. 2006, Levén et al. 2006/. The issues treated are:

- The interplay between Quaternary and bedrock hydrogeology.
- Interpretation of 5 m double-packer injection tests.
- Multi-parameter plots of primary data.

Compilation of monitoring data

Figure 2-41 shows an overview of the percussion and core drillings at Forsmark from the start of the site investigations up to the 2.1 data freeze. The progress of the Hydro Monitoring System (HMS) installations is also shown. The installations began in January 2004 and represent an important step in the site investigation programme in Forsmark.

The information from the HMS measurements to the overall conceptual hydrogeological model is important. However, for a quantitative assessment of recharge and discharge, i.e. the interplay between surface hydrology, Quaternary hydrogeology and bedrock hydrogeology, the usefulness of the acquired HMS recordings is probably quite limited. The major reason for this condition is the intense drilling programme, which in Forsmark creates significant pressure disturbances /Juston et al. 2006/. The disturbances are readily transmitted across large distances due to exceptionally high transmissivities encountered in the uppermost part of the bedrock /Gentzschein et al. 2006/.

Figure 2-42 shows the recordings available in HMS for the percussion-drilled boreholes HFM01–HFM22 between the beginning of December 2002 and the end of June 2005. Figure 2-42 reveals that the point-water heads are quite disturbed for most of the time because of the intense drilling, flushing and pumping activities. According to /Juston et al. 2006/ there are few periods, if any, when several boreholes measure natural conditions simultaneously. For instance, there is a fairly good but short period during the second half of July 2004.

One of the interesting observations by /Juston et al. 2006/ is that the horizontal component of the point-water head gradient in the uppermost part of the bedrock within the candidate area is quite flat and many head recordings appear to follow changes in sea level. The flat gradient is indicative of permeable conditions in the uppermost part of the bedrock. However, the sea level changes often coincide with changes in the barometric pressure and large precipitation, which affects the ground-water recharge. This circumstance complicates the interpretations significantly. Long time series under undisturbed conditions are needed in order to be more conclusive.

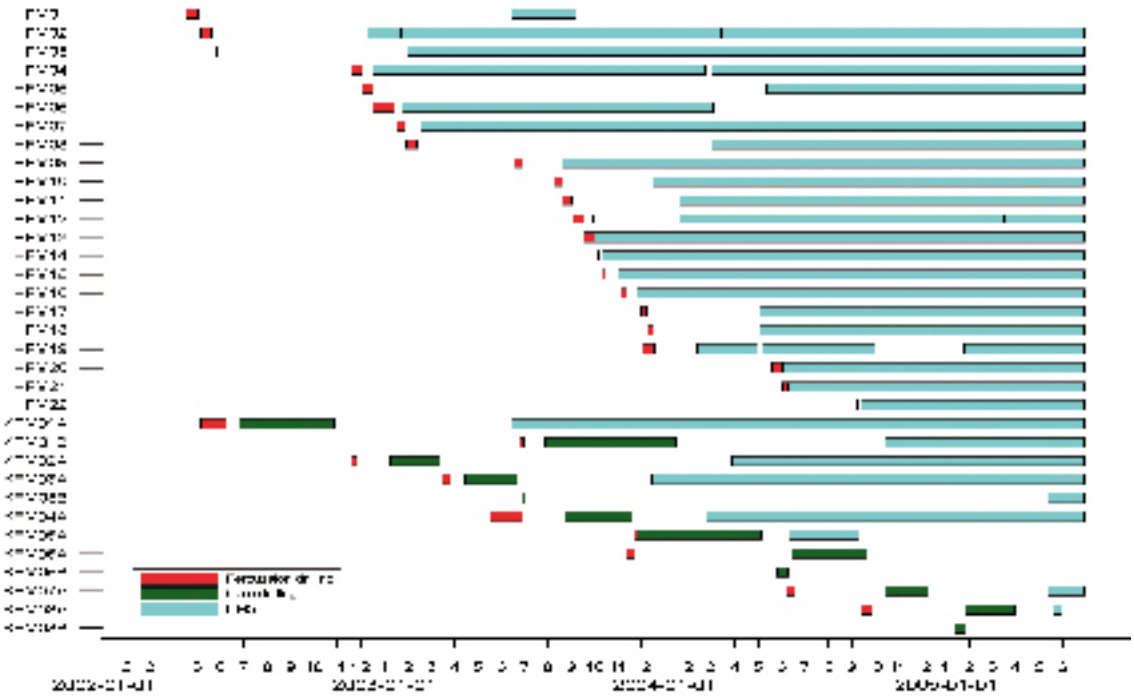

Figure 2-41. *Overview of the percussion and core drillings at Forsmark from the start of the site investigations up to the 2.1 data freeze. The progress of the Hydro Monitoring System (HMS) installations is shown in blue.*

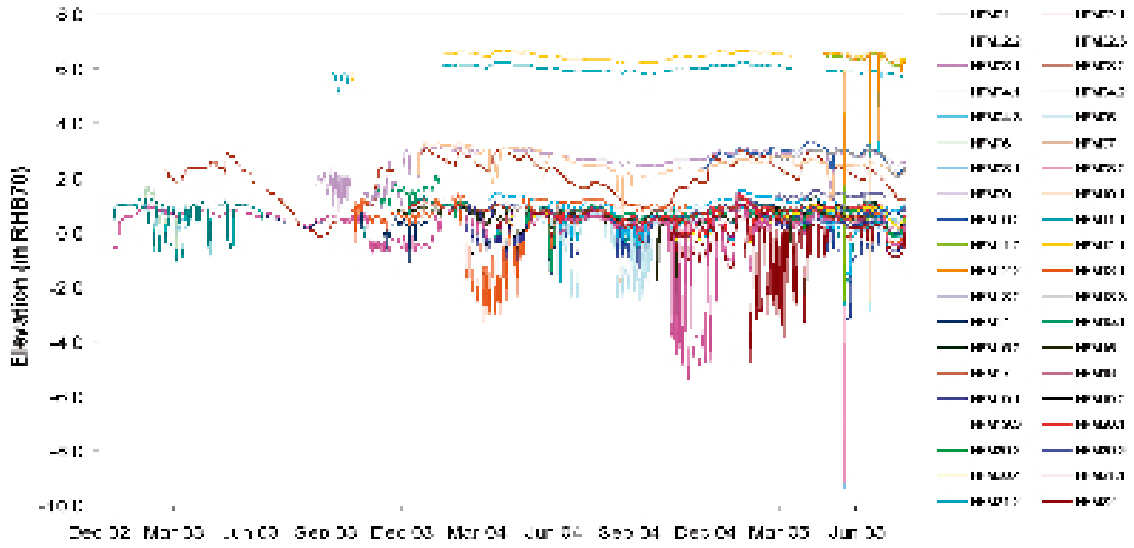

Figure 2-42. *Point-water heads available in HMS for the percussion-drilled boreholes HFM01–HFM22 between the beginning of December 2002 and the end of June 2005. Large head disturbances are due to drilling operations /Juston et al. 2006/.*

Another interesting observation by /Juston et al. 2006/ is the difference in point-water head between the Quaternary deposits and the uppermost part of the bedrock observed at a few locations where there are adjacent boreholes in the two media. Figure 2-43 shows an example from drillsite 2. The HFM05 borehole (c. 150 m long) and the SFM0005 monitoring well (c. 2–3 m long) are c. 37 m apart but have similar bedrock elevations. The HFM05 borehole is completely dry except for the base of the borehole where a high-transmissive structure is intersected /Gentzschein et al. 2006/.

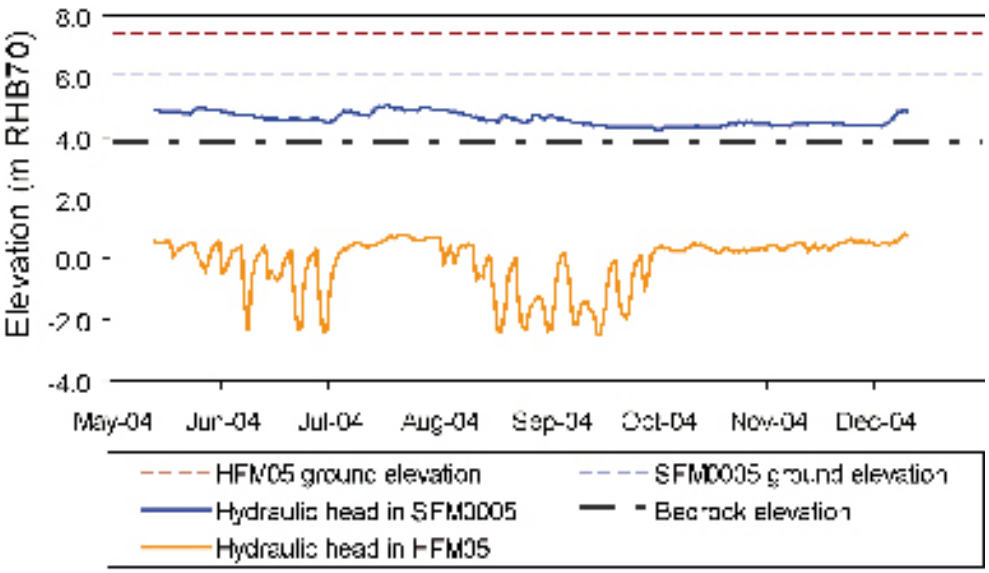

Figure 2-43. *Point-water heads observed in the bedrock (HFM05) and the glacial till (SFM0005). The two boreholes are c. 37 m apart but have the same bedrock elevation. Borehole HFM05 is c. 150 m long and has major hydraulic structure at the base. The SFM0005 monitoring well is c. 2–3 m long and barely reaches the bedrock surface. The head disturbances in borehole HFM05 are due to drilling operations at other drill sites.*

The difference in point-water head observed in the bedrock (HFM05) and the glacial till (SFM0005) may indicate an unsaturated zone in the uppermost part of the bedrock below the Quaternary deposits. However, the difference may also be due to lack of data in the "impervious" rock. More head observations at different depths (and locations) are needed in order to be more conclusive on this issue. It is also recommended to drill a deep borehole into the bedrock below the Lake Bolundsfjärden and monitor changes in the point-water head versus depth. However, in order to compare the head readings it is probably necessary to account for variable-density flow.

Yield of percussion-drilled boreholes

Figure 2-44 shows a map reported by /Gentzschein et al. 2006/ of the median yield for the HFM01–HFM22 boreholes (red dots) and nearby domestic bedrock wells (green and black dots). Figure 2-44 clearly demonstrates the anomalous hydrogeological conditions encountered in the uppermost part of the bedrock in the Forsmark area. The differences are statistically significant.

Figure 2-45 shows the inferred transmissivities in intervals of 50 m in the uppermost 200 m of bedrock. The pattern of high transmissivities in the uppermost parts of the bedrock is quite heterogeneous, i.e. high values can occur at any depth and location. This is interpreted to be due to discontinuities in the spatial extent, and/or the hydraulic properties, of a network consisting of horizontal sheet joints and outcropping deformation zones /Gentzschein el al. 2006/. Evidence for such an interpretation is presented in version 1.2 of the Forsmark SDM /SKB 2005a/.

The illustration in Figure 2-46 is a compilation of the best undisturbed point-water head data available from the uppermost packer sections in the monitored percussion-drilled boreholes in the 2.1 data freeze. The illustration reinforces the previous observation that the point-water heads in the uppermost part of the bedrock within the candidate area are governed by the high transmissivities of superficial, horizontal sheet joints and the elevation of the Baltic Sea. The majority of the percussion-drilled boreholes have no monitoring wells in the Quaternary deposits nearby, which make the correct interpretation regarding the relationship between the hydraulic head in the uppermost part of the bedrock and the hydraulic head in the Quaternary deposits difficult to conceive. For instance, are the high point-water heads in HFM11 and HFM12 (right-hand part of Figure 2-46) indicative of recharge conditions or are they indicative of unsaturated conditions in the uppermost part of the bedrock? What is the interpretation if the environmental head is considered?

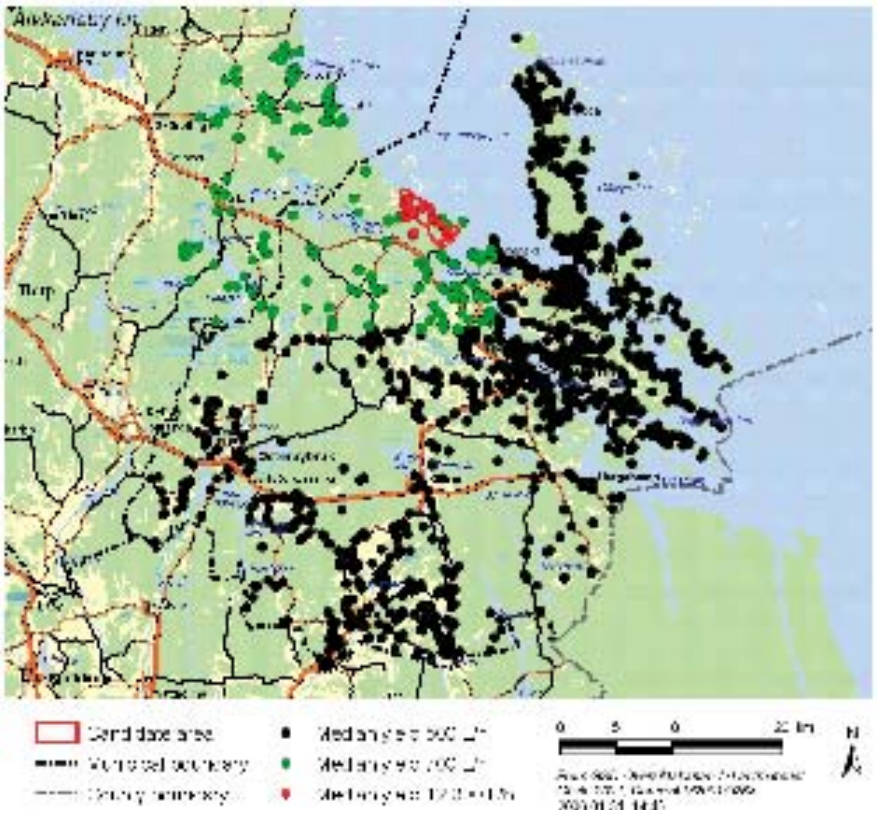

Figure 2-44. *Map of the median well yield from the HFM01–HFM22 boreholes at Forsmark (red dots) and nearby domestic wells (black and green dots) /Gentzschein et al. 2006/.*

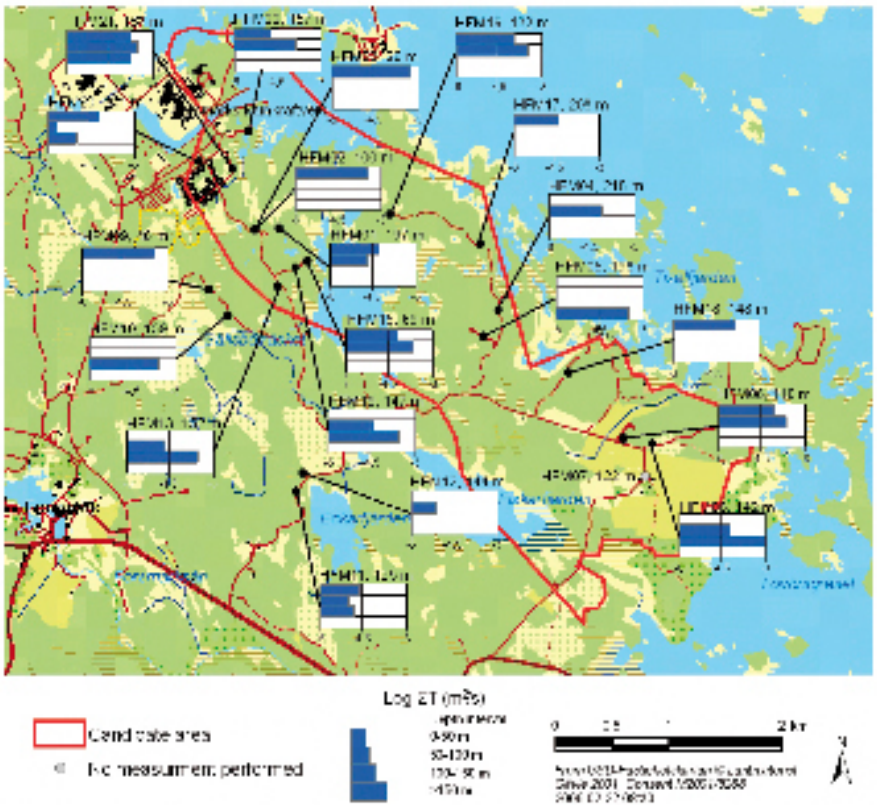

Figure 2-45. *Inferred transmissivities in intervals of 50 m in the uppermost 200 m of rock. The figure after the borehole number is the vertical penetration length /Gentzschein et al. 2006/.*

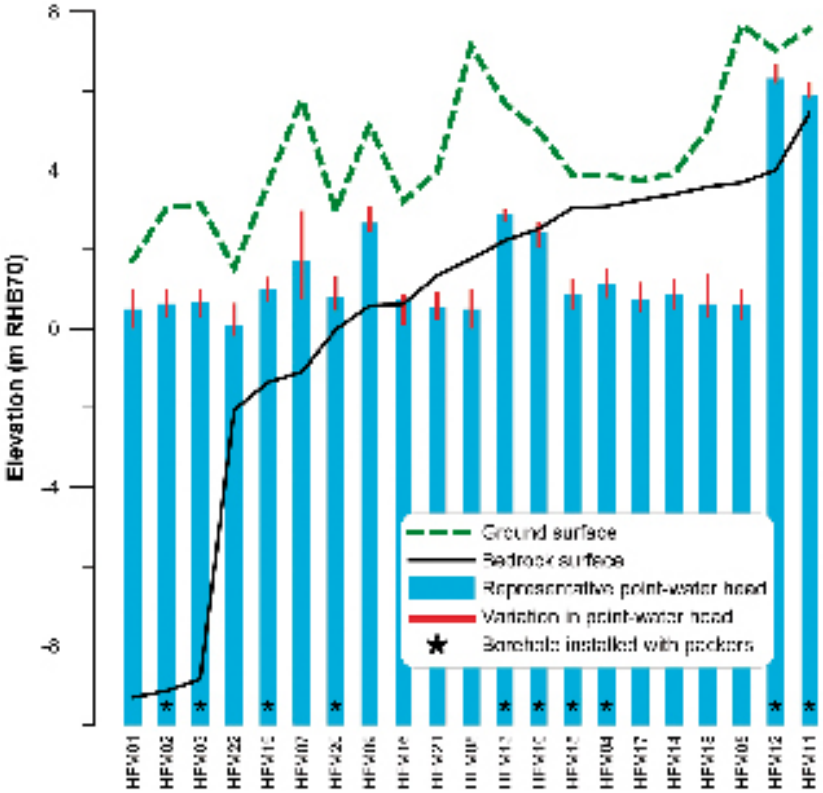

Figure 2-46. *Compilation of the best undisturbed point-water head data available from the uppermost packer sections in the monitored percussion-drilled boreholes in the 2.1 data freeze /Gentzschein et al. 2006/.*

Interpretation of single-hole double-packer injection tests

The transmissivities reported to the Sicada database from the interpretation of 5 m double-packer injection tests refer to the most representative value of each test, T_R. In general, the value deduced from the 20 minute long injection period refers to the first radial acting transient flow regime. Figure 2-47 shows a comparison between the transmissivities, T_R, reported by /Hjerne et al. 2005/ from the KFM06A borehole and generalised radial flow transmissivities, T_{GRF}, deduced from the same data as reported by /Follin et al. 2006/. The cross-plot in Figure 2-47 indicates a fairly good agreement between the T_{GRF} and the T_R values except for a few cases, where the T_{GRF} values are much greater. The cases are denoted by filled squares. The figures adjacent to the filled squares represent the associated packer positions and the interpreted fractional flow dimensions, n, using the GRF approach, respectively. The fractional flow dimensions are in general quite low, which may indicate channelling (a radial flow regime has a fractional flow dimension of two in theory).

Figure 2-48 shows a cross-plot of the fractional flow dimensions interpreted from the injection period versus the observed pressure recovery at the end of the recovery period. The pressure recoveries for the filled squares in Figure 2-48 are not very good, which suggest poorly connected fracture network geometries rather than infinite acting channels for the associated test sections. /Follin et al. 2006/ note that poorly connected networks often render low values of the flow dimension, which in turn render high T_{GRF} values. More details about the analyses behind the results displayed in Figure 2-47 and Figure 2-48 and premises for the comparison are found in /Follin et al. 2006/.

WellCad plots for improved integrated modelling

/Levén et al. 2006/ have compiled multi-parameter plots in WellCad for the percussion-drilled HFM01–HFM22 boreholes and the core-drilled KFM01A–KFM07A boreholes with the objective to facilitate the integrated modelling between disciplines. Figure 2-49 shows an example from the KFM02A borehole. The information shown in this example is of particular interest to Hydrogeology, Hydrogeochemistry and Transport Properties.

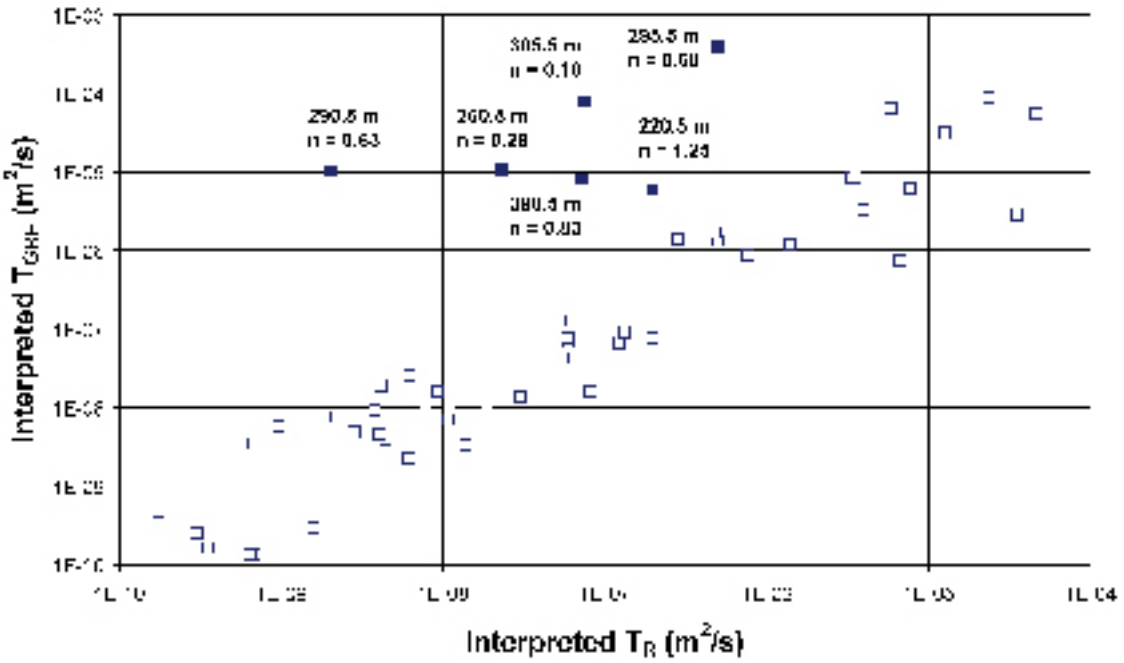

Figure 2-47. *Cross-plot of transmissivities derived with the GRF approach, T_{GRF}, versus the transmissivities T_R reported to Sicada. The data shown come from the double-packer injection tests conducted in the KFM06A borehole /Hjerne et al. 2005/. The cross-plot indicates a fairly good agreement between the T_{GRF} and the T_R values except for a few cases, where the T_{GRF} values are much greater. The cases are denoted by filled squares. The figures adjacent to the filled squares represent the associated packer positions and the interpreted fractional flow dimensions, n, using the GRF approach, respectively. Reproduced from /Follin et al. 2006/.*

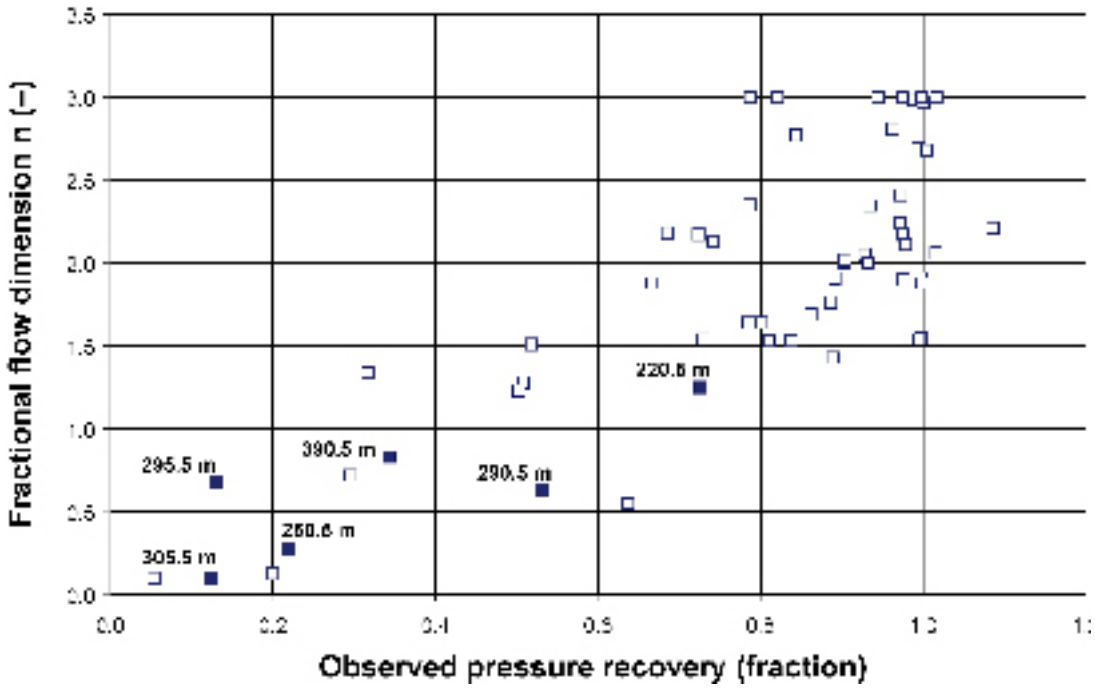

Figure 2-48. *Cross-plot of the fractional flow dimension versus the measured pressure recovery. Reproduced from /Follin et al. 2006/.*

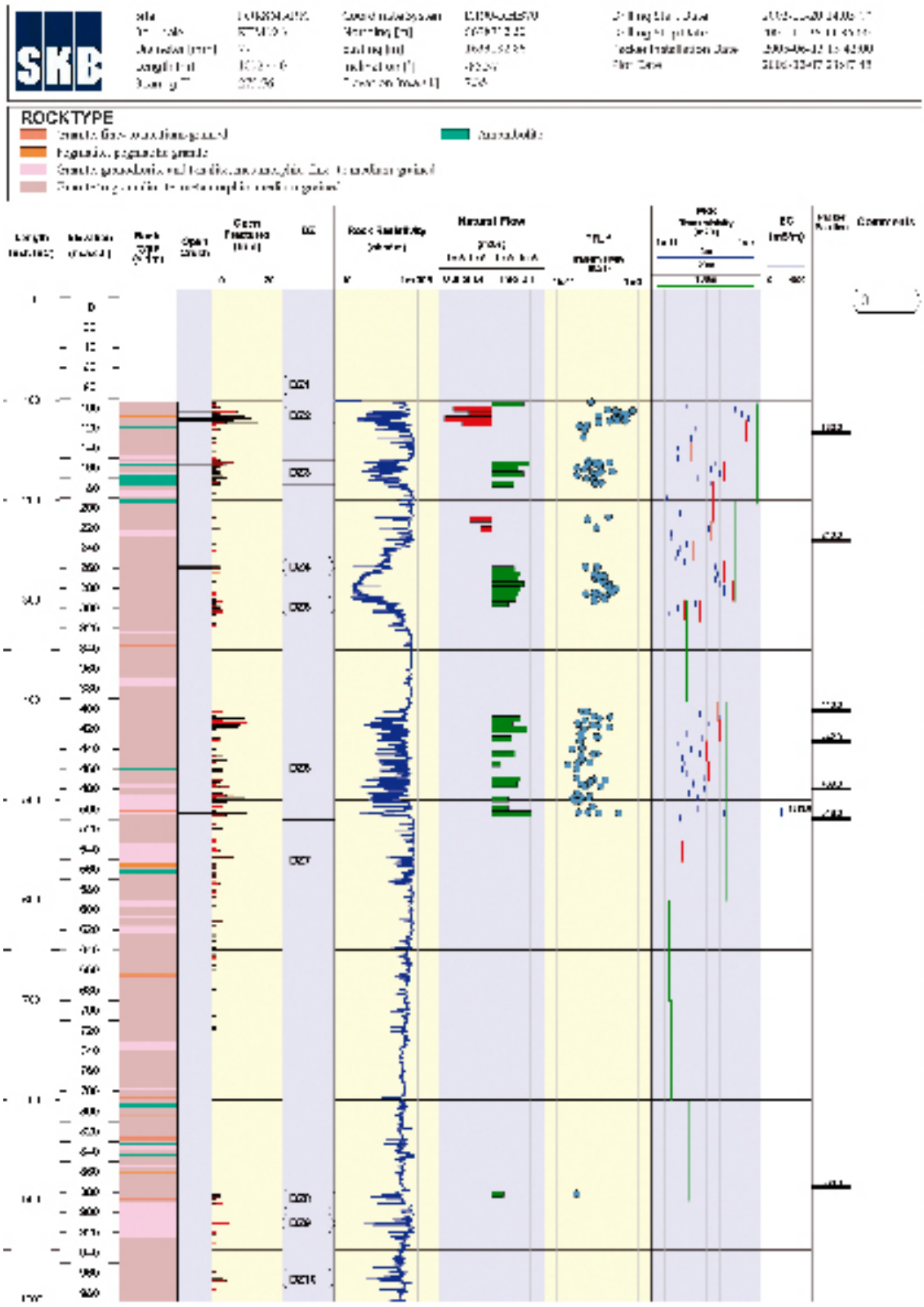

Figure 2-49. *Example of a multi-parameter plot compiled in WellCad to facilitate the integrated modelling between disciplines. Reproduced from /Levén et al. 2006/.*

2.8 Interpretation of primary hydrogeochemical data

This section presents the results of a collective effort made by the ChemNet analysis group to systematically analyse the available Forsmark 2.1 hydrogeochemical data. The work conducted has involved manual evaluation and expert judgment (Sections 2.8.2 and 2.8.3) and mathematical modelling (Sections 2.8.4, 2.8.5 and 2.8.6), all of which must be integrated when evaluating primary groundwater information. These evaluation and modelling steps were made with the purpose to highlight gaps in existing data or the need for additional data in order to provide constructive input to the site characterisation programme. New hydrogeochemical recommendations are presented in Chapters 5 and 6.

2.8.1 Available data

The Forsmark 2.1 data freeze included hydrogeochemical data derived from the drilling of three new percussion boreholes (HFM20, 21 and 22) and four new cored boreholes (KFM05A, KFM06A, KFM07A and KFM08A), and sampling from an additional 6 shallow Soil Pipe installations (SFM0022, 59, 61, 62, 63 and 64).

Surface investigations (Lake and Stream waters) have been evaluated with respect to demarcating potential recharge/discharge localities and establishing the natural (i.e. primarily precipitation source) distribution of ^{14}C and tritium in the Forsmark region. This latter issue is important since there may be some additional effects from the nearby nuclear plant facilities.

Borehole investigations have continued to further extend knowledge regarding the vertical and lateral spatial extent of the various identified hydrochemical end members, and the origin and evolution of these end members.

Anomalously high uranium concentrations, often (but not always) coinciding with the Littorina Sea groundwater component, have become a debatable issue to be resolved. Different approaches have been recommended, for example:

- Are these values an analytical artefact or due to mobilisation of uranium in connection with the drilling process?
- Have they entered the system in association with the Littorina Sea transgression?
- Do they reflect migration from some distance (i.e. from a mineralised source) through a hydraulically active fracture network which, in cases, fortuitously coincides with the entry points of the Littorina Sea component?

Characterisation of additional fractures and their infillings have added further understanding to the spatial extent and origin of specific mineral indicators that can contribute to unravelling the palaeoevolution of some groundwater types, and also in estimating the depth of redox fronts etc.

Accessible, interconnected pore water has been extracted successfully by laboratory out-diffusion methods from crystalline rocks using some 20 core samples from borehole KFM06A as part of the Forsmark hydrogeochemical site investigation programme.

The Forsmark 2.1 data extracted from the Sicada database have been screened and reviewed to produce groups of data characterised with respect to being suitable or less suitable for quantitative modelling purposes (Table 2-22).

Percussion boreholes

Chosen data have been subdivided into samples collected from: a) borehole sections < 50 m long were the groundwater data can be related approximately to a more constrained bedrock level, i.e. dominant water conducting fracture, and b) total borehole lengths which can vary from 100–300 m deep. These latter boreholes mostly represent a homogenised mixed groundwater. It is important to know the chemistry of such waters when they are used as a source of flushing water during drilling of the deep cored boreholes, but otherwise such data is of little use in understanding the groundwater stratification in the upper 300 m of bedrock. Recent information (Table 2-23) provides the approximate depth of major groundwater input to the percussion boreholes. These data may be used

Table 2-22. The total number of usable samples included in the Forsmark 2.1 data base. Orange = Most representative/suitable (relates to all water types if applicable), Green = Less suitable and to be used with caution (relates to all water types if applicable), Pink = Least suitable and to be used with caution (relates only to surface waters).

		Total number of samples	Usable samples		
			Orange	Green	Pink
Percussion boreholes		107	3	16	
Packed-off sections in cored boreholes	KFM01A	150	2	1	
	KFM02A		2	2	
	KFM03A		4	2	
	KFM04A			2	
	KFM05A				
	KFM06A		1	2	
	KFM07A			1	
Near-surface groundwater		267		231	
Sea water		255		42	106
Lake water		352		80	253
Stream water		341		74	249
Precipitation		23		19	

Table 2-23. Locations (vertical depth) indicating points of maximum water flow into the Forsmark percussion boreholes.

Borehole	Sections (vertical depth) with maximum water volume input into the borehole	Borehole	Sections (vertical depth) with maximum water volume input into the borehole
HFM01	~ 38 m	HFM12	~ 93 m
HFM02	~ 43 m	HFM13	~ 140 m
HFM03	~ 21 m	HFM14	Not determined
HFM04	~ 61 m	HFM15	Fairly uniform input along the borehole
HFM05	~ 153 m	HFM16	~ 59 m (some also from 42 m)
HFM06	~ 70 m	HFM17	~ 31 m
HFM07	Not determined	HFM18	~ 30–40 m
HFM08	~ 138 m	HFM19	~ 150 m
HFM09	~ 24 m	HFM20	~ 25 m
HFM10	~ 110 m	HFM21	~ 84–136 m
HFM11	~ 32 m (some also from 83–108 m)	HFM22	~ 53 m

qualitatively to indicate potential hydrochemical stratification in the upper bedrock. In the present Forsmark 2.1 Sicada Table, samples representing type (a) above are highlighted in orange, and those representing type (b) are highlighted in green.

Cored boreholes

Additional boreholes to those evaluated in Forsmark 1.2 are KFM05A, KFM06A, KFM07A and KFM08A; additional sampling of KFM04A is also included. Evaluation of samples from the four new boreholes made use of the published differential flow logs, hydrochemical logs and also hydrochemical characterisation of sampled groundwaters.

The final selection of data which best represents the sampled borehole section is based on identifying as near as possible a complete set of major ion and isotope (particularly tritium, ^{18}O and deuterium plus carbon isotopes when available) analytical data. This is not always the case, however, and a degree of flexibility is necessary in order to achieve an adequate dataset to work with. For example:

- A charge balance of ± 5% was considered acceptable.
- Less or close to 1% drilling water was considered acceptable for suitable (representative) groundwaters. In some cases groundwaters of limited suitability were chosen when exceeding 1% (but < 5%) to provide a wider selection of groundwater data to work with. These groundwaters should be treated with caution if used quantitatively.
- In borehole KFM03A, sections 803.20–804.20 m and 939.50–956.62 m indicate drilling water contents of 16.5% and 11.2% respectively. These have been highlighted in green although strictly speaking they should have been omitted because of high drilling water content. However, because of the general lack of deep groundwater chemistry data at Forsmark, they have been included, but should be treated with great care when used quantitatively.

Resulting from this assessment, two groundwater sample types are highlighted in the Sicada database; one type considered representative or suitable (in orange), the other type less representative or of limited suitability (in green) and should be used with caution.

Open-hole tube sampling has been carried out in the cored boreholes. Whilst this approach can be very useful in evaluating borehole groundwater circulation pathways and groundwater budgets (e.g. water in and water out between the borehole and surrounding bedrock), the fact that the these groundwaters are mixed to varying degrees due to: a) borehole hydraulics, b) borehole activities prior to sampling, and c) perturbation during lowering of the tube system into the borehole, their representativeness (or suitability) to describe the bedrock formation waters is questionable.

Consequently, groundwater samples relating to the Sicada tube sampling data contained in the Forsmark 2.1 data freeze are considered unsuitable for use.

PFM-series: private wells, unused old dug wells, natural springs and excavated trenches

Most of these surface waters have a time-series of data (most sampled on 3 occasions over the period of a year) covering autumn and spring. Some have been sampled on two occasions and some only on one occasion, but all these data still can be incorporated to some limited extent since they represent at least one season. Future data freezes should provide additional seasonal values plus outstanding ^{14}C data.

All samples have been highlighted in green to indicate:

- satisfactory charge balance (± 5%),
- good coverage of major elements,
- several trace elements,
- tritium,
- ^{18}O and D,
- No ^{14}C (exception the excavated trench).

Because of the complex nature of the near-surface environment being sampled, all samples have been highlighted in green until future interpretative studies and greater understanding of this environment suggest otherwise.

SFM-series: soil monitoring pipes

Most have a good seasonal time-series spread over a period of 1.5 years in cases, although some are restricted to only one or two sampling occasions within this period. Other locations included in the earlier 1.2 data freeze, usually restricted to one sampling occasion, have not been, and will not be, further sampled within the hydrochemical programme. However, even if there may be only one sample from a particular location collected at one season, it may have some general use when included with other better constrained seasonal values, as mentioned with the PFM-series samples above.

All suitable data, i.e. indicating at least:

- satisfactory charge balance (± 5%),
- good coverage of major elements,
- several trace elements,
- tritium,
- ^{18}O and D,

have been included and highlighted in green. Many samples also have more complete data, e.g. ^{14}C (plus boron and chlorine isotopes), REEs and the uranium/radium/radon group. These samples with more complete analytical data could have been highlighted in orange, but because of the complex nature of the near-surface environment being sampled, all samples have been highlighted in green until future interpretative studies and greater understanding of this environment suggest otherwise.

Baltic Sea water

Baltic Sea samples have been collected over a three year period. Evaluation of suitability is based on:

- satisfactory charge balance (± 5%),
- good coverage of major elements,
- within 2,500–2,800 mg/L Cl,
- tritium,
- ^{18}O and D,
- ± ^{14}C.

Samples satisfying these criteria are highlighted in green. Samples based only on the first three criteria (i.e. no isotopic data) are highlighted in pink.

Lake and stream water

Lake and stream samples have been collected over an approximately three year period. Evaluation of suitability is based on:

- satisfactory charge balance (± 5%),
- good coverage of major elements,
- tritium,
- ^{18}O and D,
- ± ^{14}C.

In common with some of the near-surface soil monitoring pipe groundwaters, these surface waters may have been subject to seasonal fluctuations, complex reaction processes in the biosphere and potential discharge influences. Consequently, in the absence of knowing what could be representative or not, all selected samples that conform to the above criteria are recommended at this juncture (highlighted in green). Samples restricted only to major ion analytical data have also been recommended for use (highlighted in pink).

Precipitation

Twenty two samples are included, collected during an approximately two year four month period. These waters have not undergone any representativity check *senso stricto*. On the other hand, the main intention has been to monitor ^{18}O, D and tritium, since these parameters are used to identify modern meteoric groundwater components at depth. Disturbances, such as unpredictable annual and seasonal trends and possible evaporation, have not been evaluated in this present representativity check. Because of the difficulty of assessing representativeness, samples with isotopic values are highlighted in green in the Forsmark 2.1 data base.

Data collected during drilling

The drilling event is considered to be the major source for contamination of the formation groundwater. During drilling, large hydraulic pressure differences can occur due to uplifting/lowering of the equipment, pumping and injection of drilling fluids etc. These events can facilitate unwanted mixing and contamination of the groundwater in the fractures, or the cutting at the drilling head itself can change the hydraulic properties of the borehole fractures. It is therefore of major importance to analyse the drilling events in detail. From this information not only can the uranine-spiked drilling water be traced, but also the major risk of contamination and disturbance from foreign water volumes can be directly identified. Insufficient or excessive extraction of water from a deformation zone prior to sampling can be determined by applying DIS (Drilling Impact Study) modelling /Gurban and Laaksoharju 2002/.

The DIS modelling requires evaluation of data that is not normally included in the hydrogeochemistry data set. The drilling rig records various parameters during the entire drilling event. This so called DMS (Drilling Machine Survey) data is recorded in separate data files that have to be requested from Sicada. In addition, for the DIS study electrical conductivity values or EC values recorded during the DIFF (Differential flow) measurements are needed. The extraction and compilation of this data has been problematic for the Forsmark 1.2 and 2.1 modelling stages. The problems can be associated with how the data files are organised, missing information concerning the meaning behind variable names, unequal dosing of uranine at times and inaccuracy in recording of the water volumes pumped in and out from the borehole during drilling. This makes the DIS study difficult or impossible and makes the determination of the disturbances from drilling inaccurate.

2.8.2 Explorative analysis

The version 2.1 hydrogeochemical explorative analysis has basically involved updating the version 1.2 major ion and environmental isotope plots. This updating confirms and strengthens existing trends, as well as the chemistry and evolution of the various groundwater types. This is exemplified in Figure 2-50 and Figure 2-51 which show the distribution of chloride with depth, and the relationship between chloride and ^{18}O, respectively. Figure 2-50 is interesting because of the anomalously high chloride content of 14,400 mg/L that occurs at a slightly shallower depth (KFM07A: 700–730 m) than the previously highest value of 9,690 mg/L (KFM03A:990.6 m). Although this high value could be explained by groundwater being brought from deeper levels during sampling, it is also noticeable that this borehole section is located entirely below the gently dipping deformation zone ZFMNE00A2, whilst KFM03A is located above. Maybe this suggests that groundwaters below zone A2 achieve greater salinity at shallower depth, or it represents a different evolutionary trend.

Figure 2-51 demonstrates four features: a) the large spread of ^{18}O values for the dilute soil pipe groundwaters, most likely reflecting seasonal precipitation variations, b) the separate group of soil pipe groundwaters at higher salinity (~ 1,000–2,500 mg/L Cl), some with a light ^{18}O signature, c) a small cluster of soil pipe (and one percussion borehole) groundwaters of more brackish composition with heavier ^{18}O signatures plotting close to the Littorina Sea type waters, and d) the continued light ^{18}O values for the deeper, more saline groundwaters, indicating a distinct cold climate recharge (glacial) component at the maximum depths sampled. A recommendation arising from these observations is to drill at least one deeper borehole to try and establish the maximum depth at which cold climate recharge is detectable.

The Forsmark area has been the focus of studying the composition of the rock matrix in situ pore water, i.e. the accessible, interconnected pore water. This has been extracted successfully by laboratory out-diffusion methods from the crystalline rocks using some 20 core samples from borehole KFM06A. With depth, these pore waters generally reflect hydrochemical trends already noted in adjacent formation groundwaters. Some insight into the palaeoevolution of the site has been obtained and there is the possibility to use the extraction method to derive rock matrix diffusion coefficients.

However, an underlining concern is the possible modification of the in situ water content during sampling. Every rock sample recovered from depth is potentially subjected to some stress release mechanisms. Such release will result in an increase of the void volume of a rock sample and thus perturb bulk density measurements and, if drilled with a drilling fluid, also the water content because some drilling fluid might enter this newly created void volume. Furthermore, small-scale

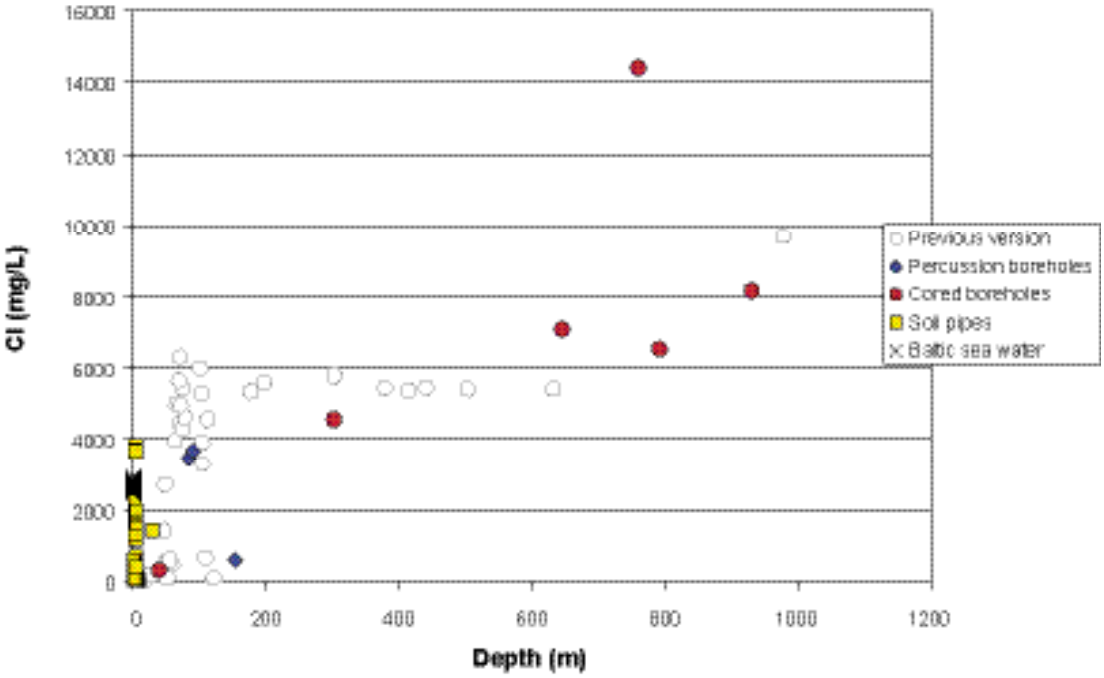

Figure 2-50. *Distribution of chloride with increasing depth.*

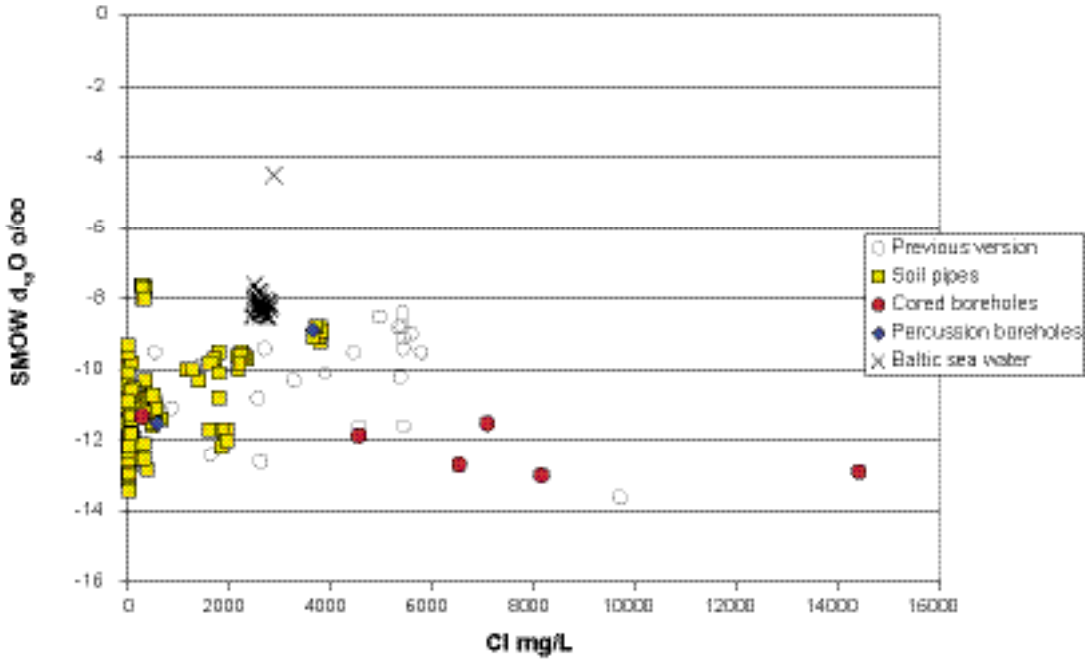

Figure 2-51. *Distribution of chloride versus* ^{18}O.

fracturing of the rock core may expose fresh faces containing ruptured quartz grains releasing fluids (potentially saline) normally trapped in inclusions. A final problem is that in rocks with such low water contents, the measurements employed in these studies might simply not be accurate enough to resolve the effects of stress release. While a fully quantitative argumentation is difficult with the data at hand, several semi-quantitative arguments have been put forward which appear to show that measurable effects of stress release are very small. Calculations based on hypothetical changes in water content show that a change of 50% caused by stress release would essentially increase the pore water chloride by a factor of 2.

To further help resolve the stress release issues, it is recommended that pore water determination from strategic boreholes at Forsmark should be carried out in close collaboration with groups involved with rock mechanic studies, solute transport modelling including rock porosity measurements, and down-hole measurements of formation factors based on electromigration. Future sampling for porewater chemistry is expected to include boreholes KFM01D and KFM08C and, in collaboration with the rock mechanic group, borehole KFM02B (see Chapter 6).

The issue with the high uranium contents (between 10–90 µg/L) in some of the groundwaters with Cl contents between 4,000–6,000 mg/L needs to be further elaborated on.

2.8.3 Microbes, gases and colloids

The suggestion described below for further detailed microbial, gas and colloid sampling will be dealt with in the ordinary CSI sampling programme.

Microbes

In their energy harvesting reactions, microbes use available energy-rich compounds as electron donors and various electron acceptors from groundwater and fracture minerals. This means that they are intimately coupled to the redox conditions in the groundwater system. Redox pair analyses described in the Forsmark 1.2 reports /SKB 2005ad/ and the present 2.1 work coincide very well with the microbial data, i.e. the physiological groups of microorganisms that are present at the different sampling sites.

Figure 2-52 shows the results from sampling in Forsmark. Data to the right of the vertical line in the figure are new in the 2.1 data freeze; this also includes a duplicate sampling at 302 m depth in KFM06A. Data from this sampling verified the Most Probable Number (MPN) method to be both confident and reproducible, and that the sampling method was accurate. In the last sampling, nitrate reducing bacteria were included in the MPN analyses. Figure 2-53 shows microbial data together with the reduction potential in groundwater at the sampled depths.

Figure 2-53 shows that when iron- and manganese-reducing bacteria dominate at 111 m depth, the redox values are below –150 mV. When the sulphate-reducing bacteria increase in numbers at 632 m depth and even more at 930 m depth, the redox values decrease to –175 and –250 mV, respectively. At depths between 200 and 600 m, the redox values are higher due to a low number of microbes and few redox-lowering reactions.

The data so far give a good overview of possible microbial processes and important microbial redox-controlling mechanisms in the depth interval 100–1,000 m. However, several of the SIERG and INSITE reviewers correctly have asked also for data and models of the processes that dominate in the region between the surface and 100 m depth, in particular information about the oxygen penetration depth. Figure 2-52 and Figure 2-53 show that data from this depth interval at Forsmark are lacking. This is problematic since this region is very important with respect to microbial processes. At this depth interval, the main inflow of meteoric water containing oxygen and organic material occurs. Organic matter input to the subsurface effectively blocks oxygen intrusion by microbial consumption of the organics with oxygen, and by that governs the redox conditions at depth.

Sampling and analysis of the presence of different microbial groups, together with oxygen and redox measurements in existing soil pipes and percussion-drilled boreholes, would provide the data required for modelling: a) the oxygen intrusion into deeper groundwaters and, b) consumption of oxygen by microorganisms in the region between the surface and the depths already sampled.

Gases

Several dissolved gases are important components in microbial redox processes. The planned sampling will give more data to be used in the models. One specific issue that has been requested by one reviewer is the stable isotope composition of methane. This information would make it possible to distinguish between biogenic and abiogenic produced methane.

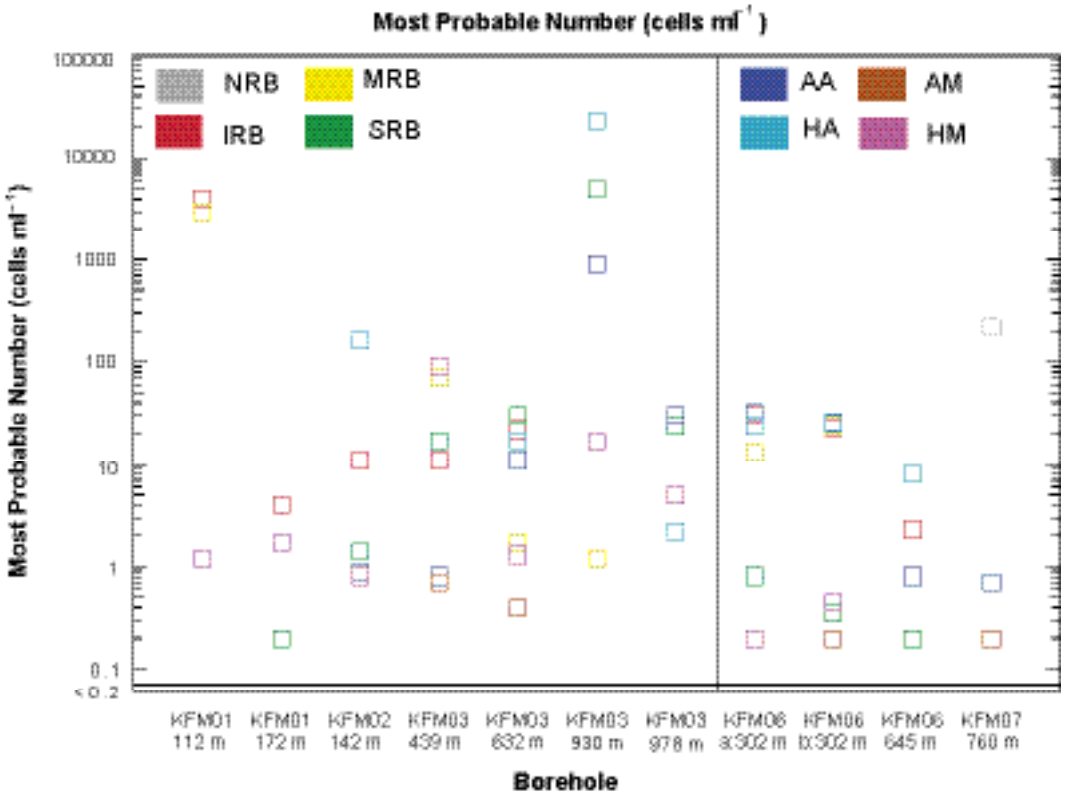

Figure 2-52. *The most probable numbers of different physiological groups of microorganisms at the Forsmark area. Data to the right of the vertical line are new in the 2.1 data freeze.*

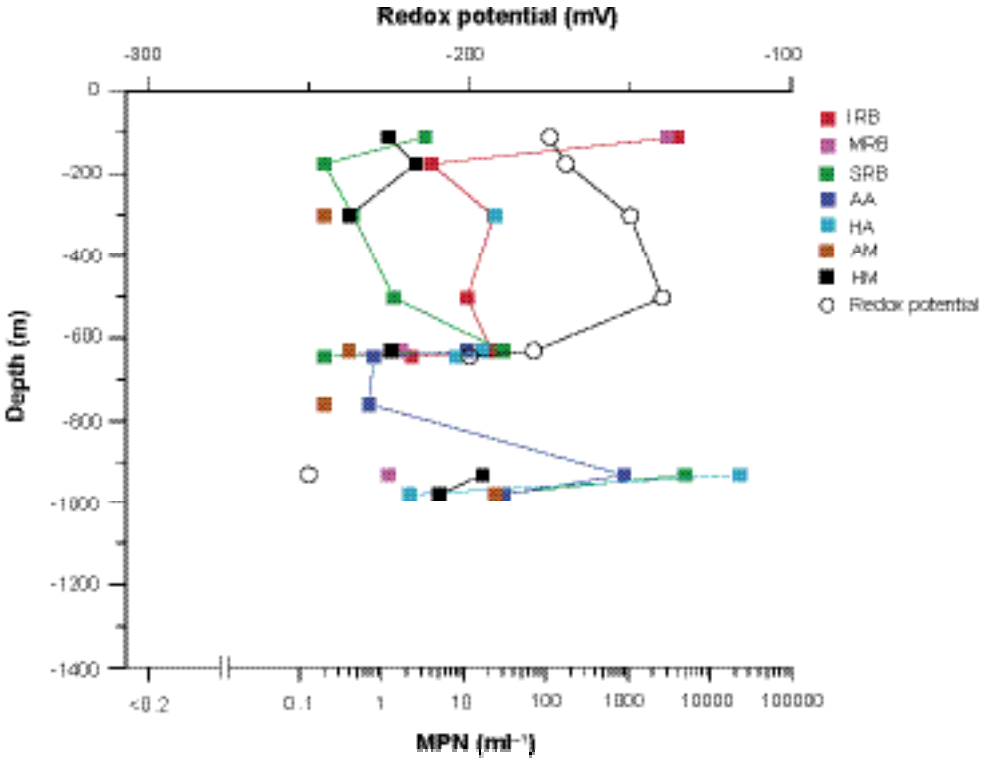

Figure 2-53. *Most probable numbers (MPN) of different physiological groups of microorganisms and redox potential against depth in the Forsmark area.*

Colloids

To obtain a clear picture of the origin and influence of colloids, the numbers of colloid particles and their mineralogical composition should be included in the programme. Measuring the number of colloid particles has commenced in Forsmark following the 2.1 data freeze. Knowledge of the colloid composition is important in the redox couple modelling and ultimately in the safety assessment modelling. Although the colloid data set is still limited, it will increase by the planned sampling campaign.

2.8.4 Water rock interactions

In version 1.2 of the SDM, the groundwaters at Forsmark were divided into three groups based on their salinity: (1) *Saline groundwaters* with a brine signature, (2) *Brackish-saline groundwaters* with an important and relatively constant Littorina component and (3) *Non saline groundwaters*. The new samples have confirmed this grouping and increased the number of samples in the more saline group (new samples with higher salinity). The mixing and reaction processes reported in version 1.2 have also been confirmed with these new data except in the case of the redox control of the system.

The data considered in the version 1.2 for the redox modelling indicated that the redox state is mainly controlled by the sulphur system. The new data concerning Eh logs, redox pairs, solubility calculations and microbiological analysis show that an active sulphate-reduction process must have been effective in the past but it is very limited at present. In this situation, the iron system could be one of the main controls of the redox state. This hypothesis will be studied in detail when new data are available.

Additionally, based on the modelling work with the new data delivered in the Forsmark 2.1 data freeze, the following 4 suggestions have been compiled to give recommendations to the site.

1. With respect to the water samples from packed off sections in cored boreholes, the new samples have extended the Cl range to higher values. However, maximum chloride values are still far from the salinities found in the Laxemar area (more than 45,000 mg/l of Cl) for comparative depths. Figure 2-54 clearly shows the two main challenges in future sampling programmes: (a) to find waters with high salinity (higher than 16,000 mg/l Cl) at depths larger than 500 m, and (b) to find samples that close the compositional gap shown in the plots.

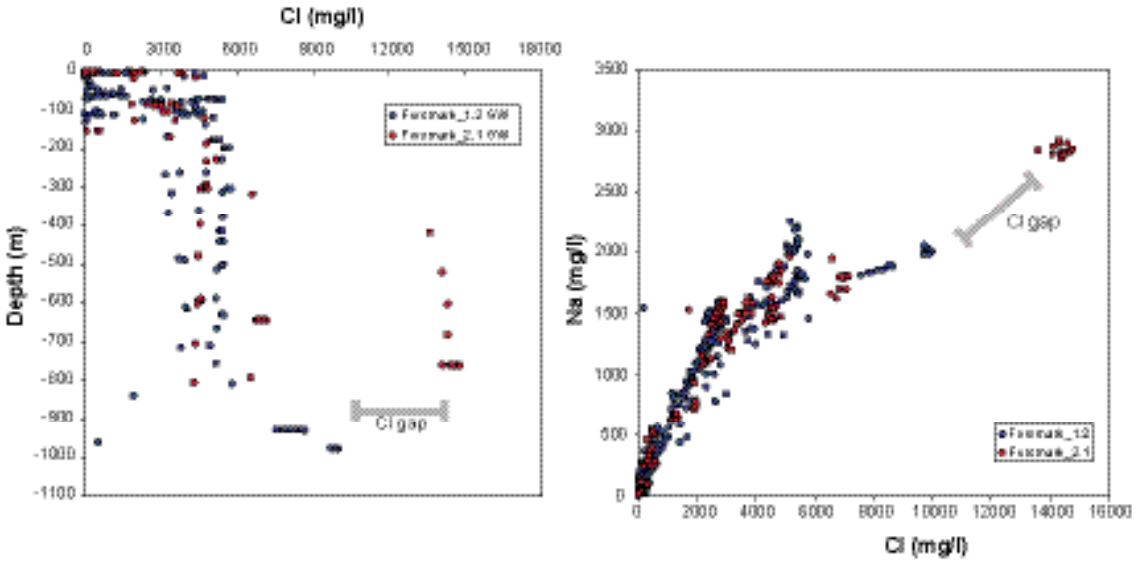

Figure 2-54. *Cl versus depth and versus Na indicates the gap where further information would be desirable.*

2. It is very important to make an effort in getting as much information as possible from each of the packed-off sections in the boreholes, including not only the chemical characterisation but also the physicochemical parameters measured by continuous logging. Analysing the samples and data already compiled, it was found that there are good and complete (i.e. representative) samples from some borehole sections where the Chemmac logging failed to reach stable readings of the physicochemical parameters (Eh and pH), or was not done (due to the use of simple equipment which on the other hand allowed contemporary investigations in two different boreholes). Although good for the chemistry, these samples do not have the essential information of Eh, pH and temperature (see Table 2-24). There are also other borehole sections with good values from Chemmac logging that do not have a completely representative sample ((because of the high percentage of drilling water or the lack of important elements like tritium at the data freeze date).

Table 2-24. Section sampled in each cored borehole, indicating information available and missing. Note that the boreholes are monitored and later stage water compositional information may support the redox modelling.

ID code	Sampling section (m)		Water sample	Chemmac			Analysed redox pairs	Missing information
				Eh	pH	T		
KFM01A	110.1	120.77	Representative[1]	2B[2], 2S[3]	2B, 1S	B	SO_4^{2-}/HS^-, $Fe^{2+}/Fe(OH)_3$, SO_4^{2-}/pyrite, SO_4^{2-}/FeS	
KFM01A	176.8	183.90	Representative	2B, 1S	2S	B	CO_2/CH_4, $Fe^{2+}/Fe(OH)_3$, SO_4^{2-}/pyrite, SO_4^{2-}/FeS	
KFM02A	106.5	126.50	Representative					Chemmac measurements, redox pairs
KFM02A	413.5	433.50	Representative				(HS^- not analysed)	Chemmac measurements, redox pairs
KFM02A	509.0	516.08	6.77% drilling water	3B	1S	B	CO_2/CH_4, $Fe^{2+}/Fe(OH)_3$, SO_4^{2-}/pyrite, SO_4^{2-}/FeS	New water sample
KFM03A	386.0	391.00	Representative		2S		$Fe^{2+}/Fe(OH)_3$, SO_4^{2-}/pyrite, SO_4^{2-}/FeS	Chemmac measurements
KFM03A	448.0	453.00	Representative	3B, 1S	1B, 2S	B	SO_4^{2-}/HS^-, $Fe^{2+}/Fe(OH)_3$, SO_4^{2-}/pyrite, SO_4^{2-}/FeS	
KFM03A	639.0	646.12	Representative	1B, 2S	1S	B	CO_2/CH_4, $Fe^{2+}/Fe(OH)_3$, SO_4^{2-}/pyrite, SO_4^{2-}/FeS	
KFM03A	803.2	804.20	16.5% drilling water					New sample, Chemmac and redox pairs
KFM03A	939.5	946.62	11.2% drilling water	3B, 2S	2B, 2S	B	SO_4^{2-}/HS^-, CO_2/CH_4, $Fe^{2+}/Fe(OH)_3$, SO_4^{2-}/pyrite, SO_4^{2-}/FeS	New water sample
KFM03A	980.0	1,001.19	Representative	1S	1S	B	SO_4^{2-}/HS^-, CO_2/CH_4, $Fe^{2+}/Fe(OH)_3$, SO_4^{2-}/pyrite, SO_4^{2-}/FeS	Chemmac measurements
KFM04A	230.5	237.64	7.45% drilling water				$Fe^{2+}/Fe(OH)_3$, SO_4^{2-}/pyrite, SO_4^{2-}/FeS	New sample and Chemmac measurements
KFM04A	354.0	361.13	6.5% drilling water	1S	2S	B	$Fe^{2+}/Fe(OH)_3$, SO_4^{2-}/pyrite, SO_4^{2-}/FeS, (HS^- not analysed)	New sample and Chemmac measurements
KFM05A	712.0	722.00	Not repres. GW	2S	2B, 2S	B	$Fe^{2+}/Fe(OH)_3$, SO_4^{2-}/pyrite, SO_4^{2-}/FeS, (HS^- not analysed)	New sample and Chemmac measurements
KFM06A	353.5	360.62	7.7% drilling water and T not analysed	3B	1S	B	$Fe^{2+}/Fe(OH)_3$, SO_4^{2-}/pyrite, SO_4^{2-}/FeS, (HS^- not analysed)	New sample
KFM06A	768.0	775.12	Representative		1B, 1S	B	SO_4^{2-}/HS^-, CO_2/CH_4, $Fe^{2+}/Fe(OH)_3$, SO_4^{2-}/pyrite, SO_4^{2-}/FeS	Chemmac measurements
KFM07A	848.0	1,001.55	Representative but T not analysed		2B, 2S	B	SO_4^{2-}/HS^-, CO_2/CH_4, $Fe^{2+}/Fe(OH)_3$, SO_4^{2-}/pyrite, SO_4^{2-}/FeS	Chemmac measurements

[1] Representative means: major and trace elements, D, T and ^{18}O, charge balance < 5%, percent of drilling water < 1% and time-series data.

[2] Down-hole measurement.

[3] Surface measurement.

As a result of necessary investigation logistics and flushing water problems, the set of complete and representative groundwater samples is smaller than the number of investigated borehole sections. However, the number of representative samples fulfilled the initial requirements stated in /SKB 2001/ already at data freeze 2.1. Table 2-24 shows the different depths studied in each cored-borehole and the missing information. The first column indicates the quality of the samples available in terms of their representativity. Columns 2, 3 and 4 show the number of stabilised values of Eh, pH and T from Chemmac: up to 3 borehole measurements (C, Pt and Au electrodes) and 2 surface measurements (C and Pt electrodes) for Eh; up to 2 borehole and 2 surface pH measurements; and 1 temperature measurement. The fifth column indicates the redox pairs with concentration values available for redox modelling, and the type of missing data is indicated in the final column. Presently the boreholes are monitored so that later stage water compositional information may support the redox modelling.

3. Another important modelling support to the ongoing site investigation programme is the need for further reliable data on:
   - Physicochemical parameters (Chemmac loggings): Eh, pH and temperature.
   - Aluminium concentration in the groundwaters.
   - Boron (total elemental concentration, not only isotopes).
   - Uranium redox pairs (if possible).
   - Br and Li contents (as conservative elements very important for the characterisation of mixing).
4. Finally, as an important need for the modelling of water-rock interaction processes, it would be very useful to have a more detailed mineralogical description of those borehole sections where a complete water sampling programme has been carried out. It should be included in the borehole information plots together with the rock matrix information. This information should contain:
   - Specific mineralogical information for each depth where water samples have been taken and analysed (mineral phases and their abundances).
   - Exchange capacity of fracture filling minerals (mainly clays and oxyhydroxides).
   - Hematite (goethite) grain size, specific surface area and abundance.

2.8.5 Mixing

There are 145 groundwater samples in the Forsmark 2.1 data set which meet the requirements to perform M3 modelling, i.e. in particular the major elements Na, K, Ca, Mg, SO_4, Cl and HCO_3, ^2H, ^{18}O and ^3H. The data from the Laxemar 2.1 data freeze were used as background and for comparison. The Glacial, Meteoric, Sea Sediment, Littorina and Brine waters are used as end members. For the Meteoric end member, a modelled value of 168TU was used. The PCA in Figure 2-55 shows that the the Forsmark 2.1 data set contains a larger number of samples with Marine, Glacial and Saline signatures compared with the 1.2 data set. Further sampling of deep groundwaters in Forsmark will strengthen the M3 modelling and site understanding. Some modelling based on the version 2.1 data set is currently undertaken and this modelling, including uncertainty analyses, will be presented in detail in a separate report during 2006 /SKB 2006b/.

2.8.6 Hydrochemical data for integration with hydrogeology

Soil pipes

As a working hypothesis, it is assumed that meteoric water recharge mainly reaches the shallow aquifer by infiltration during emergence of the landmass, and then discharges by flowing through both the granitic bedrock and the overlying Quaternary sediments towards discharge zones, located mainly in the lakes and near the Baltic coastline.

Figure 2-56 shows a plot of tritium versus Cl^- in the soil pipe samples (near surface groundwater) located at presumed discharge zones (selected on the basis of topographic and geochemical reasons). It can be seen that the lowest tritium contents are measured in soil pipes under three lakes (Bolundsfjärden, a small lake in SFM12 named Gällsboträsket and Eckarfjärden). However, groundwater under these three lakes shows very different salinities. Near-surface groundwater under Bolundsfjärden show Cl^- concentration values higher than the present Baltic Sea water, indicating

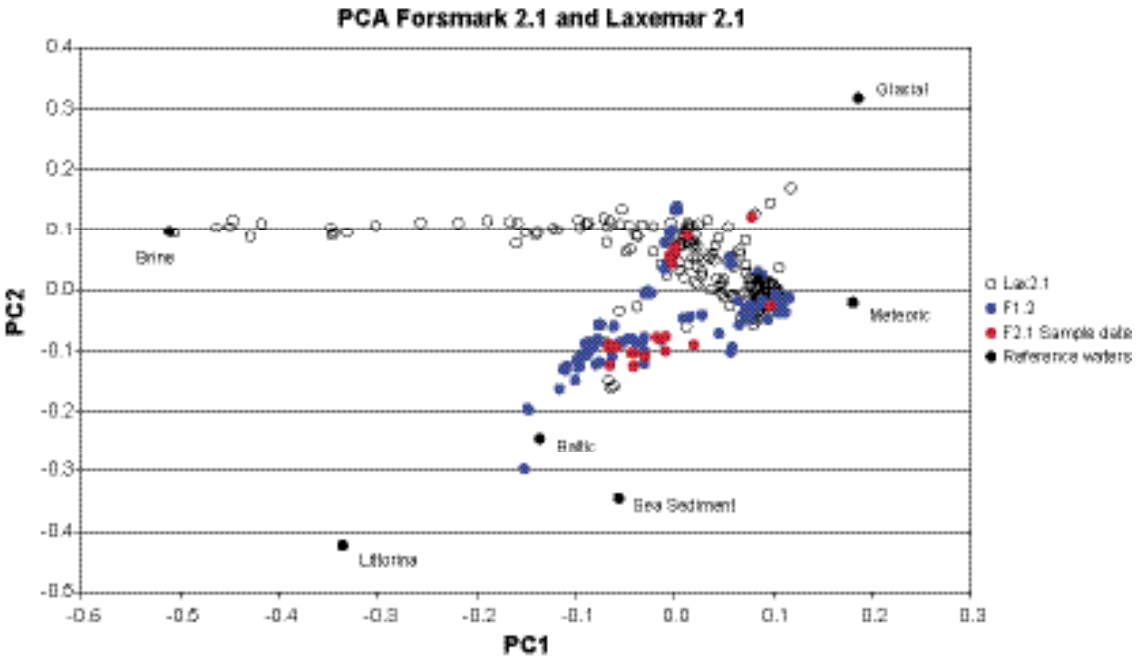

Figure 2-55. *The red dots indicates the new data obtained for Forsmark 2.1 data freeze, the blue dots the Forsmark 1.2 data and the transparent dots the Laxemar 2.1 data.*

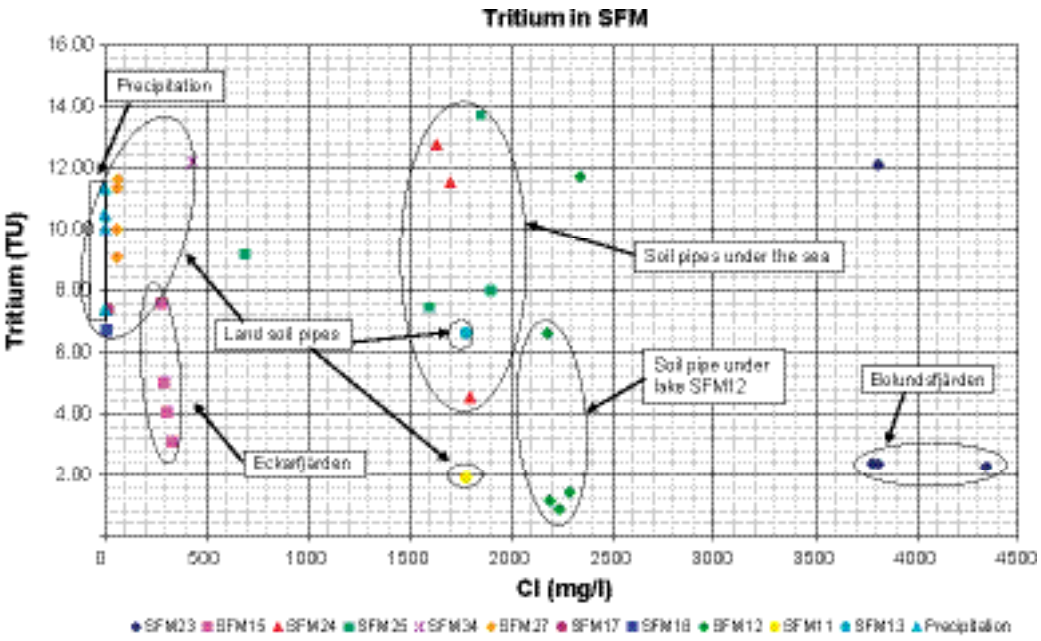

Figure 2-56. *Tritium versus Cl^- in soil pipe samples (near surface groundwater) located at presumed discharge zones.*

a significant contribution of saline water which may comprise an old relict marine water component (e.g. Littorina Sea) or a deeper non-marine groundwater component. In contrast, the shallow groundwater under Eckarfjärden shows Cl^- concentrations much lower (i.e. more diluted groundwater). Finally, shallow groundwater under Gällsboträsket (SFM12) shows an intermediate salinity. It is worth noting that groundwater sampled beneath the Baltic Sea shows Cl^- contents lower than the present sea water, which is consistent with the occurrence of local discharge of fresh groundwater under the sea.

The occurrence of brackish near-surface groundwater under Bolundsfjärden points towards the discharge of older groundwater, and/or the presence of "trapped" relict water not yet flushed out. On the contrary, the low tritium contents under Eckarfjärden indicate the influence of sub-modern groundwater close to the surface, but with no signature of older marine or non-marine deep saline components.

Figure 2-57 shows a plot of ^{18}O versus Cl^- in soil pipe samples located at presumed discharge zones. Littorina Sea and average Baltic Sea values have been included in the plot. It can be seen that near-surface groundwater at presumed discharge zones plot along a hypothetical mixing line between Littorina Sea water and fresh soil pipes water, with the exception of groundwater sampled below Eckarfjärden, which show clearly the absence of Littorina Sea influence.

The hydrochemical and isotopic patterns of near-surface hydrochemistry at the presumed discharge zones in Forsmark show differences between them. Some of the discharge zones may correspond exclusively to very shallow and local groundwater systems, probably involving flow through the Quaternary deposits only. These very local systems show dilute groundwater and ^{3}H and ^{18}O values close to modern precipitation. On the other hand, there are places where mixing between meteoric and old marine water seems clear (Bolundsfjärden being the most obvious one). Whether this indicates the discharge of deeper groundwater (dominated by a Littorina Sea component) or, may be the presence of "trapped" relict Littorina Sea water not yet flushed out, should be further investigated. In this context, it has been hypothesised that effective recharge into the granitic bedrock at Forsmark could be as low as a few millimetres/year, due to both the presence of low permeability Quaternary cover and the low topographic driving forces. This hypothesis could provide the explanation for the signatures of old marine water in the near-surface groundwater.

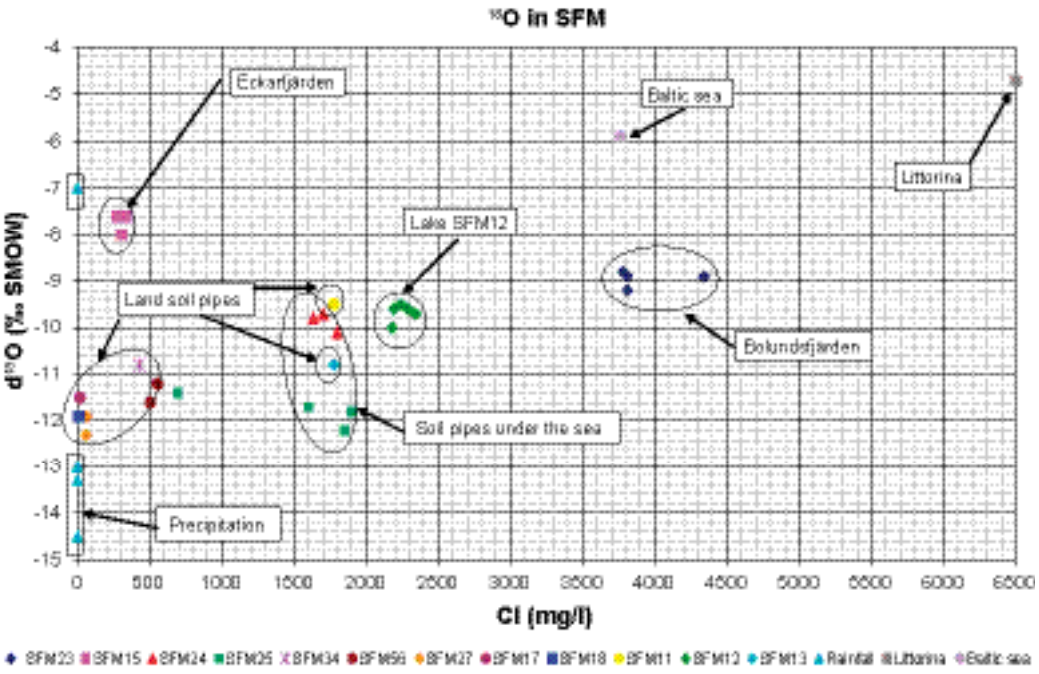

Figure 2-57. *^{18}O versus Cl^- in soil pipe samples (near surface groundwater) located at the presumably discharge zones.*

Deep boreholes

Several dissolved ions and isotopic parameters are useful in determining or verifying fluid flow directions and characteristics on a large scale, and have been applied in waste management programmes in crystalline (Canada, Sweden, Finland) and sedimentary (USA, Switzerland, France) rock types. Such understanding can be helpful for interpreting the origin and residence time of groundwater and help also the integration with hydrogeology.

Future site activities at Forsmark should focus on sampling and determination of certain isotopes in groundwater, fracture minerals and bedrock. With respect to groundwaters, taking into consideration logistical problems (e.g. large sample volumes; transport of equipment/personnel etc) and interpretative problems, it is suggested that the following approach could be feasible at the Forsmark site.

A. The selection of strategic groundwater sampling locations for use of ^{36}Cl, $^{3}He/^{4}He$ and U-series isotope studies; this already forms part of the present hydrogeochemical programme (U-series also apply to rock and fracture mineral samples).

B. A borehole where groundwater samples can be collected from shallow, intermediate and deep levels (deeper levels could overlap with the ^{36}Cl, $^{3}He/^{4}He$ and U-series samples).

C. At these borehole locations groundwater samples (200 mL volumes) could be collected and analysed for the noble gases: helium, argon, neon, krypton and xenon.

D. By deriving the total abundance of these noble gases at each depth level, it is possible to:
   – derive the noble gas infiltration (recharge) temperature (can be correlated with ^{18}O and ^{2}H data),
   – estimate the total sampled groundwater volume required if individual isotopes will be required for study,
   – provide information concerning mixing of different groundwater types (i.e. help to separate mixing proportions).

E. Based on this information, a future decision can be made to study in detail some of the individual noble gas isotopes summarised above.

Studies that already fall within the hydrogeochemical site investigation programme at Forsmark include the analyses of U-series isotopes and U and Th contents in groundwater and fracture fillings; these studies will be expanded. Ra and Rn are also part of the ongoing groundwater sampling programme and these nuclides will provide more information on groundwater circulation patterns.

To increase the database for Forsmark on U-series radionuclides and their large scale spatial behaviour, the sampling and analyses of groundwaters for U-concentration and $^{234}U/^{238}U$ activity ratios should continue, and, in selected areas (probable discharge zones and shallow sampling locations), be complemented with sampling and analyses of ^{226}Ra as an indicator of the mobility of sorbing nuclides. To further increase the understanding of the palaeohydrogeology of the area, work has commenced already on the U-series characterisation of fracture minerals, particularly calcite, haematite and clay minerals in conjunction with stable isotopic analyses of calcite and fluid inclusions.

With respect to fracture fillings, even more effort is recommended to demarcate the position of the present redox front; for this purpose U-series analyses will be combined with detailed core mapping and mineralogy in drill cores from shallow depth (0–200 m). This, in turn, will be integrated with stable isotopes analyses on calcites from the same depth in order to describe not only the redox conditions, but also the groundwater composition. Finally, to be able to describe and quantify the available reducing capacity along the water-flowing pathways, Fe^{2+}/Fe^{3+} determination of Fe-silicates and oxides in fracture minerals and wall rock should be carried out.

2.9 Interpretation of primary data on rock transport properties

2.9.1 Available data

The available site investigation data on transport properties at the data freeze 2.1 for Forsmark are summarised in /Börjesson and Gustavsson 2005, Thunehed 2005ab, Löfgren and Neretnieks 2005ab/. The data set consists largely of numerical data from water saturation porosity measurements, a small number of through-diffusion data, and formation factors obtained from laboratory

as well as in situ electrical resistivity measurements. All reported transport data not included in the above references lie outside the data freeze. No surface area or sorption data were available for the F2.1 data freeze.

The data set compiled for transport that was reported in model version 1.2 was based largely upon data specifically obtained from boreholes KFM01A and KFM02A. The data presented in version 2.1 includes the above with the addition of newly acquired data obtained from these boreholes as well as from KFM03A, KFM04A, KFM05A, KFM06A, KFM07A, and KFM08A. Only a brief account of the data is given in the following sections.

2.9.2 Porosity

The porosity of the rock matrix as discussed in this report relates to the total intergranular void space in the rock that is filled with water and available for participation in solute diffusion processes. No distinction is made between the total porosity and the transport porosity of the rock matrix. The transport porosity is always less than the total porosity and accounts for the presence of dead end pores that although contributing towards the solute storage capacity, do not contribute to the effective diffusivity of the rock. For the purposes of safety assessment, no distinction is necessary between these two types of porosity as the salient variable for estimation of the rock capacity factor is the total porosity given that the transport porosity is implicitly accounted for in the measurement of effective diffusivity (or the rock matrix formation factor).

The results of porosity measurements on samples from the boreholes in Forsmark are summarised in Table 2-25. The large standard deviations of the data, with sample mean minus the standard deviation ( ) showing negative values in some cases, indicate that a distribution in log-space is possibly more appropriate than a distribution in linear space for describing the data. This does not necessarily mean that the data are actually log-normally distributed, but rather that a distribution using log-transformed data should be used for parameterisation purposes in SA given that the porosity can vary over one or more orders of magnitude.

The geological characterisation in binocular microscope shows a great number of small cracks that are 3–15 mm in length and with a width of 0.5 mm in both fresh and altered rock samples. These cracks are larger than intragranular micro cracks /Ståhle 2001/, and cut right through mineral grains. Table 2-25 gives results where the samples with alteration or cracks have been excluded. Comparison of the filtered data with the complete datasets indicates that cracks may increase the porosity.

Other factors that may influence the measured porosity of the sample are alteration of the rock and the length of the rock sample. Samples with observed alteration were studied separately and some indications of increased porosity can be observed for these samples. Alteration of the rock has been previously shown to influence porosity /e.g. Eliasson 1993/ although there are currently not enough data to quantify this effect unambiguously for the site specific rock samples which have undergone mild alteration. The strongly altered episyenetic (vuggy metagranite) rock samples exhibit significantly higher porosities than all other rock types included in the study.

The influence of sample length is indicated in Table 2-26, where shorter sample lengths are associated with higher measured porosities. Based upon the available measurement data, the effect appears to be insignificant for core samples 1.0 cm in length. Stress release ef fects during sampling (i.e. bore core retrieval) and damage induced during sawing and sample preparation are generally thought to result in overestimation of the measured porosity and diffusivity of the samples. Damage acquired during sawing may include additional microfractures in the samples, which thus may increase the porosity in the rock closest to the edges of the sampled rock. It follows that this effect should be more pronounced in shorter rock samples. This is supported by earlier porosity measurements in connection with diffusion experiments /Johansson et al. 1997/ and is consistent with expectations based upon consideration of pore-connectivity over different length scales (i.e. it is expected that fewer pores will be connected over larger length scales). It is interesting to note that for the very porous, episyenetic rock (strongly altered vuggy metagranite) the opposite effect is observed (i.e. lower measured porosity for shorter sample lengths). The reason for this is unclear, although it is speculated that it may be due to physical draining of water from the rock pores when removing the samples from the water bath used to saturate the rock.

Table 2-25. Porosities (vol %) of different rock types from the Forsmark area (number of samples given as N_s). The values are given as mean value ± σ of the experimental dataset. Non-log (N) and log_{10} values (LN) are specified for each rock type.

Rock type		All samples	N_s	No alteration/cracks	N_s
Granite, granodiorite and tonalite, metamorphic, fine- to medium-grained (101051)	N	0.30 ± 0.27	30	0.25 ± 0.11	28
	N[A)]	0.5 ± 0.51[A)]	7[A)]	0.30 ± 0.18[A)]	5[A)]
	LN	–0.60 ± 0.23	30	–0.64 ± 0.17	28
	LN[A)]	–0.44 ± 0.36	7[A)]	–0.64 ± 0.17	5[A)]
Granite to granodiorite, metamorphic, medium-grained, episyenetic (strongly altered vuggy metagranite) samples excluded (101057)	N	0.38 ± 1.11	129	0.22 ± 0.09	119
	N[A)]	0.54 ± 0.70[A)]	29[A)]	0.62 ± 0.82[A)]	20[A)]
	LN	–0.63 ± 0.27	129	–0.67 ± 0.16	119
	LN[A)]	–0.47 ± 0.37	29[A)]	–0.46 ± 0.43	20[A)]
Granite to granodiorite, metamorphic, medium-grained, episyenite (strongly altered vuggy metagranite) (101057)	N	14 ± 6	15	No samples excluded	–
	LN	1.05 ± 0.36	15	No samples excluded	–
Pegmatite, pegmatitic granite (101061)	N	0.42 ± 0.23	3	No samples excluded	–
	LN	–0.41 ± 0.22	3	No samples excluded	–
Amphibolite (102017)	N	1.8 ± 4.0	6	0.21 ± 0.12	5
	LN	–0.46 ± 0.76	6	–0.75 ± 0.28	5
Granodiorite, metamorphic (101056)	N	0.34 ± 0.21	2	No samples excluded	–
	LN	–0.52 ± 0.28	2	No samples excluded	–
Felsic to intermediate volcanic rock, metamorphic (103076)	N	0.78	1	No samples excluded	–
	LN	–0.11	1	No samples excluded	–
Tonalite to granodiorite, metamorphic (101054)	N	0.17 ± 0.02	3	No samples excluded	–
	LN	–0.77 ± 0.04	3	No samples excluded	–
Granite, metamorphic, aplitic (101058)	N	0.22 ± 0.06	2	0.19	1
	LN	–0.66 ± 0.11	2	–0.73	1
Granite, fine to medium-grained (111058)	N	0.36	1	No samples excluded	–
	LN	–0.44	1	No samples excluded	–

[A)] altered samples only.

Table 2-26. Porosities (vol %) for rock samples of different lengths (number of samples within parenthesis). The values are given as mean value ± σ of the experimental dataset.

Rock type	Borehole	Sample length (number of samples)			
		0.5 cm (3)	1 cm (3)	3 cm (3)	5 cm (3)
Granite, granodiorite and tonalite, metamorphic, fine- to medium-grained (101051)	KFM02A, 541 m	0.34 ± 0.17	0.20 ± 0.12	0.19 ± 0.08	0.18 ± 0.10
Granite to granodiorite, metamorphic, medium-grained (101057)	KFM01A, 313 m	0.26 ± 0.11	0.18 ± 0.03	0.12 ± 0.08	0.16 ± 0.03
Granite to granodiorite, metamorphic, medium-grained, episyenetic (strongly altered vuggy metagranite) samples (101057)	KFM02A, 276 m	10.5 ± 1.1	16.5 ± 0.3	18.3 ± 1.1	18.5 ± 0.6

It should be noted that a complementary method for determining the rock porosity is also available from the through-diffusion experiments. From the fitting of measurement data to the diffusion model, a capacity factor ( ) is obtained, which for a non-reactive tracer should be identical to the porosity. Although this may not be strictly true for HTO owing to hydrogen isotope exchange with surface functional groups on the mineral surfaces, owing to the very small fraction of surface bonded hydrogen compared to that in the porewater, it is close enough to provide a reasonable comparison (see Table 2-27 in the following section).

2.9.3 Diffusion

Estimates of the effective diffusivity of the rock matrix are obtained by through-diffusion experiments carried out in the laboratory as well as from resistivity measurements that are performed both in the laboratory and in situ. The effective diffusivity can also be given in terms of the rock matrix formation factor, F_f (–) which is defined as the ratio of effective diffusivity of the solute in the rock and the diffusivity of the solute at infinite dilution in water. From the formation factor, the effective diffusivity can be calculated for all tracers or radionuclides of interest (see e.g. /Widestrand et al. 2003/).

In through-diffusion experiments, the effective diffusivity is obtained indirectly by fitting a theoretical model of solute diffusion to measurement data for HTO diffusion through a rock sample. In resistivity measurements, the effective diffusivity is obtained by an analogy between diffusion and ionic mobility as defined in the Einstein relation (see e.g. /Atkins 1999/). The formation factor is obtained directly as the ratio of the pore water resistivity and that of the saturated rock. In the laboratory, the rock samples are firstly saturated with a solution of known salinity (1 M NaCl), while in situ measurements rely upon accurate characterisation of the matrix porewater. This is typically done using flowing water in fractures as a proxy although this implicitly assumes equilibrium between the matrix porewater and that sampled in the borehole. Measurements also require a relatively high salinity (1 M NaCl or equivalent) so as to not be influenced by surface ion mobility effects /Ohlsson and Neretnieks 1997/.

Site specific rock materials from the Forsmark site have been sampled and used in through-diffusion measurements. These measurements take many months to carry out and steady state conditions (necessary for final evaluation) have not been obtained for most samples. However, for the parameterisation of the retardation model in model version 2.1, a selection of measurement data from on-going through diffusion experiments have been examined. Based on these data, preliminary diffusivities have been evaluated and are given in Table 2-27.

From the results in Table 2-27 it appears that the formation factor for the investigated rock types exhibits roughly an order of magnitude variation covering the range 4×10^{-5} to 4×10^{-4}. Although there are only two measurements for strongly-altered episyenetic rock (porosity 10%), these exhibit formation factors that are roughly one order of magnitude higher than that typical for the unaltered rock. Allowing for measurement uncertainties, there appears to be quite close correspondence between the values measured using through diffusion and electrical resistivity in the laboratory. However, in situ resistivity measurements give formation factors that are typically one order of magnitude lower than the laboratory measurements (see also Table 2-29).

A summary of the results of the electrical resistivity measurements reported by /Löfgren and Neretnieks 2005ab/ as well as of through diffusion measurements is provided in Table 2-28 sorted by rock type and in Table 2-29 sorted by borehole. The results are expressed in the form of formation factors, both in non-log and $\log_{10}$ units. Similarly to the porosity data discussed above, the standard deviations are in many cases of the same order of magnitude as the mean values.

Some general observations concerning the electrical resistivity data are made below.

Laboratory resistivity versus porosity

A tendency of increased formation factor with increasing porosity can be observed in the results. The results appear very scattered when plotted on a linear scale although seem to be better behaved when plotted on logarithmic axes. Quantification of the formation factor correlation with porosity is tenuous, however, and there is only a very vague suggestion of correspondence with a power law relation such as Archie's law. There is some suggestion of a log-normal distribution of porosities and formation factors in some of the data sets.

Table 2-27. Preliminary results from through-diffusion experiments on rock samples from KFM01A and KFM02. The effective diffusivity, D_e, and the rock capacity factor, α, were obtained from least-square fits to experimental data. Comparisons are made to the porosity obtained by water saturation measurements and to the formation factors obtained from closest available electrical resistivity measurements (Lab and in situ).

Rock type	Borehole; borehole length (m)	Sample thick-ness (mm)	Capacity factor, α (–)	Porosity[1] (water saturation), θ_m	D_e (m^2/s)	F_f (–) Through-diffusion	F_f (Resistivity in situ, closest available measurement)
Granite, granodiorite and tonalite, metamorphic, fine- to medium-grained (101051)	KFM02A; 381.01–381.04	30	3.2×10^{-3}	2.3×10^{-3}	8.7×10^{-14}	4.1×10^{-5}	(2.79×10^{-5})
	KFM02A; 554.60–554.61	10	2.0×10^{-2}	3.1×10^{-3}	3.8×10^{-13}	1.8×10^{-4}	(1.81×10^{-5})
	KFM02A; 554.61–554.64	30	1.3×10^{-2}	2.3×10^{-3}	3.4×10^{-13}	1.6×10^{-4}	(1.72×10^{-5})
	KFM02A; 554.71–554.72	10	2.0×10^{-2}	2.1×10^{-3}	3.2×10^{-13}	1.5×10^{-4}	(1.67×10^{-5})
	KFM02A; 554.72–554.75	30	8.9×10^{-3}	2.2×10^{-3}	3.6×10^{-13}	1.7×10^{-4}	(1.67×10^{-5})
	KFM02A; 554.84–554.85	10	2.1×10^{-2}	2.6×10^{-3}	3.0×10^{-13}	1.4×10^{-4}	(1.68×10^{-5})
	KFM02A; 554.86–554.89	30	5.5×10^{-3}	2.3×10^{-3}	3.1×10^{-13}	1.5×10^{-4}	(1.68×10^{-5})
	KFM05A; 570.04–570.07	30	2.3×10^{-3}	2.0×10^{-3}	3.4×10^{-13}	1.6×10^{-4}	Not measured
Granite to granodiorite, metamorphic, medium-grained (101057)	KFM01A; 312.54–312.55	10	9.6×10^{-3}	2.0×10^{-3}	2.0×10^{-13}	9.6×10^{-5}	(9.44×10^{-6})
	KFM01A; 312.56–312.59	30	6.2×10^{-3}	1.6×10^{-3}	2.7×10^{-13}	1.3×10^{-4}	(9.44×10^{-6})
	KFM01A; 312.59–312.64	50	3.5×10^{-3}	1.7×10^{-3}	2.6×10^{-13}	1.2×10^{-4}	(9.43×10^{-6})
	KFM01A; 312.66–312.67	10	1.5×10^{-2}	1.9×10^{-3}	3.0×10^{-13}	1.4×10^{-4}	(9.42×10^{-6})
	KFM01A; 312.68–312.71	30	5.0×10^{-3}	1.6×10^{-3}	3.1×10^{-13}	1.5×10^{-4}	(9.43×10^{-6})
	KFM01A; 312.77–312.78	10	1.8×10^{-2}	1.5×10^{-3}	3.2×10^{-13}	1.5×10^{-4}	(9.48×10^{-6})
	KFM01A; 539.99–540.02	30	1.7×10^{-3}	1.2×10^{-3}	1.7×10^{-13}	8.0×10^{-5}	(1.97×10^{-5})
	KFM01A; 999.96–999.99	30	8.8×10^{-3}	2.4×10^{-3}	9.2×10^{-13}	4.3×10^{-4}	Not measured
	KFM02A; 281.01–281.04[E)]	30	6.2×10^{-2}	1.1×10^{-1}	1.3×10^{-11}	5.9×10^{-3}	(4.31×10^{-3})
	KFM02A; 300.96–300.99[E)]	30	1.8×10^{-2}	1.2×10^{-2}	7.5×10^{-13}	3.5×10^{-4}	(4.66×10^{-4})
	KFM02A; 481.01–481.04	30	2.5×10^{-3}	1.7×10^{-3}	5.5×10^{-14}	2.6×10^{-4}	Not measured
	KFM05A; 168.34–168.37	30	1.6×10^{-3}	1.5×10^{-3}	9.8×10^{-14}	4.6×10^{-5}	Not measured
	KFM05A; 369.23–369.26	30	4.6×10^{-3}	1.8×10^{-3}	3.2×10^{-13}	1.5×10^{-4}	Not measured
	KFM05A; 761.07–761.10	30	4.2×10^{-3}	2.0×10^{-3}	3.4×10^{-13}	1.6×10^{-4}	Not measured

[E)] Episyenetic sample, strongly altered vuggy metagranite.

[1)] To facilitate comparison, data is given here as a volume fraction rather than percentages (%). For comparison with Table 2-25 and Table 2-26, the tabulated values above should be multiplied by a factor of 100.

Table 2-28. Summary of formation factors for the Forsmark rock types. The values are given as mean value ± σ of the considered datasets. Non-log (N) and log_{10} values (LN) are specified for each category where appropriate (number of samples is given as N_s).

Rock type		Method					
		HTO through diffusion	N_s	Electrical resistivity lab	N_s	Electrical resistivity (in situ)	N_s
Granite, granodiorite and tonalite, metamorphic, fine- to medium-grained (101051)	N	$(1.4 \pm 0.4)\times10^{-4}$	8	$(2.6 \pm 2.2)\times10^{-4}$	10	$(1.7 \pm 1.1)\times10^{-5}$	4
	LN	-3.88 ± 0.21	8	-3.71 ± 0.37	10	-4.81 ± 0.24	4
Granite to granodiorite, metamorphic, medium-grained (101057)	N	$(1.6 \pm 1.0)\times10^{-4}$	12	$(2.9 \pm 1.7)\times10^{-4}$	80	$(2.5 \pm 1.3)\times10^{-5}$	50
	LN	-3.86 ± 0.24	12	-3.61 ± 0.24	80	-4.67 ± 0.24	50
Granite to granodiorite, metamorphic, medium-grained, Episyentic (101057)	N	$(3.1 \pm 3.9)\times10^{-3}$	2	Pending	n/a	Pending	n/a
	LN	-2.84 ± 0.97	2	Pending	n/a	Pending	n/a
Pegmatite, pegmatic granite (101061)	N	Pending	n/a	$(4.8 \pm 2.9)\times10^{-4}$	4	$(1.2 \pm 0.9)\times10^{-4}$	3
	LN	Pending	n/a	-3.38 ± 0.24	4	-4.12 ± 0.62	3
Amphibolite (102017)	N	$> 2.3\times10^{-5}$ [S)]	n/a	$(5.7 \pm 3.4)\times10^{-5}$	3	$> 2.6\times10^{-5}$	1
	LN	> -4.65[S)]	n/a	-4.32 ± 0.36	3	-4.58	1

[S)] Steady state diffusion not reached, only minimum diffusion rate evaluated.

Table 2-29. Summary of formation factors compared on a borehole basis. The values are given as mean value ± σ of the considered datasets for the Granite to granodiorite, metamorphic, medium-grained samples and are compared based on the results from the boreholes KFM01A, KFM02A and KFM05A and also as the average of all boreholes used. Non-log (N) and log_{10} values (LN) are specified for each category where appropriate.

Boreholes		Method			
		HTO through diffusion	Electrical resistivity (lab)	Electrical resistivity (in situ)	$F_{m\ (lab)}/F_{m\ (in\ situ)}$
All boreholes	N	$(1.6 \pm 1.0)\times10^{-4}$	$(2.9 \pm 1.7)\times10^{-4}$	$(2.5 \pm 1.3)\times10^{-5}$	20 ± 16
	LN	–3.86 ± 0.24	–3.61 ± 0.24	–4.67 ± 0.24	n/a
KFM01A	N	$(1.6 \pm 1.1)\times10^{-4}$	$(3.6 \pm 1.9)\times10^{-4}$	$(1.5 \pm 0.6)\times10^{-5}$	30 ± 16
	LN	–3.85 ± 0.22	–3.50 ± 0.24	–4.86 ± 0.17	n/a
KFM02A	N	2.6×10^{-4}	$(2.8 \pm 1.5)\times10^{-4}$	$(3.4 \pm 0.9)\times10^{-5}$	10 ± 5
	LN	–3.58	–3.61 ± 0.24	–4.49 ± 0.12	n/a
KFM05A	N	$(1.2 \pm 0.6)\times10^{-4}$	$(2.0 \pm 1.4)\times10^{-4}$	Pending	Pending
	LN	–3.99 ± 0.30	–3.77 ± 0.26	Pending	n/a

Laboratory resistivity versus through-diffusion data

The comparison between laboratory resistivity and through-diffusion measurements on samples from similar locations indicate a very good correlation between the measurements, although with a tendency towards lower formation factors (by a factor of about 2) in the through diffusion measurements as compared with the resistivity data. There is currently, however, insufficient data to draw any clear conclusions concerning differences between the two methods.

It should be emphasised that it is intended to make electrical resistivity measurements on the samples used for through-diffusion after these tests are completed. By doing this, a more exact comparison of the two techniques should be obtained.

In situ versus laboratory-obtained data

Formation factors measured in situ are generally about an order of magnitude lower than those obtained using electrical resistivity measurements in the laboratory. The difference indicates either the effect of in situ compression or that the laboratory samples have been mechanically damaged when brought to the laboratory.

Formation factor versus borehole length

Due to some degree of scatter in the dataset, it is difficult to identify any particular trend in the in situ resistivity measurement data and for all practical purposes the formation factor appears approximately constant as a function of depth. It is noted, however, that the ratio of laboratory and in situ resistivity measurement data do show a trend of increasing formation factor for the laboratory values relative to the in situ data as a function of increasing depth in boreholes KFM01A and KFM02A. A similar trend is also apparent for porosity measurement data in KFM01A, although the effect is largely absent for the corresponding data from KFM02A. Although the trend of the data is qualitatively recognisable on a linear scale, there is much scatter and the trend is barely visible when plotted on a log-scaled axis.

The observed trend could indicate an increased effect of stress release on samples taken form greater depths owing to the greater mass of overburden. Since there is no such depth trend apparent in the in situ data this could be interpreted as sampling causing stress release of the rock samples with a concomitant pore space dilation. According to this interpretation, the stress release experienced by laboratory samples should lead to an overestimation of the porosity and diffusivity/formation factor. The fact that no tendency of increased porosity measured with depth for borehole KFM02A partially contradicts this interpretation and ratios of laboratory and in situ formation factors are quite different for KFM01A and KFM02A. The difference between the two boreholes is actually larger than the slight increase in formation factor observed with increasing sample depth.

It should be noted, however, that in situ stresses are multi-axial in nature and the effect of stress release is not only related to overburden, but also complicated by formation stresses acting along other axes. The difference in laboratory and in situ formation factors between the two boreholes could indicate that the rock stress is higher for borehole KFM01A than KFM02A. It follows that the KFM01A drill core would be more influenced by stress release than the corresponding KFM02A drill core. This explanation is also supported by the discussion in the rock mechanics chapter of the version 1.2 of the Forsmark site descriptive model report /SKB 2005a/.

Formation factor versus rock type

From the available data there is some evidence that the medium grained rock (Granite to granodiorite, metamorphic medium grained rock, 101057) exhibits slightly higher formation factors than the fine grained rock type (Granite, granodiorite and tonalite, metamorphic fine- to medium grained rock, 101051). This is as anticipated given that more finely grained rock is generally expected to have lower diffusivity than more coarsely grained varieties. It is important to note, however, that the differences are small and there is a large variation within individual rock types that is larger than the variation between different rock types. Amphibolite samples (102017) have been found to have lower formation factor than the other rock types, and the highly porous episyenetic rock (Granite to granodiorite, metamorphic, medium-grained rock, 101057) has a somewhat larger formation factor. These results are as expected based upon the texture of the rock types, although the number of measurements are few and therefore clear statistical distinctions cannot be made. The same is true for the few available samples of Pegmatite, pegmatic granite (101061) where the formation factor has been found to be in the same range as the main rock types discussed above (i.e. rock types 101051 and 101057).

2.9.4 Sorption

The notion of sorption in the context of the site descriptive model relates to the adsorptive interaction of radionuclides with the surfaces of geological materials. This occurs principally by way of the association of ionic solutes with charged mineral surfaces. In the simplified approach to sorption modelling adopted within the SDM, sorption processes are considered to be linear (no concentration dependency) as well as being fast and reversible (chemical kinetics are not considered). The concept is the same as that described in the strategy report by /Widestrand et al. 2003/.

BET surface area data

Given that the adsorption of radionuclides takes place on the surfaces of geological materials, the quantification of available surface areas is an important predictor of the sorption capacity of the rock material. Various ferric oxides, for example, have very large specific surface areas and have been shown to be strongly adsorbing minerals for cations that associate with surfaces by way of surface complexation /e.g. Jakobsson 1999/. Furthermore, the presence of clay minerals (as a group identified as a significant potential sink for Cs^+) also gives rise to increased surface areas in the measurements on rock samples.

The surface area is measured by way of the BET method using the sorption of gas molecules (typically N_2 or Ar) to a surface /Brunauer et al. 1938/. Although at this stage no method is available for establishing a quantitative relationship between specific surface areas and sorption parameters, results of BET surface area measurements are included in the retardation model as qualitative data important for the understanding of the sorption processes. The results of the measurements on the Forsmark site rock types are given in Table 2-30.

The BET measurements indicate that crushing of the rock material results in the formation of new surfaces that are non-representative for the intact rock. From the results for the samples of major rock types, the 63–125 μm size fraction typically shows as much as an order of magnitude or higher increased surface area relative to the 2–4 mm size fraction. The measured BET surface area of the crushed rock particles is interpreted as the sum of the external surface area and a contribution from internal surface areas. Only the internal surface area of the rock is of relevance for sorption within the rock matrix in situ. In order to estimate the internal surface area of the rock, an extrapolation

Table 2-30. Measured BET surface area for the fractions 0.063–0.125 mm and 2–4 mm of crushed and sieved matrix rock samples. Measured results are presented together with extrapolated inner surface area (assuming constant sphericity for all particle sizes). Values are given as mean ± σ for the considered data set where available.

Sampling location		BET surface area (m^2/g)				Extrapolated inner BET surface area (m^2/g)
Borehole	Borehole length (m)	0.063–0.125 mm		2–4 mm		
		Min	Max	Min	Max	Value ± 2σ[1)]
Granite to granodiorite, metamorphic, medium-grained (101057)						
KFM01A	103.46–103.65	0.1943	0.2085	0.0088	0.0397	0.019 ± 0.012
	312.20–312.50	0.1529	0.1881	0.0003	0.0047	< 0.01
	487.10–487.50	0.1292	0.1975	0.0444	0.0495	0.043 ± 0.025
	703.25–703.45	0.09	0.1006	0.0092	0.0147	0.0093 ± 0.0044
	908.18–908.36	0.0744	0.1563	0.0291	0.0311	< 0.06
KFM02A	350.00–350.27	0.2858	0.2935	0.0472	0.0580	0.045 ± 0.010
	711.48–711.73	0.2237	0.2372	0.0175	0.0257	0.015 ± 0.011
KFM03A	536.47–536.67	0.2041	0.2479	0.0111	0.0149	< 0.02
KFM04A	694.80–695.00	0.1577	0.1673	0.0115	0.0227	0.012 ± 0.005
KFM06A	440.13–440.60	0.2636	0.2740	0.0315	0.0381	0.027 ± 0.009
	601.86–602.26	0.2785	0.2956	0.0265	0.0448	0.028 ± 0.018
KFM07A	387.47–387.87	0.2123	0.2149	0.0262	0.0382	0.026 ± 0.009
	608.92–609.32	0.1224	0.1885	0.0208	0.0265	< 0.06
					Average:	< 0.05[2)]
KFM02A	243.50–243.70[A)]	0.7633	0.7799	0.1891	0.2019	0.18 ± 0.01
	275.22–275.45[E)]	1.5726	1.5918	0.2555	0.2847	0.23 ± 0.01
KFM08A	412.04–412.30[A)]	0.7323	0.7446	0.3348	0.3493	0.33 ± 0.01
Granite, granodiorite and tonalite, metamorphic, fine- to medium-grained (101051)						
KFM01A	520.88–521.00	0.1204	0.1352	0.0049	0.0232	0.010 ± 0.009
KFM02A	552.00–552.23	0.3401	0.3412	0.0333	0.0480	0.031 ± 0.005
	915.53–915.70	0.1621	0.1832	0.0151	n/a	< 0.025
KFM03A	311.01–311.21	0.3196	0.3205	0.0203	0.0240	0.013 ± 0.001
KFM05A	570.09–570.24	0.2059	0.2903	0.0194	0.0340	< 0.08
					Average:	< 0.04[2)]
Pegmatite, pegmatic granite (101061)						
KFM03A	367.52–367.72	0.2272	0.2394	0.0246	0.0297	0.020 ± 0.005
	660.18–660.39	0.2785	0.2956	0.0265	0.0448	0.043 ± 0.009
Tonalite and granodiorite, metamorphic (101054)						
KFM03A	242.93–243.13	0.2459	0.2903	0.0361	0.0487	0.035 ± 0.017
Amphibolite (102017)						
KFM06A	541.01–541.43	0.3042	0.3286	0.0375	0.0385	0.029 ± 0.016
Granite, metamorphic, aplitic (101058)						
KFM08A	808.54–808.70	0.1822	0.1842	0.0491	0.0549	0.048 ± 0.004
Felsic to intermediate volcanic rock, metamorphic (103076)						
KFM08A	890.90–890.21	0.2034	0.2068	0.0422	0.0513	0.042 ± 0.007

[E)] Episyenetic sample, strongly altered vuggy metagranite.

[A)] Altered sample.

[S)] Only a single sample measured.

[1)] Based on the uncertainty of the intercept obtained in linear regression of the data.

[2)] Including the 2σ error estimate yields uncertainty larger than the calculated average values and is therefore not included in the estimate of the average.

procedure is used based upon the BET surface measured for two distinct particle size fractions. Extrapolating the results to obtain an inner BET surface (assuming constant particle sphericity) gives values approximately in the range 0.01–0.06 m^2/g.

It should be noted that the formation of large amounts of additional surface area during crushing that are non-representative for intact rock introduces considerable uncertainty concerning the use of crushed rock material for the determination of sorption coefficients. Even the large particle size fraction, 2–4 mm can be expected to be mechanically damaged (in terms of additional internal microfracturing caused by crushing) as compared with undisturbed in situ rock.

This means that surface areas estimated on the basis of extrapolations using crushed rock are likely to be overestimated with respect to the undisturbed rock matrix. These are biases that will need to be addressed further in forthcoming versions of the site description when more detailed, site-specific sorption data becomes available.

Material carefully sampled from natural fractures (Table 2-31) exhibits higher BET surface areas relative to the crushed major rock types by as much as 2–3 orders of magnitude. A possible explanation for this is the presence of, for example, clay minerals and ferric oxides close to the fracture surfaces (i.e. materials that in different alteration processes have become very porous and acquired large surface areas). The large disparity between the surface areas measured for these materials and non-altered rock types indicates that the altered materials may be significant sinks for radionuclides.

Sorption data

No sorption measurement data were available for analysis in modelling stage 2.1. Based upon the BET surface area measurements, the various rock types are thought to have very similar sorption properties. Although there are large differences in sample support amongst the different rock types, which make it difficult to draw specific quantitative conclusions, the sorption property variation

Table 2-31. Measured BET surface area for rock material from open fractures and altered bedrock obtained by scraping loose fracture material and sieving into the < 0.125 mm size fraction unless contraindicated in the table. Measured results are presented together with extrapolated inner surface area (assuming constant sphericity for all particle sizes).

Sampling location		BET surface area (m^2/g)						Extrapolated inner BET surface area (m^2/g)
Borehole	Borehole length (m)	< 0.125 mm		0.063–0.125 mm		2–4 mm		
		Min	Max	Min	Max	Min	Max	Value ± 2σ[1)]
Rim zone material								
KFM01B	47.90–48.00			3.5501	3.6946	1.9367	2.0198	1.93±0.06
Altered bedrock								
KFM01B	418.29–418.43	3.6831	4.0114					
Hydraulically conductive fracture zone								
KFM03A	643.80–644.17	10.0028	10.4595					
Fracture with chlorite								
KFM04A	141.71–141.85	7.6650 [S)]						
Deformation zone, potentially water bearing[3)]								
KFM04A	414.20–414.40	1.1721	2.0412					
Brecciated, fracture Type E [3, 4)]								
KFM05A	611.68–611.91			0.6133	0.6668	0.6874	0.8757	[5)]
Altered bedrock in deformation zone, potentially water bearing, fracture Type A								
KFM05A	627.85–628.00	2.4498	2.8666					
Altered bedrock in deformation zone, hydraulically conductive								
KFM06B	56.25–56.32	7.5052	7.5830					

[S)] Only a single sample measured.

[1)] Based on the uncertainty of the intercept obtained in the linear regression of the data.

[2)] Sampled, crushed and sieved according to the procedures for the material in Table 2-30.

[3)] A significant fraction of the material was non-consolidated and could be sampled without scraping.

[4)] Material sieved into the 0.063–0.125 mm and 2–4 size fractions, respectively.

[5)] Results indicate that the BET-surface area is independent of size fraction.

within rock types appears to be equal to or greater than between different rock types. It is also noted that BET surface areas measured for materials associated with rock fractures and deformation zones indicate potentially stronger sorption on these materials than for unaltered matrix rock.

2.9.5 Field scale tracer experiments

An important element of the site descriptive modelling is the demonstration of retention processes in situ and the partial validation of laboratory data by means of different kinds of field-scale tracer tests. This section gives a brief overview of the tests that have been performed thus far within the site investigation of the Forsmark area. For further details the reader is referred to the relevant data reports.

Single well injection withdrawal (SWIW) tests

Currently, two single well injection withdrawal (SWIW) tests have been performed in the Forsmark site investigation area. One test was made in a complex fracture at 414.7–417.7 m depth within KFM02A (with a transmissivity of 9.5×10^{-7} m^2/s), whereas the other was made in a similar fracture in KFM03A at a depth of 643.5–644.5 m (with a transmissivity of 2.5×10^{-6} m^2/s). The procedure used for making a SWIW test is described in detail in /Gustafsson et al. 2005/ as well as in the background feasibility study reports /Nordqvist and Gustafsson 2002, 2004/. It comprises the following phases and typical timescales:

1) Pumping and storage of groundwater from the selected fracture for subsequent injection.
2) Pre-injection of accumulated water to establish steady state hydraulic conditions (2–3 h).
3) Active injection of one or more tracers within the packed-off borehole section (1 h).
4) Injection of groundwater (chaser fluid) after cessation of tracer injection (12–14 h).
5) Waiting phase (< 1 h).
6) Tracer recovery phase (withdrawal of water under active pumping, 100–200 h).

In both of the experiments a mixture of uranine (non-sorbing) and cesium (sorbing) were used as tracer substances. From the recovery data, clear and unambiguous indications of cesium retention were obtained. In the data report /Gustafsson et al. 2005/, a numerical model simulating radial advective flow and transport with equilibrium sorption (SUTRA /Voss 1984/) was used in a preliminary evaluation of the data.

Using the tracer recovery data for both solutes, the longitudinal dispersivity ($_L$) and linear retardation factor (R) were simultaneously fitted using a least squares approach for a range of fixed flow porosities (i.e. fracture apertures). The linear retardation factor, although not a physically meaningful entity in the presence of matrix diffusion, is operationally defined as the ratio of the delayed tracer breakthrough time relative to the water residence time. The analysis gave a retardation factor on the order of 11–12 for the borehole test section in KFM02A and a factor of 72–73 for the borehole test section in KFM03A.

2.10 Interpretation of primary data on surface system properties

No major changes or improvements in the interpretation of primary data on surface system properties have been performed since version 1.2, except for a compilation and statistical evaluation of all available data on the chemical characteristics of surface system /Tröjbom and Söderbäck 2006/. The main new results from this evaluation are presented below.

2.10.1 Chemical characteristics of shallow groundwater in the Forsmark area

The shallow groundwater in the Forsmark is characterised by high pH-values and high contents of major constituents, especially calcium and bicarbonate. ‘Lower’ located soil tubes, in presumably discharge areas, are strongly influenced by marine relics, resulting in high content of e.g. chloride,

bromide, sodium and manganese. Soil tubes at 'higher' locations, presumably in recharge areas, show clear influences of the calcite rich overburden, resulting in very high levels of calcium, bicarbonate and strontium.

Several parameters show large deviations when the Forsmark data is compared with national reference data. For calcium, bicarbonate and manganese, the median concentrations in the Forsmark area corresponds to the 90th percentile of the national reference data from Swedish wells, indicating very high values in a national context.

Summary per element

Major and minor constituent

The shallow groundwaters in the Forsmark area can be divided in two main water types with respect to the content of major constituents: the Ca-HCO_3 type that is found in 'higher' located soil tubes (presumably recharge areas) and the Na-HCO_3 or Na-Cl types that are found in most 'lower' located soil tubes (presumably discharge areas).

The calcium and bicarbonate levels deviate substantially from the levels normally found in excavated wells of Sweden. The median values in the Forsmark area corresponds to the 90th percentile of Swedish distributions. According to the classification in the Swedish Environmental Quality Criteria for groundwater /Naturvårdsverket 1999/, the alkalinity in all samples from shallow groundwater is 'very high' (the major part of the alkalinity consists of bicarbonate).

Strontium, which is closely correlated to calcium, shows elevated levels compared to the measurements in the Simpevarp area. When data from lake water in the Forsmark area is compared to other lakes in Sweden, the strontium concentrations are seven times higher, indicating that strontium occur in elevated levels.

Manganese occurs in elevated concentrations in the Forsmark area compared to the rest of Sweden. In soil tubes situated at 'higher' locations the concentrations are elevated 40 times compared to the median value of undisturbed shallow groundwaters of Sweden.

The major constituents of sea water, e.g. chloride, sodium, magnesium and sulphate occur in elevated levels in many of the soil tubes due to influences of relict marine water. This fact is also reflected in many surface waters, where elevated concentrations are measured compared to most lakes in Sweden. In the upstream sub-catchments of the Forsmark area, e.g. Eckarfjärden, there are no elevated levels of chloride, underlining the rather recent marine origin of these constituents.

Carbon, nitrogen and phosphorus

Most of the *organic carbon* occurs as dissolved carbon species. The particulate fraction usually constitutes a minor part of the total organic carbon. The lowest concentrations of organic carbon are found in 'lower' located soil tubes, especially in the groundwater in the quaternary deposits below lakes and sea. Most of the *dissolved inorganic carbon* consists of bicarbonate.

In soil tubes at 'lower' levels (presumably in discharge areas) the major part of the *total nitrogen* usually occurs as ammonium. In contrast, most of the soil tubes at 'higher' levels (presumably in recharge areas) occur as dissolved organic nitrogen. Most of *the total phosphorus* occurs as particulate species. In general, only a minor fraction of the total phosphorus consists of phosphate.

Redox potential

The coarse classification of redox potential, based on a scheme from the Swedish Environmental Quality Criteria for groundwater /Naturvårdsverket 1999/, shows that the redox potential is 'low' in most soil tubes. There are two exceptions, SFM0009 and SFM0060, where the redox potential is 'high'. These findings agree with the results of the in situ sonde measurements.

In soil tubes where the redox potential is classed as low, hydrogen sulphide concentrations are usually elevated and the fraction of Fe^{2+} of total iron is usually substantial. On the contrary, soil tubes classed as high redox potential (i.e. class 1 and 2) usually shows a fraction of Fe^{2+} lower than 50% of total iron.

Trace elements

Almost forty trace elements have been measured in samples from shallow groundwater and surface water. When the concentrations are studied along the flow paths, there are examples of both increasing and decreasing concentrations from recharging groundwater to sea water.

The concentrations of the rare earth elements (REE), e.g. lanthanum, ytterbium and lutetium, tend to occur in higher concentrations in recharge waters compared to discharge waters and surface waters. When the concentrations in the lakes in the Forsmark area are compared to other lakes in Sweden, there are no clear differences, indicating rather normal levels in a national perspective.

There is tendency that the arsenic concentration is slightly elevated in shallow groundwater in the Forsmark area. When the concentrations of lakes and streams are compared to rest of Sweden, there is no obvious elevation of the arsenic levels.

The uranium content in shallow groundwater shows rather normal values compared to other Swedish groundwaters. The concentrations in the lakes are, on the other hand, highly elevated compared to most lakes in Sweden. The latter is also seen for molybdenum, possibly indicating that the distribution of these rather mobile elements is different in the Forsmark area compared to other areas in Sweden.

Rubidium and molybdenum generally show higher concentrations in 'lower' located soil tubes compared to 'higher' located tubes, and the highest concentrations are found in sea water. This pattern is analogue to most of the major constituents of sea water.

For metals as chromium, nickel and vanadium, the differences in concentration levels are negligible when precipitation, shallow groundwater and surface waters are compared, implicating that deposition could be an important source for these elements. In some of the soil tubes, especially in 'higher' located soil tubes, the vanadium concentrations are markedly elevated, approximately 30 times compared to the lowest concentrations observed.

Isotopes of hydrogen, oxygen and carbon

Deuterium and *oxygen-18* data for precipitation and most of the observations from shallow groundwater plot on or close to the Global Meteoric Water Line (GMWL), indicating a meteoric origin of most samples from shallow groundwater.

Data from streams and lakes forms an 'evaporation line' indicating enrichments of the heavier isotopes due to evaporation. This is also seen as a gradual decrease of the deuterium deviations along the flow path from 'higher' to 'lower' located soil tubes, to streams, lakes and finally the Baltic Sea. Median values are –78 (precipitation), –85 ('higher' soil tubes), –81 ('lower' soil tubes), –74 (stream), –70 (lake) and –64 (sea) respectively.

'Lower' located soil tubes, presumably in discharge areas, usually show smaller variation of these isotopes compared to 'higher located soil tubes. This tendency is most accentuated for deuterium.

The tritium levels in most soil tubes range from 8–15 TU, an interval that overlap the range of surface waters and precipitation that are approximately 8–16 TU. In a few soil tubes low tritium values, corresponding to sub modern levels, have been observed. Of these are SFM0011, SFM0012, SFM0015, SFM0022, SFM0023 located in till below lake sediments, whereas SFM0010 and SFM0056 are located at higher topographical levels.

Most soil tubes show carbon-14 values below 100% modern carbon, whereas most surface waters exceed 100% modern carbon. The lowest proportions of modern carbon, approximately 50%, are found for SFM0012 and SFM0023 in Lake Gällsboträsket and Lake Bolundsfjärden.

In combination with carbon-14, the stable isotope of carbon-13 discriminates the soil tubes in three different groups:

- The soil tube in the quaternary deposits below Lake Eckarfjärden show unusual positive values of carbon-13 and slightly more than 80% modern carbon is observed.
- The soil tubes located in the lakes Gällsboträsket and Bolundsfjärden show low carbon-14 values in combination with carbon-14 values ranging from –10‰ to 0‰ PDB.

- In the third group, comprising most soil tubes, the content modern carbon is ranging from 80–90 pmC, whereas the carbon-13 values are generally between –15‰ and –10‰, indicating a dominantly biogenic carbon source.

Isotopes of boron, chlorine, sulphur and strontium

The boron-10 ratios found in shallow groundwater are generally higher than ratios in lake, stream and especially sea water. Boron-10 is most depleted in the soil tubes located in the till below the sediments of lakes and sea, e.g. SFM0012, SFM0015, SFM0023, SFM0024 and SFM0025, whereas it is most enriched in the soil tubes SFM0074, SFM0062 and SFM0032, all located in the catchment of Lake Bolundsfjärden.

The chlorine-37 ratios found in the Forsmark area are centred on the international standard, indicating an average ratio of about 0.324 (SMOC). The soil tubes in the catchment of Lake Fiskarfjärden are most depleted in chlorine-37 (SFM0022 and SFM0027). Soil tubes located in till below the lake sediments of Lake Eckarfjärden, Lake Gällsboträsket and Lake Bolundsfjärden (SFM0015, SFM0012 and SFM0023) are most enriched on chlorine-37. There is a tendency that streams draining topographically higher areas show some enrichments of chlorine-37.

The recorded values of sulphur-34 in shallow groundwater vary within a wide range between –17‰ to 41‰ CDT, indicating different sources of dissolved sulphate. Surface waters from lakes and streams range between –10‰ and 10‰ CDT, with most of the samples ranging between 2‰ and 8‰ CDT. All measurements from sea water are very close to 20‰ CDT (Figure 4-65). Sulphur-34 is enriched in the soil tubes located in till below the lake sediments (SFM0012, SFM0022, SFM0023, SFM0024, SFM0025), with values significantly exceeding 20‰ CDT (sea water). Also SFM0057 and SFM0049 show enriched sulphur-34 values. A number of soil tubes at 'higher' locations are depleted in sulphur-34 (e.g. SFM0008, SFM009, SFM0031, SFM0060), showing values well below 0‰ CDT. The 'higher' located soil tubes usually show sulphur-34 values in the range from –10 to 10‰ CDT, similar to values measured in the surface waters.

The stable isotope of sulphur-34 is positively correlated to calcium, strontium, chloride and sulphate, and strontium-87 negatively correlated to these ions.

Strontium-87 is generally enriched relative the natural abundance ratio by 5–40‰. The recorded ratio in the Forsmark soil tubes ranges from 0.712–0.738, compared to the natural abundance ratio of 0.712 (Sr-87/Sr-86). The spatial distribution patterns for strontium-87 differ from most patterns observed for other isotopes, as well as major and minor constituents. Strontium-87 is least enriched in SFM0015, SFM0024 and SFM0022. The highest enrichment is found in SFM0027, located near the outlet of Lake Fiskarfjärden.

Isotopes of radium, radon, thorium and uranium

The radium-226 activities are higher in the Forsmark area than the median value of the reference data from drilled wells in Sweden, whereas the radon-222 activities are in the same order of magnitude as the references. There is a weak correlation between the activities of radium and radon. SFM0027 and SFM0031 marks out by having elevated radon levels compared to the radium activity measured. SFM0002, SFM0015 and SFM0009 display the highest activity when both radium and radon are considered.

Evaluation per catchment

In this section, conclusions are summarised per catchment in order to make the compilation compatible with the corresponding work on surface waters in Forsmark /Sonesten 2005/. The compilation per catchment area is also appropriate for shallow groundwater since the catchment boundaries often coincide with the groundwater divides. The measurements from streaming waters and lakes may also be seen as the sum of groundwater discharge in the area. That is especially the case in an area were local recharge-discharge patterns dominate.

The seven different catchment areas investigated are to a large degree similar in their water chemical composition, but there are also numerous differences both between the catchment areas and within them.

A) The ***Gunnarsbo-Lillfjärden catchment (1:1–4)*** in the north-western part of the study area does not include any measurements of groundwater, except for a single private well. The surface waters in this catchment are characterised by high levels of calcium and alkalinity. The alkalinity measured in this catchment is the highest of all investigated fresh waters in the Forsmark area /Sonesten 2005/. The concentrations of most other ions as sodium and chloride are low compared to other fresh surface waters in the area. Based on the conditions observed in the surface waters, the discharging groundwater in this area probably show low concentrations of ions of marine origin and is probably dominated by Ca-HCO_3 groundwater types.

B) The chemical composition of both shallow groundwater and surface waters varies considerably in the large ***catchment of Norra Bassängen (2:1–11)***. This catchment, which is the largest of the investigated areas, can be divided into three different sub-catchments.

The ***Lake Eckarfjärden sub-catchment (2:10)*** constitutes the upper part of the Norra Bassängen catchment. The soil tubes in this catchment deviates considerably with respect to several parameters. In the Piper plot, all soil tubes in this sub-catchment are classed as Na-HCO_3 type. Compared to most other catchments, the concentrations of several ions, e.g. calcium, potassium, chloride and sulphate, are significantly lower in most soil tubes except for SFM0015, located in the till below the sediments of Lake Eckarfjärden. SFM0015 shows instead high concentrations of magnesium, potassium, iodine, lithium, manganese, barium, rubidium and bicarbonate, and especially low values of sulphate and uranium. Among the isotopes, this soil tube also shows deviating high values of carbon-13, chlorine-37, deuterium and oxygen-18, and low values of tritium and strontium-87. The deviating major and minor constituents observed in SFM0015 are also found in surface water from the outlet of the lake, but not from the inlet, indicating that discharging groundwater in the lake may be important for the water chemical composition of Lake Eckarfjärden /Sonesten 2005/.

The soil tubes in the ***sub-catchment of Bolundskogen/Lake Gällsboträsket (2:8)*** show elevated levels of most ions, e.g. sodium, magnesium, chloride, sulphate, bromide, and uranium, in the 'lower' located soil tubes SFM0011 and SFM0012. These tubes also show low pH-values and low values of tritium, carbon-14 and strontium-87. The streams draining this catchment show elevated concentrations of major and minor constituents.

Most soil tubes in the ***sub-catchment of Norra Bassängen and Bolundsfjärden (2:1–3)*** show normal values compared to most soil tubes in the Forsmark area, except for SFM0023 located in till below the sediments of Lake Bolundsfjärden. This soil tube deviates from all other soil tubes in the Forsmark area by showing a very high salinity, even higher than the present sea water. Besides high chloride concentration, also sulphate, bromide, lithium, strontium, rubidium, deuterium and sulphur-34 show high values. Low values are found for bicarbonate, barium, pH, uranium, vanadium, tritium and carbon-14.

C) Of the three soil tubes situated in the ***catchment of Fiskarfjärden (8:1)***, SFM0022 which is located in till below the lake sediments, show a deviating pattern compared to SFM0026 and SFM0027. The latter two tubes are characterised by low calcium and TOC contents and high silicon content compared to most other soil tubes. SFM0027, located in a thick layer of till, displays the highest radon-222 activities measured in the Forsmark area. SFM0022 shows, except for generally elevated levels of most major constituents, also high levels of iodide, strontium, strontium-87, and low levels of chlorine-37, tritium and carbon-14. The iodine concentration in Lake Fiskarfjärden also show outstanding high values compared to all other surface water sampling sites in the area, analogue to the elevated iodine levels in the soil tube SFM0022. The saturation indices calculated for several minerals show the highest values in the soil tube SFM0022. For example is calcite oversaturated in all observations of SFM0022.

D) The shallow groundwater in the small ***catchment of Bredviken (5:1)*** show deviating chemical composition compared to most other catchments. The soil tubes SFM0006 and SFM0008 are characterised by rather low concentrations of marine ions as chloride, bromide, magnesium and sodium. Instead, elevated levels are found for calcium, potassium, barium and uranium, compared to most other soil tubes. The corresponding pattern is seen in the measurements of streaming water in the inlet of Lake Bredviken.

E) The soil tubes in the small ***catchment of Lake Vambörsfjärden (2:6)*** (SFM0009 and SFM0020), as well as those in the ***catchment of Lake Märrbadet (7:1–4)*** (SFM0059 and SFM0061), show no considerable deviations in their water chemical characteristics compared to typical shallow groundwater in the Forsmark area.

F) There are a number of soil tubes which fall outside the catchments above. These are lumped in the supplementary category 'Coastal areas'. Of these are SFM0024 and SFM0025 located in shallow bays of brackish water. These soil tubes show very similar patterns with a few exceptions: SFM0024 show higher content of magnesium, potassium, deuterium and lower strontium-87. SFM0025 show elevated levels of strontium, calcium, iodine and lower levels of carbon-14 and bicarbonate compared to SFM0024.

2.10.2 Chemical characteristics of the regolith in the Forsmark area

The chemical investigations of the regolith in the Forsmark area have hitherto included analyses of till, soil and sediment samples.

Till

The majority of the elements in the till samples from the Forsmark area occur in normal concentrations, compared to Swedish reference data. Calcium and strontium are two exceptions, where the content is markedly elevated compared to normal till in Sweden.

Most till samples in the Forsmark area contain between 10–30% calcite (calcium carbonate) per dry weight, which is about 30 times higher than the median value of the Swedish reference data. The calcite in the Forsmark area originates from the seafloor of Gävlebukten, a bay of the Baltic Sea which is located about 100 km north of the Forsmark site and which is covered by Cambrian and Ordovician sedimentary bedrock. The calcium-rich material was transported from Gävlebukten and deposited in the Forsmark area during the latest glacial period /Ingemar and Moreborg 1976/. This explanation is supported by the fact that extraordinary high contents of calcite is measured in till, whereas the bedrock dominated by granite lacks calcite. The shallow groundwater in the area also shows highly elevated concentrations of calcium and bicarbonate, the products formed by the dissolution processes of calcite in the Quaternary deposits.

The strontium content in till from the Forsmark area is about seven times higher than normal values of Swedish till. A similar elevation is also seen when surface waters in the Forsmark area are compared to most Swedish surface waters. The elevated strontium concentration in surface water is likely caused by the high content of strontium in the till, and similar to calcium the high strontium content probably originates from the sedimentary bedrock of Gävlebukten.

The variation in bedrock geochemistry is reflected in the chemical composition of the till. In the vicinity of Lake Eckarfjärden, in the south-western part of the Forsmark area, the deviating rock composition is probably reflected by the elevated contents of aluminium, magnesium, iron and some trace elements as e.g. bismuth, uranium and vanadium.

Sediments

The content of calcium carbonate shows considerable variation both within and among the five marine and lacustrine sediment sampling sites in the Forsmark area. There are examples of both very low and very high content of calcium carbonate, reflecting varying conditions during the formation of the sediments. The calcareous gyttja of Lake Stocksjön shows extremely high content of calcium carbonate (60%), originating from precipitation of dissolved calcium carbonate.

The content of organic carbon, sulphur and nitrogen usually shows a decreasing trend from younger (superficial) to older (deeper) sediments. There are usually distinct transitions in the concentrations at certain depths, coinciding with the successions from sea bottom, to brackish lagoon and finally a fresh water lake.

In a sediment profile from Lake Stocksjön most elements occur at higher levels in the marine sediments, except for e.g. calcium, manganese, mercury, antimony and lead which show higher levels in the superficial lacustrine sediments. Strontium, phosphorus and sulphur show only minor correlations to the transition from marine to fresh water. At a depth of 15–20 cm in the sediment profile, air transported pollutants, e.g. mercury, zinc, cadmium, lead and antimony, occur at higher levels compared to both more superficial and deeper layers.

Peat

Most major constituents and trace elements occur at normal concentrations when the three available peat samples are compared to Swedish reference data. One of the peat samples from Lersättermyran show high contents of calcium, indicating that this fen is strongly influenced by the calcareous soils in the vicinity. The concentration of trace elements in the two mires shows normal values, except for lead and zinc that occur in 10–50 times higher concentrations compared to the median of the Swedish reference data /Fredriksson 2004/.

Soil

The pH in the top soil in the Forsmark area is in general high with values around six, whereas Swedish soils on average show values between four and five. The humus layer is influenced by the underlying calcareous mineral soil and the pH value is 6.5 on average, to be compared to values around 5 for most of Sweden.

Carbon concentrations in the humus layer are in accordance with ordinary Swedish conditions, but in the mineral soil the influence of $CaCO_3$ makes the concentration of carbon higher compared to typical values for Sweden. Nitrogen concentrations in the soil agree fairly well with most parts of Sweden, but are lower than usually observed in the Uppsala County.

Element contents in amphibious plants

The content of calcium is markedly elevated in the roots of amphibious plants in the Forsmark area, compared to both Uppsala County and Sweden. The remaining major constituents occur in approximately normal concentrations.

Most trace metals occur in normal or slightly lower concentrations compared to the normal levels in Uppsala county and Sweden. An exception is arsenic that shows tendencies for slightly increased concentrations in plant roots in the Forsmark area.

3 Modelling, implications of data evaluation and modifications since version 1.2

3.1 Rock domains

Relative to the previous rock domain models in SDM versions 1.1 and 1.2, no modifications have been carried out either to the tectonic lens concept (Figure 3-1) or to the assumptions utilised in the modelling work. Both features steer the modelling and are described in /SKB 2005a/. As in earlier models, rock domains have been defined using a combination of the composition, grain size, homogeneity, and style and inferred degree of ductile deformation of various rock units. Minor modifications in the geometry of some rock domains have emerged solely on the basis of new borehole data. A modified regional model and, for the first time, a local model are presented in model version 2.1. The motivation for the choice of the local model volume is presented in Section 2.3.2.

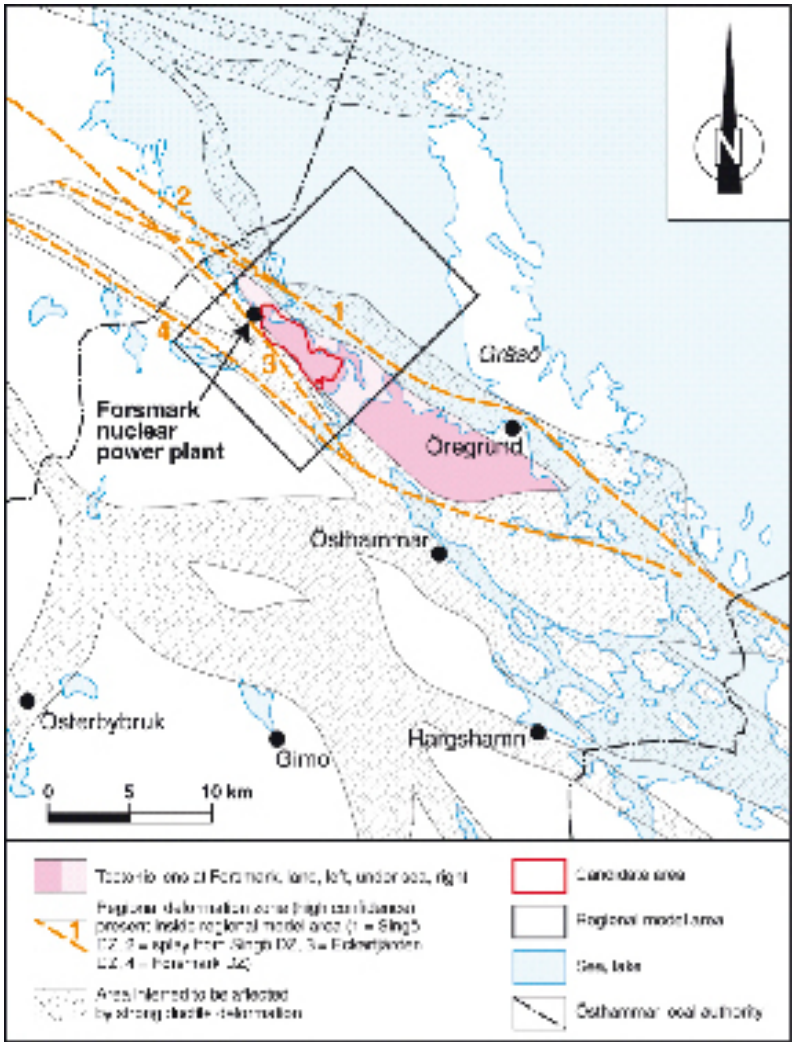

Figure 3-1. *Structural geological map of the coastal area in the local authority of Östhammar, showing the extension of the tectonic lens within which the candidate area at Forsmark is situated (based on /Bergman et al. 1996, 1999/). The regional deformation zones with high confidence that transect the regional model area are also shown (adapted from Figure 5-51 in /SKB 2005a/).*

The properties assigned in the geological modelling work to each rock domain and to the dominant rock type in each domain are identical to those presented in previous models (see, for example, Tables 5-21 and 5-22 in /SKB 2005a/). As emphasised above, the limited amount of new data bearing on rock characteristics precludes an updating of the properties of the different rock types at the site. For this reason, only minor adjustments have been made to the properties of the domains recognised earlier in SDM version 1.2. These adjustments concern changes in the quantitative estimates of the proportions of different rock types in domain RFM029, i.e. the rock domain of prime importance in, for example, rock engineering work. Properties are also provided for the domains that have been restored or added to the regional model, version 1.2. It is worth emphasising that the contents of quartz in the 15 new modal analyses fall within the respective ranges for different rock types that were established during SDM version 1.2.

The correlation of rock units that have emerged during the single hole interpretation of new boreholes with rock domains is shown in Table 3-1. The modelling work is described in more detail in Appendix 2. The text below summarises the key changes that have occurred relative to the earlier model version, the level of confidence for the modelling work, and the remaining uncertainties.

Table 3-1. Correlation of rock units in the single hole interpretation of the boreholes analysed for the first time in model version 2.1 and rock domains. A similar table for the data in boreholes KFM01A, KFM01B, KFM02A, KFM03A, KFM03B, KFM04A, KFM05A and HFM01–19, which were analysed in SDM version 1.2, is presented in /SKB 2005a/.

Borehole	Rock unit (single hole interpretation)	Rock domain in model version 2.1
KFM06A	RU1a, RU2, RU3, RU1b, RU5	RFM029
KFM06A	RU4	RFM045
KFM06B	RU1	RFM029
KFM07A	RU1a, RU1b, RU1c	RFM029
KFM07A	RU2a, RU3, RU2b	RFM044
KFM08A	RU1	RFM029
KFM08A	RU2, RU3	RFM032
KFM08A	RU4	RFM034
KFM08B	RU1	RFM029
HFM20	RU1a, RU2, RU1b	RFM029
HFM21	RU1	RFM029
HFM22	RU1	RFM029

3.1.1 Updated regional model

The regional rock domain model version 2.1 strongly resembles that presented in earlier modelling work /SKB 2004, 2005a/. Minor modifications have been carried out in the geometry of domains RFM029 and RFM032 in the north-western part of the candidate volume. Furthermore, revised estimates of the proportions of different rock types in domain RFM029 have been calculated from the borehole data. Both the dominant rock type and the rock occurrences that are less than 1 m in borehole length have been included in the analysis (cf. SDM version 1.2 in /SKB 2005a/). Domain RFM034 in SDM version 1.1 /SKB 2004/ has been restored into the regional model and two new domains, RFM043 and RFM044, have been added. Since the geometry and character of rock domain RFM043 cannot have any consequences in, for example, repository engineering work (Figure 3-2), the text below only addresses the revisions in the other four domains.

The new data from borehole KFM08A (Figure 2-13) have provided tighter constraints on the down-dip extension of the fine-grained, felsic meta-igneous rocks in rock domain RFM032, the upper boundary to rock domain RFM029, and the lower boundary to rock domain RFM034. On the basis of these data, it can be inferred with high confidence that the synformal structure in the north-westernmost part of the candidate volume /Stephens et al. 2003, SKB 2005a/ plunges 55° towards the south-east. This plunge is 10° gentler compared to that in SDM version 1.2 /SKB 2005a/. It is in good agreement with the calculations that emerge from an analysis of mesoscopic structural data (Appendix 2).

The lower part of borehole KFM07A (< 657 m depth) is dominated by strongly foliated metagranite (Figure 2-15). The conspicuous ductile structures in this borehole interval are vertical or sub-vertical and this new domain (RFM044) has been modelled to intersect the surface close to and south of the reactors 1 and 2 (Appendix 2). In the present model, domain RFM044 separates metagranite, which dominates in the target area in domain RFM029, from the same type of bedrock to the north-west of the nuclear power plant, in the restored domain RFM034 (Figure 3-2).

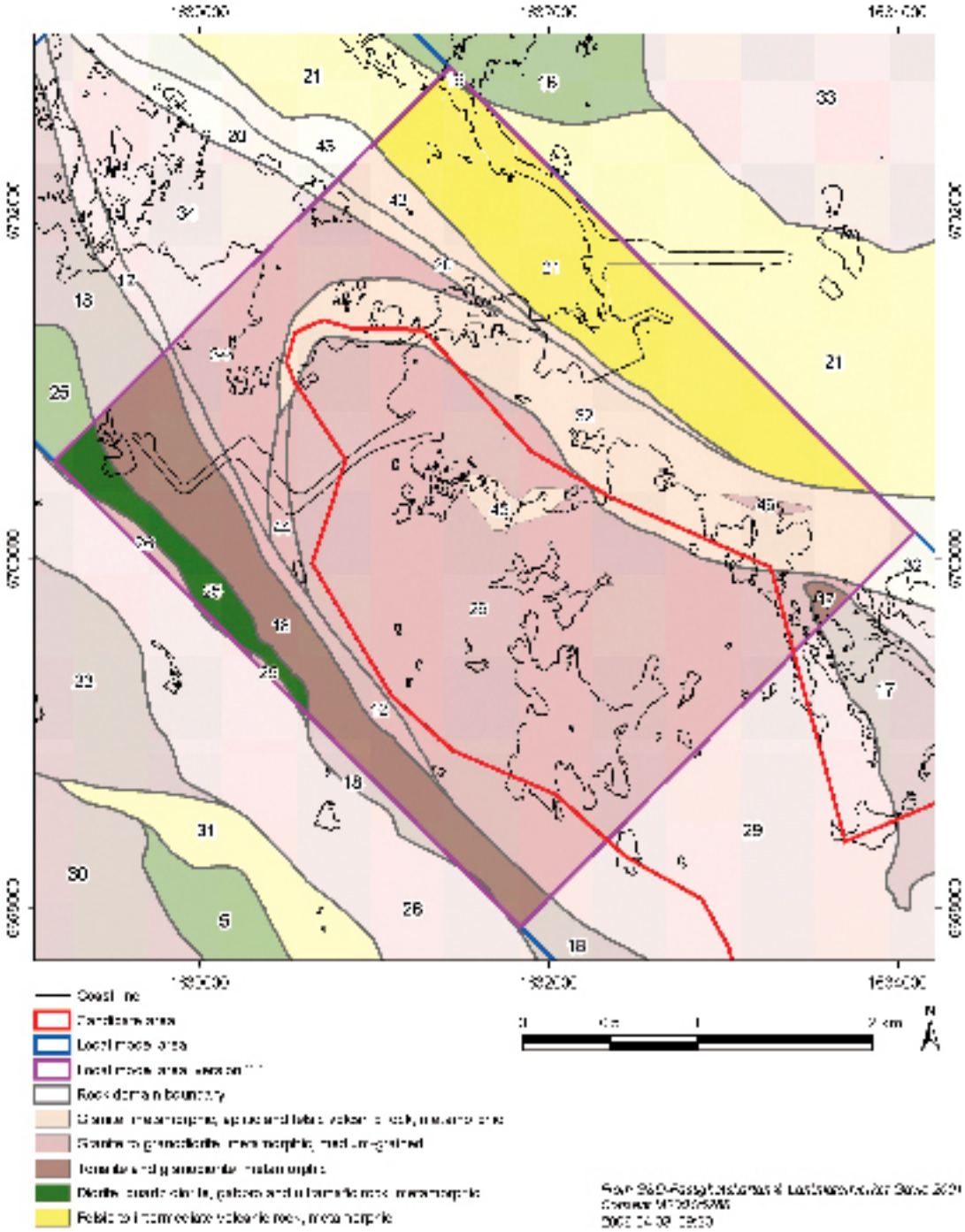

Figure 3-2. *Two dimensional model at the surface for rock domains inside and immediately around the local model area, version 2.1. Rock domains further away from this area are identical to SDM version 1.2 (see also Figure 1 in Appendix 2). The colours represent the composition of the dominant rock type in each domain, if necessary, in combination with the grain size of this rock. As in previous models, the degree of homogeneity and the style and degree of ductile deformation (not shown here) have also been used to distinguish domains. Coordinates are provided using the RT90 (RAK) system.*

The geometric modelling, around and south of the nuclear power plant, resembles that completed in SDM version 1.1 /SKB 2004/. However, domain RFM044 bears compositional (Table 3-2), homogeneity and deformational characteristics somewhat intermediate between domains RFM012 and RFM029, and not to RFM032 as was inferred in /SKB 2004/. Domains RFM032 and RFM044 pass laterally in to each other close to and beneath the nuclear power plant. Domains RFM012 and RFM044 have been separated from each other in the present model, primarily due to their different structural positions relative to the major synform, in the north-westernmost part of the candidate volume.

The estimated proportion of medium-grained metagranite (101057) in domain RFM029 has reduced somewhat relative to that presented in SDM version 1.2 (Table 3-2). This is primarily due to the more precise methodology employed in the calculations in the present work (see above). There is also a slightly higher proportion of this rock type and a lower proportion of the fine- to medium-grained metagranitoid (101051) in the local relative to the regional model volume (Table 3-2).

3.1.2 Local model

The local model aims to provide more detail of the geological relationships inside the target area that has been chosen for the nuclear waste repository /SKB 2005c/. The local model for rock domains differs from its regional equivalent by the addition of two minor domains, RFM045 and RFM046. However, only one of these domains (RFM045) occurs in the central part of the local model volume, where the repository target area is located.

The altered (bleached) rocks in the lower part of borehole KFM06A consist of aplitic metagranite with subordinate medium-grained metagranite and fine-grained, banded felsic rock that is possibly volcanic in origin (Figure 2-15). This unit has been modelled (Appendix 2) by linking the rocks in this borehole intersection with the aplitic metagranite unit, which is exposed in the coastal area south of Asphällsfjärden (Bedrock geological map, Forsmark, version 1.2). Together, these units define domain RFM045. Estimates of the proportions of different rock types in this rock domain, based on the data in borehole KFM06A, are shown in Table 3-2. In accordance with the conceptual understanding of the site, this domain is modelled as a rod that plunges to the south-east, parallel to the mineral stretching lineation inside the tectonic lens (Figure 3-3).

Strongly deformed metagranite dominates the minor domain RFM046 in the coastal area (Figure 3-2). It has been modelled in the same manner as domain RFM045, i.e. as a constrained rod that plunges to the south-east, parallel to the mineral stretching lineation.

Table 3-2. Quantitative estimates of the proportions of different rock types in domains RFM029 (regional and local model volumes), RFM044 and RFM045. For comparison purposes, the revised values for domain RFM012, which take into account rock occurrences less than 1 m in borehole length, are also included (cf. Table 5-23 in /SKB 2005a/).

Code (SKB)	Composition and grain size	RFM029 (regional)	RFM029 (local)	RFM044	RFM012	RFM045
101057	Granite (to granodiorite), metamorphic, medium-grained	73%	76%	64%	57%	8%
101061	Pegmatitic granite, pegmatite	10%	10%	29%	12%	18%
101051	Granodiorite to tonalite, metamorphic, fine- to medium-grained	8%	5%		21%	4%
102017	Amphibolite	5%	5%	5%	6%	4%
111058	Granite, fine- to medium-grained	2%	2%			
101058	Granite, metamorphic, aplitic. Altered (bleached) in RFM045	1%	1%			66%
103076	Felsic to intermediate volcanic rock, metamorphic				3%	
Other rock types		1%	1%	2%	1%	

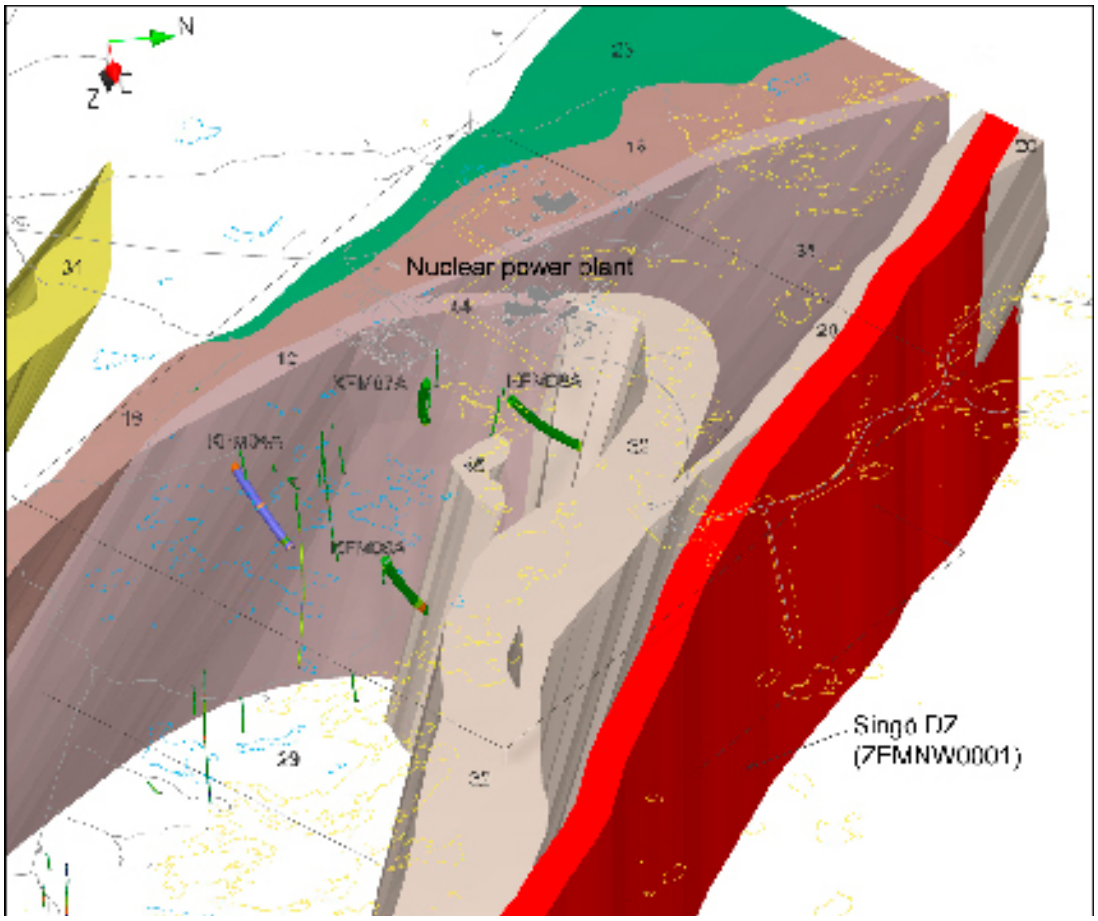

Figure 3-3. *Three dimensional model for rock domains (numbered) inside the target area, in the north-western part of the candidate volume. The model is viewed to the west from approximately the position of SFR. The regionally significant Singö deformation zone is shown in the foreground. Several domains, including RFM029, are unshaded, in order to display the structural style at the Forsmark site. Note especially the moderately to steeply plunging synform that is defined by the boundary between domain RFM029 and domains RFM032 and RFM044. The dominant rock type in each domain is depicted by different colours (see Figure 3-2). Boreholes marked with the help of larger cylinders (KFM04A, KFM06A, KFM07A and KFM08A) constrain the boundaries between different domains.*

3.1.3 Uncertainties

The following more significant uncertainties were noted after the development of the rock domain model, version 1.2.

1. The composition, degree of homogeneity and degree of ductile deformation in the rock domains at the surface in the sea areas, especially Öregrundsgrepen.
2. The location of the boundaries between rock units under Asphällsfjärden, which lies east of the nuclear power plant, and around Storskäret.
3. The extension at depth of all rock domains except RFM017, RFM029 and to some extent RFM007, RFM012, RFM018 and RFM023.
4. The quantitative estimates of the proportions of different rock types in all rock domains except RFM012 and RFM029.

The data acquired in connection with model version 2.1 has improved our understanding of the geometric relationships between domain RFM029 and the bordering domains to the north-west and west. Confidence in both the existence and the geometry of the rock domains that have so far been recognised within or immediately around the target area, in the local model volume, are now judged

to be high down to c. 1,000 m depth. Furthermore, quantitative estimates of the proportions of different rock types have emerged in a few more domains in the present modelling work. In contrast, no new data have been and only a few data will be acquired that affect the uncertainties in the rock domains in the sea areas (point 1 above), around Storskäret (part of point 2), and at depth outside the candidate volume (point 3). However, these uncertainties are, for the most part, of minor importance for the understanding of the geological relationships inside the target area.

It is anticipated that forthcoming data from boreholes KFM06C, KFM08C and KFM09A will provide refined geometric constraints on the boundaries of domain RFM029 (parts of point 2 and point 3 above). Furthermore, data from the new boreholes KFM01C, KFM01D, KFM07B, KFM07C, KFM09B and KFM10A (see Chapter 6) will provide considerably more data that will constrain the properties of this key domain (point 4). Integration work with the modelling of thermal properties has recognised the need for a better understanding of the thickness, the frequency of different thickness classes, and the orientation of the metamorphosed dykes and lenses that occur as amphibolite in rock domain RFM029. In the local model area, version 2.1, this subordinate rock type is estimated to form c. 5% of the total rock volume. An analysis that is focused on these questions will be carried out in connection with model version 2.2.

3.2 Deterministic deformation zones

3.2.1 Methodology

A revised regional model and a new local model, which is situated in the same volume as for the rock domains, have been completed for the deterministic deformation zones in model version 2.1. This approach provides an improved treatment of the variation in data resolution inside the regional model volume, compared to that used in SDM version 1.2 /SKB 2005a/. The revised regional model has several similarities to the base model in SDM version 1.2. However, there are significant changes in the cut-off length of especially the gently dipping deformation zones. Zones in the local model that are not truncated at depth by an adjacent zone have been allowed to extend to the base of the model, irrespective of their length. Apart from this change, all other assumptions used in the modelling work are identical to those used in SDM version 1.2 (see p. 228–229 in /SKB 2005a/).

As in previous modelling work, gently dipping zones have been detected by an integration of data from boreholes with the interpretation of seismic reflectors. By contrast, vertical and steeply dipping zones have been recognised by an integration of data from boreholes with the interpretation of lineaments. Data bearing on fracture orientation, fracture mineralogy and bedrock alteration inside each of the possible deformation zones in the single hole interpretations, or the modified version of these zones (see Section 2.4.5), have been utilised. Some examples of the analysis of these data were presented in Section 2.4.5. The adjustments in the boundaries of deformation zone intersections that were recognised in the single hole interpretations are shown in Table 3-3. Several possible zones recognised in the lower part of KFM08A (DZ5, DZ6 and DZ7) have not been modelled. Fine-grained, felsic meta-igneous rocks are conspicuous at these depths in this borehole and the higher fracture frequency along DZ5, DZ6 and DZ7 is possibly related to the character of the rock type rather than to the occurrence of deformation zones.

Table 3-3. Comparison of deformation zones (DZ) as inferred from the single hole interpretation (SHI) of cored boreholes with deformation zones as modelled in version 2.1.

Borehole	DZ in SHI	Borehole length (m)	Extension or reduction in SHI during modelling work	DZ in model version 2.1
KFM01A (percussion)	DZ1	36–48	29–36 m and 48–51 m added	ZFMNE00A2
KFM01A	DZ2	386–412		ZFMNE1192
KFM01A	DZ3	639–684		ZFMNE0061C
KFM01B	DZ1	16–53		ZFMNE00A2
KFM01B	DZ2	107–135		ZFMNE1194
KFM01B	DZ3	415–454		ZFMNW0404
KFM02A (percussion)	DZ1	79–91		ZFMNE0866

Borehole	DZ in SHI	Borehole length (m)	Extension or reduction in SHI during modelling work	DZ in model version 2.1
KFM02A	DZ2	110–122		ZFMNE0866
KFM02A	DZ3	160–184		ZFMNE00A3
KFM02A	DZ4	266–267		No zone modelled
KFM02A	DZ5	303–310		ZFMNE1189
KFM02A	DZ6	415–520		ZFMNE00A2
KFM02A	DZ7	520–600		No zone modelled
KFM02A	DZ8	893–905		ZFMNE1195
KFM02A	DZ9	922–925		ZFMNE1195
KFM02A	DZ10	976–982		ZFMNE00B4
KFM03B	DZ1	24–42		ZFMNE00A5
KFM03B	DZ2	62–67		ZFMNE00A5
KFM03A	DZ1	356–399		ZFMNE00A4
KFM03A	DZ2	448–455		ZFMNE00A7
KFM03A	DZ3	638–646		ZFMNE00B1
KFM03A	DZ4	803–816		ZFMNE00A3
KFM03A	DZ5	942–949		ZFMNE1207
KFM04A	DZ1	169–176	125–169 m added	ZFMNW1200/ZFMNE00A2
KFM04A	DZ2	202–213		ZFMNE00A2
KFM04A	DZ3	232–242		ZFMNE00A2
KFM04A			290–370 m inferred to part of a DZ. Not recognised in SHI	ZFMNE1188
KFM04A	DZ4	412–462		ZFMNE1188
KFM04A	DZ5	654–661		ZFMNW0123
KFM04A			980–984 m inferred to part of a DZ. Not recognised in SHI	ZFMNW0133
KFM05A	DZ1	102–114		ZFMNE00A2
KFM05A	DZ2	416–436	395–416 m added	ZFMNE0401
KFM05A	DZ3	590–796	Only borehole intervals 590–616 m and 685–720 m included as DZ. Note minor additions relative to SDM version 1.2	ZFMNE0103A (685–720 m)/ ZFMNE0103B (590–616 m)
KFM05A	DZ4	892–916		ZFMNE0062B
KFM05A	DZ5	936–950	950–992 m added	ZFMNE0062A
KFM06B	DZ1	55–93	93–98 m added	ZFMNE00A2
KFM06A	DZ1	126–148	102–126 m added	ZFMNE00A2
KFM06A	DZ2	195–245	245–260 m added	ZFMNE0060B
KFM06A	DZ3	260–278		ZFMNE0060B
KFM06A	DZ4	318–358		ZFMNE0060A. Interference also with ZFMNS00B7
KFM06A	DZ5	619–624	624–652 m added	ZFMNE0061C
KFM06A	DZ6	652–656		ZFMNE0061C
KFM06A	DZ7	740–775	775–788 m added	ZFMNE0061A
KFM06A	DZ8	788–810		ZFMNE0061A
KFM06A	DZ9	882–905	905–925 m added	ZFMNE0061B
KFM06A	DZ10	925–933	933–950 m added	ZFMNE0061B
KFM06A	DZ11	950–990		ZFMNE0061B
KFM07A	DZ1	108–183	Only borehole interval 108–142 m included as DZ	ZFMNE1203
KFM07A	DZ2	196–205		ZFMNE1206
KFM07A	DZ3	417–422		ZFMNE0159
KFM07A	DZ4	803–999	Only borehole interval 873–999 m included as DZ	ZFMNS0100. Possible interference also with ZFMNE1061, ZFMNS1072 and ZFMNW1068
KFM08A	DZ1	172–342	Only borehole interval 250–315 m included as DZ	ZFMNE1061
KFM08A	DZ2	479–496		ZFMNS1204
KFM08A	DZ3	528–557		No zone modelled. Possibly related to ZFMNS1204

Borehole	DZ in SHI	Borehole length (m)	Extension or reduction in SHI during modelling work	DZ in model version 2.1
KFM08A	DZ4	672–693		No zone modelled
KFM08A	DZ5	775–840		No zone modelled. High frequency of fractures along and close to rock domain boundary RFM029–RFM032. Fine-grained rocks in RFM032
KFM08A	DZ6	915–946		No zone modelled. High frequency of fractures along and close to rock domain boundary RFM032– RFM034. Fine-grained rocks in RFM032
KFM08A	DZ7	967–976		No zone modelled. High frequency of fractures in RFM034
KFM08B	DZ1	133–140		No zone modelled. Possibly related to ZFMNS1205
KFM08B	DZ2	167–185		ZFMNS1205

Considerations of respect distance /Munier and Hökmark 2004/, and the significant discrepancy in geometry between the topographic surface and the disconformity between the crystalline bedrock and the Quaternary cover sequence at Forsmark /Lindborg 2005/, have motivated two key changes in the modelling procedure. The latter has provoked an alternative treatment of lineaments relative to that used in SDM version 1.2.

Firstly, in order to focus attention on the zones that require a respect distance in the rock engineering work, all steeply dipping zones that are inferred to be longer than 3,000 m at the surface are included in the regional model (cf. base model in /SKB 2005a/). Since gently dipping zones are important from a hydrogeological viewpoint /SKB 2005a/, and since the length of these zones is difficult to assess, it has also been decided to include all gently dipping zones in the regional model. For this reason, even gently dipping zones that are geologically minor structures, based, for example, on characters such as fracture frequency and thickness, are included in the regional model. Zones that are shorter than 3,000 m and longer than 200 m are included, naturally with varied confidence, in the local model. Bearing in mind the data available, it is considered that the deterministic approach has been driven to its absolute limit in model version 2.1.

Secondly, there are considerable uncertainties at the Forsmark site to interpret topographic lineaments that are based on surface data. For this reason, attention has been addressed in model version 2.1 on lineaments defined solely by magnetic minima. The character of the wall rock alteration associated with zone intersections in boreholes (see Section 2.4.5), as well as the results of the excavation work (see Section 2.4.2), support this modification. However, the results of the excavation work also indicate that some lineaments defined by magnetic minima may be related to changes in rock type. For this reason, there is probably an overestimation of zones that are based solely on this criterion. Lineaments based on depressions in the bedrock disconformity have also been utilised in especially the areas where the magnetic data is of poorer quality, for example in the vicinity of the nuclear power plants /SKB 2005a/.

The geological properties assigned to each deformation zone are shown in Table 3-4. These are identical to those presented in previous work and have been assigned using the same type of data. One exception concerns the estimation of the thickness of deformation zones that lack data from borehole and tunnel intersections. The thickness of these zones has been estimated using a length-thickness correlation plot that has been derived with the help of data from zones, where both ground surface length and thickness have been determined (Appendix 2). The details of the modelling procedure carried out for each deformation zone, the confidence level for the occurrence of each zone, and the geological properties of each zone are presented in Appendix 2.

The text below focuses attention firstly on the present conceptual understanding of the deformation zones at the Forsmark site. Furthermore, the behaviour of different sets of geologically ancient structures in the current (Quaternary) stress regime is discussed. The text also summarises the key changes in the models relative to SDM version 1.2 /SKB 2005a/. Finally, the progress made with the reduction of uncertainties in the modelling work as well as the remaining uncertainties are addressed.

Table 3-4. Properties assigned to deterministic deformation zones in the geological modelling work.

Property	Comment
Deformation zone ID code	ZFM******.
Position	With numerical estimate of uncertainty.
Orientation (strike/dip)	With numerical estimate of uncertainty.
Thickness	With numerical estimate of uncertainty.
Length[1]	With numerical estimate of uncertainty.
Ductile deformation	Indicated if present along the zone.
Brittle deformation	Indicated if present along the zone.
Alteration	Indicated if present along the zone. Type of alteration specified.
Fracture orientation	With numerical estimate of uncertainty.
Fracture frequency	With numerical estimate of uncertainty.
Fracture filling	Mineral coating or filling specified.

[1] Length refers to the inferred length of the deformation zone at the ground surface. No length is provided for the deformation zones that fail to intersect the ground surface. The parts of zones that intersect the ground surface outside the model volume are included in the length estimate.

3.2.2 Conceptual understanding of the site

Sets of deformation zones

Analysis of data bearing on the character of deformation zones in combination with the geometric modelling work indicate that four distinctive sets of deformation zones are present at the Forsmark site. Each set is associated with altered bedrock that contains a fine-grained hematite dissemination.

- Vertical and steeply, SW-dipping deformation zones that strike WNW and NW. These zones contain mylonites, cataclastic rocks and cohesive breccias, and are dominated by sealed fractures. They initiated their development in the ductile regime but continued to be active in the brittle regime, i.e. they are composite structures. Epidote, quartz, chlorite and calcite are conspicuous along the fractures in these zones. Regional zones that are longer than 10 km (e.g. Forsmark, Singö and Eckarfjärden deformation zones, see /SKB 2005a/) are restricted to this set which is the master set at the site.
- Vertical and steeply dipping fracture zones that strike ENE to NNE and formed in the brittle regime, referred to here as the NE set. These zones are dominated by sealed fractures. Laumontite, hematite-stained adularia, chlorite, calcite and quartz are conspicuous along the fractures in these zones.
- Vertical and steeply dipping fracture zones that strike NNW to NS and formed in the brittle regime, referred to here as the NS set. These zones are dominated by sealed fractures. Fillings and coatings along the fractures in these zones are similar to those observed in the NE set. Clay minerals are also present along steeply dipping fractures with NNW strike in some zones. On the basis of their low frequency of occurrence, this set is judged to be of lower significance at the Forsmark site relative to the other three sets. Nevertheless, the version 2.1 modelling work has indicated the existence of such zones in the local model volume.
- Gently S-, SE- and W-dipping fracture zones that formed in the brittle regime and, relative to all the other sets, contain a higher frequency of open fractures and incoherent crush material. Chlorite, calcite and clay minerals are conspicuous along the fractures in these zones. Locally, epidote, quartz, prehnite and laumontite are present.

Formation and reactivation during Precambrian tectonic events

On the basis of the properties of the deformation zones, the relative time relationships between different mineral sets (see Section 2.4.3), and the $^{40}Ar/^{39}Ar$ cooling ages /Page et al. 2004/, a working conceptual model for the formation of the zones during the later part of the Svecokarelian orogeny was presented in SDM version 1.2 /SKB 2005a/. The version 2.1 work:

- Reinforces the concept that the composite WNW and NW regional deformation zones truncate all the other sets of zones, indicating that the WNW and NW zones are the oldest structures.
- The gently dipping zones in places truncate against steeply dipping zones with NE strike, indicating that at least some of the steeply dipping structures in the NE set are older than the gently dipping zones.
- Epidote fills gently dipping fractures within or immediately beneath the gently dipping zones, indicating that the latter are geologically ancient structures.

If it is assumed that all four sets formed in the same tectonic regime, the geometric relationships between the different sets are consistent with their formation in a strike-slip tectonic regime (Figure 3-4). As argued in /SKB 2004, 2205a/, the Fennoscandian Shield was subject to bulk crustal shortening in a NNW direction during the later part of the Svecokarelian orogeny. In such a tectonic regime, a dextral component of movement would have occured, for example, along the WNW and NW structures (Figure 3-4). This is consistent with the older ductile deformation observed in the region /SKB 2004, 2005a/.

Reactivation of these zones at temperatures under c. 300–350°C (growth of prehnite) and under 250°C (growth of laumontite) is apparent during one or more events after 1,700 million years ago /SKB 2005a/. This is especially relevant for the steeply dipping NE set. Indeed, the widespread occurrence of lower temperature minerals such as laumontite along the fractures in these zones holds open the possibility that these structures actually formed later than 1,700 million years ago. However, there is the added complication with reactivation that fluid movement during the reactivation event may have destroyed the mineral traces that formed during older events.

Deformation during the time period 1,700–1,560 million years ago, in connection with a far-field response to Gothian tectonic events, is one of the candidates for early reactivation. Regional considerations indicate bulk crustal shortening in a NE direction at this stage in the geological history

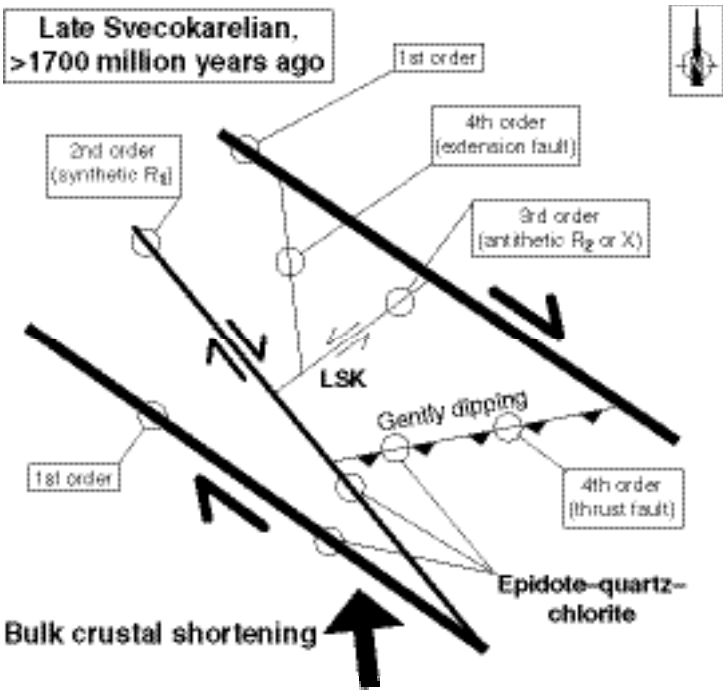

Figure 3-4. *Two-dimensional cartoon illustrating the regional scale kinematics during the formation of the different sets of deformation zones at the Forsmark site. In this conceptual model, it is assumed that all structures formed in response to the same tectonic event during the later part of the Svecokarelian orogeny. A bulk crustal shortening in an approximately NNW direction is envisaged. For further comments, see /SKB 2005a/.*

/SKB 2004, 2005a/. In such a tectonic framework, movement along steeply dipping zones with strike directions ENE and NS would have occurred with sinistral and dextral strike-slip components of movement, respectively.

The disturbance of the U-Pb isotope system for titanite in the Forsmark area /Page et al. 2004/ indicates that a second reactivation episode may have occured after c. 1,100 million years ago, in connection with Sveconorwegian tectonic reworking. As argued in /SKB 2004, 2005a/, the Fennoscandian Shield was subject to bulk crustal shortening in a WNW direction during the later part of the Sveconorwegian orogeny. In such a tectonic regime, a dextral component of movement would have occurred along the steep NE set of structures at this time (Figure 3-5). This type of kinematics has been observed along one of the steeply dipping zones with NE strike at drill site 4 (ZFMNE1188 in /SKB 2005a/). In such a tectonic regime, sinistral strike-slip motion along the WNW and NW structures would have occured (Figure 3-5).

Loading and unloading cycles during the Phanerozoic

It is of interest to assess the behaviour of these different sets of ancient structures during the Phanerozoic and, not least, during the Quaternary in the current stress regime. Disturbance of the sub-Cambrian peneplain /Lidmar-Bergström 1994/ along the regionally important Forsmark deformation zone /Bergman et al. 1999/ suggests a component of vertical motion after the establishment of this ancient, erosional surface. Furthermore, Phanerozoic reactivation of older fractures (or possibly even the formation of new fractures) is suggested by the occurrence of sulphides and organic asphaltite along fractures in the upper part of the bedrock /Sandström and Tullborg 2005/. Downward migration of, for example, hydrocarbon-bearing fluids from a source rock that covered

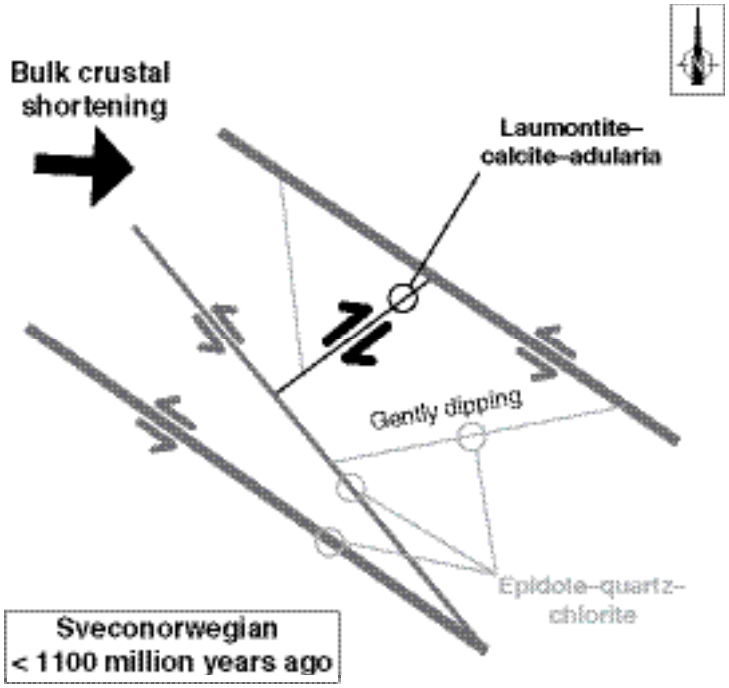

Figure 3-5. *Two-dimensional cartoon illustrating the regional scale kinematics in connection with a possible phase of reactivation of the different sets of deformation zones at the Forsmark site during the Sveconorwegian orogeny. A bulk crustal shortening in an approximately WNW direction is envisaged. In this conceptual model, significant deformation is suggested along the steeply dipping NE zones (black line) and even along the steeply dipping WNW and NW zones (dark grey line). The steeply dipping NS and gently dipping zones (pale grey line) are also shown. Note the major change in the kinematics of the structures relative to that seen in Figure 3-4.*

the crystalline bedrock during the earlier part of the Phanerozoic is envisaged (see Section 2.4.5). It is uncertain to what extent Phanerozoic tectonic events south and west of the Fennoscandian Shield /SKB 2004, 2005a/ or simply the effects of loading and unloading have steered the development of these structures.

In situ stress measurements at the Forsmark site /Carlsson and Christiansson 1987, SKB 2004, 2005a/ show that the current, maximum principal stress ($_1$) is sub-horizontal with a mean orientation in a NW-SE (c. 140°) direction (Figure 3-6). This orientation has been related to ongoing ridge-push tectonics. High rock stresses also prevail at the site (approximate value for $_1$ is 45 MPa at a depth of 500 m, see /SKB 2005a/). It has been suggested that build-up of rock stresses at Forsmark is related, in part, to the loading effect of Quaternary ice sheets /Carlsson and Olsson 1982/. Stress modelling work indicates that there appears to be a build-up of higher rock stresses in the bedrock beneath the gently dipping deformation zones /SKB 2005a/. The current minimum principal stress ($_3$) is vertical with the implications that, at shallow crustal levels in bedrock blocks beneath the gently dipping deformation zones, the differential stress ($_1 - _3$) is high. Furthermore, $_3$ would have decreased dramatically, following the rapid removal of ice after a Quaternary glaciation, including the latest Weichselian glaciation /Carlsson 1979/.

The changes in the stress regime following the latest glaciation event have been invoked as an explanation for the sub-horizontal joints in the uppermost (< few tens of metres) crustal levels at the Forsmark site /Carlsson 1979, Leijon 2005/. These joints represent reactivated, ancient, gently dipping or sub-horizontal fractures, or newly formed sheet joints with apertures sub-parallel to the ground surface. Block uplift and rotation have also been documented at drill site 5 /Leijon 2005/. It is suggested here that the same processes, i.e. rapid unloading and significant changes in the differential stress regime during the Quaternary, can explain the increased frequency of open fractures and the increased hydraulic transmissivity in the gently dipping fracture zones. In this context, a high frequency of ancient fractures along these zones, which lie at a high angle to the current $_3$ (Figure 3-6) and can, thus, open as stress-release joints, is a key factor.

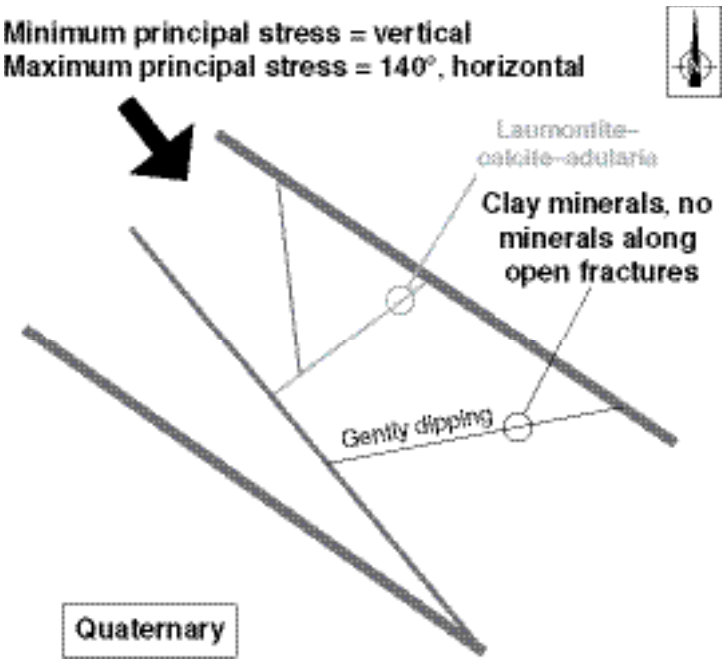

Figure 3-6. *Two-dimensional cartoon illustrating the current conceptual model for a reactivation of the different sets of deformation zones at the Forsmark site, in the current stress regime (Quaternary). The maximum principal stress is oriented 140° and is horizontal. The different colour shadings along the zones indicate a variable degree of response to this stress field. The black line along the gently dipping structures indicates a considerable change in aperture development along the fractures in these zones; the dark grey line indicates a moderate change and the pale grey line little change.*

One corollary of these considerations is that the steeply dipping NE zones which are oriented at a high angle to $_1$ (Figure 3-6), should not, in general, be prone to reactivation in the current stress regime. However, the aperture and, as a consequence, the hydraulic transmissivity of subordinate gently dipping fractures along these zones (see Section 2.4.5) may be modified in the current stress field. An important implication of this observation is that the orientation of water-bearing fractures along an ancient deformation zone is not necessarily an indication of the orientation of the zone itself. The remaining steeply dipping zones at the Forsmark site, with a high frequency of ancient fractures that strike WNW-NW and NNW-NS, should also be prone to some reactivation in the current stress field, but not to the same extent as the gently dipping structures (Figure 3-6).

A second corollary concerns the relationship between the occurrence of gently dipping zones and the in situ stress magnitudes in the bedrock. Since the south-eastern part of the candidate volume contains a high frequency of gently dipping fracture zones at regular intervals at depth /SKB 2005a/, it is predicted that there would have been little build-up of stress in this volume during the Quaternary. By contrast, the high, relic in situ stresses in the north-western part of the candidate volume, beneath zone ZFMNE00A2, are steered by the absence of such gently dipping structures. Ancient sub-horizontal or gently dipping fractures in this bedrock volume, especially such fractures that lie close to the surface, would be highly susceptible to modification of aperture in connection with the release of the high in situ stress in the bedrock. At the highest crustal levels, even formation of new sub-horizontal sheet joints is likely.

Since the present topographic surface is more or less identical to the ancient, erosional surface represented by the sub-Cambrian peneplain, it is possible that stress build-up and changes in the aperture characteristics of fractures during the subsequent release of stress are also related to earlier loading and unloading cycles, respectively. For example, sedimentation and subsequent removal of the Phanerozoic sedimentary cover rocks, with its significant component of dense limestone, is potentially of considerable importance /SKB 2005a/.

Fracture domains and implications for future work

These considerations have provoked a division of the bedrock at the Forsmark site into domains that are defined on the basis of different fracture intensities. A preliminary example of such a division is presented here for the candidate volume (Figure 3-7). This bedrock volume is dominated by rock domain RFM029 and has been divided into three separate fracture domains. The division of the bedrock at Forsmark into fracture domains will be developed further during modelling stage 2.2, with a principal aim to assist in the development of the new DFN modelling.

The ongoing study that characterises, in more detail, the deformation zones at the Forsmark site, in particular the kinematics of the zones, will provide a solid test and hopefully a significant refinement of the working conceptual model described above. The modelling of bedrock stresses within the rock mechanics programme should also provide a closer insight into the development of the deformation zones. Furthermore, it is recommended that future DFN work include analyses of the following features in each fracture domain.

- The orientation of fractures with apertures.
- The variation with depth of the occurrence of gently dipping and sub-horizontal fractures.
- The variation with depth of the size of fracture apertures.
- The variation with depth of the occurrence of younger fracture minerals.
- The variation with depth of the occurrence of open fractures devoid of minerals.

Such analyses will help to test some of the hypotheses put forward here.

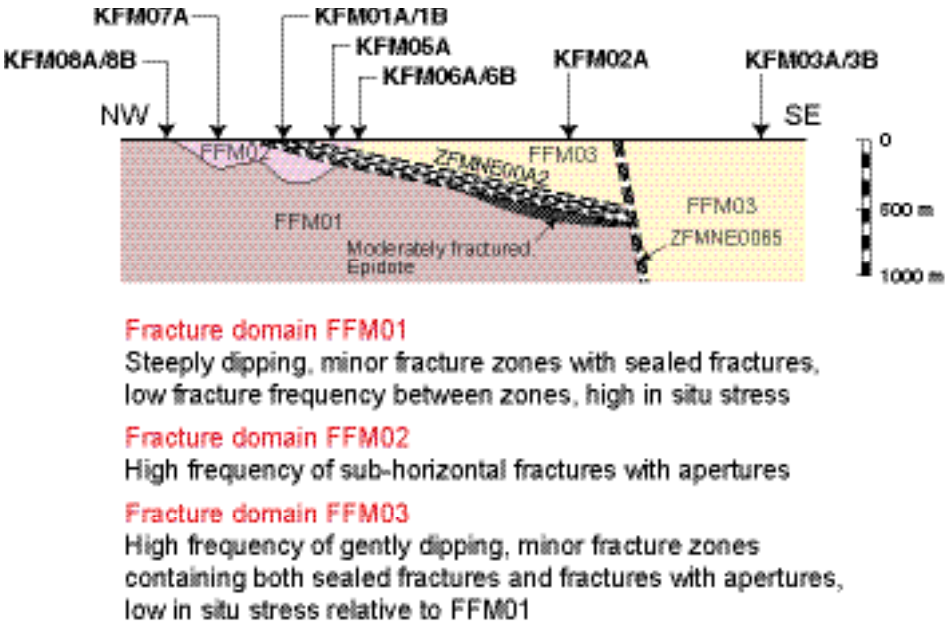

Figure 3-7. *A possible division of the candidate volume at Forsmark, which is dominated by rock domain RFM029, into three fracture domains. The domains are shown on a simplified NW-SE cross-section along the candidate volume. Only two fracture zones, the gently dipping fracture zone ZFMNE00A2 and the steeply dipping zone ZFMNE0065, against which zone ZFMNE00A2 appears to truncate to the south-east, are shown.*

3.2.3 Updated regional model

Relative to SDM version 1.2, there are no changes in the degree of resolution of geophysical data that have been used to identify magnetic lineaments in the regional model area. However, new surface reflection seismic data are now available outside the candidate area (see Section 2.4.2). These data improve the ability to assess the occurrence and extension of gently dipping fracture zones. The new borehole data are restricted to the local model volume.

73 deformation zones are present in the regional deformation zone model, version 2.1. 47 of these zones are steeply dipping, while the remainder are gently dipping. All except 15 zones, most of which are gently dipping, intersect the surface and are included in the two dimensional model for the site (Figure 3-8). Steeply dipping zones longer than 3,000 m and all the gently dipping zones are included in the regional model.

The use of magnetic rather than linked lineaments (Appendix 2), in combination with the identification of corridors, across which seismic reflectors can not be traced (Appendix 2), have resulted in modifications in the length and orientation of virtually all the deformation zones presented in earlier regional models. In particular, this new modelling routine has resulted in a reduction in the along-strike extension of the gently dipping zones and a rejection of the model referred to as base model variant in SDM version 1.2. Nevertheless, most of the changes, especially for the steeply dipping zones, are relatively minor in character.

A NW-SE cross-section down to 1,000 m depth, which passes close to drill sites 1, 2, 3, 5 and 7, is shown in Figure 3-9. A comparison with Figure 11-3 in /SKB 2005a/ illustrates the changes that have occurred between model versions 1.2 and 2.1 inside the candidate volume. The cross-section illustrates the regular spacing of gently dipping fracture zones to the south-east of the steeply dipping zone ZFMNE0065. The absence of gently dipping zones in the north-western part of the candidate volume at depths from c. 200 m down to greater than 1,000 m is also apparent. A bedrock with somewhat intermediate character where it concerns the occurrence of gently dipping structures is present in the bedrock block between the steeply dipping zones ZFMNE0062A and ZFMNE0065. The text that follows focuses attention on the more significant changes that have occurred after SDM version 1.2.

Steeply dipping fracture zones

Zones ZFMNE0060A and -B, zones ZFMNE0062A and -B, and zone ZFMNW0123 are all longer than 3,000 m and all transect the target area. Only minor changes in the length, orientation and thickness of zones ZFMNE0062A and -B have occurred in the present model and the excavation work (see Section 2.4.2) confirms the occurrence of this zone. The other zones as well as zone ZFMNW1200 are addressed below.

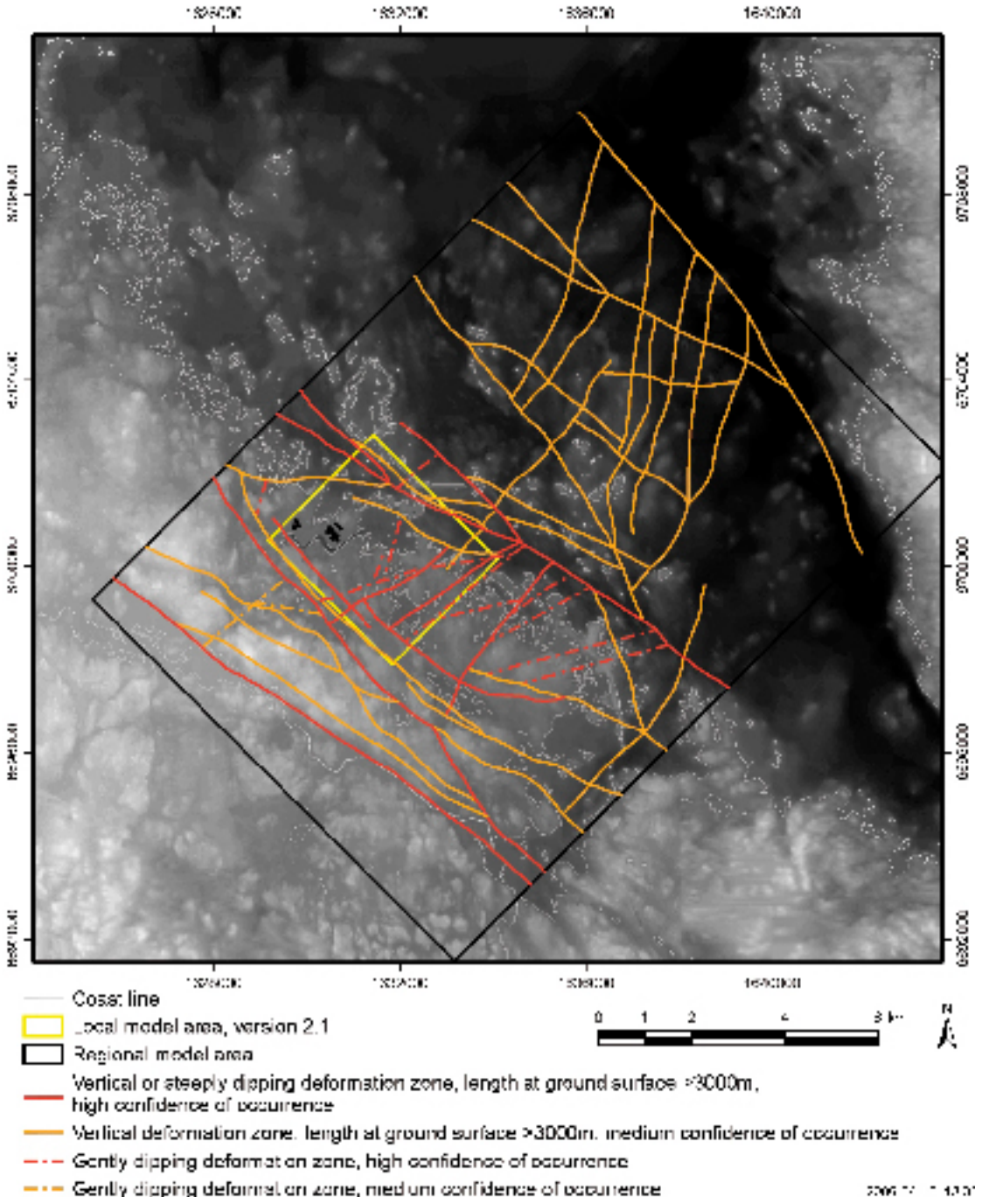

Figure 3-8. *Surface intersection of deformation zones in the regional model area (version 2.1). The background corresponds to the digital elevation model for the site. Coordinates are provided using the RT90 (RAK) system.*

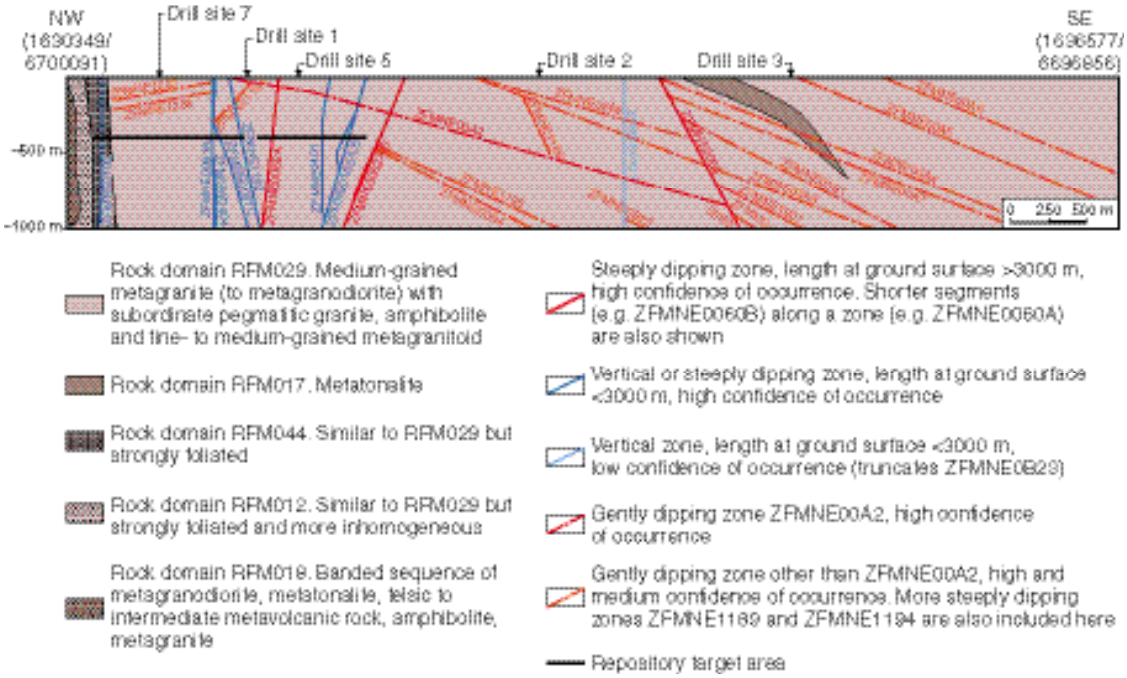

Figure 3-9. *NW-SE cross-section that passes close to drill sites 1, 2, 3, 5 and 7 inside the candidate volume (version 2.1). This two-dimensional structural model shows the steeply dipping deformation zones that strike NE and the gently dipping zones that dip to the south-east and south. All these zones transect the candidate volume. They are sandwiched between regionally more significant, vertical and steeply dipping deformation zones that strike WNW or NW and are not able to be shown in this cross-section.*

The data from KFM06A confirm that the magnetic lineament 60 corresponds to a fracture zone that contains a high frequency of steeply dipping, sealed fractures with NE strike (ZFMNE0060A and -B). The results of the drilling work have permitted an upgrading in the confidence level for the existence of zone 60 from medium in model version 1.2 to high in version 2.1. This structure is still inferred to be longer than 3,000 m (3,120 m) and, for this reason, is included in the regional model. Bearing in mind the uncertainties in the orientation, it shows a strike and dip (c. 240/85) that is identical to that in SDM version 1.2. The acquisition of high-resolution, ground magnetic data, which is in progress at the present time, will provide more constraints on the character of this zone.

A reassessment of the structural data in KFM04A and the magnetic lineaments (Appendix 2) has permitted an upgrading of the confidence level for zone ZFMNW0123, relative to SDM version 1.2. Based on the length of the magnetic lineament, this zone is inferred to be longer than 5,000 m. Sealed fractures that dip steeply to the south-west are prominent in the borehole intersection in KFM04A (DZ5). Quartz, epidote, prehnite and some clay minerals together with chlorite and calcite are conspicuous along the fractures.

A third, more significant change in the regional model for steeply dipping zones concerns the linking of a magnetic lineament with NW trend at the surface (MFM1200) with DZ1 (extended) in the upper part of KFM04A (Appendix 2). The occurrence of fractures, both sealed and open/partly open, that dip steeply to the south-west and an alteration, which involves a hematisation of the bedrock, support this correlation. Based on the length of the lineament and its inferred continuation along a topographic lineament south-west of reactor 3, where the magnetic data are of poor quality /SKB 2005a/, this zone (ZFMNW1200) is inferred to be slightly longer than 3,000 m.

Gently dipping fracture zones

As predicted from SDM version 1.2, fracture zone ZFMNE00A2 intersects borehole KFM06B (DZ1) and the upper part of KFM06A (DZ1). The orientation of zone A2 in the present model is identical to that in SDM version 1.2 (080/24). It has been truncated in a down-dip direction to the

south (Figure 3-9) along a steeply dipping zone with NE strike (ZFMNE0065) and to the south-west along an inferred deformation zone with WNW strike (ZFMNW0017). These modifications in the truncation of zone A2 are motivated by the implications of the new reflection seismic data (Appendix 2). Relative to SDM version 1.2, only minor changes have been carried out in the properties of this zone.

Zone A2 is a composite zone that consists of several, narrower high-strain segments (sub-zones) that are inferred to diverge and converge in a complex pattern /SKB 2005a/. These sub-zones separate less deformed bedrock segments. In KFM02A, the uppermost (415–430 m) and lowermost (480–520 m) parts display bedrock alteration and highest fracture frequency. In KFM04A, three separate sub-zones that vary in thickness from 5–10 m are present over an interval of 67 m perpendicular to the zone. Thus, the overall estimated thickness of 70 m includes intervals of bedrock considerably less affected by deformation relative to, for example, the uppermost and lowermost parts in borehole KFM02A.

Reflector B8 intersects the older borehole KFK001 (DBT1) close to the minor, gently dipping zone in the interval 316–322 m /Carlsson and Christiansson 1987/, which was identified as ZFMNE1193 in SDM version 1.2. For this reason, this zone is renamed ZFMNS00B8 in the present model. With the help of the reflection seismic data, there are now far better constraints on the orientation of this gently dipping zone (015/22) relative to the model version 1.2. Furthermore, the reflection seismic data indicate that it does not extend eastwards beneath reactors 1–2 (cf. Figure 3-9 in this report with Figure 11-3 in /SKB 2005a/). Further drilling work is in progress to provide better constraints on its properties.

A new assessment of the fracture data from zone ZFMNW1194 in SDM version 1.2, which intersects borehole KFM01B (DZ2) directly beneath ZFMNE00A2, has provoked a remodelling of this zone. Epidote-filled fractures that strike S to SW and dip gently to moderately to the W to NW are conspicuous. A high frequency of epidote-filled fractures with a similar orientation is also present directly beneath ZFMNE00A2 in borehole KFM02A. Based on these observations, zone 1194 has been remodelled as a minor zone with SW strike and NW dip that is conjugate to the more important zone ZFMNE00A2 (Figure 3-9). Minor fracture zones (ZFMNS1203, ZFMNS1206) that dip more gently (10°) to the west occur in the upper part of borehole KFM07A. The upper zone (DZ1 in KFM07A) contains sub-horizontal fractures that are also sealed with epidote.

Zone ZFMNE1195 was identified near the base of borehole KFM02A (DZ8 and DZ9 in KFM02A) during SDM version 1.2 /SKB 2005a/. No seismic reflector was recognised at this depth. Sealed fractures dominate in this zone but a transmissivity anomaly has been documented /Forsman et al. 2004/ along the thicker segment in DZ8. The orientation of the zone (065/30) has been modelled primarily on the basis of the orientation of the main set of fractures within the zone and it has been truncated against surrounding steeply dipping structures (Figure 3-9). Although there is a high confidence for the existence of this zone along KFM02A, its orientation and its extension both along strike and down dip are highly uncertain.

A gently dipping fracture zone (ZFMNE1207), which corresponds to DZ5 in KFM03A, has been added to the regional model (Figure 3-9). This zone has been modelled with the same orientation and using similar truncation principles as for zone ZFMNE00B1 (DZ3 in KFM03A). Reflectors J1, J2 and K1 have been modelled as moderately dipping zones with a medium degree of confidence. No borehole data are available from these structures. All these structures are located in the south-eastern part of or outside the candidate volume.

Minor modifications in the version 1.2 modelling of the gently dipping zones ZFMNE00A3, ZFMNE00B6 and ZFMNE0866 in the upper part of borehole KFM02A and in boreholes HFM04 and HFM05 have been carried out (Appendix 2). These changes are of minor significance and have no implications for the repository target area. In SDM version 1.2, the gently dipping reflectors C1 and C2, which occur close to the base of the regional model volume, were modelled as deformation zones with a medium degree of confidence. Since these reflectors are curved and occur on both sides of the Singö deformation zone, it is now considered that they are related to a lithological velocity contrast and may be related to mafic sills. For this reason, these two zones have been removed from the deformation zone model. Once again, this change has no implications for the relationships inside the repository target area.

3.2.4 Local model

Data from boreholes are, as yet, the prime feature that permits an improved degree of resolution for the recognition of deformation zones within the local model volume. These data also provide a much better insight into the character of the deformation zones that occur within the local model volume relative to those that occur outside this volume. Inside the local model area, the helicopter-borne geophysical data and the earlier lineament interpretation work have been reassessed, with an aim to identify all possible deformation zones that are related to magnetic minima, irrespective of their length (Appendix 2).

89 deformation zones are present in the local deformation zone model, version 2.1. The vast majority of these zones (75) are steeply dipping, while the remainder are gently dipping. All except 14 zones, which are predominantly gently dipping or occur as subordinate segments that are attached to a larger zone, intersect the surface and are included in the two dimensional model for the site (Figure 3-10).

30 zones in the regional model also intersect the local model volume (Table 3-5). Since the characteristics of these zones have been determined predominantly from data acquired inside the local model volume, there are no differences in the properties of these zones in the two models. These zones are treated in the comments on the regional model and are not addressed further here. Bearing in mind the proposed repository layout at 400 m depth (Figure 3-11), only zones ZFMNE00A2, ZFMNE0060A and -B, ZFMNE0062A and -B, ZFMNW0123, and possibly the poorly constrained zone ZFMNE1195 in this group are of critical importance (Table 3-5).

Steeply dipping zones that are less than 3,000 m in length are also included in the local model. Most of these are inferred solely from the interpretation of lineaments that are based on magnetic minima (Appendix 2). Direct data from boreholes or surface outcrops are lacking and, for this reason, they are registered with a low degree of confidence for their occurrence. Due to their low degree of confidence, such zones have not been included in the cross-section in Figure 3-9 or in the geological map at 400 m depth in the target area (Figure 3-11). Furthermore, they are not discussed further here. The properties of the respective lineaments are presented in Appendix 2.

The text below focuses attention on a few changes in fracture zones (< 3,000 m in length) that have occurred on the basis of a reassessment of the borehole data used in SDM version 1.2 and on some additions based on the data from the new boreholes.

Steeply dipping fracture zones

Minor changes in the orientation, length and thickness of the steeply dipping fracture zones ZFMNE0103A and ZFMNE0401, which were recognised in KFM05A during SDM version 1.2 /SKB 2005a/, have been carried out. Furthermore, zone 404 has been remodelled as a minor zone that strikes NW (Appendix 2).

The data from the lower part of KFM06A (DZ5–DZ11) confirm that the minor fracture zone ZFMNE0061, which contains a high frequency of steeply dipping, sealed fractures with NE strike, transects the target area. In the same manner as other steeply dipping structures with NE strike, it consists of several segments where the bedrock is more intensely fractured and intermediate intervals where the deformation in the bedrock is lower. The model involves an intricate network of subordinate fracture zones (e.g. ZFMNE0061B1) that are attached to a main zone (e.g. ZFMNE0061A). Two zones with similar orientation and character of fractures as the steeply dipping NE zones (ZFMNE0159 and ZFMNE1061) have been modelled in the north-westernmost part of the candidate area.

An important development in model version 2.1 concerns the establishment of fracture zones in the local model volume that can be linked to lineaments that trend NS. Steeply dipping fractures and zones of low confidence that belong to this orientation set were recognised in SDM version 1.2 /SKB 2005a/. There is now stronger evidence that such zones exist inside the local model volume. The most conspicuous example intersects the lower part of borehole KFM07A (major part of DZ4) with the identification number ZFMNS0100 and transects the north-western corner of the repository target area. Adularia, laumontite, chlorite and calcite are common minerals along the fractures in

this zone. It corresponds at the surface to a lineament defined by a magnetic minimum as well as to a low velocity anomaly in older seismic refraction data /SKB 2005a/. Other minor zones that strike NS (ZFMNS0431, ZFMNS1204 and ZFMNS1205) have been modelled, primarily on the basis of borehole intersections in HFM22 (DZ1), KFM08A (DZ2) and KFM08B (DZ2), respectively.

A reassessment of the structural data in KFM04A and the magnetic lineaments (Appendix 2) has resulted in the inclusion of a minor zone with NW strike referred to as ZFMNW0133. Sealed fractures that dip steeply to the north-east dominate in this minor structure. Laumontite is conspicuous along the fractures.

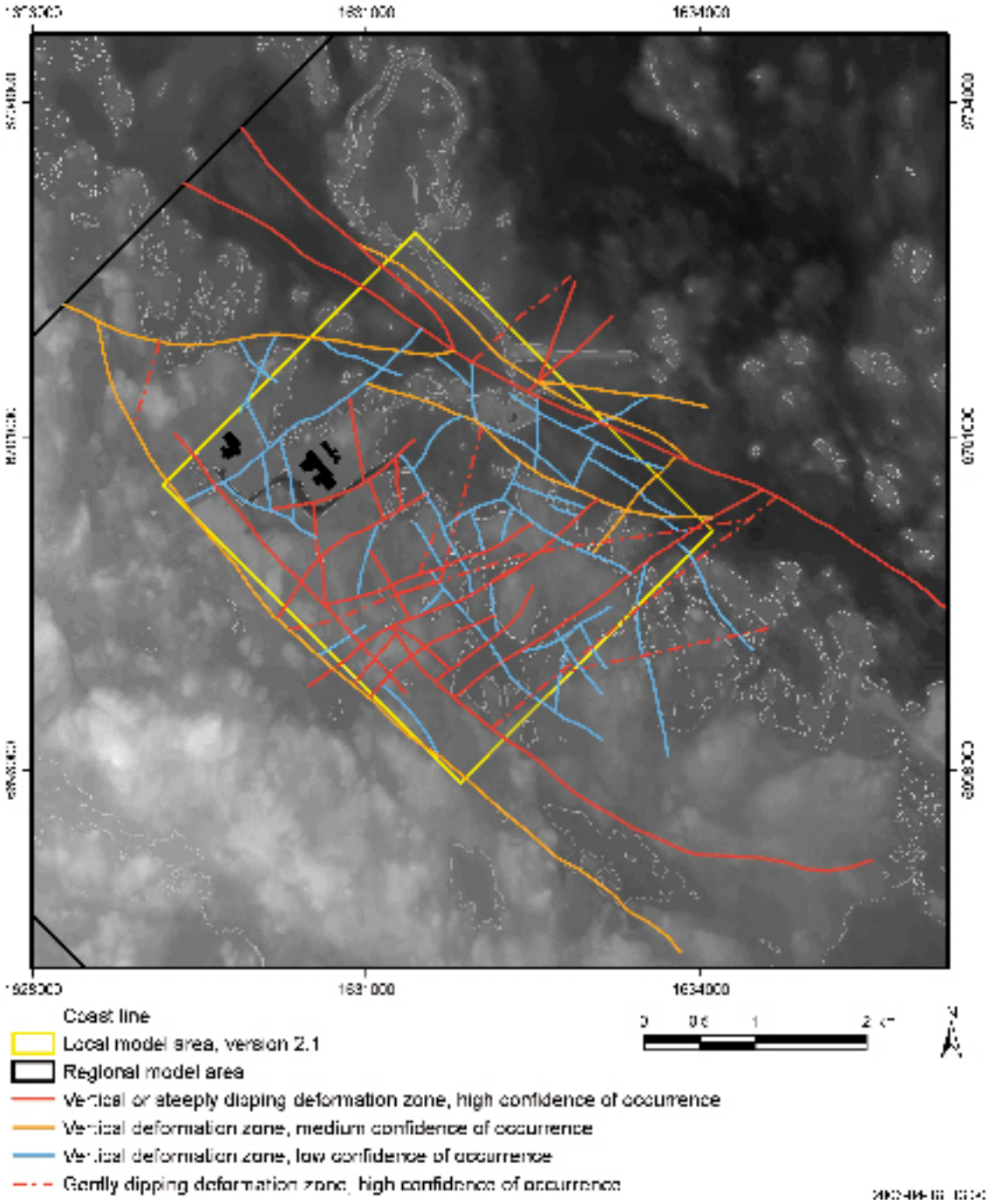

Figure 3-10. *Surface intersection of deformation zones in the local model area (version 2.1). The background corresponds to the digital elevation model for the site. Coordinates are provided using the RT90 (RAK) system.*

Table 3-5. Deformation zones in both the regional and local models. The steeply dipping zones in this table are all longer than 3,000 m. Zones of importance for the proposed repository layout are ZFMNE00A2, ZFMNE0060A and -B, ZFMNE0062A and -B, ZFMNW0123, and possibly the poorly constrained zone ZFMNE1195 (see comments in table).

Deformation zone ID	Confidence of occurrence	Basis for interpretation (for details, see Appendix 2)	Comment
Steeply dipping, WNW and NW zones			
ZFMNW0001 (Singö deformation zone)	High	Tunnels, borehole intersections, seismic refraction data, low magnetic lineament	Regionally important zone that is situated outside the target area at 400 m depth. New cored and percussion boreholes planned (see Chapter 6).
ZFMNW0002 (splay from Singö deformation zone through tunnel 3)	High	Tunnel, seismic refraction data, low magnetic lineament	Outside the target area at 400 m depth.
ZFMNW0017	Medium	Low magnetic lineament	Outside the target area at 400 m depth. Percussion drilling planned.
ZFMNW0123	High	Borehole intersection, low magnetic lineament	Intersects south-western corner of target area at 400 m depth. One inferred borehole intersection (KFM04A). Percussion drilling planned.
ZFMNW0137	Medium	Low magnetic lineament	Outside the target area at 400 m depth.
ZFMNW0809	Medium	Low magnetic lineament	Outside the target area at 400 m depth.
ZFMNW0835B	Medium	Low magnetic lineament	Outside the target area at 400 m depth.
ZFMNW1127	Medium	Low magnetic lineament	Outside the target area at 400 m depth.
ZFMNW1200	High	Borehole intersection, low magnetic lineament	Outside the target area at 400 m depth.
Steeply dipping, NE zones			
ZFMNE0060A	High	Borehole intersection, low magnetic lineament	Transects target area at 400 m depth. Inferred borehole intersections in KFM06A. New cored borehole planned (see Chapter 6).
ZFMNE0060B1	High	Borehole intersection	Transects target area at 400 m depth. Inferred borehole intersections in KFM06A. New cored borehole planned (see Chapter 6).
ZFMNE0060B2	High	Borehole intersection	Transects target area at 400 m depth. Inferred borehole intersections in KFM06A. New cored borehole planned (see Chapter 6).
ZFMNE0062A	High	Borehole intersection, low magnetic lineament	Together with ZFMNE00A2 forms the south-eastern border of the target area at 400 m depth. Inferred borehole intersections in KFM05A. Percussion drilling planned.
ZFMNE0062B1	High	Borehole intersection	Together with ZFMNE00A2 forms the south-eastern border of the target area at 400 m depth. Inferred borehole intersections in KFM05A. Percussion drilling planned.
ZFMNE0062B2	High	Borehole intersection	Together with ZFMNE00A2 forms the south-eastern border of the target area at 400 m depth. Inferred borehole intersections in KFM05A. Percussion drilling planned.
ZFMNE0808C	Medium	Low magnetic lineament	Outside the target area at 400 m depth.
Gently dipping zones			
ZFMNE00A1	Medium	Seismic reflector	Outside the target area at 400 m depth.
ZFMNE00A2	High	Borehole intersections, seismic reflector	Together with ZFMNE0062A forms the south-eastern border of the target area at 400 m depth. Inferred borehole intersections in several boreholes close to the surface and at c. 405–510 m depth in KFM02A. New cored boreholes planned (see Chapter 6).
ZFMNE00A3	High	Borehole intersections, seismic reflector	Outside the target area at 400 m depth.
ZFMNE00B4	High	Borehole intersections, seismic reflector	Outside the target area at 400 m depth.
ZFMNE0B23	Medium	Seismic reflector	Outside the target area at 400 m depth.
ZFMNS00B7	High	Borehole intersections, seismic reflector	Outside the target area at 400 m depth.
ZFMNE00B8	High	Borehole intersections, seismic reflector	Outside the target area at 400 m depth.

ZFMNE00J1	Medium	Seismic reflector	Outside the target area at 400 m depth.
ZFMNE0866	High	Borehole intersections	Outside the target area at 400 m depth.
ZFMNE0871 (Zone H2, SFR)	High	Tunnel, borehole intersections	Outside the target area at 400 m depth.
ZFMNE1194	High	Borehole intersections	Minor zone with predominantly sealed fractures that transects the western part of the target area at 400 m depth, between ZFMNE0061A and ZFMNW1200.
ZFMNE1195	High	Borehole intersections	Minor zone that is situated outside but close to the eastern part of the target area at 400 m depth. One inferred borehole intersection (KFM02A). Uncertain along-strike and down-dip extension.
ZFMNE1203	High	Borehole intersections	Outside the target area at 400 m depth.
ZFMNE1206	High	Borehole intersections	Outside the target area at 400 m depth.

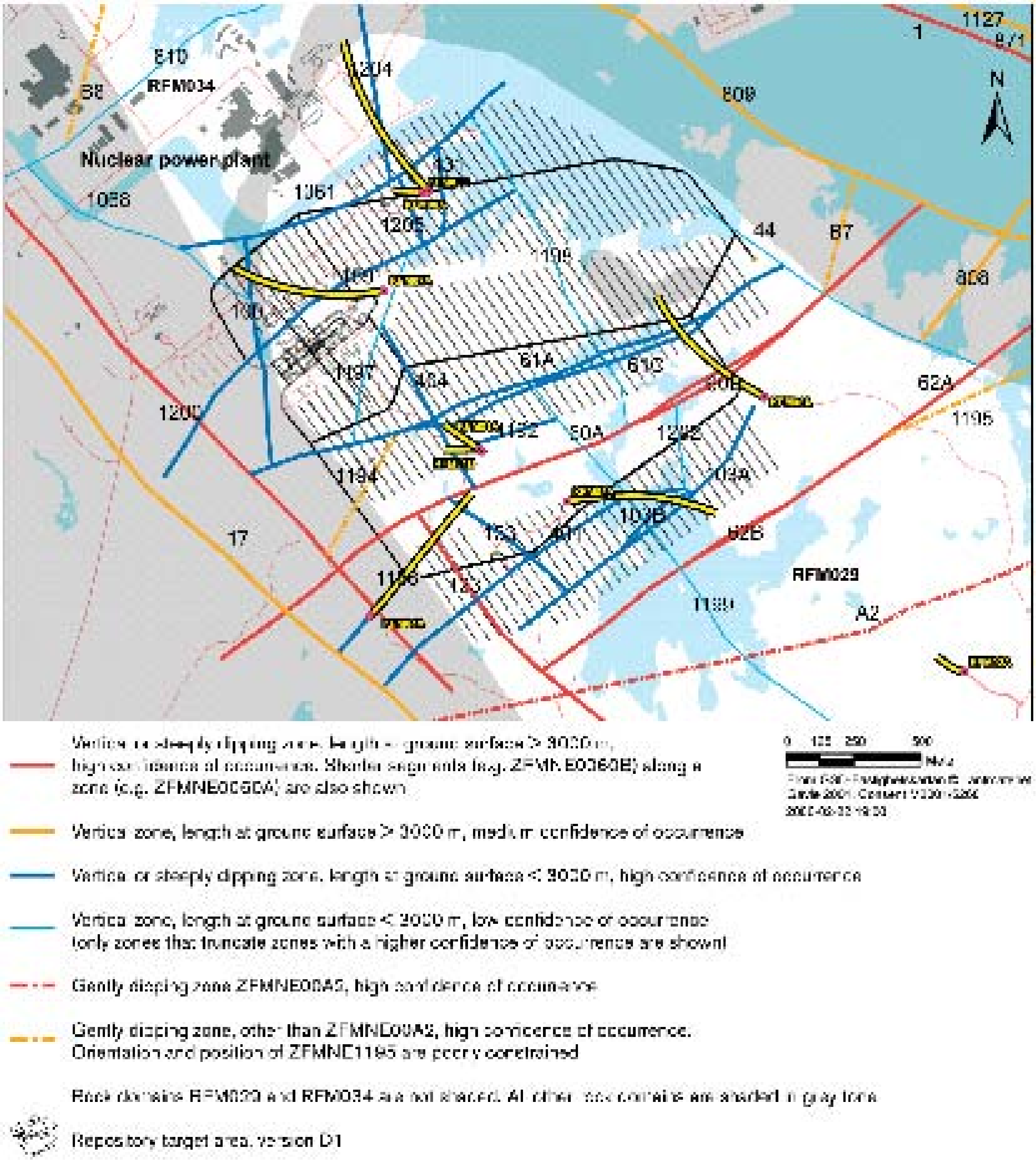

Figure 3-11. *Distribution of rock domains and deformation zones in the target area at 400 m depth within the local model volume (version 2.1).*

Gently dipping fracture zones

The gently dipping zones in the local model volume (Table 3-4) are addressed above in the discussion of the regional model.

3.2.5 Uncertainties

The following more significant uncertainties were noted after the development of the deterministic deformation zone model, version 1.2.

1. The presence of undetected deformation zones.
2. The character of the geological feature that is represented in an inferred lineament.
3. The length and down-dip extension, the dip and the thickness of deformation zones interpreted with the help of linked lineaments.
4. The length and down-dip extension, and the thickness of the gently dipping zones that are based, to a large extent, on the seismic reflection data.

More deformation zones are now present in the regional model volume compared to that in the SDM version 1.2 base model. However, a shorter cut-off length, 3,000 m rather than 4,000 m, has been adopted in the present model version and this accounts for the increase. The only changes of significance that have occurred inside the repository target area concern the presence of a high confidence zone longer than 3,000 m close to the south-western margin of the area (ZFMNW0123), and the occurrence of shorter, high confidence zones with NS strike, partly or entirely within the target area (e.g. ZFMNS0100). These considerations suggest that the occurrence of undetected deformation zones inside the repository target area that are longer than 3,000 m (point 1) is unlikely at this stage in the investigations.

Both the excavation work and the new boreholes analysed during modelling stage 2.1 have strengthened our understanding of the geological character of lineaments. However, they also demonstrate the difficulties to predict their character. Uncertainty remains for all the zones defined solely on the basis of lineaments and comparative studies and, for this reason, such zones continue to be classified as low confidence structures in the present model. The results of further excavation work and an extensive drilling programme across lineaments in the target area is planned for model version 2.2. It is anticipated that this programme will further diminish these uncertainties (point 2).

Many of the uncertainties in points 3 and 4 above remain. However, an analysis of all the surface seismic reflection data has provided better constraints on the extension of the gently dipping zones, both along strike and down dip (Appendix 2). For this reason, there is now a somewhat higher confidence in the truncation procedures for these zones. A study of the relationship between length and thickness of deformation zones has demonstrated a poor correlation between these two parameters, with a large variation in the thickness of a zone with a given length (Appendix 2). This feature once again demonstrates the major difficulties to establish the size of structures in the bedrock, when the degree of surface exposure is poor and only limited borehole data and a few profiles for the acquisition of seismic reflection data are available. In this respect, the estimates of the length of zones from the length of magnetic lineaments are more confident, as long as the correct inference has been made concerning the geological character of the lineament.

3.3 Rock mechanics properties

The rock mechanics studies during modelling stage 2.1 have been carried out with the purpose of:

- Reducing the uncertainties in the mechanical properties of intact rock and fractures regarding spatial and depth variations, homogeneity within rock domain RFM029 and the target area, variation between different fracture sets, and influence of the testing techniques.
- Reducing the uncertainties in the mechanical properties of the deformation zones by using the empirical and theoretical approach, including the identification and description of minor fracture/deformation zones not included in the earlier version 1.2 of the deterministic deformation zone model.

- Reducing the uncertainties in the rock stress field by analysing the structural geological model for the site and by modelling the three-dimensionality of the stress field at different scales.

The results of the analyses of the mechanical properties of intact rock and fractures are described in Section 2.5. The following sub-sections summarise the results of the analyses of the mechanical properties of the deformation zones and the rock stress modelling as obtained at the time of compilation of this report. More details are given in Appendix 3.

3.3.1 Mechanical properties of the rock mass – minor fracture/ deformation zones

The empirical characterisation of boreholes KFM01A, KFM02A, KFM03A and KFM04A conducted in version 1.2 /SKB 2005a/ shows that there are sections where the rock mass quality quantified by the empirical methods Q and RMR is comparable with that of the deterministic deformation zones. This indicates that there are features present in the rock, which were not included in the version 1.2 deterministic deformation zone model. In order to ensure mechanical stability of the rock surrounding a canister, the canister must not be deposited in a hole that is intersected by longer fractures or minor deformation zones. Therefore, attention has to be devoted to smaller structures in the rock mass along the boreholes where rock mass quality is low. The length of these structures might range from the length of a single fracture (typically some metres) to the length of the deterministic deformation zones (typically longer than 1 km in version 1.2 of the deformation zone model. It needs to be noted that a cut-off of 200 m has been employed in the local model version 2.1 for zones with varied degree of conficence of occurrence (see Section 3.2)).

Some limitations affect the determination of minor deformation zones from borehole information.

- Only the width of the intersection between a zone and a borehole is known. Furthermore, the empirical characterisation of the rock mass quality is performed in a discrete way (i.e. the length of the borehole sections along which the rock mass quality is determined is typically 5 m). For this reason, averaging processes of the local rock mass quality can lead to imprecision in the localisation of zones and in the estimation of their thickness.
- The width of the intersections gives a measure of apparent thickness of the zone since the zones are often inclined with respect to the borehole axis. Some methods are available for inferring the intersection angle (e.g. RAMAC – radar logging).
- There are uncertainties in the relation between the thickness and the trace length of the zones (see also Appendix 2). As a first approximation, the relation can be determined by plotting the length versus thickness of the deterministic deformation zones, and extrapolating it to the scale of relevance for minor zones. However, it needs to be demonstrated that the relation is scale independent and applicable for structures with a length as short as approximately 200 m.

Empirical modelling

The location of the minor deformation zones is determined by identifying all borehole sections where Q and RMR are smaller than certain thresholds. At Forsmark, these thresholds are assumed to be $Q < 10$ and $RMR < 65$. Contiguous sections are grouped together so that the apparent thickness of the zones can be estimated. Considering that the estimated thickness can only increase discretely, the thickness could be overestimated by about 25%.

By checking the radar reflectors in the loggings taken from the sections with low rock mass quality, the intersection angle with the borehole axis is determined. Locally, the uncertainty of this angle is estimated to be about ± 2°.

From the thickness and the trace length of all the deterministic deformation zones in the Forsmark SDM version 1.2, /Follin et al. 2005/ tested the correlation between thickness and trace length of the deterministic deformation zones. Figure 3-12 shows the resulting power-law fitting curve. This correlation is assumed to apply for the minor deformation zones. However, it should be noted that a corresponding plot between the trace length and thickness of the deformation zones in version 2.1 of the deformation zone model shows a poorer correlation (see Appendix 2). This new analysis had not been completed when the present work was carried out.

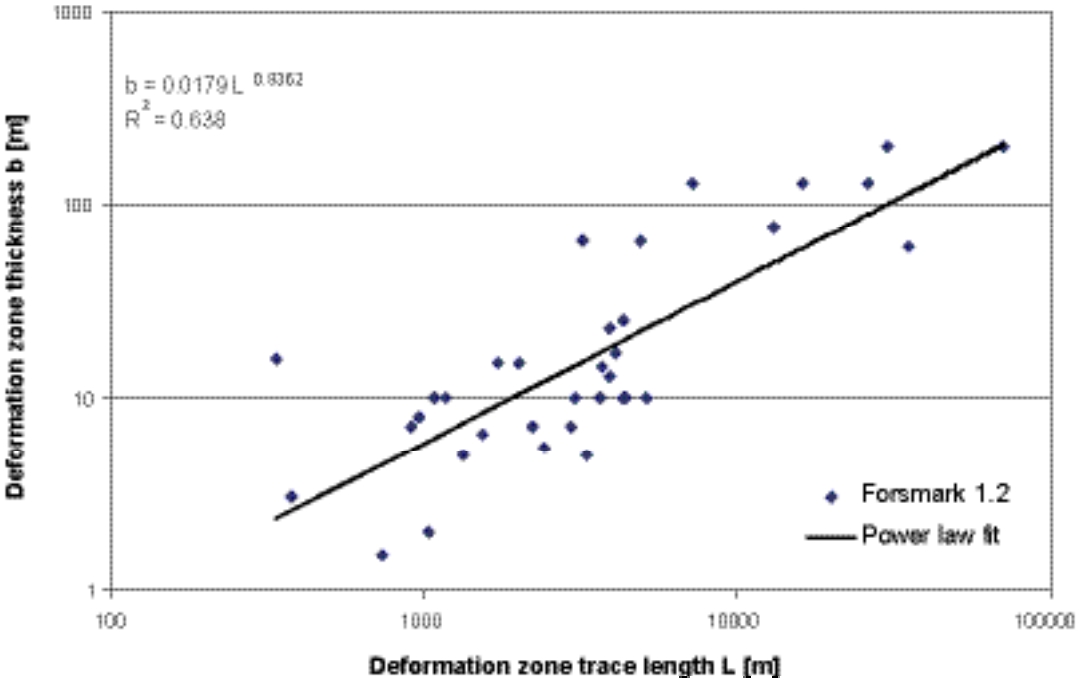

Figure 3-12. *Plot of the lineament trace length versus geological thickness of the deterministic deformation zones in the Forsmark SDM version 1.2 /Follin et al. 2005/.*

Applying the technique described above to the available data from the Forsmark local model volume (version 1.2) produces the results summarised in Table 3-6. Seven minor zones are identified in the four boreholes. One of these zones (ZFMNE1207) is now included in version 2.1 of the deterministic deformation zone model (see Section 3.2). The estimated thickness of these zones ranges between 2.5 and 7.5 m, with an average uncertainty of about ± 25%. The related estimated trace lengths obtained from the power-law fit in Figure 3-12 vary between 240 and 1,240 m. However, due to the uncertainty given above, the range of possible trace lengths could span between 160 and 1,700 m, which corresponds to an uncertainty of about ± 40% of the estimated length.

Figure 3-13 shows the location of the minor zones along the length of the boreholes as identified by means of the empirical rock mass quality ratings. It can be seen that the minor zones occur rather sporadically, and that the majority of them is located in the upper 300 m of the vertical boreholes. Above this depth, and outside the deterministic deformation zones, the spacing of these minor zones ranges between 20 and 200 m.

In Figure 3-14, the orientation of deterministic deformation zones intercepting the four analysed boreholes, as reported in /SKB 2005a/, is shown. Considering that the inclination of the boreholes is prevalently between 60° and 86°, the interception angle between the zones and the borehole axis would typically be 10°, 40° and 60°. Since the boreholes are rather steep, the interception angles between the boreholes and the deterministic deformation zones can be approximated by the intersection angles for the minor zones given in Table 3-6 and obtained by RAMAC radar loggings (revised values). Thus, in the boreholes, the minor zones seem to have roughly the same orientation as the deterministic deformation zones. These similarities support the assumption that the minor zones have geometrical properties similar to the deterministic zones and that the correlation between thickness and trace length for deterministic deformation zones should also apply to the minor zones. In other words, the minor zones can be considered as shorter zones in the same group as the deterministic deformation zones.

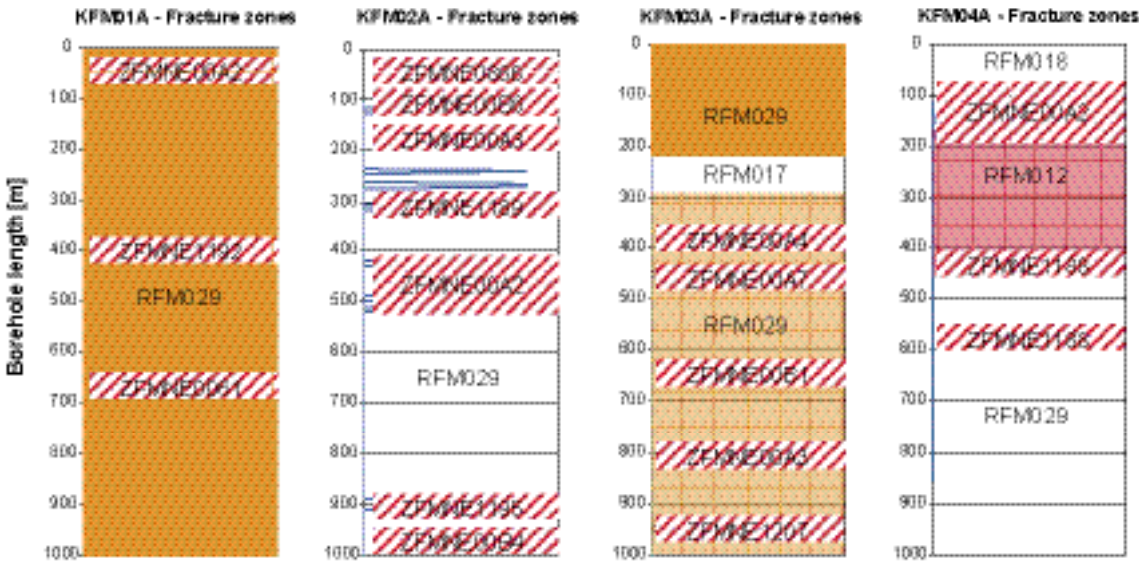

Figure 3-13. *Plot of the minor deformation zones identified by means of the empirical methods Q and RMR along the length of the boreholes (Q < 10 and/or RMR < 65). The deterministic deformation zones in version 2.1 are also indicated.*

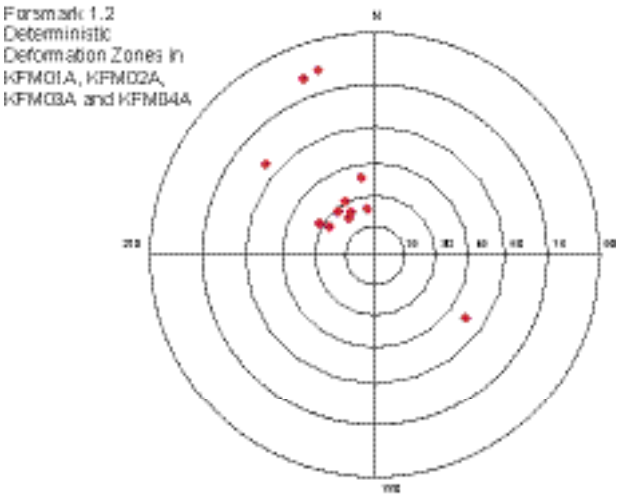

Figure 3-14. *Pole orientation of the deterministic deformation zones in borehole KFM01A, KFM02A, KFM03A and KFM04A (from /SKB 2005a/). Zone ZFMNE1207 is not plotted here.*

Despite the large uncertainty in the mechanical properties of the minor zones (e.g. deformation modulus, uniaxial compressive strength, cohesion and friction angle), the mean values do not vary very much from zone to zone and almost coincide with the properties of the deterministic deformation zones shorter than 10 km reported in Forsmark version 1.2 /SKB 2005a/. Only one zone in KFM02A (DZ4, 260–270 m) seems to have much poorer mechanical properties than the other zones. This zone is located within a section of vuggy metagranite /SKB 2005a/.

Theoretical modelling

One of the deformation zones in Table 3-6, ZFMNE1207 in KFM03A, as well as ZFMNE00A4, have been numerically modelled according to the methodology presented by /Olofsson and Fredriksson 2005/. An empirical characterisation of zone ZFMNE00A4 was made in version 1.2 of the Forsmark SDM /SKB 2005a/, but no theoretical modelling of the behaviour of the zone was undertaken at that time. Since the theoretical methodology is designed for characterisation of the

Table 3-6. Summary of the geometrical properties of the minor zones identified by means of the empirical methods Q and RMR: fracture sets, zone intersection with the borehole axis, estimated thickness and trace length. Zone DZ5 in KFM03A is now included in the deformation zone model version 2.1 (see Section 3.2).

Borehole	Borehole length	Fracture sets	Intersection angle	Estimated thickness	Estimated trace length
KFM01A	155–175 m	145/36, 104/02	22°	6 m (4–7 m)	970 m (660–1,225 m)
(inclination 85°)	230–235 m	013/40, 054/11	40°	2.5 m (1.5–3 m)	240 m (160–315 m)
KFM02A	235–240 m	344/86, 347/14	50°	3 m (2–4 m)	434 m (275–590 m)
(inclination 85°)	260–270 m (DZ4)	027/18	67°	7 m (4.5–9 m)	1,240 m (775–1,715 m)
KFM03A	105–110 m	295/80, 040/29	50°	3 m (2–3.5 m)	435 m (275–590 m)
(inclination 86°)	940–950 m (DZ5 = ZFMNE1207)	046/76, 031/10	76°	7.5 m (5–9.5 m)	1,320 m (820–1,840 m)
KFM04A (inclination 60°)	140–145 m	141/85, 233/74, 311/06	40°	2.5 m (1.7–3 m)	350 m (225–471 m)

bedrock outside the deformation zones, it has been necessary to make some adjustments, especially concerning the generation of fracture networks. Currently, no DFN model is available for the deformation zones due to the scarcity of the available fracture data. To overcome this problem, it has been assumed that the fracture sets recognized in rock domain RFM029 /LaPointe et al. 2005/ also describe the orientation of the fractures in the deformation zones. Furthermore, the fracture frequency within the deformation zones is often higher than in the rest of the rock mass and has, therefore, been increased based on the available local borehole information. The following procedure has been followed to overcome the limitations:

- The fractures mapped within the deformation zones were assigned to the different fracture sets by using the hard sector technique applied to the Boremap data from RFM029 (Figure 3-15, left).
- The target P_{10} for each fracture set within the deformation zones was calculated based on the Boremap data.
- A number of realisations of the DFN model with different P_{32} was produced and sampled by means of synthetic boreholes to determine the relation between P_{10} and P_{32}.
- The value of P_{32} that gives the P_{10} observed for each fracture set in the Boremap data was determined (Figure 3-15, right).

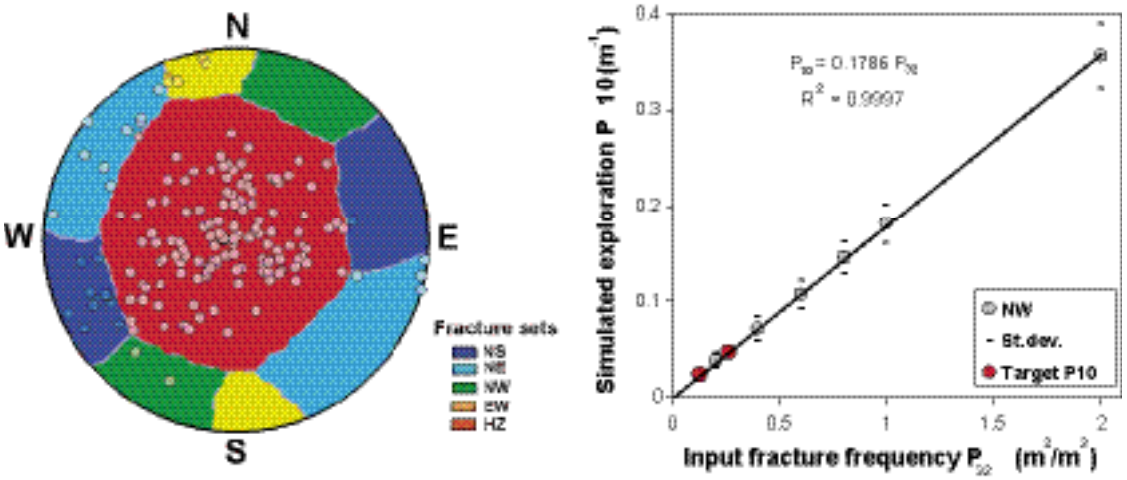

Figure 3-15. *Hard fracture set sector assignation of the fractures within deformation zone ZFM-NE00A4 in KFM03A (left) and relation between P_{32} in the DFN realisations and the target P_{10} obtained from the Boremap data for the same zone (right).*

All the other DFN parameters (e.g. minimum fracture radius, exponent of the size distribution, and orientation) were also taken from Table 9-1 in /LaPointe et al. 2005/. The results reported here are obtained using the values of the mechanical properties evaluated for intact rock and fractures reported in Section 2.5.1 and 2.5.2, respectively.

Twenty 3D realisations of the fracture network were produced with the DFN model adapted to the deformation zones (Figure 3-16). From these realisations, twenty vertical and planar cross sections were generated in the direction parallel to the maximum principal stress at Forsmark /SKB 2005a/. Examples are shown in Figure 3-16. In the code 3DEC, these cross-sections were represented by 1 m thick slices. Loading of the models was carried out by assigning lateral boundary stresses and by moving the upper boundary of the model downward at constant velocity, in "plane strain" conditions.

The numerical models were used to analyse deformability, by calculating the equivalent deformation modulus and Poisson's ratio (Figure 3-17), and strength, by determining the maximum vertical stress calculated by the models for each level of lateral confining stress. Thirteen out of the twenty simulations were considered in the analysis of the mechanical properties of the rock mass, since seven of the configurations failed to provide stable numerical 3DEC results.

The results of the numerical modelling are summarised in Table 3-7 and Table 3-8, where the strength parameters are given in terms of equivalent cohesion and friction angle of the rock mass for a certain range of confinement stress. From the strength envelope obtained by the different models, RMR can be back-calculated according to the relation between the Hoek and Brown's Criterion /Hoek et al. 2002/, the Geological Strength Index and RMR /Hoek and Brown 1997/. Table 3-7 and Table 3-8 also show that ZFMNE00A4 has slightly better equivalent mechanical properties than ZFMNE1207.

Figure 3-17 shows the influence of the confinement stress on the equivalent deformation modulus and Poisson's ratio of the rock mass obtained by numerical modelling. The increase of the deformation modulus with an increase of the confining stress is in agreement with the description of the deformation modulus provided in Forsmark and Simpevarp SDM version 1.2 /SKB 2005ae/. However, the variation of the Poisson's ratio differs. In version 1.2, an increase of the Poisson's ratio as the confinement stress increases was reported rather than a decrease as shown in Figure 3-17 (lower). Although values of the Poisson's ratio in the range of 0.35 and 0.55 appear to be rather high compared to the values usually used in engineering practice, the issue has not been resolved at the time of completion of this report.

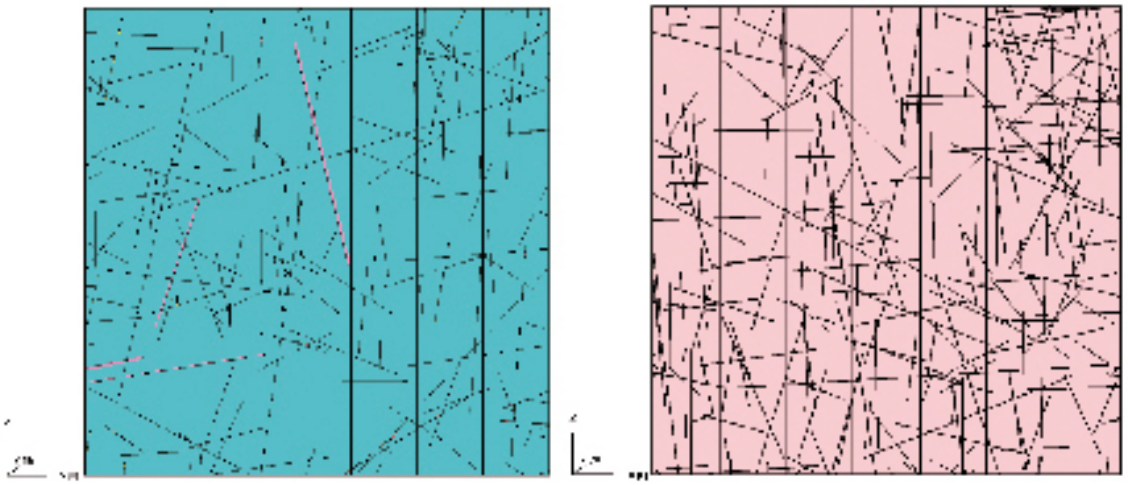

Figure 3-16. *Example of fracture pattern for ZFMNE00A4 in KFM03A (left) and for ZFMNE1207 in KFM03A (right).*

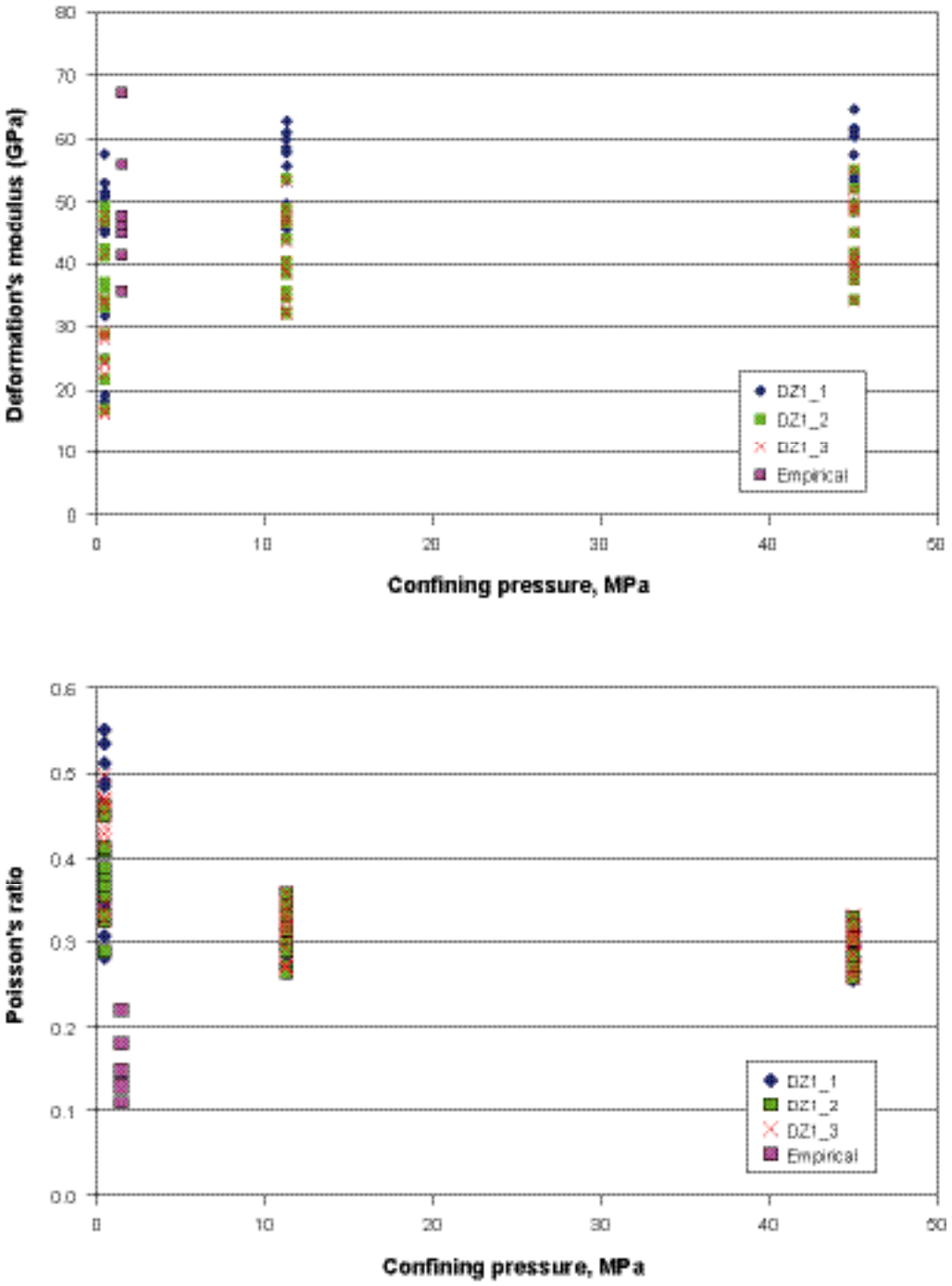

Figure 3-17. *Variation of the equivalent deformation modulus (upper) and Poisson's ratio (lower) as a function of the confining stress obtained by empirical methods and numerical simulation of the rock mass as within zone ZFMNE1207 (DZ1) in KFM03A.*

Table 3-7. Summary of the deformability parameters of deformation zone ZFMNE00A4 and ZFMNE1207 in KFM03A obtained by empirical estimation and numerical modelling for low confinement stress.

	ZFMNE00A4 – KFM03A				ZFMNE1207 – KFM03A			
	Empirical[1]		Numerical[2]		Empirical[1]		Numerical[2]	
	Mean/ St. dev.	Possible Min–Max	Mean/ St. dev.	Possible Min–Max	Mean/ St. dev.	Possible Min–Max	Mean/ St. dev.	Possible Min–Max
E_m (GPa)	48.0/9.0	12.2–85.0	40.8/13.7	18.3–57.6	45.1	15.2–85.0	33.1/8.3	20.9–54.8
ν_m (–)	0.15/0.03	0.05–0.31	0.41/0.09	0.28–0.55	0.14	0.06–0.31	0.45/0.06	0.33–0.54

[1] for confinement stress of about 1.5 MPa.
[2] for confinement stress of 0.5 MPa.

Table 3-8. Summary of the strength of deformation zones ZFMNE00A4 and ZFMNE1207 in KFM03A obtained by empirical estimation and numerical modelling.

	ZFMNE00A4 – KFM03A				ZFMNE1207 – KFM03A			
	Empirical[1]		Numerical[2]		Empirical[1]		Numerical[2]	
	Mean/ St. dev.	Possible Min–Max	Mean/ St. dev.	Possible Min–Max	Mean/ St. dev.	Possible Min–Max	Mean/ St. dev.	Possible Min–Max
c_m (MPa)	20/1.1	11–35	14.5/4.5	5.5–21	20	12–32	12.5/3.4	7.6–21
ϕ_m (°)	47/0.8	32–55	52.1/3.0	46–55	46	34–54	49.7/2.7	43–54
RMR	77/3.1	54–93	78.1/9.4	64–91	76	57–90	74.8/8.3	56–91

[1] for confinement stresses between 10 and 30 MPa.
[2] for confinement stresses between 0.5 and 45 MPa.

Another important aspect concerns the effect of the fracture normal stiffness on the numerical results. In fact, as reported in Section 2.5.2, due to a change in the laboratory testing technique, the obtained new stiffness values are about 6–8 times larger than the values reported in SDM version 1.2 /SKB 2005a/. The consequence of this change is that some of the strength (friction angle) and deformability parameters (Poisson's ratio) obtained by numerical modelling of the deformation zones approach the results reported in version 1.2 for the competent rock, despite that the rock mass quality in the zones is poorer than for the competent rock.

Comparison of the empirical and theoretical modelling results

When comparing the results of the empirical and numerical methods, it should be remembered that the available data on minor zones is rather scarce. Thus, i) the empirical evaluation is made for a few short sections of a borehole, and ii) the DFN model is extrapolated from a model derived for the rock outside the deformation zones. Thus, the representativity of the results cannot be guaranteed.

This study is a first attempt, within the frame of site descriptive modelling, to correlate the deformability and strength properties of the deformation zones obtained by empirical estimations with those obtained by numerical modelling. Since some of the results were obtained for comparably low stress conditions (0.5–1.5 MPa), a comparison of the equivalent deformation modulus, Poisson's ratio, friction angle and cohesion can be made.

Table 3-7 shows the deformability parameters for ZFMNE00A4 and ZFMNE1207. Both these simulations were obtained by assuming the average mechanical properties of the intact rock and rock fractures, as reported in Section 2.5, and by modelling a series of fracture patterns.

The deformation modulus obtained from the empirical method is between 17 and 36% higher than that obtained by numerical modelling (Figure 3-17, upper). Despite this difference, the ranges of possible variation in this parameter obtained by the two methods are in good agreement. For the Poisson's ratio (Figure 3-17, lower), there seems to be a larger discrepancy because the range of possible variation obtained by one method does not overlap the mean value obtained by the other method.

The discrepancy in the Poisson's ratio can be explained by the relation between the particular fracture pattern at the site (as shown in Figure 3-16) and the direction along which the Poisson's ratio is calculated with respect to the loading direction.

- If loading is exercised parallel to the average fracture planes, it is expected that the Poisson's ratio will decrease by increasing the confinement stress. This hypothesis would coincide with the numerical modelling results.
- If, instead, loading is exercised with an angle with respect to the fracture planes, the Poisson's ratio is expected to increase by increasing the confinement stress. This hypothesis could relate to the results of the empirical methods, where the direction of loading is not explicitly given.

Thus, it cannot be excluded that the results of both methods are realistic, but associated with different loading directions. This also leads to the conclusion that the equivalent Poisson's ratio of the rock mass might be anisotropic (see also /Min 2004/). This possibility is not covered by the assumptions presently made in modelling stage 2.1 on the behaviour of the rock mass as an equivalent medium (elastic and isotropic). In conclusion, both the directional variations of the Poisson's ratio listed above are accounted for by assigning a wide range of variation of the Poisson's ratio. Otherwise, a more sophisticated model that describes the directional variation of this parameter has to be adopted.

The strength parameters of the deformation zones from empirical and numerical results are summarised in Table 3-8, where the values of the equivalent cohesion and friction angle are given. Moreover, the empirically determined RMR values are flanked by the RMR obtained by back-calculation of the numerical modelling results of rock mass strength.

For the overlapping range of confinement stress, the Coulomb's Criterion from the empirical and numerical methods almost coincide (Figure 3-18). A very good agreement can also be observed when comparing the RMR values obtained by the two methods.

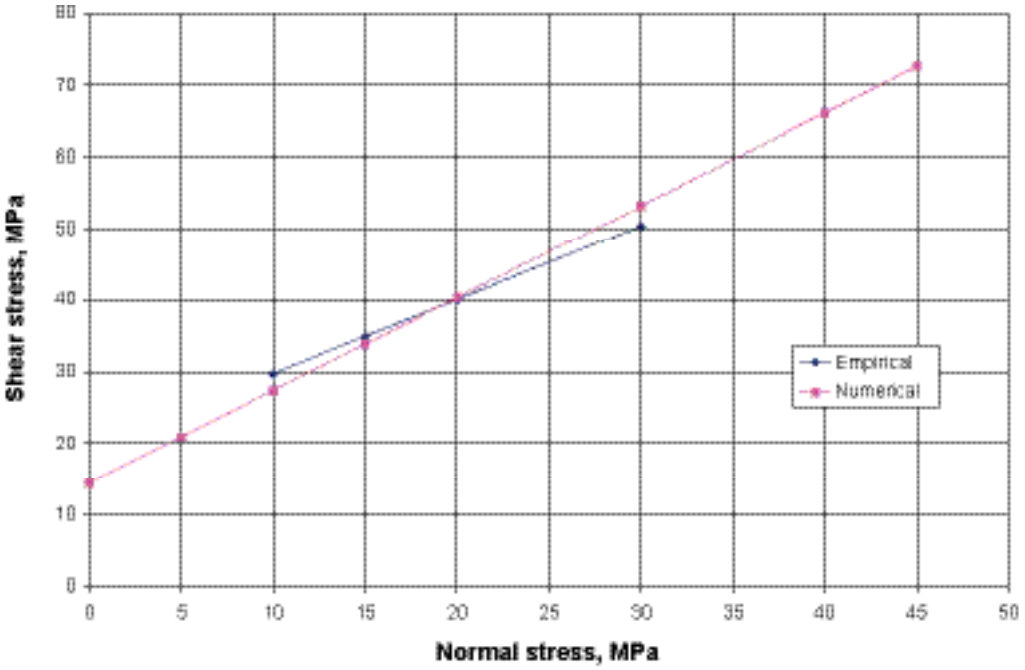

Figure 3-18. *Comparison of the empirical and numerical Coulomb's failure criterion for deformation zone ZFMNE1207 in KFM03A.*

The uncertainty of the values of the parameters for the deformation zones given in Table 3-7 and Table 3-8 almost coincide with that determined in the Forsmark SDM version 1.2 /SKB 2005a/, which was based on a larger data set. This results in an uncertainty of the deformation modulus and Poisson's ratio of about ± 40%, and of the cohesion and the friction angle of about ± 40% and about ± 14%, respectively.

3.3.2 Modelling of in situ stress

Based on the status of the structural geological investigations reported in version 1.1 of the Forsmark SDM /SKB 2004/ and in parallel with the at-the-time ongoing investigations later reported in version 1.2 /SKB 2005a/, a pre-study of the rock stress field at Forsmark was carried out /Mas Ivars and Hakami 2005/. The aim of that study was to investigate how two site-specific features, the existence of a central "tectonic lens" between the Singö and Forsmark deformation zones and the presence of a gently dipping deformation zone (ZFMNE00A2), would influence the stress field at the site. This study is currently being re-evaluated in order to identify which features have to be included and what geometrical layout should be given to the planned detailed numerical modelling of the site. The modelling will address the following aspects:

- Evaluate the current state of knowledge regarding the structural geology of the site from a rock mechanics standpoint.
- Establish complementary numerical investigations focusing on the influential site-specific features, for example the sub-horizontal fractures in the uppermost 200–300 m of the bedrock.
- Analyse the effect of those features, transformed into numerical entities, on the global stress model of the site.
- Provide a new stress field model for the Forsmark site.

The work comprises the conversion of the current working concepts for the formation and reactivation of different sets of deformation zones at Forsmark, as illustrated in Figure 3-4 to Figure 3-6, and the division of the bedrock into fracture domains, as illustrated in Figure 3-7, into a three-dimensional model that can explain the actual stress field. This important aspect calls upon an introductory numerical investigation to find out how changes in the direction of the major principal stress over geological times would relate to the direction of the inferred shearing along the major discontinuities at the site. Hopefully, an adequate relation will be found.

More studies are to be conducted in order to identify the critical aspects and the sources of uncertainties affecting the rock stress field determination. Furthermore, the vertical sections of the structural geological model have to be transformed into viable rock mechanics features entering the numerical simulations. Numerical modelling may even necessitate the inclusion of depths beyond 1,000 m and the uncertainty in the orientation of the deformation zones. Plausible extrapolations may be needed and this may be done by resorting to the findings from geophysical investigations or consulting the regional geological maps.

3.3.3 Summary

In modelling stage 2.1, the focus of the rock mechanics analyses and modelling work has been on special topics remaining from the work with previous model versions as well as on issues arising as a result of the progress in developing an integrated understanding of the site and as a result of the repository design work.

One improvement during modelling stage 2.1 concerns the size of the data sets of the mechanical properties of the intact rock and fractures, and the way these sets are analysed. The new data on mechanical properties have been analysed by studying the variation with rock type, depth, degree of alteration and orientation. In summary, some differences in the properties of the intact rock and rock fractures from the rock mass in the upper 200 m have been observed. It is also concluded that some subordinate rock types remain to be tested and that a representative set of samples should be selected (e.g. pegmatite, granodiorite, amphibolite). The stress-strain curves for granite and granodiorite show that most of the samples behave in a brittle way, and that this can be assigned to "class II" behaviour.

More representative samples for some of the fracture sets at the site (sub-vertical EW and sub-horizontal) are also needed. Although still based on few samples from the deformation zones, the results show that the difference in properties between samples taken within and outside the deformation zones appears to be negligible. This can be explained by the fact that sampling of the deformation zones was not intentional, and when it happened, it was performed to reflect the properties of the fractures outside the zones, thus probably ignoring most of the altered, clay-infilled and multiple fractures that are more common inside the deformation zones.

Minor deformation zones, both included and not included in version 2.1 of the deformation zone model and intercepting borehole KFM01A, KFM02A, KFM03A, and KFM04A, have been analysed from an empirical point of view. Based on the relation between the thickness and the trace length of zones provided in version 1.2, an attempt has been made to estimate the trace length of the minor zones.

The determination of the mechanical properties of the minor zones by empirical methods (Q and RMR) and by numerical simulation of a series of fracture patterns gives results that are in good agreement, especially for strength at confining stresses between 10 and 30 MPa. The analyses of the deformational properties seem to indicate that there is a certain influence of the orientation of loading with respect to the fracture orientation that might require an anisotropic description of the equivalent deformation modulus and Poisson's ratio. At this stage of the site descriptive modelling work, possible directional properties are handled by widening the range of variation in the parameter values to be able to include the suspected anisotropy depending on the angle between the fracture planes and the loading direction.

The numerical study on the mechanical properties of the deformation zones provides information about the variation of the deformability properties of the rock mass with increasing confinement stress, and thus, with increasing depth. This aspect is very important for the modelling of the rock stresses at the site. In fact, the displacements along the major deformation zones determines the stress redistributions and stress gradients. Thus, the modelling has to involve larger depth than those usually observable in the boreholes. By knowing the behaviour of the deformation zones with depth/high stresses, prediction of the stresses at the site can be made by numerical modelling.

Ongoing rock stress modelling addresses various topics to seek support for the current conceptual models for the formation and reactivation of deformation zones and fracture domains at the site. Regional modelling will be carried out in order to test the hypothesis of a strike-slip regime for the formation of the regional deformation zones. In addition, numerical modelling of the rock stresses will be attempted based on the regional deformation zone model version 2.1, to study the local variation of the stresses induced by the deformation zones in the target area. This reconnects to the problem of scale dependency of the rock mass material properties. Although aware of the influence of scale on the mechanical properties at Forsmark, no further steps have yet been taken, awaiting potential requirements arising from the repository design applications.

Most of the described rock mechanics activities were already completed at the time of compilation of this report, whereas others are planned and will be reported separately or included in stage 2.2 of the Forsmark site descriptive modelling.

3.4 Thermal properties

3.4.1 Rock type models: evaluation of model version 1.2

In model version 1.2 /Sundberg et al. 2005/, rock type models of thermal conductivity were produced by combining the available data from TPS measurements and SCA calculations. The rock type models used in version 1.2 were examined in the light of the new data made available in version 2.1, and a judgement was made as to whether the models required revision, see Table 3-9.

The most important conclusions of this verification process are as follows.

- A model based on 4 SCA values can be established for amphibolite (102017). With only one sample available in version 1.2, this was not previously possible.
- The model for aplitic granite (101058) used in version 1.2 should be modified.

Table 3-9. Model properties (normal distributed) of thermal conductivity (W/(m·K)) for rock types according to model version 1.2. TPS and SCA refer to the type of data used as a basis for the models. Comments refer to impact of new data on models.

Rock code (type)	Rock models, version 1.2	Arithmetic mean	St. dev.	Comments
101057 (granite to granodiorite)	TPS+SCA	3.63	0.22	
101056 (granodiorite)	TPS+SCA	3.10	0.15	
101054 (tonalite to granodiorite)	TPS+SCA	2.96	0.41	
101051 (granite, granodiorite and tonalite)	TPS+SCA	3.02	0.31	Still large uncertainty; see discussion below.
101061 (pegmatite, pegmatitic granite)	SCA	3.54	0.12	
103076 (felsic to inter-mediate volcanic rock)	SCA	3.01	0.37	
101058 (granite, metamorohic, aplitic)	SCA	3.47	0.12	New data requires revised model. Mean = 3.79, std. dev. = 0.27.
111058 (granite, fine- to medium-grained)	SCA	3.35	0.05	
101033 (diorite, quartz diorite and gabbro)	TPS+SCA	2.33	0.16	
102017 (amphibolite)	No model			New data allows construction of a model. Mean 2.41 W/(m·K), std. dev. 0.08 W/(m·K).

- The rock type models for the other rock types are judged not to require significant modification in the light of the new data.
- The reliability of some rock type models, e.g. for granite, granodiorite and tonalite (101051), is still fairly low, see discussion below.

The model used for granite, granodiorite and tonalite (101051) in model version 1.2 was established using results of both TPS measurements and SCA calculations. However, there are some uncertainties concerning the reliability of the data used for the rock type model, a situation that has not improved with the limited amount of additional data obtained within data freeze 2.1. Firstly, the representativity of TPS data is very poor, there being only three TPS data values available, all from samples from the same 1 m borehole section. Secondly, there is a question of reliability concerning the more plentiful SCA data (25 samples, Table 2-13). The lowest SCA value (2.61 W/(m·K)) is higher than all three of the TPS values (Figure 3-19). Furthermore, a comparison of one sample for which both measured (TPS) and calculated (SCA) values are available shows a large deviation, 2.47 W/(m·K) and 3.15 W/(m·K), respectively. Given the compositional diversity inherent in this rock type, from granite through granodiorite to tonalite, a correspondingly large range in thermal conductivities is to be expected. It should be noted that the three samples measured by the TPS method come from borehole KFM03A, which lies outside the local model area, as defined by model version 2.1. A thin-section analysis of a sample from KFM03A /Petersson et al. 2004/ indicates a more tonalitic composition, which suggests that this borehole may not be representative with respect to rock type 101051.

3.4.2 Thermal properties at domain level

Rock domain model

The rock domain model version 2.1 (see 3.1) forms the basis for the following discussion concerning the thermal properties of the rock mass within the local model volume at Forsmark. Thermal properties of four rock domains within the Forsmark area are evaluated within modelling stage 2.1; domains RFM029, RFM012, RFM044 and RFM045 (Figure 3-2). Domain RFM029 makes up the major part of the local model volume and will constitute the bulk of any future repository volume. The much smaller domain RFM045 is also located within the candidate volume. Domains RFM012 and RFM044 are marginal to domain RFM029 and, although within the local model volume, are unlikely to impact on the repository volume. A lithological domain classification of borehole intervals is presented in Table 3-10.The dominating rock type in domains RFM029, RFM012 and RFM044 is granite to granodiorite (101057). In domain RFM045, the dominating rock type is aplitic granite (101058). For a more detailed description of the rock type composition in the different domains, see Table 3-2.

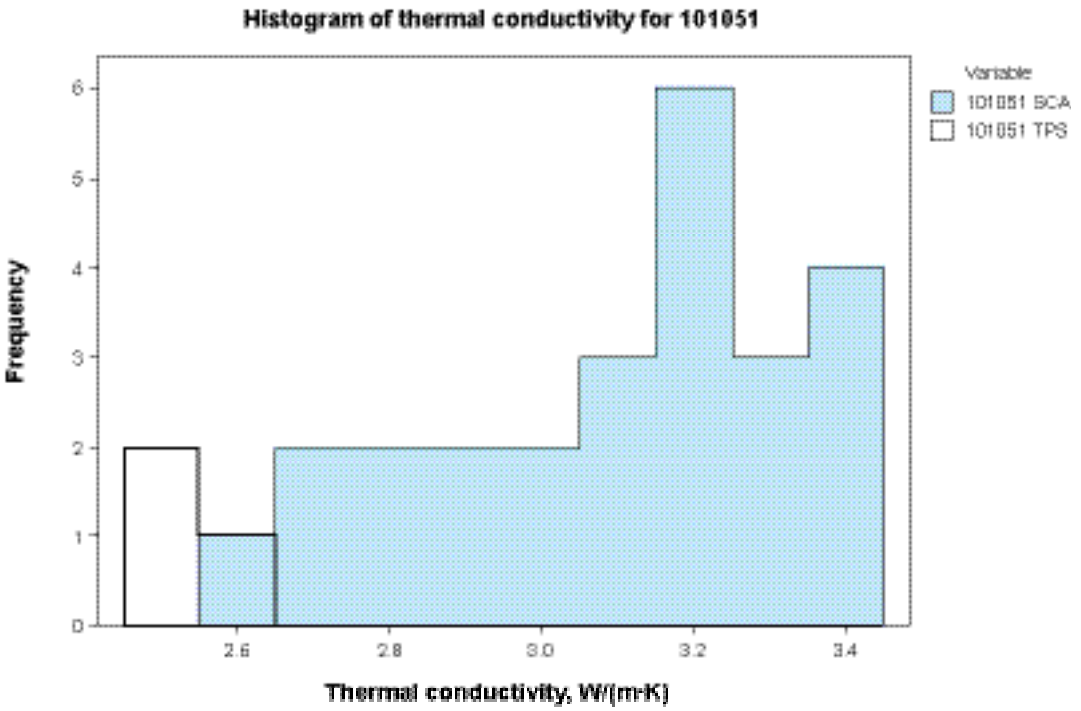

Figure 3-19. *Histogram of thermal conductivities for rock type 101051 showing both TPS and SCA data.*

Table 3-10. Boreholes classified by domain (see Appendix 2).

Domain	Dominant rock type	Borehole
RFM029	Granite to granodiorite (101057)	KFM01A
		KFM02A
		KFM03A, 102–220 m and 293–1,000 m
		KFM04A, 500–1,001.5 m
		KFM05A
		KFM06A, 102–751 m and 966–998 m
		KFM07A, 102–793 m
		KFM08A, 102–781 m
RFM012	Granite to granodiorite (101057)	KFM04A 177–500 m
RFM018	Tonalite to granodiorite (101054)	KFM04A 12–177 m
RFM044		KFM07A, 793–999 m
RFM045		KFM06A, 751–966 m

New boreholes in red.

Method

Modelling of the thermal transport properties of the rock domains has not been performed as part of version 2.1. However, for each domain a judgement of the thermal conductivity distribution has been made based on the new data together with the results of the modelling efforts made in model version 1.2 /Sundberg et al. 2005/.

For model version 2.1, the thermal conductivity properties at domain level were assessed in the following way.

- The rock type models used in model version 1.2 were evaluated in the light of the new TPS and SCA data, and new rock type models was constructed for amphibolite (102017) and aplitic granite (101058), see Table 3-9.

- The rock type abundances for domains RFM029, RFM044 and RFM045 in boreholes KFM05A–08A were approximated and for domain RFM029 compared to those based on the boreholes used in version 1.2.
- Based on the rock type models and rock type abundances, the thermal conductivity distributions of these domains were approximated.

Judgement of domain properties

Domain RFM029 makes up the greater part of the rock mass within the local model volume and is represented in all investigated boreholes. The dominant rock type, granite to granodiorite (101057), makes up approximately 75% of this domain. Other important rock types are granite, granodiorite and tonalite (101051), pegmatite (101061) and amphibolite (102017). A comparison of updated rock type abundances based on all available boreholes (Table 3-2) with results from boreholes available in model version 1.2 /Sundberg et al. 2005/ shows only small differences. The main discrepancy is a slightly lower proportion of granite, granodiorite and tonalite (101051) in the local volume version 2.1 relative to version 1.2. Therefore, these new boreholes are unlikely to significantly change the outcome of thermal modelling as presented in model version 1.2. On the other hand, one important subordinate rock type, amphibolite, was, due to lack of data, not included in the previous modelling versions. Incorporating this rock type, which compared to other rock types within domain RFM029 has considerably lower thermal conductivity (mean: 2.41 W/(m·K)), may have an important impact on the modelling results.

Domain RFM012 outcrops along the western margin of the local model area and is represented by section 177–500 m in borehole KFM04A. Domain RFM012 is, in common with domain KFM029, dominated by granite to granodiorite (101057), but includes a greater proportion of granite, granodiorite and tonalite (101051) /Sundberg et al. 2005/. There are no new borehole data for domain RFM012 in the newly available boreholes. However, once again, amphibolite, an important subordinate rock type in domain RFM012, must be incorporated into thermal modelling.

Thermal modelling was performed for both domain RFM012 and domain RFM029 in model version 1.2 /Sundberg et al. 2005/. The main modelling approach did not take into account spatial variability within rock types, so this was estimated separately for the dominant rock type, 101057, and added to the between rock variability. The results at the 0.7 m scale for model version 1.2 are summarised in Table 3-11.

Limited modelling work was performed for domains RFM029 and RFM012 using only the boreholes modelled in version 1.2 but, this time, incorporating a rock type model for amphibolite, which comprises about 5% of the rock volume in the above domains. At the 0.8 m scale, the mean thermal conductivities are somewhat lower (about 0.1 W/(m·K)) and standard deviations considerably larger than the results given in version 1.2, see Table 3-11. Based on one realisation only, it is speculated that the 2.5 percentiles may be up to 0.3 W/(m·K) lower than that reported in version 1.2, whereas the upper tail percentiles remain essentially unchanged.

Domain RFM045 is represented by a c. 200 m long borehole section (751–966 m) in KFM06A. The dominant rock type in domain RFM045 is aplitic granite (101058), which occurs both as altered (albitized) and unaltered varieties. This domain, new for model version 2.1, has been identified within the local model volume only, and not in the regional model volume. No thermal modelling

Table 3-11. Mean and standard deviation of thermal conductivity (W/(m·K)) for domains RFM029 and RFM012 according to model version 1.2. Also given are the adopted 2.5 and 97.5 percentiles of thermal conductivity (W/(m·K)). Comments refer to impact of incorporating a rock type model for amphibolite.

Domain	Scale (m)	Arithmetic mean	St. dev.	2.5 percentiles	97.5 percentiles	Comment
RFM029	0.7	3.55	0.22	2.9	3.8	Lower mean, lower 2.5 percentiles
RFM012	0.7	3.46	0.28	2.9	3.8	Lower mean, lower 2.5 percentiles

has been performed for this domain, either as part of this version or previous versions. Nevertheless, a judgement of the thermal conductivity distribution of this domain is attempted based on rock type abundances (Table 3-2) and summary statistics of thermal conductivity for the different rock types making up this domain (Table 3-9). The mean thermal conductivity is judged to be between 3.5 and 3.7 W/(m·K). With reservation for rock type 101051, which makes up less than 5% of the domain, rock types with low thermal conductivities, for example amphibolite, are absent as occurrences thicker than 1 m.

Domain RFM044 occurs in borehole KFM07A between 793 and 999 m in the north-western part of the local model volume. The dominant rock type is granite to granodiorite (101057). Subordinate rock types are pegmatite and amphibolite (see Table 3-2). Domain RFM045 is considered to be lithologically similar to domain RFM029, but differs from this domain with respect to its stronger degree of ductile deformation (see 3.1). The stronger penetrative fabric within this domain may produce a greater anisotropy in thermal properties. No modelling has been performed, but it is reasonable to assume that the mean thermal conductivity for domain RFM044 is similar to that for domain RFM029, i.e. approximately 3.5 W/(m·K).

3.4.3 Conclusions

Thermal conductivity

Based on modelling performed as part of model version 1.2 /Sundberg et al. 2005/ and thermal conductivity data acquired as part of version 2.1, it can be concluded that the thermal conductivity distributions at domain level for domains RFM029 and RFM012 require revision. For both domains, the mean thermal conductivity is likely to be lower (up to 0.1 W/(m·K)) than indicated in model version 1.2. At the 0.8 m scale, the 2.5 percentiles of thermal conductivity may be up to 0.3 W/(m·K) lower than reported in version 1.2, whereas the 97.5 percentiles remain unchanged. These modifications are the result of taking into account the presence of amphibolite, which based on calculations from modal analyses gives a mean thermal conductivity of about 2.4 W/(m·K), considerably lower than all other common rock types present at the Forsmark site.

For domains RFM044 and RFM045, not modelled in version 1.2, estimates of mean thermal conductivities are 3.5 W/(m·K) and 3.6 W/(m·K), respectively.

Heat capacity

Domain modelling of heat capacity was not performed. The new data for granite to granodiorite (101057) does not significantly influence the rock type model used in version 1.2. Therefore, the modelling results presented in version 1.2 for domain RFM029 and RFM012 are still considered valid.

Thermal expansion

Domain modelling of thermal expansion was not performed. The new data does not affect the conclusions presented in model version 1.2.

In situ temperature

Means of the in situ temperature at 400 m, 500 m and 600 m depth are estimated at 9.3, 10.5 and 11.8°C, respectively, from boreholes KFM05A–08A, which compares with 10.6, 11.7 and 12.8°C for boreholes KFM01A–04A reported in version 1.2 /Sundberg et al. 2005/. The large differences in temperature between boreholes at the same depth indicate large errors in the temperature measurements. Some of the boreholes have recently been re-logged. Preliminary results indicate that the data is of better quality.

3.4.4 Remaining uncertainties

The evaluation of thermal properties performed as part of model version 2.1 suggests that the results of thermal conductivity modelling presented in model version 1.2 for domains RFM029 and RFM012 should be revised. Amphibolite, omitted from modelling in version 1.2 due to lack of data, has a considerable influence on the nature of the lower tails of the modelled distributions. Additional modelling efforts incorporating all available boreholes within the new local model volume are required.

Considerable uncertainties remain. The estimated thermal properties at domain level are very dependant on the robustness of the rock type models. In general, data based on calculations from mineral composition (SCA method) are considered to be less reliable than data based on direct measurement (TPS method). Rock types for which the data are particularly inadequate are amphibolite (102017) and granite, granodiorite and tonalite (101051). Thus, uncertainties in rock type models for these rock types are correspondingly large. This is all the more important since both of these rock types have thermal conductivities that are potentially much lower than the dominant rock type, granite to granodiorite (101057), in the local model volume. For amphibolite, thermal conductivity values are available from calculations based on mineral composition (SCA method) only. Given the importance of amphibolite (makes up approx. 5% of the rock mass in domain RFM029), and its low thermal conductivity, as indicated by SCA calculations (mean 2.4 W/(m·K)), it is important that direct measurements (TPS method) are performed on a number of samples of this rock type.

For rock type granite, granodiorite and tonalite (101051), which comprises approximately 8% of the rock mass in domain RFM029, the picture is less clear. The few available TPS values give thermal conductivities of about 2.5 W/(m·K), which is much lower than the mean of 3.0 W/(m·K) calculated from the more plentiful SCA data. The samples used for direct measurement are probably not representative of the rock type as a whole, which, based on studies of mineral composition, has been shown to be compositionally diverse, comprising granite, granodiorite and tonalite. Clearly, there is a need for more direct measurements on a representative number of samples. TPS measurements should be supplemented by modal analysis of the same samples.

As mentioned above, a better understanding of the thermal properties of the amphibolites is necessary in order to more accurately describe the distribution of thermal conductivities at domain level. It is not only their anomalously low thermal conductivity that is of importance. Their mode of occurrence as dykes may create large-scale anisotropies in thermal properties, an aspect that should be incorporated into future modelling efforts. In this regard, the thickness of the amphibolite dykes, their frequency and their orientation are of significance. Moreover, a better understanding is needed of the significance of anisotropic thermal properties for the temperature distribution in a repository.

Small-scale anisotropy of thermal conductivity may be produced by ductile structures such as foliation and lineation. Determinations of anisotropy on core samples presented in model version 1.2 have been revised. Results are preliminary and have not been delivered to Sicada.

There is a lack of knowledge regarding the impact of alteration, oxidation in particular, on the thermal properties of the rocks. To resolve this issue, the mineralogy of rock described in the Boremap as oxidised should be investigated. It may also be worthwhile to determine the thermal properties of oxidised samples by direct measurement in the laboratory.

Bias may be present in the heat capacity results determined using the TPS method. For this reason, direct determinations are planned.

3.5 Bedrock hydrogeology, hydrogeochemistry and bedrock transport properties

3.5.1 Bedrock hydrogeology

The transmissivity observations reported by /Gentzschein et al. 2006/ demonstrate that the hydrogeological conditions in the uppermost c. 200 m of the bedrock in the candidate area are quite complex and much different from the conditions outside the tectonic lens as well as at greater depths within

the tectonic lens. Most likely, the uppermost part of the bedrock is much more anisotropic and heterogeneous hydraulically than modelled in the 1.2 modelling stage. For instance, Figure 2-45 indicates that the occurrence of high transmissive sub-horizontal fractures/fracture zones/sheet joints may vary considerably over the model area, in particular with regard to the foot/hang walls of the gently dipping ZFMNE00A2 deformation zone, with a tentative maximum depth of c. 200 m.

The point-water head observations by /Gentzschein et al. 2006/ and /Juston et al. 2006/ confirm that the hydrogeological conditions in the uppermost c. 200 m of rock indeed are difficult to readily conceive. The horizontal component of the point-water head gradient in the uppermost part of the bedrock is quite flat and appears to be independent of the topography of the surface as well as the bedrock surface. The available data lead to questions how to best describe and model the top boundary hydrologic condition in Forsmark in the modelling stages yet to be.

A tentative, preliminary interpretation may be expressed as follows (cf. Figure 3-20):

- In monitoring section intersected by highly transmissive and connected horizontal sheet joints and/or outcropping gently-dipping deformation zones, the resistance against flow is so low that almost no gradients can be observed. Most of the monitored sections shown in Figure 2-46 belong to this category of data.
- At locations where the uppermost part of the bedrock below the Quaternary deposits is of low conductivity (but not impervious) the resistance against flow causes a higher head in the uppermost monitoring section in the percussion-drilled boreholes. A typical example of this situation is borehole HFM13, see Figure 2-46. The monitoring section below the uppermost section has a much higher transmissivity (see Figure 2-45) and, consequently, a much lower head.
- Some of the boreholes shown in Figure 2-46 intersect the bedrock outside the tectonic lens, i.e. HFM09, HFM10, HFM11 and HFM12. The transmissivities in these boreholes are probably better associated with fractures belonging to the steeply-dipping structures that strike NW, e.g. the Eckarfjärden deformation zone. Hence, they are not readily associated with the sub-horizontal fractures and gently dipping deformation zones within the tectonic lens.
- Borehole HFM07, which is located within the tectonic lens, is close to impervious. It has a very low yield, because the intersected gently dipping deformation zone at c. 50–70 m depth was completely filled with glacial sediments.

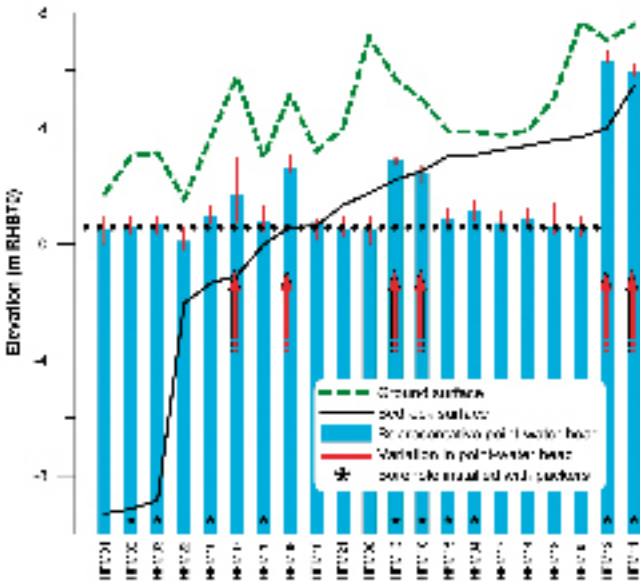

Figure 3-20. *Preliminary interpretation of Figure 2-46. The dotted line indicates the point-water heads associated within the tectonic lens. The boreholes indicated with arrows are commented in the text.*

If this tentative description is correct it suggests that there can be a “hydraulic cage” in the target volume within the tectonic lens. The sub-horizontal fractures that occur in the uppermost part of the bedrock above the “hydraulic cage” short circuit the recharge from above and constitutes the real discharge elevation for deeper groundwater flows. Indeed, the “Natural Flow” data from the PFL measurements in the KFM02A borehole shown in Figure 2-49 suggest that there is a discharge zone below the casing in this borehole for the deep and more saline groundwater entering the borehole as a result of the core-drilling. Whether or not the hydraulic cage is in good or poor contact with the Eckarfjärden deformation zone, which may act as an upstream hydraulic boundary, remains to be tested. The hydraulic interference test conducted in KFM04A /Gokall-Norman et al. 2005b/ was a good attempt to answer this question, but unfortunately the configuration of the test equipment in the pumped borehole was not optimal. Probably, we need to wait until the intense drilling programme is completed before detailed hydraulic responses can be resolved.

The recommendation made here is to take a closer look at the existing data and continue the very important monitoring of meteorological, hydrological and hydrogeological data in the surface waters, in the Quaternary deposits and in the bedrock until the interference test programme at the end of the site investigations has been completed and the results properly understood.

The hydrogeological model for the tectonic lens presented in the 1.2 modelling stage divided the rock mass in rock domain RFM029 below –100 m above sea level into different sub-volumes, cf. /SKB 2005a/. Though not presented in Figure 2-34, the data from the 2.1 investigations in boreholes KFM06A and KFM07A support the reasoning. It was recommended that the sub-volume approach suggested by hydrogeology is revisited in the 2.2 modelling stage, however, in close co-operation with geology and rock mechanics. Also, it was recommended that both the PFL method and the PSS method are used in the most important future boreholes. The comparisons between double-packer injection tests and difference flow logging tests reported in the P-report series from Forsmark are very useful for the development of the conceptual hydrogeological model of the bedrock at depth. The analysis of PSS data conducted by /Follin et al. 2006/ using the GRF approach suggests that the interpretation scheme of PSS data used in Forsmark is in order, at least from a practical point of view.

The information in Table 2-21 and Figure 2-36 through Figure 2-40 is primary input to the hydrogeological DFN modelling that will be undertaken in the 2.2 modelling stage. The stereo nets of flowing features shown in Figure 2-38 indicate that the observations reported by /Follin et al. 2005/ may be valid also for the KFM06A and KFM07A boreholes. That is, the majority (75–80%) of the PFL-f transmissivities are associated with gently dipping fractures. Second and third in number to the horizontal set come the NE (10–15%) and the NW (5–10%) fracture sets. It is noteworthy that these three sets gather almost all flowing fractures in the central part of the target volume and that the differences in the first (mean) and second moments (variance) in the log transmissivity between the three sets are small. It is also noteworthy that there are very few flow anomalies below c. –400 m above sea level in the target volume. This observation is supported by the double-packer injection tests.

The flow anomalies observed at depth in Figure 2-36 and Figure 2-37 are generally associated with deterministically interpreted deformation zones. The hydraulic character of these zones is surprisingly discrete. In general, there is one or a few flow anomalies only that are situated within the deterministically interpreted deformation zones (see Figure 2-36 and Figure 2-37).

The multi-parameter plot suggested by /Levén et al. 2006/ is extremely useful for the integrated modelling. It is recommended that this kind of work is carried on throughout the future modelling work, including parameters as requested by the different disciplines. However, it is noted that the WellCad plotting program cannot access data outside the Sicada database. Possible implications for the integration due to this limitation need to be discussed. For instance, will the WellCad plotting program access the 2.1 deformation zone model if this model version is reported outside the Sicada database?

3.5.2 Bedrock hydrogeochemistry

The Forsmark 2.1 data imply relatively small modifications to the version 1.2 hydrogeochemical site description /SKB 2005ad/, but the overall geochemical understanding of the site has improved. This includes confirmation of previous findings from version 1.2 and also support for the predictions made in version 1.2 based on the limited knowledge at that time. The confidence concerning the three-dimensional variability of processes and properties has also improved due to the addition of both new data in previously drilled boreholes and from new boreholes in specific key areas.

Figure 3-21 shows the spatial distribution of chloride concentration values (only representative values) available in bedrock water samples. It can be seen that there is a strong salinity contrast between the groundwaters in the upper 100 m of the bedrock and that below this depth; moreover, there are very few representative samples available below the gently dipping deformation zone ZFMN002A. This fact is related to the lower hydraulic conductivity of the bedrock below this deformation zone which hinders normal hydrochemical sampling. Therefore, it should be borne in mind that the hydrochemical evaluation provides a biased "picture", basically representing information only coming from the most conductive part of the bedrock. In this respect, the results of the matrix fluid characterisation programme is expected to be an extremely useful tool to approach a proper ("unbiased") conceptualisation of the hydrogeochemical system.

The most conductive part of the upper 100 m in the bedrock is supported by the tritium contents measured in groundwater samples (Figure 3-22). Samples taken above 100 m show high tritium contents typical of modern water; available data show that these decrease to below 4 TU at around the 100 m depth. It can be stated, therefore, that even in the most conductive zones of the bedrock, groundwater deeper than 100 m is, at least, sub-modern.

Stable isotopes indicate that glacial signatures can be recognised in the bedrock, in general at depths greater than 500–600 m. Figure 3-23 shows the spatial distribution of ^{18}O values.

It is worth noting that there are two main exceptions to the low stable isotope values (potentially indicative of glacial signatures) in shallow groundwater samples. They correspond to groundwater samples collected in percussion boreholes, located between Bolundsfjärden and Fiskarfjärden. The boreholes HFM11 and HFM12 should be re-sampled and modelled to exclude possible input from recent snow melt.

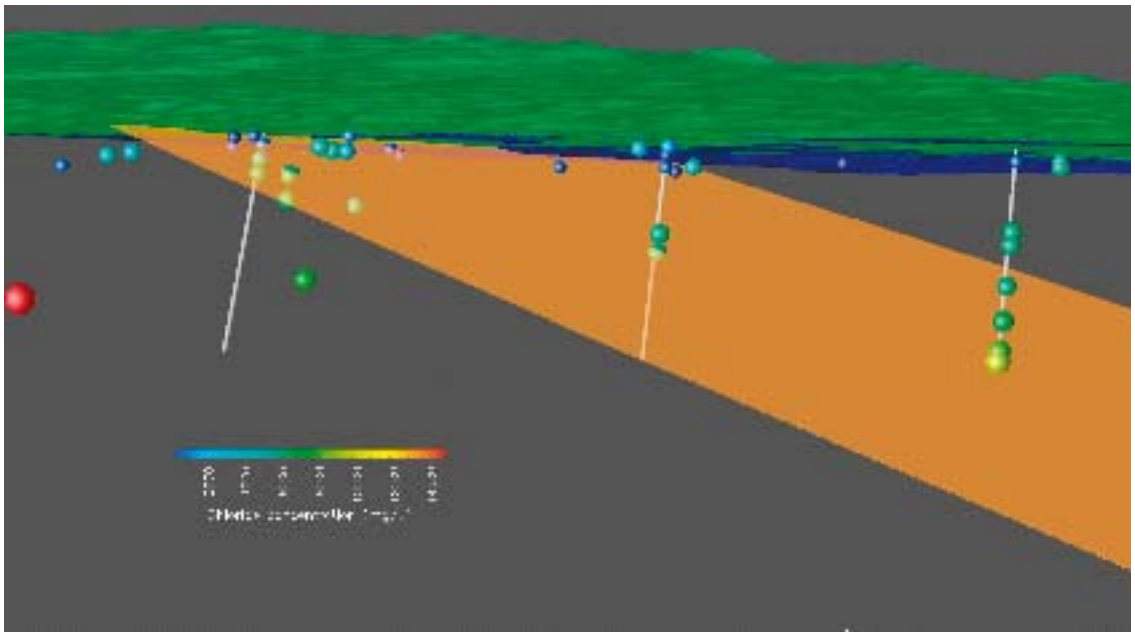

Figure 3-21. *Spatial distribution of the chloride concentrations in the bedrock groundwater samples available in Forsmark, and its relation with the gently dipping deformation zone ZFMNE002A. Boreholes KFM01A, KFM02A and KFM03A (from left to right) have been included for location purposes.*

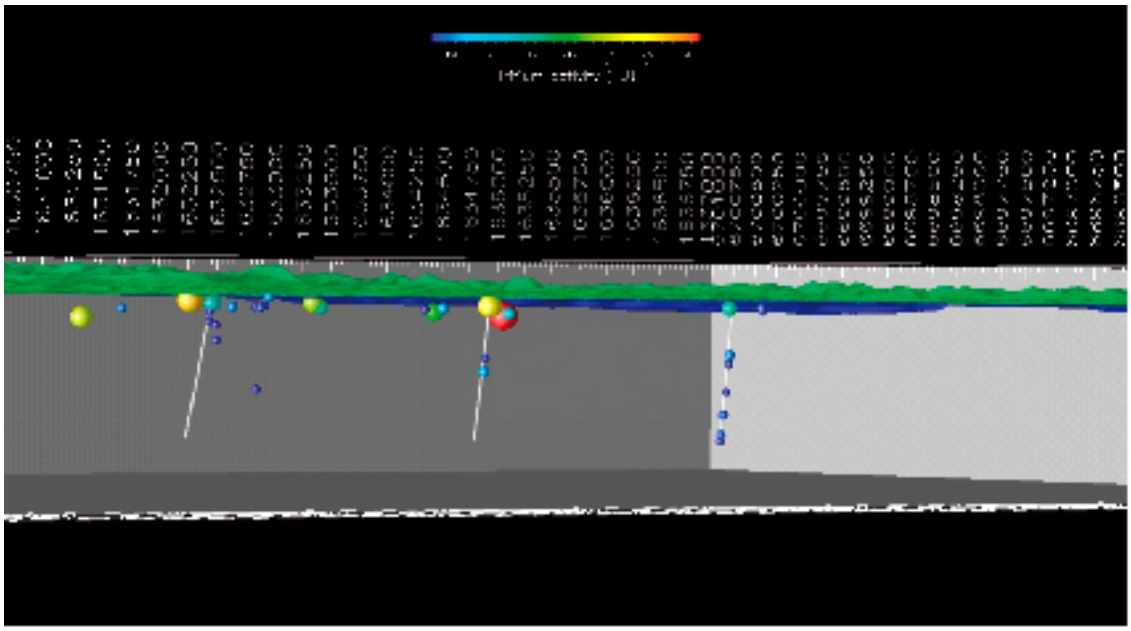

Figure 3-22. *Spatial distribution of the tritium activities in the bedrock groundwater samples available in Forsmark. Boreholes KFM01A, KFM02A and KFM03A (from left to right) have been included for location purposes.*

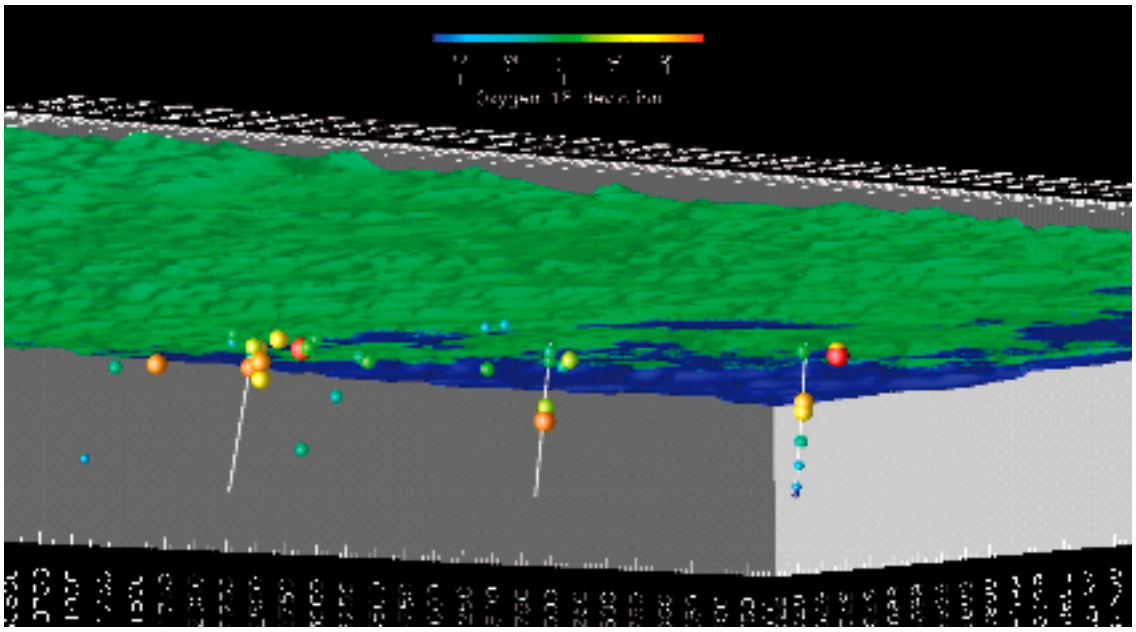

Figure 3-23. *Spatial distribution of the ^{18}O deviations in the bedrock groundwater samples available in Forsmark. Boreholes KFM01A, KFM02A and KFM03A (from left to right) have been included for location purposes.*

In general, the new Forsmark 2.1 data have allowed for a more detailed geochemical process modelling and redox description. This work will be presented in a separate issue report during 2006 /SKB 2006b/.

3.5.3 Bedrock transport properties

The Forsmark 2.1 model has undergone only minor changes relative to the 1.2 model version. The overall organisation and structure of the retardation model is essentially unchanged since Forsmark 1.2, although altered to accommodate newly acquired site-specific data.

The main uncertainty identified in previous model versions was the lack of site specific transport data. Although data support is improving for the major rock types, there are still gaps and omissions that will need to be filled in forthcoming model versions. There were no sorption data available for inclusion in this model version, although the BET surface area (see Section 2.9 for explanation) has been measured for a number of major and minor rock types and is used as a qualitative indicator of relative sorption affinity.

Transport properties of rock domains

The geological model in the site description is based upon the concept of rock domains (cf. Section 3.1) whereas the sampling for the transport programme is based on rock types. The proportions of different rock types in each of the cored boreholes, as reported in version 1.2 of the Forsmark SDM /SKB 2005a/, are given in Table 3-12. The major rock type is granite (to granodiorite), metamorphic, medium-grained rock (101057). All other rock types given in the table are considered to be minor.

Table 3-13 gives selected transport parameters for the fresh and altered rock types that have been scrutinised thus far in the site investigation. The only alteration form for which data is currently available is for the episyenetic (hydrothermally altered and porous) form of the major rock type (101057).

Table 3-12. Proportions of different rock types that occupy more than 1 m contiguous borehole length in the cored boreholes (Chapter 5 Forsmark SDM1.2 /SKB 2005a/).

Code (SKB)	Composition and grain size	KFM01A	KFM01B	KFM02A	KFM03A	KFM03B	KFM04A	KFM05A
103076	Felsic to intermediate volcanic rock, metamorphic	×	×	×	×	×	4.2%	0.3%
108019	Calc-silicate rock (skarn)	0.2%	×	×	×	×	×	×
102017	Amphibolite (group C)	1.9%	0.3%	4.1%	1.9%	8.5%	2.8%	3.4%
101054	Tonalite and grano-diorite, metamorphic (group B)	×	×	×	4.2%	×	×	×
101056	Granodiorite, metamorphic	×	×	×	×	×	10.8%	×
101057	Granite (to grano-diorite), metamorphic, medium-grained (group B)	85.3%	92.6%	79.5%	74.8%	50.3%	68.3%	89.2%
101051	Granodiorite, tonalite and granite, meta-morphic, fine- to medium-grained (group C)	10.0%	6.1%	14.3%	9.9%	1.2%	10.5%	5.0%
101061	Pegmatitic granite, pegmatite (group D)	1.4%	1.0%	0.9%	6.8%	38.7%	2.3%	1.2%
111058	Granite, fine- to medium-grained	1.2%	×	1.2%	2.4%	1.3%	1.1%	0.8%
No information		×	×	×	×	×	×	0.1%

× No occurrence with a contiguous length > 1 m for given borehole.

Table 3-13. Suggested transport parameters for the most common rock types in the Forsmark area (water saturation based porosities and formation factors derived from in situ electrical resistivity measurements). All data are given as log_{10} mean values ± σ for the considered data set where available.

Rock type (SKB code)	Porosity (vol %)	Formation factor (–)
Granite to granodiorite, metamorphic, mediumgrained (101057)	–0.67 ± 0.16	–4.67 ± 0.28
Granite to granodiorite, metamorphic, mediumgrained (101057), episyenetic samples	1.05 ± 0.36	–2.84 ± 0.97[1)]
Granite, granodiorite and tonalite, metamorphic, fine- to medium-grained (101051)	–0.64 ± 0.17	–4.81 ± 0.24
Pegmatite, pegmatic granite (101061)	–0.41 ± 0.22	–4.12 ± 0.62
Amphibolite (101217)	–0.75 ± 0.28	–4.58
Granodiorite metamorphic (101056)	–0.52 ± 0.28	Pending
Felsic to intermediate volcanic rock, metamorphic (103076)	–0.11	Pending
Tonalite to granodiorite, metamorphic (101054)	–0.77 ± 0.04	Pending
Granite, metamorphic, aplitic (101058)	–0.73	Pending
Granite, fine- to medium-grained (111058)	–0.44	Pending

[1)] Based on through-diffusion measurement result.

Transport properties of fractures

The samples selected for laboratory investigation represent both fresh rock and altered forms obtained in the immediate vicinity of, or within, fractures.

Wall rock alteration is not always visible as red staining or feldspar bleaching, but is typically present in the form of altered plagioclase and chlorite resulting from the weathering of biotite. Chlorite is present in 70–80% of the open fractures in KFM01A–KFM06A. Calcites are found in varying amounts in the chlorite coated fractures, although are not ubiquitous. Clay minerals are found in 2–18% of the open fractures. X-ray identification shows, however, that corrensite (a swelling, mixed-layer clay) is present in many of the open, chlorite-coated fractures, which indicates that the frequency of clay minerals identified from the core mapping is probably an underestimate.

Laumontite + calcite ± chlorite/corrensite is a common coating in open fractures (mostly steep fractures usually trending NE). It is, however, difficult to determine whether these fractures are originally open or sealed. This means that the frequency of open, laumontite coated fractures is very uncertain and could range anywhere from < 1–19% in boreholes KFM01A to KFM06A. It is therefore possible that the observed large variation could be a result of the different locations and directions of the boreholes /Sandström and Tullborg 2005/. Thin, although continuous coatings of euhedral quartz crystals are found in many reactivated fractures. Such fractures are also frequently associated with calcite and often pyrite mineralisations.

According to the presently available data, the presence of different fracture coatings cannot be related to specific rock types. This may be of some importance for the application of the identified fracture types in transport models. It is noted that only a small proportion of the fractures (< 10%) are accompanied by altered wall rock according to the core logging. However, this may be an underestimation, particularly considering the nearest cm to the fracture, owing to the nature of the alteration processes and that most fractures appear to have mineral coatings (e.g. epidote, prehnite, and laumontite) that are formed hydrothermally.

Five different, principal fracture types are currently considered in the retardation model for transport within fractures. For the most part these differ only by type and depth of alteration, although provision is made in the conceptual model for inclusion of relations between material properties and transmissivity (or even fracture orientation) if these are subsequently shown to be relevant. The quantification and description of the different fracture types were previously documented in the site descriptive model version 1.2 for Forsmark /SKB 2005a/ and will not be repeated here. Based upon the updated core mapping data and detailed fracture mineral studies, there is currently no reason to implement any changes to the conceptual retardation model for fractures.

Although there is a general paucity of data for altered wall rock materials (with the possible exception of episyenetic (strongly altered) granite to granodiorite, metamorphic, medium-grained rock (101057)), it should be noted that the present safety assessment transport modelling principally uses retardation parameters for fresh (non-altered) rock, as it is the parameterisation of the unaltered rock that is generally thought to be of overwhelming importance for radionuclide transport retardation at such timescales. The Safety Assessment modelling at this present time is, therefore, not directly dependent on the availability of parameter values for fault gouge, fracture coatings, and altered wall rock. The continuing limited availability of data for altered rock types also implies that the same parameter values that were missing from the fracture type descriptions in SDM version 1.2 are currently still missing. These gaps will be filled in forthcoming versions of the Forsmark SDM.

Transport properties of fracture zones

Based on the information available at this stage in the site investigation, it is not possible to provide a retardation model for the local minor and local major deformation zones. This is partly due to a lack of transport data, although also related to uncertainties in the classification of deformation zones. Although no retardation model has been developed, it is implicitly assumed that deformation zones consist of one or several types of altered wall rock (i.e. layers of hydrothermal and tectonic alteration that extend from fracture surfaces to some distance within the host rock). The conductive parts of the zones are conceptualised to consist of multiple fractures and regions with crushed material that can be classified as belonging to one of the main fracture types or a broader fault gouge classification.

3.6 Surface system

No new modelling of the surface system properties has been performed since SDM version 1.2. For a summary of the current knowledge, the reader is referred to Section 4.1 in this report and to Chapter 11 in /SKB 2005a/.

4 Summary of current understanding of the Forsmark site

4.1 Topography and the surface system

The landscape in Forsmark is a relatively flat peneplain, which dips gently towards the east. The whole area is situated below the highest coastline. Despite the modest topography, the upper surface of the bedrock is found to undulate over small distances implying large variation in thickness of the Quaternary cover.

In northern Uppland, the coastline has been continually regressive since the last deglaciation about 10,800 years ago. Most of the Forsmark area has emerged from the Baltic Sea during the last 1,000 years, and today's landscape is strongly influenced by the ongoing shoreline displacement which measures c. 6 mm per year. This means that processes such as chemical weathering and peat formation has affected the area during a relatively short period of time. The till and the glacial clay are rich in $CaCO_3$, emanating from Palaeozoic limestone that occurs at the sea bottom north of the area. This, together with the recent emergence of the area above sea level, affects the chemistry of both surface water and shallow groundwater, giving rise to high pH, high alkalinity and high contents of major constituents. Furthermore, the surface waters are high in nitrogen and low in phosphorous, a characteristics of the oligotrophic hardwater lakes which are typical for the Forsmark area.

The vegetation is affected by the bedrock, the quaternary deposits and human land use. The Quaternary deposits consist mainly of wave-washed till, where conifer forests are common. In depressions, a deeper regolith layer with relatively high lime content is found. The calcareous influence is typical for the north-eastern part of the Uppsala County and is manifested in the flora. The Forsmark area has a long history of forestry which is seen today as a fairly high percentage of younger and older clear-cuts in the landscape.

The land use within the Forsmark area differs from the average land use in the Uppsala County, as there is proportionally more forest, wetland and water in the Forsmark area, and the area of agricultural and developed land is smaller. Arable land, pastures and clear cuts are mainly found close to settlements. The pastures were earlier intensively used, but are today a part of the abandoned farmland following the nationwide general regression of agriculture activities. Wetlands are frequent and are characterised by a strong calcareous influence. Bogs are found in the more elevated parts of the area, but they are rare, mainly due to the young age of wetlands. The population density in the Forsmark parish is low, on average1.8 inhabitants per square kilometre, but has been fairly stable during the last decades.

4.2 Rock type and associated thermal and rock mechanics properties

In the regional structural context of the coastal area in northern Uppland, the tectonic lens in which the candidate area is located is considered to be well established, see Figure 3-1. The lens developed more than 1,850 million years ago, when the rock units were situated at mid-crustal depths and were affected by penetrative but variable degrees of ductile deformation under amphibolite-facies metamorphic conditions. The bedrock inside the lens is relatively homogeneous and is dominated by a metagranite, whereas the lithology and deformation is more complex outside the lens.

A substantial amount of geologic data, both at the surface (mapping and geophysics) and from depth in the form of information from cored and percussion boreholes, underpins the version 2.1 of the rock domain model. Cored borehole data confirm that the character of the bedrock at c. 1,000 m depth inside the candidate volume is identical to that observed at the surface. Hence, the surface geology is the key to the composition and homogeneity of the bedrock at depths down to at least 1,000 m in the candidate volume at Forsmark.

Due to its internal homogeneity, most of the lens is possible to describe as a single rock domain, RFM029. The dominant rock type in this rock domain is medium-grained granite to granodiorite (c. 75% of the domain volume). Subordinate rock types are fine- to medium-grained metagranodiorite or metatonalite, amphibolite, pegmatitic granite or pegmatite, and fine- to medium-grained granite. With the exception of amphibolite that contains little or no quartz, the dominant rock type and the subordinate rock types have high quartz content, c. 20–50%.

The lens is surrounded by various domains that strike north-west, dip steeply to the south-west and are dominated by SL-tectonites, i.e. contain both planar and linear ductile mineral fabrics. In general, the rocks in these domains show a considerably higher degree of ductile deformation relative to that observed inside the tectonic lens and the bedrock is heterogeneous and composed of various types of felsic to intermediate metavolcanic rocks and metagranitoids. In the model, this is described as rock domains with strongly deformed, and also in part, banded and inhomogeneous rocks that occur along the south-western and the north-eastern margins of the lens.

Confidence in both the existence and geometry of rock domains within or immediately around the target area is high down to a depth of 1,000 m, whereas significant uncertainties still remain where it concerns the character and geometry of rock domains outside the candidate area, e.g. in the sea area.

4.2.1 Ore potential

The ore potential in the coastal area in northern Uppland is correlated to the rock types and their characteristics. An assessment of the ore potential carried out in support of model version 1.1 came to the conclusion that there is no potential for metallic and industrial mineral deposits within the candidate area at Forsmark. A potential for iron oxide mineralisation was recognised in an area south-west of the candidate area, predominantly in the felsic to metavolcanic rock, but the mineral deposits are small and have been assessed to be of no economic value /Lindroos et al. 2004/.

Based on data from the islands outside the Forsmark candidate area, a new rock domain (RFM021), dominated by felsic to metavolcanic rock, was recognised in version 1.2 of the site descriptive model. This rock domain is located north of the candidate area (Figure 3-2). There is no documented iron mineralisation in data available from the islands, but since most part of this rock domain is located beneath the Baltic Sea from where no mineralogical data exist, the potential for iron oxide mineralisation in rock domain RFM021 cannot be totally excluded.

4.2.2 Thermal properties

The rock types in rock domain RFM029 have typically high quartz content, which favours high values of the thermal conductivity. Measurements at the cm-scale show values in the range 3.4 to 4 $W \cdot m^{-1} \cdot K^{-1}$ for the dominant rock type in rock domain RFM029, whereas some subordinate rock types yield significantly lower values. Although the picture of high thermal conductivity for domain RFM029 as described in model version 1.2 is largely retained, the new data indicate that the mean thermal conductivity at a scale of 0.8 m is slightly lower than the value of 3.55 W/(m·K) reported in version 1.2. This is primarily due to the impact of amphibolite, which comprises about 5% of the rock volume in the domain, and based on calculations from mineral composition has a low thermal conductivity (mean value of 2.4 W/(m·K)). Preliminary results indicate that the impact of amphibolite at the 0.8 m scale is a somewhat lower (about 0.1 W/(m·K)) mean thermal conductivity, whereas the 2.5 percentiles may be up to 0.3 W/(m·K) lower. However, the upper tail percentiles remain essentially unchanged.

There is generally a high confidence in the modelled distribution of the thermal properties, due to its strong correlation to the well understood lithology and also supported by the low spatial variability of the data. The main remaining uncertainties in thermal properties of the rock in the target area concern the impact of subordinate rock types, primarily amphibolite, both in terms of their thermal conductivity and their spatial distribution. In addition, some measured data indicate anisotropy in thermal conductivity in foliated parts of the rock with higher conductivity parallel to foliation. However, the interpretation of these data is uncertain.

4.2.3 Rock mechanics properties

Measurements of the mechanical strength of the dominant rock type (granite to granodiorite) within rock domain RFM029 show high values for the uniaxial compressive strength (UCS) of intact rock sampled at the depth interval 400–550 m in boreholes in the candidate area. The mean values for samples from boreholes in the target area (north-western part of the candidate area) are all above 220 MPa (Figure 2-20). Samples from larger depths have lower mechanical strength and deformability (Young's modulus) than samples from the depth interval 400–550 m, which can be explained by microcracking induced by the drilling in a high-stress environment. This is supported by results from P-wave velocity measurements.

There is generally a high confidence in the modelled distribution of the strength of the intact rock, at least inside rock domain RFM029, due to its strong correlation to the well understood lithology and also supported by the low spatial variability of the data. In a similar manner to the thermal properties, the main remaining uncertainties concern the potential impact of subordinate rock types.

4.3 Deformation zones and fractures

4.3.1 Deformation zones and deformation history

Three major sets of deformation zones with distinctive orientations have been recognized with high confidence at the Forsmark site. Vertical and steeply, SW-dipping zones with WNW and NW strike show complex, ductile and brittle deformation. Regional zones longer than 10 km (e.g. Forsmark, Singö and Eckarfjärden deformation zones at the boundary of the candidate area) are restricted to this set which is the master set at the site. Vertical and steeply-dipping, brittle deformation zones with NE strike transect the candidate volume at Forsmark and are prominent in the Bolundsfjärden area. This set is strongly dominated by sealed fractures and sealed fracture networks. Gently SE- and S- and W-dipping brittle deformation zones occur more frequently in the south-eastern part of the candidate volume. Relative to the other three sets, there is an increased frequency of open fractures along the gently dipping set. These gently dipping zones seem to play an important role in determining the properties of the Forsmark site (see further below). A fourth set of zones that strikes NS and is vertical or steeply dipping has also been recognized. These zones formed in the brittle regime and are dominated by sealed fractures. Relative to the other three sets, there is a limited number of such zones.

The properties of the deformation zones and geochronological data have been used to establish a working conceptual model for the formation and reactivation of these zones. This model attempts to address the deformation zones in the context of changes in stress regimes from the later part of the Svecokarelian orogeny, c. 1,800–1,750 million years ago, until the current time (Quaternary). This understanding of the tectonic evolution of the site has had important implications for the development of the current deterministic deformation zone model. For example, deformation zones and most of the fractures are inferred to be geologically ancient structures and the inferred structural hierarchy has provided a procedure for truncation of deformation zones. Kinematic data and more geochronological data are needed to test and hopefully refine the working conceptual model. It is proposed that more than one fracture set is present along a deformation zone. Furthermore, rapid changes in the magnitude of the differential stress, during the Quaternary, can explain the increased frequency of open fractures and the increased hydraulic transmissivity of the gently dipping zones.

The deterministic deformation zone model builds on an integration of the understanding of the deformation history in the region with surface seismic reflection data, lineaments, and fracture orientation, fracture mineralogical and bedrock alteration data from especially the cored boreholes. Gently dipping zones have mainly been detected by an integration of data from boreholes with the interpretation of seismic reflectors. By contrast, vertical and steeply dipping zones have been recognised by an integration of data from boreholes and the surface with the interpretation of magnetic lineaments.

Confidence in the occurrence of deterministics deformation zones in the target area is high and the occurrence of undetected deformation zones inside the repository target area that are longer than 3,000 m is judged unlikely at this stage in the investigations. However, uncertainty remains for all the deformation zones defined solely on the basis of lineaments, both what regards their occurrence

and their geometry. There are also remaining uncertainties in the geometry of the gently dipping zones, although analysis of all the surface seismic reflection data has provided better constraints on the extension of the gently dipping zones, both along strike and down dip.

4.3.2 Fractures and fracture domains

The analysis of fracture data indicates a large spatial variability in the size, intensity and properties between different rock domains, but also within rock domain RFM029. For example, the frequency of open and partly open fractures is markedly higher in the upper part (< c. 300 m) of the bedrock in the north-western part of rock domain RFM029, relative to that observed in deeper sections in this part of domain RFM029. By contrast, there is no simple depth dependence in the frequency of such fractures in the south-eastern part of rock domain RFM029. Furthermore, fracturing is affected by the proximity to deformation zones. This is indicated, for example, by the higher frequency of fractures immediately beneath the gently dipping deformation zone ZFMNE00A2 that outcrops in the target area, and very few fractures at greater depth beneath this zone. These features together with the inferred relationship between the occurrence of gently dipping fracture zones and in situ stress magnitudes in the bedrock, suggest that rock domain RFM029 in the candidate area should be subdivided into different fracture domains, as indicated in Figure 3-7.

4.3.3 Rock mechanics properties

The fractures in rock domain RFM029 are prevalently rough, planar, fresh and unaltered. Although some of the fracture sets are underrepresented in the laboratory samples for testing of rock mechanics properties, the difference between the mechanical properties of the fracture sets is not statistically significant. In addition, there seems not to be any difference between the properties of the fracture samples taken from the rock mass within and outside the deformation zones.

Empirical and numerical analyses of the data conducted so far indicate that the mechanical properties of the naturally fractured rock mass outside deformation zones in rock domain RFM029 are very close to those of the intact rock and are therefore considered to be constant for all levels of confining stress. The deformation modulus of the rock mass outside the deformation zones is estimated at 67 GPa with a standard deviation of 10 GPa.

At low confining stress, the mechanical properties of the rock mass within deformation zones shorter than 10 km are lower than those of the rock mass outside deformation zones. However, for confining stresses larger than about 10 MPa, these values approach the values determined for the rock mass outside the deformation zones. Although Figure 3-14 shows that the zones analysed from a rock mechanics point of view all strike NE, the results so far indicate small differences in mechanical properties between the different zones. One exception concerns a minor deformation zone identified in the strongly altered vuggy metagranite in borehole KFM02A, which seems to have lower deformability and strength than the other zones because of lower rock matrix strength of this metagranite. Analyses of regional deformation zones longer than 10 km (e.g. the Singö and Forsmark deformation zones) are planned for the coming modelling work.

4.4 Stress conditions

The current estimates of the state of stress at Forsmark show that the maximum horizontal stress trends NW-SE, sub-parallel to the direction of plate-ridge push and to the regional deformation zones at the site. Furthermore, the few measurements of stress currently available indicate that the magnitude is significantly higher, at least at some 200–500 m depth, compared with other sites in Scandinavia.

Stress data from borehole DBT-1 demonstrate a stress jump at the same depth at which a fracture zone has been detected. New reflection seismic data indicate that this, water-bearing, minor fracture zone at c. 320 m depth in borehole DBT-1, corresponds to a gently dipping zone (ZFMNS00B8) that is partly similar in character to ZFMNE00A2. The reflector dies out to the south-east and does not transect the candidate volume. Similar observations of variation of in situ stress across geologically

old thrust faults have also been made in the URL in Canada, where the rock above a gently dipping fracture zone at about 300 m depth is low-to moderately stressed and the rock below this zone is highly stressed /Martin et al. 2001 and references therein/.

The orientation of the major deformation zones relative to the current regional stress orientation, given by the plate-ridge push, offer a conceptual explanation for the high stress levels found. Especially the rock volume below deformation zone ZFMNE00A2 would be subject to the full thrust of the regional stress, whereas rock volumes above the zone would be relaxed and thus show comparably lower stress levels. However, it should be noted that all stress data collected so far in the candidate volume are from the bedrock below the gently dipping deformation zone ZFMNE00A2. More stress data, especially above deformation zone ZFMNE00A2, are needed before a full confidence stress model can be established.

4.5 Hydraulic properties and groundwater flow

Analyses of hydraulic data from the boreholes in the target area reveal that the geological structures in the uppermost part of the bedrock are highly transmissive in the horizontal plane and in good hydraulic contact over large distances (~2 km). In contrast, the body of the geological structures at depth appears to be of significantly lower transmissivity. This strongly suggests that the rock mass between the deterministically modelled deformation zones in rock domain RFM029 contains sub-domains with different hydraulic properties. The exact division of the different volumes remains to be defined. The relationship between fracture domains and sub-domains with different transmissivities is presently under review in preparation for modelling stage 2.2. A tentative proposal for such a division is envisaged in Figure 3-7.

The presence of highly transmissive structures in the uppermost c. 200 m of the bedrock is potentially of importance for the groundwater flow pattern within the target volume. For instance, point-water head data suggest a “hydraulic cage” scenario where the recharge of meteoric water from above is short circuited by sub-horizontal fractures/fracture zones/sheet joints in the uppermost part of the rock and outcropping gently dipping deformation zones. In effect, these sub-horizontal fractures may also constitute the real discharge elevation for some of the deeper groundwater flows. However, this working hypothesis remains to be elaborated and tested.

Furthermore, it is currently not fully established how to describe the hydraulics of the low permeability rock mass encountered below the foot wall of the gently dipping deformation zone ZFMNE00A2. Transmissivity data from structures outside deterministically modelled deformation zones are, in general, rare, and depending on the assumptions made in the DFN modelling, alternative interpretations are possible ranging from a sparsely connected DFN with a rather high transmissivity field to a well connected DFN with a very low transmissivity, i.e. close to the lower measurement limit of the hydraulic test equipment. Both interpretations results in a rather low percolating medium on a large scale, but one is geometrically constrained and the other hydraulically.

An interesting observation made is that the transmissivity of the deterministically modelled deformation zones seems to depend on depth and dip, with higher transmissivities in the gently dipping zones than in the steeply dipping zones at comparable depths. However, down to c. 200 m depth, the zones may be hydraulically very heterogeneous with transmissivities that vary over three orders of magnitude. These observations are based on results of hydraulic testing of 27 of the 44 deformation zones included in the version 1.2 deformation zone base model.

Transient, density dependent, groundwater flow calculations carried out in the 1.2 modelling stage suggest that the flow field in the target volume is mainly local. The presence and properties of deformation zones outside RFM029 have little effect on flow and salt transport inside rock domain RFM029. In contrast, deformation zone heterogeneity within the candidate area presumably has a greater effect on the local flow distribution. However, it should be noted that these simulations do not consider the anisotropy and heterogeneity of the hydraulic properties of the near-surface rock as indicated by the hydraulic data from the site. According to Figure 2-38, it is possible that horizontal anisotropy also prevails at depth.

4.6 Groundwater composition

Data on groundwater composition show an increase in salinity down to a depth of about 200 m. This combined with the finding that ^{3}H data show no input of modern water at depths greater than 200 m indicates that groundwaters in the uppermost parts of the bedrock are of meteoric origin. At depths between 200 and 800 m, the salinity remains fairly constant at a level between 5,000 and 6,000 $mg \cdot L^{-1}$, which together with high Mg concentrations indicate input of Littorina waters at these depths. At depths between 800 and 1,000 m, the salinity increases to high values. Furthermore, there are some weak indications that the salinity is higher at large depths in the rock in the north-western part of the candidate area (i.e. in the target area) as compared with that in the south-eastern part.

Analyses of groundwater chemistry data have also revealed an anomaly in uranium concentration. Large variations in uranium content in surface waters are common and are usually ascribed to various redox states (oxidation will facilitate mobilisation of uranium) and various contents of complexing agents, normally bicarbonate (which will keep the uranium mobile). Lower uranium content with depth is expected due to decreasing redox potential and decreasing bicarbonate content. This trend is not seen in the data collected so far at Forsmark. Instead, most of the data indicate high values at depths between 200 and 600 m. The reason for this anomaly is presently under investigation.

The hydrogeochemical data evaluation and modelling has revealed that the main compositional changes in groundwater composition at Forsmark are related to mixing of water with various origin. However, microbial processes and rock-water interactions are important in controlling certain parameters such as redox, pH and certain trace elements.

According to current understanding of the past evolution, the Forsmarks site has been transgressed by different non-saline and brackish lake/sea stages since c. 11,000 years BP, which have affected the hydrogeochemical conditions at the site. Of these periods, the Littorina Sea period, with a salinity maximum of about twice the present salinity of the Baltic Sea, is judged to have had largest impact by penetrating down into the rock and by mixing with glacial/brine groundwater already present in the bedrock. During the last 1,500 years, the Forsmark region has gradually emerged above the sea and recharging fresh meteoric water have formed a lens on top of the more saline water. Since the topography of the Forsmark area is flat, and the time elapsed since the area emerged above the sea is short, the outflushing of saline water has been limited and the freshwater lens remains at shallow depths.

Hydrogeological simulations of the past evolution of groundwater composition show good agreement between simulated and measured hydrogeochemical data at depth, whereas poorer matches were obtained in the upper 100 m of the rock. Furthermore, these hydrogeological simulations support the occurrence of Littorina Sea water in the upper 500 m of the bedrock. An explanation to the poor match in the upper part of the rock can be that the uppermost part of the bedrock is much more anisotropic and hydraulically heterogeneous than that predicted in the version 1.2 hydrogeological model.

4.7 Bedrock transport properties

There is currently good data support for the diffusive properties of the major rock type; granite (to granodiorite), metamorphic, medium-grained rock (101057). Some data values are available for minor rock types, although they are associated with greater uncertainty owing to the smaller number of samples that have been investigated (in some cases only single measurements). It is therefore not possible at this time to make unequivocal quantitative distinctions between the diffusive properties of the different rock types in the Forsmark area. Notwithstanding this, there does not currently appear to be large differences between the diffusive properties of the various unaltered rock types.

In situ measurements of formation factors are thought to be more relevant for model parameterisation owing to that they are obtained under prevailing formation stresses and are less subject to stress release and drill bit induced damage than core samples used in laboratory measurements. An epistemic uncertainty exists relating to a lack of knowledge concerning the actual pore water composition relative to that sampled in the borehole, although this is thought to be less than the uncertainty introduced by stress release and artefacts relating to mechanically induced damage.

There are currently no sorption data available for parameterisation of any of the rock types in the retardation model. This is a major weakness that will need to be rectified in the next model version. Although it is not possible to extract quantitative estimates of sorption properties from the data at this time, an indication of the relative sorption properties of the rock is given by the relative surface areas measured using BET. Making allowances for differences in sample support, it appears that the different rock types should have substantially similar sorption properties with only minor differences between rock types that are typically less than the spatial variability and measurement uncertainty inherent in the data itself.

The available data also indicate that altered forms most likely exhibit significantly stronger solute sorption than the unaltered matrix rock. The relatively high formation factors measured for episyenetic, strongly altered metagranite, samples as well as their typically high BET surface area suggests that they have substantially enhanced retention properties relative to unaltered rock.

5 Remaining critical site-specific issues and their handling

The identification and compilation of remaining important issues/uncertainties and suggestions for handling these uncertainties was carried out in a series of seminars/workshops, with joint participation from the Forsmark modelling project, the site investigation team, repository engineering and safety assessment. Based on uncertainties in the preliminary site description for Forsmark /SKB 2005a/, the results of analyses carried out in modelling stage 2.1, the experience from the work with repository layout D1 and the PSE for Forsmark, the remaining site-specific issues/uncertainties were compiled and documented in a protocol. These issues were then explored with the purpose to:

- provide a motivation for the issue to occur on the list and, if possible, prioritise the importance of the issue for the current stage of the site investigations, i.e. before conducting underground investigations,
- identify potential modelling actions to resolve the issue, and
- propose investigations that could produce data to resolve the issue, separating between investigations already decided upon and new investigations.

The results were documented in the protocol and are presented in the following sub-sections.

Using the completed protocol, necessary modifications to the CSI programme /SKB 2005c/ were subsequently discussed. These implications are presented in Chapter 6.

5.1 Geological issues and their handling

The remaining geological issues identified concern:

- Occurrence, geometry and properties of deformation zones (DZ) inside the target area.
- Occurrence, geometry and properties of DZ bounding the target area.
- Fractures and fracture domains including sub-horizontal fractures inside the candidate volume.
- Geological conditions that bound the extent of the repository.
- Timing of brittle deformation in the bedrock around the Forsmark site.
- Feedback to geology from rock mechanics on stress orientation in relation to fracture sets.

The two last issues, timing of brittle deformation and orientation of rock stress in relation to fracture sets, were judged as important for improving the conceptual understanding of the geological features at the Forsmark site. Reducing uncertainties associated with these issues do not require any additional site-specific data, apart from that already specified in the CSI programme /SKB 2005c/. For this reason, they are not further addressed here. Instead, the text below focus on the remaining issues in the list above.

5.1.1 Occurrence, geometry and properties of deformation zones inside the target area

The occurrence, geometry and properties of deformation zones inside the target area, especially, so far, unidentified steeply dipping zones that strike NS or NW and gently dipping zones, is assessed as an issue of high priority. Deformation zones in the target area and their geometry affect the repository layout in terms of location of suitable rock volumes for deposition holes. Especially the occurrence of zones longer than 3,000 m is important since such zones requires a respect distance to deposition holes. The current layout, layout D1, based on SDM version 1.2, is directly affected by its adaptation to three such deformation zones, ZFMNE00A2, ZFMNE0060A and ZFMNE062A (see Figure 3-11).

Since the new data included in data freeze 2.1 have resulted in only minor changes to the deformation zone model where it concerns zones longer than 3,000 m, one new zone cutting the south-western corner of the target are (see Section 3.2), it seems very likely that all existing regional deformation zones crossing the target area are already known. However, it cannot be totally excluded that there still are undetected features in smaller scale. Furthermore, the geometry and character of some of the confirmed deformation zones are still an issue of concern, e.g. a NS trending zone observed at the bottom of the cored borehole KFM07A in the north-western corner of the target area. In addition, there are still some uncertainties regarding the truncation of gently dipping zones, although the new reflection seismic data provide strong support to the current view that the gently dipping zones terminate against adjacent, longer steeply dipping zones with NW or WNW strike.

The location of deformation zones and their properties are also of importance for characterising groundwater flow and chemistry and especially the gently dipping zones seem to play a dominant role in determining the hydrogeological character of the bedrock at Forsmark (see Section 5.3.2) and also for rock stresses (see Section 5.2.1).

Modelling actions to reduce uncertainty

If new data become available, see next section, continued modelling of deformation zones, using basically the same approach as for 1.1–2.1, will decrease the uncertainties associated with the occurrence, geometry and properties of deformation zones in the target area. In addition, the importance of uncertainties associated with deformation zones in the target area for groundwater flow and chemistry can be explored by numerical simulations (see also Section 5.3.2)

Site data requirements for reducing uncertainty

Current plans already contain a number of investigations that will provide a valuable input to the characterisation of deformation zones in the target area. These include surface excavation of representative lineaments, high resolution surface magnetic measurements, reflection and refraction seismics, and a number of cored- and percussion-drilled boreholes (Figure 5-1). One of these boreholes is not included in the CSI programme /SKB 2005c/. This borehole, KFM01C, is designed to investigate the character of zone ZFMNE0060A and the gently dipping zone ZFMNE00A2, both of which are important for the repository layout. This borehole is drilled from drillsite 1 towards the south.

In order to obtain a good coverage of the rock in all parts of the repository area, the need for an additional cored borehole is identified (KFM01D). This borehole should be designed to investigate the central part of the target area, including lineaments that trend NS and NW. In addition to geological information, this hole should provide hydrogeological and hydrogeochemical data from the central part of the target area (see Section 5.3). The borehole will also be used as a verification tool to test the character of the bedrock in the central part of the target area, as predicted in previous model versions.

Since the representativity of NS lineaments as being deformation zones is a remaining issue of concern, it is also suggested that the possibility of surface excavation of such a lineament in the north-western part of the target area should be investigated.

In essence, new seismic reflection data analysed in modelling stage 2.1 support the existence of gently dipping fracture zones in the south-eastern part of the candidate area. In addition, these data indicate the presence of a separate group of gently dipping zones that strike NE and ESE and dip moderately southwards in the domain south-west of the tectonic lens. Furthermore, the new data show that the earlier detected minor fracture zone at c. 320 m depth in borehole DBT1, close to reactor 3, corresponds to a reflector that dies out to the south-east and does not transect the candidate volume. According to current understanding, none of these new, gently and moderately dipping zones transect the rock volume proposed for the repository location. However, in order to get more strong support for the concept concerning the truncation of the gently dipping zone in DBT-1, it is suggested to conduct some minor additional reflection seismic measurements from the surface (extension of seismic profile #6 towards the north-west) as recommended by /Juhlin and Palm 2005/.

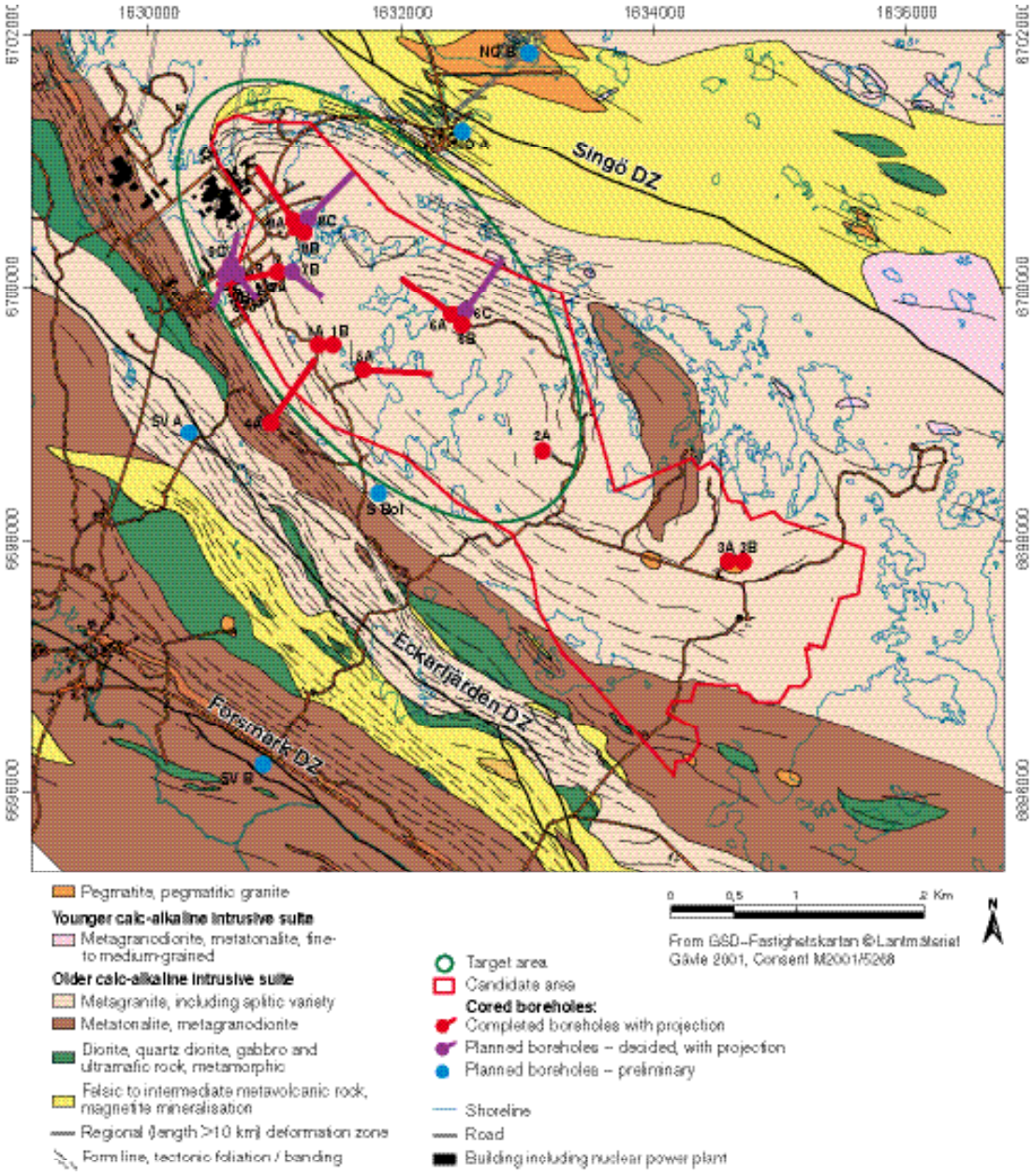

Figure 5-1. *The target area (green) and drilled (red) and planned boreholes in June 2005.*

5.1.2 Occurrence, geometry and properties of deformation zones bounding the target area

Uncertainties in the occurrence, geometry and properties of the regional deformation zones bounding the target area, i.e. the Singö, Forsmark and Eckarfjärden deformation zones, is judged as an issue of medium priority. The geometry of the regional zones is fairly well established, but there are uncertainties in the properties of the zones at repository depth. More data on properties can give support to the current conceptual model for the formation and development of deformation zones, which implies that all zones are geologically ancient structures and that the tectonic lens has been stable over a long time period.

Although sensitivity analyses conducted within SDM version 1.2 demonstrated that the geometry and hydraulic properties of these zones only have minor influence on the flow conditions in the target area and on the retention of radionuclides potentially released from a repository within the target area, uncertainties in these properties may affect the regional groundwater flow and possibly the location of the end points for radionuclides if released from a repository.

Modelling actions to reduce uncertainty

As for deformation zones in the target area and if new data become available, continued deformation zone modelling, using basically the same approach as for 1.1–2.1, will decrease the uncertainties associated with the occurrence, geometry and properties of deformation zones bounding the target area. In addition, the importance of these uncertainties for groundwater flow and chemistry can be explored by numerical simulations. However, already performed analyses strongly suggest that the uncertainties are of low importance, implying a limited need for additional sensitivity analyses.

Site data requirements for reducing uncertainty

Plans for drilling through the Singö, Eckarfjärden and Forsmark deformation zones are already outlined in the CSI programme /SKB 2005c/ (Figure 5-1). It is judged that drilling through the Singö Forsmark deformation zones is still motivated, since these investigations can provide data that contribute to geological and hydrogeological understanding of the role of these boundary zones for the conditions inside the target area. Investigation of especially the Singö zone can be of some importance, since it is located down-stream of the target area and, therefore, could affect the potential path of the discharge from a repository. Geological, hydrogeological and hydrogeochemical data from the zone and from the surrounding rock will thus aid to the understanding of the role of the Singö zone in the hydrogeological system. In addition to this, data on the composition of groundwater below the Baltic Sea can give indications on the importance of past transients, e.g. land rise, for groundwater flow and chemistry.

Further investigations of the Eckarfjärden deformation zone are judged less motivated. There are already two percussion holes drilled through the zone.

5.1.3 Fractures and fracture domains, including sub-horizontal fractures, inside the candidate volume

In the site description, minor deformation zones and fractures are handled statistically by discrete fracture network (DFN) modelling. There are several uncertainties associated with the description of the fracturing of the rock that concerns both the understanding and conceptualisation of the fracturing and the quantitative DFN modelling approach.

Although not implemented yet in quantitative DFN modelling, a conceptual model for division of rock domain RFM029 into fracture domains has been developed. This model is based on: 1) observations of an increased frequency of fractures with apertures in the uppermost c. 300 m of the bedrock, 2) observations of very few fractures with apertures at depth in the volume beneath the influence of the gently dipping deformation zone ZFMNE00A2, and 3) adaption of the hypothesis that there is some correlation between the development of fractures with apertures, the occurrence of gently dipping deformation zones and the current rock stress regime (see Section 3.2). However, the correlation of fracturing to rock stress and gently dipping deformation zones remains to be tested (see also Section 5.2.1).

One specific feature of the more fractured near-surface bedrock concerns sub-horizontal fractures with large apertures which potentially can bear much groundwater. Resolving uncertainties regarding the characteristics of these structures and their potential connectivity and interplay with other water-bearing structures, e.g. the gently dipping deformation zone ZFMNE00A2, is of importance for the hydrogeological conditions in the uppermost part of the rock and the potential draw-down effects of a repository at the site.

The principal remaining uncertainties in the DFN model where it concerns the fracturing of the bedrock at depth below the gently dipping deformation zone ZFMNE00A2 concern the size and intensity distribution, especially of sub-horizontal fractures, and the correlation between the geometrical DFN and the hydraulic properties of the fractured rock (hydraulic DFN). These issues are of high priority to resolve, especially since, in order to ensure long term mechanical stability, canisters must not be deposited in deposition holes intersecting too long fractures, see e.g. /SKB 2005b/. Proper estimates of the fracture size distribution thus both effects the percentage of useable deposition positions and the probability of erroneously placing canister in a deposition hole intersected by a

too long fracture. Understanding the correlation between the geometrical and the hydrological DFN is of importance for understanding the groundwater flow in the rock (Section 5.3.1) as well as the groundwater chemistry (Section 5.3.5).

Modelling actions to reduce uncertainty

Assessment of available and new data and further modelling will be undertaken in order to reduce uncertainties in the DFN model. Evaluation of so far applied modelling strategies and assumptions made in the site descriptive modelling will, together with experience from parallel projects conducted within SKB (Project Expect /SKB 2006c/ and Project RecovereD), provide input to improvements of the DFN modelling approach. In addition, the need for a closer and more integrated evaluation of the present concept of fracture domains between geology, rock mechanics and hydrogeology has been identified.

It is further recognised that it most probably will be difficult to resolve uncertainties in the size and intensity distribution of sub-horizontal fractures with site data from boreholes alone. Current intensities are probably overestimated, but it is more difficult to bound the size distribution. Sensitivity analyses, testing different distributions in the Safety Assessment context may be needed. Data from underground investigations will increase the possibility of detecting these features, but it may still be a difficult task. In addition, it may be worthwhile to analyse old data from mapping of the underground tunnels in SFR, alternatively to collect new fracture data from the tunnels in SFR (see below).

Site data requirements for reducing uncertainty

Boremap mapping of all on-going, planned and new cored boreholes suggested will provide additional fracture data to support the DFN analysis and modelling. This includes the proposed additional cored borehole through the central part of the target area that will provide fracture data needed to test the present hypothesis of fracture domains within rock domain RFM029 and give input to an assessment of their geometrical extension. More fracture data in the near-surface rock above deformation zone ZFMNE00A2 can be obtained from a new cored borehole at drill site 2, suggested for rock stress measurements (see 5.2.1).

Excavation and fracture mapping at the surface can provide additional information on the fracturing of the rock at depth below the gently dipping deformation zone ZFMNE00A2, provided that the surface mapping is carried out at a location outside the influence of this zone. A detailed surface mapping has been carried out at an excavation close to drill site 7 and results from this mapping indicate that the fracture intensity is much lower than at other localities at, or closer to, the outcropping of zone ZFMNE00A2. Evaluation of these data will show whether this locality is distant enough from zone ZFMNE00A2 for the rock to be considered as structurally representative for the rock at depth below zone ZFMNE00A2. If not, another locality still further away from zone ZFMNE00A2 should be selected for excavation and detailed surface mapping.

It is also suggested that a new mapping of fractures along the walls of the tunnels in SFR should be undertaken in order to obtain more information on the size and intensity distributions from a well defined window at an underground facility. This would provide data down to a depth of 140 m.

5.1.4 Geological conditions that bound the extent of the repository

In the current repository layout at Forsmark, all deposition tunnels are located in rock domain RFM029 and below the gently dipping deformation zone ZFMNE00A2. Therefore, remaining uncertainties in the location of boundaries of rock domain RFM029 are important to resolve in addition to uncertainties in the geometry of ZFMNE00A2, as already mentioned above.

Analyses of data and modelling carried out so far have increased the confidence in the location of the boundaries of rock domain RFM029 in the target area, and another, already planned, borehole (KFM08C) will provide still more data to constrain the location of the boundaries under Asphällsfjärden (see Figure 5-1). Therefore, it is not found motivated to require more data above those already included in present plans.

Another issue concerns whether the rock domains surrounding RFM029 and the deformation zone ZFMNE00A2 are real boundaries for construction of the repository. It is argued that the properties of rock domains surrounding domain RFM029 might well be good enough for hosting parts of a repository, but it will not be possible to get enough data during the CSI stage to evaluate whether this is the case. In addition, the main reason to keep the current boundary for construction for now is the potential for iron oxide mineralisation in the rock bounding the candidate area (and RFM029), identified already during the pre-investigation stage and later confirmed in a separate study /Lindroos et al. 2004/. Resolving this specific issue can await underground investigations.

5.2 Rock mechanics and thermal issues and their handling

The remaining rock mechanics and thermal issues identified concern:

- Rock stresses in terms of magnitude and variability.
- Rock mechanics properties in terms of spatial variability and scale effects.
- Thermal properties in terms of spatial variability and upscaling.
- Bias in measurements of thermal expansion on stress-released samples.

The last issue in the list above could to some extent affect the reliability in thermal expansion data, but this could be compensated for in the analysis of data. Therefore, this is considered to be a methodology issue rather than an issue of collecting more data and is not further addressed here.

5.2.1 Rock stresses

Data and modelling carried out so far indicate that rock stresses at Forsmark are high, but there are still considerable uncertainties associated with both the magnitude of stress and its potential spatial variability. The main reason for this is the difficulty in obtaining reliable measurement data because of limitations in the measurement techniques at high rock stresses. Resolving uncertainties in rock stresses is of importance for repository engineering, since high rock stresses may imply stability problems when constructing a repository at the site. It is also of importance for safety assessment of a repository at the site, since rock stress is input to the assessment of thermal spalling in deposition holes after canister emplacement. Furthermore, the evolving conceptual site model suggests different stress regimes below and above the gently dipping deformation zone ZFMNE00A2. Data in support of this hypothesis would thus strengthen the confidence in the overall conceptual model of the site.

Modelling actions to reduce uncertainty

There is a need for numerical stress modelling to study the influence of deformation zones on the stress regime. In addition, the stress modelling should investigate the origin and extension in depth of the sub-horizontal superficial fracturing and the link to past and present state of stress. Such modelling is presently on-going, utilising the geological models of lithology and deformation zones and available stress data (see Section 3.2.2).

Site data requirements for reducing uncertainty

A number of on-going and already planned stress measurements in cored boreholes will provide additional stress data. These include over-coring in KFM07C and hydraulic testing of pre-existing fractures (HTPF) in boreholes at drill site 7 and drill site 9. In addition to this, rock stress measurements by hydraulic methods could be conducted in the new borehole KFM01D.

In order to test the hypothesis of different stress regimes above and below the gently dipping deformation zone ZFMNE00A2, stress data from the rock above this zone are needed. This requirement could be met by conducting stress measurements in a new cored borehole at drill site 2 (KFM02B).

In order to overcome problems associated with the measurement techniques, a feasibility study on high-capacity hydro-fracturing equipment is under way. In addition, analyses of breakouts in boreholes at Forsmark will provide data on stress levels and on the orientation of stress.

5.2.2 Rock mechanics properties

Although the rock mechanics properties in the target area seem to be rather well known (see Section 3.2.1), there is still some uncertainty related to the spatial variability in the target area and effects of scale at which the properties are evaluated. These uncertainties have some impact on repository design, but the importance depends on the construction criteria, which is different for different parts of the repository (shafts, central area, and deposition areas). This could be considered in future modelling.

Underlying the uncertainty in spatial variability and scaling is the issue of representativity of the samples collected for laboratory testing of rock mechanics properties of intact rock and fractures. This potential bias in sampling is currently the focus of a separate study (see Section 2.5) and the result may define a need for new data.

The analyses undertaken in modelling stage 2.1 have identified the need for additional sampling and rock mechanics testing of some of the subordinate rock types, e.g. amphibolite. Such sampling is already included in the current plans.

5.2.3 Thermal properties

Uncertainties remaining in the site descriptive model of thermal properties concern spatial variability and scaling of thermal conductivity. Issues of special concern are related to thermal properties and size distribution of subordinate rock types in rock domain RFM029 and the potential anisotropy of thermal data and its relation to the foliation/lineation of the rock. The preliminary safety evaluation, PSE, /SKB 2005b/ has shown that all thermal requirements and preferences are met for a repository at Forsmark. This indicates that further reduction of these uncertainties is not of high priority, but would allow for a more efficient repository design.

It should be noted that the preliminary safety evaluation, PSE, is based on model version 1.2. The evaluation of thermal properties undertaken as a part of modelling stage 2.1 indicates that the rock type amphibolite has low thermal conductivity and that this can have impact on the thermal conductivity distributions for rock domain RFM029 (see Section 3.3)

Modelling actions to reduce uncertainty

Further analyses of new data and thermal modelling will aid in reducing remaining uncertainties. This includes evaluation of the on-going field and laboratory tests addressing anisotropy of thermal properties in a foliated rock. In addition to this, an improved integration with geology what concerns the identification of important sub-ordinate rock types, their spatial variability and large-scale anisotropy, will aid in reducing remaining uncertainties in the thermal model.

The methodology applied for scaling of thermal properties will also be evaluated and updated as necessary in order to resolve remaining uncertainties inherent in the approach.

Site data requirements for reducing uncertainty

In addition to on-going and already planned laboratory and field measurements, including the on-going study on anisotropy of thermal properties in foliated rocks, there is a need for more data from laboratory measurements on subordinate rock types. Of special concern are the rock types granite, granodiorite and tonalite (rock code 101051) and amphibolite (rock code 102017) for which few or no data from measurements are currently available.

5.3 Hydrogeological and hydrogeochemical issues and their handling

The remaining hydrogeological and hydrogeochemical issues identified concern:

- Hydraulic properties of the rock mass in rock domain RFM029 (target area).
- Hydraulic properties of the deformation zones in rock domain RFM029 (target area).
- Hydraulic properties of rock mass and deformation zones in rock domains other than RFM029.
- Hydraulic properties of near-surface rock.
- Groundwater composition and interactions between surface and groundwater.
- Anomalies in uranium concentration.
- Redox and alkalinity buffering capacity of the bedrock.
- Hydrogeological confirmation and indications of structures (hydraulic contacts or not) and control of the hydraulic applicability of the DFN model.
- Consistency between stress magnitudes and orientation and anisotropy of hydraulic conductivity.

All issues in the above list are important integration aspects related to the conceptual understanding of the site. The last two issues will be further handled in the modelling work by e.g. analysing signals/responses from the hydraulic monitoring system and by evaluation of correlation between rock stresses, fracture minerals and hydraulic properties. However, these activities do not require any new data or investigations above those already in the current plans. Therefore, they are not further discussed here.

5.3.1 Hydraulic properties of rock mass in rock domain RFM029 (target area)

Current hydrogeological data and modelling strongly indicates that the rock mass in the target area (north-western part of rock domain RFM029) comprises sub-domains of different hydraulic properties (see Sections 2.7 and 3.5.1). However, there are still uncertainties in the geometrical extension of these sub-volumes as well as in the spatial variability of hydraulic properties within these sub-domains. Especially, reducing uncertainties in the distribution of flow in the low-transmissive rock volume at depth below the deformation zone ZFMNE00A2 is of high priority primarily because of the implications on a potential future release of radionuclides. Furthermore, these uncertainties affect the prediction of inflow to the open repository and the assessment of resaturation after closure. Uncertainties in the description of the flow also affect the understanding and description of the groundwater composition in this rock volume and thereby indirectly also uncertainties in the assessment of the future, long-term stability of the engineered repository barriers (see also Section 5.3.5).

Modelling actions to reduce uncertainty

Further analyses of hydrological data from new and planned boreholes and hydrogeological DFN modelling are required for reducing the uncertainty in the description of hydraulic properties of the rock mass. Different hypotheses in subdividing the model domain should be tested. Another aim should be to eventually be able to distinguish between the two alternative concepts propagated into the SR-Can assessment, a sparsely connected DFN with a rather high transmissivity field and a well connected DFN with a very low transmissivity, since these two different concepts result in quite different flow distribution around individual deposition holes as well as distribution of transport resistance (F-factor) in fluid pathways from deposition holes.

A potential additional source of information is contained in the resistivity logs of the boreholes. These logs indicate the presence of water-filled, but not necessarily water-flowing, fractures, and the frequency of water-filled fractures might also be useful information for the hydraulic DFN modelling.

Site data requirements for reducing uncertainty

In addition to on-going and planned hydrogeological tests in existing and new boreholes, it is essential to get hydrogeological data from the central part of the repository volume in order to confirm the geometrical extent of the low-permeable volume of the rock at depth. Such data could be obtained from the proposed new cored borehole, KFM01D, by flow logging of individual fractures, which implies that logging with the Posiva flow log (PFL) is required.

Carrying out dilution tests with the purpose to analyse open, but non-flowing fractures could provide input to assessments of whether the system is advection or diffusion dominated. Such tests have been considered and there are still some practical issues to resolve, but, considering the importance of the results of such tests, planning should proceed.

Analyses of the composition of water samples collected from very low transmissive fractures (see Section 5.3.5) would potentially also be important for characterising the flow system, since very different chemistry in these fractures would indicate hydraulic isolation.

It is further concluded that it will not be possible to fully characterise the flow distribution in the rock mass or the deformation zones (see also Section 5.3.2) by hydraulic tests conducted from the surface. A final verification of the existence of the low-permeability volume must, therefore, await results of hydraulic testing conducted during underground investigations, although noting that it will never be possible to obtain a complete characterisation of the flow path distribution in the rock.

5.3.2 Hydraulic properties of deformation zones in rock domain RFM029 (target area)

Hydraulic data analysed so far indicate large variability in transmissivity of deformation zones, both horizontally and with depth, but there are still large uncertainties in describing this spatial variability in the scale appropriate for a safety assessment of a repository. Sensitivity analyses reported in version 1.2 of the Forsmark SDM /SKB 2005a/ show that uncertainties in transmissivity of the zones in the candidate volume affect the groundwater flow in this volume and thereby the spatial distribution of migration paths from a repository, although with small impact on the transport resistance statistics. Reducing these uncertainties would improve the site-scale groundwater flow modelling and the possibility to utilise groundwater chemistry data to increase the confidence in the groundwater flow model and thus also in the predictions of potential future radionuclide releases. The impact of uncertainties in deformation zone transmissivity for repository engineering is judged to be of limited importance, but could have some influence on the assessment of issues related to the construction of shafts and ramps, e.g. extent of grouting needed.

Modelling actions to reduce uncertainty

Further evaluation and comparison of data from on-going and planned hydraulic testing in existing and new boreholes at different locations will help in reducing the uncertainties. Also vertical seismic profile data (VSP) could give indications as to whether zones are carrying water or are tight. Continued modelling, where different hypothesis of the spatial variability in transmissivity of the zones are tested by checking against groundwater chemistry, is another action proposed for reducing the uncertainty.

Site data requirements for reducing uncertainty

On-going and planned hydrogeological tests in existing and new boreholes will provide more data on the zones in the vicinity of the repository, i.e. zone ZFMNE0060A (see Figure 3-11) and the gently dipping zone ZFMNE00A2. Furthermore, extending the proposed new cored borehole KFM02B such that it intersects zone ZFMNE00A2 would allow for another transmissivity characterisation of this zone.

5.3.3 Hydraulic properties of rock mass and deformation zones in rock domains other than RFM029

Hydraulic properties and geometries of deformation zones and rock mass fracturing in rock domains other than RFM029 are uncertain, but, according to current modelling results, of less importance for the hydrogeological conditions in the target area. One exception is the hydraulic character of the near-surface rock, which seems to be highly transmissive and in hydraulic contact over long distances. This is further discussed in Section 5.3.4) below.

Modelling actions to reduce uncertainty

The importance of uncertainties in hydraulic properties and geometries of deformation zones and rock mass fracturing for groundwater flow can be explored by further sensitivity analyses, building on the analyses carried out in version 1.2 of the SDM for Forsmark and utilising groundwater chemistry data from the site for calibration purposes.

Site data requirements for reducing uncertainty

Drilling through the Singö and Forsmark deformation zones and hydraulic as well as hydrogeochemical characterisation of these zones and the surrounding rock will provide information that will contribute to the understanding of the regional hydrogeological conditions at Forsmark (see also Section 5.1.2). Also other hydraulic tests outside the target area would improve the understanding.

5.3.4 Hydraulic properties of near-surface rock

The current understanding of the groundwater flow in the high-transmissive near-surface rock structures is gradually improving. Although results of hydraulic tests indicate hydraulic connections over long distances (see Sections 2.7.5 and 3.5.1), there are still uncertainties in the lateral extension of this near-surface flow system, local or connected to the regional system, and whether it is connected to the deeper system or not.

Resolving uncertainties associated with the hydraulic properties and groundwater flow in the near-surface rock is important for repository engineering when assessing inflow and grouting requirements in shaft and access tunnels. It is also of importance for environmental impact assessments and assessment of long-term safety of a repository at the site, since the character of the near-surface flow will influence the drawdown created by the repository and it can also affect the location of entrance points in the surface system for radionuclides, if released from the repository.

A better understanding of the hydrogeological properties of the near-surface rock is also important for understanding near-surface chemistry and for enhancing confidence in the hydrogeological model of the deep system.

Modelling actions to reduce uncertainty

Analyses of data from on-going and planned hydrogeological tests in existing and new boreholes and further hydrogeological modelling will be carried out in order to decrease uncertainties in hydraulic properties of the near-surface rock. Modelling carried out so far has not acknowledged the presence of sub-horizontal, high-transmissive fractures in the near-surface rock. This should be done in forthcoming modelling and various hypotheses that could explain differences in fracture properties should be formulated and tested by simulations/calibrations against groundwater chemistry data and results of pumping tests.

A better understanding of the hydrogeological properties of the near-surface rock would also contribute to improvements in the description of the deep system by allowing for inclusion of the high-transmissive near-surface fractures in forthcoming modelling of the deep hydrogeological system.

Site data requirements for reducing uncertainty

Monitoring of pressure responses in existing and new boreholes and pumping/interference tests between boreholes will provide additional information to the evaluation of the properties of the near-surface rock. In addition, there is an extended chemical sampling on-going in existing percussion-drilled holes that can provide chemistry data to support an integrated hydrogeological and hydrogeochemical interpretation (see Section 5.3.5).

It is further noted that flow measurements in the near-surface rock possibly would show if natural flows are too high to support a hypothesis of a local flow system.

Currently, there are less data at the potential shaft positions, but the main reason to characterise the near-surface flow at these positions would be for construction planning, e.g. assessing grouting needs etc. Such characterisation can probably await underground investigations.

5.3.5 Groundwater composition and interactions between surface and groundwater

The groundwater chemistry and its spatial variability is of importance for understanding the present hydrogeochemical and hydrogeological system and, thus, also affects the confidence in predictions of future changes, which is of importance for safety assessment of a repository at the site. In this context, there are still considerable uncertainties remaining concerning the groundwater composition in the low-conductive part of the rock at depth in the target area, i.e. in the potential repository volume, and in the potential influence on this water chemistry by both surface water and deeper groundwater that has taken place in the past and that may take place in the future. However, as noted in the PSE /SKB 2005b/, even if the exact future evolution of groundwater composition is uncertain, due to uncertainties in future groundwater flow, it is highly likely that the groundwater composition will remain within the range of the required and preferred criteria also in the future. However, further reduction of uncertainties in the spatial distribution at depth is desirable to improve the understanding of the hydrogeochemistry and thus to enhance the safety case.

The main reason to the uncertainties in the description of the present groundwater chemistry is the lack of data from depth in the rock. This in turn is due to both the difficulty in collecting water samples, especially in the low-conductive parts, and to obtain samples that are representative for the natural conditions in the rock.

Modelling actions to reduce uncertainty

Analyses of new data from water chemistry characterisation in existing and new boreholes will be conducted and provide additional information to the description of groundwater chemistry conditions. In addition to this, a more thorough evaluation of data for samples judged as non-representative will be undertaken in order to find out whether there is relevant information that could be extracted from these data. This could include, for example, an evaluation of the impact of test conditions prior and during sampling.

Earlier data have indicated the presence of an old marine (Littorina Sea) water signature beneath Lake Bolundsfjärden. Further assessment of data from samples taken from soil tubes in Bolundsfjärden will be carried out to investigate whether this is a discharge area for deep groundwater. This will be complemented by analyses of data obtained from a percussion hole (c. 200 m deep) drilled at a small island in Lake Bolundsfjärden.

Based on assessment of the representativity and spatial precision of chemical data, further modelling activities will be undertaken in order to obtain an integrated picture of the hydrogeology and hydrogeochemistry at the Forsmark site.

The possibility that pumping tests could provide chemical responses in addition to hydrogeological was raised. This could be explored by simulating the chemical evolution of a pumping test in order to study what pumping rates would be needed and which issues could be addressed by measuring chemical responses of such a test.

Site data requirements for reducing uncertainty

In order to get a better understanding of the groundwater composition in the potential repository rock volume, there is a need for data from this low-conductive part of the rock. This includes data on water chemistry in both low-conductive fractures and the rock matrix. Sampling and analyses of porewater in the rock matrix have been conducted in several of the existing cored boreholes and should continue in conjunction with the drilling of new cored boreholes (see also Section 5.4.2). Of special interest would be to obtain a chemical profile of the matrix pore water away from a strongly water conducting fracture as this may potentially show evidence of relict palaeo-interaction between the water in the fractures and in the rock matrix. However, this requires that the position of this water conductive feature is known at the time of collecting the core samples for matrix water analyses, i.e. at the time of the drilling. Sampling of water in low-conductive fractures has so far not been conducted, but the possibility should be evaluated and the applicability of potential methods should be tested.

An on-going programme for regular registration of water chemistry in some of the existing core-drilled and percussion-drilled holes will provide more chemical data both from depth and from the near-surface rock. In addition, the percussion-drilled borehole at the island in Lake Bolundsfjärden can provide information on water chemistry in the near-surface rock, and this can also be the case for the shallow soil pipes in Lake Bolundsfjärden, unless they are too shallow.

It is further suggested that the chemical characterisation programme should be extended to include also analyses of natural tracers like ^{36}Cl and noble gases, both in the near-surface waters and deeper groundwaters.

Conducting pumping tests over long periods can possibly give information on possible interactions between groundwater at repository level and the surface system and the deep system, respectively, and potential changes over time. However, such tests can imply many practical problems and can also have a negative impact on other investigations and tests at the site. Therefore, the idea has been put on hold for the time being for possible activation at a later stage.

5.3.6 Anomalies in uranium concentration

Analyses of groundwater chemistry data have revealed an anomaly in uranium concentration in the groundwaters at Forsmark. Large variations in uranium content in surface waters are common, but lower uranium content with depth is expected due to decreasing redox potential and decreasing bicarbonate content. This trend is not seen in the data collected so far at Forsmark. Instead, most of the data indicate high uranium values at depths between 200 and 600 m.

It is very important to understand the cause of these high uranium concentrations. Some pegmatites in the Forsmark area have elevated U-contents, which is documented in version 1.2 of the Forsmark SDM /SKB 2005a/, and a few fracture fillings have been found showing U contens up to 2,300 ppm /Sandström and Tullborg 2005/. Despite this, the reducing groundwater is expected to ensure low uranium concentrations in the groundwater. If the elevated concentrations are connected to the occurrence of glacial meltwater it could raise questions regarding the redox conditions during glaciation and the potential for deep penetration of oxygenated water during glaciation, which is an important issue to consider in the safety assessment of a repository at the site

Modelling actions to reduce uncertainty

The reason for this anomaly is presently under investigation by conducting hydrogeochemical analyses and modelling, including also evaluation of trace element analyses in soil samples. Different hypothesis are tested, e.g. whether the anomaly is of colloidal nature, which it does not seem to be, whether there are trends with distance to the Baltic Sea, whether there is a correlation to the transmissivity distribution, or whether it is a result of drilling.

Site data requirements for reducing uncertainty

On-going and planned hydrogeochemical sampling and analyses, including also analyses of fracture minerals, will provide additional data for exploring the anomalies in uranium concentration. In addition, the on-going programme for regular registration of water chemistry in some of the existing core-drilled and percussion-drilled holes will provide an opportunity to follow potential changes in uranium concentration over time in some of the sampling points.

5.3.7 Redox and alkalinity buffering capacity of the bedrock

The redox and alkalinity buffering capacity of the rock is important input to the safety assessment of a repository at the site when evaluating the potential impact of the operational phase on the hydrogeochemical conditions. In addition, the consequences of intruding oxygenated melt water during glacial conditions will depend on the redox buffering of fracture minerals and rock matrix minerals. The main redox buffering parameters of interest are the content of Fe (II) and sulphide, whereas calcite is of importance for pH. So far, there have not been enough detailed mineralogical data available to provide a confident description of the redox- and alkalinity buffering capacity of fracture minerals and rock matrix, so this issue remains to be solved.

Modelling actions to reduce uncertainty

Evaluating the redox and alkalinity buffering capacity of the rock and its impact on present groundwater chemistry is part of the established methodology for developing a geochemical description of the site, and this work will proceed as new data become available.

Site data requirements for reducing uncertainty

On-going and already planned activities for characterisation of fracture minerals include the evaluation of mineralogical entities of importance for determining the redox- and alkalinity buffering capacity of fracture minerals.

Conducting tests with injection of oxygenated water and low-pH water at depth in the rock with the purpose to measure the buffering capacity might be possible. Such tests could possibly be combined with SWIW tests and/or with in situ test of sorption properties (K_d), but the experimental feasibility needs first to be assessed.

5.4 Issues related to bedrock transport properties

The remaining issues related to the bedrock transport properties concern both flow-related transport properties, especially channeling, and migration properties of the rock matrix. These issues are further described below.

5.4.1 Flow-related transport properties – Channeling

The transport resistance, or F-factor, is a measure of the potential for solute retention along flow paths in the fractured rock and is simply defined as the flow-wetted surface to flow ratio. For fractured rock systems where diffusive exchange with the rock matrix dominates the solute residence time distribution, the magnitude of the surface area over which matrix diffusion takes place is a key entity governing solute transport. Indeed, it is the F-factor and a materials property group, combining both diffusive and sorptive properties of the rock, which are the central parameters for the estimation of the solute residence time distribution.

The F-factor is not a directly measurable parameter in the same sense as material properties such as effective diffusivity or sorption K_d. Therefore, the correct estimation of this entity from hydrogeological flow models is crucial for solute transport calculations. Given that the F-factor is strongly dependent upon modelling assumptions that are not easily verifiable, uncertainties concerning the transport resistance in the rock surrounding a repository are important to resolve as much as possible

owing to the large impact this may have on the transport of radionuclides, if such releases will occur from a repository at the site. As the transport resistance is dependent on both the magnitude and the geometry of the flow field, remaining uncertainties are closely related to the uncertainties in hydraulic properties of the rock mass in rock domain RFM029 (see Section 5.3.1), i.e. whether flow and transport occurs in a very sparsely connected network of fractures (or channels), as indicated from data so far, or more evenly distributed in the rock.

Modelling actions to reduce uncertainty

Further modelling activities that will be carried out to reduce uncertainties in the estimation of the transport resistance involve analyses of the sensitivity to different assumptions concerning flow path geometry and transmissivity, building on the analyses carried out in the PSE for Forsmark /SKB 2005b/ and in version 1.2 of the Laxemar site descriptive model /SKB 2006a/. In addition, a more complex analysis will be undertaken using DFN models as a complementary activity to the above.

Two activities of a more strategic character are also underway. The first activity is aimed at providing a common framework for the disciplines hydrogeology, hydrogeochemistry and bedrock transport properties and to produce a methodology detailing how partially validated and discipline consistent models can be produced. The second activity will result in a "position paper" that will address different types of in situ tests, the type of information such tests can provide, and how this information can be utilised for determining transport properties of the rock.

Site data requirements for reducing uncertainty

Flow data (PFL) from the new borehole suggested in the centre of the repository (KFM01D) are directly relevant for determining the flow distribution and thus also for estimation of the transport resistance in this part of the rock. In addition, chemical data from this borehole and other boreholes are important insofar that they provide information concerning natural tracers. This also includes the composition of matrix porewater, although problems relating to the representativity of the chemical data need further attention.

It is difficult to carry out more experiments from the surface to characterise flow-related transport parameters, especially channelling within individual fractures. Large scale tracer tests can possibly indicate if there are some very fast flow paths, but the result cannot be used to quantify channelling effects. This issue will be further addressed in the position paper under preparation (see above) and also using tracer tests that may be relevant during underground investigations.

5.4.2 Migration properties of the rock matrix

The retention properties of the rock matrix, porosity, diffusivity and sorption, are important inputs to the safety assessment analyses of radionuclide migration from a repository at the site. Furthermore, these properties are important for understanding the water chemistry at the site and thus also for enhancing confidence in the hydrogeological model.

The diffusivity in the rock matrix is quantified through the formation factor, which is determined both by measurements in situ and in the laboratory. Although both provide results that are internally consistent, there is a considerable systematic difference between the results obtained in the in situ measurements and the corresponding laboratory measurements. One explanation for this difference can be that the laboratory samples have undergone stress release. However, the in situ measured formation factors are also uncertain due to difficulties in specifying the in situ pore water concentration. The potential impact of stress release on laboratory samples may also introduce uncertainties in the laboratory measurements of matrix porosity and possibly also sorption (see below). In addition, the still rather limited data set is another source of uncertainty when describing the spatial variability and up-scaling of matrix retention properties, including conceptual uncertainties in describing the sorption process.

Modelling actions to reduce uncertainty

Analyses of new results from on-going and planned laboratory and in situ experiments in combination with further hydrogeological and hydrogeochemical modelling will contribute to reduce uncertainties in bedrock transport properties. One specific issue of importance in this context is related to the composition of the pore water in the rock matrix and the possibility to quantify uncertainties in the analyses of this water. This should be further explored. Another issue concerns the applicability of the simplified K_d-concept for describing retention in the bedrock. To deal with this uncertainty, alternative models for describing sorption can be explored as well as the relevance of additional processes for retention, such as precipitation and co-precipitation.

Site data requirements for reducing uncertainty

Already on-going and planned in situ and laboratory experiments for measuring matrix retention properties will provide a data set that is judged sufficient for handling present uncertainties. Concerning sorption it is concluded that on-going and planned SWIW tests can demonstrate the existence of solute retention and give an indication of its magnitude, at least over the short time scales and matrix penetration depths characteristic of the tracer test.

Conducting a test to measure K_d in situ can also demonstrate the existence of sorption, but owing to the fact that this can realistically only be done at a limited number of locations over a limited period of time, it will probably be difficult to quantify sorption on a site-wide basis from the results of such a test. At this time it therefore seems most appropriate to continue with laboratory measurements of sorption, but to complement measurements on crushed material with measurements on larger samples combined with an assessment of the potential impact of stress relaxation on the samples. Measurements of K_d on larger samples from boreholes KFM01A and 02A are already planned.

Another essential issue which needs further attention concerns the uncertainties associated with sampling and analyses of the composition of the pore water in the rock matrix and the implications for the evaluation of matrix retention properties and the understanding of the hydrogeochemistry and hydrogeology at the site. It is probably difficult to fully quantify the uncertainty and representativity of the pore-water analyses, but further sampling and analyses of pore-water composition could still be very valuable, especially if sampling can be carried out at different distances from water-conducting fractures. Even if evaluated concentrations are uncertain, any gradients in element concentrations away from the water-conducting fracture can give indications of the presence and importance of matrix diffusion. Since sampling for analyses of pore-water composition is conducted during drilling, sampling for determining chemical gradients away from a water-conducting feature requires that this feature is known prior to, or can be identified during, drilling. One such feature is the gently dipping zone ZFMNE00A2. Therefore, the new borehole at drill site 2 (KFM02B) would be appropriate for such sampling and analyses if it could be drilled through and an additional few tens of metres below deformation zone ZFMNE00A2.

In order to get more information on the potential impact of stress relaxation on the porosity and pore-water composition of samples brought to the laboratory it is suggested to use tracers in the drilling water at such concentrations that these tracers could be analysed in the matrix pore water obtained from samples of the drill core.

6 Implications for the site investigation programme

The implications for the site investigation programme concerning the need for additional data to resolve remaining critical site-specific issues are summarised in this chapter, with focus on modifications compared with the CSI programme /SKB 2005c/. These modifications concern boreholes and investigations in boreholes as well as surface-based investigations. They are the result of the cooperative work of the Forsmark modelling team and the Forsmark investigation team conducted during modelling stage 2.1.

The text in this chapter is intended to give an overview of the investigations proposed, with short reference to the issues in Chapter 5. Complementary to this, extended motivations and recommendations for the location of cored boreholes and investigation in these boreholes have been provided in separate motivation documents. This complement also includes motivation documents for investigation of lineaments in the north-western part of the candidate area by percussion drilling, core drilling and surface excavations. All these documents are enclosed as appendices to this report. Details of the different measuring programmes are not given in this report, but in separate activity plans (AP) developed by the site investigation team following recommendations given in this report and in the appended motivation documents.

6.1 Cored boreholes

Compared with the CSI programme /SKB 2005c/, four new core-drilled boreholes in the north-western part of the candidate area (target area) are suggested. These are boreholes KFM01C, KFM01D, KFM02B and KFM07C (see Figure 6-1). One of these four holes, KFM07C, is primarily intended for rock stress measurements by the over-coring method. The motive for this additional hole at drill site 7 is to try to compensate for the very limited results of stress measurements obtained in the cored borehole KFM07B. Since borehole KFM07B was included and motivated in the CSI programme /SKB 2005c/ and this new borehole KFM07C can be considered as a replacement of borehole KFM07B, borehole KFM07C is not further discussed here.

In the CSI programme, the need for three boreholes for collection of data required for more detailed planning of the repository design was indicated. Three holes were planned for this purpose, KFM09A–C, and two of them are drilled. The third hole, KFM09C, is specifically designed to investigate the rock at the border of the current layout (see Appendix 5.7). Since the current view is that the need for such details is of lower priority at the present stage of site investigations compared with the information that can be obtained from the proposed new holes in the target area, it is suggested that drilling of KFM09C should be assigned a lower priority at the present stage of the site investigation.

What concerns cored boreholes outside the target area (Figure 6-1), the location of the cored borehole south of Bolundsfjärden (KFM10A) is now specified and somewhat modified compared with the planned location outlined in the CSI programme /SKB 2005c/.

The earlier plans for drilling to characterise the boundary areas are now detailed. The north-eastern boundary will be characterised by drilling through the Singö deformation zone, whereas drilling beneath the SFR repository presently is not considered. Of the two alternatives for investigation of the south-western boundary outlined in the CSI programme /SKB 2005c/, drilling through the Forsmark deformation zone is prioritised. Investigating the Eckarfjärden deformation zone is presently less motivated, since there already are percussion holes drilled through the zone. Furthermore, sensitivity analyses conducted in version 1.2 of the SDM show that the hydraulic character of up-stream zones are less important than those of down-stream zones for the groundwater flow in the target area. More about the motives for the proposed borehole plans are given in the following sub-sections.

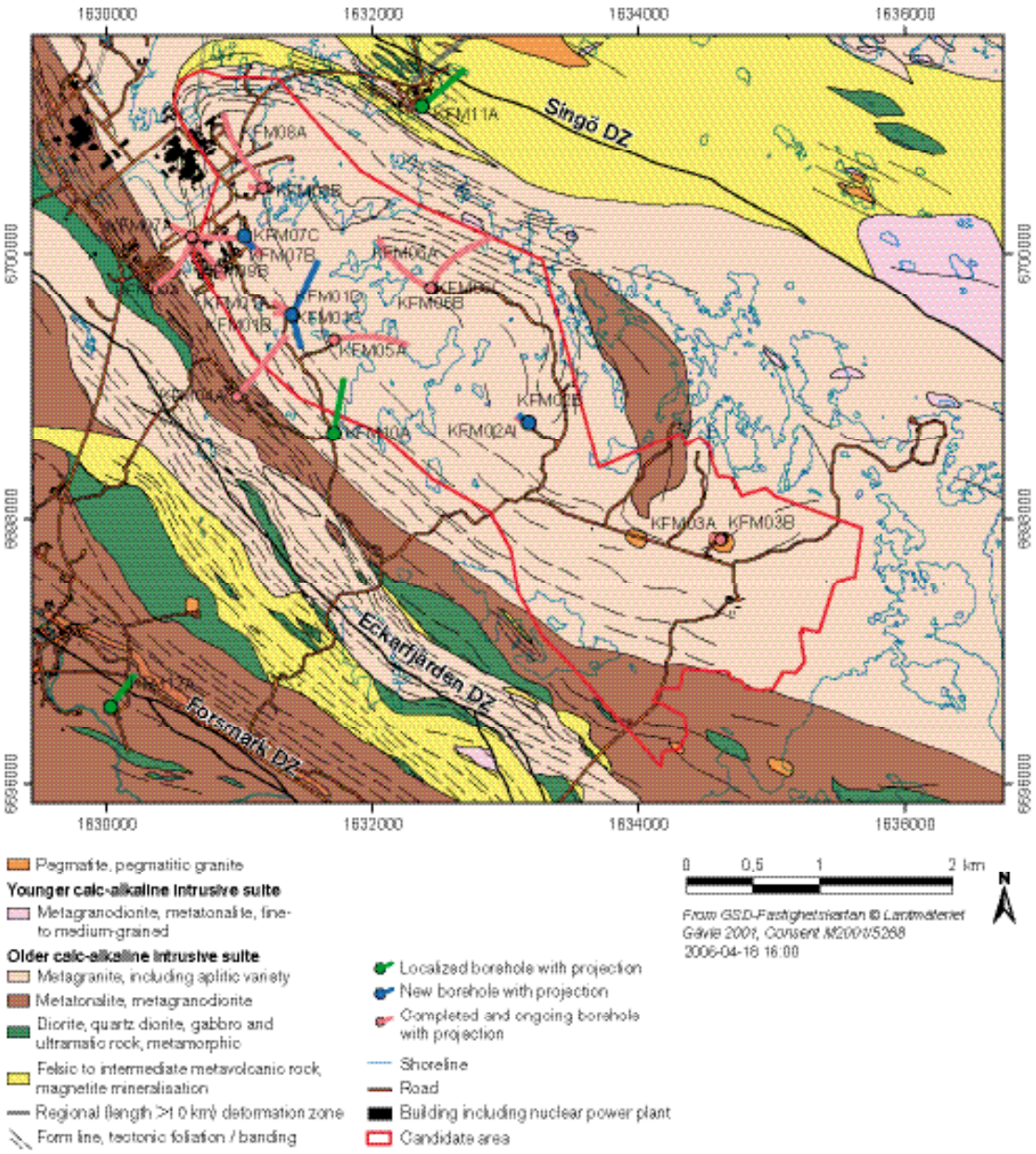

Figure 6-1. *New and localised cored boreholes compared with the CSI programme /SKB 2005c/ (see Figure 5-1).*

6.1.1 Borehole KFM01C

The main purpose of drilling this cored borehole is to investigate lineament XFM0060A0 in order to improve the confidence level of the inferred deformation zone ZFMNE0060A and to establish its geological characteristics, see Section 5.1.1. This deformation zone is of importance for the repository layout, since it, according to current interpretation, transects the target area and creates a corridor in the current layout due to its inferred length being longer than 3,000 m (see Figure 3-11). Information from the cored borehole KFM06A confirms the existence of this zone north of Lake Bolundsfjärden. By drilling borehole KFM01C, the south-western extension of the lineament can be investigated.

Drilling of borehole KFM01C is part of an extensive programme aimed at investigating lineaments in the target area. This programme also includes investigations of lineaments by percussion-hole drilling and by surface excavation. Motives for drilling borehole KFM01C and its location are specified in a motivation document for the first phase of the lineament investigation programme, see Appendix 5 (Section 5.1).

6.1.2 Borehole KFM01D

The purpose of drilling this borehole is primarily to obtain geological, hydrogeological, and hydrogeochemical data from the bedrock volume that includes the central part of the proposed repository, since such data are lacking, see Sections 5.1.1, 5.1.3, 5.3.1, 5.3.5 and 5.4.2. A separate motivation document for the location of these boreholes and which investigations should be carried out has been prepared, see Appendix 5 (Section 5.3).

The borehole is oriented such that it will intersect zone ZFMNE0061 close to repository depth and also the gently dipping zone ZFMNE00A2 in the upper part of the borehole. This means that this borehole can provide data on the character of these zones. Furthermore, it can confirm if lineaments LL0060 and XFM0099A0 are related to deformation zones that are vertical, in addition to provide base geological data. These objectives can be met by conducting the standard geological investigation programme for cored boreholes.

From a hydrogeological perspective, this borehole is important for confirmation of the existence of high-transmissive structures in the upper part of the bedrock as well as for confirmation of low-conductive rock at depth in the central part of the proposed repository. Investigations suggested to be carried out for meeting these objectives are pressure monitoring in nearby boreholes during drilling and measurements with the Posiva flow log (PFL) as well as single-hole hydraulic testing with the Pipe String System (PSS) after drilling.

Hydrogeochemically, the objective of the suggested investigations in this borehole is to obtain data from the potential repository volume, but also to provide hydrogeochemical data from different parts of the rock with different hydraulic transmissivity. This will contribute to the understanding of the hydrogeochemistry at the site, but will also support the hydrogeological analyses and the assessment of the transport properties in the rock volume of interest. To achieve this, it is suggested that the normal routine groundwater sampling and complete chemical characterisation from water-conducting zones is supplemented by sampling and characterisation of water from low-conductive zones and by sampling and chemical characterisation of porewaters from the rock matrix.

Sampling of water from low-conductive zones implies implementation of new measurement equipment. Thus, the possibility to conduct sampling in low-conductive zones in this borehole will depend on the feasibility of this equipment for this purpose (a feasibility study in KFM06C is planned) and the presence of suitable low-conductive zones, indicated by the PFL logs.

Sampling for characterisation of rock matrix porewater is conducted during drilling. In addition to sampling at regular intervals along the borehole, it is recommended that sampling should be conducted from a water-conducting zone, if such a zone is intersected, and further out into the rock matrix in order to allow for detection of possible diffusion profiles in the rock matrix adjacent to a water-conducting zone.

6.1.3 Borehole KFM10A

Borehole KFM10A is intended for geological and hydrogeological characterisation of the gently dipping zone ZFMNE00A2, see Sections 5.1.1 and 5.3.2. In addition, its location is selected to provide information to improve the understanding of the character of north-westerly trending lineaments in the south-western part of the target area and potential repository area. The motives for this hole and its location are specified in a separate motivation document, see Appendix 5 (Section 5.4).

For geological characterisation, a standard geological/geophysical investigation programme is recommended. For hydrogeological characterisation, pressure monitoring in nearby boreholes during drilling and measurements with the Posiva flow log (PFL) as well as single-hole hydraulic testing with the Pipe String System (PSS) after drilling, are recommended. Hydrogeochemical sampling and characterisation will be undertaken depending on the outcome of the PFL measurements.

6.1.4 Borehole KFM02B

The main purpose of this borehole is to provide rock stress data above the gently dipping zone ZFMNE00A2, see Section 5.2.1, but also to obtain information on groundwater composition in low-conductive zones of the rock and on porewater composition in the rock matrix, Sections 5.3.5 and 5.4.2, respectively. In addition, this borehole will be drilled through the gently dipping zone ZFMNE00A2 and thereby allow for hydraulic testing of this zone, see Section 5.3.2. The motives for this hole and its location are specified in a separate motivation document, see Appendix 5 (Section 5.5).

In order to test the current hypothesis that the rock fracturing is different above and below the gently dipping deformation zone ZFMNE00A2 and that this is correlated to rock stresses, stress data from measurements in the rock above zone A2 are needed. For this purpose, it is recommended that rock stress measurements are conducted by the overcoring method down to the intersection with zone A2. At a later stage, these measurements can be supplemented by hydraulic fracturing tests of the entire borehole.

Due to the closeness to borehole KFM02A, it should be possible to predict in advance at what depth borehole KFM02B will intersect zone ZFMNE00A2. This makes this borehole suitable for sampling and characterisation of rock matrix porewater with the purpose to obtain data for evaluation of the potential existence of diffusion profiles in the rock beneath the zone. Therefore, it is recommended that such sampling is undertaken. It is also recommended that sampling and characterisation of groundwater in low-conductive zones are made, provided that such zones can be identified at suitable depths and that the feasibility test of the equipment has shown to be successful.

It is further suggested that the drilling water is marked with higher concentrations of uranine than normally used, and also with Iodide, in order to test if this could be an appropriate method to trace effects of stress relaxation on the porosity and porewater composition of rock samples.

In addition to the above mentioned investigations, geological characterisation by the standard geological/geophysical programme should be conducted. Furthermore, pressure monitoring in nearby boreholes during drilling and measurements with the Posiva flow log (PFL) as well as single-hole hydraulic testing with the Pipe String System (PSS) after drilling, are recommended.

6.1.5 Boreholes KFM11A (Singö) and KFM12A (Forsmark)

The main purpose of these two boreholes is to provide a hydrogeological and hydrogeochemical characterisation of the north-eastern and south-western boundary areas to the target (repository) area, see Sections 5.1.2 and 5.3.3. This includes the regional deformation zones Singö and Forsmark and surrounding rock.

The Singö deformation zone is located downstream of the target area and below the Baltic Sea mainly, whereas the Forsmark deformation zone is (nowadays) a terrestrial zone located upstream of the target area. Moreover, the Forsmark deformation zone is located in a valley below one of the major streams in northern Uppland, Forsmarksån. Between the Forsmark deformation zone and the target area there is a regional water divide with a fairly high topography.

The characterisation of the Singö zone is judged more important since it could interfere with a potential future release of radionuclides from the repository. Questions of importance to address by these investigations concern the hydraulic character of the Singö zone, e.g. in terms of heterogeneity and potential anisotropy in transmissivity, as well as potential differences in hydraulic characteristics of the rock inside (south-west of) the zone compared to outside (north-east of) the zone and if there is any hydraulic contact through the zone.

Hydrochemical sampling is recommended at every opportunity at these locations since these large-scale deformation zones are the main penetration pathways of percolating groundwaters to depth. Such waters do not refer only to modern meteoric water recharge, but also the possibility of detecting the extent and depth of preserved palaeo-recharged glacial, Littorina Sea and old Baltic Sea waters.

The characterisation of the Forsmark zone is of interest for several reasons as already indicated. One particular interest is the comparison with the data aquired from the Singö deformation zone. Both zones are of similar regional character and tectonic regime, e.g. they are orientated more or less parallel to the principal horizontal stress component.

More details on the motives for these holes and their locations as well as suggested supplementary drilling and investigations are specified in a separate motivation document, see Appendix 5 (Section 5.6).

6.2 Other investigations

6.2.1 Percussion-drilled holes

The extensive programme aimed at investigating lineaments includes investigations by percussion-hole drilling. In Stage I of this programme, percussion drilling is conducted to confirm the extension of deformation zones in target area and to investigate the characters of these zones, see Section 5.1.1. Further details are given in the motivation document, see Appendix 5 (Section 5.1).

In Stage II of the lineament programme, percussion holes are drilled to test whether some long lineaments along the south-western boundary of the target area correspond to deformation zones as well as to study the character of seismic reflector B8 north-west of the candidate area close to the reactor 3 site, see Section 5.1.1. In addition, the programme includes drilling of a percussion hole in the central part of Bolundsfjärden with the purpose to investigate the groundwater flow above the deformation zone ZFMNE00A2 beneath Bolundsfjärden. This is of interest for establishing whether Bolundsfjärden and the rock beneath is a discharge area for deeper groundwater, see Section 5.3.5. For further details, see the motivation document in Appendix 5 (Section 5.2).

6.2.2 Surface investigations

In order to obtain more information as to the characters of north-south trending lineaments in the target area, see Section 5.1.1, it is suggested that surface excavation of at least one such lineament is carried out. Although recognising the difficulty associated with surface excavations in the area due to environmental concerns, the importance of obtaining information on the characters of these lineaments motivates an effort on finding an appropriate place for a trench. One possibility could be to find a suitable location near the Forsmark NPP's temporary housing.

A second recommendation concerns a supplementary study in the lineament trench close to drill site 7. This surface excavation has exposed a small northeast trending zone. In order to obtain more information for different fracture sets in northeast zones, it is suggested that a detailed fracture mapping is conducted at this locality.

A minor addition to complement the seismic reflection data is further proposed. By extending profile 6 /Juhlin and Palm 2005/ to the north-west, along the road south of the power plant, additional information concerning the extension of the gently dipping zone that intersects the old borehole DBT-1 could be attained.

Finally, it is recommendation that one or more surface excavations should be carried out to assess the character of low velocity anomalies in the seismic refraction data.

6.2.3 Sampling for laboratory measurements of thermal and rock mechanics properties

The current database available for evaluation of thermal and rock mechanics properties contains too few or no measurements results from some subordinate rock types of potential importance for domain scale properties, see Sections 5.2.2 and 5.2.3. To overcome this, sampling and lab measurements on the group C rocks (101051) and the amphibolite (102017) should be carried out.

6.2.4 Other hydraulic and tracer tests

Dilution tests to analyse open, non-flowing fractures would be useful for assessing whether the system is advection or diffusion dominated, see Section 5.4.1. Equipment for such measurements is available and testing of the equipment should be initiated as soon as possible, for example in the cored borehole KFM04A.

There are currently plans for conducting tracer tests in the more surficial parts of the gently dipping zone ZFMNE00A2. In addition, the possibility of conducting tracer test at larger depth in zone A2 between the two cored boreholes KFM02A and 02B at drill site 2 will be evaluated when borehole 02B is drilled and more information about the hydraulics is available. Section 5.4.1 outlines the motivation for these tests.

The possibility of conducting test for measuring sorption in situ, see Section 5.4.2, is also under consideration. However, both equipment and procedures for such measurements need to be developed and tested. Furthermore, it is not obvious, at present, if in situ measurements are capable to provide more reliable sorption data compared with laboratory measurements on larger samples, since quantification of sorption in situ will require injection of tracer and sampling of rock and thus also disturbances caused by drilling. Therefore, for the current stage of the site investigation at Forsmark, any in situ sorption tests conducted will primarily be aimed at demonstrating sorption.

6.3 Proposed investigations of low priority

Based on the interpretation of primary data and modelling undertaken during stage 2.1 some of the earlier planned investigations are judged less or no longer motivated. As already mentioned above, this concerns drilling and investigation of the Eckarfjärden deformation zone as well as the earlier planned cored borehole KFM09C.

In the CSI programme /SKB 2005c/, the need for additional bedrock mapping in the north-western part of the tectonic lens, southeast of Kallrigafjärden, was identified. The purpose of this investigation was to provide information on the large-scale fold structures in order to improve the understanding of the geometry of rock domain RFM029 in that part of the lens. Since data from drilling in the north-western part, combined with modelling, have made it possible to constrain the geometry of the folding in the target area, there is no longer any need for conducting this planned bedrock mapping.

7 Conclusions

In general, the stage 2.1 objectives of the site descriptive modelling for Forsmark have been achieved. On the basis of version 1.2 of the site descriptive model /SKB 2005a/, repository layout D1 /Brantberger et al. 2006/ and the preliminary safety evaluation (PSE) /SKB 2005b/, data requirements and modelling actions to resolve remaining issues of importance for site understanding, repository engineering and long-term safety of a repository at the site have been identified. The work has been conducted in close cooperation with the site investigation team at Forsmark and representatives from repository engineering and safety assessment. The results of the work are compiled in this report as additions and modifications to the Complete Site Investigation (CSI) programme /SKB 2005c/. In addition, the analysis and modelling work carried out so far has been evaluated and remaining modelling issues identified during previous modelling stages have been addressed. The outcome of these latter activities have to some extent been reported here, but more complete accounts will be given in separate issue reports and as updates of the discipline-specific methodologies for site descriptive modelling.

In order to meet the primary objectives of the stage 2.1 work, data available in data freeze 2.1 have been analysed and updated versions of the geological models for rock domains and deterministic deformation zones have been developed. Local models for the geometry of rock domains and deterministic deformation zones, with a higher resolution, are presented for the first time. The version 2.1 local model volume covers the northwestern part of the candidate area, which is the target area for a repository at the site.

On the basis of the observed spatial variability of fracturing, which was already recognised in model version 1.2, and the inferred relationship between the occurrence of gently dipping zones and the in situ stress magnitudes in the bedrock, a working conceptual model for division of the critical rock domain RFM029 into separate fracture domains has been developed. This approach was originally suggested by hydrogeology in the version 1.2 modelling stage and the concept will be further developed and tested during stage 2.2 of the modelling work as an integrated issue between geology, rock mechanics, hydrogeology and hydrogeochemistry.

In summary, it can be concluded that interpretations of site data and the modelling undertaken have, in general, confirmed the version 1.2 results. No new site-specific issues of decisive importance for the conceptual understanding of the Forsmark site have been identified. In addition, more focus on interdisciplinary feedback and consistency in the results of the data interpretation and modelling have improved our understanding of the Forsmark site. However, it needs to be kept in mind that there was no ambition within the framework of modelling stage 2.1 to complete a fully integrated site description.

8 References

Adl-Zarrabi B, 2004a. Drill hole KFM02A Thermal properties: heat conductivity and heat capacity determined using the TPS method and mineralogical composition by modal analysis. Forsmark site investigation. SKB P-04-161, Svensk Kärnbränslehantering AB.

Adl-Zarrabi B, 2004b. Drill hole KFM04A Thermal properties: heat conductivity and heat capacity determined using the TPS method and mineralogical composition by modal analysis. Forsmark site investigation. SKB P-04-199, Svensk Kärnbränslehantering AB.

Adl-Zarrabi B, 2005. Drill hole KFM06A. Thermal properties: heat conductivity and heat capacity determined using the TPS method. Forsmark site investigation. SKB P-05-123, Svensk Kärnbränslehantering AB.

Andersson J, Christiansson R, Hudson J, 2002. Site Investigations. Strategy for Rock Mechanics Site Descriptive Model. SKB TR-02-01, Svensk Kärnbränslehantering AB.

Andersson J, 2003. Site descriptive modelling – strategy for integrated evaluation. SKB R-03-05, Svensk Kärnbränslehantering AB.

Atkins P W, 1999. Physical Chemistry 6 ed. Oxford University Press, ISBN 0-19-850102-1.

Axelsson C-L, Hansen L M, 1997. Update of structural models at SFR nuclear waste repository, Forsmark, Sweden. SKB R-98-05, Svensk Kärnbränslehantering AB.

Balu L, Cosma C, 2005. Estimation of 3D positions and orientations of reflectors based on an updated interpretation of Stage 1 reflection seismic data. Preliminary site description of the Forsmark area – version 1.2. SKB R-05-39, Svensk Kärnbränslehantering AB.

Bergman S, Isaksson H, Johansson R, Lindén A, Persson Ch, Stephens M, 1996. Förstudie Östhammar. Jordarter, bergarter och deformationszoner. SKB PR-D-96-016, Svensk Kärnbränslehantering AB (in Swedish).

Bergman T, Isaksson H, Johansson R, Lindèn A H, Lindroos H, Rudmark L, Stephens M, 1999. Förstudie Tierp. Jordarter, bergarter och deformationszoner. SKB R-99-53, Svensk Kärnbränslehantering AB.

Brantberger M, Zetterqvist A, Arnbjerg-Nielsen T, Olsson T, Outters N, Syrjänen P, 2006. Final repository for spent nuclear fuel. Underground design Forsmark, Layout D1. SKB R-06-34, Svensk Kärnbränslehantering AB.

Brunauer S, Emmet P H, Teller E, 1938. Adsorption of gases in multimolecular layers. J. Am. Chem. Soc., 60: 309–319.

Börjesson S, Gustavsson E, 2005. Laboratory data from the site investigation programme for the transport properties of the rock. Data delivery for data freeze Forsmark 2.1. Forsmark site investigation. SKB P-05-109, Svensk Kärnbränslehantering AB.

Carlsson A, 1979. Characteristic features of a superficial rock mass in southern central Sweden – Horizontal and subhorizontal fractures and filling material. Striae 11.

Carlsson A, Christiansson R, 1987. Geology and tectonics at Forsmark, Sweden. SKB SFR-87-04, Svensk Kärnbränslehantering AB.

Carlsson A, Olsson T, 1982. High rock stresses as a consequence of glaciation. Nature, 298, 739–742.

Carlsten S, Gustafsson J, Mattsson H, Petersson J, Stephens M, 2005a. Geological single-hole interpretation of KFM06A and KFM06B (DS6). Forsmark site investigation. SKB P-05-132, Svensk Kärnbränslehantering AB.

Carlsten S, Gustafsson J, Mattsson H, Petersson J, Stephens M, 2005b. Geological single-hole interpretation of KFM07A and HFM20–21 (DS7). Forsmark site investigation. SKB P-05-157, Svensk Kärnbränslehantering AB.

Carlsten S, Gustafsson J, Mattsson H, Petersson J, Stephens M, 2005c. Geological single-hole interpretation of KFM08A, KFM08B and HFM22 (DS8). Forsmark site investigation. SKB P-05-262, Svensk Kärnbränslehantering AB.

Cosma C, Enescu N, 2001. Characterization of fractured rock in the vicinity of tunnels by the swept impact seismic technique. International Journal of Rock Mechanics and Mining Sciences, 38, 815–821.

Cosma C, Balu L, Enescu N, 2003. Estimation of 3D positions and orientations of reflectors identified in the reflection seismic survey at the Forsmark area. SKB R-03-22, Svensk Kärnbränslehantering AB.

Cosma C, Balu L, Enescu N, 2006 (manuscript submitted). Estimation of 3D positions and orientations of reflectors identified in the reflection seismic survey at Forsmark, stage 2. SKB R-06-xx, Svensk Kärnbränslehantering AB.

Cronquist T, Forssberg O, Maersk Hansen L, Jonsson A, Leiner P, Vestgård J, Petersson J, Skogsmo G, 2005. Detailed fracture mapping of two trenches at Forsmark. Forsmark site investigation. SKB P-04-88, Svensk Kärnbränslehantering AB.

Eliasson T, 1993. Mineralogy, geochemistry and petrophysics of red coloured granite adjacent to fractures. SKB TR-93-06, Svensk Kärnbränslehantering AB.

Fairhurst CE, Hudson JA, 1999. Draft ISRM suggested methods for the complete stress-strain curve fro intact rock in uniaxial compression, International Society for Rock Mechanics Commission on Testing Methods, I.J.R.M. and Min. Sci., Vol.36, p. 279–289.

Follin S, Stigsson M, Svensson U, 2005. Regional hydrogeological simulations for Forsmark – numerical modelling using Darcy Tools. Preliminary site description Forsmark area – version 1.2. SKB R-05-60, Svensk Kärnbränslehantering AB.

Follin S, Ludvigson J-E, Levén J, 2006. A comparison between standard well test evaluation methods used in SKB's site investigations and the Generalised Radial Flow concept. SKB P-06-54, Svensk Kärnbränslehantering AB.

Forsman I, Zetterlund M, Rhén I, 2004. Correlation of Posiva Flow Log anomalies to core mapped features in Forsmark (KFM01A to KFM05A). SKB R-04-77, Svensk Kärnbränslehantering AB.

Forssman I, Zetterlund M, Forsmark T, Rhén I, 2006. Correlation of Posiva Flow Log anomalies to core mapped fractures in KFM06A and KFM07A. SKB P-06-56, Svensk Kärnbränslehantering AB.

Fredriksson D, 2004. Peatland investigation Forsmark. Forsmark site investigation. SKB P-04-127, Svensk Kärnbränslehantering AB.

Gentzschein B, Levén J, Follin S, 2006. A comparison between well yield data from the site investigation in Forsmark and domestic wells in northern Uppland. SKB P-06-53, Svensk Kärnbränslehantering AB.

Gokall-Norman K, Svensson T, Ludvigson L-E, Jönsson S, 2004. Hydraulic interference test. Boreholes HFM18 and KFM03A. Forsmark site investigation. SKB P-04-307, Svensk Kärnbränslehantering AB.

Gokall-Norman K, Ludvigson J-E, 2005. Hydraulic interference test. Boreholes HFM16, HFM19 and KFM02A. Forsmark site investigation. SKB P-05-78, Svensk Kärnbränslehantering AB.

Gokall-Norman K, Ludvigson J-E, Hjerne C, 2005a. Single-hole injection tests in borehole KFM05A. Forsmark site investigation. SKB P-05-56, Svensk Kärnbränslehantering AB.

Gokall-Norman K, Ludvigson J-E, Jönsson S, 2005b. Hydraulic interference test. Boreholes KFM04A, HFM10, HFM13, HFM19 and HFK252. Forsmark site investigation. SKB P-05-186, Svensk Kärnbränslehantering AB.

Gokall-Norman K, Svensson T, Ludvigson L-E, 2005c. Single-hole injection tests in borehole KFM07A. Forsmark site investigation. SKB P-05-133, Svensk Kärnbränslehantering AB.

Gurban I, Laaksoharju M, 2002. Drilling Impact Study (DIS); Evaluation of the influences of drilling, in special on the changes on groundwater parameters. SKB PIR-03-02, Svensk Kärnbränslehantering AB.

Gustafsson E, Nordqvist R, Thur P, 2005. Groundwater flow measurements in boreholes KFM01A, KFM02A, KFM03A, KFM03B and SWIW tests in KFM02A, KFM03A. Forsmark site investigation. SKB P-05-77, Svensk Kärnbränslehantering AB.

Hakami E, Johansson M, 2006. PM – Bias in rock mechanics sampling, document in preparation, Svensk Kärnbränslehantering AB.

Hjerne C, Jönsson J, Ludvigson J-E, 2004. Single-hole injection tests in borehole KFM03B. Forsmark site investigation. SKB P-04-278, Svensk Kärnbränslehantering AB.

Hjerne C, Ludvigson J-E, 2005. Single-hole injection tests in borehole KFM04A. Forsmark site investigation. SKB P-04-293, Svensk Kärnbränslehantering AB.

Hjerne C, Ludvigson J-E, Lindquist A, 2005. Single-hole injection tests in boreholes KFM06A and KFM06B. Forsmark site investigation. SKB P-05-165, Svensk Kärnbränslehantering AB.

Hoek E, Brown E T, 1997. Practical estimates of rock mass strength, Int. J. Rock Mech. Min. Sci. Vol. 34, p. 1165–1186.

Hoek E, Carranza-Torres C, Corkum B, 2002. The Hoek-Brown Failure Criterion – 2002 Edition. 5th North American Rock Mechanics Symposium and 17th Tunneling Association of Canada Conference: NARMS-TAC, p. 267–271.

Holmén J G, Stigsson M, 2001. Modelling of future hydrogeological conditions at SFR. SKB R-01-02, Svensk Kärnbränslehantering AB.

Ingemar T, Moreborg K, 1976. The leaching and original content of calcium carbonate in till in Northern Uppland, Sweden. Geol. Fören. Stockh. Förh. 98:120–132. (The Geological Society, Stockholm, Sweden).

Isaksson H, Thunehed H, Keisu M, 2004. Interpretation of airborne geophysics and integration with topography. Forsmark site investigation. SKB P-04-29, Svensk Kärnbränslehantering AB.

Isaksson H, Keisu M, 2005. Interpretation of airborne geophysics and integration with topography. Stage 2 (2002–2004). Forsmark site investigation. SKB P-04-282, Svensk Kärnbränslehantering AB.

Jakobsson A-M, 1999. Measurement and modelling using surface complexation of cation (II to IV) sorption onto mineral oxides. Ph.D. Thesis. Chalmers University of Technology, Department of Nuclear Chemistry, Göteborg, Sweden.

Jacobsson L, 2005. Borehole KFM07A – Uniaxial compression test of intact rock – Forsmark site investigation P-05-211, Svensk Kärnbränslehantering AB.

Johansson H, Byegård J, Skarnemark G, Skålberg M, 1997. Matrix diffusion of some alkali and alkaline earth metals in granitic rock. Mat. Res. Soc. Symp. Proc. 465: 871–878.

Juhlin C, Bergman B, Palm H, 2002. Reflection seismic studies in the Forsmark area – stage 1. SKB R-02-43, Svensk Kärnbränslehantering AB.

Juhlin C, Bergman B, 2004. Reflection seisimics in the Forsmark area. Updated interpretation of Stage 1 (previous report R-02-43). Updated estimate of bedrock topography (previous report P-04-99). SKB P-04-158, Svensk Kärnbränslehantering AB.

Juhlin C, Palm H, 2005. Reflection seismic studies in the Forsmark area, 2004: Stage 2. Forsmark site investigation. SKB R-05-42, Svensk Kärnbränslehantering AB.

Juhlin C, Stephens M B, in press. Gently dipping fracture zones in Paleoproterozoic metagranite, Sweden: Evidence from reflection seismic and cored borehole data, and implications for the disposal of nuclear waste. Journal of Geophysical Research − Solid Earth.

Juston J, Johansson P-O, Levén J, Follin S, 2006. Analysis of meteorological, hydrological and hydrogeological monitoring data, December 2002–July 2005. Forsmark site investigation. SKB R-06-49, Svensk Kärnbränslehantering AB.

Jönsson J, Hjerne C, Ludvigson J-E, 2005. Pumping tests and flow logging. Boreholes HFM20, HFM21 and HFM22. Forsmark site investigation. SKB P-05-14, Svensk Kärnbränslehantering AB.

LaPointe P, Olofsson I, Hermanson J, 2005. Statistical model of fractures and deformation zones for Forsmark. Preliminary site description Forsmark area – version 1.2, SKB R-05-26, Svensk Kärnbränslehantering AB.

Leijon, Bengt (ed.), 2005. Investigations of superficial fracturing and block displacements at drill site 5. Forsmark site investigation. SKB P-05-199, Svensk Kärnbränslehantering AB.

Levén J, Carlberg T, Follin S, 2006. Compilation and visualisation of cross discipline borehole data using WellCad. SKB P-06-55, Svensk Kärnbränslehantering AB.

Lidmar-Bergström K, 1994. Morphology of the bedrock surface. In C. Fredèn (ed.), Geology. National Atlas of Sweden.

Lindborg T (ed.), 2005. Description of the surface systems, Forsmark area – version 1.2. SKB R-05-03. Svensk Kärnbränslehantering AB.

Lindroos H, Isaksson H, Thunehed H, 2004. The potential for ore and industrial minerals in the Forsmark area. SKB R-04-18, Svensk Kärnbränslehantering AB.

Lundin L, Stendahl J, Lode E, 2005. Soils in two large trenches. Forsmark site investigation. SKB P-05-166, Svensk Kärnbränslehantering AB.

Löfgren M, Neretnieks I, 2005a. Formation factor logging in-situ and in the laboratory by electrical methods in KFM01A and KFM02A. Measurements and evaluation of methodology. Forsmark site investigation. SKB P-05-29, Svensk Kärnbränslehantering AB.

Löfgren M, Neretnieks I, 2005b. Formation factor logging in-situ by electrical methods in KFM03A and KFM04A. Forsmark site investigation. SKB P-05-108, Svensk Kärnbränslehantering AB.

Martin C D, Christiansson R, Söderhäll J, 2001. Rock stability considerations for siting and constructing a KBS-3 repository. Based on experiences from Äspö HRL, AECL's URL, tunnelling and mining. SKB TR-01-38, Svensk Kärnbränslehantering AB.

Mas Ivars D, Hakami H, 2005. Effect of a sub-horizontal fracture zone and rock mass heterogeneity on the stress field in Forsmark area – A numerical study using 3DEC. Preliminary site description Forsmark area – version 1.2, R-05-59, Svensk Kärnbränslehantering AB.

Mattsson H, Thunehed H, Isaksson H, 2005. Interpretation of petrophysical data from the cored boreholes KFM04A, KFM05A and KFM06A. Forsmark site investigation. SKB P-05-204, Svensk Kärnbränslehantering AB.

Min K-B, 2004. Fractured Rock Masses as Equivalent Continua – A Numerical Study, Ph.D. Thesis, Royal Institute of Technology, Stockholm, Sweden.

Munier R, Stenberg L, Stanfors R, Milnes A G, Hermanson J, Triumf C-A, 2003. Geological Site Descriptive Model. A strategy for the model development during site investigations. SKB R-03-07, Svensk Kärnbränslehantering AB.

Munier R, Hökmark H, 2004. Respect distances. Rationale and means of computation. SKB R-04-17, Svensk Kärnbränslehantering AB.

Möller C, Snäll S, Stephens M B, 2004. Dissolution of quartz, vug formation and new grain growth associated with post-metamorhic hydrothermal alteration in KFM02A. Forsmark site investigation. SKB P-03-77, Svensk Kärnbränslehantering AB.

Naturvårdsverket, 1999. Environmental Quality Criteria – Groundwater. Swedish Environmental Protection Agency Report 4915.

Nordqvist R, Gustafsson E, 2002. Single-well injection-withdrawal tests (SWIW). Literature review and scoping calculations for homogeneous crystalline bedrock conditions. SKB R-02-34, Svensk Kärnbränslehantering AB.

Nordqvist R, Gustafsson E, 2004. Single-well injection-withdrawal tests (SWIW). Investigation of evaluation aspects under heterogeneous crystalline bedrock conditions. SKB R-04-57, Svensk Kärnbränslehantering AB.

Nyberg G, Wass E, 2005. Hydro Monitoring Program. Report for August 2004–July 2005. Forsmark site investigation. SKB P-05-245, Svensk Kärnbränslehantering AB.

Nyberg G, Wass E, Askling P, Johansson P-O, 2005. Hydro monitoring programme. Report for June 2002 – July 2004. Forsmark site investigation. SKB P-04-313, Svensk Kärnbränslehantering AB.

Ohlsson Y, Neretnieks I, 1997. Diffusion data in granite – recommended values. SKB TR 97-20, Svensk Kärnbränslehantering AB.

Olofsson I, Fredriksson A, 2005. Strategy for a numerical Rock Mechanics Site Descriptive Model. Further development of the theoretical/numerical approach. SKB R-05-43, Svensk Kärnbränslehantering AB.

Page L, Hermansson T, Söderlund P, Andersson J, Stephens M B, 2004. Bedrock mapping U/Pb, 40Ar/39Ar and (U-Th)/He geochronology. Forsmark site investigation. SKB P-04-126, Svensk Kärnbränslehantering AB.

Park C B, Miller R D, Steeples D W, Black R A, 1996. Swept impact seismic technique (SIST). Geophysics, 61, 1789–1803.)

Petersson J, Berglund J, Danielsson P, Wängnerud A, Tullborg E-L, Mattsson H, Thunhed H, Isaksson H, Lindroos H, 2004. Petrography,geochemistry, petrophysics and fracture mineralogy of boreholes KFM01A, KFM02A and KFM03A + B. Forsmark site investigation. SKB P-04-103, Svensk Kärnbränslehantering AB.

Petersson J, Berglund J, Danielsson P, Skogsmo G, 2005. Petrographic and geochemical characteristics of bedrock samples from boreholes KFM04A–06A, and a whitened alteration rock. Forsmark site investigation. SKB P-05-156, Svensk Kärnbränslehantering AB.

Pöllänen J, Sokolnicki M, 2004. Difference flow logging in borehole KFM03A, Forsmark site investigation. SKB P-04-189, Svensk Kärnbränslehantering AB.

Rouhiainen P, Sokolnicki M, 2005a. Difference flow logging in borehole KFM06A. Forsmark site investigation. SKB P-05-15, Svensk Kärnbränslehantering AB.

Rouhiainen P, Sokolnicki M, 2005b. Difference flow logging in borehole KFM02A during pumping in HFM16. Forsmark site investigation. SKB P-05-37, Svensk Kärnbränslehantering AB.

Sandström B, Savolainen M, Tullborg E-L, 2004. Fracture mineralogy. Results from fracture minerals and wall rock alteration in boreholes KFM01A, KFM02A, KFM03A and KFM03B. Forsmark site investigation. SKB P-04-149, Svensk Kärnbränslehantering AB.

Sandström B, Tullborg E-L, 2005. Fracture mineralogy. Results from fracture minerals and wall rock alteration in boreholes KFM01B, KFM04A, KFM05A and KFM06A. Forsmark site investigation. SKB P-05-197, Svensk Kärnbränslehantering AB.

Sandström B, Tullborg E-L, de Torres T, Ortiz J E, 2006. (Avsnitt 2.4) The occurrence and potential origin of asphaltite in bedrock fractures, Forsmark, central Sweden. Bulletin of the Geological Society of Finland, Special Issue 1, 2006, 140 (extended abstract).

SKB, 2001. Site investigations. Investigation methods and general execution programme. SKB TR-01-29, Svensk Kärnbränslehantering AB.

SKB, 2002. Forsmark – site descriptive model version 0. SKB R-02-32, Svensk Kärnbränslehantering AB.

SKB, 2004. Preliminary site description Forsmark area–version 1.1. SKB R-04-15, Svensk Kärnbränslehantering AB.

SKB, 2005a. Preliminary site description Forsmark area – version 1.2. SKB R-05-18, Svensk Kärnbränslehantering AB.

SKB, 2005b. Preliminary safety evaluation for the Forsmark area. Based on data and site descriptions after the initial site investigation stage. SKB TR-05-16, Svensk Kärnbränslehantering AB.

SKB, 2005c. Programme for further investigations of geosphere and biosphere. Forsmark site investigation. SKB R-05-14, Svensk Kärnbränslehantering AB.

SKB, 2005d. Hydrochemical evaluation. Preliminary site description Forsmark area – version 1.2. SKB R-05-17, Svensk Kärnbränslehantering AB.

SKB, 2005e. Preliminary site description Simpevarp subarea – version 1.2. SKB R-05-08, Svensk Kärnbränslehantering AB.

SKB, 2006a. Preliminary site description Laxemar subarea – version 1.2. SKB R-06-10, Svensk Kärnbränslehantering AB.

SKB, 2006b. Forsmark 2.1 hydrogeochemical issues. SKB report in preparation.

SKB, 2006c. Geological characteristics of large fractures and minor deformation zones and strategy for their detection in a repository. SKB R-06-39, Svensk Kärnbränslehantering AB.

Sokolnicki M, Rouhiainen P, 2005. Difference flow logging in borehole KFM07A. Forsmark site investigation. SKB P-05-63, Svensk Kärnbränslehantering AB.

Sonesten L, 2005. Chemical characteristics of surface waters in the Forsmark area. Evaluation of data from lakes, streams, and coastal sites. SKB R-05-41. Svensk Kärnbränslehantering AB.

Stephens M B, Lundqvist S, Ekström M, Bergman T, Andersson J, 2003. Bedrock mapping. Rock types, their petrographic and geochemical characteristics, and a structural analysis of the bedrock based on stage 1 (2002) surface data. Forsmark site investigation. SKB P-03-75, Svensk Kärnbränslehantering AB.

Stephens M B, Lundqvist S, Bergman T, Ekström M, 2005. Bedrock mapping. Petrographic and geochemical characteristics of rock types based on Stage 1 (2002) and Stage 2 (2003) surface data. Forsmark site investigation. SKB P-04-87, Svensk Kärnbränslehantering AB.

Streckeisen A, 1976. To each plutonic rock its proper name. Earth Science Reviews 12.

Stråhle A, 2001. Definition och beskrivning av parametrar för geologisk, geofysisk och bergmekanisk kartering av berg. SKB R-01-19, Svensk Kärnbränslehantering AB.

Sundberg J, 1988. Thermal properties of soils and rocks, Publ. A 57 Dissertation. Department of Geology, Chalmers University of Technology and university of Göteborg, Sweden.

Sundberg J, 2003. A strategy for the model development during site investigations version 1.0. SKB R-03-10, Svensk Kärnbränslehantering AB.

Sundberg J, Back P, Bengtsson A, Ländell M, 2005. Thermal modelling, Preliminary site description Forsmark area – version 1.2. SKB R-05-31. Svensk Kärnbränslehantering AB.

Thunehed, 2005a. Resistivity measurements on samples from KFM01A and KFM02A. Forsmark site investigation. SKB P-05-26, Svensk Kärnbränslehantering AB.

Thunehed, 2005b. Resistivity measurements and determination of formation factors on samples from KFM03A, KFM04A and KFM05A. Forsmark site investigation. SKB P-05-76, Svensk Kärnbränslehantering AB.

Tröjbom M, Söderbäck B, 2006. Chemical characteristics of surface systems in the Forsmark area. Visualisation and statistical evaluation of data from shallow groundwater, precipitation and regolith. SKB R-06-19, Svensk Kärnbränslehantering AB.

Voss C I, 1984. SUTRA – Saturated-Unsaturated Transport. A finite element simulation model for saturated-unsaturated fluid-density-dependent ground-water flow with energy transport or chemically-reactive single-species solute transport. U.S: Geological Survey Water-Resources Investigations Report 84-4369.

Wern L, Jones J, 2006. Meteorological monitoring at Forsmark, June 2003 until July 2005. SKB P-06-49. Svensk Kärnbränslehantering AB. (Avsnitt 2.7)

Widestrand H, Byegård J, Ohlsson Y, Tullborgh E-L, 2003. Strategy for the use of laboratory methods in the site investigations programme fort the transport properties of the rock. SKB R-03-20, Svensk Kärnbränslehantering AB.

Åkesson U, 2004. Drill hole KFM04A: Extensometer measurement of the coefficient of thermal expansion of rock. Forsmark site investigation. SKB P-04-198, Svensk Kärnbränslehantering AB.

Appendix 1

Tables with primary data

The data that were available at the time of data freeze 1.2 are compiled in tables in this appendix. The purpose of these tables is to give a reference and account of which data were considered in the work conducted in modelling stage 2.1. However, data per se are not provided. For simplification and traceability reasons, the information is split into different tables, one for each discipline, and complete references to the site-data reports are given in the last table in this appendix. Since no major changes or improvements in the interpretation of primary data on surface system properties have been performed since version 1.2, these data are not reported here, other than those of relevance for the hydrogeological interpretations, which are included in Table 4.

Table 1. Available bedrock geological and geophysical data and their handling in Forsmark modelling step 2.1. Report numbers in italics show data available already at data freeze 1.2.

Available data Data specification	Ref	Usage in F2.1 Analysis/Modelling	cf. section	Not utilised in F2.1 Motivation/Comment
Data from core-drilled boreholes				
Technical data in connection with drilling (KFM01A, KFM01B, KFM02A, KFM03A and KFM03B, KFM04A, KFM05A, KFM06A and KFM06B, KFM07A, KFM08A and KFM08B)	*P-03-32* *P-04-302* *P-03-52* *P-03-59* *P-03-82* *P-04-222* P-05-50 P-05-142 P-05-172	Siting and orientation of boreholes in modelling work.	Appendix 2	
Radar and BIPS logging, and interpretation of radar logs (KFM01A, KFM01B, KFM02A, KFM03A and KFM03B, KFM04A, KFM05A, KFM06A, KFM06B, KFM07A, KFM08A, KFM08B)	*P-03-45* *P-04-79* *P-04-40* *P-04-41* *P-04-67* *P-04-152* P-05-01 P-05-53 P-05-52 P-05-158 P-05-58	Data used in borehole mapping (BIPS) and in single hole interpretation (radar logging) with focus on identification of brittle deformation zones. Input for both rock domain and DZ modelling.	2.4, Appendix 2	
Geophysical logging (KFM01A, KFM01B, KFM02A and KFM03A/KFM03B, KFM04A, KFM05A, KFM06A, KFM07A, KFM08A and KFM08B)	*P-03-103* *P-04-145* *P-04-97* *P-04-144* *P-04-153* P-05-17 P-05-159	Data used in borehole mapping and in single hole interpretation. Input for both rock domain and DZ modelling.	2.4, Appendix 2	
Interpretation of geophysical logs (KFM01A and KFM01B, KFM02A and KFM03A/ KFM03B, KFM04A, KFM05A, KFM06A, KFM07A, KFM08A and KFM08B)	*P-04-80* *P-04-98* *P-04-143* *P-04-154* P-05-51 P-05-119 P-05-202	Used in single hole interpretation. Input for both rock domain and DZ modelling.	2.4, Appendix 2	

Available data Data specification	Ref	Usage in F2.1 Analysis/Modelling	cf. section	Not utilised in F2.1 Motivation/Comment
Vertical seismic profiling, KFM01A and KFM02A (including interpretation)	P-05-168			Data and interpretation not used during version 2.1. Closer integration with geological and other geophysical data from KFM01A and KFM02A required. Planned to be carried out in version 2.2.
Boremap mapping (KFM01A, KFM01B, KFM02A, KFM03A and KFM03B, KFM04A, KFM05A, KFM06A and KFM06B, KFM07A, KFM08A and KFM08B)	*P-03-23* *P-04-114* *P-03-98* *P-03-116* *P-04-115* *P-04-295* P-05-101 P-05-102 P-05-203	Rock type, ductile deformation in the bedrock, fracture statistics. Data used in identification of rock units and brittle deformation zones in single hole interpretation. Input for both rock domain and DZ modelling.	2.4, Appendix 2	
Mineralogical and geochemical analyses of rock types and fracture fillings (KFM01A, KFM02A, and KFM03A/ KFM03B, KFM01B, KFM04A, KFM05A and KFM06A)	*P-04-103* *P-04-149* P-05-156 P-05-197	Mineralogical and geochemical properties of rock types and mineral fracture fillings. Input for rock domain and DZ modelling	2.4, Appendix 2	No update of rock type properties completed during version 2.1, on the basis of results in P-05-156. Update is planned in version 2.2.
Petrophysical and in situ gamma-ray spectrometric data from rock types (KFM01A, KFM02A and KFM03A/ KFM03B, KFM04A, KFM05A and KFM06A)	*P-04-103* *P-04-107* P-05-204	Physical properties of rock types. Input for rock domain modelling. Comment: Data also utilised for the interpretation of geophysical logs.	Appendix 2	No update of rock type properties completed during version 2.1, on the basis of results in P-05-204. Update is planned in version 2.2.
Mineralogical and microstructural analyses of vuggy metagranite in KFM02A	*P-03-77*			No further assessment of the vuggy metagranite in KFM02A and zone ZFMNE1189. No new data.
Single hole interpretation (KFM01A and KFM01B, KFM02A, KFM03A and KFM03B, KFM04A, KFM05A, KFM06A and KFM06B, KFM07A, KFM08A and KFM08B)	*P-04-116* *P-04-117* *P-04-118* *P-04-119* *P-04-296* P-05-132 P-05-157 P-05-262	Interpretation used in rock domain and DZ modelling.	2.4, Appendix 2	
Data from percussion-drilled boreholes				
Technical data in connection with drilling (HFM01–HFM03, HFM04–HFM05, HFM06–HFM08, HFM09–HFM10, HFM13–HFM15, HFM16, HFM11–HFM12 and HFM17–HFM19, HFM20–22)	*P-03-30* *P-03-51* *P-03-58* *P-04-76* *P-04-85* *P-04-94* *P-04-106* P-04-245	Siting and orientation of boreholes in modelling work.	Appendix 2	
Radar and BIPS logging, and interpretation of radar logs (KFM01A and HFM01–HFM03, KFM02A and HFM04–HFM05, HFM06–HFM08, KFM04A/4B and HFM09–HFM10, HFM11–HFM12, HFM13–HFM15, HFM16–HFM19, KFM07A and HFM20–HFM21, HFM22, HFK248–250)	*P-03-39* *P-03-53* *P-03-54* *P-04-67* *P-04-39* *P-04-68* *P-04-69* P-05-64 P-05-01 P-05-176	Data used in borehole mapping (BIPS) and in single hole interpretation (radar logging) with focus on identification of brittle deformation zones. Input for both rock domain and DZ modelling.	2.4, Appendix 2	Data from KFM04B and HFK248–250 not used. Percussion boreholes neither mapped nor interpreted.

Available data	Ref	Usage in F2.1	cf. section	Not utilised in F2.1
Data specification		**Analysis/Modelling**		**Motivation/Comment**
Geophysical logging (KFM01A and HFM01–HFM03, repeat HFM01–HFM02, KFM02A and HFM04–HFM05, HFM06–HFM08, HFM10–HFM13, HFM14–HFM18, HFM19, HFM20–HFM22)	*P-03-39* *P-03-103* *P-03-53* *P-03-54* *P-04-144* *P-04-145* *P-04-153* P-05-17	Data used in borehole mapping and in single hole interpretation. Input for both rock domain and DZ modelling.	2.4, Appendix 2	Geophysical data in P-03-39 not used. Poor quality.
Interpretation of geophysical logs (HFM01–HFM03, HFM04–HFM08, HFM10–HFM13 and HFM16–HFM18, HFM14–HFM15 and HFM19, HFM20–HFM22)	*P-04-80* *P-04-98* *P-04-143* *P-04-154* P-05-51	Used in single hole interpretation. Input for both rock domain and DZ modelling.	2.4, Appendix 2	
Boremap mapping (HFM01–HFM03, HFM04–HFM05, HFM06–HFM08, HFM09–HFM12, HFM13–15 and HFM19, HFM16–HFM18, HFM20–HFM22)	*P-03-20* *P-03-21* *P-03-22* *P-04-101* *P-04-112* *P-04-113* P-05-103	Data mainly used in identification of rock units and brittle deformation zones in single hole interpretation. Input for rock domain and DZ modelling. Comment: Difficulties with the recognition of rock types and mineral coatings along fractures. Also underestimation of fractures. Latter derived solely from BIPS images.	2.4, Appendix 2	
Single hole interpretation (HFM01–HFM03, HFM04–HFM05, HFM06–HFM08, HFM09–HFM10, HFM11–13 and HFM16–HFM18, HFM14–HFM15 and HFM19, HFM20–HFM22)	*P-04-116* *P-04-117* *P-04-118* *P-04-119* *P-04-120* *P-04-296* P-05-157 P-05-262	Interpretation used in rock domain and DZ modelling.	2.4, Appendix 2	
Older borehole, tunnel and surface data				
Older geological and geophysical data from the Forsmark nuclear power plant and SFR, including seismic refraction data	*P-04-81*	Rock type data from boreholes and tunnels, lineament identification at the nuclear power plant, brittle structures at or close to the surface in the vicinity of the nuclear power plant, and identification of brittle deformation zones. Input for both rock domain and DZ modelling. Comment: Data acquisition in P-04-81.	Appendix 2	
Surface-based data				
Bedrock mapping − outcrop data. Rock type and ductile structures at 2,119 outcrops; frequency and orientation of fractures at 44 outcrops	*P-03-09* *P-04-91* *Bedrock geological map, Forsmark, version 1.2 (SKB GIS database)*	Rock type, rock type distribution, ductile deformation in the bedrock, fracture statistics, and identification of deformation zones at the surface. Input for both rock domain and DZ modelling. Comment: Data also utilised for the interpretation of helicopter-borne geophysical data.	Appendix 2	

Available data Data specification	Ref	Usage in F2.1 Analysis/Modelling	cf. section	Not utilised in F2.1 Motivation/Comment
Detailed bedrock mapping with special emphasis on fractures (drill sites 2, 3, 4 and 5, and coastal outcrop at Klubbudden)	*P-03-12* *P-03-115* *P-04-90*			No further assessment of detailed bedrock mapping data carried out during version 2.1. No new data. No DFN modelling work completed during version 2.1.
Detailed bedrock mapping of excavations across lineaments	P-04-88	Assessment of the geological character of lineaments. Input especially for DZ modelling	2.4 and Appendix 2	
Geochemical analyses of till	*P-03-118*			No further assessment of the mineral resources potential at the site completed during version 2.1. No new data.
Evaluation of the occurrence of late- or post-glacial faulting	*P-03-76* *P-04-123*			No further assessment of late- or post-glacial faulting completed during version 2.1. No new data.
Mineralogical and geochemical analyses of rock types	*P-03-75* *P-04-87*	Mineralogical and geochemical properties of rock types. Input for rock domain modelling.	Appendix 2	
Petrophysical and in situ gamma-ray spectrometric data from rock types	*P-03-26* *P-03-102* *P-04-155*	Physical properties of rock types. Input for rock domain modelling. Comment: Data also utilised for the interpretation of helicopter-borne geophysical data.	Appendix 2	
U-Pb, $^{40}Ar/^{39}Ar$ and (U-Th)/He geochronological data	*P-04-126*	Input for conceptual understanding of the DZ modelling work.	3.1 and Appendix 2	
Production of orthorectified aerial photographs and digital terrain model	*P-02-02*			Except around the nuclear power plant, where helicopter-borne geophysical data are absent, only lineaments based on magnetic data have been used in version 2.1.
Methodology for construction of digital terrain model for the site	*P-04-03*			Same comment as for P-02-02.
Marine geological survey of the sea bottom off Forsmark	*P-03-101*			Same comment as for P-02-02.
Water depth in shallow lakes	*P-04-25*			Same comment as for P-02-02.
Water depth in shallow bays	P-04-125			Same comment as for P-02-02.
Helicopter-borne, geophysical data (magnetic, EM, VLF and gamma-ray spectrometry data)	*P-03-41*			No further assessment of airborne geophysical data in version 2.1. No new data.
Electric soundings	*P-03-44*			Lineaments based on helicopter-borne EM data have not been used in version 2.1.
Inversion of helicopter-borne EM measurements	*P-04-157*			Same comments as for P-02-02 and P-03-44.
Interpretation of topographic, bathymetric and helicopter-borne geophysical data. Alternative interpretation in and immediately around the candidate area. Assessment of all lineaments in the target area	*P-03-40* *P-04-29* *P-04-282* *P-04-241* P-05-261	Identification of magnetic lineaments. Input for DZ modelling work.	3.1 and Appendix 2	

Available data	Ref	Usage in F2.1	cf. section	Not utilised in F2.1
Data specification		**Analysis/Modelling**		**Motivation/Comment**
High-resolution seismic reflection data carried out during Stage I and Stage II (including interpretation)	*R-02-43* *P-04-158* R-05-42	Identification of seismic reflectors in the bedrock that may correspond to deformation zones or boundaries between different types of bedrock. Input for DZ modelling.	2.4 and Appendix 2	
Seismic refraction data	P-05-12			Data not used during version 2.1. Await completion of the complementary seismic refraction study 2005–2006. All data planned to be used in version 2.2.
Seismic velocity measurements along excavations across lineaments	P-05-46			Data not used during version 2.1. Await completion of the complementary seismic refraction study 2005–2006. All data planned to be used in version 2.2.
Ground geophysical data (magnetic and EM data) close to drill sites 1, 2, 3, 4 and 5, and several lineaments (including Interpretation)	*P-02-01* *P-03-55* *P-03-104*			No further assessment of these ground geophysical data completed during version 2.1. No new data.
Mise-à-la-masse data from DS5	P-04-305			Method test.
Regional gravity data	*P-03-42*			The data have not yet been interpreted. They are of broad, regional significance. Results of modelling work will be available in version 2.2.
Previous models				
SFR structural models	*R-98-05* *R-01-02*	DZ modelling. The sub-vertical zones 3, 8 and 9 have been extracted from /Axelsson and Hansen 1997/. The sub-horizontal zone H2 has been extracted from the SAFE model /Holmén and Stigsson 2001/.	Appendix 2	
Forsmark site descriptive models version 0, version 1.1 and version 1.2	*R-02-32* *R-04-15* R-05-18	Comparison of models.	3.1	

Table 2. Available rock mechanics data and their handling in Forsmark modelling step 2.1. Report numbers in italics show data available already at data freeze 1.2.

Available data	Ref	Usage in F2.1	cf. section	Not utilised in F2.1
Data specification		**Analysis/Modelling**		**Motivation/Comment**
Data from core-drilled boreholes				
Uniaxial compressive strength – Intact rock		Characterisation of the intact rock; Empirical determination of the rock mass mechanical properties by means of RMR and Q; Theoretical determination of the rock mass mechanical properties by means of numerical modelling.	2.5 and Appendix 3	
KFM01A	P-04-223			
KFM02A	P-04-224			
KFM03A	P-04-225			
KFM04A	P-04-226			
KFM01A – Independent determination	P-04-176			
KFM05A	P-05-97			
KFM06A	P-05-120			

Available data	Ref	Usage in F2.1	cf. section	Not utilised in F2.1
Data specification		**Analysis/Modelling**		**Motivation/Comment**
Triaxial compressive strength – Intact rock		Characterisation of the intact rock; Empirical determination of the rock mass mechanical properties by means of RMR and Q; Theoretical determination of the rock mass mechanical properties by means of numerical modelling.	2.5 and Appendix 3	
KFM01A	P-04-227			
KFM02A	P-04-228			
KFM03A	P-04-229			
KFM04A	P-04-230			
KFM01A – Independent determination	P-04-177			
KFM05A	P-05-100			
Indirect tensile strength		Characterisation of the intact rock; Theoretical determination of the rock mass mechanical properties by means of numerical modelling.	2.5 and Appendix 3	
KFM01A	P-04-170			
KFM02A	P-04-172			
KFM03A	P-04-173			
KFM04A	P-04-174			
KFM01A – Independent determination	P-04-171			
KFM05A	P-05-98			
Direct shear tests on rock fractures		Characterisation of the rock fractures – strength and stiffness; Theoretical determination of the rock mass mechanical properties by means of numerical modelling.	2.5 and Appendix 3	
KFM01A	P-04-175			
	P-05-08			
KFM02A	P-05-09			
KFM03A	P-05-10			
KFM04A	P-05-11			
KFM05A	P-05-99			
	P-05-141			
KFM06A	P-05-122			
Crack initiation stress		Evaluation of the elastic limit of deformation – for addressing spalling and core discing problems.	2.5 and Appendix 3	
KFM01A	P-04-223			
KFM02A	P-04-224			
KFM03A	P-04-225			
KFM04A	P-04-226			
KFM05A	SICADA			
KFM06A	SICADA			
Q-logging from KFM01A	*P-03-29*		R-05-18	Not included in new analyses
Tilt tests on fractures		Characterisation of the rock fracture properties and of the rock mass by RMR and Q.	2.5 and Appendix 3	
KFM01A	P-03-108			
KFM02A	P-04-08			
KFM03A	P-04-178			
KFM04A	P-04-179			
KFM05A	P-04-205			
P-wave velocity measurements		Correlation between rock mass stresses and foliation.	2.5 and Appendix 3	
KFM01A	P-03-38			
KFM02A	P-04-09			
KFM03A	P-04-180			
KFM04A	P-04-181			
KFM05A	P-04-203			
KFM06A	P-05-04			
Sonic velocity measurements along		Correlation with P-velocity along the cores and consideration about damage of the core	2.5 and Appendix 3	
KFM01A	Sicada			
KFM02A	Sicada			
KFM03A	Sicada			
KFM04A	Sicada			
KFM05A	Sicada			
KFM06A	Sicada			

Available data	Ref	Usage in F2.1	cf. section	Not utilised in F2.1
Data specification		**Analysis/Modelling**		**Motivation/Comment**
KFM07A	Sicada			
KFM08A	Sicada			
Empirical characterisation		Characterisation of the rock mass (RMR, Q) – rock mass mechanical properties.	3.2 and Appendix 3	
KFM01A	P-05-112			
KFM02A	P-05-113			
KFM03A	P-05-114			
KFM04A	*P-05-115*			
Overcoring measurements – KFM01B	P-04-83		R-05-18	No new evaluation of rock stresses included in 2.1 work
Evaluation of overcoring result – KFM01B	*P-05-66*			
HF and HTPF measurements – KFM01A, KFM01B, KFM02A, KFM04A	*P-04-311*			
HF and HTPF measurements – KFM01A, KFM01B, KFM02A, KFM04A – laboratory testing on cores	*P-04-312*			
RAMAC and BIPS logging in		Dip direction of minor deformation zones	3.2 and Appendix 3	
KFM01A	P-03-45			
KFM02A	P-04-40			
KFM03A	P-04-41			
KFM04A	P-04-67			
Other borehole and tunnel data				
Young´s modulus, Poisson´s ratio of intact rock. Point load tests on fractures. Point load tests on core samples from SFR boreholes.	Sicada		R-05-18	Not included in new analyses
Stress measurements in DBT1, DBT3	Sicada		R-05-18	No new evaluation of rock stresses included in 2.1 work
Stress measurements in KB-21, KB-22, KBS-7, SFR 1/177	Sicada	.		

Table 3. Available rock thermal data and their handling in Forsmark modelling step 2.1. Report numbers in italics show data available already at data freeze 1.2.

Available data			Usage in F2.1		Not utilised in F2.1
Data specification	**Ref**		**Analysis/Modelling**	**cf. section**	**Motivation/Comment**
Data from core-drilled boreholes					
Temperature logging	Results	Interpret.	Temperature variation with depth		Temperature gradient distribution not evaluated due to errors in data.
KFM01A	*P-03-103*	*P-04-80*			
KFM01B	*P-04-145*	*P-04-80*			
KFM02A	*P-04-97*	*P-04-98*			
KFM03A	*P-04-97*	*P-04-98*			
KFM04A	*P-04-144*	*P-04-143*			
KFM05A	*P-04-153*	*P-04-154*			
KFM06A	P-05-17	P-05-51			
KFM07A	P-05-159	P-05-119			
KFM08A	P-05-159	P-05-202			

Available data		Usage in F2.1		Not utilised in F2.1
Data specification	**Ref**	**Analysis/Modelling**	**cf. section**	**Motivation/Comment**
Difference-flow logging (PFL)		PFL-temperature compared with temperature logging data	2.6	
KFM01A	P-03-28 P-04-193			
KFM02A	P-04-188			
KFM03A	P-04-189			
KFM04A	P-04-190			
KFM05A	P-04-191			
KFM06A	P-05-15			
KFM07A	P-05-63			
Boremap logging		Dominant and subordinate rock type distribution	2.6	
KFM01A	P-03-23			
KFM01B	P-04-114			
KFM02A	P-03-98			
KFM03A	P-03-116			
KFM04A	P-04-115			
KFM05A	P-04-295			
KFM06A	P-05-101			
KFM07A	P-05-102			
KFM08A	P-05-203			
Laboratory measurements of thermal properties		Estimation of thermal conductivity and specific heat capacity.	2.6	
KFM01A	P-04-159			
KFM02A	P-04-161			
KFM03A	P-04-162			
KFM04A	P-04-199			
KFM06A	P-05-123			
Anisotropy in thermal properties for KFM04A	Sicada	Estimation of anisotropy in thermal properties.	2.6	
Modal analysis		Estimation of thermal conductivity from mineralogical properties of the bedrock. Statistical analysis.	2.6	
KFM01A	P-04-103, P-04-159			
KFM02A	P-04-103, P-04-161			
KFM03A	P-04-103, P-04-162			
KFM03B	P-04-103			
KFM04A	*P-04-199*, P-05-156			
KFM05A	P-05-156			
KFM05A	P-05-156			
Laboratory test of thermal expansion		Estimation of the thermal expansion coefficient.	2.6	
KFM01A	P-04-163			
KFM02A	P-04-164			
KFM03A	P-04-165			
KFM04A	P-04-198			
Surface-based data				
Modal analyses	*P-03-75, P-04-87*	Estimation of thermal conductivity from mineralogical properties of the bedrock. Statistical analysis.	2.6	
Laboratory measurement of thermal properties	*P-03-08*	Estimation of thermal conductivity and specific heat capacity.	2.6	

Table 4. Available meteorological, hydrological and hydrogeological data and their handling in Forsmark bedrock hydrogeological modelling step 2.1. Report numbers in italics show data available already at data freeze 1.2.

Available data		Usage in F2.1		Not utilised in F2.1
Data specification	**Ref**	**Analysis/Modelling**	**cf. section**	**Motivation/Comment**
Single-hole data from core-drilled boreholes				
Double-packer injection tests (PSS)		Lumped characterisation of rock fracture transmissivities in terms of different test section length transmissivities (5 m, 20 m and 100 m).	2.7, 3.4	
KFM01A	P-04-95			
KFM02A	P-04-100			
KFM02A – re-measurement after hydraulic fracturing	P-05-145			
KFM03A	P-04-194			
KFM03B	P-04-278			
KFM04A	P-04-293			
KFM05A	P-05-56			
KFM06A and 06B	P-05-165			
KFM07A	P-05-133			
Difference-flow logging (PFL)		Detailed characterisation of individual rock fracture transmissivities in terms of high-resolution test section length transmissivities (0.1 m).	2.7, 3.4	
KFM01A	P-03-28 P-04-193			
KFM02A	P-04-188			
KFM03A	P-04-189			
KFM04A	P-04-190			
KFM05A	P-04-191			
KFM06A	P-05-15			
KFM07A	P-05-63			
Single-hole data from percussion-drilled boreholes				
Pumping tests and impeller flow logging		Characterisation of superficial rock fracture transmissivities in terms of borehole specific capacity and cumulative flow logging.	2.7, 3.4	
HFM01, -02, -03	P-03-33			
HFM04, -05	P-03-34			
HFM06, -07, -08	P-03-36			
HFM09, -10	P-04-74			
HFM11, -12	P-04-64			
HFM13, -14, -15	P-04-71			
HFM16	P-04-65			
HFM17, -18, -19	P-04-72			
HFM20, -21, -22	P-05-14			
Cross-hole (interference) data				
HFM01, -02, -03	*P-03-35*	Characterisation of the hydraulic contact between boreholes presumably intersected by a swarm of connected fractures forming a transmissive deformations zone.	2.7, 3.4	
HFM11, -12	P-04-200			
HFM18, KFM03A	P-04-307			
HFM16, KFM02A	P-05-78			
	P-05-37			
KFM04A, HFM10, -13 -19, HFK252	P-05-186			
Correlation of structural, hydraulic and hydrogeochemical data				
KFM01A, -02A, -03A, -04A, -05A	*R-04-77*	Correlation of Posiva Flow Log anomalies to core mapped features.	2.7	
KFM06A, -07A	P-06-56	Correlation of Posiva Flow Log anomalies to core mapped features	2.7	
HFM16, KFM02A	*Sicada field note Forsmark 437*	Hydraulic responses during drilling of HFM16.	2.7, 3.4	

Available data		Usage in F2.1		Not utilised in F2.1
Data specification	**Ref**	**Analysis/Modelling**	**cf. section**	**Motivation/Comment**
KFM03A	*P-04-96*	Hydraulic evaluation of pumping activities prior to hydrogeochemical sampling – indications of upconing.	2.7, 3.4	
KFM02A, -03A, -04A	*P-05-21*	Comparison of measured EC in selected fractures – indications of upconing.	2.7, 3.4	
KFM01B, HFM01, -02, -03, KFM01A	*P-04-135*	Hydraulic responses during drilling of KFM01B.	2.7, 3.4	
Surface data				
Meteorological data	P-05-134 P-05-152 P-06-49	General description and quantitative modelling of groundwater and surface water flow. Snow measurements. Meteorological monitoring.	2.7, 3.4	
Hydrological data	P-05-153	Delineation of catchment areas.	2.7, 3.4	
	P-05-154 P-04-313	Specific discharge in conceptual and quantitative modelling.		
	P-05-245	Brook measurements.		
Hydrogeological data	P-05-166 R-06-49	General description, conceptual and quantitative modelling.	2.7, 3.4	
		Description of soil depth, basis for groundwater level measurements and hydraulic tests.		
		Basis for assigning hydraulic conductivity of Quaternary deposits in conceptual and quantitative models. Head measurements.		
Supplemenatry information and models				
SFR	R-02-14	General description, conceptual and quantitative modelling.	2.7, 3.4	
		Basis for assigning transmissivity data to some of the deterministically treated deformation zones.		
Forsmark Reactor area	SSPB, 1982 SSPB, 1996 /Carlsson 1979/	General description, conceptual and quantitative modelling.	2.7, 3.4	
SDM version 0	R-02-32	General description, conceptual and quantitative modelling.	2.7, 3.4	
SDM version 1.1	R-04-15	General description, conceptual and quantitative modelling.	2.7, 3.4	
SDM version 1.2	R-05-18	General description, conceptual and quantitative modelling.	2.7, 3.4	

Table 5. Available hydrogeochemical data and their handling in Forsmark modelling step 2.1. Report numbers in italics show data available already at data freeze 1.2.

Available data	Ref	Usage in F2.1	cf. section	Not utilised in F2.1
Data specification		**Analysis/Modelling**		**Motivation/Comment**
Complete chemical characterisation (class 4 and 5) in		Manual evaluation and mathematical modelling such as PHREEQC, M3 and coupled transport modelling. The results of the modelling is presented in the conceptual model of the site. The use of the data in the specific modelling approaches are described in ChemNet's issue report (in preparation)	2.8	Non representative samples were not used in the detailed modelling (see motivation in ChemNet's Issue report in preparation)
KFM01A	P-03-94			
KFM02A	P-04-70			
KFM03A	P-04-108			
KFM04A	P-04-109			
KFM05A	P-05-79			
KFM06A	P-05-178			
KFM07A	P-05-170			
Sampling during drilling and Uranine analyses	Drilling reports			
Hydrochemical logging in				
KFM02A	P-03-95			
KFM03A	P-03-96			
KFM04A	P-04-47			
KFM06A	P-05-33			
KFM07A	P-05-187			
KFM08A	P-05-206			
Sampling in percussion-drilled boreholes and monitoring wells				
Drillsite 1	P-03-47			
Drillsite 2	P-03-48			
Drillsite 3	P-03-49			
HFM09–HFM19	P-04-92			
HFM20–HFM22	P-05-48			
Sampling/analyses of shallow groundwaters; May 2003–April 2005	P-05-171			
Samling/analyses of surface waters	P-03-27			
	P-04-146			
	P-05-274			
Sampling/analysis of precipitation	P-05-142			
Other available data: Swedish and Nordic site data				

Table 6. Available data on transport properties and their handling in Forsmark modelling step 2.1. Report numbers in italics show data available already at data freeze 1.2.

Available data	Ref	Usage in F2.1	cf. section	Not utilised in F2.1
Data specification		**Analysis/Modelling**		**Motivation/Comment**
Data from core-drilled boreholes				
Results from porosity measurements and through-diffusion test on samples from boreholes KFM01A, KFM02A, KFM03A, KFM04A, KFM05A, KFM06A, KFM06B and KFM07A.	P-05-109	Assignment of porosity and diffusion parameters.	2.9, 3.5.3	
Formation factors from electrical resistivity measurements in the laboratory on samples from boreholes KFM01A, KFM02A, KFM03A, KFM04A and KFM05A.	*P-05-26* P-05-76	Assignment of diffusion parameters.	2.9, 3.5.3	
Formation factors from in situ electrical resistivity measurements in boreholes KFM01A, KFM02A, KFM03A and KFM04A.	*P-05-29* P-05-108	Assignment of diffusion parameters.	2.8, 3.5.3	

Available data	Ref	Usage in F2.1	cf. section	Not utilised in F2.1
Data specification		Analysis/Modelling		Motivation/Comment
Results from BET surface area measurements on crushed material	P-report not yet published	Qualitative assessment of sorption properties.	2,8, 3.5.3	
Fracture mineralogy	*P-04-103* P-04-149 P-05-197	Identification of site-specific fracture and fracture zone properties as a basis for a conceptual transport model	2.8, 3.5.3	

Table 7. Reports in the SKB series P-, R- and TR that are referred to in Table 1 to Table 6. Reports with numbers in italics contain data available already at data freeze 1.2.

P-02-01	**Thunehed H, Pitkänen T.** Markgeofysiska mätningar inför placering av de tre första kärnborrhålen i Forsmarksområdet.
P-02-02	**Wiklund S.** Digitala ortofoton och höjdmodeller. Redovisning av metodik för platsundersökningsområdena Oskarshamn och Forsmark samt förstudieområdet Tierp Norra.
P-03-08	**Adl-Zarrabi B.** Outcrop samples from Forsmark. Determination of thermal properties by the TPS-method.
P-03-09	**Stephens M B, Bergman T, Andersson J, Hermansson T, Wahlgren C-H, Albrecht L, Mikko H.** Bedrock mapping. Stage 1 (2002) – Outcrop data including fracture data. Forsmark.
P-03-10	**Gren M.** Fågelundersökningar inom SKB:s platsundersökningar 2002. Forsmark.
P-03-11	**Sohlenius G, Rudmark L, Hedenström A.** Forsmark. Mapping of unconsolidated Quaternary deposits. Field data 2002.
P-03-12	**Hermanson J, Hansen L, Olofsson J, Sävås J, Vestgård J.** Detailed fracture mapping at the KFM02 and KFM03 drill sites. Forsmark
P-03-14	**Sohlenius G, Rudmark L.** Forsmark site investigation. Mapping of unconsolidated Quaternary deposits. Stratigraphical and analytical data.
P-03-18	**Cederlund G, Hammarström A, Wallin K.** Surveys of mammal populations in the areas adjacent to Forsmark and Tierp
P-03-20	**Nordman C.** Forsmark site investigation. Boremap mapping of percussion boreholes HFM01–03.
P-03-21	**Nordman C.** Forsmark site investigation.Boremap mapping of percussion boreholes HFM04 and HFM05.
P-03-22	**Nordman C.** Forsmark site investigation. Boremap mapping of percussion boreholes HFM06–08.
P-03-23	**Petersson J, Wägnerud A.** Forsmark site investigation. Boremap mapping of telescopic drilled borehole KFM01A.
P-03-24	**Hedenström A.** Forsmark site investigation. Investigation of marine and lacustrine sediments in lakes. Field data 2003.
P-03-26	**Mattsson H, Isaksson H, Thunehed H.** Forsmark site investigation. Petrophysical rock sampling, measurements of petrophysical rock parameters and in situ gamma-ray spectrometry measurements on outcrops carried out 2002.
P-03-27	**Nilsson A-C, Karlsson S, Borgiel M.** Forsmark site investigation. Sampling and analysis of surface waters. Results from sampling in the Forsmark area, March 2002 to March 2003.
P-03-28	**Rouhiainen P, Pöllänen J.** Forsmark site investigation. Difference flow logging of borehole KFM01A.
P-03-29	**Barton N.** KFM01A. Q-logging.
P-03-30	**Claesson L-Å, Nilsson G.** Forsmark site investigation. Drilling of a flushing water well, HFM01, and two groundwater monitoring wells, HFM02 and HFM03 at drillsite DS1.
P-03-32	**Claesson L-Å, Nilsson G.** Forsmark site investigation. Drilling of the telescopic borehole KFM01A at drilling site DS1.
P-03-33	**Ludvigson J-E, Jönsson S, Levén, J.** Forsmark site investigation. Pumping tests and flow logging. Boreholes KFM01A (0–100 m), HFM01, HFM02 and HFM03.
P-03-34	**Ludvigson J-E, Jönsson S, Svensson T.** Forsmark site investigation. Pumping tests and flow logging. Boreholes KFM02A (0–100 m), HFM04 and HFM05.
P-03-35	**Ludvigson J-E, Jönsson S.** Forsmark site investigation. Hydraulic interference tests. Boreholes HFM01, HFM02 and HFM03.
P-03-36	**Källgården J, Ludvigson J-E, Jönsson S.** Forsmark site investigation. Pumping tests and flow logging. Boreholes KFM03A (0–100 m), HFM06, HFM07 and HFM08.
P-03-38	**Tunbridge L, Chryssanthakis P.** Forsmark site investigation. Borehole KFM01A. Determination of P-wave velocity, transverse borehole core.
P-03-39	**Gustafsson C, Nilsson P.** Forsmark site investigation. Geophysical, radar and BIPS logging in boreholes HFM01, HFM02, HFM03 and the percussion drilled part of KFM01A.
P-03-40	**Isaksson H.** Forsmark site investigation. Interpretation of topographic lineaments 2002.
P-03-41	**Rønning H J S, Kihle O, Mogaard J O, Walker P, Shomali H, Hagthorpe P, Byström S, Lindberg H, Thunehed H.** Forsmark site investigation. Helicopter borne geophysics at Forsmark, Östhammar, Sweden.
P-03-42	**Aaro S.** Forsmark site investigation. Regional gravity survey in the Forsmark area, 2002 and 2003.

P-03-44 **Thunehed H, Pitkänen, T.** Forsmark site investigation. Electric soundings supporting inversion of helicopterborne EM-data.

P-03-45 **Aaltonen J, Gustafsson C.** Forsmark site investigation. RAMAC and BIPS logging in borehole KFM01A.

P-03-47 **Nilsson A-C.** Forsmark site investigation. Sampling and analyses of groundwater in percussion drilled boreholes and shallow monitoring wells at drillsite DS1. Results from the percussion boreholes HFM01, HFM02, HFM03, KFM01A (borehole section 0–100 m) and the monitoring wells SFM0001, SFM0002 and SFM 0003.

P-03-48 **Nilsson A-C.** Forsmark site investigation. Sampling and analyses of groundwater in percussion drilled boreholes and shallow monitoring wells at drillsite DS2. Results from the percussion boreholes HFM04, HFM05, KFM02A (borehole section 0–100 m) and the monitoring wells SFM0004 and SFM0005.

P-03-49 **Nilsson A-C.** Forsmark site investigation. Sampling and analyses of groundwater in percussion drilled boreholes at drillsite DS3. Results from the percussion boreholes HFM06 and HFM08.

P-03-51 **Claesson L-Å, Nilsson, G.** Forsmark site investigation. Drilling of a flushing water well, HFM05, and a groundwater monitoring well, HFM04, at drillsite DS2.

P-03-52 **Claesson L-Å, Nilsson, G.** Forsmark site investigation. Drilling of the telescopic borehole KFM02A at drilling site DS 2.

P-03-53 **Nilsson P, Gustafsson C.** Forsmark site investigation. Geophysical, radar and BIPS logging in boreholes HFM04, HFM05, and the percussion drilled part of KFM02A.

P-03-54 **Nilsson P, Aaltonen J.** Forsmark site investigation. Geophysical, radar and BIPS logging in boreholes HFM06, HFM07 and HFM08.

P-03-55 **Pitkänen T, Isaksson H.** Forsmark site investigation. A ground geophysical survey prior to the siting of borehole KFM04A.

P-03-58 **Claesson L-Å, Nilsson, G.** Forsmark site investigation. Drilling of a flushing water well, HFM06 and two groundwater monitoring wells, HFM07 and HFM08, at drillsite DS3.

P-03-59 **Claesson L-Å, Nilsson, G.** Forsmark site investigation. Drilling of the telescopic borehole KFM03A and the core drilled borehole KFM03B at drilling site DS3.

P-03-64 **Johansson P-O.** Forsmark site investigation. Slug tests in groundwater monitoring wells in soil.

P-03-65 **Werner K, Johansson P-O.** Forsmark site investigation. Slug tests in groundwater monitoring wells in soil.

P-03-75 **Stephens M B, Lundqvist S, Bergman T, Anderson J, Ekström M.** Forsmark site investigation. Bedrock mapping. Rock types, their petrographic and geochemical characteristics, and a structural anaysis of the bedrock based on Stage 1 (2002) surface data.

P-03-76 **Lagerbäck R, Sundh M.** Forsmark site investigation. Searching for evidence of late- or post-glacial faulting in the Forsmark region. Results from 2002.

P-03-77 **Möller C, Snäll S, Stephens M B.** Forsmark site investigation. Dissolution of quartz, vug formation and new grain growth associated with post-metamorphic hydrothermal alteration in KFM02A.

P-03-81 **Abrahamsson T.** Forsmark site investigation. Vegetation inventory in part of the municipality of Östhammar.

P-03-82 **Claesson L-Å, Nilsson, G.** Forsmark site investigation. Drilling of the telescopic borehole KFM04A and the percussion drilled borehole KFM04B at drilling site DS4.

P-03-90 **Fridriksson G, Öhr J.** Forsmark site investigations. Assessment of plant biomass of the ground, field and shrub layers of the Forsmark area.

P-03-94 **Wacker P, Bergelin A, Nilsson, A-C.** Forsmark site investigation. Complete hydrochemical characterisation in KFM01A. Results from two investigated sections, 110.1-120,8 and 176.8-183.9 m.

P-03-95 **Wacker P, Nilsson A-C.** Forsmark site investigation. Hydrochemical logging and “clean up” pumping in KFM02A.

P-03-96 **Berg C, Nilsson A-C.** Forsmark site investigation. Hydrochemical logging in KFM 03A.

P-03-98 **Petersson J, Wängnerud A, Stråhle A.** Forsmark site investigation. Boremap mapping of telescopic drilled borehole KFM02A.

P-03-101 **Elhammer et al.** Forsmark site investigation. Detailed marine geological mapping (in prep).

P-03-102 **Isaksson H, Mattsson H,Thunehed H, Keisu M**. Forsmark site investigation. Interpretation of petrophysical surface data. Stage 1 (2002).

P-03-103 **Nielsen U T, Ringgaard J.** Forsmark site investigation. Geophysical borehole logging in borehole KFM01A, HFM01 and HFM02.

P-03-104 **Pitkänen T, Thunehed H, Isaksson H.** Forsmark site investigation. A ground geophysical survey prior to the siting of borehole KFM05A and KFM06A and control of the character of two SW-NE oriented lineaments.

P-03-108 **Chryssanthakis P.** Forsmark site investigation.Borehole KFM01A. Results of tilt testing.

P-03-115 **Hermanson J, Hansen L, Vestgård J, Leiner P.** Forsmark site investigation. Detailed fracture mapping of the outcrops Klubbudden, AFM001098 and drill site 4, AFM001097.

P-03-116 **Petersson J, Wängnerud A, Danielsson P, Stråhle A.** Forsmark site investigation. Boremap mapping of telescopic drilled borehole KFM03A and core drilled borehole KFM03B.

P-03-117 **Aquilonius K, Karlsson S.** Forsmark site investigation. Snow depth, frost in ground and ice cover during the winter 2002/2003.

P-03-118 **Nilsson B.** Forsmark site investigation. Element distribution in till at Forsmark – a geochemical study.

P-04-03 **Brydsten L.** A method for construction of digital elevation models for site investigation program at Forsmark and Simpevarp.

P-04-04 **Cederlund G, Hammarström A, Wallin K.** Survey of mammal populations in the areas adjacent to Forsmark and Oskarshamn. Results from 2003.

P-04-05 **Borgiel M.** Forsmark site investigation. Sampling and analyses of surface sediment in lakes and shallow bays.

P-04-07 **Andrén C.** Forsmark site investigation. Amphibians and reptiles.

P-04-08 **Chryssanthakis P.** Forsmark site investigation. Borehole KFM02A. Results of tilt testing.

P-04-09 **Chryssanthakis P, Tunbridge L.** Forsmark site investigation. Borehole KFM02A. Determination of P-wave velocity, transverse borehole core.

P-04-25 **Brunberg A-K, Carlsson T, Blomqvist P, Brydsten L, Strömgren M.** Forsmark site investigation. Identification of catchments, lake-related drainage parameters and lake habitats.

P-04-29 **Isaksson H, Thunehed H, Keisu M.** Forsmark site investigation. Interpretation of airborne geophysics and integration with topography.

P-04-30 **Gren M.** Forsmark site investigation. Bird monitoring in Forsmark 2002–2003.

P-04-34 **Sundh M, Sohlenius G, Hedenström A.** Forsmark site investigation. Stratigraphical investigation of till in machine cut trenches.

P-04-39 **Gustafsson J, Gustafsson C.** Forsmark site investigation. RAMAC and BIPS logging in borehole HFM11 and HFM12.

P-04-40 **Gustafsson J, Gustafsson C.** Forsmark site investigation. RAMAC and BIPS logging in borehole KFM02A.

P-04-41 **Gustafsson J, Gustafsson C.** Forsmark site investigation. RAMAC and BIPS logging in borehole KFM03A and KFM03B.

P-04-47 **Berg C, Nilsson A-C.** Forsmark site investigation. Hydrochemical logging of KFM04A.

P-04-64 **Ludvigson J-E, Jönsson S, Jönsson J.** Forsmark site investigation. Pumping tests and flow logging. Boreholes HFM11 and HFM12.

P-04-65 **Ludvigson J-E, Jönsson S, Hjerne C.** Forsmark site investigation. Pumping tests and flow logging. Boreholes KFM06A (0-100m) and HFM16.

P-04-67 **Gustafsson J, Gustafsson C.** Forsmark site investigation. RAMAC and BIPS logging in borehole KFM04A, KFM04B, HFM09 and HFM10.

P-04-68 **Gustafsson J, Gustafsson C.** Forsmark site investigation. RAMAC and BIPS logging in borehole HFM13, HFM14 and HFM 15.

P-04-69 **Gustafsson J, Gustafsson C.** Forsmark site investigation. RAMAC and BIPS logging in borehole KFM06A, HFM16, HFM17, HFM18 and HFM19.

P-04-70 **Wacker P, Bergelin A, Nilsson A-C.** Forsmark site investigation. Hydrochemical characterisation in KFM02A. Results from three investigated borehole sections; 106.5-126.5, 413.5-433.5 and 509.0-516.1 m.

P-04-71 **Ludvigson J-E, Jönsson S, Jönsson J.** Forsmark site investigation. Pumping tests and flow logging. Boreholes HFM13, HFM14 and HFM15.

P-04-72 **Ludvigson J-E, Källgården J, Hjerne C.** Forsmark site investigation. Pumping tests and flow logging. Boreholes HFM17, HFM18 and HFM19.

P-04-74 **Ludvigson J-E, Källgården J, Jönsson J.** Forsmark site investigation. Pumping tests and flow logging. Boreholes HFM09 and HFM10.

P-04-76 **Claesson L-Å, Nilsson, G.** Forsmark site investigation. Drilling of a flushing water well, HFM10, a groundwater monitoring well in solid bedrock, HFM09, and a groundwater monitoring well in soil, SFM0057, at drilling site DS4.

P-04-78 **Marek R.** Forsmark site investigation. Ground penetrating radar survey 2003.

P-04-79 **Gustafsson J, Gustafsson C.** Forsmark site investigation. RAMAC and BIPS logging in borehole KFM01B and RAMAC directional re-logging in borehole KFM01A.

P-04-80 **Mattsson H, Thunehed H, Keisu M.** Forsmark site investigation. Interpretation of borehole geophysical measurements in KFM01A, KFM01B, HFM01, HFM02 and HFM03.

P-04-81 **Keisu M, Isaksson H.** Forsmark site investigation. Acquisition of geological information from Forsmarksverket. Information from the Vattenfall archive, Råcksta.

P-04-83 **Sjöberg J.** Forsmark site investigation. Overcoring rock stress measurements in borehole KFM01B.

P-04-85 **Claesson L-Å, Nilsson, G.** Forsmark site investigation. Drilling of a flushing water well, HFM13, two groundwater monitoring wells in solid bedrock, HFM14-15, and one groundwater monitoring well in soil, SFM0058, at and close to drilling site DS5.

P-04-86 **Hedenström A.** Forsmark site investigation. Investigation of marine and lacustrine sediments in lakes. Stratigraphical and analytical data.

P-04-87 **Stephens M B, Lundqvist S, Bergman T, Ekström M.** Forsmark site investigation. Bedrock mapping. Petrographic and geochemical characteristics of rock types based on Stage 1 (2002) and Stage 2 (2003) surface data.

P-04-88 **Cronqvist T, Forssberg O, Mærsk Hansen L, Jonson A, Koyi S, Leiner P, Vestgård J, Petersson J, Skogsmo G.** Forsmark site investigation. Detailed fracture mapping of two trenches at Forsmark.

P-04-90 **Hermanson J, Hansen L, Vestgård J, Leiner, P.** Forsmark site investigation. Detailed fracture mapping of excavated rock outcrop at drilling site 5, AFM100201.

P-04-91 **Bergman T, Andersson J, Hermansson T, Zetterström Evins L, Albrecht L,Stephens M, Petersson J, Nordman C.** Forsmark site investigation. Bedrock mapping. Stage 2 (2003) - bedrock data from outcrops and the basal parts of trenches and shallow boreholes through the Quaternary cover.

P-04-92 **Nilsson D.** Forsmark site investigation. Sampling and analyses of groundwater from percussion drilled boreholes. Results from the percussion boreholes HFM09 to HFM19 and the percussion drilled part of KFM06A.

P-04-94 **Claesson L-Å, Nilsson G.** Forsmark site investigation. Drilling of a monitoring well, HFM16, at drilling site DS6.

P-04-95 **Ludvigson J-E, Levén J, Jönsson S.** Forsmark site investigation. Single-hole injection tests in borehole KFM01A.

P-04-96 **Ludvigson J-E, Jönsson S, Levén J.** Forsmark site investigation. Hydraulic evaluation of pumping activities prior to hydro-geochemical sampling in borehole KFM03A – Comparison with results from difference flow logging.

P-04-97 **Nielsen U T, Ringgaard J.** Forsmark site investigation. Geophysical borehole logging in borehole KFM02A, KFM03A and KFM03B.

P-04-98 **Thunehed H.** Forsmark site investigation. Interpretation of borehole geophysical measurements in KFM02A, KFM03A, KFM03B and HFM04 to HFM08.

P-04-99 **Bergman B, Palm H, Juhlin C.** Forsmark site investigation. Estimate of bedrock topography using seismic tomography along reflection seismic profiles.

P-04-100 **Källgården J, Ludvigson J-E, Jönsson J.** Forsmark site investigation. Single-hole injection tests in borehole KFM02A.

P-04-101 **Nordman C.** Forsmark site investigation. Boremap mapping of percussion holes HFM09-12.

P-04-103 **Petersson J, Berglund J, Danielsson P, Wängnerud A, Tullborg E-L, Mattsson H, Thunehed H, Isaksson H, Lindroos, H.** Forsmark site investigation. Petrography, geochemistry, petrophysics and fracture mineralogy of boreholes KFM01A, KFM02A and KFM03A+B.

P-04-106 **Claesson L-Å, Nilsson G.** Forsmark site investigation. Drilling of five percussion boreholes, HFM11-12 and HFM17-19, on different lineaments.

P-04-107 **Mattsson H, Thunehed H, Isaksson H, Kübler L.** Forsmark site investigation. Interpretation of petrophysical data from the cored boreholes KFM01A, KFM02A, KFM03A and KFM03B.

P-04-108 **Wacker P, Bergelin A, Berg C, Nilsson A-C.** Forsmark site investigation. Hydrochemical characterisation in KFM03A. Results from six investigated borehole sections: 386.0-391.0 m, 448.0-453.0 m, 448.5-455.6 m, 639.0–646.1 m, 939.5–946.6 m, 980.0–1,001.2 m.

P-04-109 **Wacker P, Bergelin A, Berg C, Nilsson A-C.** Forsmark site investigation. Hydrochemical characterisation in KFM04A. Results from two investigated borehole sections, 230.5–237.6 and 354.0–361.1 m.

P-04-110 **Robertsson A-M.** Microfossil analyses of till and sediment samples from Forsmark, northern Uppland.

P-04-111 **Hedenström A, Sohlenius G, Albrecht J.** Forsmark site investigation. Stratigraphical and analytical data from auger drillings and pits.

P-04-112 **Nordman C.** Forsmark site investigation. Boremap mapping of percussion boreholes HFM13–15 and HFM19.

P-04-113 **Nordman C, Samuelsson E.** Forsmark site investigation. Boremap mapping of percussion boreholes HFM16–18.

P-04-114 **Berglund J, Petersson J, Wängnerud A, Danielsson P.** Forsmark site investigation. Boremap mapping of core drilled borehole KFM01B.

P-04-115 **Petersson J, Wängnerud A, Berglund J, Danielsson P, Stråhle A.** Forsmark site investigation. Boremap mapping of telescopic drilled borehole KFM04A.

P-04-116 **Carlsten S, Petersson J, Stephens M, Mattsson H, Gustafsson J.** Forsmark site investigation. Geological single-hole interpretation of KFM01A, KFM01B and HFM01–03 (DS1).

P-04-117 **Carlsten S, Petersson J, Stephens M, Mattsson H, Gustafsson J.** Forsmark site investigation. Geological single-hole interpretation of KFM02A and HFM04–05 (DS2).

P-04-118 **Carlsten S, Petersson J, Stephens M, Thunehed H, Gustafsson J.** Forsmark site investigation. Geological single-hole interpretation of KFM03B, KFM03A and HFM06–08 (DS3).

P-04-119 **Carlsten S, Petersson J, Stephens M, Mattsson H, Gustafsson J.** Forsmark site investigation. Geological single-hole interpretation of KFM04A and HFM09–10 (DS4).

P-04-120 **Carlsten S, Petersson J, Stephens M, Thunehed H, Gustafsson J.** Forsmark site investigation. Geological single-hole interpretation of HFM11–13 and HFM16–18.

P-04-123 **Lagerbäck R, Sundh M, Johansson H.** Forsmark site investigation. Searching for evidence of late- or post-glacial faulting in the Forsmark region. Results from 2003.

P-04-124 **Andersson J.** Forsmark site investigation. Investigation of the amount of dead wood.

P-04-125 **Brydsten L, Strömgren M**. Forsmark site investigation. Water depth soundings in shallow bays in Forsmark.

P-04-126 **Page L, Hermansson T, Söderlund P, Andersson J, Stephens M B.** Forsmark site investigation. Bedrock mapping U-Pb, 40Ar/39Ar and (U-Th)/He geochronology.

P-04-127 **Fredriksson D.** Forsmark site investigation. Peatland investigation Forsmark.

P-04-135 **Levén J, Ludvigson J-E.** Forsmark site investigation. Hydraulic interferences during the drilling of borehole KFM01B. Boreholes HFM01, HFM02, HFM03 and KFM01A.

P-04-136 **Johansson P-O.** Forsmark site investigation. Undisturbed pore water sampling and permeability measurements with BAT filter tips. Soil sampling for pore water analyses.

P-04-137 **Heneryd N.** Forsmark site investigation. Snow depth, frost in ground and ice cover during the winter 2003/2004.

P-04-138 **Werner K, Lundholm L, Johansson P-O.** Forsmark site investigation. Drilling and pumping test of wells at Börstilåsen.

P-04-139 **Werner K, Lundholm L.** Forsmark site investigation. Supplementary drilling and soil sampling, installation of groundwater monitoring wells, a pumping well and surface water level gauges.

P-04-140 **Werner K.** Forsmark site investigation. Supplementary slug tests in groundwater monitoring wells in soil.

P-04-142 **Werner K, Lundholm L.** Forsmark site investigation. Pumping test in wells SFM0074.

P-04-143 **Mattsson H, Keisu M.** Forsmark site investigation. Interpretation of borehole geophysical measurements in KFM04A, KFM06A (0–100 m), HFM10, HFM11, HFM12, HFM13, HFM16, HFM17 and HFM18.

P-04-144 **Nielsen U T, Ringgaard J.** Forsmark site investigation. Geophysical borehole logging in borehole KFM04A, KFM06A, HFM10, HFM11, HFM12 and HFM13.

P-04-145 **Nielsen U T, Ringgaard J.** Forsmark site investigation. Geophysical borehole logging in borehole KFM01B, HFM14, HFM15, HFM16, HFM17 and HFM18.

P-04-146 **Nilsson A-C, Borgiel M.** Forsmark site investigation. Sampling and analyses of surface waters. Results from sampling in the Forsmark area, March 2003 to March 2004.

P-04-148 **Hedenström A.** Forsmark site investigation. Stratigraphical and analytical data of Quaternary deposits.

P-04-149 **Sandström B, Savolainen M, Tullborg E-L.** Forsmark site investigation. Fracture mineralogy. Results from fracture minerals and wall rock alteration in boreholes KFM01A, KFM02A, KFM03A and KFM03B.

P-04-152 **Gustafsson J, Gustafsson C.** Forsmark site investigation. RAMAC and BIPS logging in borehole KFM05A.

P-04-153 **Nielsen U T, Ringgaard J.** Forsmark site investigation. Geophysical borehole logging in borehole KFM05A and HFM19.

P-04-154 **Thunehed H, Keisu M.** Forsmark site investigation. Interpretation of borehole geophysical measurements in KFM05A, HFM14, HFM15 and HFM19.

P-04-155 **Isaksson H, Mattsson H, Thunehed H, Keisu M.** Forsmark site investigation. Petrophysical surface data Stage 2 – 2003 (including 2002).

P-04-156 **Marek R.** Forsmark site investigation. A co-ordinated interpretation of ground penetrating radar data from the Forsmark site.

P-04-157 **Thunehed H.** Forsmark site investigation. Inversion of helicopterborne electromagnetic measurements.

P-04-158 **Juhlin C, Bergman B.** Reflection seismics in the Forsmark area. Updated interpretation of Stage 1 (previous report R-02-43). Updated estimate of bedrock topography (previous report P-04-99).

P-04-159 **Adl-Zarrabi B.** Forsmark site investigation. Drill hole KFM01A. Thermal properties: heat conductivity and heat capacity determined using the TPS method and mineralogical composition by modal analysis.

P-04-161 **Adl-Zarrabi B.** Forsmark site investigation. Drill hole KFM02A. Thermal properties: heat conductivity and heat capacity determined using the TPS method and mineralogical composition by modal analysis.

P-04-162 **Adl-Zarrabi B.** Forsmark site investigation. Drill hole KFM03A. Thermal properties: heat conductivity and heat capacity determined using the TPS method and mineralogical composition by modal analysis.

P-04-163 **Åkesson U.** Forsmark site investigation. Drill hole KFM01A. Extensometer measurements of the coefficient of thermal expansion of rock.

P-04-164 **Carlsson L.** Forsmark site investigation. Drill hole KFM02A. Extensometer measurements of the coefficient of thermal expansion of rock.

P-04-165 **Liedberg L.** Forsmark site investigation. Drill hole KFM03A. Extensometer measurements of the coefficient of thermal expansion of rock.

P-04-170 **Jacobsson L.** Forsmark site investigation. Drill hole KFM01A. Indirect tensile strength test.

P-04-171 **Eloranta P.** Forsmark site investigation. Drill hole KFM01A. Indirect tensile strength test (HUT).

P-04-172 **Jacobsson L.** Forsmark site investigation. Drill hole KFM02A. Indirect tensile strength test.

P-04-173 **Jacobsson L.** Forsmark site investigation. Drill hole KFM03A. Indirect tensile strength test.

P-04-174 **Jacobsson L.** Forsmark site investigation. Drill hole KFM04A. Indirect tensile strength test.

P-04-175 **Chryssanthakis P.** Forsmark site investigation. Drill hole KFM01A. The normal stress and shear tests on joints.

P-04-176 **Eloranta P.** Forsmark site investigation. Drill hole KFM01A. Uniaxial compression test (HUT).

P-04-177 **Eloranta P.** Forsmark site investigation. Drill hole KFM01A. Triaxial compression test (HUT).

P-04-178 **Chryssanthakis P.** Forsmark site investigation. Boreholes KFM03A and KFM03B Tilt testing.

P-04-179 **Chryssanthakis P, Tunbridge L.** Forsmark site investigation. Borehole KFM04A Tilt testing.

P-04-180 **Chryssanthakis P, Tunbridge L.** Forsmark site investigation. Borehole KFM03A. Determination of P-wave velocity, transverse borehole core.

P-04-181 **Chryssanthakis P, Tunbridge L.** Forsmark site investigation. Borehole KFM04A. Determination of P-wave velocity, transverse borehole core.

P-04-186 **Dinges C.** Forsmark site investigation. Drill hole KFM01A. Thermal properties: heat conductivity and heat capacity determined using the TPS method – compared test.

P-04-188 **Rouhiainen P, Pöllänen J.** Forsmark site investigation. Difference flow logging in borehole KFM02A.

P-04-189 **Pöllänen J, Sokolnicki M.** Forsmark site investigation. Difference flow logging in borehole KFM03A.

P-04-190 **Rouhiainen P, Pöllänen J.** Forsmark site investigation. Difference flow logging in borehole KFM04A.

P-04-191 **Pöllänen J, Sokolnicki M, Rouhiainen P.** Forsmark site investigation. Difference flow logging in borehole KFM05A.

P-04-193 **Rouhiainen P, Pöllänen J, Ludvigson J-E.** Forsmark site investigation. Addendum to Difference flow logging in borehole KFM01A.

P-04-194 **Källgården J, Ludvigson J-E, Hjerne C.** Forsmark site investigation. Single-hole injection tests in borehole KFM03A.

P-04-198 **Åkesson U.** Forsmark site investigation. Drill hole KFM04A: Extensometer measurement of the coefficient of thermal expansion of rock.

P-04-199 **Adl-Zarrabi B.** Forsmark site investigation. Drill hole KFM04A. Thermal properties: heat conductivity and heat capacity determined using the TPS method and mineralogical composition by modal analysis.

P-04-200 **Jönsson S, Ludvigson J-E, Svensson T.** Forsmark site investigation. Hydraulic interference tests. Boreholes HFM11 and HFM12.

P-04-203 **Chryssanthakis P, Tunbridge L.** Forsmark site investigation. Borehole: KFM05A. Determination of P-wave velocity, transverse borehole core.

P-04-205 **Chryssanthakis P, Tunbridge L.** Forsmark site investigation. Borehole: KFM05A. Tilt testing.

P-04-222 **Claesson L-Å, Nilsson G.** Forsmark site investigation. Drilling of the telescopic borehole KFM05A at drilling site DS5.

P-04-223 **Jacobsson L.** Forsmark site investigation. Borehole KFM01A. Uniaxial compression test of intact rock.

P-04-224 **Jacobsson L.** Forsmark site investigation. Borehole KFM02A. Uniaxial compression test of intact rock.

P-04-225 **Jacobsson L.** Forsmark site investigation. Borehole KFM03A. Uniaxial compression test of intact rock.

P-04-226 **Jacobsson L.** Forsmark site investigation. Borehole KFM04A. Uniaxial compression test of intact rock.

P-04-227 **Jacobsson L.** Forsmark site investigation. Borehole KFM01A. Triaxial compression test of intact rock.

P-04-228 **Jacobsson L.** Forsmark site investigation. Borehole KFM02A. Triaxial compression test of intact rock.

P-04-229 **Jacobsson L.** Forsmark site investigation. Borehole KFM03A. Triaxial compression test of intact rock.

P-04-230 **Jacobsson L.** Forsmark site investigation. Borehole KFM04A. Triaxial compression test of intact rock.

P-04-241 **Korhonen K, Paananen M, Paulamäki S.** Interpretation of lineaments from airborne geophysical and topographic data. An alternative model within version 1.2 of the Forsmark modelling project

P-04-245 **Claesson L-Å, Nilsson G.** Forsmark site investigation. Drilling of two flushing water wells, HFM21 and HFM22, one groundwater monitoring well in solid bedrock, HFM20, and one groundwater monitoring well in soil, SFM0076.

P-04-278 **Hjerne C, Jönsson J, Ludvigson J-E.** Forsmark site investigation. Single-hole injection tests in borehole KFM03B.

P-04-282 **Isaksson H, Keisu M.** Forsmark site investigation. Interpretation of airborne geophysics and integration with topography. Stage 2 (2002–2004).

P-04-293 **Hjerne C, Ludvigson J-E.** Forsmark site investigation. Single-hole injection tests in borehole KFM04A.

P-04-295 **Petersson J, Berglund J, Wängnerud A, Danielsson P, Stråhle A.** Forsmark site investigation. Boremap mapping of telescopic drilled borehole KFM05A.

P-04-296 **Carlsten S, Petersson J, Stephens M, Thunehed H, Gustafsson J.** Forsmark site investigation. Geological single-hole interpretation of KFM05A, HFM14–15 and HFM19 (DS5).

P-04-302 **Claesson L-Å, Nilsson G.** Forsmark site investigation. Drilling of borehole KFM01B at drilling site DS1.

P-04-305 **Gustafsson J, Nissen J.** Forsmark site investigation. Mise-á-la-masse measurements. An experiment to test the possibility for detecting the outcropping of the fracture zone DZ2 in HFM14.

P-04-307 **Gokall-Norman K, Svensson T, Ludvigson L-E, Jönsson S.** Forsmark site investigation. Hydraulic interference test. Boreholes HFM18 and KFM03A.

P-04-311 **Klee G, Rummel F.** Forsmark site investigation. Rock stress measurements with hydraulic fracturing and hydraulic testing of pre-existing fractures in borehole KFM01A, KFM01B, KFM02A and KFM04A. Results from in situ tests.

P-04-312 **Rummel F, Weber U.** Forsmark site investigation. Rock stress measurements with hydraulic fracturing and hydraulic testing of pre-existing fractures in borehole KFM01A, KFM01B, KFM02A and KFM04A. Laboratory Core Investigations.

P-04-313 **Nyberg G, Wass E, Askling P, Johansson P-O.** Forsmark site investigation. Hydro monitoring programme. Report for June 2002–July 2004.

P-05-01 **Gustafsson J, Gustafsson C.** Forsmark site investigation. RAMAC and BIPS logging in boreholes KFM06A and HFM22.

P-05-04 **Chryssanthakis P, Tunbridge L.** Forsmark site investigation. Borehole KFM06A. Determination of P-wave velocity, transverse borehole core.

P-05-08 **Ljunggren B.** Forsmark site investigation. Drill hole KFM01A. Normal loading and shear tests on joints

P-05-09 **Ljunggren B.** Forsmark site investigation. Drill hole KFM02A. Normal loading and shear tests on joints

P-05-10 **Ljunggren B.** Forsmark site investigation. Drill hole KFM03A. Normal loading and shear tests on joints

P-05-11 **Ljunggren B.** Forsmark site investigation. Drill hole KFM04A. Normal loading and shear tests on joints

P-05-12 **Toresson B.** Forsmark site investigation. Seismic refraction survey 2004.

P-05-14 **Jönsson J, Hjerne C, Ludvigson J-E.** Forsmark site investigation. Pumping tests and flow logging. Boreholes HFM20, HFM21 and HFM22.

P-05-15 **Rouhiainen P, Sokolnicki M.** Forsmark site investigation. Difference flow logging in borehole KFM06A.

P-05-17 **Nielsen U T, Ringgaard J, Horn F.** Forsmark site investigation. Geophysical borehole logging in borehole KFM06A, HFM20, HFM21, HFM22 and SP-logging in KFM01A and KFM04A.

P-05-21 **Ludvigson J-E, Levén J.** Forsmark site investigation. Comparison of measured EC in selected fractures in boreholes KFM02A, KFM03A and KFM04A from difference flow logging and hydro-geochemical characterization – Analysis of observed discrepancies in KFM03A.

P-05-26 **Thunehed H.** Forsmark site investigation. Resistivity measurements on samples from KFM01A and KFM02A.

P-05-29 **Löfgren M, Neretnieks I.** Forsmark site investigation. Formation factor logging in situ and in the laboratory by electrical methods in KFM01A and KFM02A. Measurements and evaluation of methodology.

P-05-33 **Berg C.** Forsmark site investigation. Hydrochemical logging in KFM06A.

P-05-37 **Rouhiainen P, Sokolnicki M.** Forsmark site investigation. Difference flow logging in borehole KFM02A during pumping in HFM16.

P-05-46 **Toresson B.** Forsmark site investigation. Seismic velocity analysis in excavated trenches.

P-05-48 **Nilsson D.** Forsmark site investigation. Sampling and analyses of groundwater from percussion drilled boreholes Results from the percussion drilled boreholes HFM20, HFM21 and HFM22.

P-05-50 **Claesson L-Å, Nilsson G.** Forsmark site investigation. Drilling of the telescopic borehole KFM06A and the core drilled borehole KFM06B at drill site DS6.

P-05-51 **Mattsson H, Keisu M.** Forsmark site investigation. Interpretation of geophysical borehole measurements from KFM06A and HFM20, HFM21 and HFM22.

P-05-52 **Gustafsson J, Gustafsson C.** Forsmark site investigation. RAMAC and BIPS logging in borehole KFM07A.

P-05-53 **Gustafsson J, Gustafsson C.** Forsmark site investigation. RAMAC and BIPS logging in borehole KFM06B.

P-05-56 **Gokall-Norman K, Ludvigson J-E, Hjerne C.** Forsmark site investigation. Single-hole injection tests in borehole KFM05A.

P-05-58 **Gustafsson J, Gustafsson C.** Forsmark site investigation. RAMAC and BIPS logging in borehole KFM08B.

P-05-63 **Sokolnicki M, Rouhiainen P.** Forsmark site investigation. Difference flow logging in borehole KFM07A

P-05-64 **Gustafsson J, Gustafsson C.** Forsmark site investigation. RAMAC and BIPS logging in borehole KFM07A (0–100 m), HFM20 and HFM21.

P-05-66 **Lindfors U, Perman F, Sjöberg J.** Forsmark site investigation. Evaluation of the overcoring results from borehole KFM01B.

P-05-76 **Thunehed H.** Forsmark site investigation. Resistivity measurements and determination of formation factors on samples from KFM03A, KFM04A and KFM05A.

P-05-78 **Gokall-Norman, Ludvigson J-E.** Forsmark site investigation. Hydraulic interference test. Boreholes HFM16, HFM19 and KFM02A.

P-05-97 **Jacobsson L.** Forsmark site investigation. Borehole KFM05A. Uniaxial compression test of intact rock.

P-05-98 **Jacobsson L.** Forsmark site investigation. Borehole KFM05A. Indirect tensile strength test.

P-05-99 **Jacobsson L.** Forsmark site investigation. Borehole KFM05A. Normal stress and shear test on joints

P-05-100 **Jacobsson L.** Forsmark site investigation. Borehole KFM05A. Triaxial compression test of intact rock.

P-05-101 **Petersson J, Skogsmo G, Berglund J, Wängnerud A, Stråhle A.** Forsmark site investigation. Boremap mapping of telescopic drilled borehole KFM06A and core drilled borehole KFM06B.

P-05-102 **Petersson J, Skogsmo G, Wängnerud A, Berglund J, Stråhle A.** Forsmark site investigation. Boremap mapping of telescopic drilled borehole KFM07A.

P-05-103 **Berglund J, Döse C.** Forsmark site investigation. Boremap mapping of percussion boreholes HFM20, HFM21 and HFM22.

P-05-108 **Löfgren M, Neretnieks I.** Forsmark site investigation. Formation factor logging in situ by electrical methods in KFM03A and KFM04A.

P-05-109 **Börjesson S, Gustavsson E.** Forsmark site investigation. Laboratory data from the site investigation programme for the transport properties of the rock. Data delivery for data freeze Forsmark 2.1.

P-05-112 **Lanaro F.** Forsmark site investigation. Rock mechanics characterisation of borehole KFM01A.

P-05-113 **Lanaro F.** Forsmark site investigation. Rock mechanics characterisation of borehole KFM02A.

P-05-114 **Lanaro F.** Forsmark site investigation. Rock mechanics characterisation of borehole KFM03A.

P-05-115 **Lanaro F.** Forsmark site investigation. Rock mechanics characterisation of borehole KFM04A.

P-05-119 **Mattson H.** Forsmark site investigation. Interpretation of geophysical borehole measurements from KFM07A.

P-05-120 **Jacobsson L.** Forsmark site investigation. Borehole KFM06A. Uniaxial compression test of intact rock.

P-05-122 **Jacobsson L, Flansbjer M.** Forsmark site investigation. Borehole KFM06A. Normal loading and shear test on joints

P-05-123 **Adl-Zarrabi B.** Forsmark site investigation. Drill hole KFM06A Thermal properties: heat conductivity and heat capacity determined using the TPS method.

P-05-132 **Carlsten S, Gustafsson J, Mattsson H, Petersson J, Stephens M.** Forsmark site investigation. Geological single-hole interpretation of KFM06A and KFM06B (DS6).

P-05-133 **Gokall-Norman K, Svensson T, Ludvigson.** Forsmark site investigation. Single-hole injection tests in borehole KFM07A.

P-05-134 **Heneryd N.** Forsmark site investigation. Snow depth, ground frost and ice cover during the winter 2004/2005.

P-05-141 **Jacobsson L, Flansbjer M.** Forsmark site investigation. Borehole KFM05A Normal stress test with direct and indirect deformation measurement together with shear tests on joints.

P-05-142 **Claesson L-Å, Nilsson G.** Forsmark site investigation. Drilling of the telescopic borehole KFM07A at drill site DS7.

P-05-143 **Nilsson D.** Forsmark site investigation. Sampling and analysis of precipitation, years 2002 to 2005.

P-05-145 **Svensson T, Ludvigson J-E, Hjerne C.** Forsmark site investigation. Single-hole injection tests in borehole KFM02A, re-measurements after hydraulic fracturing.

P-05-152 **Juston J, Johansson P-O.** Forsmark site investigation. Analysis of meteorological data, surface water level data, and groundwater level data.

P-05-153 **Johansson P-O.** Forsmark site investigation. Manual discharge measurements in brooks, April 2002–April 2005.

P-05-154 **Johansson P-O.** Forsmark site investigation. Installation of brook discharge gauging stations.

P-05-156 **Petersson J, Berglund J, Danielsson P, Skogsmo G.** Forsmark site investigation. Petrographic and geochemical characteristics of bedrock samples from boreholes KFM04A–06A, and a whitened alteration rock.

P-05-157 **Carlsten S, Gustafsson J, Mattsson H, Petersson J, Stephens M.** Forsmark site investigation. Geological single-hole interpretation of KFM07A and HFM20–21 (DS7).

P-05-158 **Gustafsson J, Gustafsson C.** Forsmark site investigation. RAMAC and BIPS logging in borehole KFM08A.

P-05-159 **Nielsen U T, Ringgaard J, Fris Dahl J.** Forsmark site investigation. Geophysical borehole logging in the boreholes KFM07A, KFM08A and KFM08B.

P-05-165 **Hjerne C, Ludvigson J-E, Lindquist A.** Forsmark site investigation. Single-hole injection tests in boreholes KFM06A and KFM06B.

P-05-166 **Lundin L, Stendahl J, Lode E.** Forsmark site investigation. Soils in two large trenches.

P-05-168 **Cosma C, Enescu N, Balu L.** Forsmark site investigation. Vertical seismic profiling from the boreholes KFM01A and KFM02A.

P-05-170 **Berg C, Wacker P, Nilsson A-C.** Forsmark site investigation. Chemical characterisation in borehole KFM07A Results from the investigated section at 848.0–1,001.6 m.

P-05-171 **Nilsson A-C, Borgiel M.** Forsmark site investigation. Sampling and analyses of near surface groundwaters Results from sampling of shallow soil monitoring wells, BAT pipes, a natural spring and private wells, May 2003–April 2005.

P-05-172 **Claesson L-Å, Nilsson G.** Forsmark site investigation. Drilling of the telescopic borehole KFM08A and the core drilled borehole KFM08B at drill site DS8.

P-05-176 **Gustafsson J, Gustafsson C.** Forsmark site investigation. BIPS logging in the boreholes HFK248, HFK249 and HFK250.

P-05-178 **Berg C, Wacker P, Nilsson A-C.** Forsmark site investigation. Chemical characterisation in borehole KFM06A. Results from the investigated sections at 266.0–271.0 m, 353.5–360.6 m and 768.0–775.1 m.

P-05-186 **Gokall-Norman K, Ludvigson J-E, Jönsson S.** Forsmark site investigation. Hydraulic interference test. Boreholes KFM04A, HFM10, HFM13, HFM19 and HFK252.

P-05-187 **Berg C, Levén J, Nilsson A-C.** Forsmark site investigation. Hydrochemical logging in KFM07A.

P-05-197 **Sandström B, Tullborg E-L.** Forsmark site investigation. Fracture mineralogy Results from fracture minerals and wall rock alteration in boreholes KFM01B, KFM04A, KFM05A and KFM06A.

P-05-202 **Mattsson H, Keisu M.** Forsmark site investigation. Interpretation of geophysical borehole measurements from KFM08A and KFM08B.

P-05-203 **Petersson J, Berglund J, Skogsmo G, Wängnerud A.** Forsmark site investigation. Boremap mapping of telescopic drilled borehole KFM08A and cored drilled borehole KFM08B

P-05-204 **Mattsson H, Thunehed H, Isaksson H.** Forsmark site investigation. Interpretation of petrophysical data from the cored boreholes KFM04A, KFM05A and KFM06A.

P-05-206 **Berg C.** Forsmark site investigation. Hydrochemical logging in KFM08A.

P-05-245 **Nyberg G, Wass E.** Forsmark site investigation. Hydro Monitoring Program. Report for August 2004–July 2005.

P-05-261 **Johansson R, Isaksson H.** Forsmark site investigation. Assessment of inferred lineaments in the northwestern part of the Forsmark site investigation area. Present knowledge and recommendations for further investigations

P-05-262 **Carlsten S, Gustafsson J, Mattsson H, Petersson J, Stephens M.** Forsmark site investigation. Geological single-hole interpretation of KFM08A, KFM08B and HFM22 (DS8).

P-06-49 **Wern L, Jones J.** Meteorological monitoring at Forsmark, June 2003 until July 2005.

P-06-56 **Forssman I, Zetterlund M, Forsmark T, Rhén I.** Correlation of Posiva Flow Log anomalies to core mapped features in Forsmark in KFM06A and KFM07A.

R-98-05 **Axelsson C-L; Hansen L M.** Update of structural models at SFR nuclear waste repository, Forsmark, Sweden

R-99-08 **Stigsson M, Follin S, Andersson J.** On the simulation of variable density flow at SFR, Sweden.

R-99-69 **Kautsky H, Plantman P, Borgiel M.** Quantitative distribution of aquatic plant and animal communities in the Forsmark area.

R-99-70 **Lindell S, Ambjörn C, Juhlin B, Larsson-McCann S, Lindquist K.** Available climatological and oceanographical data for site investigation programme.

R-01-02 **Holmén J G, Stigsson M.** Modelling of future hydrogeological conditions at SFR

R-01-12 **Bergström E.** Late Holocene distribution of lake sediment and peat in NE Uppland.

R-02-06 **Boresjö Bronge L, Wester K.** Vegetation mapping with satellite data of the Forsmark and Tierp regions.

R-02-08 **Berggren J, Kyläkorpi L.** Ekosystemen i Forsmarksområdet. Sammanställning av befintlig information.

R-02-17 **Ludvigson J-E.** Brunnsinventering I Forsmark.

R-02-14 **Axelsson C-L, Ekstav A, Lindblad Påsse A**. SFR – Utvärdering av hydrogeologi.

R-02-32 **SKB.** Forsmark – site descriptive model version 0.

R-02-41 **Blomqvist P, Nilsson E, Brunberg A-K.** Habitat distribution, water chemistry, and biomass and production of pelagic and benthic microbiota in Lake Eckarfjärden, Forsmark.

R-02-43 **Juhlin C, Bergman B, Palm H.** Reflection seismic studies in the Forsmark area – stage 1.

R-03-27 **Andersson E, Tudorancea M-M, Tudorancea C, Brunberg A-K, Blomqvist P.** Water chemistry, biomass and production of biota in Lake Eckarfjärden during 2002.

R-04-08 **Lundin L, Lode E, Stendahl J, Melkerud P A, Björkvald L, Thorstensson A.** Soils and site types in the Forsmark area.

R-04-10 **Miliander S, Punakivi M, Kyläkorpi L, Rydgren B.** Human population and activities in Forsmark. Site description.

R-04-15 **SKB.** Preliminary site description Forsmark area – version 1.1

R-04-77 **Forssman I, Zetterlund M, Rhén I.** Correlation of Posiva Flow Log anomalies to core mapped features in Forsmark (KFM01A to KFM05A).

R-04-39 **Sohlenius G, Hedenström A, Rudmark L.** Forsmark site investigation. Mapping of unconsolidated Quaternary deposits 2002–2003. Map description.

R-04-70 **Brydsten L.** Digital elevation models for site investigation program in Forsmark.

R-05-18 **SKB.** Preliminary site description Forsmark area – version 1.2.

R-05-42 **Juhlin C, Palm H.** Forsmark site investigation. Reflection seismic studies in the Forsmark area, 2004: Stage 2.

R-06-49 **Juston J, Johansson P-O, Levén J, Follin S.** Analysis of meteorological, hydrological and hydrogeological monitoring data, December 2002–July 2005. Forsmark site investigation.

TR-91-24 **Andersson J-E, Nordqvist R, Nyberg G, Smellie J, Tirén S.** Hydrogeological conditions in the Finnsjön area. Compilation of data and conceptual model.

TR-92-07 **Geir J E, Axelsson C-E, Hässler L, Benabderrahmane A.** Discrete fracture modelling of the Finnsjön rock mass: Phase 2.

TR-92-33 **Ahlbom K, Andersson J-E, Andersson P, Ittner T, Ljunggren C, Tirén S.** Finnsjön study site. Scope of activities and main results.

TR-96-24 **Påsse T.** A mathematical model of the shore level displacement in Fennoscandia.

TR-97-28 **Påsse T.** A mathematical model of past, present and future shore level displacement in Fennoscandia.

TR-99-11 **Engqvist A, Andrejev O.** Water exchange of Öregrundsgrepen. A baroclinic 3D-model study.

TR-99-16 **Brydsten L.** Shore line displacement in Öregrundsgrepen.

TR-99-18 **Gylling B, Walker D, Hartley L.** Site-scale groundwater flow modelling of Beberg.

TR-99-38 **Westman P, Wastegård S, Schoning K, Gustafsson B, Omstedt A.** Salinity change in the Baltic Sea during the last 8,500 years: evidence, causes and models.

TR-00-02 **Brunberg A-K, Blomqvist P.** Post-glacial, land rise-induced formation and development of lakes in the Forsmark area, central Sweden.

TR-02-02 **Larsson-McCann S, Karlsson A, Nord M, Sjögren J, Johansson L, Ivarsson M, Kindell S.** Meteorological, hydrological and oceanographical information and data for the site investigation program in the communities of Östhammar and Tierp in the northern part of Uppland.

TR-03-17 **Hedenström A, Risberg J.** Shore displacement in northern Uppland during the last 6,500 calender years.

TR-04-12 **Gustafsson B G.** Millenial changes of the Baltic Sea salinity. Studies of the sensitivity of the salinity to climate change.

Appendix 2

Geological modelling

1 Rock domains

Relative to the regional model in SDM version 1.2, minor modifications in rock domains have emerged on the basis of new borehole data. These data have led to better constraints on the geometry of domain RFM032 and the addition of two, new domains with identification codes RFM043 and RFM044. This exercise has resulted in minor changes in the geometry of domain RFM029 and the reinstallation of domain RFM034 from SKB version 1.1, both of which share the same compositional, homogeneity and deformational characteristics /SKB 2004/. In summary, 38 rock domains are present in the regional domain model, version 2.1. The geometry and properties of 33 domains have been retained from version 1.2, i.e. all domains except RFM029 and RFM032.

For the first time, a local rock domain model is presented for the Forsmark site. The motivation for the choice of the local model area is presented in Section 2.3.2. 13 rock domains in the regional domain model are also present in the local model volume (RFM012, RFM016, RFM017, RFM018, RFM020, RFM021, RFM025, RFM026, RFM029, RFM032, RFM034, RFM043 and RFM044. See Figure 3-2 in main text). Rock domain RFM026 occurs in two, small separate volumes inside the local model volume. The geometry of these domains in the regional model has been retained in the local model. Two minor domains with identification codes RFM045 and RFM046 have also been added in the local model. The former occurs in the central part of the local model volume and is the only one that is relevant for, for example, repository engineering. In summary, 16 rock domains are present in the local model. Minor changes to the properties of rock domain RFM029 have been made in the local model and the properties of the two new domains are also presented. Otherwise the properties of the domains in the local model are inherited from the regional model.

Some remarks concerning the modelling procedure and property assignment are provided in the text below for the modified domains RFM029 and RFM032, for the reinstalled domain RFM034, and for the new domains RFM043, RFM044, RFM045 and RFM046. The translation of rock codes to rock type is provided in Appendix 2.1. Confidence assessment and uncertainties are addressed in the main part of the report. The geometry, confidence level and properties of the rock domains in model version 2.1 are archived in SKB's database for modelling activities.

1.1 RFM029

Rock domain RFM029 dominates the tectonic lens at Forsmark /SKB 2004, 2005/ and is of prime importance in, for example, the rock engineering work. It has been modelled in model version 2.1 by simply infilling the volume that is situated between domains RFM012, RFM013, RFM017, RFM018, RFM032 and RFM044 (Figure 1-1). Minor changes in the geometry of this domain have only occurred in the north-westernmost part of the candidate area, along the boundaries to domains RFM032 and RFM044.

In agreement with earlier work /SKB 2004, 2005/, the ductile planar structures, which have been measured both at the surface and at depth, define a great-circle distribution pattern on the lower hemisphere of an equal-area stereographic projection (Figure 1-2). This pattern confirms large-scale folding of the planar structures inside the domain. The integrated surface and borehole data from the local model volume indicate a fold axis that plunges 166/56 (Figure 1-2). This value differs somewhat from that calculated from the equivalent surface data (Figure 1-2). However, the quantity of surface data is considerably less and, for this reason, the significance of this difference is difficult to interpret. The mean value of the mineral lineation data from the surface plunges slightly more to the east and more gently than the inferred fold axis from the local model volume (Figure 1-2). A linear anisotropy, with both folding and stretching that plunge moderately to the SSE and SE, respectively, is apparent in domain RFM029.

Quantitative estimates of the different rock types in rock domain RFM029 are provided with the help of the borehole data. Both the dominant rock type and the rock occurrences that are less than 1 m in borehole length have been included in the analysis (cf. SDM version 1.2). There are very minor differences between the proportions of rock types between the regional and local model volumes

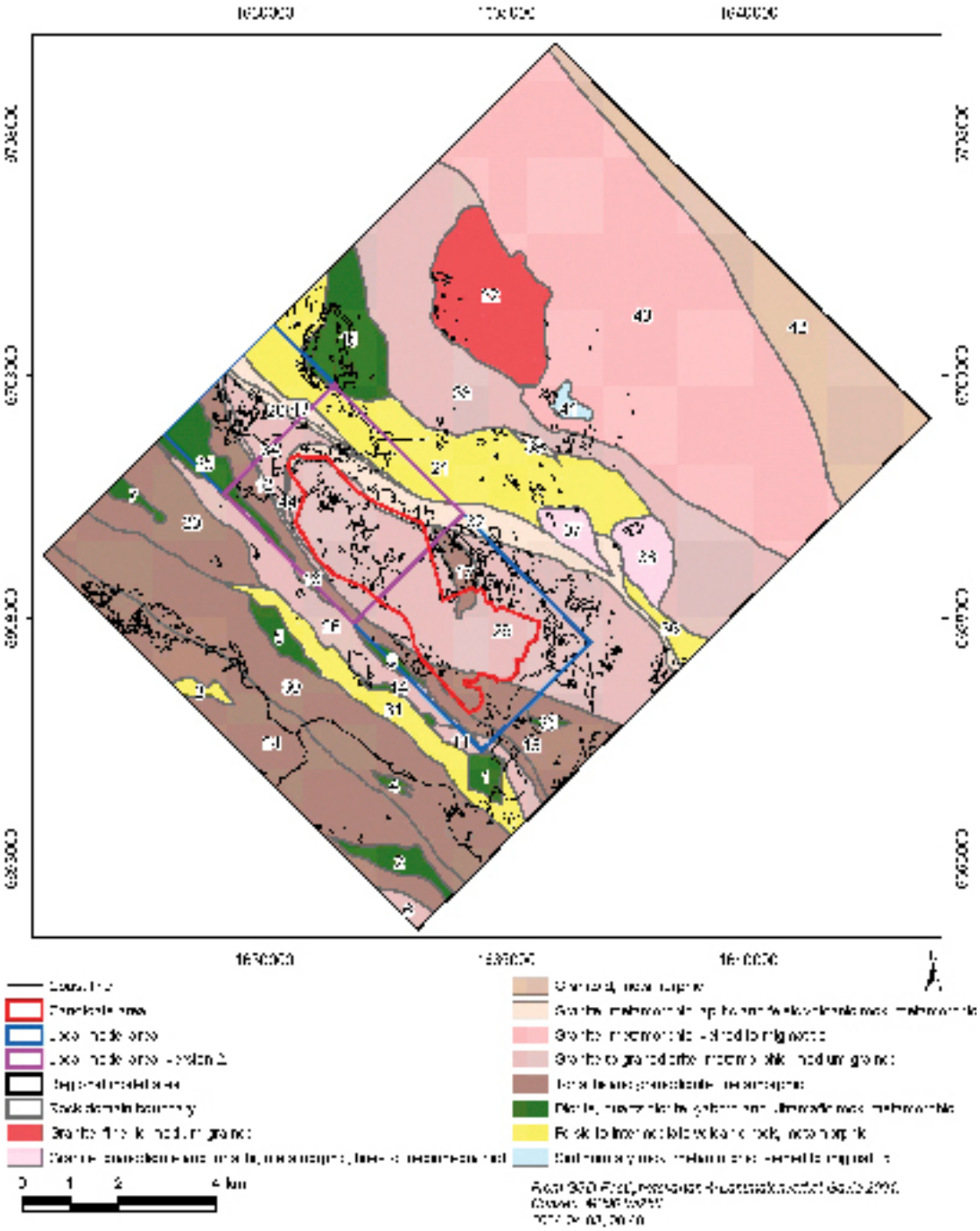

Figure 1-1. *Two-dimensional model at the surface for rock domains inside the regional model area, version 2.1. The colours represent the composition of the dominant rock type in each domain, if necessary, in combination with the grain size of this rock. As in previous models, the degree of homogeneity and the style and degree of ductile deformation (not shown here) have also been used to distinguish domains.*

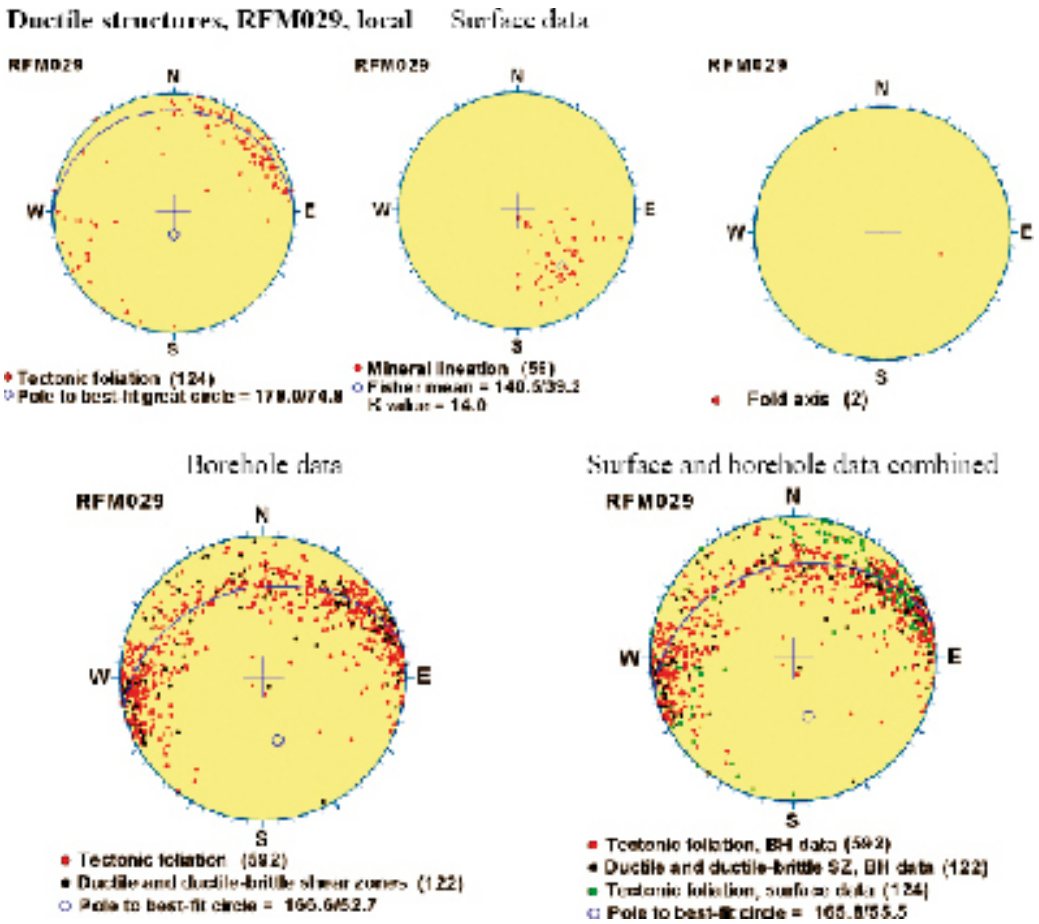

Figure 1-2. *Orientation of ductile structures from the surface and at depth inside rock domain RFM029 in the local model volume. All structures are plotted in the lower hemisphere of an equal-area stereographic plot. Planar structures are plotted as poles.*

(Figure 1-3). A slight increase in the proportion of medium-grained metagranite (101057, 73% and 76%, respectively), which is the dominant rock type, combined with a slight decrease in the proportion of fine- to medium-grained metagranitoid (101051, 78% and 75%, respectively) is apparent. The proportion of amphibolite yields a stable value of 5%, irrespective of which model volume is considered.

1.2 RFM032 and RFM043

Domain RFM032 is dominated by aplitic metagranite and is commonly banded together with amphibolite, pegmatitic granite, medium-grained metagranite and felsic metavolcanic rock. It forms a marginal geological unit that borders rock domain RFM029 (Figure 1-1). In SDM version 1.2, a part of domain RFM032 is folded in a major synform, the hinge of which is situated in the north-westernmost part of the candidate volume (see Figure 5-54 in /SKB 2005/). A second part of this domain extends at the surface, in a north-west strike direction, from close to the entrance to the SFR tunnel system, more or less along the Singö deformation zone (see Figure 5-54 in /SKB 2005/). These two segments have been separated in model version 2.1, in order to take account of their different structural positions relative to the major synform and to the Singö zone. The folded segment, where virtually all data have been acquired, has retained the name RFM032, while the north-western segment has acquired the new term RFM043. This division has no consequences in, for example, repository engineering work.

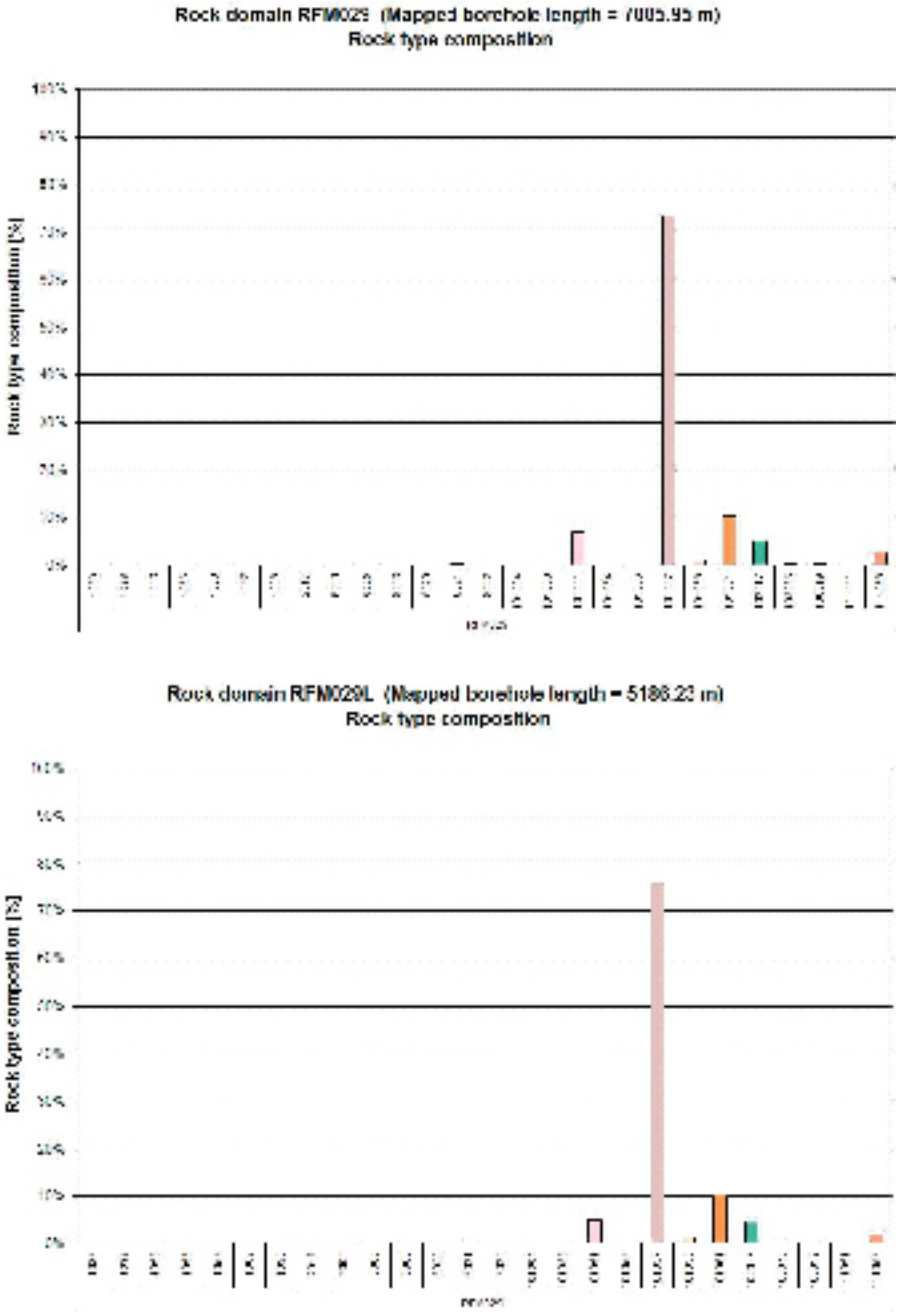

Figure 1-3. *Quantitative estimates of the proportions of different rock types in rock domain RFM029 in the regional (a) and local (b) model volumes. The translation of rock codes to rock type is provided in Appendix 2.1.*

The fine-grained felsic meta-igneous rocks with amphibolite and pegmatitic rock in the lower part of borehole KFM08A have been modelled together with similar rocks at the surface, in the coastal area between SFR and reactors 1 and 2, which were included in rock domain RFM032 in earlier studies /SKB 2004, 2005/. This modelling provides a firm control on the orientation of both the upper boundary of domain RFM032 with RFM029 and the lower boundary with domain RFM034, in the hinge zone of the synform north-west of Asphällsfjärden (Figure 1-1). A plunge of 55° to the SE for this fold structure is inferred from the model. This is in good agreement with the moderate plunge to the SE or SSE that has been inferred from the analysis of planar ductile structures, both from the surface and in boreholes, in domains RFM032 (Figure 1-4) and RFM029 (Figure 1-2), respectively. The new rock domain RFM043 has been modelled in the same manner as the north-western segment of RFM032 in SDM version 1.2.

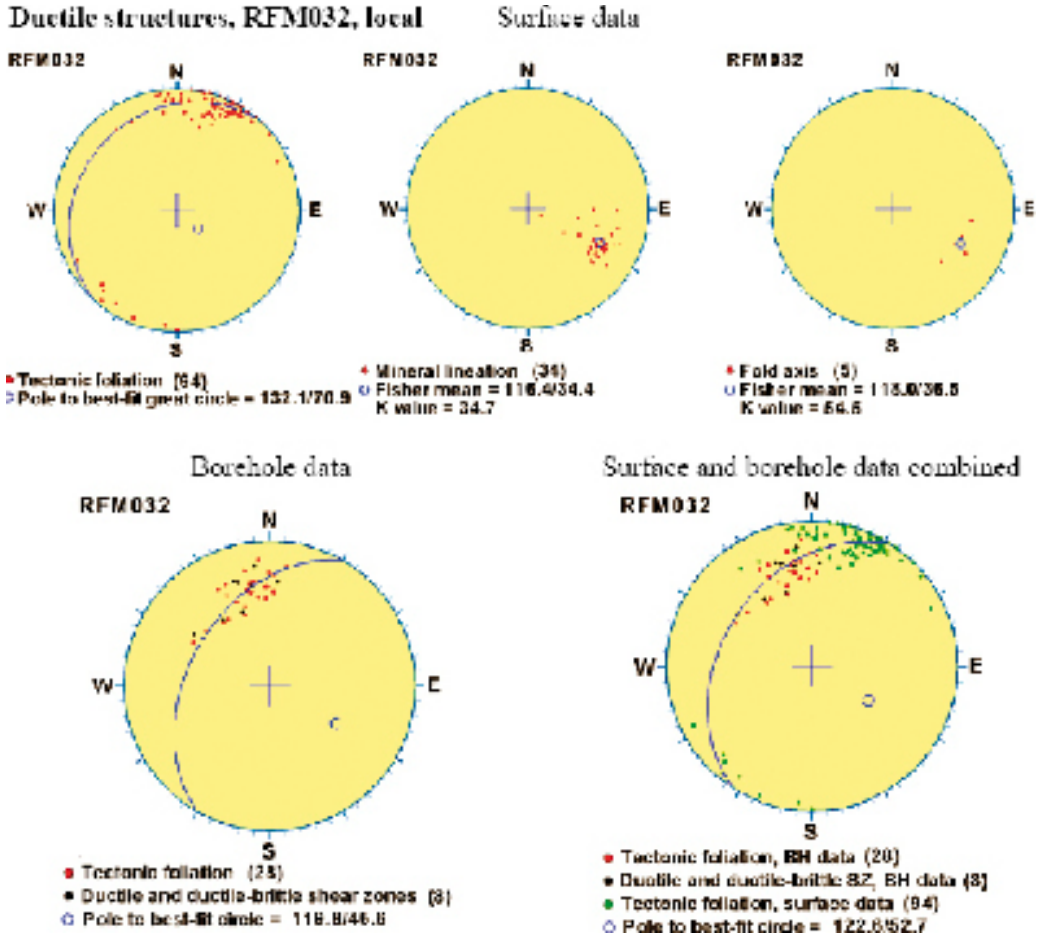

Figure 1-4. *Orientation of ductile structures from the surface and at depth inside rock domain RFM032 in the local model volume. All structures are plotted in the lower hemisphere of an equal-area stereographic plot. Planar structures are plotted as poles.*

1.3 RFM034

Rock domain RFM034 is situated in the north-westernmost part of the tectonic lens at Forsmark and lies outside both the candidate volume and the target area. It was defined in SDM version 1.2 on the basis of outcrop data and consists of medium-grained metagranite with subordinate aplitic metagranite, pegmatitic granite and amphibolite /SKB 2004/. In several aspects, it resembles domain RFM029. Domain RFM034 has been modelled in version 2.1 by infilling the volume that is situated between domains RFM012, RFM020, RFM032 and RFM044 (Figure 1-1). It is inferred that the medium-grained metagranite with subordinate amphibolite, felsic metavolcanic rocks and pegmatitic granite, which is situated structurally beneath domain RFM032 at the base of borehole KFM08A, belongs to domain RFM034.

1.4 RFM044

In the same manner as rock domain RFM032, domain RFM044 forms a marginal geological unit that borders rock domain RFM029 (Figure 1-1). It has been recognised for the first time in model version 2.1 on the basis of the data beneath 657 m depth in borehole KFM07A. Metagranite with subordinate pegmatitic granite and amphibolite at this depth in KFM07A display strong ductile deformation. The planar structures, with a high proportion of ductile and ductile-brittle shear zones, strike NNW and are vertical or sub-vertical (Figure 1-5). On the basis of this observation and in accordance with the methods employed in the extrapolation of surface data in earlier models /SKB 2004, 2005/, domain RFM044 has been modelled with the same orientation as the mesoscopic structures. It is predicted to intersect the surface close to and south of the reactors 1 and 2. The borehole data provide some quantitative estimates of the different rock types in this domain (Figure 1-6).

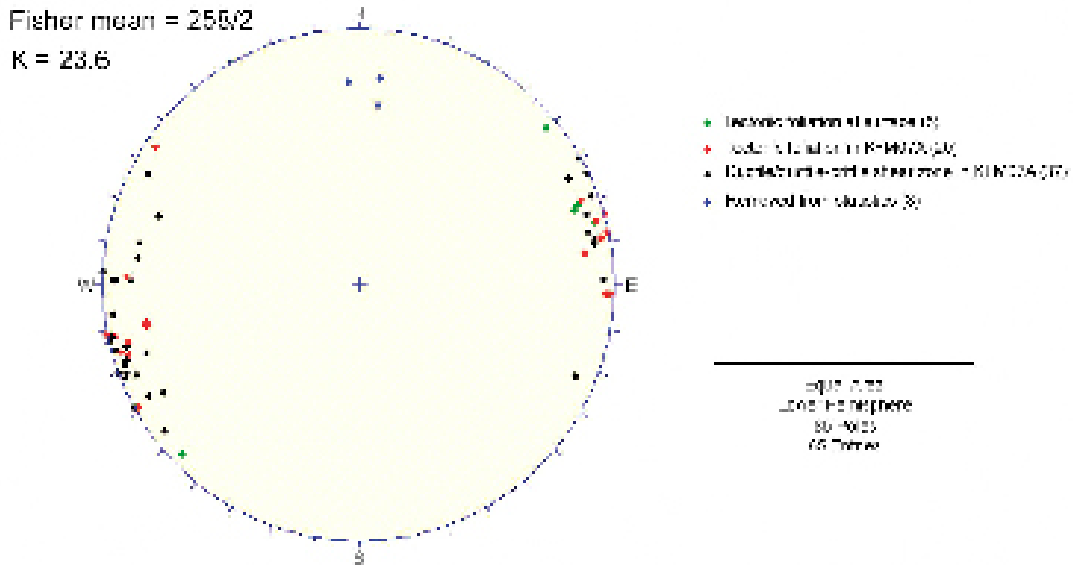

Figure 1-5. *Orientation of planar ductile structures from rock domain RFM044. 60 of the 65 data points are from the inferred occurrence of this domain in the lower part of borehole KFM07A (RU2a, RU2b and RU3). The remaining data points are from surface observations. The structures are plotted as poles in the lower hemisphere of an equal-area stereographic plot.*

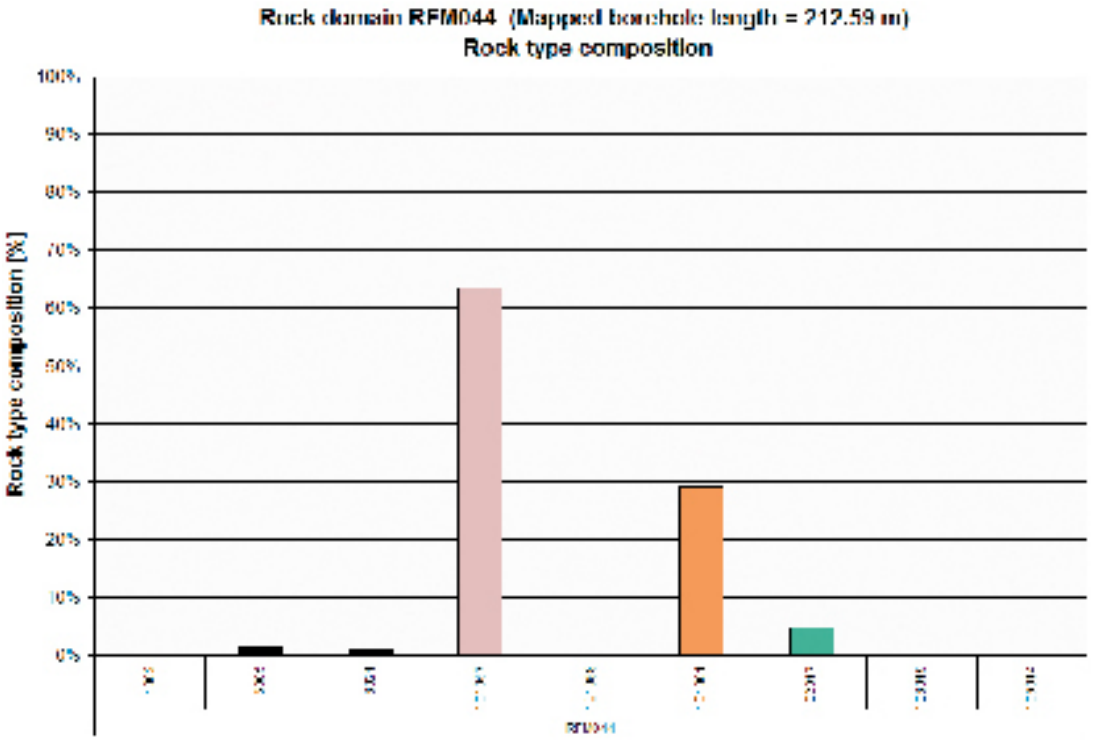

Figure 1-6. *Quantitative estimates of the proportions of different rock types in rock domain RFM044. The values have been obtained from borehole KFM07A inside the local model volume. The translation of rock codes to rock type is provided in Appendix 2.1.*

1.5 RFM045

Rock domain RFM045 has only been modelled inside the local model volume (see Figure 3-2 in the main report) and is based on a combination of borehole and surface data. It is situated inside both the candidate volume and the repository target area, and is of significance for, for example, the repository engineering work. The metamorphosed and altered (bleached) aplitic granite, which dominates borehole KFM06A between 629 and 801 m depth, has been modelled together with a minor unit of aplitic metagranite and subordinate pegmatitic granite that is exposed in the coastal area south of Asphällsfjärden (Bedrock geological map, Forsmark, version 1.2).

In accordance with the principles adopted for isolated bodies of ultramafic, mafic and intermediate rocks at the surface in earlier models /SKB 2004, 2005/, domain RFM045 has been modelled as a rod that plunges to the south-east, parallel to the mineral stretching lineation at the Forsmark site. Mineral lineation data are unfortunately lacking in this domain. However, the orientation of the rod structure is similar to the orientation of the mineral stretching lineation in rock domain RFM029 (Figure 1-2). The domain is modelled to extend to the base of the local model volume. The borehole data from KFM06A provide some quantitative estimates of the different rock types in domain RFM045 (Figure 1-7). Whole-rock analytical data /Petersson et al. 2005/ indicate that the alteration in these rocks leads to a small increase in the quartz content and a marked decrease in the content of K-feldspar relative to the equivalent unaltered rocks.

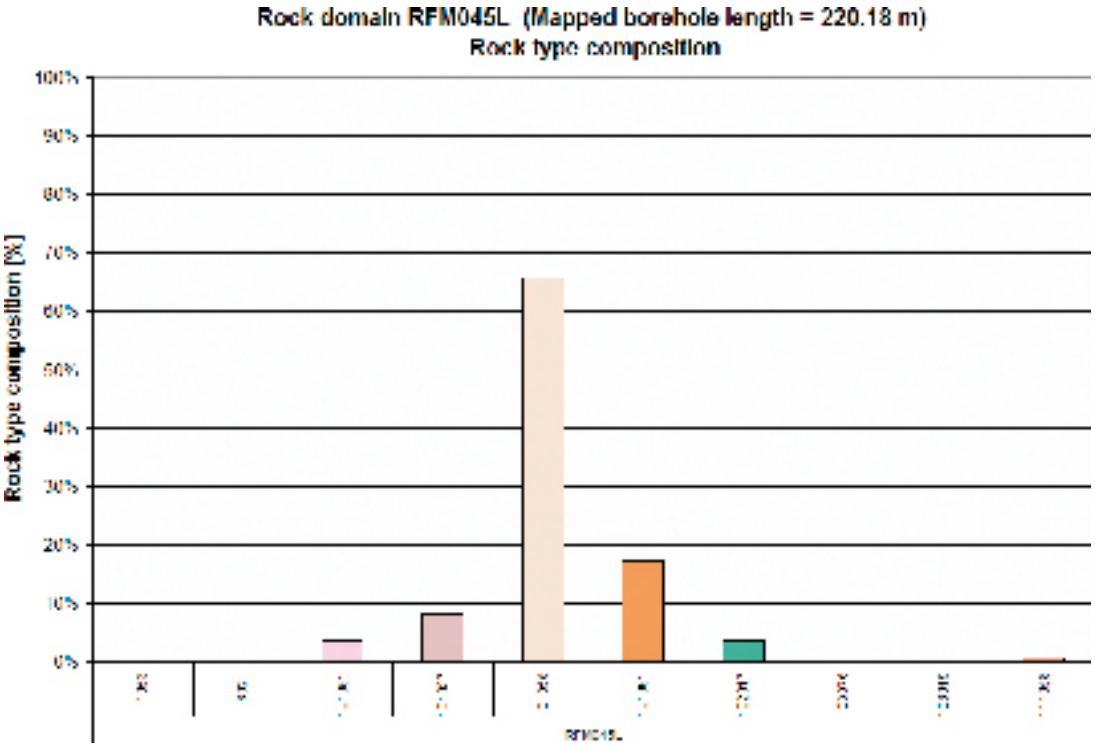

Figure 1-7. *Quantitative estimates of the proportions of different rock types in rock domain RFM045 inside the local model volume. The translation of rock codes to rock type is provided in Appendix 2.1.*

1.6 RFM046

Rock domain RFM046 has only been modelled inside the local model volume (see Figure 3-2 in the main report) and is based solely on limited surface data. This domain is situated outside both the candidate volume and target area, and has no influence on the repository engineering work. In accordance with the principles adopted for isolated bodies of ultramafic, mafic and intermediate rocks at the surface in earlier models /SKB 2004, 2005/, domain RFM046 has been modelled as a rod that plunges to the south-east, parallel to the mineral stretching lineation at the Forsmark site.

2 Deformation zones

Apart from the use of available borehole data, the version 2.1 modelling of deformation zones has included the use of magnetic lineaments, the identification of reflection seismic corridors to constrain the length of zones based on seismic reflection data, and an assessment of the relationship between length and thickness of deformation zones. Each of these aspects of the modelling work is described below. The modelling procedure applied to each deformation zone in the local model, as well as the confidence of occurrence and geological properties of each zone are also presented below.

2.1 Magnetic lineaments

As pointed out and argued for in the main text of this report (Section 3.1.2), magnetic rather than linked lineaments have been used at the surface in the modelling work. Each lineament is identified using the identification code MFMxxxx(xx). The identification and character of the magnetic lineaments are presented in a PM in Appendix 2.2 and the position and properties of these lineaments have been delivered to SKB's GIS database. Lineaments based on depressions in the bedrock disconformity beneath the Quaternary cover /Isaksson and Keisu 2005/ have also been utilised in especially the areas where the magnetic data is of poorer quality, for example in the vicinity of the nuclear power plants /SKB 2005/.

The magnetic lineament MFM0137B0 in the regional model area has not been modelled as a separate deformation zone, since it possibly represents the surface expression of zone ZFMNE0871 (zone H2 at SFR). This zone has been modelled with the help of tunnel and borehole data from SFR (see also /SKB 2005/). The magnetic lineament MFM0126 in the local model area has not been modelled, since the results from the excavation work along AFM001244 (Section 2.4.2) indicate that this lineament does not represent a deformation zone. Since the magnetic lineaments MFM1064 and MFM1035 are both less than 200 m in length, modelling work was not carried out on these two structures. All other magnetic lineaments have been incorporated in the version 2.1 modelling work for deformation zones.

2.2 Reflection seismic corridors and truncation of gently dipping deformation zones

In order to obtain a more confident basis for the truncation of gently dipping deformation zones, an attempt has been made to identify sub-vertical corridors that define the along-strike and down-dip extent of the seismic reflectors identified during both the stage 1 /Juhlin et al. 2002, Juhlin and Bergman 2004/ and stage 2 /Juhlin and Palm 2005/ activities. This procedure is motivated, since many of these reflectors correspond to gently dipping deformation zones /SKB 2005/. The results of this work are presented in a PM in Appendix 2.3.

The gently dipping C reflectors are curved /Juhlin et al. 2002/. They also extend over most of the Forsmark area (Figure 1 in Appendix 2.3) and are only limited to the south-west against the Forsmark deformation zone (ZFMNW0004). The different character and spatial behaviour of these reflectors relative to, for example, the A and B reflectors at the site suggest that they are related to a lithological velocity contrast, possibly flat-lying basic sills. For this reason, the zones inferred to be related to these reflectors in SDM version 1.2 /SKB 2005/ have been removed from the deformation zone model. This modification has no implications for the relationships inside the repository target area.

Three, possible, reflection seismic corridors have been identified (Figure 3 in Appendix 2.3). Two of these corridors trend WNW. They correspond to the Forsmark deformation zone (ZFMNW0004) and to a group of inferred, vertical deformation zones (e.g. ZFMNW0023, ZFMNW0123, ZFMNW0017), which partly lie within the south-eastern part of the candidate area and partly fringe and lie outside the candidate area to the north-west. A third corridor trends NE and corresponds to an inferred vertical zone located between the nuclear power plants 1–2 and 3 (ZFMNE0810). All these structures have been used in the present model to truncate gently dipping zones.

The important reflector A2 can not be observed along profile 3 and appears to die out south-east of drill site 2 /Juhlin and Palm 2005/. A possible candidate for the truncation of the corresponding gently dipping deformation zone (ZFMNE00A2), which corresponds to this reflector, is the inferred, steeply dipping zone ZFMNE0065 that transects the candidate area between drill sites 2 and 3. There remains some uncertainty concerning whether or not reflector A0–A1 transects the Singö deformation zone (ZFMNW0001), as inferred in Figure 2 in Appendix 2.3. Furthermore, there are, at present, no data that allow other A and B reflectors to transect the Singö zone. For these reasons, the Singö deformation zone is also considered to truncate gently dipping deformation zones to the north-east of the candidate area.

In summary, the gently dipping deformation zones that are related to seismic reflectors are inferred to be enclosed within different bedrock blocks. These blocks are bordered by vertical or steeply dipping zones that belong to the WNW and NE sets (see Section 3.1.2). The intensity of gently dipping deformation zones varies between the different blocks, with a strong intensity in the south-eastern part of the candidate volume.

2.3 Length-thickness correlation

Using the geological data in SDM version 1.2, /Follin et al. 2005/ tested a possible correlation between the ground surface length and the thickness of deterministic deformation zones. The new data in model version 2.1 have been used with an aim to refine the possible correlation and to estimate, with better confidence relative to SDM version 1.2 /SKB 2005/, the thickness of deformation zones where borehole and tunnel data are lacking. In the earlier modelling work, the thickness of these zones was estimated simply by a crude comparison with high confidence, vertical and steeply zones of similar length.

Since the length of gently dipping zones is highly uncertain, only vertical and steeply dipping deformation zones have been included in the present study. A prerequisite for inclusion of a zone in the analysis is that estimates of both ground surface length and thickness are available for the zone. The ground surface length of virtually all these structures corresponds closely to the length of the corresponding magnetic lineament. Thickness is derived from borehole and tunnel intersections. There are two major limitations with this type of analysis. Firstly, it is not known where, along a deformation zone, the ground surface intersects the zone and, thus, how representative the ground surface length is for the length of the zone. Secondly, the estimate of the thickness of virtually all the zones at Forsmark is based on a single borehole intersection. For these two reasons, there is considerable uncertainty in the significance of the correlation plot.

The results of the analysis are shown in Figure 2-1. The version 2.1 data indicate a poor correlation between the ground surface length and the thickness of deformation zones. For example, there appears to be a large variation in thickness for a given zone length. For this reason, it is recommended that extreme care is applied when using such a correlation. Notwithstanding this restriction, the thickness of deformation zones where only ground surface length is known has been estimated from Figure 2-1 in the present modelling work. The property table for a deformation zone indicates when this procedure has been followed.

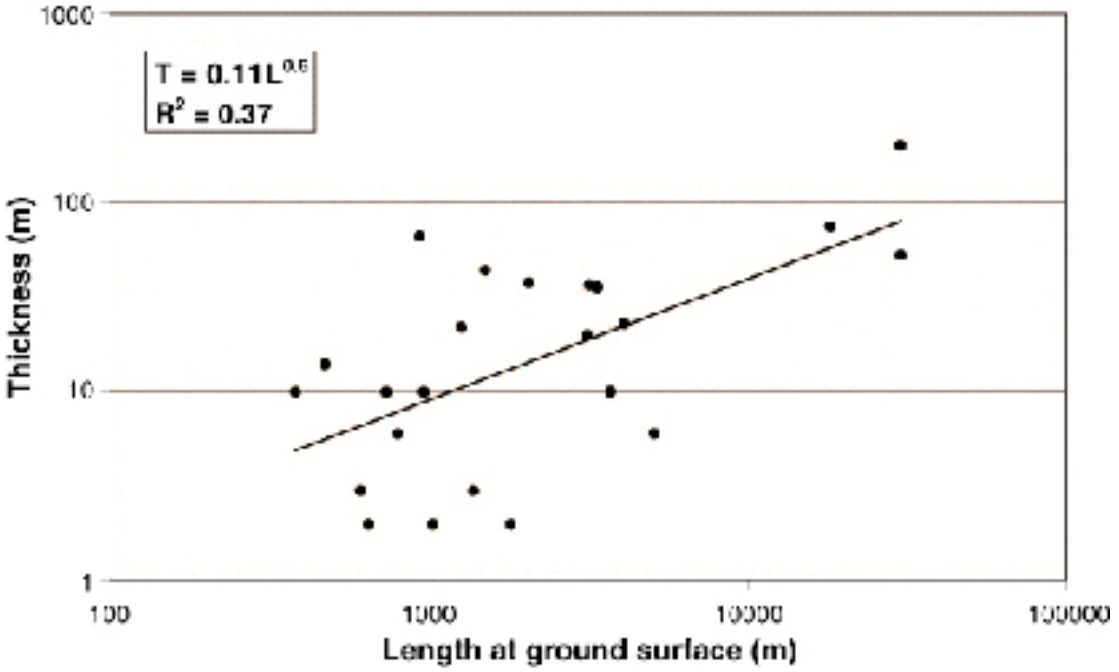

Figure 2-1. *Power law correlation diagram between ground surface length and thickness of deterministic deformation zones based on version 2.1 data.*

2.4 Modelling procedure, confidence of occurrence and geological properties of deformation zones in the local model volume

The details of the modelling procedure carried out for each deformation zone in the local model volume, the confidence level for the occurrence of each zone, and the geological properties of each zone are presented in Appendix 2.4. A high confidence of occurrence is applied to all zones that have been confirmed directly by geological data from a borehole or tunnel or from the surface. In general, indirect data (e.g. a seismic reflector, a magnetic lineament) are also present. It is important to keep in mind that the majority of high confidence zones at Forsmark are based on a single borehole intersection along a cored borehole.

A medium confidence zone lacks direct confirmatory data. The zone has been identified solely by a seismic reflector or with the help of a long (> 3,000 m), continuous magnetic lineament. A low confidence of occurrence is applied to the zones that have been identified solely from a short (< 3,000 m) magnetic lineament. Once again, direct confirmatory data are lacking.

Estimates of the span of numerical data as well as a judgement of the level of confidence for the estimation of each geological property (for example, position, orientation, thickness, length) are provided in each table. The character of the zone (ductile, brittle, composite), the type of bedrock alteration along the zone, and the results of the analysis of fracture orientation, fracture frequency and fracture mineral filling or coating are also presented in the property table for each zone. The orientation of a deformation zone and the mean values of fracture sets are given in the form of strike and dip using the right-hand-rule. For example, 108/75 corresponds to a strike and dip of N72°W/75°SW. The geometry, confidence level of occurrence and geological properties of the deformation zones in both the version 2.1 local and regional models are archived in SKB's database for modelling activities.

3 References

Axelsson C-L, Hansen L M, 1997. Update of structural models at SFR nuclear waste repository, Forsmark, Sweden. SKB R-98-05, Svensk Kärnbränslehantering AB.

Carlsson A, Christiansson R, 1987. Geology and tectonics at Forsmark, Sweden. SKB SFR-87-04, Svensk Kärnbränslehantering AB.

Follin S, Stigsson M, Svensson U, 2005. Regional hydrogeological simulations for Forsmark – numerical modelling using DarcyTools. Preliminary site description Forsmark area – version 1.2. SKB R-05-60, Svensk Kärnbränslehantering AB.

Holmén J G, Stigsson M, 2001. Modelling of future hydrogeological conditions at SFR. SKB R-01-02, Svensk Kärnbränslehantering AB.

Isaksson H, Keisu M, 2005. Interpretation of airborne geophysics and integration with topography. Stage 2 (2002–2004). SKB P-04-282, Svensk Kärnbränslehantering AB.

Juhlin C, Bergman B, Palm H, 2002. Reflection seismic studies in the Forsmark area – stage 1. SKB R-02-43, Svensk Kärnbränslehantering AB.

Juhlin C, Bergman B, 2004. Reflection seisimics in the Forsmark area. Updated interpretation of Stage 1 (previous report R-02-43). Updated estimate of bedrock topography (previous report P-04-99). SKB P-04-158, Svensk Kärnbränslehantering AB.

Juhlin C, Palm H, 2005. Reflection seismic studies in the Forsmark area, 2004: Stage 2. Forsmark site investigation. SKB R-05-42, Svensk Kärnbränslehantering AB.

Petersson J, Berglund J, Danielsson P, Skogsmo G, 2005. Petrographic and geochemical characteristics of bedrock samples from boreholes KFM04A–06A, and a whitened alteration rock. Forsmark site investigation. SKB P-05-156, Svensk Kärnbränslehantering AB.

SKB, 2004. Preliminary site description. Forsmark area – version 1.1. SKB R-04-15, Svensk Kärnbränslehantering AB.

SKB, 2005. Preliminary site description. Forsmark area – version 1.2. SKB R-05-18, Svensk Kärnbränslehantering AB.

Stephens M B, Lundqvist S, Bergman T, Andersson J, Ekström M, 2003. Rock types, their petrographic and geochemical characteristics, and a structural analysis of the bedrock based on stage 1 (2002) surface data. SKB P-03-75, Svensk Kärnbränslehantering AB.

Appendix 2.1

Translation of rock codes to rock type

The table below translates the various rock codes used at Forsmark to rock names. The different groups (A to D), which are essentially a stratigraphic classification of the rocks, are described in /Stephens et al. 2003/ and are summarised in Table 2-2 in the main text in this report. The oldest rocks of supracrustal character are included in Group A. The rocks in Groups B and C belong to different generations of younger, calc-alkaline intrusive rocks. The youngest intrusive rocks are included in Group D.

Rock code	Rock composition	Complementary characteristics		
Rock codes and rock names adopted by SKB				
111058	Granite		Fine- to medium-grained	Group D
101061	Pegmatite, pegmatitic granite			Group D
101051	Granite, granodiorite and tonalite	Metamorphic	Fine- to medium-grained	Group C
111051	Granitoid	Metamorphic		Group B
101058	Granite	Metamorphic	Aplitic	Group B
111057	Granite to granodiorite	Metamorphic, veined to migmatitic		Group B

Rock code	Rock composition	Complementary characteristics		
Rock codes and rock names adopted by SKB				
101057	Granite to granodiorite	Metamorphic	Medium-grained	Group B
101056	Granodiorite	Metamorphic		Group B
101054	Tonalite to granodiorite	Metamorphic		Group B
101033	Diorite, quartz diorite, gabbro	Metamorphic		Group B
102017	Amphibolite			Group B
101004	Ultramafic rock	Metamorphic		Group B
108019	Calc-silicate rock (skarn)			Group A
109014	Magnetite mineralisation associated with calc-silicate rock (skarn)			Group A
109010	Sulphide mineralisation			Group A
103076	Felsic to intermediate volcanic rock	Metamorphic		Group A
106001	Sedimentary rock	Metamorphic, veined to migmatitic		Group A
106000	Sedimentary rock	Metamorphic		Group A

Rock code	Rock composition	Complementary characteristics		
Additional rock codes and rock names of strongly subordinate character				
1051	Granitoid	Metamorphic	Uncertain classification 101051, 111051	Group B or Group C
1053	Tonalite	Metamorphic	Uncertain classification 101051 or 101054	Group B or Group C
1054	Tonalite to granodiorite	Metamorphic	Uncertain classification 101051 or 101054	Group B or Group C
1056	Granodiorite	Metamorphic	Uncertain classification 101051 or 101056	Group B or Group C
1057	Granite to granodiorite	Metamorphic	Uncertain classification 101051 or 101057	Group B or Group C
1058_120	Granite	Metamorphic	Uncertain classification 101057 or 101058	Group B
1058	Granite		Uncertain classification 101051, 101057, 101058 or 111058	Group B, Group C or Group D
1059	Leucocratic granite		Uncertain classification 101058 or 111058	Group B or Group D
1062	Aplite		Uncertain classification 101058 or 111058	Group B or Group D
111058_ 101051	Granite		Uncertain classification 101051 or 111058	Group C or Group D
5103	Felsic rock	Metamorphic	Uncertain classification 103076 or 101058	Group A or Group B
6053	Quartz-hematite rock			
8003	Cataclastic rock			
8004	Mylonite			
8011	Gneiss			
8020	Hydrothermal vein or segregation			
8021	Quartz-rich hydrothermal vein or segregation			
8023	Hydrothermally altered rock			

Appendix 2.2

PM: Identification and character of magnetic lineaments

This section presents the methodology used to determine lineaments based only on magnetic characteristics. The purpose of the work is to delineate and compile linear magnetic features that are most probably caused by brittle and ductile deformation in the bedrock. The work has comprised a compilation of previous work presented in /1, 2/. The basis for the work has been linked, co-ordinated and magnetic lineaments from /1/. Furthermore, basic data including processed airborne

magnetics (NGU, SGU) from /1/ have been used. Lineaments identified by Korhonen et al. /3/ have not been included in this compilation. The identification has been carried out by visually comparing the previous lineament sets and the magnetic data. This has resulted in a compilation of new lineament sets based solely on magnetic features.

In most cases, the magnetic lineaments follow previous linked lineaments and only minor adjustments of the position have been necessary. Due to this fact, a magnetic lineament has been named with the same suffix as for the previous linked lineament and a new prefix MFM ("Magnetic – Forsmark") has been introduced, i.e. "MFM0015" mainly originating from "XFM0015A0". However, the decision to combine lineaments has been different from the previous work where other methods were also considered (e.g. topography). This means that a new MFM lineament can be composed of several different XFM lineaments and, in this case, the most prominent lineament has provided the name. In the local model area, previous work in /2/ has provided a segment numbering for each individual co-ordinated lineament segment, which, in some cases, has been used in this work (see Figure 2 and Table 2). In the local model area, a few new, longer magnetic lineaments have been identified. They originate from small magnetic lineament segments and most of them are characterized as magnetic minima connections with rather high uncertainty.

The magnetic lineament tables follow the same structure as the previous linked lineament tables /1/. In cases where the lineament adjustment has been minor, the calculated properties for the linked lineament have been maintained (see Tables 1 and 2). In cases where the adjustments have been more comprehensive, foundations for these estimates are lacking and hence, the properties have been erased. The properties Method, Character, Process, Platform, Width, Date and Signature, are not presented in Tables 1 and 2, since they only describe more general information. The final stage of the compilation has been to recalculate the length and direction of each lineament.

The magnetic linked lineaments are divided into two major groups:

MFM_3 km, with magnetic lineaments longer than 3,000 m and covering the regional model area (Figure 1 and Table 1). A total of 43 lineaments have been complied and characterized.

MFM_0-3 km equal to or shorter than 3,000 m, and covering the local model area (Figure 2 and Table 2). A total of 51 lineaments have been complied and characterized of which 7 lineaments are mostly new.

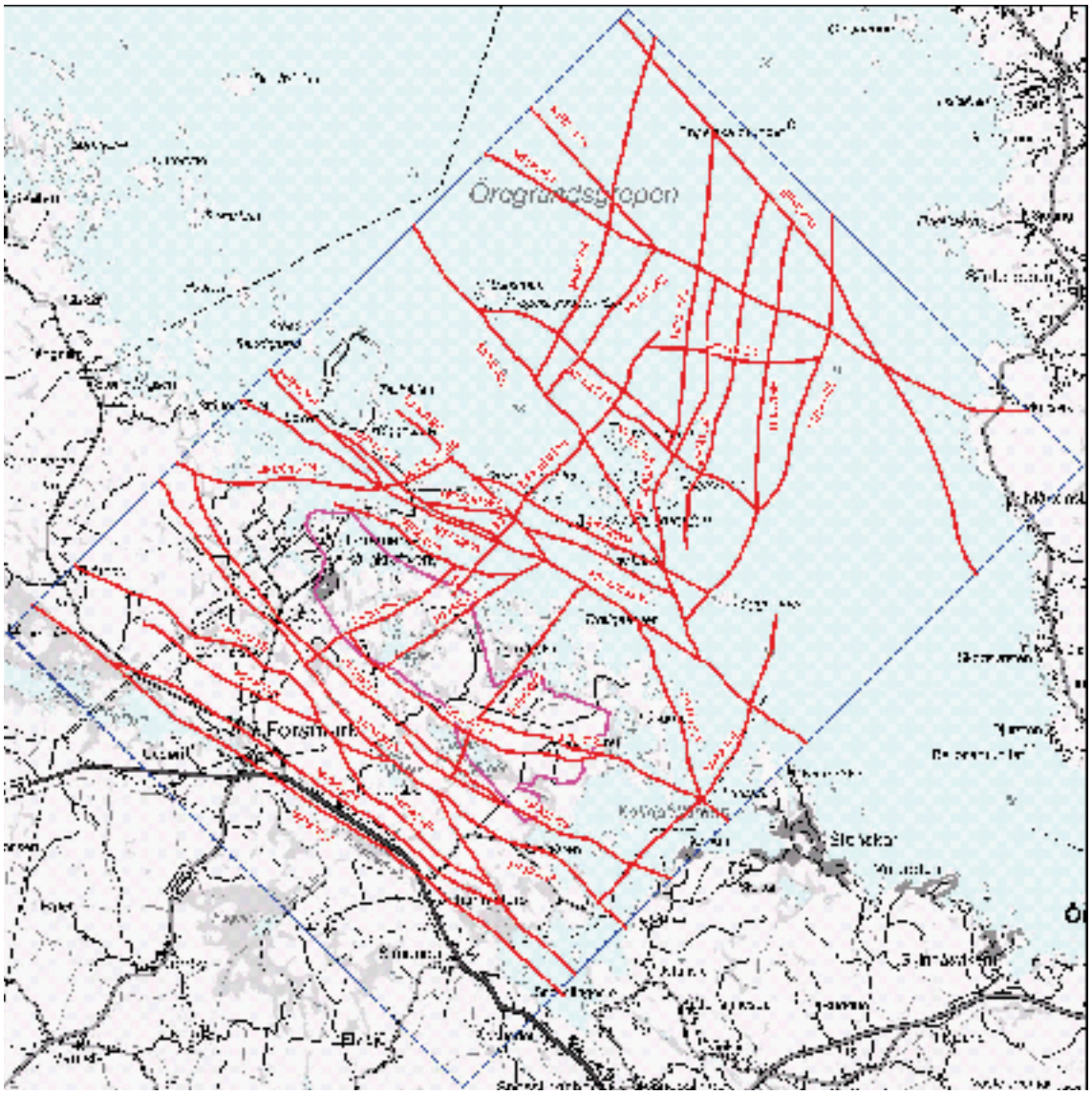

Figure 1. *Magnetic linked lineaments, longer than 3,000 m, in the regional model area. Forsmark candidate area shown as magenta, solid line.*

Table 1. Magnetic linked lineaments, longer than 3,000 m, in the regional model area.

ID_T	ORIGIN_T	CLASS_T	WEIGHT_N	UN-CERT_T	COMMENT_T	SCALE_T	PRE-CIS_N	COUNT_N	COND_N	MAGN_N	TOPO_N	TOPOG_N	TOPOR_N	PROP_N	LENGTH_N	DIRECT_N
MFM0014	XFM0014A0	Regional			modified 14 with magnetic priority	10000	20			1.00					11,302	306.3
MFM0015	XFM0015A0	Regional	3.90	1.20	baty in Kallrigafjarden	10000	20	20	0.40	1.00	0.70	0.70	0.00	2.10	11,191	319.9
MFM0016	XFM016A0 + part of 15A2	Local major			16 extended with N part of 15A2	10000	40			1.00					4,118	305.2
MFM0017	XFM0017A0 + 18A0	Local major			shortened 17 modified and extended with 18	20000	20			1.00					7,925	317.2
MFM0019	XFM019A0 + 21A0	Local major	1.89	2.33	19A0 extended with 21A0	10000	20	7	0.03	1.00	0.17	0.17	0.00	1.22	5,269	297.6
MFM0023	XFM0023A0	Local major	3.27	1.77		10000	20	13	0.46	1.00	0.58	0.58	0.08	2.04	4,690	292.0
MFM0024	XFM0024A0	Local major	1.50	2.70		10000	20	10	0.10	1.00	0.20	0.20	0.00	1.30	7,985	301.7
MFM0029	XFM0029A0	Local major	2.60	2.20		10000	20	7	0.20	1.00	0.60	0.60	0.00	1.80	3,798	313.3
MFM0035	XFM0035A0	Local major	1.20	2.90		10000	20	5	0.00	1.00	0.00	0.00	0.00	1.10	3,502	299.6
MFM0036	XFM0036A0 + 32A0+34A0	Local major			36 extented with 32 and 34	10000	20			1.00					6,641	301.6
MFM0060	XFM0060A0	Local major				10000	20			1.00			0.00		3,116	57.1
MFM0062	XFM0062A0	Local major	3.59	1.62		10000	20	7	0.35	0.94	0.85	0.85	0.06	2.15	3,372	56.2
MFM0065	XFM0065A0	Local major	4.35	1.11		10000	20	5	0.68	1.00	0.79	0.79	0.00	2.46	4,086	35.1
MFM0123	XFM0123A0 + 136A0	Local major			123 extened towards NW with 136	10000	20			1.00					5,067	296.1
MFM0137A0	XFM0137A0 + 46A0	Local major			137A0 much shorter and partly exchanged with 46A0	10000	20			1.00					3,608	276.8
MFM0137B0	XFM0137B0	Local major	2.58	1.97	Link to Singö zone XFM0137 segment 10	20000	20	4	0.00	1.00	0.55	0.24	0.55	1.55	1,305	67.3
MFM0803	XFM0803A0	Regional	3.60	1.28	Singö-line	20000	20	17	0.00	1.00	0.88	0.83	0.77	1.88	11,435	301.2
MFM0804	XFM0804A0	Local major	3.71	1.29	rock_surface also from refraction seism	20000	20	6	0.00	1.00	1.00	0.96	0.53	2.00	2,806	316.4
MFM0805	XFM0805A0	Local major	3.54	1.46		20000	20	6	0.00	1.00	1.00	1.00	0.38	2.00	3,701	314.8
MFM0806	XFM0806A0	Local major	3.14	1.67	irregular shape	20000	20	15	0.00	0.94	0.87	0.87	0.48	1.81	8,996	326.6
MFM0808A0	XFM0808A0	Local major			Split of 808A0	20000	20		0.00	1.00					4,105	38.3
MFM0808B0	XFM0808B0	Local major			Split of 808A0	20000	20		0.00	1.00					451	45.8
MFM0808C0	XFM0808C0	Local major			Split of 808A0	20000	20		0.00	1.00					1,165	40.9
MFM0809	XFM0809A0	Local major	3.16	1.00	magnetic 10 m grid	20000	20	5	0.00	1.00	0.16	0.16	0.00	1.16	3,428	291.3

ID_T	ORIGIN_T	CLASS_T	WEIGHT_N	UN-CERT_T	COMMENT_T	SCALE_T	PRE-CIS_N	COUNT_N	COND_N	MAGN_N	TOPO_N	TOPOG_N	TOPOR_N	PROP_N	LENGTH_N	DIRECT_N
MFM0823	XFM0823A0 + 824A0	Local major			823 extended towards SSE and 824 added in NNW	20000	20	5	0.00	1.00					3,265	340.5
MFM0828	XFM0828A0	Local major	3.48	1.24	propagation uncertainty in rock_surface	20000	20	7	0.00	0.97	0.75	0.75	0.19	1.72	5,949	31.9
MFM0835A0	XFM0835A0	Local major	2.41	2.00	new XFM0835B0 = XFM1033A0	20000	20	4	0.00	1.00	0.41	0.41	0.34	1.41	2,813	293.3
MFM0835B0	XFM1033A0	Local major			change of Identity (new extension of MFM0835A0)	20000	20			1.00					1,534	278.5
MFM0836	XFM0836A0	Local major	2.28	2.00		20000	20	8	0.00	0.92	0.36	0.36	0.31	1.28	4,508	296.0
MFM0842	XFM0842A0	Local major				20000	20	3	0.00	1.00	1.00	1.00	0.00	2.00	3,171	37.0
MFM0851	XFM0851A0	Local major	2.81	1.90	Magnetic edge in NW segment	50000	50	3	0.00	0.71	1.00	1.00	0.00	1.71	3,112	306.6
MFM0853	XFM0853A0	Regional	2.30	1.80		50000	50	6	0.00	1.00	0.10	0.10	0.00	1.10	10,392	295.3
MFM0854	XFM0854A0	Regional	3.00	1.00		50000	50	2	0.00	1.00	0.00	0.00	0.00	1.00	11,389	327.3
MFM0860	XFM0860A0	Local major	2.87	1.51	slightly shorter in SSW	20000	20	7	0.00	0.94	0.43	0.43	0.07	1.38	6,262	19.5
MFM0929	XFM0929A0	Local major	1.65	2.52		20000	20	5	0.00	0.81	0.35	0.35	0.13	1.17	5,220	10.4
MFM0974	XFM0974A0	Local major	1.92	2.16	inphase 880 Hz anomaly	20000	30	3	0.08	0.84	0.16	0.16	0.00	1.08	4,099	302.4
MFM1127	XFM1127A0	Local major	2.94	1.23	Poor data coverage	20000	20	4	0.00	1.00	0.18	0.18	0.00	1.18	3,652	303.2
MFM1132	XFM1132A0	Local major	2.00	2.00	XFM0859A0	50000	50	2	0.00	1.00	0.00	0.00	0.00	1.00	5,484	8.4
MFM1133	XFM1133A0 + 858A0	Local major			1133 shortened in SSW and exchanged/extended with 858	50000	50			1.00					6,288	12.7
MFM1134	XFM1134A0 + 850A0	Local major			1134 extended towards SSW with 850	50000	50			1.00					7,287	15.1
MFM1135	XFM1135A0	Local major	1.66	2.34		50000	50	4	0.00	1.00	0.00	0.00	0.00	1.00	5,376	14.2
MFM1156	XFM1156A0	Local major	1.00	3.00		50000	50	3	0.00	1.00	0.00	0.00	0.00	1.00	3,025	273.5
MFM1173	XFM1173A0	Local major	2.00	2.00		50000	50	1	0.00	1.00	0.00	0.00	0.00	1.00	3,226	317.9

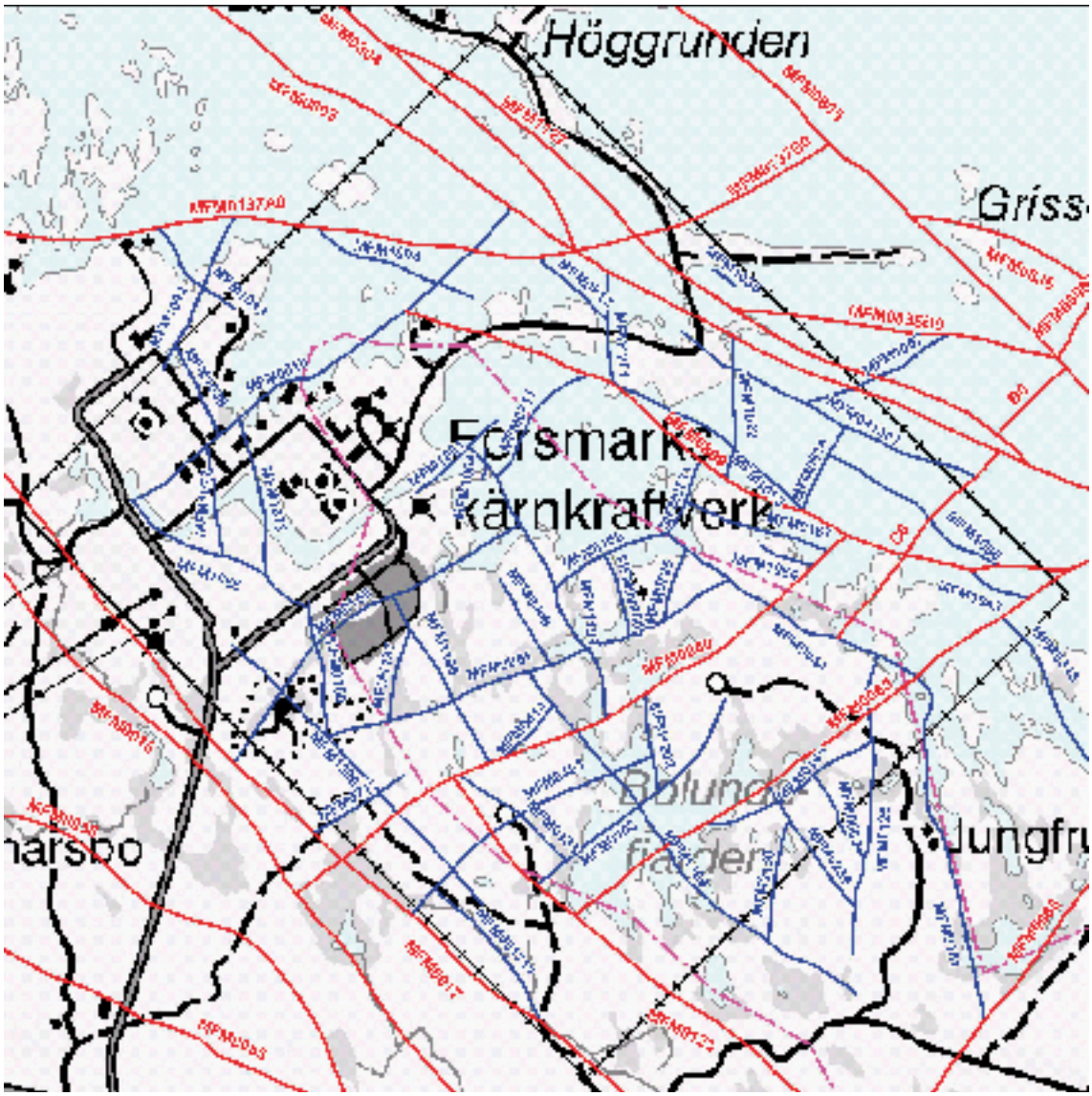

Figure 2. *Magnetic linked lineaments, in the local model area (black, fence line). Lineaments longer than 3,000 m as red, solid lines and lineaments equal to or shorter than 3,000 m as blue, solid lines. Forsmark candidate area shown as magenta, dot-dashed line.*

Table 2. Magnetic linked lineaments, equal to or shorter than 3,000 m, in the local model area.

ID_T	ORIGIN_T	CLASS_T	WEIGHT_N	UNCERT_T	COMMENT_T	SCALE_T	PRECIS_N	COUNT_N	COND_N	MAGN_N	TOPO_N	TOPOG_N	TOPOR_N	PROP_N	LENGTH_N	DIRECT_N
MFM001711	XFM001711	Local minor	5.00	1.00	part of previous XFM0017A0	20000	30	1	1.00	1.00	1.00	1.00	0.00	3.00	815.62	321.30
MFM0044	XFM004401	Local major			segment 4407-4408 cut out	10000	30	6		1.00	1.00	1.00	0.00		1,482.59	301.40
MFM0061	XFM006101	Local major	3.79	1.61	4401 extended 262 m towards SW	10000	30	6	0.61	1.00	0.87	0.87	0.00	2.30	2,039.00	68.60
MFM009805	XFM0098A0 segment 05	Local minor	4.00	1.00	segm 05 extended towards NNW to MFM0168	10000	30	2	0.00	1.00	1.00	1.00	0.00	2.00	401.13	343.40
MFM0100	XFM010003	Local minor			30 m, 3,000–4,000 m/s, P20	10000	30	2	0.00	1.00	1.00	1.00	0.00	2.00	648.78	352.10
MFM0101	XFM010101	Local major	4.20	1.50		10000	40	4	0.90	1.00	0.80	0.80	0.00	2.60	1,580.38	351.20
MFM0103	XFM010302, 010303, 010304	Local major				10000	30	3		1.00					1,262.62	45.60
MFM0126	XFM012601	Local major		1.70	extended towards north to MFM0044	10000	30	5	0.00	1.00	0.30	0.30	0.00	1.30	1,431.02	4.80
MFM0130	XFM0130A0	Local minor		2.10	shortened towards N, extended towards S	10000	30	3	0.60	0.60	0.90	0.90	0.00	2.20	574.54	10.40
MFM0159	XFM015901	Local major			central section in Barackbyn less certain,	10000	30	6		1.00					1,794.99	50.10
MFM0167	XFM0167A0	Local minor	2.40	2.00		10000	30	2	0.00	1.00	0.40	0.40	0.00	1.40	714.57	288.70
MFM0168	XFM0168A0	Local minor	3.00	2.00	baty in the Sea area, part shoreline	10000	30	1	0.00	1.00	1.00	1.00	0.00	2.00	592.23	63.90
MFM0169	XFM0169A0	Local minor	2.00	2.00		10000	30	2	0.00	1.00	0.00	0.00	0.00	1.00	899.02	63.30
MFM0236	XFM0236A0	Local minor		2.00	extended towards NW to MFM0062	10000	30	4		1.00		1.00	0.00	1.90	699.68	324.20
MFM0401A0	XFM040101	Local major			401 extended with 713	10000	30	5	0.00	1.00			0.00		1,372.08	56.70
MFM0408	XFM0408A0	Local minor	2.50	2.50		10000	30	2	0.00	1.00	1.00	1.00	0.00	2.00	466.00	328.30
MFM0683	XFM0683A0	Local minor	1.00	3.00	on topo high (and ridge ?)	10000	20	1	0.00	1.00	0.00	0.00	0.00	1.00	458.64	328.80
MFM0717	XFM0717A0	Local minor	1.00	3.00		10000	30	1	0.00	1.00	0.00	0.00	0.00	1.00	504.16	57.40
MFM0725	XFM0725A0	Local minor	2.10	2.50		10000	20	2	0.00	1.00	0.50	0.50	0.00	1.50	354.26	16.10
MFM0731	XFM0731A0	Local minor	3.00	2.00	baty in Asphallefjarden, shoreline to Sea	10000	30	3	0.00	1.00	1.00	1.00	0.00	2.00	376.28	24.80
MFM0810	XFM081001	Local major	1.87	2.56	NE part magnetic low-	20000	30	4	0.11	0.51	0.82	0.44	0.38	1.44	2,286.87	52.30
MFM0811	XFM0811A0	Local minor				20000	30	2	0.00	1.00	0.00	0.00	0.00	1.00	666.92	42.40
MFM0812	XFM0812A0	Local minor	2.00	2.00		20000	30	1	0.00	1.00	0.00	0.00	0.00	1.00	448.52	313.00
MFM081301	XFM0813A0	Local major	2.00	2.00	extended ca 300 m towards WNW	20000	30	1	0.00	1.00	0.00	0.00	0.00	1.00	1,548.34	296.10
MFM0814	XFM0814A0	Local minor	1.00	3.00		20000	30	1	0.00	1.00	0.00	0.00	0.00	1.00	440.92	26.50

ID_T	ORIGIN_T	CLASS_T	WEIGHT_N	UNCERT_T	COMMENT_T	SCALE_T	PRECIS_N	COUNT_N	COND_N	MAGN_N	TOPO_N	TOPOG_N	TOPOR_N	PROP_N	LENGTH_N	DIRECT_N
MFM0818	XFM081801	Local major			segment 81804-81805 cut out	20000	30	3	0.00	1.00	1.00	1.00	0.00	2.00	1,952.71	318.00
MFM1022	XFM102201	Local minor	3.00	1.00		10000	30	1	0.00	0.78	1.00	1.00	1.00	1.00	675.44	2.90
MFM1035	XFM1035A0	Local minor	3.00	1.00	low velocity, 10-23 m, 3700	10000	20	1	0.00	0.00	1.00	0.00	1.00	1.00	129.68	308.10
MFM1043	XFM1043A0	Local minor	3.00	1.00		20000	30	1	0.00	1.00	1.00	1.00	1.00	2.00	304.18	296.80
MFM1053	XFM105301	Local major	2.80	1.60		20000	40	2	0.00	1.00	0.40	0.40	0.00	1.40	1,071.44	303.80
MFM1054	XFM1054A0	Local minor	2.00	3.00	magnetic 10 m grid	20000	30	1	0.00	1.00	1.00	0.00	0.00	2.00	262.42	290.80
MFM1056	XFM1056A0	Local minor			extended towards SE with piece of XFM081805	20000	30	2	0.00	1.00	1.00	1.00	0.00	2.00	967.72	303.20
MFM1057	XFM1057A0	Local minor	4.00	1.00	dredge and landfill ?, part magnetic	20000	30	1	0.00	1.00	1.00	1.00	1.00	2.00	766.21	64.60
MFM1061	XFM1061A0	Local minor	2.00	2.00		10000	30	1	0.00	0.48	1.00	1.00	1.00	1.00	508.14	48.10
MFM1064	XFM1064A0	Local minor	3.00	1.00	low velocity, 4,000 m/s, 5	10000	20	1	0.00	0.00	1.00	0.00	1.00	1.00	151.83	3.80
MFM1068	XFM106801	Local major	2.00	2.00	low velocity, 5–10 m 3800	10000	30	1	0.00	0.00	1.00	0.00	1.00	1.00	1,001.98	301.10
MFM1072	XFM1072A0	Local minor	2.00	2.00		10000	30	1	0.00	0.00	1.00	1.00	1.00	1.00	751.97	350.30
MFM1077	XFM1077A0	Local minor	2.00	2.00		10000	30	2	0.00	0.00	1.00	1.00	1.00	1.00	521.64	352.00
MFM1088	XFM1088A0	Local minor	2.00	3.00	Old FMV ground geophysical survey	10000	20	1	1.00	1.00	0.00	0.00	0.00	2.00	476.25	334.50
MFM1092	XFM1092A0	Local minor	2.56	1.44	ytberg, low velocity	10000	40	2	0.00	0.00	1.00	1.00	1.00	1.00	788.83	25.00
MFM1093	XFM1093A0	Local minor	2.00	2.00		10000	40	2	0.00	0.00	1.00	1.00	1.00	1.00	531.87	317.40
MFM1094	XFM1094A0	Local minor			east segment exchanged for ESE new segment	20000	40	3	0.00	1.00					812.56	294.20
MFM1201	XFM0098A0, segment 08	Local minor	2.00	2.00	across roadbank	20000	30	1	0.00	0.00	1.00	1.00	1.00	1.00	536.18	356.10
MFM1202	XFM0098A0 segment 03	Local minor			Magnetic piece of XFM0098A0	10000	40		0.34	1.00	0.83	0.83	0.17	1.34	462.80	351.90
MFM0133	XFM0133A0	Local minor				20000	30	3		1.00	1.00	1.00	0.00		644.72	309.40
MFM0414	XFM0414A0	Local minor	2.00	3.00	splay to MFM0060? parallell 70 m towards SE	20000	30	1	0.00	1.00	1.00	1.00	0.00	1.00	340.57	43.50
MFM1196	Magnetic 10 m grid	Local minor	3.00	1.00	partly XFM0404A0	20000	40	1		1.00					904.67	329.90
MFM1197	XFM0412A0 + 158	Local minor	2.00	2.00	extended with piece of 158	20000	30	1		1.00			0.00		440.35	13.30
MFM1198	XFM0127, 166, 45 (all parts)	Local major			linking of 12711, 12712, 166A0 (part), 4501, 450	20000	30			1.00			0.00		1,460.60	332.80
MFM1199	LowMagn + XFM...	Local major	2.00	2.00	XFM:4706, 134, 9802, 733, 12710, 402, 163	20000	40			1.00					2,200.03	314.60
MFM1200	XFM0425A0, 421A0, 711A0	Local major	1.00	3.00		20000	40	2	0.00	1.00			0.00		1,697.61	315.90

References

/1/ **Isaksson H, Keisu M, 2005.** Interpretation of airborne geophysics and integration with topography. Stage 2 (2002–2004). SKB P-04-282, Svensk Kärnbränslehantering AB.

/2/ **Johansson R, Isaksson H, 2006.** Assessment of inferred lineaments in the north-western part of the Forsmark site investigation area. Present knowledge and recommendations for further investigations. SKB P-05-261, Svensk Kärnbränslehantering AB.

/3/ **Korhonen K, Paananen M, Paulamäki S, 2004.** Interpretation of lineaments from airborne geophysical and topographic data. An alternative model within version 1.2 of the Forsmark modelling project. SKB P-04-241, Svensk Kärnbränslehantering AB.

Hans Isaksson

Luleå, 2006-02-14

Appendix 2.3

PM: Possible transparent reflection seismic corridors at Forsmark

In an effort to identify near-vertical zones or corridors from the reflection seismic data acquired during stage 1 and stage 2, maps of important reflectors have been produced. The limits of reflections were determined from the various profiles and these points were then migrated into the subsurface using the already estimated strike and dip of the equivalent reflector. When making the maps, no distinction was made as to whether a reflection terminated due to that it could not be followed further on the section or that it terminated due to that the profile ended. However, consideration of these two alternatives has been taken into account when making the interpretation.

Reflectors were grouped into sub-horizontal and gently dipping reflectors and their areal extent mapped (Figures 1 and 2). In general, only one reflector was mapped from a group of reflectors with similar orientation. For example, only the C1 reflector is mapped out of the C group. The C reflectors extend over most of the area, but are limited to the southwest where they cannot be followed on the seismic profiles.

From the mapping and taking into account the reason why a reflector terminates (either the profile is not long enough or it cannot be followed any further on the profile) three corridors have been identified that may form physical boundaries for reflectors (Figure 3). Out of these three corridors only corridor 3 coincides with an existing well defined deformation zone, the Forsmark zone, Corridor 2 is sub-parallel to the Eckarfjärden zone, but cuts across it. Also, both the J1 and J2 reflectors cut across the Eckarfjärden zone. Finally, note that corridor 2 does not extend all the way down to the set C reflectors since these cut across it. Corridor 1 runs perpendicular to the three deformation zones and appears to limit the A1 reflector to the west and the B8 and B9 reflectors to the east. It may also limit the C reflectors to the west, but this is not clear from the existing set of profiles. Both the M and C sets of reflectors appear to cut across the Singö deformation zone.

In conclusion, given the present data set, only the Forsmark zone appears to cut reflectors vertically below it, the other two major deformation zones are cut by reflectors at various depths.

Christopher Juhlin

Uppsala, 2005-10-03

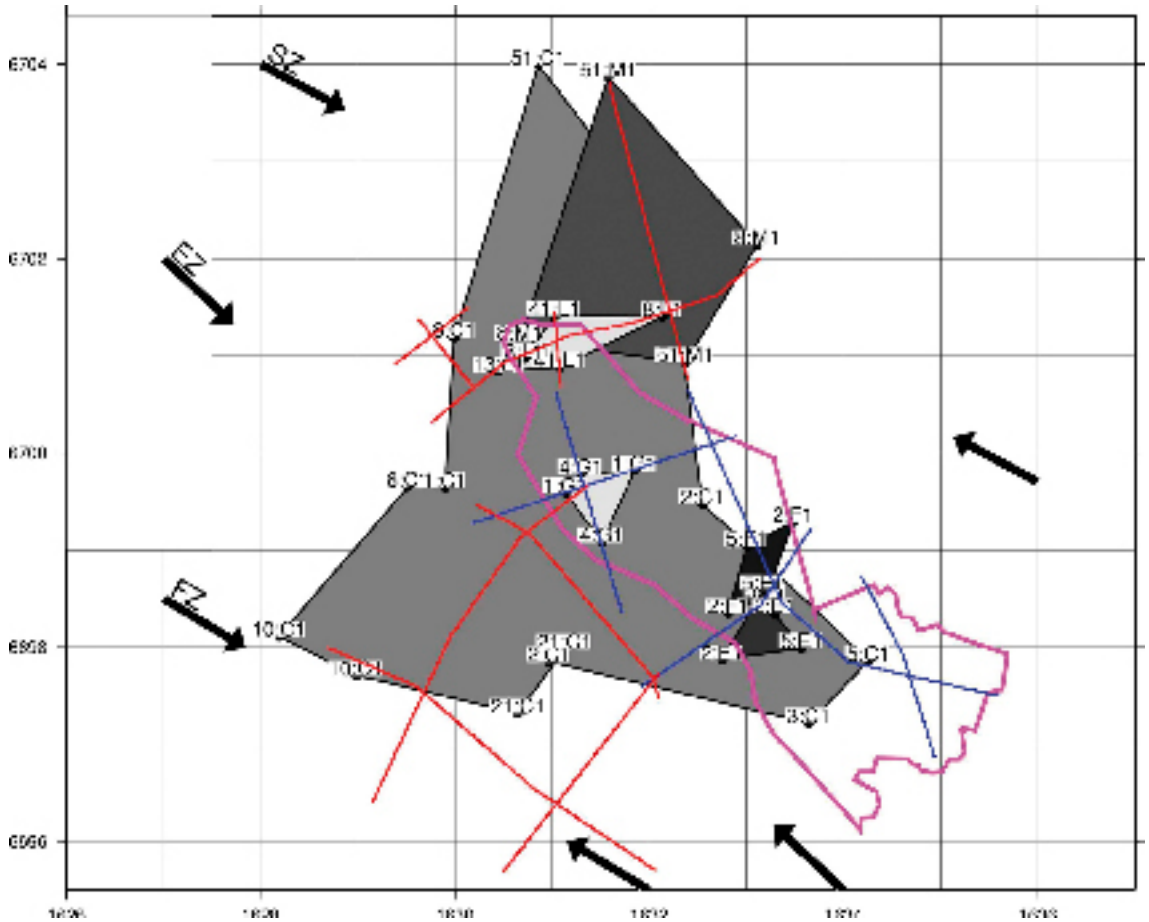

Figure 1. *Limits of a number of sub-horizontal reflectors identified on the reflection seismic profiles. View is from above and the dip and strike of the reflectors have been taken into account. No distinction is made in defining the limits between where the profiles end and where the reflections cannot be followed further on the profiles. Reflectors are coded at the corners of the polygons as profile:reflector.*

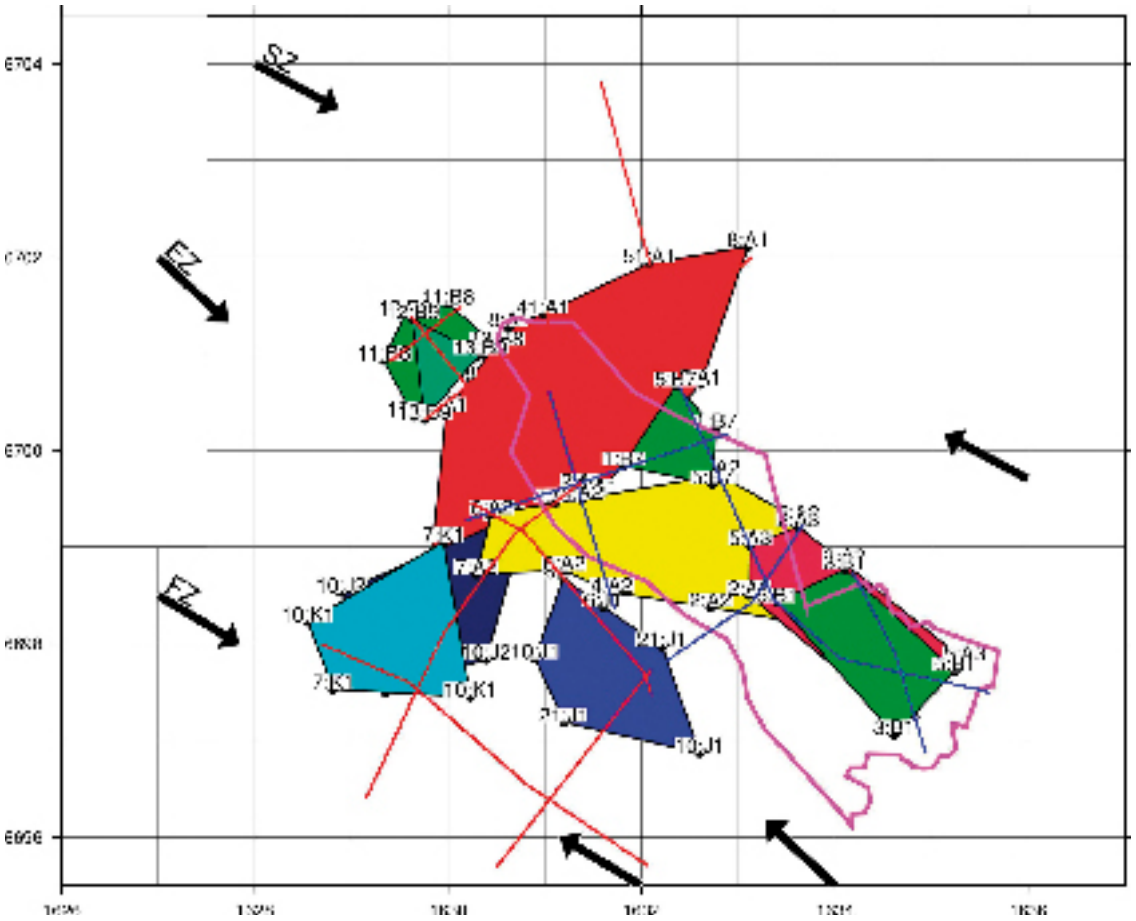

Figure 2. *Limits of a number of gently dipping reflectors identified on the reflection seismic profiles. View is from above and the dip and strike of the reflectors have been taken into account. No distinction is made in defining the limits between where the profiles end and where the reflections cannot be followed further on the profiles. Reflectors are coded at the corners of the polygons as profile:reflector.*

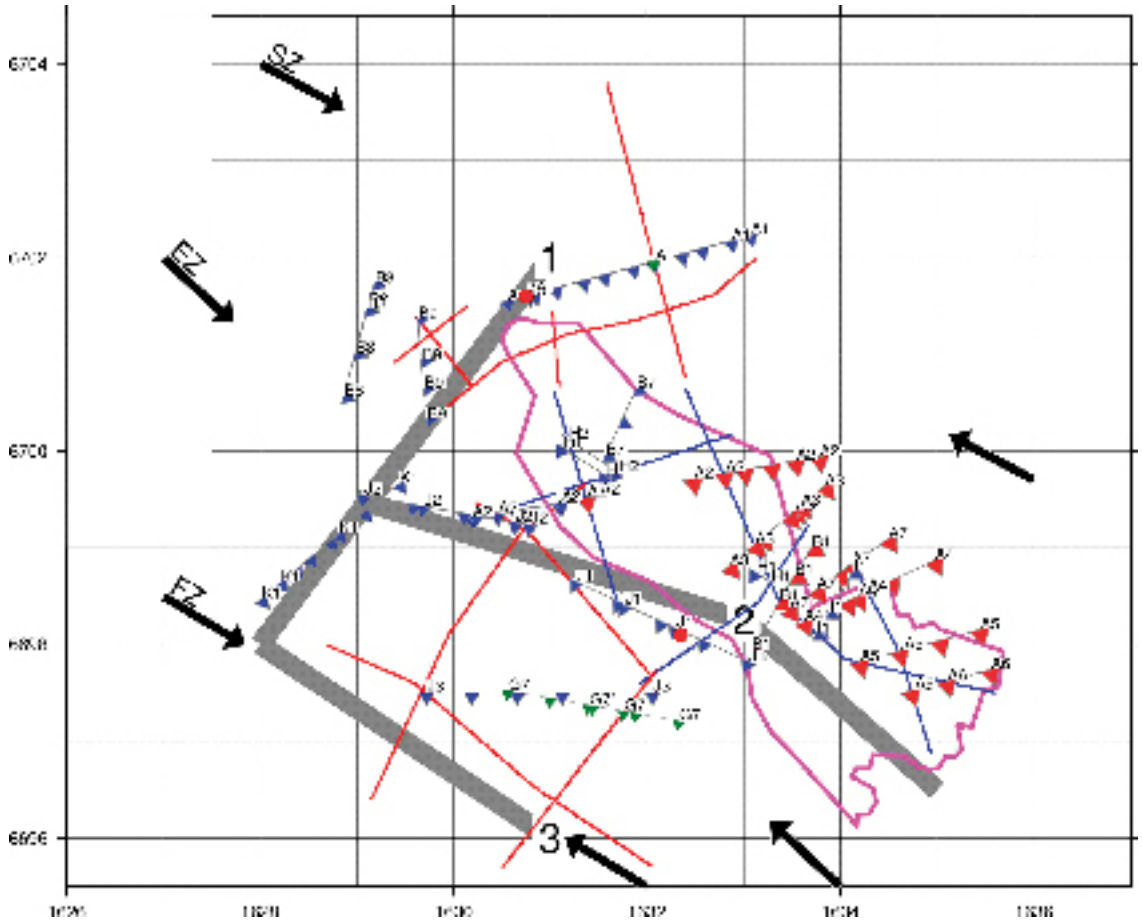

Figure 3. *Three possible sub-vertical corridors that cut across reflectors. Only corridor 3 appears to definitely cut the deep C1 and C2 reflectors. The C1 and C2 reflectors are present below corridor 2 and may also extend below corridor 1.*

Appendix 2.4

Modelling procedure, confidence of occurrence and geological properties of deformation zones in the local model volume

The modelling procedure used, the confidence of occurrence, and the geological properties of deformation zones that have been modelled in the local model volume (SDM stage 2.1) are presented here. The equivalent information for the regional model volume can be found in SKB's database for modelling activities.

Vertical and steeply, SW-dipping brittle and ductile deformation zones with NW strike

ZFMNW0001 (Singö deformation zone)

Property	Quantitative estimate	Span	Confidence level	Basis for interpretation	Comments
At the surface, replaced linked lineament XFM0803A0 by low magnetic lineament MFM0803. Modelled at depth using dip estimated from data along near-surface tunnels and boreholes					
Confidence of occurrence: High					
Position		± 20 m	High	Intersections along tunnels 1–2, 3 and SFR, and boreholes along tunnels, seismic refraction data, low magnetic lineament MFM0803	Span refers to the general position of the zone core on the surface. Span reduces to ± 1 m in the bedrock volume close to the tunnels and boreholes. Lineament is also defined by a bathymetric depression along the boundary between the Quaternary cover and the crystalline bedrock
Orientation (strike/dip)	120/90	± 10/± 10	High for strike, medium for dip	Strike based on trend of lineament MFM0803. Dip based on data from intersections along tunnels 1–2, 3 and SFR, and boreholes along tunnels	
Thickness	200 m	± 50 m	Medium	Intersections along tunnels 1–2, 3 and SFR, and boreholes along tunnels	/Carlsson and Christiansson 1987/. Thickness refers to total zone thickness (ductile and brittle, transition zone and core). Approximately 80 m along SFR tunnels
Length	30 km	+25 km	Medium	Low magnetic lineament MFM0803	Total length at ground surface. Extends outside regional model volume
Ductile deformation			High	Intersections along tunnels 1–2, 3 and SFR, and boreholes along tunnels	Present
Brittle deformation			High	Intersections along tunnels 1–2, 3 and SFR, and boreholes along tunnels	Present
Alteration			Medium	Character of lineament MFM0803	Red-stained bedrock with fine-grained hematite dissemination
Fracture orientation	125/80 (schistosity), 140/80 (schistosity), 210/75, 055/75, 170/40, sub-horizontal		High	Intersections along tunnels 1–2, 3 and SFR, and boreholes along tunnels	/Carlsson and Christiansson 1987/
Fracture frequency	10 m^{-1}	± 4 m^{-1}	High	Intersections along tunnels 1–2, 3 and SFR, and boreholes along tunnels	
Fracture filling			High	Intersections along tunnels 1–2, 3 and SFR, and boreholes along tunnels	Chlorite, calcite, quartz, clay minerals, sandy material

Vertical and steeply, SW-dipping brittle and ductile deformation zones with NW strike

ZFMNW0002 (splay from Singö deformation zone through tunnel 3)

Property	Quantitative estimate	Span	Confidence level	Basis for interpretation	Comments
At the surface, replaced linked lineament XFM0804A0 by low magnetic lineament MFM0804. Modelled at depth using dip estimated from data along the near-surface tunnel 3					
Confidence of occurrence: High					
Position		± 20 m	High	Intersection along tunnel 3, seismic refraction data, low magnetic lineament MFM0804	Span refers to the general position of the zone core on the surface. Span reduces to ± 1 m in the bedrock volume close to tunnel 3. Lineament is also defined by a bathymetric depression along the boundary between the Quaternary cover and the crystalline bedrock
Orientation (strike/dip)	135/90	± 10/± 10	High for strike, medium for dip	Strike based on trend of lineament MFM0804. Dip based on data from intersection along tunnel 3	
Thickness	75 m	± 10 m	Medium	Intersection along tunnel 3	Thickness refers to total zone thickness (ductile and brittle, transition zone and core)
Length	18 km	± 1 km	Medium	Low magnetic lineament MFM0804. Truncated to the south-east against ZFMNW0001	Total length at ground surface. Extends to the north-west outside regional model volume
Ductile deformation			High	Intersection along tunnel 3	Present. Zones of foliated rocks and chlorite schist documented during mapping of tunnel 3
Brittle deformation			Medium	Intersection along tunnel 3	Present. However, note low fracture frequency
Alteration			High	Intersection along tunnel 3, character of lineament MFM0804	Chloritization, red-stained bedrock with fine-grained hematite dissemination
Fracture orientation	NW/70S, NE/90, NNW/90		High	Intersection along tunnel 3	
Fracture frequency	1 m^{-1}	0.5 m^{-1}	Low	Intersection along tunnel 3	
Fracture filling			High	Intersection along tunnel 3	Chlorite, calcite

Vertical and steeply, SW-dipping brittle and ductile deformation zones with NW strike

ZFMNW0123 (DZ5 in KFM04A)

Property	Quantitative estimate	Span	Confidence level	Basis for interpretation	Comments
At the surface, replaced linked lineaments XFM0123A0 and XFM0136A0 by low magnetic lineament MFM0123. Modelled at depth using dip estimated by connecting lineament MFM0123 at the surface with the borehole intersection 654–661 m (DZ5) in KFM04A					
Confidence of occurrence: High					
Position		± 20 m	High	Intersection along DZ5 in KFM04A, low magnetic lineament MFM0123	Span refers to general position of the zone core on surface. Span reduces to ± 1 m in the bedrock volume close to borehole KFM04A
Orientation (strike/dip)	118/82	± 5/± 10	High for strike, low for dip	Strike based on trend of lineament MFM0123. Dip based on linking MFM0123 at the surface with borehole intersection along KFM04A (DZ5)	
Thickness	6 m		Medium	Intersection along DZ5 in KFM04A	Thickness refers to total zone thickness (transition zone and core). Borehole intersection is close to the north-western end of the structure
Length	5,064 m	± 200 m	Medium	Low magnetic lineament MFM0123. Truncated against ZFMNW0023 and ZFMNE0060A	Total length at ground surface
Ductile deformation			High	Intersection along DZ5 in KFM04A	Strongly foliated bedrock present
Brittle deformation			High	Intersection along DZ5 in KFM04A	Present
Alteration			High	Intersection along DZ5 in KFM04A, character of lineament MFM0123	Red-stained bedrock with fine-grained hematite dissemination
Fracture orientation	Fisher mean of NW fracture set = 140/80	K value of NW fracture set = 39	Medium	Intersection along DZ5 in KFM04A, N=65	Few fractures with other orientations are present
Fracture frequency	Mean 10 m^{-1}	Span 5–17 m^{-1}	Medium	Intersection along DZ5 in KFM04A	Dominance of sealed fractures. Quantitative estimate and span exclude sealed fracture network at 656–657 m, due to uncertainty in the estimation of fracture frequency in sealed networks
Fracture filling			Medium	Intersection along DZ5 in KFM04A	Chlorite, calcite, quartz epidote, prehnite, clay minerals

Vertical and steeply, SW-dipping brittle and ductile deformation zones with NW strike

ZFMNW0133 (borehole interval 980–984 m in KFM04A)

Property	Quantitative estimate	Span	Confidence level	Basis for interpretation	Comments
At the surface, replaced linked lineament XFM0133A0 by low magnetic lineament MFM0133. Modelled at depth using dip estimated by connecting lineament MFM0133 at the surface with the borehole intersection 980–984 m in KFM04A					
Confidence of occurrence: High					
Position		± 20 m	High	Intersection along borehole KFM04A (980–984 m), magnetic lineament MFM0133	Span estimate refers to the general position of the central part of the zone on the surface. Span reduces to ± 1 m in the bedrock volume close to KFM04A
Orientation (strike/dip)	309/83	± 5/± 10	High	Intersection along borehole KFM04A (980–984 m), magnetic lineament MFM0133	
Thickness	2 m		Medium	Intersection along borehole KFM04A (980–984 m)	Thickness refers to total zone thickness (transition zone and core)
Length	643 m	± 50 m	Medium	Magnetic lineament MFM0133. Truncated against ZFMNE0060A and ZFMNE0103A	Total length at ground surface
Ductile deformation			Low	Comparison with high confidence, vertical and steeply-dipping zones with NW strike	Assumed to be present. Data not available in borehole interval 980–984 m in KFM04A (p_rock_struct_feat)
Brittle deformation			High	Intersection along borehole KFM04A (980–984 m)	Present
Alteration			High	Intersection along borehole KFM04A (980–984 m)	Oxidized bedrock with fine-grained hematite dissemination
Fracture orientation				Intersection along borehole KFM04A (980–984 m)	Fractures that strike NW and dip steeply to the NE dominate. Insufficient data to calculate Fisher mean and K value (N=20)
Fracture frequency	Mean 8 m^{-1}	Span 2–16 m^{-1}	Medium	Intersection along borehole KFM04A (980–984 m)	Occurrence throughout the zone of sealed fracture networks. Estimate and span exclude these sealed networks, due to uncertainty in the estimation of fracture frequency in these networks
Fracture filling			Low	Intersection along borehole KFM04A (980–984 m)	Laumontite, chlorite, calcite. Few data

Vertical and steeply, SW-dipping brittle and ductile deformation zones with NW strike

ZFMNW0404 (DZ3 in KFM01B)

Property	Quantitative estimate	Span	Confidence level	Basis for interpretation	Comments
At the surface, recognised low magnetic lineament MFM0404 that, in part, corresponds to the linked lineament XFM0404A0. Modelled at depth using dip estimated by connecting lineament MFM0404 at the surface with the borehole intersection 415–454 m (DZ3) in KFM01B. This zone was modelled in SDM version 1.2 as a NS zone					
Confidence of occurrence: High					
Position		± 20 m	High	Intersection along DZ3 in borehole KFM01B, magnetic lineament MFM0404	Span estimate refers to the general position of the central part of the zone on the surface. Span reduces to ± 1 m in the bedrock volume close to KFM01B
Orientation (strike/dip)	150/90	± 5/± 10	High	Intersection along DZ3 in borehole KFM01B, magnetic lineament MFM0404	
Thickness	10 m		Medium	Intersection along DZ3 in borehole KFM01B	Thickness refers to total zone thickness (transition zone and core)
Length	729 m	± 25 m	Medium	Magnetic lineament MFM0404. Truncated against ZFMNE0060 and ZFMNE1197	Total length at ground surface
Ductile deformation			High	Intersection along DZ3 in borehole KFM01B	Not present
Brittle deformation			High	Intersection along DZ3 in borehole KFM01B	Present
Alteration			High	Intersection along DZ3 in borehole KFM01B	Oxidized bedrock with fine-grained hematite dissemination
Fracture orientation	Fisher mean of NNW fracture set = 340/85	K value of NNW fracture set = 20	Medium	Intersection along DZ3 in borehole KFM01B (N=219)	Fracture set with NNW strike and steep dip to the east is dominant. A subordinate fracture set that is sub-horizontal and fractures with steeper, more variable orientation are also present
Fracture frequency	Mean 8 m^{-1}	Span 1–14 m^{-1}	Medium	Intersection along DZ3 in borehole KFM01B	Dominance of sealed fractures. Quantitative estimate and span exclude sealed fracture networks and two crush zones in the borehole interval 431–443 m, due to uncertainty in the estimation of fracture frequency in these networks/zones
Fracture filling			Medium	Intersection along DZ3 in borehole KFM01B	Chlorite, calcite, laumontite, prehnite, quartz, hematite/ adularia, epidote

Vertical and steeply, SW-dipping brittle and ductile deformation zones with NW strike

ZFMNW1200 (DZ1 and extension 125–169 m in KFM04A)

Property	Quantitative estimate	Span	Confidence level	Basis for interpretation	Comments
At the surface, recognised low magnetic lineament MFM1200 that, in part, corresponds to the linked lineaments XFM0425A0, XFM0421A0 and XFM0711A0. Mylonitic rocks observed at the surface along this lineament (e.g. PFM001257). Zone extended to the north-west, where it also corresponds to the linked lineament with NW trend, XFM0789A0. Modelled at depth using dip estimated by connecting lineament MFM01200 at the surface with the borehole intersection 125–176 m in KFM04A (DZ1 and extension in interval 125–169 m). A segment of zone ZFMNE00A2 has also been modelled to intersect KFM04A along DZ1					
Confidence of occurrence: High					
Position		± 20 m	High	Intersection along DZ1 and its extension (125–169 m) in KFM04A, low magnetic lineament MFM1200	Span refers to general position of the zone core on surface. Span reduces to ± 1 m in the bedrock volume close to borehole KFM04A
Orientation (strike/dip)	138/78	± 5/± 10	High for strike, low for dip	Strike based on trend of lineament MFM1200. Dip based on linking MFM1200 at the surface with borehole intersection along KFM04A (DZ1 and extension 125–169 m)	
Thickness	37 m		Medium	Intersection along DZ1 and its extension (125–169 m) in KFM04A	Thickness refers to total zone thickness (transition zone and core)
Length	3,179 m	± 200 m	Medium	Low magnetic lineament MFM1200 and its extension to the north-west. Truncated at depth against ZFMNW0017	Total length at ground surface
Ductile deformation			High	Surface geology and intersection along DZ1 and its extension (125–169 m) in KFM04A	Present
Brittle deformation			High	Intersection along DZ1 and its extension (125–169 m) in KFM04A	Present
Alteration			High	Intersection along DZ1 and its extension (125–169 m) in KFM04A	Red-stained bedrock with fine-grained hematite dissemination
Fracture orientation	Fisher mean of NW fracture set = 140/85	K value of NW fracture set = 24	Medium	Intersection along DZ1 and its extension (125–169 m) in KFM04A, N=418	Fractures that belong to gently dipping and NE steeply dipping fracture sets are also present
Fracture frequency	Mean 8 m^{-1}	Span 1–26 m^{-1}	Medium	Intersection along DZ1 and its extension (125–169 m) in KFM04A	Quantitative estimate and span exclude three sealed fracture networks, due to uncertainty in the estimation of fracture frequency in these networks
Fracture filling			Medium	Intersection along DZ1 and its extension (125–169 m) in KFM04A	Chlorite, calcite, prehnite, hematite/adularia, clay minerals, epidote

Vertical and steeply, SW-dipping brittle and ductile deformation zones with NW strike, based solely on lineament and comparison studies

ZFMNW0017

Property	Quantitative estimate	Span	Confidence level	Basis for interpretation	Comments
At the surface, replaced linked lineaments XFM0017A0 and XFM0018A0 by low magnetic lineament MFM0017. Modelled at depth using an assumed dip of 90° based on a comparison with high confidence, vertical and steeply dipping zones with NW strike					
Confidence of occurrence: Medium					
Position		± 20 m	High	Low magnetic lineament MFM0017	Span estimate refers to the general position of the central part of the zone on the surface
Orientation (strike/dip)	135/90	± 5/± 10	High for strike, low for dip	Strike based on trend of lineament MFM0017. Dip based on comparison with high confidence, vertical and steeply-dipping zones with NW strike	
Thickness	25 m	± 10 m	Low	Estimated on basis of length – thickness correlation diagram	Thickness refers to total zone thickness (ductile and brittle, transition zone and core)
Length	7,898 m	± 500 m	Medium	Low magnetic lineament MFM0017. Truncated against ZFMNW0019 and ZFMNW0137	Total length at ground surface
Ductile deformation			Low	Comparison with high confidence, vertical and steeply-dipping zones with NW strike	Assumed to be present
Brittle deformation			Low	Comparison with high confidence, vertical and steeply-dipping zones with NW strike	Assumed to be present
Alteration			Medium	Character of lineament MFM0017	Red-stained bedrock with fine-grained hematite dissemination
Fracture orientation					
Fracture frequency					
Fracture filling					

Vertical and steeply, SW-dipping brittle and ductile deformation zones with NW strike, based solely on lineament and comparison studies

ZFMNW0137

Property	Quantitative estimate	Span	Confidence level	Basis for interpretation	Comments
At the surface, replaced linked lineaments XFM0137A0 and XFM0046A0 by low magnetic lineament MFM0137A0. Modelled at depth using an assumed dip of 90° based on a comparison with high confidence, vertical and steeply dipping zones with NW strike					
Confidence of occurrence: Medium					
Position		± 20 m	High	Low magnetic lineament MFM0137A0	Span estimate refers to the general position of the central part of the zone on the surface
Orientation (strike/dip)	095/90	± 5/± 10	High for strike, low for dip	Strike based on trend of lineament MFM0137A0. Dip based on comparison with high confidence, vertical and steeply-dipping zones with NW strike	
Thickness	15 m	± 10 m	Low	Estimated on basis of length – thickness correlation diagram	Thickness refers to total zone thickness (ductile and brittle, transition zone and core)
Length	4,300 m	± 200 m	Medium	Low magnetic lineament MFM0137A0. Truncated to east against ZFMNW0001	Total length at ground surface. Extends to the west and to the south-east outside regional model volume
Ductile deformation			Low	Comparison with high confidence, vertical and steeply-dipping zones with NW strike	Assumed to be present
Brittle deformation			Low	Comparison with high confidence, vertical and steeply-dipping zones with NW strike	Assumed to be present
Alteration			Medium	Character of lineament MFM0137A0	Red-stained bedrock with fine-grained hematite dissemination
Fracture orientation					
Fracture frequency					
Fracture filling					

Vertical and steeply, SW-dipping brittle and ductile deformation zones with NW strike, based solely on lineament and comparison studies

ZFMNW0809

Property	Quantitative estimate	Span	Confidence level	Basis for interpretation	Comments
At the surface, replaced linked lineament XFM0809A0 by low magnetic lineament MFM0809. Modelled at depth using an assumed dip of 90° based on a comparison with high confidence, vertical and steeply dipping zones with NW strike					
Confidence of occurrence: Medium					
Position		± 20 m	High	Low magnetic lineament MFM0809	Span estimate refers to the general position of the central part of the zone on the surface
Orientation (strike/dip)	115/90	± 5/± 10	High for strike, low for dip	Strike based on trend of lineament MFM0809. Dip based on comparison with high confidence, vertical and steeply-dipping zones with NW strike	
Thickness	15 m	± 10 m	Low	Estimated on basis of length – thickness correlation diagram	Thickness refers to total zone thickness (ductile and brittle, transition zone and core)
Length	3,401 m	± 200 m	Medium	Low magnetic lineament MFM0809. Truncated against ZFMNE062A and ZFMNE0810	Total length at ground surface
Ductile deformation			Low	Comparison with high confidence, vertical and steeply-dipping zones with NW strike	Assumed to be present
Brittle deformation			Low	Comparison with high confidence, vertical and steeply-dipping zones with NW strike	Assumed to be present
Alteration			Medium	Character of lineament MFM0809	Red-stained bedrock with fine-grained hematite dissemination
Fracture orientation					
Fracture frequency					
Fracture filling					

Vertical and steeply, SW-dipping brittle and ductile deformation zones with NW strike, based solely on lineament and comparison studies

ZFMNW0835A, -0835B

Property	Quantitative estimate	Span	Confidence level	Basis for interpretation	Comments
At the surface, replaced linked lineament XFM0835A0 by low magnetic lineament MFM0835A0, and linked lineament XFM1033A0 by low magnetic lineament MFM0835B0. Modelled at depth using an assumed dip of 90° based on a comparison with high confidence, vertical and steeply dipping zones with NW strike. Only zone ZFMNW0835B lies inside the local model volume					
Confidence of occurrence: Medium					
Position		± 20 m	High	Low magnetic lineaments MFM0835A0 and MFM0835B0	Span estimate refers to the general position of the central part of the zone on the surface
Orientation (strike/dip)	ZFMNW0835A = 114/90 ZFMNW0835B = 098/90	± 5/± 10	High for strike, low for dip	Strike based on trend of lineaments MFM0853A0 and MFM0835B0. Dip based on comparison with high confidence, vertical and steeply-dipping zones with NW strike	
Thickness	15 m for ZFMNW0835A and 10 m for ZFMNW0835B	± 10 m	Low	Estimated on basis of length – thickness correlation diagram	Thickness refers to total zone thickness (ductile and brittle, transition zone and core)
Length	ZFMNW0835A is 2,816 m and ZFMNW0835B is 1,532 m	± 200 m for zone ZFMNW0835A and ± 100 m for zone ZFMNW0835B	Medium	Low magnetic lineaments MFM0835A0 and MFM0835B0. Zone ZFMNW0835A truncated against ZFMNW0805 and ZFMNW0806. Zone ZFMNW0835B truncated against ZFMNW0805 and ZFMNW1127	Length of both components at ground surface exceeds 3,000 m
Ductile deformation			Low	Comparison with high confidence, vertical and steeply-dipping zones with NW strike	Assumed to be present
Brittle deformation			Low	Comparison with high confidence, vertical and steeply-dipping zones with NW strike	Assumed to be present
Alteration			Medium	Character of lineaments MFM0835A0 and MFM0835B0	Red-stained bedrock with fine-grained hematite dissemination
Fracture orientation					
Fracture frequency					
Fracture filling					

Vertical and steeply, SW-dipping brittle and ductile deformation zones with NW strike, based solely on lineament and comparison studies

ZFMNW1127

Property	Quantitative estimate	Span	Confidence level	Basis for interpretation	Comments
At the surface, replaced linked lineament XFM1127A0 by low magnetic lineament MFM1127. Modelled at depth using an assumed dip of 90° based on a comparison with high confidence, vertical and steeply dipping zones with NW strike					
Confidence of occurrence: Medium					
Position		± 20 m	High	Low magnetic lineament MFM1127	Span estimate refers to the general position of the central part of the zone on the surface
Orientation (strike/dip)	124/90	± 5/± 10	High for strike, low for dip	Strike based on trend of lineament MFM1127. Dip based on comparison with high confidence, vertical and steeply-dipping zones with NW strike	
Thickness	15 m	± 10 m	Low	Estimated on basis of length – thickness correlation diagram	Thickness refers to total zone thickness (ductile and brittle, transition zone and core)
Length	3,645 m	± 200 m	Medium	Low magnetic lineament MFM1127. Truncated by ZFMNW0001 and ZFMNW0002	Total length at ground surface
Ductile deformation			Low	Comparison with high confidence, vertical and steeply-dipping zones with NW strike	Assumed to be present
Brittle deformation			Low	Comparison with high confidence, vertical and steeply-dipping zones with NW strike	Assumed to be present
Alteration			Medium	Character of lineament MFM1127	Red-stained bedrock with fine-grained hematite dissemination
Fracture orientation					
Fracture frequency					
Fracture filling					

Vertical and steeply, SW-dipping brittle and ductile deformation zones with NW strike, based solely on lineament and comparison studies

ZFMNW0044

Property	Quantitative estimate	Span	Confidence level	Basis for interpretation	Comments
At the surface, replaced various segments of the linked lineament XFM0044A0 by low magnetic lineament MFM0044. Modelled at depth using an assumed dip of 90° based on a comparison with high confidence, vertical and steeply dipping zones with NW strike					
Confidence of occurrence: Low					
Position		± 20 m	High	Low magnetic lineament MFM0044	Span estimate refers to the general position of the central part of the zone on the surface
Orientation (strike/dip)	120/90	± 5/± 10	High for strike, low for dip	Strike based on trend of lineament MFM0040. Dip based on comparison with high confidence, vertical and steeply-dipping zones with NW strike	
Thickness	10 m	± 5 m	Low	Estimated on basis of length – thickness correlation diagram	Thickness refers to total zone thickness (ductile and brittle, transition zone and core)
Length	1,340 m	± 100 m	Medium	Low magnetic lineament MFM0044. Truncated by ZFMNE0168 and ZFMNE0062A	Total length at ground surface
Ductile deformation			Low	Comparison with high confidence, vertical and steeply-dipping zones with NW strike	Assumed to be present
Brittle deformation			Low	Comparison with high confidence, vertical and steeply-dipping zones with NW strike	Assumed to be present
Alteration			Medium	Character of lineament MFM0044	Red-stained bedrock with fine-grained hematite dissemination
Fracture orientation					
Fracture frequency					
Fracture filling					

Vertical and steeply, SW-dipping brittle and ductile deformation zones with NW strike, based solely on lineament and comparison studies

ZFMNW0167

Property	Quantitative estimate	Span	Confidence level	Basis for interpretation	Comments
At the surface, replaced linked lineament XFM0167A0 by low magnetic lineament MFM0167. Modelled at depth using an assumed dip of 90° based on a comparison with high confidence, vertical and steeply dipping zones with NW strike					
Confidence of occurrence: Low					
Position		± 20 m	High	Low magnetic lineament MFM0167	Span estimate refers to the general position of the central part of the zone on the surface
Orientation (strike/dip)	110/90	± 5/± 10	High for strike, low for dip	Strike based on trend of lineament MFM0167. Dip based on comparison with high confidence, vertical and steeply-dipping zones with NW strike	
Thickness	5 m	± 3 m	Low	Estimated on basis of length – thickness correlation diagram	Thickness refers to total zone thickness (ductile and brittle, transition zone and core)
Length	712 m	± 50 m	Medium	Low magnetic lineament MFM0167. Truncated by ZFMNE0731 and ZFMNE0060A	Total length at ground surface
Ductile deformation			Low	Comparison with high confidence, vertical and steeply-dipping zones with NW strike	Assumed to be present
Brittle deformation			Low	Comparison with high confidence, vertical and steeply-dipping zones with NW strike	Assumed to be present
Alteration			Medium	Character of lineament MFM0167	Red-stained bedrock with fine-grained hematite dissemination
Fracture orientation					
Fracture frequency					
Fracture filling					

Vertical and steeply, SW-dipping brittle and ductile deformation zones with NW strike, based solely on lineament and comparison studies

ZFMNW0171

Property	Quantitative estimate	Span	Confidence level	Basis for interpretation	Comments
At the surface, replaced part of linked lineament XFM0017A0 by low magnetic lineament MFM001711. Modelled at depth using an assumed dip of 90° based on a comparison with high confidence, vertical and steeply dipping zones with NW strike					
Confidence of occurrence: Low					
Position		± 20 m	High	Low magnetic lineament MFM001711	Span estimate refers to the general position of the central part of the zone on the surface
Orientation (strike/dip)	140/90	± 5/± 10	High for strike, low for dip	Strike based on trend of lineament MFM001711. Dip based on comparison with high confidence, vertical and steeply-dipping zones with NW strike	
Thickness	5 m	± 3 m	Low	Estimated on basis of length – thickness correlation diagram	Thickness refers to total zone thickness (ductile and brittle, transition zone and core)
Length	828 m	± 50 m	Medium	Low magnetic lineament MFM001711. Truncated by ZFMNW0017 and ZFMNE0401	Total length at ground surface
Ductile deformation			Low	Comparison with high confidence, vertical and steeply-dipping zones with NW strike	Assumed to be present
Brittle deformation			Low	Comparison with high confidence, vertical and steeply-dipping zones with NW strike	Assumed to be present
Alteration			Medium	Character of lineament MFM001711	Red-stained bedrock with fine-grained hematite dissemination
Fracture orientation					
Fracture frequency					
Fracture filling					

Vertical and steeply, SW-dipping brittle and ductile deformation zones with NW strike, based solely on lineament and comparison studies

ZFMNW0236

Property	Quantitative estimate	Span	Confidence level	Basis for interpretation	Comments
At the surface, replaced and extended to NW linked lineament XFM0236A0 by low magnetic lineament MFM0236. Modelled at depth using an assumed dip of 90° based on a comparison with high confidence, vertical and steeply dipping zones with NW strike					
Confidence of occurrence: Low					
Position		± 20 m	High	Low magnetic lineament MFM0236	Span estimate refers to the general position of the central part of the zone on the surface
Orientation (strike/dip)	145/90	± 5/± 10	High for strike, low for dip	Strike based on trend of lineament MFM0236. Dip based on comparison with high confidence, vertical and steeply-dipping zones with NW strike	
Thickness	5 m	± 3 m	Low	Estimated on basis of length – thickness correlation diagram	Thickness refers to total zone thickness (ductile and brittle, transition zone and core)
Length	714 m	± 50 m	Medium	Low magnetic lineament MFM0236. Truncated by ZFMNE0062A	Total length at ground surface
Ductile deformation			Low	Comparison with high confidence, vertical and steeply-dipping zones with NW strike	Assumed to be present
Brittle deformation			Low	Comparison with high confidence, vertical and steeply-dipping zones with NW strike	Assumed to be present
Alteration			Medium	Character of lineament MFM0236	Red-stained bedrock with fine-grained hematite dissemination
Fracture orientation					
Fracture frequency					
Fracture filling					

Vertical and steeply, SW-dipping brittle and ductile deformation zones with NW strike, based solely on lineament and comparison studies

ZFMNW0408

Property	Quantitative estimate	Span	Confidence level	Basis for interpretation	Comments
At the surface, replaced linked lineament XFM0408A0 by low magnetic lineament MFM0408. Modelled at depth using an assumed dip of 90° based on a comparison with high confidence, vertical and steeply dipping zones with NW strike					
Confidence of occurrence: Low					
Position		± 20 m	High	Low magnetic lineament MFM0408	Span estimate refers to the general position of the central part of the zone on the surface
Orientation (strike/dip)	150/90	± 5/± 10	High for strike, low for dip	Strike based on trend of lineament MFM0408. Dip based on comparison with high confidence, vertical and steeply-dipping zones with NW strike	
Thickness	5 m	± 3 m	Low	Estimated on basis of length – thickness correlation diagram	Thickness refers to total zone thickness (ductile and brittle, transition zone and core)
Length	463 m	± 25 m	Medium	Low magnetic lineament MFM0408. Truncated by ZFMNE0061A	Total length at ground surface
Ductile deformation			Low	Comparison with high confidence, vertical and steeply-dipping zones with NW strike	Assumed to be present
Brittle deformation			Low	Comparison with high confidence, vertical and steeply-dipping zones with NW strike	Assumed to be present
Alteration			Medium	Character of lineament MFM0408	Red-stained bedrock with fine-grained hematite dissemination
Fracture orientation					
Fracture frequency					
Fracture filling					

Vertical and steeply, SW-dipping brittle and ductile deformation zones with NW strike, based solely on lineament and comparison studies

ZFMNW0683

Property	Quantitative estimate	Span	Confidence level	Basis for interpretation	Comments
At the surface, replaced linked lineament XFM0683A0 by low magnetic lineament MFM0683. Modelled at depth using an assumed dip of 90° based on a comparison with high confidence, vertical and steeply dipping zones with NW strike					
Confidence of occurrence: Low					
Position		± 20 m	High	Low magnetic lineament MFM0683	Span estimate refers to the general position of the central part of the zone on the surface
Orientation (strike/dip)	150/90	± 5/± 10	High for strike, low for dip	Strike based on trend of lineament MFM0683. Dip based on comparison with high confidence, vertical and steeply-dipping zones with NW strike	
Thickness	5 m	± 3 m	Low	Estimated on basis of length – thickness correlation diagram	Thickness refers to total zone thickness (ductile and brittle, transition zone and core)
Length	465 m	± 25 m	Medium	Low magnetic lineament MFM0683. Truncated by ZFMNE0169	Total length at ground surface
Ductile deformation			Low	Comparison with high confidence, vertical and steeply-dipping zones with NW strike	Assumed to be present
Brittle deformation			Low	Comparison with high confidence, vertical and steeply-dipping zones with NW strike	Assumed to be present
Alteration			Medium	Character of lineament MFM0683	Red-stained bedrock with fine-grained hematite dissemination
Fracture orientation					
Fracture frequency					
Fracture filling					

Vertical and steeply, SW-dipping brittle and ductile deformation zones with NW strike, based solely on lineament and comparison studies

ZFMNW0812

Property	Quantitative estimate	Span	Confidence level	Basis for interpretation	Comments
At the surface, replaced linked lineament XFM0812A0 by low magnetic lineament MFM0812. Modelled at depth using an assumed dip of 90° based on a comparison with high confidence, vertical and steeply dipping zones with NW strike					
Confidence of occurrence: Low					
Position		± 20 m	High	Low magnetic lineament MFM0812	Span estimate refers to the general position of the central part of the zone on the surface
Orientation (strike/dip)	135/90	± 5/± 10	High for strike, low for dip	Strike based on trend of lineament MFM0812. Dip based on comparison with high confidence, vertical and steeply-dipping zones with NW strike	
Thickness	5 m	± 3 m	Low	Estimated on basis of length – thickness correlation diagram	Thickness refers to total zone thickness (ductile and brittle, transition zone and core)
Length	445 m	± 25 m	Medium	Low magnetic lineament MFM0812. Truncated by ZFMNW0137 and ZFMNS1201	Total length at ground surface
Ductile deformation			Low	Comparison with high confidence, vertical and steeply-dipping zones with NW strike	Assumed to be present
Brittle deformation			Low	Comparison with high confidence, vertical and steeply-dipping zones with NW strike	Assumed to be present
Alteration			Medium	Character of lineament MFM0812	Red-stained bedrock with fine-grained hematite dissemination
Fracture orientation					
Fracture frequency					
Fracture filling					

Vertical and steeply, SW-dipping brittle and ductile deformation zones with NW strike, based solely on lineament and comparison studies

ZFMNW0813

Property	Quantitative estimate	Span	Confidence level	Basis for interpretation	Comments
At the surface, replaced and extended to the WNW linked lineament XFM0813A0 by low magnetic lineament MFM081301. Modelled at depth using an assumed dip of 90° based on a comparison with high confidence, vertical and steeply dipping zones with NW strike					
Confidence of occurrence: Low					
Position		± 20 m	High	Low magnetic lineament MFM081301	Span estimate refers to the general position of the central part of the zone on the surface
Orientation (strike/dip)	115/90	± 5/± 10	High for strike, low for dip	Strike based on trend of lineament MFM081301. Dip based on comparison with high confidence, vertical and steeply-dipping zones with NW strike	
Thickness	10 m	± 5 m	Low	Estimated on basis of length – thickness correlation diagram	Thickness refers to total zone thickness (ductile and brittle, transition zone and core)
Length	1,541 m	± 100 m	Medium	Low magnetic lineament MFM081301. Truncated by ZFMNE0808C and ZFMNE0062A	Total length at ground surface
Ductile deformation			Low	Comparison with high confidence, vertical and steeply-dipping zones with NW strike	Assumed to be present
Brittle deformation			Low	Comparison with high confidence, vertical and steeply-dipping zones with NW strike	Assumed to be present
Alteration			Medium	Character of lineament MFM081301	Red-stained bedrock with fine-grained hematite dissemination
Fracture orientation					
Fracture frequency					
Fracture filling					

Vertical and steeply, SW-dipping brittle and ductile deformation zones with NW strike, based solely on lineament and comparison studies

ZFMNW0818

Property	Quantitative estimate	Span	Confidence level	Basis for interpretation	Comments
At the surface, replaced part of linked lineament XFM0818A0 by low magnetic lineament MFM0818. Modelled at depth using an assumed dip of 90° based on a comparison with high confidence, vertical and steeply dipping zones with NW strike					
Confidence of occurrence: Low					
Position		± 20 m	High	Low magnetic lineament MFM0818	Span estimate refers to the general position of the central part of the zone on the surface
Orientation (strike/dip)	140/90	± 5/± 10	High for strike, low for dip	Strike based on trend of lineament MFM0818. Dip based on comparison with high confidence, vertical and steeply-dipping zones with NW strike	
Thickness	10 m	± 5 m	Low	Estimated on basis of length – thickness correlation diagram	Thickness refers to total zone thickness (ductile and brittle, transition zone and core)
Length	1,200 m	± 50 m	Medium	Low magnetic lineament MFM0818. Truncated by ZFMNE0062A and ZFMNE0065	Total length at ground surface
Ductile deformation			Low	Comparison with high confidence, vertical and steeply-dipping zones with NW strike	Assumed to be present
Brittle deformation			Low	Comparison with high confidence, vertical and steeply-dipping zones with NW strike	Assumed to be present
Alteration			Medium	Character of lineament MFM0818	Red-stained bedrock with fine-grained hematite dissemination
Fracture orientation					
Fracture frequency					
Fracture filling					

Vertical and steeply, SW-dipping brittle and ductile deformation zones with NW strike, based solely on lineament and comparison studies

ZFMNW1043

Property	Quantitative estimate	Span	Confidence level	Basis for interpretation	Comments
At the surface, replaced linked lineament XFM1043A0 by low magnetic lineament MFM1043. Modelled at depth using an assumed dip of 90° based on a comparison with high confidence, vertical and steeply dipping zones with NW strike					
Confidence of occurrence: Low					
Position		± 20 m	High	Low magnetic lineament MFM1043	Span estimate refers to the general position of the central part of the zone on the surface
Orientation (strike/dip)	115/90	± 5/± 10	High for strike, low for dip	Strike based on trend of lineament MFM1043. Dip based on comparison with high confidence, vertical and steeply-dipping zones with NW strike	
Thickness	5 m	± 3 m	Low	Estimated on basis of length – thickness correlation diagram	Thickness refers to total zone thickness (ductile and brittle, transition zone and core)
Length	310 m	± 25 m	Medium	Low magnetic lineament MFM1043. Truncated by ZFMNW0809 and ZFMNE0062A	Total length at ground surface
Ductile deformation			Low	Comparison with high confidence, vertical and steeply-dipping zones with NW strike	Assumed to be present
Brittle deformation			Low	Comparison with high confidence, vertical and steeply-dipping zones with NW strike	Assumed to be present
Alteration			Medium	Character of lineament MFM1043	Red-stained bedrock with fine-grained hematite dissemination
Fracture orientation					
Fracture frequency					
Fracture filling					

Vertical and steeply, SW-dipping brittle and ductile deformation zones with NW strike, based solely on lineament and comparison studies

ZFMNW1053

Property	Quantitative estimate	Span	Confidence level	Basis for interpretation	Comments
At the surface, replaced part of linked lineament XFM1053A0 by low magnetic lineament MFM1053. Modelled at depth using an assumed dip of 90° based on a comparison with high confidence, vertical and steeply dipping zones with NW strike					
Confidence of occurrence: Low					
Position		± 20 m	High	Low magnetic lineament MFM1053	Span estimate refers to the general position of the central part of the zone on the surface
Orientation (strike/dip)	125/90	± 5/± 10	High for strike, low for dip	Strike based on trend of lineament MFM1053. Dip based on comparison with high confidence, vertical and steeply-dipping zones with NW strike	
Thickness	10 m	± 5 m	Low	Estimated on basis of length – thickness correlation diagram	Thickness refers to total zone thickness (ductile and brittle, transition zone and core)
Length	1,108 m	± 50 m	Medium	Low magnetic lineament MFM1053. Truncated at both ends by ZFMNW0809	Total length at ground surface
Ductile deformation			Low	Comparison with high confidence, vertical and steeply-dipping zones with NW strike	Assumed to be present
Brittle deformation			Low	Comparison with high confidence, vertical and steeply-dipping zones with NW strike	Assumed to be present
Alteration			Medium	Character of lineament MFM1053	Red-stained bedrock with fine-grained hematite dissemination
Fracture orientation					
Fracture frequency					
Fracture filling					

Vertical and steeply, SW-dipping brittle and ductile deformation zones with NW strike, based solely on lineament and comparison studies

ZFMNW1054

Property	Quantitative estimate	Span	Confidence level	Basis for interpretation	Comments
At the surface, replaced linked lineament XFM1054A0 by low magnetic lineament MFM1054. Modelled at depth using an assumed dip of 90° based on a comparison with high confidence, vertical and steeply dipping zones with NW strike					
Confidence of occurrence: Low					
Position		± 20 m	High	Low magnetic lineament MFM1054	Span estimate refers to the general position of the central part of the zone on the surface
Orientation (strike/dip)	110/90	± 15± 10	High for strike, low for dip	Strike based on trend of lineament MFM1054. Dip based on comparison with high confidence, vertical and steeply-dipping zones with NW strike	
Thickness	5 m	± 3 m	Low	Estimated on basis of length – thickness correlation diagram	Thickness refers to total zone thickness (ductile and brittle, transition zone and core)
Length	262 m	± 25 m	Medium	Low magnetic lineament MFM1054. Truncated by ZFMNE0060A	Total length at ground surface
Ductile deformation			Low	Comparison with high confidence, vertical and steeply-dipping zones with NW strike	Assumed to be present
Brittle deformation			Low	Comparison with high confidence, vertical and steeply-dipping zones with NW strike	Assumed to be present
Alteration			Medium	Character of lineament MFM1054	Red-stained bedrock with fine-grained hematite dissemination
Fracture orientation					
Fracture frequency					
Fracture filling					

Vertical and steeply, SW-dipping brittle and ductile deformation zones with NW strike, based solely on lineament and comparison studies

ZFMNW1056

Property	Quantitative estimate	Span	Confidence level	Basis for interpretation	Comments
At the surface, replaced and extended to the SE linked lineament XFM1056A0 by low magnetic lineament MFM1056. Modelled at depth using an assumed dip of 90° based on a comparison with high confidence, vertical and steeply dipping zones with NW strike					
Confidence of occurrence: Low					
Position		± 20 m	High	Low magnetic lineament MFM1056	Span estimate refers to the general position of the central part of the zone on the surface
Orientation (strike/dip)	125/90	± 5/± 10	High for strike, low for dip	Strike based on trend of lineament MFM1056. Dip based on comparison with high confidence, vertical and steeply-dipping zones with NW strike	
Thickness	5 m	± 3 m	Low	Estimated on basis of length – thickness correlation diagram	Thickness refers to total zone thickness (ductile and brittle, transition zone and core)
Length	975 m	± 50 m	Medium	Low magnetic lineament MFM1056. Truncated by ZFMNW809, ZFMNE0814 and, at depth, by ZFMNE0062A	Total length at ground surface
Ductile deformation			Low	Comparison with high confidence, vertical and steeply-dipping zones with NW strike	Assumed to be present
Brittle deformation			Low	Comparison with high confidence, vertical and steeply-dipping zones with NW strike	Assumed to be present
Alteration			Medium	Character of lineament MFM1056	Red-stained bedrock with fine-grained hematite dissemination
Fracture orientation					
Fracture frequency					
Fracture filling					

Vertical and steeply, SW-dipping brittle and ductile deformation zones with NW strike, based solely on lineament and comparison studies

ZFMNW1068

Property	Quantitative estimate	Span	Confidence level	Basis for interpretation	Comments
At the surface, replaced part of linked lineament XFM1068A0 by lineament MFM1068. This lineament is defined by a depression in the bedrock surface, the form of which has been recognised on the basis of an analysis of old refraction seismic data /Isaksson and Keisu 2005/. Possible correlation also with a low velocity seismic refraction anomaly (/Isaksson and Keisu 2005/, RSLV02 in Figure 5-33 in /SKB 2005a/). Modelled at depth using an assumed dip of 90° based on a comparison with high confidence, vertical and steeply dipping zones with NW strike					
Confidence of occurrence: Low					
Position		± 20 m	High	Bedrock surface lineament MFM1068, seismic refraction data	Span estimate refers to the general position of the central part of the zone on the surface
Orientation (strike/dip)	120/90	± 5/± 10	High for strike, low for dip	Strike based on trend of bedrock surface lineament MFM1068. Dip based on comparison with high confidence, vertical and steeply-dipping zones with NW strike	
Thickness	5 m	± 3 m	Low	Estimated on basis of length – thickness correlation diagram	Thickness refers to total zone thickness (ductile and brittle, transition zone and core)
Length	994 m	± 50 m	Medium	Bedrock surface lineament MFM1068. Truncated by ZFMNS0100 and ZFMNE0810	Total length at ground surface
Ductile deformation			Low	Comparison with high confidence, vertical and steeply-dipping zones with NW strike	Assumed to be present
Brittle deformation			Medium	Seismic refraction data, comparison with high confidence, vertical and steeply-dipping zones with NW strike	Assumed to be present
Alteration					
Fracture orientation					
Fracture frequency					
Fracture filling					

Vertical and steeply, SW-dipping brittle and ductile deformation zones with NW strike, based solely on lineament and comparison studies

ZFMNW1088

Property	Quantitative estimate	Span	Confidence level	Basis for interpretation	Comments
At the surface, replaced and extended to SE linked lineament XFM1088A0 by low magnetic lineament MFM1088. Old ground geophysical data from FMV utilised /Isaksson and Keisu 2005/. Modelled at depth using an assumed dip of 90° based on a comparison with high confidence, vertical and steeply dipping zones with NW strike					
Confidence of occurrence: Low					
Position		± 20 m	High	Low magnetic lineament MFM1088	Span estimate refers to the general position of the central part of the zone on the surface
Orientation (strike/dip)	155/90	± 5/± 10	High for strike, low for dip	Strike based on trend of lineament MFM1088. Dip based on comparison with high confidence, vertical and steeply-dipping zones with NW strike	
Thickness	5 m	± 3 m	Low	Estimated on basis of length – thickness correlation diagram	Thickness refers to total zone thickness (ductile and brittle, transition zone and core)
Length	470 m	± 25 m	Medium	Low magnetic lineament MFM1088. Truncated by ZFMNE0810 and ZFMNE1092	Total length at ground surface
Ductile deformation			Low	Comparison with high confidence, vertical and steeply-dipping zones with NW strike	Assumed to be present
Brittle deformation			Low	Comparison with high confidence, vertical and steeply-dipping zones with NW strike	Assumed to be present
Alteration			Medium	Character of lineament MFM1088	Red-stained bedrock with fine-grained hematite dissemination
Fracture orientation					
Fracture frequency					
Fracture filling					

Vertical and steeply, SW-dipping brittle and ductile deformation zones with NW strike, based solely on lineament and comparison studies

ZFMNW1093

Property	Quantitative estimate	Span	Confidence level	Basis for interpretation	Comments
At the surface, replaced linked lineament XFM1093A0 by lineament MFM1093. This lineament is defined by a depression in the bedrock surface, the form of which has been recognised on the basis of an analysis of old refraction seismic data /Isaksson and Keisu 2005/. Modelled at depth using an assumed dip of 90° based on a comparison with high confidence, vertical and steeply dipping zones with NW strike					
Confidence of occurrence: Low					
Position		± 20 m	High	Bedrock surface lineament MFM1093	Span estimate refers to the general position of the central part of the zone on the surface
Orientation (strike/dip)	135/90	± 5/± 10	High for strike, low for dip	Strike based on trend of bedrock surface lineament MFM1093. Dip based on comparison with high confidence, vertical and steeply-dipping zones with NW strike	
Thickness	5 m	± 3 m	Low	Estimated on basis of length – thickness correlation diagram	Thickness refers to total zone thickness (ductile and brittle, transition zone and core)
Length	529 m	± 25 m	Medium	Bedrock surface lineament MFM1093. Truncated by ZFMNW0137	Total length at ground surface
Ductile deformation			Low	Comparison with high confidence, vertical and steeply-dipping zones with NW strike	Assumed to be present
Brittle deformation			Low	Comparison with high confidence, vertical and steeply-dipping zones with NW strike	Assumed to be present
Alteration					
Fracture orientation					
Fracture frequency					
Fracture filling					

Vertical and steeply, SW-dipping brittle and ductile deformation zones with NW strike, based solely on lineament and comparison studies

ZFMNW1094

Property	Quantitative estimate	Span	Confidence level	Basis for interpretation	Comments
At the surface, replaced part of linked lineament XFM1094A0 by low magnetic lineament MFM1094. New segment added to the ESE. Modelled at depth using an assumed dip of 90° based on a comparison with high confidence, vertical and steeply dipping zones with NW strike					
Confidence of occurrence: Low					
Position		± 20 m	High	Low magnetic lineament MFM1094	Span estimate refers to the general position of the central part of the zone on the surface
Orientation (strike/dip)	115/90	± 5/± 10	High for strike, low for dip	Strike based on trend of lineament MFM1094. Dip based on comparison with high confidence, vertical and steeply-dipping zones with NW strike	
Thickness	5 m	± 3 m	Low	Estimated on basis of length – thickness correlation diagram	Thickness refers to total zone thickness (ductile and brittle, transition zone and core)
Length	810 m	± 50 m	Medium	Low magnetic lineament MFM1094. Truncated by ZFMNW0137	Total length at ground surface
Ductile deformation			Low	Comparison with high confidence, vertical and steeply-dipping zones with NW strike	Assumed to be present
Brittle deformation			Low	Comparison with high confidence, vertical and steeply-dipping zones with NW strike	Assumed to be present
Alteration			Medium	Character of lineament MFM1094	Red-stained bedrock with fine-grained hematite dissemination
Fracture orientation					
Fracture frequency					
Fracture filling					

Vertical and steeply, SW-dipping brittle and ductile deformation zones with NW strike, based solely on lineament and comparison studies

ZFMNW1198

Property	Quantitative estimate	Span	Confidence level	Basis for interpretation	Comments
At the surface, replaced parts of linked lineaments XFM0045A0, XFM0127A0 and XFM0166A0 by low magnetic lineament MFM1198. Possible correlation also with low velocity seismic refraction anomalies at the north-western end of the lineament (/Isaksson and Keisu 2005/, RSLV04 in Figure 5-33 in /SKB 2005a/). Modelled at depth using an assumed dip of 90° based on a comparison with high confidence, vertical and steeply dipping zones with NW strike					
Confidence of occurrence: Low					
Position		± 20 m	High	Low magnetic lineament MFM1198	Span estimate refers to the general position of the central part of the zone on the surface
Orientation (strike/dip)	155/90	± 5/± 10	High for strike, low for dip	Strike based on trend of lineament MFM1198. Dip based on comparison with high confidence, vertical and steeply-dipping zones with NW strike	
Thickness	10 m	± 5 m	Low	Comparison with high confidence, vertical and steeply-dipping, regional zones with NW strike	Thickness refers to total zone thickness (ductile and brittle, transition zone and core)
Length	1,433 m	± 100 m	Medium	Low magnetic lineament MFM1198. Truncated by ZFMNE1061 and ZFMNE0060A	Total length at ground surface
Ductile deformation			Low	Comparison with high confidence, vertical and steeply-dipping zones with NW strike	Assumed to be present
Brittle deformation			Low	Comparison with high confidence, vertical and steeply-dipping zones with NW strike	Assumed to be present
Alteration			Medium	Character of lineament MFM1198	Red-stained bedrock with fine-grained hematite dissemination
Fracture orientation					
Fracture frequency					
Fracture filling					

Vertical and steeply, SW-dipping brittle and ductile deformation zones with NW strike, based solely on lineament and comparison studies

ZFMNW1199

Property	Quantitative estimate	Span	Confidence level	Basis for interpretation	Comments
At the surface, replaced parts of linked lineaments XFM0047A0, XFM0098A0, XFM0127A0, XFM0134A0, XFM0163A0, XFM0402A0 and XFM0733A0 by low magnetic lineament MFM1199. Correlates to part of lineament LL0060 in the alternative lineament interpretation /Korhonen et al. 2004/. Modelled at depth using an assumed dip of 90° based on a comparison with high confidence, vertical and steeply dipping zones with NW strike					
Confidence of occurrence: Low					
Position		± 20 m	High	Low magnetic lineament MFM1199	Span estimate refers to the general position of the central part of the zone on the surface
Orientation (strike/dip)	135/90	± 5/± 10	High for strike, low for dip	Strike based on trend of lineament MFM1199. Dip based on comparison with high confidence, vertical and steeply-dipping zones with NW strike	
Thickness	10 m	± 5 m	Low	Comparison with high confidence, vertical and steeply-dipping, regional zones with NW strike	Thickness refers to total zone thickness (ductile and brittle, transition zone and core)
Length	2,192 m	± 100 m	Medium	Low magnetic lineament MFM1199. Truncated to east against ZFMNE0061A and ZFMNE0061C	Total length at ground surface
Ductile deformation			Low	Comparison with high confidence, vertical and steeply-dipping zones with NW strike	Assumed to be present
Brittle deformation			Low	Comparison with high confidence, vertical and steeply-dipping zones with NW strike	Assumed to be present
Alteration			Medium	Character of lineament MFM1199	Red-stained bedrock with fine-grained hematite dissemination
Fracture orientation					
Fracture frequency					
Fracture filling					

Vertical and steeply-dipping brittle deformation zones with NE strike

ZFMNE0060A (DZ4 in KFM06A)/ZFMNE0060B1 and ZFMNE0060B2 (DZ2/DZ3 and borehole interval 245–260 m in KFM06A)

Property	Quantitative estimate	Span	Confidence level	Basis for interpretation	Comments
At the surface, replaced linked lineament XFM0060A0 by low magnetic lineament MFM0060. ZFMNE060A modelled at depth by connecting lineament MFM0060 at the surface with the borehole interval 318–358 m in KFM06A (DZ4). ZFMNE0060B modelled as a structure that, at depth, diverges and attaches to ZFMNE0060A along its eastern side (synthetic Reidel and P shears?). For this reason, ZFMNE0060B is made up of two components in the model, ZFMNE0060B1 and ZFMNE0060B2. It intersects KFM06A along borehole interval 195–278 m, including DZ2, DZ3 and the less fractured rock along the short interval 245–260 m. The gently dipping zone ZFMNS00B7 is also modelled to intersect borehole KFM06A along DZ4. For this reason, there are difficulties to separate the influence of zones ZFMNE0060A and ZFMNS00B7 along this borehole interval					
Confidence of occurrence: High					
Position		± 20 m	High	ZFMNE0060A: Intersection along KFM06A (DZ4), low magnetic lineament MFM0060. ZFMNE0060A also intersects HFM09 (DZ1)	Span estimate refers to the general position of the central part of the zone ZFMNE0060A on the surface. Span reduces to ± 1 m in the bedrock volume close to KFM06A.
Orientation (strike/dip)	ZFMNE0060A = 239/85	± 5/± 10	High	Strike based on trend of lineament MFM0060. Dip based on linking MFM0060 at the surface with borehole intersection DZ4 in KFM06A	
Thickness	ZFMNE0060A = 20 m ZFMNE0060B = 29 m		Medium	Intersections along KFM06A (DZ2, DZ3 and DZ4 and less fractured rock along borehole interval 245–260 m)	Thickness refers to total zone thickness (transition zone and core)
Length	ZFMNE0060A = 3,120 m ZFMNE0060B = 377 m	ZFMNE0060A = ± 200 m	Medium	Low magnetic lineament MFM0060. Truncated by ZFMNW0809 and ZFMNW0003	Total length at ground surface
Ductile deformation			High	Intersections along KFM06A (DZ2, DZ3 and DZ4)	Not present
Brittle deformation			High	Intersections along KFM06A (DZ2, DZ3 and DZ4)	Present
Alteration			High	Intersections along KFM06A (DZ2, DZ3 and DZ4), character of lineament MFM0060	Red-stained bedrock with fine-grained hematite dissemination
Fracture orientation	Fisher mean of NE fracture set = 210/85 Fisher mean of sub-horizontal set = 070/5	K value of NE fracture set = 17 K value of sub-horizontal fracture set = 12	Medium	Intersections along KFM06A (DZ2, DZ3 and DZ4), N=835	Two sets of fractures are conspicuous. One of these sets strikes NE and dips steeply to the NW, the other is sub-horizontal. Fractures that strike NS and dip steeply to the east are also present
Fracture frequency	ZFMNE0060A Mean = 10 m^{-1} ZFMNE0060B Mean = 7 m^{-1}	ZFMNE0060A 2–20 m^{-1} ZFMNE0060B 1–18 m^{-1}	Medium	Intersections along KFM06A (DZ2, DZ3 and DZ4)	Dominance of sealed fractures. Open fractures only significant in the sub-horizontal set. Mean value and span exclude sealed fracture networks at several short intervals. Note especially borehole intervals 268–271 m along DZ3 and 323–326 m along DZ4. Crushed rock also excluded. Procedure implemented due to uncertainty in the estimation of fracture frequency in these structures
Fracture filling			Medium	Intersections along KFM06A (DZ2, DZ3 and DZ4)	Calcite and chlorite in all sets of fractures; hematite/ adularia, quartz, and prehnite predominantly in the steeply dipping fractures but also in the sub-horizontal fractures; clay minerals predominantly in the sub-horizontal fractures but also in the steeply dipping fractures

Vertical and steeply-dipping brittle deformation zones with NE strike

ZFMNE0061A (DZ7/DZ8 and borehole interval 775–788 m in KFM06A)/ZFMNE0061B1 and ZFMNE0061B2 (DZ9/DZ10/DZ11 and borehole intervals 905–925 m and 933–950 m in KFM06A)/ZFMNE0061C (DZ3 in KFM01A and DZ5/DZ6 and borehole interval 624–652 m in KFM06A)

Property	Quantitative estimate	Span	Confidence level	Basis for interpretation	Comments
At the surface, replaced linked lineament XFM0061A0 by low magnetic lineament MFM0061. ZFMNE061A modelled at depth by connecting lineament MFM0061 at the surface with the borehole interval 740–810 m in KFM06A (DZ7, DZ8 and the less fractured rock along the short interval 775–788 m). ZFMNE0061B modelled as a structure that, at depth, diverges and attaches to ZFMNE0061A along its western side (synthetic Reidel and P shears?). For this reason, ZFMNE0061B is made up of two components in the model, ZFMNE0061B1 and ZFMNE0061B2. It intersects KFM06A along borehole interval 882–990 m (DZ9, DZ10, DZ11 and the less fractured rock along the short intervals 905–925 m and 933–950 m). ZFMNE0061C modelled as a minor, transfer structure between zones ZFMNE0060A and ZFMNE0061A. Zone ZFMNE0061C intersects borehole KFM01A along the borehole interval 639–684 m (DZ3) and borehole KFM06A along the interval 619–656 m (DZ5, DZ6 and the less fractured rock along the short borehole interval 624–652 m). Only zone ZFMNE0061A is inferred to intersect the surface					
Confidence of occurrence: High					
Position		± 20 m	High	ZFMNE0061A: Intersection along KFM06A (DZ7 and DZ8 and the short borehole interval 775–788 m), linked lineament XFM0061A0	Span estimate refers to the general position of the central part of zone ZFMNE0061A on the surface. Span reduces to ± 1 m in the bedrock volume close to KFM06A
Orientation (strike/dip)	ZFMNE0061A = 069/90	± 5/± 10	High	Strike based on trend of lineament MFM0061. Dip based on linking MFM0061 at the surface with borehole intersection DZ7, DZ8 and the short borehole interval 775–788 m in KFM06A	
Thickness	ZFMNE0061A = 38 m ZFMNE0061B = 40 m ZFMNE0061C = 14 m		Medium	Intersections along KFM01A (DZ3) and KFM06A (DZ5, DZ6, DZ7, DZ8, DZ9, DZ10 DZ11 and less fractured rock along borehole intervals between DZ5 and DZ6, between DZ7 and DZ8, and between DZ9 and DZ11)	Thickness refers to total zone thickness (transition zone and core)
Length	ZFMNE0061A = 2,046 m	± 100 m	Medium	Linked lineament XFM0061A0. Truncated at depth against ZFMNW0044 and ZFMNW1200	Total length at ground surface
Ductile deformation			High	Intersections along KFM01A (DZ3) and KFM06A (DZ5, DZ6, DZ7, DZ8, DZ9, DZ10 DZ11)	Not present
Brittle deformation			High	Intersections along KFM01A (DZ3) and KFM06A (DZ5, DZ6, DZ7, DZ8, DZ9, DZ10 DZ11)	Present
Alteration			High	Intersections along KFM01A (DZ3) and KFM06A (DZ5, DZ6, DZ7, DZ8, DZ9, DZ10 DZ11), character of lineament MFM0061	Red-stained bedrock with fine-grained hematite dissemination

Fracture orientation	ZFMNE0061A: Fisher mean of NE fracture set = 030/90 ZFMNE0061A: Fisher mean of ENE fracture set = 255/80 ZFMNE0061B: Fisher mean of NE fracture set = 025/85 ZFMNE0061B: Fisher mean of ENE fracture set = 250/75 ZFMNE0061C: Fisher mean of NE fracture set = 040/80	ZFMNE0061A: K value of NE fracture set = 30 ZFMNE0061A: K value of ENE fracture set = 30 ZFMNE0061B: K value of ENE fracture set = 20 ZFMNE0061B: K value of ENE fracture set = 55 ZFMNE0061C: K value of NE fracture set = 40	Medium	ZFMNE0061A: Intersection along KFM06A (DZ7, DZ8), N=452 ZFMNE0061B: Intersection along KFM06A (DZ9, DZ10, DZ11), N=359 ZFMNE0061C: Intersections along KFM01A (DZ3) and KFM06A (DZ5, DZ6), N=330	Steeply dipping fracture set with NE strike dominates in all the zones. In both ZFMNE0061A and ZFMNE0061B, a subordinate steeply dipping set with ENE strike is also present. Fractures in other orientations, including a gently dipping fracture set, are also present in all three zones
Fracture frequency	ZFMNE0061A: Mean 6 m^{-1} ZFMNE0061B: Mean 9 m^{-1} ZFMNE0061C: Mean 6 m^{-1}	ZFMNE0061A: Span 0–17 m^{-1} ZFMNE0061B: Span 2–18 m^{-1} ZFMNE0061C: Span 0–15 m^{-1}	Medium	ZFMNE0061A: Intersection along KFM06A (DZ7, DZ8) ZFMNE0061B: Intersection along KFM06A (DZ9, DZ10, DZ11) ZFMNE0061C: Intersections along KFM01A (DZ3) and KFM06A (DZ5, DZ6)	Dominance of sealed fractures. Mean value and span exclude sealed fracture networks at several intervals in KFM06A. Crushed rock along interval 770–771 m in DZ7 (ZFMNE0061A) also excluded. Procedure implemented due to uncertainty in the estimation of fracture frequency in these structures
Fracture filling			Medium	ZFMNE0061A, -61B: Intersection along KFM06A (DZ7, DZ8, DZ9, DZ10, DZ11) ZFMNE0061C: Intersections along KFM01A (DZ3) and KFM06A (DZ5, DZ6)	ZFMNE0061A, -61B: Chlorite, calcite, quartz, hematite/ adularia, laumontite. Note in ZFMNE0061B, hematite/ adularia is conspicuous in the NE and gently dipping sets, while laumontite is conspicuous in all sets ZFMNE0061C: Laumontite, chlorite, calcite, quartz, hematite/adularia

Vertical and steeply-dipping brittle deformation zones with NE strike

ZFMNE0062A (DZ5 and borehole interval 950–992 m in KFM05A)/ZFMNE0062B1 and ZFMNE0062B2 (DZ4 in KFM05A)

Property	Quantitative estimate	Span	Confidence level	Basis for interpretation	Comments
At the surface, replaced linked lineament XFM0062A0 by low magnetic lineament MFM0062. ZFMNE062A modelled at depth by connecting lineament MFM0062 at the surface with the borehole interval 936–992 m in KFM05A (DZ5 and extension 950–992 m). ZFMNE0062B modelled as a structure that, at depth, diverges and attaches to ZFMNE0062A along its western side (synthetic Reidel and P shears?). For this reason, ZFMNE0062B is made up of two components in the model, ZFMNE0062B1 and ZFMNE0062B2. It intersects KFM05A along the borehole interval 892–916 m (DZ4)					
Confidence of occurrence: High					
Position		± 20 m	High	ZFMNE0062A: Intersection along KFM05A (DZ5 and borehole interval 950–992 m), low magnetic lineament MFM0060. ZFMNE0062B: Intersection along KFM05A (DZ4).	Span estimate refers to the general position of the central part of the zone on the surface. Span reduces to ± 1 m in the bedrock volume close to KFM05A
Orientation (strike/dip)	ZFMNE0062A = 236/70	± 5/± 10	High	Strike based on trend of lineament MFM0062. Dip based on linking MFM0062 at the surface with borehole intersection DZ5 in KFM05A	
Thickness	ZFMNE0062A = 36 m ZFMNE0060B = 19 m		Medium	Intersections along KFM05A (DZ4, DZ5 and borehole interval 950–992 m)	Thickness refers to total zone thickness (transition zone and core)
Length	ZFMNE0062A = 3,358 m	± 200 m	Medium	Low magnetic lineament MFM0062. Truncated against ZFMNW0001 and ZFMNW0123	Total length at ground surface
Ductile deformation			High	Intersections along KFM05A (DZ4, DZ5 and borehole interval 950–992 m)	Not present
Brittle deformation			High	Intersections along KFM05A (DZ4, DZ5 and borehole interval 950–992 m)	Present
Alteration			High	Intersections along KFM05A (DZ4, DZ5 and borehole interval 950–992 m), character of lineament MFM0062	Red-stained bedrock with fine-grained hematite dissemination
Fracture orientation	Fisher mean of NE fracture set = 050/90	K value of NE fracture set = 35	Medium	Intersections along KFM05A (DZ4, DZ5 and borehole interval 950–992 m), N=467	Only one fracture set in a NE strike direction is prominent. Other fracture orientations are present
Fracture frequency	ZFMNE062A Mean = 7 m^{-1} ZFMNE062B Mean = 8 m^{-1}	ZFMNE062A 0–19 m^{-1} ZFMNE062B 0–16 m^{-1}	Medium	Intersections along KFM05A (DZ4, DZ5 and borehole interval 950–992 m)	Dominance of sealed fractures. Quantitative estimate and span exclude several sealed fracture networks in both sub-zones, due to uncertainty in the estimation of fracture frequency in these networks
Fracture filling			Medium	Intersections along KFM05A (DZ4, DZ5 and borehole interval 950–992 m)	Calcite, chlorite, hematite/ adularia, laumontite, quartz

Vertical and steeply-dipping brittle deformation zones with NE strike

ZFMNE0103A, ZFMNE0103B1 and ZFMNE0103B2 (part of DZ3 in KFM05A)

Property	Quantitative estimate	Span	Confidence level	Basis for interpretation	Comments
At the surface, replaced part of linked lineament XFM0103A0 by low magnetic lineament MFM0103. ZFMNE0103A modelled at depth by connecting lineament MFM0103 at the surface with the borehole interval 685–720 m in KFM05A (part of DZ3). ZFMNE0103B modelled as a structure that, at depth, diverges and attaches to ZFMNE0103A along its western side (synthetic Reidel and P shears?). For this reason, ZFMNE0103B is made up of two components in the model, ZFMNE0103B1 and ZFMNE0103B2. It intersects KFM05A along the borehole interval 590–616 m (also part of DZ3)					
Confidence of occurrence: High					
Position		± 20 m	High	Intersections along KFM05A (590–616 m and 685–720 m borehole intervals in DZ3), low magnetic lineament MFM0103	Span estimate refers to the general position of the central part of the zone on the surface. Span reduces to ± 1 m in the bedrock volume close to KFM05A
Orientation (strike/dip)	ZFMNE0103A = 227/75	± 5/± 10	High	Strike based on trend of lineament MFM0103. Dip based on linking MFM0103 at the surface with borehole interval 685–720 m in KFM05A (part of DZ3)	
Thickness	22 m in sub-zone ZFMNE0103A and 14 m in sub-zone ZFMNE0103B		Medium	Intersections along KFM05A (590–616 m and 685–720 m borehole intervals in DZ3)	Thickness refers to total zone thickness (transition zone and core)
Length	ZFMNE0103A = 1,259 m	± 50 m	Medium	Low magnetic lineament MFM0103. ZFMNE103A truncated against ZFMNW0123	Total length at ground surface
Ductile deformation			High	Intersections along KFM05A (590–616 m and 685–720 m borehole intervals in DZ3)	Not present
Brittle deformation			High	Intersections along KFM05A (590–616 m and 685–720 m borehole intervals in DZ3)	Present
Alteration			High	Intersections along KFM05A (590–616 m and 685–720 m borehole intervals in DZ3), character of lineament MFM0103	Oxidized bedrock with fine-grained hematite dissemination. Consistent with low magnetic anomaly
Fracture orientation	Fisher mean of NE fracture set = 220/90 Fisher mean of NW fracture set = 330/85	K value of NE fracture set = 19 K value of NW fracture set = 15	Medium	Intersections along KFM05A (590–616 m and 685–720 m borehole intervals in DZ3), N=444	Fracture set with NE strike and steep dip is dominant. Subordinate fracture set with NW strike and steep dip, as well as fractures with more gentle dips are also present
Fracture frequency	Mean = 7 m^{-1} in sub-zone ZFMNE0103A and 11 m^{-1} in sub-zone ZFMNE0103B	Span = 0–18 m^{-1} in sub-zone ZFMNE0103A, 2–24 m^{-1} in sub-zone ZFMNE0103B	Medium	Intersections along KFM05A (590–616 m and 685–720 m borehole intervals in DZ3)	Dominance of sealed fractures. Quantitative estimate and span exclude several sealed fracture networks along predominanly the lower parts of both sub-zones, due to uncertainty in the estimation of fracture frequency in these networks
Fracture filling			Medium	Intersections along KFM05A (590–616 m and 685–720 m borehole intervals in DZ3)	Calcite, chlorite, laumontite, hematite/adularia, quartz

Vertical and steeply-dipping brittle deformation zones with NE strike

ZFMNE0159 (DZ3 in KFM07A)

Property	Quantitative estimate	Span	Confidence level	Basis for interpretation	Comments
At the surface, replaced the major part of linked lineament XFM0159A0 and the short linked lineament XFM0419A0 by low magnetic lineament MFM0159. ZFMNE0159A modelled at depth by connecting lineament MFM0159 at the surface with the borehole interval 417–422 m in KFM07A					
Confidence of occurrence: High					
Position		± 20 m	High	Intersection along DZ3 in KFM07A, low magnetic lineament MFM0159	Span estimate refers to the general position of the central part of the zone on the surface. Span reduces to ± 1 m in the bedrock volume close to KFM07A
Orientation (strike/dip)	231/87	± 5/± 10	High	Strike based on trend of lineament MFM0159. Dip based on linking MFM0159 at the surface with DZ3 in KFM07A	
Thickness	2 m		Medium	Intersection along DZ3 in KFM07A	Thickness refers to total zone thickness (transition zone and core)
Length	1,790 m	± 100 m	Medium	Low magnetic lineament MFM0159. ZFMNE0159 truncated against ZFMNW0017 and ZFMNW1198	Total length at ground surface
Ductile deformation			High	Intersection along DZ3 in KFM07A	Not present
Brittle deformation			High	Intersection along DZ3 in KFM07A	Present
Alteration			High	Intersection along DZ3 in KFM07A, character of lineament MFM0159	Oxidized bedrock with fine-grained hematite dissemination. Consistent with low magnetic anomaly
Fracture orientation	Fisher mean of NS fracture set = 355/90	K value of NS fracture set = 23	Low	Intersection along DZ3 in KFM07A, N=57	Few data. Fracture set with steeply dipping fractures with NS strike dominates. Steeply dipping fractures with NE strike and some gently dipping fractures are also present
Fracture frequency	Mean = 13 m^{-1}	Span = 8–23 m^{-1}	Medium	Intersection along DZ3 in KFM07A	Dominance of sealed fractures. Quantitative estimate and span exclude a sealed fracture network at 419–420 m, due to uncertainty in the estimation of fracture frequency in these networks
Fracture filling			Low	Intersection along DZ3 in KFM07A	Few data. Calcite, chlorite, hematite/adularia, clay minerals

Vertical and steeply-dipping brittle deformation zones with NE strike

ZFMNE0401 (DZ2 and borehole interval 395–416 m in KFM05A)

Property	Quantitative estimate	Span	Confidence level	Basis for interpretation	Comments
At the surface, replaced the major part of linked lineament XFM0401A0 and the short linked lineament XFM0713A0 by low magnetic lineament MFM0401. ZFMNE0401A modelled at depth by connecting lineament MFM0401 at the surface with the borehole interval 395–436 m in KFM05A (DZ2 and borehole interval 395–416 m)					
Confidence of occurrence: High					
Position		± 20 m	High	Intersections along DZ2 and its extension (395–436 m) in KFM05A and DZ1 in HFM13, low magnetic lineament MFM0401	Span estimate refers to the general position of the central part of the zone on the surface. Span reduces to ± 1 m in the bedrock volume close to KFM05A
Orientation (strike/dip)	237/90	± 5/± 10	High	Strike based on trend of lineament MFM0401. Dip based on linking MFM0401 at the surface with borehole intersections DZ2 and its extension (395–436 m) in KFM05A and DZ1 in HFM13	
Thickness	3 m		Medium	Intersections along DZ2 and its extension (395–436 m) in KFM05A and DZ1 in HFM13	Thickness refers to total zone thickness (transition zone and core)
Length	1,371 m	± 50 m	Medium	Low magnetic lineament MFM0401. ZFMNE0401 truncated against ZFMNW0017, ZFMNS1202 and at depth against ZFMNE0103A	Total length at ground surface
Ductile deformation			High	Intersections along DZ2 and its extension (395–436 m) in KFM05A and DZ1 in HFM13	Not present
Brittle deformation			High	Intersections along DZ2 and its extension (395–436 m) in KFM05A and DZ1 in HFM13	Present
Alteration			High	Intersections along DZ2 and its extension (395–436 m) in KFM05A and DZ1 in HFM13	Oxidized bedrock with fine-grained hematite dissemination. Consistent with low magnetic anomaly
Fracture orientation	Fisher mean of NE fracture set = 235/85	K value of NE fracture set = 26	Medium	Intersections along DZ2 and its extension (395–436 m) in KFM05A and DZ1 in HFM13, N=268	Fracture set with NE strike direction and steep dip is dominant. Fractures with more gentle dips as well as steeply dipping fractures that strike NW and NS are also present
Fracture frequency	Mean = 7 m^{-1}	Span = 0–26 m^{-1}	Medium	Intersection along DZ2 and its extension (395–436 m) in KFM05A	Dominance of sealed fractures in KFM05A (DZ2 and extension). Approximately equal amounts of open and sealed fractures in HFM13 (DZ1). Quantitative estimate and span exclude some sealed fracture networks at several locations along KFM05A (DZ2 and extension), due to uncertainty in the estimation of fracture frequency in these networks
Fracture filling			Medium	Intersection along DZ2 and its extension (395–436 m) in KFM05A	Calcite, chlorite, hematite/ adularia, prehnite, laumontite, epidote (steeply dipping NW and gently dipping fractures) and clay minerals (steeply dipping NW and NE fractures, few gently dipping fractures)

Vertical and steeply-dipping brittle deformation zones with NE strike

ZFMNE0869 (Zone 3, SFR)

Property	Quantitative estimate	Span	Confidence level	Basis for interpretation	Comments
Adopted from structural geological model for SFR /Axelsson and Hansen 1997/					
Confidence of occurrence: High					
Position		± 1 m	High	Intersection along SFR tunnel and boreholes, seismic refraction data	Span estimate refers to the position of the central part of the zone in SFR tunnel and boreholes
Orientation (strike/dip)	200/90	± 5/± 10	Medium	Intersection along SFR tunnel	SSW/steep W in /Axelsson and Hansen 1997/
Thickness	10 m	± 1 m	High	Intersection along SFR tunnel	Composite zone consisting of several narrower high-strain segments (sub-zones) that diverge and converge in a complex pattern (see /Axelsson and Hansen 1997/). Thickness refers to total zone thickness (transition zone and core)
Length	958 m	± 50 m	High	Intersection along SFR tunnel and boreholes. Truncated along strike against ZFMNW0001 and ZFMNW0805	Total length at ground surface
Ductile deformation			High	Intersection along SFR tunnel and boreholes	Not present
Brittle deformation			High	Intersection along SFR tunnel and boreholes, seismic refraction data	Present
Alteration					
Fracture orientation					
Fracture frequency	15 m^{-1}	± 5/ m	High	Intersection along SFR boreholes	
Fracture filling					

Vertical and steeply-dipping brittle deformation zones with NE strike

ZFMNE0870 (Zone 9, SFR)

Property	Quantitative estimate	Span	Confidence level	Basis for interpretation	Comments
Adopted from structural geological model for SFR /Axelsson and Hansen 1997/					
Confidence of occurrence: High					
Position		± 1 m	High	Intersection along SFR tunnel and boreholes	Span estimate refers to the position of the central part of the zone in SFR tunnel and boreholes
Orientation (strike/dip)	230/90	± 5/± 10	Medium	Intersection along SFR tunnel	ENE/steep in /Axelsson and Hansen 1997/
Thickness	2 m	± 1 m	High	Intersection along SFR tunnel and boreholes	Thickness refers to total zone thickness (transition zone and core)
Length	1,022 m	± 50 m	High	Intersection along SFR tunnel and boreholes. Truncated along strike against ZFMNW0001 and ZFMNW0805	Total length at ground surface
Ductile deformation			Low	Intersection along SFR tunnel	Mylonite present. Significance uncertain
Brittle deformation			High	Intersection along SFR tunnel and boreholes	Present. Water-bearing, clayey gouge
Alteration					
Fracture orientation					
Fracture frequency	15 m^{-1}	± 5/ m	High	Intersection along SFR boreholes	
Fracture filling			High	Intersection along SFR tunnel	Clay minerals, chlorite, calcite, Fe-bearing mineral

Vertical and steeply-dipping brittle deformation zones with NE strike

ZFMNE1061 (borehole interval 250–315 m along DZ1 in KFM08A)

Property	Quantitative estimate	Span	Confidence level	Basis for interpretation	Comments
At the surface, replaced linked lineament XFM1061A0 by lineament MFM1061. This lineament is defined by a depression in the bedrock surface, the form of which has been recognised on the basis of an analysis of old refraction seismic data /Isaksson and Keisu 2005/. Possible correlation also with a low velocity seismic refraction anomaly (see /Isaksson and Keisu 2005/, Figure 5-33 in /SKB 2005a/). Zone ZFMNE1061 extended to the south-west as far as zone ZFMNW1068 and modelled at depth by connecting lineament MFM1061 at the surface with the borehole interval 250–315 m in KFM08A (part of DZ1). Possible interference with a zone related to linked lineament XFM1063A0 with NS trend (not modelled). Zone lies within and close to the area with poorer quality, airborne magnetic data					
Confidence of occurrence: High					
Position		± 20 m	Low	Intersection along borehole interval 250–315 m in KFM08A (part of DZ1), lineament MFM1061, seismic refraction data	Span estimate refers to the general position of the central part of the zone on the surface. Span reduces to ± 1 m in the bedrock volume close to KFM08A
Orientation (strike/dip)	060/78	± 5/± 10	Low	Strike based on trend of lineament MFM1061. Dip based on linking MFM1061 at the surface with borehole interval 250–315 m in KFM08A (part of DZ1)	See fracture orientation data
Thickness	44 m		Low	Intersection along borehole interval 250–315 m in KFM08A (part of DZ1)	Thickness refers to total zone thickness (transition zone and core). Anomalously high compared to length
Length	1,496 m	± 100 m	Low	Lineament MFM1061. ZFMNE1061 truncated against ZFMNW1068	Total length at ground surface
Ductile deformation			High	Intersection along borehole interval 250–315 m in KFM08A (part of DZ1)	Not present
Brittle deformation			High	Intersection along borehole interval 250–315 m in KFM08A (part of DZ1)	Present
Alteration			High	Intersection along borehole interval 250–315 m in KFM08A (part of DZ1)	Oxidized bedrock with fine-grained hematite dissemination
Fracture orientation	Fisher mean of SSW fracture set = 200/90 Fisher mean of NNW fracture set = 335/85	K value of SSW fracture set = 17 K value of NNW fracture set = 16	Medium	Intersection along borehole interval 250–315 m in KFM08A (part of DZ1), N=565	Variable fracture orientation. Steeply dipping SSW and NNW fractures as well as gently dipping fractures dominate
Fracture frequency	Mean = 10 m^{-1}	Span = 1–28 m^{-1}	Medium	Intersection along borehole interval 250–315 m in KFM08A (part of DZ1)	Dominance of sealed fractures. Quantitative estimate and span include a few sealed fracture networks with a fracture frequency up to 14 m^{-1}
Fracture filling			Medium	Intersection along borehole interval 250–315 m in KFM08A (part of DZ1)	Calcite, chlorite, laumontite, hematite/adularia, quartz

Vertical and steeply-dipping brittle deformation zones with NE strike

ZFMNE1188 (surface at drill site 4/DZ4 and borehole interval 290–370 m in KFM04A)

Property	Quantitative estimate	Span	Confidence level	Basis for interpretation	Comments
Zone ZFMNE1188 has been identified at the surface (drill site 4). Modelled at depth by connecting surface occurrence with borehole interval 290–370 m and DZ4 (borehole interval 412–462 m) in KFM04A. Zone strikes more or less parallel to borehole KFM04A and is situated along or close to the borehole					
Confidence of occurrence: High					
Position		± 1 m	High	Surface geology (drill site 4) and intersections along KFM04A (borehole interval 290–370 m and DZ4)	Span estimate refers to the position of the central part of the zone at drill site 4 and close to borehole KFM04A. Zone is located close to and strikes more or less parallel to borehole KFM04A
Orientation (strike/dip)	220/88	± 5/ ± 10	High	Surface geology (drill site 4) and intersections along KFM04A (290–370 m and DZ4)	
Thickness	3 m		High	Surface geology (drill site 4) and intersections along KFM04A (290–370 m and DZ4)	Thickness refers to total zone thickness (transition zone and core)
Length	607 m	± 25 m	Medium	Estimated length at surface after truncation along strike against ZFMNW0017 and ZFMNW0123	
Ductile deformation			High	Surface geology (drill site 4) and intersections along KFM04A (290–370 m and DZ4)	Present in KFM04A. NW strike. Surface data indicates that this deformation is probably older than and is not related to zone ZFMNE1188
Brittle deformation			High	Surface geology (drill site 4) and intersections along KFM04A (290–370 m and DZ4)	Present. Dextral horizontal component of movement at surface
Alteration			High	Surface geology (drill site 4) and intersections along KFM04A (290–370 m and DZ4)	Oxidized bedrock with fine-grained hematite dissemination
Fracture orientation	Fisher mean of NW fracture set = 135/85 Fisher mean of NE fracture set = 235/85	K value of NW fracture set = 16 K value of NE fracture set = 16	Medium	Intersections along KFM04A (290–370 m and DZ4), N=1022	Fracture set with NW strike dominates. Steeply dipping fractures with NE strike and more gently-dipping fractures are also present. Difficulties to interpret significance of fracture orientation data, since zone strikes more or less parallel to borehole KFM04A and is situated along or close to the borehole
Fracture frequency	Mean 10 m^{-1}	Span 2–24 m^{-1}	Medium	Intersections along KFM04A (290–370 m and DZ4)	Dominance of sealed fractures. Quantitative estimate and span exclude sealed fracture networks with abundant fractures along both the borehole interval 290–370 m and DZ4
Fracture filling			Medium	Intersections along KFM04A (290–370 m and DZ4)	Chlorite, calcite, hematite/ adularia, laumontite, clay minerals, quartz, prehnite, epidote (steeply dipping NW fractures)

Vertical and steeply-dipping brittle deformation zones with NE strike

ZFMNE1192 (DZ2 in KFM01A)

Property	Quantitative estimate	Span	Confidence level	Basis for interpretation	Comments
On the basis of fracture orientation, borehole interval 386–412 m in borehole KFM01A (DZ2) is modelled as a steeply dipping zone with NE strike. Zone fails to reach the surface. Truncated at depth against the adjacent zones ZFMNE0060A, ZFMNW0404, ZFMNW1199 and ZFMNE00A2					
Confidence of occurrence: High					
Position		± 1 m	High	Intersection along KFM01A (DZ2)	Span estimate refers to the position of the central part of the zone close to borehole KFM01A
Orientation (strike/dip)	073/82	± 5/± 10	Medium	Orientation of fractures along DZ2 in KFM01A	
Thickness	5 m		Medium	Intersection along KFM01A (DZ2)	Thickness refers to total zone thickness (transition zone and core)
Length	392 m	± 25 m		Truncated at depth against ZFMNE0060A, ZFMNW0404, ZFMNW1199 and ZFMNE00A2	Total length at ground surface
Ductile deformation			High	Intersection along KFM01A (DZ2)	Not present
Brittle deformation			High	Intersection along KFM01A (DZ2)	Present
Alteration			High	Intersection along KFM01A (DZ2)	Oxidized bedrock with fine-grained hematite dissemination
Fracture orientation	Fisher mean of NE fracture set = 070/80	K value of NE fracture set = 101	Medium	Intersection along KFM01A (DZ2), N=	Fracture set with NE strike and steep dip to the south-east is prominent. Gently dipping fractures are also present
Fracture frequency	Mean 4.5 m^{-1}	Span 1–8 m^{-1}	Medium	Intersection along KFM01A (DZ2)	Sealed and open fractures
Fracture filling			Medium	Intersection along KFM01A (DZ2)	Chlorite, laumontite, hematite/ adularia, calcite, quartz along NE steeply dipping fractures. Chlorite and occasional occurrences of other minerals along gently dipping fractures

Vertical and steeply-dipping brittle deformation zones with NE strike, based solely on lineament and comparison studies

ZFMNE0808A, -0808B, -0808C

Property	Quantitative estimate	Span	Confidence level	Basis for interpretation	Comments
At the surface, replaced linked lineament XFM0808A0 by low magnetic lineaments MFM0808A0, MFM0808B0 and MFM0808C0. Modelled to base of regional model volume using an assumed dip of 90° based on a comparison with high confidence, vertical and steeply dipping zones with NE strike. Only zone ZFMNW0808C lies inside the local model volume					
Confidence of occurrence: Medium					
Position		± 20 m	High	Low magnetic lineaments MFM0808A0, -0808B0 and -0808C0	Span estimate refers to the general position of the central part of the zone on the surface
Orientation (strike/dip)	ZFMNE0808A = 219/90, ZFMNE0808B = 226/90, ZFMNE0808C = 221/90	± 10/± 10	High for strike, low for dip	Strike based on trend of lineaments MFM0808A0, -0808B0 and -0808C0. Dip based on comparison with high confidence, vertical and steeply-dipping zones with NE strike	
Thickness	ZFMNE0808A 15 m, ZFMNE0808B 5 m, ZFMNE0808C 10 m	ZFMNE0808A ± 10 m, ZFMNE0808B ± 3 m, ZFMNE0808C ± 5 m	Low	Comparison with high confidence, vertical and steeply-dipping zones with NE strike	Thickness refers to total zone thickness (transition zone and core)
Length	ZFMNE0808A 4,080 m, ZFMNE0808B 452 m, ZFMNE0808C 1,157 m	ZFMNE0808A ± 200 m, ZFMNE0808B ± 100 m, ZFMNE0808C ± 100 m	Medium	Low magnetic lineaments MFM0808A0, -0808B0 and -0808C0. ZFMNE0808A truncated against ZFMNW0805. ZFMNE0808B truncated against ZFMNW0805 and ZFMNW1127. ZFMNE0808C truncated against ZFMNW0001 and ZFMNE0062A	Length of all components together at the ground surface
Ductile deformation			Low	Comparison with high confidence, vertical and steeply-dipping zones with NE strike	Assumed not to be present
Brittle deformation			Low	Comparison with high confidence, vertical and steeply-dipping zones with NE strike	Assumed to be present
Alteration			Medium	Character of lineaments MFM0808A0, -0808B0 and -0808C0	Red-stained bedrock with fine-grained hematite dissemination
Fracture orientation					
Fracture frequency					
Fracture filling					

Vertical and steeply-dipping brittle deformation zones with NE strike, based solely on lineament and comparison studies

ZFMNE0168

Property	Quantitative estimate	Span	Confidence level	Basis for interpretation	Comments
At the surface, replaced linked lineament XFM0168A0 by low magnetic lineament MFM0168. Modelled at depth using an assumed dip of 90° based on a comparison with high confidence, vertical and steeply dipping zones with NE strike					
Confidence of occurrence: Low					
Position		± 20 m	High	Low magnetic lineament MFM0168	Span estimate refers to the general position of the central part of the zone on the surface
Orientation (strike/dip)	245/90	± 5/± 10	High for strike, low for dip	Strike based on trend of lineament MFM0168. Dip based on comparison with high confidence, vertical and steeply-dipping zones with NE strike	
Thickness	5 m	± 3 m	Low	Estimated on basis of length – thickness correlation diagram	Thickness refers to total zone thickness (transition zone and core)
Length	604 m	± 25 m	Medium	Low magnetic lineament MFM0168. ZFMNW1198, ZFMNW0044 and ZFMNE0731	Total length at ground surface
Ductile deformation			Low	Comparison with high confidence, vertical and steeply-dipping zones with NE strike	Assumed not to be present
Brittle deformation			Low	Comparison with high confidence, vertical and steeply-dipping zones with NE strike	Assumed to be present
Alteration			Medium	Character of lineament MFM0168	Red-stained bedrock with fine-grained hematite dissemination
Fracture orientation					
Fracture frequency					
Fracture filling					

Vertical and steeply-dipping brittle deformation zones with NE strike, based solely on lineament and comparison studies

ZFMNE0169

Property	Quantitative estimate	Span	Confidence level	Basis for interpretation	Comments
At the surface, replaced linked lineament XFM0169A0 by low magnetic lineament MFM0169. Modelled at depth using an assumed dip of 90° based on a comparison with high confidence, vertical and steeply dipping zones with NE strike					
Confidence of occurrence: Low					
Position		± 20 m	High	Low magnetic lineament MFM0169	Span estimate refers to the general position of the central part of the zone on the surface
Orientation (strike/dip)	245/90	± 5/± 10	High for strike, low for dip	Strike based on trend of lineament MFM0169. Dip based on comparison with high confidence, vertical and steeply-dipping zones with NE strike	
Thickness	5 m	± 3 m	Low	Estimated on basis of length – thickness correlation diagram	Thickness refers to total zone thickness (transition zone and core)
Length	925 m	± 50 m	Medium	Low magnetic lineament MFM0169. Truncated by ZFMNE0062A and ZFMNW1199	Total length at ground surface
Ductile deformation			Low	Comparison with high confidence, vertical and steeply-dipping zones with NE strike	Assumed not to be present
Brittle deformation			Low	Comparison with high confidence, vertical and steeply-dipping zones with NE strike	Assumed to be present
Alteration			Medium	Character of lineament MFM0169	Red-stained bedrock with fine-grained hematite dissemination
Fracture orientation					
Fracture frequency					
Fracture filling					

Vertical and steeply-dipping brittle deformation zones with NE strike, based solely on lineament and comparison studies

ZFMNE0414

Property	Quantitative estimate	Span	Confidence level	Basis for interpretation	Comments
At the surface, replaced linked lineament XFM0414A0 by low magnetic lineament MFM0414. Modelled at depth using an assumed dip of 90° based on a comparison with high confidence, vertical and steeply dipping zones with NE strike					
Confidence of occurrence: Low					
Position		± 20 m	High	Low magnetic lineament MFM0414	Span estimate refers to the general position of the central part of the zone on the surface
Orientation (strike/dip)	225/90	± 5/± 10	High for strike, low for dip	Strike based on trend of lineament MFM0414. Dip based on comparison with high confidence, vertical and steeply-dipping zones with NE strike	
Thickness	5 m	± 3 m	Low	Estimated on basis of length – thickness correlation diagram	Thickness refers to total zone thickness (transition zone and core)
Length	336 m	± 25 m	Medium	Low magnetic lineament MFM0414. Truncated by ZFMNE0060A, ZFMNE0061C and ZFMNW1199	Total length at ground surface
Ductile deformation			Low	Comparison with high confidence, vertical and steeply-dipping zones with NE strike	Assumed not to be present
Brittle deformation			Low	Comparison with high confidence, vertical and steeply-dipping zones with NE strike	Assumed to be present
Alteration			Medium	Character of lineament MFM0414	Red-stained bedrock with fine-grained hematite dissemination
Fracture orientation					
Fracture frequency					
Fracture filling					

Vertical and steeply-dipping brittle deformation zones with NE strike, based solely on lineament and comparison studies

ZFMNE0717

Property	Quantitative estimate	Span	Confidence level	Basis for interpretation	Comments
At the surface, replaced linked lineament XFM0717A0 by low magnetic lineament MFM0717. Modelled at depth using an assumed dip of 90° based on a comparison with high confidence, vertical and steeply dipping zones with NE strike					
Confidence of occurrence: Low					
Position		± 20 m	High	Low magnetic lineament MFM0717	Span estimate refers to the general position of the central part of the zone on the surface
Orientation (strike/dip)	235/90	± 5/± 10	High for strike, low for dip	Strike based on trend of lineament MFM0717. Dip based on comparison with high confidence, vertical and steeply-dipping zones with NE strike	
Thickness	5 m	± 3 m	Low	Estimated on basis of length – thickness correlation diagram	Thickness refers to total zone thickness (transition zone and core)
Length	505 m	± 25 m	Medium	Low magnetic lineament MFM0717. Truncated by ZFMNW0017	Total length at ground surface
Ductile deformation			Low	Comparison with high confidence, vertical and steeply-dipping zones with NE strike	Assumed not to be present
Brittle deformation			Low	Comparison with high confidence, vertical and steeply-dipping zones with NE strike	Assumed to be present
Alteration			Medium	Character of lineament MFM0717	Red-stained bedrock with fine-grained hematite dissemination
Fracture orientation					
Fracture frequency					
Fracture filling					

Vertical and steeply-dipping brittle deformation zones with NE strike, based solely on lineament and comparison studies

ZFMNE0725

Property	Quantitative estimate	Span	Confidence level	Basis for interpretation	Comments
At the surface, replaced linked lineament XFM0725A0 by low magnetic lineament MFM0725. Modelled at depth using an assumed dip of 90° based on a comparison with high confidence, vertical and steeply dipping zones with NE strike					
Confidence of occurrence: Low					
Position		± 20 m	High	Low magnetic lineament MFM0725	Span estimate refers to the general position of the central part of the zone on the surface
Orientation (strike/dip)	195/90	± 5/± 10	High for strike, low for dip	Strike based on trend of lineament MFM0725. Dip based on comparison with high confidence, vertical and steeply-dipping zones with NE strike	
Thickness	5 m	± 3 m	Low	Estimated on basis of length – thickness correlation diagram	Thickness refers to total zone thickness (transition zone and core)
Length	351 m	± 25 m	Medium	Low magnetic lineament MFM0725. Truncated by ZFMNE0061A and ZFMNW0044	Total length at ground surface
Ductile deformation			Low	Comparison with high confidence, vertical and steeply-dipping zones with NE strike	Assumed not to be present
Brittle deformation			Low	Comparison with high confidence, vertical and steeply-dipping zones with NE strike	Assumed to be present
Alteration			Medium	Character of lineament MFM0725	Red-stained bedrock with fine-grained hematite dissemination
Fracture orientation					
Fracture frequency					
Fracture filling					

Vertical and steeply-dipping brittle deformation zones with NE strike, based solely on lineament and comparison studies

ZFMNE0731

Property	Quantitative estimate	Span	Confidence level	Basis for interpretation	Comments
At the surface, replaced linked lineament XFM0731A0 by low magnetic lineament MFM0731. Modelled at depth using an assumed dip of 90° based on a comparison with high confidence, vertical and steeply dipping zones with NE strike					
Confidence of occurrence: Low					
Position		± 20 m	High	Low magnetic lineament MFM0731	Span estimate refers to the general position of the central part of the zone on the surface
Orientation (strike/dip)	205/90	± 5/± 10	High for strike, low for dip	Strike based on trend of lineament MFM0731. Dip based on comparison with high confidence, vertical and steeply-dipping zones with NE strike	
Thickness	5 m	± 3 m	Low	Estimated on basis of length – thickness correlation diagram	Thickness refers to total zone thickness (transition zone and core)
Length	381 m	± 25 m	Medium	Low magnetic lineament MFM0731. ZFMNW0044, ZFMNW0809 and ZFMNE0168	Total length at ground surface
Ductile deformation			Low	Comparison with high confidence, vertical and steeply-dipping zones with NE strike	Assumed not to be present
Brittle deformation			Low	Comparison with high confidence, vertical and steeply-dipping zones with NE strike	Assumed to be present
Alteration			Medium	Character of lineament MFM0731	Red-stained bedrock with fine-grained hematite dissemination
Fracture orientation					
Fracture frequency					
Fracture filling					

Vertical and steeply-dipping brittle deformation zones with NE strike, based solely on lineament and comparison studies

ZFMNE0810

Property	Quantitative estimate	Span	Confidence level	Basis for interpretation	Comments
At the surface, replaced linked lineament XFM0810A0 by lineament MFM0810. This lineament is defined partly by a magnetic minimum and partly by a depression in the bedrock surface, the form of which has been recognised on the basis of an analysis of old refraction seismic data /Isaksson and Keisu 2005/. Modelled at depth using an assumed dip of 90° based on a comparison with high confidence, vertical and steeply dipping zones with NE strike					
Confidence of occurrence: Low					
Position		± 20 m	High	Lineament MFM0810	Span estimate refers to the general position of the central part of the zone on the surface
Orientation (strike/dip)	230/90	± 5/± 10	High for strike, low for dip	Strike based on trend of lineament MFM0810. Dip based on comparison with high confidence, vertical and steeply-dipping zones with NE strike	
Thickness	15 m	± 5 m	Low	Estimated on basis of length – thickness correlation diagram	Thickness refers to total zone thickness (transition zone and core)
Length	2,676 m	± 200 m	Medium	Lineament MFM0810. Truncated by ZFMNW0001 and ZFMNW0017	Total length at ground surface
Ductile deformation			Low	Comparison with high confidence, vertical and steeply-dipping zones with NE strike	Assumed not to be present
Brittle deformation			Low	Comparison with high confidence, vertical and steeply-dipping zones with NE strike	Assumed to be present
Alteration			Medium	Character of lineament MFM0810	Red-stained bedrock with fine-grained hematite dissemination
Fracture orientation					
Fracture frequency					
Fracture filling					

Vertical and steeply-dipping brittle deformation zones with NE strike, based solely on lineament and comparison studies

ZFMNE0811

Property	Quantitative estimate	Span	Confidence level	Basis for interpretation	Comments
At the surface, replaced linked lineament XFM0811A0 by low magnetic lineament MFM0811. Modelled at depth using an assumed dip of 90° based on a comparison with high confidence, vertical and steeply dipping zones with NE strike					
Confidence of occurrence: Low					
Position		± 20 m	High	Low magnetic lineament MFM0811	Span estimate refers to the general position of the central part of the zone on the surface
Orientation (strike/dip)	220/90	± 5/± 10	High for strike, low for dip	Strike based on trend of lineament MFM0811. Dip based on comparison with high confidence, vertical and steeply-dipping zones with NE strike	
Thickness	5 m	± 3 m	Low	Estimated on basis of length – thickness correlation diagram	Thickness refers to total zone thickness (transition zone and core)
Length	682 m	± 25 m	Medium	Low magnetic lineament MFM0811. Truncated by ZFMNW0809 and ZFMNW1198	Total length at ground surface
Ductile deformation			Low	Comparison with high confidence, vertical and steeply-dipping zones with NE strike	Assumed not to be present
Brittle deformation			Low	Comparison with high confidence, vertical and steeply-dipping zones with NE strike	Assumed to be present
Alteration			Medium	Character of lineament MFM0811	Red-stained bedrock with fine-grained hematite dissemination
Fracture orientation					
Fracture frequency					
Fracture filling					

Vertical and steeply-dipping brittle deformation zones with NE strike, based solely on lineament and comparison studies

ZFMNE0814

Property	Quantitative estimate	Span	Confidence level	Basis for interpretation	Comments
At the surface, replaced linked lineament XFM0814A0 by low magnetic lineament MFM0814. Modelled at depth using an assumed dip of 90° based on a comparison with high confidence, vertical and steeply dipping zones with NE strike					
Confidence of occurrence: Low					
Position		± 20 m	High	Low magnetic lineament MFM0814	Span estimate refers to the general position of the central part of the zone on the surface
Orientation (strike/dip)	205/90	± 5/± 10	High for strike, low for dip	Strike based on trend of lineament MFM0814. Dip based on comparison with high confidence, vertical and steeply-dipping zones with NE strike	
Thickness	5 m	± 3 m	Low	Estimated on basis of length – thickness correlation diagram	Thickness refers to total zone thickness (transition zone and core)
Length	459 m	± 25 m	Medium	Low magnetic lineament MFM0814. Truncated by ZFMNW0809 and ZFMNW0813	Total length at ground surface
Ductile deformation			Low	Comparison with high confidence, vertical and steeply-dipping zones with NE strike	Assumed not to be present
Brittle deformation			Low	Comparison with high confidence, vertical and steeply-dipping zones with NE strike	Assumed to be present
Alteration			Medium	Character of lineament MFM0814	Red-stained bedrock with fine-grained hematite dissemination
Fracture orientation					
Fracture frequency					
Fracture filling					

Vertical and steeply-dipping brittle deformation zones with NE strike, based solely on lineament and comparison studies

ZFMNE1057

Property	Quantitative estimate	Span	Confidence level	Basis for interpretation	Comments
At the surface, replaced linked lineament XFM1057A0 by lineament MFM1057. This lineament is defined partly by a magnetic minimum and partly by a depression in the bedrock surface /Isaksson and Keisu 2005/. Modelled at depth using an assumed dip of 90° based on a comparison with high confidence, vertical and steeply dipping zones with NE strike					
Confidence of occurrence: Low					
Position		± 20 m	High	Lineament MFM1057	Span estimate refers to the general position of the central part of the zone on the surface
Orientation (strike/dip)	245/90	± 5/± 10	High for strike, low for dip	Strike based on trend of lineament MFM1057. Dip based on comparison with high confidence, vertical and steeply-dipping zones with NE strike	
Thickness	5 m	± 3 m	Low	Estimated on basis of length – thickness correlation diagram	Thickness refers to total zone thickness (transition zone and core)
Length	753 m	± 50 m	Medium	Lineament MFM1057. Truncated by ZFMNW0813 and ZFMNW0835B	Total length at ground surface
Ductile deformation			Low	Comparison with high confidence, vertical and steeply-dipping zones with NE strike	Assumed not to be present
Brittle deformation			Low	Comparison with high confidence, vertical and steeply-dipping zones with NE strike	Assumed to be present
Alteration			Medium	Character of lineament MFM1057	Red-stained bedrock with fine-grained hematite dissemination
Fracture orientation					
Fracture frequency					
Fracture filling					

Vertical and steeply-dipping brittle deformation zones with NE strike, based solely on lineament and comparison studies

ZFMNE1092

Property	Quantitative estimate	Span	Confidence level	Basis for interpretation	Comments
At the surface, replaced linked lineament XFM1092A0 by lineament MFM1092. This lineament is defined by a depression in the bedrock surface, the form of which has been recognised on the basis of an analysis of old refraction seismic data /Isaksson and Keisu 2005/. Possible correlation also with a low velocity seismic refraction anomaly /Isaksson and Keisu 2005/. Modelled at depth using an assumed dip of 90° based on a comparison with high confidence, vertical and steeply dipping zones with NE strike.					
Confidence of occurrence: Low					
Position		± 20 m	High	Bedrock surface lineament MFM1092, seismic refraction data	Span estimate refers to the general position of the central part of the zone on the surface
Orientation (strike/dip)	205/90	± 5/± 10	High for strike, low for dip	Strike based on trend of bedrock surface lineament MFM1092. Dip based on comparison with high confidence, vertical and steeply-dipping zones with NW strike	
Thickness	5 m	± 3 m	Low	Estimated on basis of length – thickness correlation diagram	Thickness refers to total zone thickness (ductile and brittle, transition zone and core)
Length	785 m	± 50 m	Medium	Bedrock surface lineament MFM1092. Truncated by ZFMNW0137	Total length at ground surface
Ductile deformation			Low	Comparison with high confidence, vertical and steeply-dipping zones with NE strike	Assumed not to be present
Brittle deformation			Medium	Seismic refraction data, comparison with high confidence, vertical and steeply-dipping zones with NE strike	Assumed to be present
Alteration					
Fracture orientation					
Fracture frequency					
Fracture filling					

Vertical and steeply-dipping brittle deformation zones with NE strike, based solely on lineament and comparison studies

ZFMNE1197

Property	Quantitative estimate	Span	Confidence level	Basis for interpretation	Comments
At the surface, replaced linked lineament XFM0412A0 and part of linked lineament XFM0158A0 by low magnetic lineament MFM1197. Zone extended at surface as far as zone ZFMNE0159. Modelled at depth using an assumed dip of 90° based on a comparison with high confidence, vertical and steeply dipping zones with NE strike					
Confidence of occurrence: Low					
Position		± 20 m	High	Low magnetic lineament MFM1197	Span estimate refers to the general position of the central part of the zone on the surface
Orientation (strike/dip)	200/90	± 5/± 10	High for strike, low for dip	Strike based on trend of lineament MFM1197 and zone extension to ZFMNE0159. Dip based on comparison with high confidence, vertical and steeply-dipping zones with NE strike	
Thickness	5 m	± 3 m	Low	Estimated on basis of length – thickness correlation diagram	Thickness refers to total zone thickness (transition zone and core)
Length	697 m	± 50 m	Medium	Low magnetic lineament MFM1197. Truncated by ZFMNE0061A and ZFMNE0159	Total length at ground surface
Ductile deformation			Low	Comparison with high confidence, vertical and steeply-dipping zones with NE strike	Assumed not to be present
Brittle deformation			Low	Comparison with high confidence, vertical and steeply-dipping zones with NE strike	Assumed to be present
Alteration			Medium	Character of lineament MFM1197	Red-stained bedrock with fine-grained hematite dissemination
Fracture orientation					
Fracture frequency					
Fracture filling					

Vertical and steeply-dipping brittle deformation zones with NS strike

ZFMNS0100 (borehole interval 873–999 m along part of DZ4 in KFM07A)

Property	Quantitative estimate	Span	Confidence level	Basis for interpretation	Comments
At the surface, replaced linked lineament XFM0100A0 by low magnetic lineament MFM0100. Correlation also with a low velocity seismic refraction anomaly (/Isaksson and Keisu 2005/, RSLV01 in Figure 5-33 in /SKB 2005a/). Modelled at depth using dip estimated by connecting lineament MFM0100 at the surface with the borehole interval 873–999 m in KFM07A (part of DZ4). Possible interference along DZ4 also with the steeply dipping zones ZFMNE1061, ZFMNS1072 and ZFMNW1068. This interference may account for the anomalously high thickness estimate					
Confidence of occurrence: High					
Position		± 20 m	High	Intersection along borehole interval 873–999 m in KFM07A (part of DZ4), low magnetic lineament MFM0100, seismic refraction data	Span refers to general position of the zone core on surface. Span reduces to ± 1 m in the bedrock volume close to borehole KFM07A
Orientation (strike/dip)	172/88	± 5/± 10	High	Strike based on trend of lineament MFM0100. Dip based on linking MFM0100 at the surface with borehole intersection 873–999 m in KFM07A (part of DZ4)	
Thickness	67 m		Low	Intersection along borehole interval 873–999 m in KFM07A (part of DZ4)	Thickness refers to total zone thickness (transition zone and core). Possible interference with ZFMNE1061, ZFMNS1072 and ZFMNW1068 may explain the anomalously high thickness estimate
Length	931 m	± 50 m	Medium	Low magnetic lineament MFM0100. Truncated against ZFMNE0061A, ZFMNE1061 and ZFMNW1200	Total length at ground surface
Ductile deformation			High	Intersection along borehole interval 873–999 m in KFM07A (part of DZ4)	Present
Brittle deformation			High	Intersection along borehole interval 873–999 m in KFM07A (part of DZ4)	Present
Alteration			High	Intersection along borehole interval 873–999 m in KFM07A (part of DZ4), character of lineament MFM0100	Red-stained bedrock with fine-grained hematite dissemination
Fracture orientation	Fisher mean of NNW fracture set = 345/90 Fisher mean of NE fracture set = 215/90	K value of NNW fracture set = 20 K value of NE fracture set = 15	Medium	Intersection along borehole interval 873–999 m in KFM07A (part of DZ4), N=756	Variable orientation of fractures. Steeply dipping fractures that strike NNW dominate. Steeply dipping NE and gently dipping fractures are also present
Fracture frequency	Mean 10 m^{-1}	Span 0–30 m^{-1}	Medium	Intersection along borehole interval 873–999 m in KFM07A (part of DZ4)	Dominance of sealed fractures. Quantitative estimate and span exclude several sealed fracture networks and two crush zones (883 and 990 m), due to uncertainty in the estimation of fracture frequency in these structures
Fracture filling			Medium	Intersection along borehole interval 873–999 m in KFM07A (part of DZ4)	Chlorite, calcite, hematite/ adularia, laumontite, quartz. Clay minerals also present along steeply dipping NNW fractures

Vertical and steeply-dipping brittle deformation zones with NS strike

ZFMNS0431 (DZ1 in HFM22)

Property	Quantitative estimate	Span	Confidence level	Basis for interpretation	Comments
Modelled at depth using dip estimated by connecting lineament XFM0431A0 at the surface with DZ1 in HFM22. Possible interference of a minor zone that corresponds to linked lineament XFM00429A0					
Confidence of occurrence: High					
Position		± 20 m	High	Intersection along DZ1 in HFM22, linked lineament XFM0431A0	Span refers to general position of the zone core on surface. Span reduces to ± 1 m in the bedrock volume close to borehole HFM22
Orientation (strike/dip)	177/84	± 5/± 10	High	Strike based on trend of lineament XFM0431A0. Dip based on linking XFM0431A0 at the surface with DZ1 in HFM22	
Thickness	14 m		Medium	Intersection along DZ1 in HFM22	Thickness refers to total zone thickness (transition zone and core)
Length	470 m	± 25 m	Medium	Linked lineament XFM0431A0. Truncated against ZFMNE0159, ZFMNE1061 and ZFMNS1205	Total length at ground surface
Ductile deformation			Medium	Intersection along DZ1 in HFM22	Not present
Brittle deformation			High	Intersection along DZ1 in HFM22	Present
Alteration			High	Intersection along DZ1 in HFM22	Red-stained bedrock with fine-grained hematite dissemination. Lineament XFM0431A0 only recognised on the basis of topographic data
Fracture orientation	Fisher mean of NE fracture set = 050/85	K value of NE fracture set = 15	Medium	Intersection along DZ1 in HFM22, N=95	Two sets of fractures present. Both sets dip steeply and strike NE and NS
	Fisher mean of NS fracture set = 355/80	K value of NS fracture set = 70			
Fracture frequency	Mean 5 m^{-1}	Span 0–13 m^{-1}	Low	Intersection along DZ1 in HFM22	Open and partly open fractures dominate in the NS set. Both sealed and open/partly open fractures are present in the steeply dipping NE set. Estimate probably too low (percussion borehole)
Fracture filling			Low	Intersection along DZ1 in HFM22	Unknown mineral. Poor quality data (percussion borehole)

Vertical and steeply-dipping brittle deformation zones with NS strike

ZFMNS1204 (DZ2 in KFM08A)

Property	Quantitative estimate	Span	Confidence level	Basis for interpretation	Comments
On the basis of fracture orientation, borehole interval 479–496 m in borehole KFM08A (DZ2) is modelled as a steeply dipping NS zone. Truncated against ZFMNE1061 and ZFMNE0810. DZ3 in KFM08A (borehole interval 528–557 m) is possibly related to zone ZFMNS1204					
Confidence of occurrence: High					
Position		± 1 m	Medium	Intersection along DZ2 in KFM08A	Span refers to position of the zone in borehole KFM08A
Orientation (strike/dip)	350/80	± 10/± 10	Medium	Strike and dip based on orientation of fractures along DZ2 in KFM08A	
Thickness	6 m		Medium	Intersection along DZ2 in KFM08A	Thickness refers to total zone thickness (transition zone and core)
Length	794 m	± 50 m	Medium	Intersection along DZ2 in KFM08A and inferred truncation against ZFMNE1061 and ZFMNE0810	Total length at ground surface
Ductile deformation			High	Intersection along DZ2 in KFM08A	Not present
Brittle deformation			High	Intersection along DZ2 in KFM08A	Present
Alteration			High	Intersection along DZ2 in KFM08A	Red-stained bedrock with fine-grained hematite dissemination
Fracture orientation	Fisher mean of NS fracture set = 345/85	K value of NS fracture set = 10	Medium	Intersection along DZ2 in KFM08A, N=107	Fractures that strike NS dominate. Steeply dipping NE fractures and some gently dipping fractures are also present
Fracture frequency	Mean 10 m^{-1}	Span 4–19 m^{-1}	Medium	Intersection along DZ2 in KFM08A	Sealed fractures dominate. Quantitative estimate and span exclude some sealed fracture networks and a crush zone (495 m), due to uncertainty in the estimation of fracture frequency in these structures
Fracture filling			Medium	Intersection along DZ2 in KFM08A	Calcite, chlorite, hematite/adularia. Clay minerals present in a few fractures, both NS steeply dipping and gently dipping

Vertical and steeply-dipping brittle deformation zones with NS strike

ZFMNS1205 (DZ2 in KFM08B)

Property	Quantitative estimate	Span	Confidence level	Basis for interpretation	Comments
On the basis of fracture orientation, borehole interval 167–185 m in borehole KFM08B (DZ2) is modelled as a steeply dipping NS zone. Truncated against ZFMNE0159 and ZFMNE1061. Linked lineaments XFM1063A0 (NS trend) and XFM0430A0 (NW trend) are situated at the surface above KFM08B. DZ1 in KFM08B (borehole interval 133–140 m) is possibly related to zone ZFMNS1205					
Confidence of occurrence: High					
Position		± 1 m	Medium	Intersection along DZ2 in KFM08B	Span refers to position of the zone in borehole KFM08A
Orientation (strike/dip)	340/85	± 10/± 10	Medium	Strike and dip based on orientation of fractures along DZ2 in KFM08B	
Thickness	10 m		Medium	Intersection along DZ2 in KFM08B	Thickness refers to total zone thickness (transition zone and core)
Length	380 m	± 25 m	Medium	Intersection along DZ2 in KFM08B and inferred truncation against ZFMNE0159 and ZFMNE1061	Total length at ground surface
Ductile deformation			High	Intersection along DZ2 in KFM08B	Not present
Brittle deformation			High	Intersection along DZ2 in KFM08B	Present
Alteration			High	Intersection along DZ2 in KFM08B	Red-stained bedrock with fine-grained hematite dissemination. Poor quality magnetic data in the area
Fracture orientation	Fisher mean of NNW fracture set = 160/80	K value of NNW fracture set = 49	Medium	Intersection along DZ2 in KFM08B, N=142	Fractures that strike NNW dominate. Gently dipping fractures and steeply dipping NE fractures are also present
Fracture frequency	Mean 10 m^{-1}	Span 2–28 m^{-1}	Medium	Intersection along DZ2 in KFM08B	Sealed fractures dominate. Quantitative estimate and span exclude some sealed fracture networks, due to uncertainty in the estimation of fracture frequency in sealed networks
Fracture filling			Medium	Intersection along DZ2 in KFM08B	Calcite, chlorite, laumontite, hematite/adularia, quartz

Vertical and steeply-dipping brittle deformation zones with NS strike, based solely on lineament and comparison studies

ZFMNS0098

Property	Quantitative estimate	Span	Confidence level	Basis for interpretation	Comments
At the surface, replaced part of linked lineament XFM0098A0 by low magnetic lineament MFM009805. This segment also extended to NNW. Modelled at depth using an assumed dip of 90° based on a comparison with high confidence, vertical and steeply dipping zones with NS strike					
Confidence of occurrence: Low					
Position		± 20 m	High	Low magnetic lineament MFM009805	Span estimate refers to the general position of the central part of the zone on the surface
Orientation (strike/dip)	345/90	± 5/± 10	High for strike, low for dip	Strike based on trend of lineament MFM009805. Dip based on comparison with high confidence, vertical and steeply-dipping zones with NS strike	
Thickness	5 m	± 3 m	Low	Comparison with high confidence, vertical and steeply-dipping, regional zones with NS strike	Thickness refers to total zone thickness (transition zone and core)
Length	396 m	± 25 m	Medium	Low magnetic lineament MFM009805. Truncated against ZFMNE0061A and ZFMNE0168	Total length at ground surface
Ductile deformation			Low	Comparison with high confidence, vertical and steeply-dipping zones with NS strike	Assumed not to be present
Brittle deformation			Low	Comparison with high confidence, vertical and steeply-dipping zones with NS strike	Assumed to be present
Alteration			Medium	Character of lineament MFM009805	Red-stained bedrock with fine-grained hematite dissemination
Fracture orientation					
Fracture frequency					
Fracture filling					

Vertical and steeply-dipping brittle deformation zones with NS strike, based solely on lineament and comparison studies

ZFMNS0101

Property	Quantitative estimate	Span	Confidence level	Basis for interpretation	Comments
At the surface, replaced linked lineament XFM0101A0 by low magnetic lineament MFM0101. Modelled at depth using an assumed dip of 90° based on a comparison with high confidence, vertical and steeply dipping zones with NS strike					
Confidence of occurrence: Low					
Position		± 20 m	High	Low magnetic lineament MFM0101	Span estimate refers to the general position of the central part of the zone on the surface
Orientation (strike/dip)	350/90	± 5/± 10	High for strike, low for dip	Strike based on trend of lineament MFM0101. Dip based on comparison with high confidence, vertical and steeply-dipping zones with NS strike	
Thickness	10 m	± 5 m	Low	Comparison with high confidence, vertical and steeply-dipping, regional zones with NS strike	Thickness refers to total zone thickness (transition zone and core)
Length	1,788 m	± 100 m	Medium	Low magnetic lineament MFM0101. Truncated against ZFMNE0062A and ZFMNE0065	Total length at ground surface
Ductile deformation			Low	Comparison with high confidence, vertical and steeply-dipping zones with NS strike	Assumed not to be present
Brittle deformation			Low	Comparison with high confidence, vertical and steeply-dipping zones with NS strike	Assumed to be present
Alteration			Medium	Character of lineament MFM0101	Red-stained bedrock with fine-grained hematite dissemination
Fracture orientation					
Fracture frequency					
Fracture filling					

Vertical and steeply-dipping brittle deformation zones with NS strike, based solely on lineament and comparison studies

ZFMNS0130

Property	Quantitative estimate	Span	Confidence level	Basis for interpretation	Comments
At the surface, replaced linked lineament XFM0130A0 by low magnetic lineament MFM0130. Lineament shortened towards north and extended towards south. Modelled at depth using an assumed dip of 90° based on a comparison with high confidence, vertical and steeply dipping zones with NS strike					
Confidence of occurrence: Low					
Position		± 20 m	High	Low magnetic lineament MFM0130	Span estimate refers to the general position of the central part of the zone on the surface
Orientation (strike/dip)	010/90	± 5/± 10	High for strike, low for dip	Strike based on trend of lineament MFM0130. Dip based on comparison with high confidence, vertical and steeply-dipping zones with NS strike	
Thickness	5 m	± 3 m	Low	Comparison with high confidence, vertical and steeply-dipping, regional zones with NS strike	Thickness refers to total zone thickness (transition zone and core)
Length	586 m	± 25 m	Medium	Low magnetic lineament MFM0130. Truncated against ZFMNW0236 and ZFMNW1199	Total length at ground surface
Ductile deformation			Low	Comparison with high confidence, vertical and steeply-dipping zones with NS strike	Assumed not to be present
Brittle deformation			Low	Comparison with high confidence, vertical and steeply-dipping zones with NS strike	Assumed to be present
Alteration			Medium	Character of lineament MFM0130	Red-stained bedrock with fine-grained hematite dissemination
Fracture orientation					
Fracture frequency					
Fracture filling					

Vertical and steeply-dipping brittle deformation zones with NS strike, based solely on lineament and comparison studies

ZFMNS1022

Property	Quantitative estimate	Span	Confidence level	Basis for interpretation	Comments
At the surface, replaced part of linked lineament XFM1022A0 by lineament MFM1022. This lineament is defined by a depression in the bedrock surface, the form of which has been recognised on the basis of an analysis of old refraction seismic data /Isaksson and Keisu 2005/. Modelled at depth using an assumed dip of 90° based on a comparison with high confidence, vertical and steeply dipping zones with NS strike					
Confidence of occurrence: Low					
Position		± 20 m	High	Bedrock surface lineament MFM1022	Span estimate refers to the general position of the central part of the zone on the surface
Orientation (strike/dip)	005/90	± 5/± 10	High for strike, low for dip	Strike based on trend of bedrock surface lineament MFM1022. Dip based on comparison with high confidence, vertical and steeply-dipping zones with NS strike	
Thickness	5 m	± 3 m	Low	Estimated on basis of length – thickness correlation diagram	Thickness refers to total zone thickness (transition zone and core)
Length	670 m	± 25 m	Medium	Bedrock surface lineament MFM1022. Truncated by ZFMNW0001 and ZFMNW0809	Total length at ground surface
Ductile deformation			Low	Comparison with high confidence, vertical and steeply-dipping zones with NS strike	Assumed not to be present
Brittle deformation			Low	Comparison with high confidence, vertical and steeply-dipping zones with NS strike	Assumed to be present
Alteration					
Fracture orientation					
Fracture frequency					
Fracture filling					

Vertical and steeply-dipping brittle deformation zones with NS strike, based solely on lineament and comparison studies

ZFMNS1072

Property	Quantitative estimate	Span	Confidence level	Basis for interpretation	Comments
At the surface, replaced linked lineament XFM1072A0 by lineament MFM1072. This lineament is defined by a depression in the bedrock surface, the form of which has been recognised on the basis of an analysis of old refraction seismic data /Isaksson and Keisu 2005/. Modelled at depth using an assumed dip of 90° based on a comparison with high confidence, vertical and steeply dipping zones with NS strike					
Confidence of occurrence: Low					
Position		± 20 m	High	Bedrock surface lineament MFM1072	Span estimate refers to the general position of the central part of the zone on the surface
Orientation (strike/dip)	350/90	± 5/± 10	High for strike, low for dip	Strike based on trend of bedrock surface lineament MFM1072. Dip based on comparison with high confidence, vertical and steeply-dipping zones with NS strike	
Thickness	5 m	± 3 m	Low	Estimated on basis of length – thickness correlation diagram	Thickness refers to total zone thickness (transition zone and core)
Length	765 m	± 25 m	Medium	Bedrock surface lineament MFM1072. Truncated by ZFMNW1068 and ZFMNE0810	Total length at ground surface
Ductile deformation			Low	Comparison with high confidence, vertical and steeply-dipping zones with NS strike	Assumed not to be present
Brittle deformation			Low	Comparison with high confidence, vertical and steeply-dipping zones with NS strike	Assumed to be present
Alteration					
Fracture orientation					
Fracture frequency					
Fracture filling					

Vertical and steeply-dipping brittle deformation zones with NS strike, based solely on lineament and comparison studies

ZFMNS1077

Property	Quantitative estimate	Span	Confidence level	Basis for interpretation	Comments
At the surface, replaced linked lineament XFM1077A0 by lineament MFM1077. This lineament is defined by a depression in the bedrock surface, the form of which has been recognised on the basis of an analysis of old refraction seismic data /Isaksson and Keisu 2005/. Modelled at depth using an assumed dip of 90° based on a comparison with high confidence, vertical and steeply dipping zones with NS strike					
Confidence of occurrence: Low					
Position		± 20 m	High	Bedrock surface lineament MFM1077	Span estimate refers to the general position of the central part of the zone on the surface
Orientation (strike/dip)	350/90	± 5/± 10	High for strike, low for dip	Strike based on trend of bedrock surface lineament MFM1077. Dip based on comparison with high confidence, vertical and steeply-dipping zones with NS strike	
Thickness	5 m	± 3 m	Low	Estimated on basis of length – thickness correlation diagram	Thickness refers to total zone thickness (transition zone and core)
Length	520 m	± 25 m	Medium	Bedrock surface lineament MFM1077. Truncated by ZFMNW1068 and ZFMNE0810	Total length at ground surface
Ductile deformation			Low	Comparison with high confidence, vertical and steeply-dipping zones with NS strike	Assumed not to be present
Brittle deformation			Low	Comparison with high confidence, vertical and steeply-dipping zones with NS strike	Assumed to be present
Alteration					
Fracture orientation					
Fracture frequency					
Fracture filling					

Vertical and steeply-dipping brittle deformation zones with NS strike, based solely on lineament and comparison studies

ZFMNS1201

Property	Quantitative estimate	Span	Confidence level	Basis for interpretation	Comments
At the surface, replaced part of linked lineament XFM0098A0 by lineament MFM1201. This lineament is defined by a depression in the bedrock surface, the form of which has been recognised on the basis of an analysis of old refraction seismic data /Isaksson and Keisu 2005/. Modelled at depth using an assumed dip of 90° based on a comparison with high confidence, vertical and steeply dipping zones with NS strike					
Confidence of occurrence: Low					
Position		± 20 m	High	Bedrock surface lineament MFM1201	Span estimate refers to the general position of the central part of the zone on the surface
Orientation (strike/dip)	355/90	± 5/± 10	High for strike, low for dip	Strike based on trend of bedrock surface lineament MFM1201. Dip based on comparison with high confidence, vertical and steeply-dipping zones with NS strike	
Thickness	5 m	± 3 m	Low	Estimated on basis of length – thickness correlation diagram	Thickness refers to total zone thickness (transition zone and core)
Length	543 m	± 25 m	Medium	Bedrock surface lineament MFM1201. Truncated by ZFMNW0001 and ZFMNW0809	Total length at ground surface
Ductile deformation			Low	Comparison with high confidence, vertical and steeply-dipping zones with NS strike	Assumed not to be present
Brittle deformation			Low	Comparison with high confidence, vertical and steeply-dipping zones with NS strike	Assumed to be present
Alteration					
Fracture orientation					
Fracture frequency					
Fracture filling					

Vertical and steeply-dipping brittle deformation zones with NS strike, based solely on lineament and comparison studies

ZFMNS1202

Property	Quantitative estimate	Span	Confidence level	Basis for interpretation	Comments
At the surface, replaced part of linked lineament XFM0098A0 by low magnetic lineament MFM1202. Modelled at depth using an assumed dip of 90° based on a comparison with high confidence, vertical and steeply dipping zones with NS strike					
Confidence of occurrence: Low					
Position		± 20 m	High	Low magnetic lineament MFM1202	Span estimate refers to the general position of the central part of the zone on the surface
Orientation (strike/dip)	350/90	± 5/± 10	High for strike, low for dip	Strike based on trend of lineament MFM1202. Dip based on comparison with high confidence, vertical and steeply-dipping zones with NS strike	
Thickness	5 m	± 3 m	Low	Comparison with high confidence, vertical and steeply-dipping, regional zones with NS strike	Thickness refers to total zone thickness (transition zone and core)
Length	465 m	± 25 m	Medium	Low magnetic lineament MFM1202. Truncated against ZFMNE0060A and ZFMNE0103A	Total length at ground surface
Ductile deformation			Low	Comparison with high confidence, vertical and steeply-dipping zones with NS strike	Assumed not to be present
Brittle deformation			Low	Comparison with high confidence, vertical and steeply-dipping zones with NS strike	Assumed to be present
Alteration			Medium	Character of lineament MFM1202	Red-stained bedrock with fine-grained hematite dissemination
Fracture orientation					
Fracture frequency					
Fracture filling					

Gently-dipping brittle deformation zones

ZFMNE00A2 (type intersection DZ6 in KFM02A)

Property	Quantitative estimate	Span	Confidence level	Basis for interpretation	Comments
Remodelled to take account of: 1. intersections along boreholes KFM06A (DZ1 and extension along borehole interval 102–126 m) and KFM06B (DZ1 and extension along borehole interval 93–98 m) and 2. the revised truncations to the south-west and south-east based on the stage 2 seismic reflection data. Zone ZFMNE00A2 is a composite zone that consists of narrower, high-strain segments (sub-zones) that are inferred to diverge and converge in a complex pattern. These sub-zones separate less deformed bedrock segments. In KFM02A, the uppermost (borehole interval 415–430 m) and lowermost (borehole interval 480–520 m) parts display bedrock alteration and highest fracture frequency. According to /Juhlin et al. 2002/, reflectors A2 and F1 intersect KFM02A at borehole intervals 480 m and 510 m, respectively (470 m and 500 m depth, respectively). In KFM04A, three separate sub-zones that vary in thickness from 5–10 m are present over an interval of 67 m perpendicular to the zone. Thus, thickness refers to total zone thickness (bedrock little affected by deformation between sub-zones, transition zones and cores). ZFMEW0865 in model version 1.1 also included as a sub-zone within ZFMNE00A2. The bedrock c. 75 m beneath ZFNE00A2 (measured perpendicular to the zone) contains a high frequency of sealed fractures that dip moderately to the north-west and are welded by chlorite, epidote, prehnite and calcite (DZ7 in the single-hole interpretation of KFM02A). Possibly related to ZFMNE00A2 in the same manner as ZFMNE1194					
Confidence of occurrence: High					
Position		± 15 m	High	Borehole intersections along KFM01A (DZ1), KFM01B (DZ1), KFM02A (DZ6), KFM04A (DZ1 and extension along borehole interval 125–169 m, DZ2 and DZ3), KFM05A (DZ1), KFM06A (DZ1 and borehole interval 102–126 m), KFM06B (DZ1 and borehole interval 93–98 m), HFM01 (DZ1), HFM02 (DZ1), HFM14 (DZ1 and DZ2), HFM15 (DZ1), HFM16 (DZ1), HFM19 (DZ1 and DZ2) in combination with seismic reflectors A2 and F1	Span estimate refers to the general position of the central part of the zone and is based on /Cosma et al. 2003/. Span reduces to ± 1 m in the bedrock volume close to the boreholes. Modelling work has made use of a fixed point intersection for the central part of the zone at borehole length 499 m in KFM02A. Lower boundary placed at 520 m borehole length in KFM02A
Orientation (strike/dip)	080/24	+15/–10	High	Seismic reflector A2 in combination with borehole intersections listed against “Position”	Strike and dip after /Juhlin et al. 2002/. Span estimate based on both /Juhlin et al. 2002/ and /Cosma et al. 2003/
Thickness	70 m	± 30 m	High	Borehole intersections along KFM02A (DZ6), KFM04A (DZ1 and extension along borehole interval 125–169 m, DZ2 and DZ3), KFM06A (DZ1 and borehole interval 102–126 m), KFM06B (DZ1 and borehole interval 93–98 m), HFM14 (DZ1 and DZ2). Other borehole intersections listed against “Position” start or finish within the zone	Total zone thickness including cores, transition zones and even some bedrock little affected by deformation between sub-zones (see comments above)
Length	4,283 m	± 200 m	Medium	Seismic reflector A2 and borehole intersections listed against “Position”. Truncated against ZFMNW0001 and ZFMNW0017, ZFMNE0065 and ZFMNE00A3	Total length at ground surface
Ductile deformation			High	Borehole intersections listed against “Position”	Not present
Brittle deformation			High	Borehole intersections listed against “Position”	Present
Alteration			High	Borehole intersections listed against “Position”	Oxidized bedrock with fine-grained hematite dissemination
Fracture orientation	Fisher mean of gently-dipping fracture set = 030/15 Fisher mean of NE fracture set = 060/85 Fisher mean of NW fracture set = 145/90	K value of gently-dipping fracture set = 10 K value of NE fracture set = 16 K value of NW fracture set = 16	High	Borehole intersections along KFM02A (DZ6), KFM04A (DZ1 and extension along borehole interval 125–169 m, DZ2 and DZ3) and HFM19 (DZ1 and DZ2), N=1169	Data only from deeper borehole intersections to avoid influence of sub-horizontal sheet joints in the uppermost part of the bedrock, close to drill sites 1, 5 and 6. Three fracture sets are conspicuous, a gently-dipping fracture set and steeply-dipping NE and NW sets.

Fracture frequency	Mean 7 m^{-1}	Span 0–29 m^{-1}	High	Borehole intersections along KFM02A (DZ6), KFM04A (DZ1 and extension along borehole interval 125–169 m, DZ2 and DZ3) and HFM19 (DZ1 and DZ2)	Data only from deeper borehole intersections to avoid influence of sub-horizontal sheet joints in the uppermost part of the bedrock, close to drill sites 1, 5 and 6. Open and sealed fractures. Quantitative estimate and span exclude a crush zone along DZ2 in HFM19 and several sealed fracture networks along KFM04A, due to uncertainty in the estimation of fracture frequency in such structures
Fracture filling			High	Borehole intersections along KFM02A (DZ6), KFM04A (DZ1 and extension along borehole interval 125–169 m, DZ2 and DZ3) and HFM19 (DZ1 and DZ2)	Data only from deeper borehole intersections to avoid influence of sub-horizontal sheet joints in the uppermost part of the bedrock, close to drill sites 1, 5 and 6. Chlorite, calcite, hematite/ adularia, clay minerals (gently dipping and steeply dipping NW sets, mainly open fractures), prehnite, laumontite, quartz. Asphaltite also present along fractures at shallow depths. Note high frequency of fractures with no mineral coating/filling

Gently-dipping brittle deformation zones

ZFMNE00A3 (DZ3 in KFM02A/DZ4 in KFM03A/DZ2 in HFM04; association with vuggy metagranitoid)

Property	Quantitative estimate	Span	Confidence level	Basis for interpretation	Comments
Remodelled by taking account of an inferred intersection in HFM04 (DZ2) and by applying a different truncation to the south-west. Hydraulic contact between KFM02A and KFM03A via ZFMNE00B1 that splays off ZFMNE00A3. Borehole intersections at 160–184 m (DZ3) in KFM02A, 803–816 m (DZ4) in KFM03A and 183–187 m (DZ2) in HFM04					
Confidence of occurrence: High					
Position		± 15 m	High	Intersections along KFM02A (DZ3), KFM03A (DZ4) and HFM04 (DZ2), seismic reflector A3	Span estimate refers to the general position of the central part of the zone and is based on /Cosma et al. 2003/. Span reduces to ± 1 m in the bedrock volume close to the boreholes
Orientation (strike/dip)	050/22	± 10 /± 2	High	Intersections along KFM02A (DZ3), KFM03A (DZ4) and HFM04 (DZ2), seismic reflector A3	Consistent with orientation estimates in both /Juhlin et al. 2002, Cosma et al. 2003/
Thickness	13 m	± 9	Medium	Intersections along KFM02A (DZ3), KFM03A (DZ4) and HFM04 (DZ2)	Thickness refers to total zone thickness (transition zone and core)
Length	3,325 m	± 200 m	Medium	Intersections along KFM02A (DZ3), KFM03A (DZ4) and HFM04 (DZ2), seismic reflector A3. Truncated against ZFMNW0001, ZFMNW0023, ZFMNW0123 and ZFMNE0828	Total length at ground surface
Ductile deformation			High	Intersections along KFM02A (DZ3), KFM03A (DZ4) and HFM04 (DZ2)	Not present
Brittle deformation			High	Intersections along KFM02A (DZ3), KFM03A (DZ4) and HFM04 (DZ2)	Present
Alteration			Medium	Intersections along KFM02A (DZ3), KFM03A (DZ4) and HFM04 (DZ2)	Red-stained bedrock with fine-grained hematite dissemination in central part of the zone in KFM02A. Association here with vuggy metagranitoid
Fracture orientation	Fisher mean of gently dipping fracture set = 025/5	K value of gently dipping fracture set = 7	Medium	Intersections along KFM02A (DZ3), KFM03A (DZ4) and HFM04 (DZ2), N=193	Gently dipping fractures dominate. Variable orientation
Fracture frequency	Mean 6 m^{-1}	Span 0–15 m^{-1}	Medium	Intersections along KFM02A (DZ3) and KFM03A (DZ4)	Sealed and open fractures. Quantitative estimate and span exclude crush zone in the upper part of the zone in KFM02A, , due to uncertainty in the estimation of fracture frequency in such structures
Fracture filling			Medium	Intersections along KFM02A (DZ3) and KFM03A (DZ4)	Calcite, chlorite, quartz, hematite/ adularia, clay minerals, prehnite. Note high frequency of fractures with no mineral coating/filling

Gently-dipping brittle deformation zones

ZFMNE00B4 (DZ10 in KFM02A)

Property	Quantitative estimate	Span	Confidence level	Basis for interpretation	Comments
Remodelled by applying different truncations to the south-west and south-east. Borehole intersection at 976–982 m (DZ10) in KFM02A					
Confidence of occurrence: High					
Position		± 15 m	High	Intersection along KFM02A (DZ10), seismic reflector B4	Span estimate refers to the general position of the central part of the zone and is based on /Cosma et al. 2003/. Span reduces to ± 1 m in the bedrock volume close to borehole KFM02A
Orientation (strike/dip)	050/29		High	Seismic reflector B4	Strike and dip after /Cosma et al. 2003/. Consistent with /Juhlin et al. 2002/. Only 1° difference in dip value in these two contributions
Thickness	5 m		Medium	Intersection along KFM02A (DZ10)	Thickness refers to total zone thickness (transition zone and core).
Length					ZFMNE00B4 does not extend to the surface. Truncated against ZFMNW0001, ZFMNW0123, ZFMNE0062A, ZFMNE0065 and ZFMNE1195. Truncation to the north-west takes account of recommendation in /Juhlin and Bergman 2004/
Ductile deformation			High	Intersection along KFM02A (DZ10)	Not present
Brittle deformation			High	Intersection along KFM02A (DZ10)	Present
Alteration			Medium	Intersection along KFM02A (DZ10)	Oxidized bedrock with fine-grained hematite dissemination
Fracture orientation				Intersection along KFM02A (DZ10)	Most fractures dip gently- to moderately to the south-east and south. Insufficient data to calculate Fisher mean and K value (N=26)
Fracture frequency	4.5 m^{-1}	Span 1–11 m^{-1}	Medium	Intersection along KFM02A (DZ10)	Sealed and open fractures
Fracture filling			Medium	Intersection along KFM02A (DZ10)	Chlorite, prehnite, calcite

Gently-dipping brittle deformation zones

ZFMNS00B7

Property	Quantitative estimate	Span	Confidence level	Basis for interpretation	Comments
Remodelled by taking account of inferred intersection along borehole interval 318–356 m (DZ4) in KFM06A and by applying different truncations. ZFMNE0060A also modelled to intersect KFM06A in the borehole interval 318–356 m (DZ4). For this reason, there are difficulties to separate the influence of zones ZFMNE0060A and ZFMNS00B7 along this borehole interval					
Confidence of occurrence: High					
Position		± 15 m	High	Intersection along KFM06A (DZ4), seismic reflector B7	Span estimate refers to the general position of the central part of the zone. Estimate based on /Cosma et al. 2003/
Orientation (strike/dip)	015/25	–9/ +2	High	Seismic reflector B7	Strike and dip after /Balu and Cosma 2005/. Span estimate makes use of both /Juhlin and Bergman 2004/ and /Balu and Cosma 2005/
Thickness	38 m		Medium	Intersection along KFM06A (DZ4)	Thickness refers to total zone thickness (transition zone and core)
Length	1,431 m	± 100 m	Medium	Intersection along KFM06A (DZ4), seismic reflector B7. Truncated against ZFMNW0809, ZFMNE0060A and ZFMNE00A2	Total length at ground surface
Ductile deformation			High	Intersection along KFM06A (DZ4)	Not present
Brittle deformation			High	Intersection along KFM06A (DZ4)	Present
Alteration			High	Intersection along KFM06A (DZ4)	Red-stained bedrock with fine-grained hematite dissemination
Fracture orientation	Fisher mean of NE fracture set with steep dip = 210/85	K value of NE fracture set with steep dip = 17	Medium	Intersection along KFM06A (DZ4), N=390	Two sets of fractures are conspicuous. One of these sets strikes NE and dips steeply to the NW, the other is gently dipping
	Fisher mean of gently dipping fracture set = 050/10	K value of gently dipping fracture set = 11			
Fracture frequency	10 m^{-1}	2–20 m^{-1}	Medium	Intersection along KFM06A (DZ4)	Dominance of sealed fractures. Open fractures only significant in the sub-horizontal set. Mean value and span exclude sealed fracture networks at several short intervals. Note especially borehole interval 323–326 m along DZ4. Procedure implemented due to uncertainty in the estimation of fracture frequency in sealed networks
Fracture filling			Medium	Intersection along KFM06A (DZ4)	Calcite, chlorite and clay minerals in the sub-horizontal fractures. Note also fractures with no mineral coating/filling are present

Gently-dipping brittle deformation zones

ZFMNS00B8 (316–322 m level in DBT1/KFK001)

Property	Quantitative estimate	Span	Confidence level	Basis for interpretation	Comments
Remodelled by taking account of seismic reflector B8 in combination with borehole intersection along interval 316–322 m in DBT1/KFK001. Identified as ZFMNE1193 in SDM version 1.2					
Confidence of occurrence: High					
Position		± 15 m	High	Intersection along borehole length 316–322 m in DBT1/KFK001, seismic reflector B8	Span estimate refers to the general position of the central part of the zone and is based on /Cosma et al. 2003/. Span reduces to ± 1 m in the bedrock volume close to borehole DBT1/KFK001
Orientation (strike/dip)	015/22		High	Seismic reflector B8	/Juhlin and Palm 2005/. Consistent with /Cosma et al. 2006/
Thickness	6 m		Medium	Intersection along borehole length 316–322 m in DBT1/KFK001	Thickness refers to total zone thickness (transition zone and core)
Length	808 m	± 100 m	Medium	Intersection along borehole length 316–322 m in DBT1/KFK001, seismic reflector B8. Truncated against ZFMNW0017, ZFMNW0137 and ZFMNE0810	Total length at ground surface
Ductile deformation			High	Intersection along borehole length 316–322 m in DBT1/KFK001	Not present
Brittle deformation			High	Intersection along borehole length 316–322 m in DBT1/KFK001	Present
Alteration					
Fracture orientation					
Fracture frequency					
Fracture filling					

Gently-dipping brittle deformation zones

ZFMNE0866 (DZ1 and DZ2 in KFM02A/DZ1 in HFM04/DZ1 in HFM05)

Property	Quantitative estimate	Span	Confidence level	Basis for interpretation	Comments
Remodelled by combining borehole interval 110–122 m (DZ2) in KFM02A, borehole interval 61–64 m (DZ1) in HFM04 and borehole interval 153–154 m (DZ1) in HFM05. The borehole interval 79–91 m (DZ1) in KFM02A is treated as a sub-zone related to ZFMNE0866 (see also SDM version 1.2)					
Confidence of occurrence: High					
Position		± 1 m	High	Intersections along KFM02A (DZ1 and DZ2), HFM04 (DZ1) and HFM05 (DZ1)	Span estimate refers to the position of the central part of the zone close to the boreholes
Orientation (strike/dip)	078/24	± 5/± 5	High	Intersections along KFM02A (DZ1 and DZ2), HFM04 (DZ1) and HFM05 (DZ1)	
Thickness	6 m	± 5 m	Medium	Intersections along KFM02A (DZ1 and DZ2), HFM04 (DZ1) and HFM05 (DZ1)	Thickness refers to total zone thickness (transition zone and core)
Length	1,908 m	± 100 m	Medium	Intersections along KFM02A (DZ1 and DZ2), HFM04 (DZ1) and HFM05 (DZ1). Truncated against ZFMNE00A3 and ZFMNE0065	Total length at ground surface
Ductile deformation			High	Intersections along KFM02A (DZ1 and DZ2), HFM04 (DZ1) and HFM05 (DZ1)	Not present
Brittle deformation			High	Intersections along KFM02A (DZ1 and DZ2), HFM04 (DZ1) and HFM05 (DZ1)	Present
Alteration			Medium	Intersections along KFM02A (DZ1 and DZ2), HFM04 (DZ1) and HFM05 (DZ1)	Red-stained bedrock with fine-grained hematite dissemination, clay alteration
Fracture orientation	Fisher mean of gently dipping fracture set = 040/15	K value of gently dipping fracture set = 11	Medium	Intersections along KFM02A (DZ1 and DZ2), HFM04 (DZ1) and HFM05 (DZ1), N=132	Gently dipping fractures dominate. Steeply dipping fractures with variable strike are also present
Fracture frequency	Mean 5 m^{-1}	Span 0–15 m^{-1}	Medium	Intersections along KFM02A (DZ1 and DZ2), HFM04 (DZ1) and HFM05 (DZ1)	Sealed and open fractures. Quantitative estimate and span exclude crush zones near the base of DZ2 in KFM02A and along DZ1 in HFM05. Procedure implemented due to uncertainty in the estimation of fracture frequency in crush zones
Fracture fillings			Medium	Intersections along KFM02A (DZ1 and DZ2), HFM04 (DZ1) and HFM05 (DZ1)	Calcite, clay minerals, chlorite. Note high frequency of fractures with no mineral coating/filling

Gently-dipping brittle deformation zones

ZFMNE0871 (Zone H2, SFR)

Property	Quantitative estimate	Span	Confidence level	Basis for interpretation	Comments
Modelled in same manner as in SDM version 1.2. No truncation against ZFMNW0002					
Confidence of occurrence: High					
Position		± 1 m	High	Intersection along SFR tunnel and boreholes	Span estimate refers to the position of the central part of the zone in SFR tunnel and boreholes Projection to surface differs in /Axelsson and Hansen 1997, Holmén and Stigsson 2001/. Possible correlation with low magnetic lineament MFM0137B0. Bathymetric anomaly also along this lineament
Orientation (strike/dip)	048/16	± 5/± 15	Medium	Intersection along SFR tunnel	ENE/20 in /Axelsson and Hansen 1997/. NE/15–20 in /Holmén and Stigsson 2001/
Thickness	10 m	± 9 m	High	Intersection along SFR tunnel and boreholes	Thickness refers to total zone thickness (transition zone and core)
Length	1,172 m	± 100 m	Medium	Intersection along SFR tunnel and boreholes. Truncated against ZFMNW0001 and ZFMNW0805	Total length at ground surface
Ductile deformation			High	Intersection along SFR tunnel and boreholes	Not present
Brittle deformation			High	Intersection along SFR tunnel and boreholes	Present
Alteration			High	Intersection along SFR boreholes	Present
Fracture orientation					
Fracture frequency	15 m^{-1}	± 5 m^{-1}	High	Intersection along SFR boreholes	
Fracture filling			High	Intersection along SFR boreholes	Clay minerals

Gently-dipping brittle deformation zones

ZFMNE1194 (DZ2 in KFM01B and DZ1 in HFM01)

Property	Quantitative estimate	Span	Confidence level	Basis for interpretation	Comments
On the basis of fracture orientation, borehole interval 107–135 m in borehole KFM01B (DZ2) is modelled as a moderately dipping, brittle deformation zone that is located close to but beneath zone ZFMNE00A2. This zone possibly formed as a conjugate structure to zone ZFMNE00A2. Truncated at depth against the adjacent zones ZFMNW1200, ZFMNE0060A, ZFMNE0061A and ZFMNE00A2. Possible intersection also along borehole interval 35–44 m (DZ1) in HFM01					
Confidence of occurrence: High					
Position		± 1 m	High	Intersections along KFM01B (DZ2) and HFM01 (DZ1)	Span estimate refers to the position of the central part of the zone close to borehole KFM01B
Orientation (strike/dip)	210/45	± 5/± 5	Medium	Orientation of fractures in KFM01B (DZ2) and HFM01 (DZ1)	
Thickness	11 m	± 4 m	Medium	Intersections along KFM01B (DZ2) and HFM01 (DZ1)	Thickness refers to total zone thickness (transition zone and core)
Length	73 m	± 25 m		Length on ground surface following truncation against ZFMNW1200, ZFMNE0060A, ZFMNE0061A and ZFMNE00A2	Total length at ground surface
Ductile deformation			High	Intersections along KFM01B (DZ2) and HFM01 (DZ1)	Not present
Brittle deformation			High	Intersections along KFM01B (DZ2) and HFM01 (DZ1)	Present
Alteration			High	Intersections along KFM01B (DZ2) and HFM01 (DZ1)	Oxidized bedrock with fine-grained hematite dissemination along fractures that dip moderately to the NW and along fractures that strike NW
Fracture orientation	Fisher mean of moderately-dipping and sub-horizontal fractures = 185/15 Fisher mean of NW fracture set = 135/85	K value of moderately-dipping and sub-horizontal fractures = 11 K value of NW fracture set = 14	Medium	Intersections along KFM01B (DZ2) and HFM01 (DZ1), N=254	Fractures that dip moderately to the NW and are sub-horizontal dominate. Fractures that strike NW and show variable dips are also present
Fracture frequency	Mean 8 m^{-1}	Span 2–20 m^{-1}	Medium	Intersections along KFM01B (DZ2) and HFM01 (DZ1)	Dominance of sealed fractures. Open fractures predominantly sub-horizontal. Quantitative estimate and span exclude several sealed fracture networks, due to uncertainty in the estimation of fracture frequency in these structures
Fracture filling			Medium	Intersection along KFM01B (DZ2)	Chlorite, calcite, epidote (fractures that dip moderately to the NW and that strike NW), quartz, clay minerals (sub-horizontal fractures). Note also high frequency of sub-horizontal fractures with no mineral coating/filling

Gently-dipping brittle deformation zones

ZFMNE1195 (DZ8 and DZ9 in KFM02A)

Property	Quantitative estimate	Span	Confidence level	Basis for interpretation	Comments
Modelled on the basis of the orientation of the main set of fractures (gently dipping) along the borehole intervals 893–905 m (DZ8) and 922–925 m (DZ9) in KFM02A, in combination with a truncation of zone ZFMNE00B4 against zone ZFMNE1195. Zone DZ9 that occurs along the borehole interval 922–925 m in KFM02A is treated as a sub-zone related to ZFMNE1195. Zone ZFMNE1195 does not intersect the surface.					
Confidence of occurrence: High					
Position		± 1 m	High	Intersection along KFM02A (DZ8 and DZ9)	Span estimate only refers to the position of the central part of the zone close to borehole KFM02A
Orientation (strike/dip)	065/30	± 10/± 10	Low	Orientation of gently dipping fracture set along DZ8 and DZ9 in KFM02A, truncation of ZFMNE00B4 against ZFMNE1195	
Thickness	11 m		Medium	Intersection along KFM02A (DZ8)	Thickness refers to total zone thickness (transition zone and core)
Length					ZFMNE1195 does not intersect the surface. Truncated against ZFMNW0001, ZFMNW0123, ZFMNE0062A ZFMNE0065
Ductile deformation			High	Intersection along KFM02A (DZ8 and DZ9)	Not present
Brittle deformation			High	Intersection along KFM02A (DZ8 and DZ9)	Present
Alteration					
Fracture orientation	Fisher mean of gently dipping fracture set = 060/25	K value of gently dipping fracture set = 8	Medium	Intersection along KFM02A (DZ8 and DZ9), N=73	Gently dipping fractures form the most prominent fracture set. Fractures with other orientations are also present. Variable orientation
Fracture frequency	Mean 6 m^{-1}	Span 0–21 m^{-1}	Medium	Intersection along KFM02A (DZ8 and DZ9)	Dominance of sealed fractures
Fracture filling			Medium	Intersection along KFM02A (DZ8 and DZ9)	Chlorite, calcite

Gently-dipping brittle deformation zones

ZFMNE1203 (DZ1 in KFM07A and DZ1 in HFM21)

Property	Quantitative estimate	Span	Confidence level	Basis for interpretation	Comments
Modelled as a near-surface, sub-horizontal fracture zone, on the basis of the orientation of the main set of fractures along the borehole interval 108–142 m in KFM07A (part of DZ1) and an inferred intersection along the borehole interval 94–102 m (DZ1) in HFM21. Fractures along DZ1 in HFM21 are also predominantly sub-horizontal. Remainder of DZ1 along KFM07A (142–183 m) contains sealed fracture networks and red-stained bedrock with fine-grained hematite dissemination					
Confidence of occurrence: High					
Position		± 1 m	High	Intersections along KFM07A (DZ1) and HFM21 (DZ1)	Span estimate refers only to the position of the central part of the zone close to boreholes KFM07A and HFM21
Orientation (strike/dip)	200/10	± 10/± 10	Low	Orientation of fractures in KFM07A (DZ1) and inferred intersection along HFM21 (DZ1)	
Thickness	26 m		Medium	Intersection along KFM07A (DZ1)	Thickness refers to total zone thickness (transition zone and core)
Length	532 m	± 25 m		Length on ground surface following truncation against ZFMNW1198, ZFMNW1200, ZFMNE0061A, ZFMNE0159, ZFMNS00B7	Total length at ground surface
Ductile deformation			High	Intersection along KFM07A (DZ1)	Not present
Brittle deformation			High	Intersection along KFM07A (DZ1)	Present
Alteration			Medium	Intersection along KFM07A (DZ1)	Red-stained bedrock with fine-grained hematite dissemination
Fracture orientation	Fisher mean of gently dipping to sub-horizontal fracture set = 035/5	K value of gently dipping to sub-horizontal fracture set = 20	Medium	Intersections along KFM07A (DZ1) and HFM21 (DZ1), N=269	Gently dipping and sub-horizontal fractures dominate. Steeply dipping fractures are also present
Fracture frequency	Mean 9 m^{-1}	Span 0–32 m^{-1}	Medium	Intersection along KFM07A (DZ1)	Sealed and open fractures. Quantitative estimate and span exclude a crush zone, due to uncertainty in the estimation of fracture frequency in this structure
Fracture filling			Medium	Intersection along KFM07A (DZ1)	Calcite, chlorite, laumontite, hematite/adularia, prehnite, clay minerals (sub-horizontal and gently dipping fractures). Note also some gently dipping fractures with no mineral coating/filling

Gently-dipping brittle deformation zones

ZFMNE1206 (DZ2 in KFM07A and DZ2 in HFM21)

Property	Quantitative estimate	Span	Confidence level	Basis for interpretation	Comments
Modelled in the same manner as ZFMNE1203 as a near-surface, sub-horizontal fracture zone, on the basis of the orientation of the main set of fractures along the borehole interval 196–205 m in KFM07A (DZ2) and an inferred intersection along the borehole interval 160–177 m (DZ2) in HFM21. Fractures along DZ2 in HFM21 are also, in part, gently dipping					
Confidence of occurrence: High					
Position		± 1 m	High	Intersections along KFM07A (DZ2) and HFM21 (DZ2)	Span estimate refers only to the position of the central part of the zone close to boreholes KFM07A and HFM21
Orientation (strike/dip)	200/10	± 10/± 10	Low	Orientation of fractures in KFM07A (DZ2) and inferred intersection along HFM21 (DZ2)	
Thickness	6 m		Medium	Intersection along KFM07A (DZ2)	Thickness refers to total zone thickness (transition zone and core)
Length					ZFMNE1206 does not intersect the surface. Truncation in same manner as ZFMNE1203 against ZFMNW1198, ZFMNW1200, ZFMNE0061A, ZFMNE0159, ZFMNS00B7
Ductile deformation			High	Intersection along KFM07A (DZ2)	Not present
Brittle deformation			High	Intersection along KFM07A (DZ2)	Present
Alteration			Medium	Intersection along KFM07A (DZ2)	Red-stained bedrock with fine-grained hematite dissemination
Fracture orientation	Fisher mean of gently dipping to sub-horizontal fracture set = 005/5	K value of gently dipping to sub-horizontal fracture set = 17	Medium	Intersections along KFM07A (DZ2) and HFM21 (DZ2), N=86	Gently dipping and sub-horizontal fractures dominate. Steeply dipping fractures are also present, especially with ENE strike
Fracture frequency	Mean 10 m^{-1}	Span 3–18 m^{-1}	Medium	Intersection along KFM07A (DZ2)	Sealed and open fractures
Fracture filling			Medium	Intersection along KFM07A (DZ2)	Chlorite, calcite, hematite/ adularia, clay minerals

Gently-dipping brittle deformation zones, based solely on seismic reflection data and comparison study

ZFMNE00A1

Property	Quantitative estimate	Span	Confidence level	Basis for interpretation	Comments
Remodelled by applying different truncations to the south-west and north-west. An alternative interpretation of the seismic reflector A1/A0 is that it is related to compositional variations in the bedrock (possibly RFM032)					
Confidence of occurrence: Medium					
Position		± 15 m	High	Seismic reflector A1/A0	Span estimate refers to the general position of the central part of the zone. Estimate based on /Cosma et al. 2003/
Orientation (strike/dip)	082/45	–7/± 5	High	Seismic reflector A1/A0	Strike and dip based on /Cosma et al. 2003/. Span estimate makes use of both /Juhlin et al. 2002, Cosma et al. 2003/
Thickness	70 m	± 30 m	Low	Comparison with ZFMNE00A2	Thickness refers to total zone thickness (transition zone and core)
Length					ZFMNE00A1 is modelled so that it does not intersect the surface, since it has proven difficult to follow seismic reflector A1/A0 to the surface. Truncated against ZFMNW0001, ZFMNW0017 and ZFMNE0810
Ductile deformation			Low	Comparison with high confidence, gently dipping zones	Not present
Brittle deformation			Low	Comparison with high confidence, gently dipping zones	Present
Alteration					
Fracture orientation					
Fracture frequency					
Fracture filling					

Gently-dipping brittle deformation zones, based solely on seismic reflection data and comparison study

ZFMNE0B23

Property	Quantitative estimate	Span	Confidence level	Basis for interpretation	Comments
Remodelled by applying different truncations to the south-west					
Confidence of occurrence: Medium					
Position		± 15 m	High	Seismic reflectors B2 and B3	Seismic reflectors B2 and B3 have been treated together to form a single zone. Span estimate refers to the general position of the central part of the zone. Estimate based on /Cosma et al. 2003/
Orientation (strike/dip)	028/25	± 3/ ± 3	High	Seismic reflectors B2 and B3	/Cosma et al. 2003/. Consistent with /Juhlin et al. 2002/
Thickness	15 m	± 10 m	Low	Comparison with high confidence, gently dipping zones except ZFMNE00A2	Thickness refers to total zone thickness (transition zone and core)
Length					ZFMNEB023 does not intersect the surface. Truncated against ZFMNW0001, ZFMNW023, ZFMNW0123, ZFMNE0062A and ZFMNS0101
Ductile deformation			Low	Comparison with high confidence, gently dipping zones	Not present
Brittle deformation			Low	Comparison with high confidence, gently dipping zones	Present
Alteration					
Fracture orientation					
Fracture frequency					
Fracture filling					

Gently-dipping brittle deformation zones, based solely on seismic reflection data and comparison study

ZFMNW00J1

Property	Quantitative estimate	Span	Confidence level	Basis for interpretation	Comments
Modelled solely on the basis of the seismic reflection data from /Juhlin and Palm 2005, Cosma et al. 2006/ and a comparison study with high confidence, gently- and moderately-dipping zones					
Confidence of occurrence: Medium					
Position		± 15 m	High	Seismic reflector J1	Span estimate refers to the general position of the central part of the zone. Estimate based on /Cosma et al. 2003/
Orientation (strike/dip)	118/45	± 5/ ± 5	High	Seismic reflector J1	Strike and dip after /Juhlin and Palm 2005/. Span estimate makes use of both /Juhlin and Palm 2005/ and /Cosma et al. 2006/
Thickness	15 m	± 10 m	Low	Comparison with high confidence, gently dipping zones except ZFMNE00A2	Thickness refers to total zone thickness (transition zone and core)
Length					ZFMNE00J1 does not intersect the surface. Truncated against ZFMNW0017, ZFMNW0029 and ZFMNW0036
Ductile deformation			Low	Comparison with high confidence, gently dipping zones	Not present
Brittle deformation			Low	Comparison with high confidence, gently dipping zones	Present
Alteration					
Fracture orientation					
Fracture frequency					
Fracture filling					

Appendix 3

Rock mechanics studies

This Appendix contains the results of the rock mechanics studies carried out during modelling stage 2.1 for Forsmark. These studies concern the following main topics:

- Analysis of the results on the laboratory tests carried out on core samples of intact rock.
- Analysis of the results on the laboratory tests carried out on core samples of rock fractures.
- Empirical study on the characterisation of the rock mass in the deformation zones by means of empirical methods.
- Determination of the mechanical properties of two zones in borehole KFM03A by means of numerical method.
- Conceptual and numerical studies about the regional stress field at Forsmark.

A section is dedicated to each of these studies. Comparison and integration of the results contained in each section is contained in the rock mechanics sections in the main text of this report (Sections 2.5 and 3.2).

1 Location of the boreholes

The map in Figure 1-1 will help the reader to locate the position of boreholes where the rock and fracture samples were collected, where the empirical and numerical characterisation was performed, and the central volume for which the rock stresses were modelled.

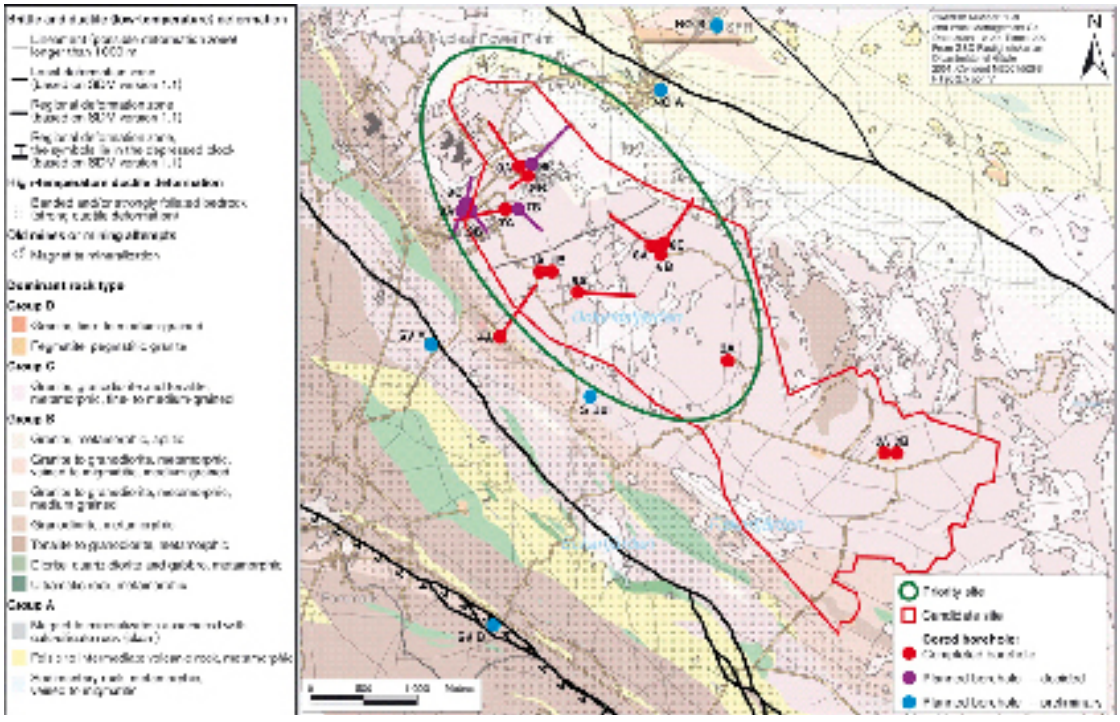

Figure 1-1. *Map of the Forsmark site with indication of the boreholes considered in the analyses in the following sections.*

2 Mechanical properties of the intact rock

Table 2-1 summarises the number of laboratory test results on intact rock available for the present version of Site Descriptive Modelling for Forsmark. Compared to the data set available for version 1.2, new data from testing of several samples of intact rock from borehole KFM05A and KFM06A were available in data freeze 2.1. References to the reports containing the laboratory results are listed in Appendix 1.

In the following sections, the results for each testing technique and tested material are summarised and sometimes compared with the results reported in Forsmark SDM version 1.2 /SKB 2005/.

Table 2-1. Laboratory tests carried out for the Forsmark site descriptive modelling stage 2.1.

Laboratory test	KFM01A[1)]	KFM02A[1)]	KFM03A[1)]	KFM04A[1)]	KFM05A	KFM06A
Uniaxial compressive tests	21	15	17	15	10	16
Triaxial tests	19	12	16	12	8	–
Indirect tensile tests	40	30	40	33	20	5
P-wave velocity on core samples	34	79	68	37		

[1)] Available for version 1.2.

2.1 Uniaxial compressive strength

Table 2-2. Summary of the results of Uniaxial Compressive Strength tests (UCS) performed on intact rock samples from boreholes KFM01A, KFM02A, KFM03A, KFM04A, KFM05A and KFM06A.

Rock type	Number of samples	Minimum UCS (MPa)	Mean UCS (MPa)	Frequent UCS (MPa)	Maximum UCS (MPa)	UCS's Std. dev. (MPa)
Granite to granodiorite, metamorphic, medium-grained	68	166	227	227	289	24
Granodiorite, metamorphic*	4	222	236	236	249	12
Tonalite to granodiorite, metamorphic**	8	140	156	155	176	13
Aplitic granite***	7	157	274	282	371	79
Pegmatite****	2	214	223	223	232	13
Only samples with sealed fractures[a)]	5	127	164	170	188	27

* Samples collected along borehole KFM04A (161–164 m depth).

** Samples collected along borehole KFM03A (278–310 m depth).

*** Samples collected along borehole KFM06A (449 and 818–820 m depth).

**** Samples collected along borehole KFM06A (483 m depth).

[a)] The presence of sealed fractures was observed in the samples after failure.

Table 2-3. Comparison of the results of Uniaxial Compressive Strength tests (UCS) performed on intact rock samples for Forsmark SDM version 1.2 and modelling stage 2.1.

Rock type	Number of samples	Minimum UCS (MPa)	Mean UCS (MPa)	Frequent UCS (MPa)	Maximum UCS (MPa)	UCS's Std. dev. (MPa)
Granite to granodiorite Forsmark 1.2	52	166	225	223	289	22
Granite to granodiorite Forsmark 2.1	68	166	227	227	289	24
Only samples with sealed fractures Forsmark 1.2[a)]	4	145	173	179	188	20
Only samples with sealed fractures Forsmark 2.1[a)]	5	127	164	170	188	27

[a)] The presence of sealed fractures was observed in the samples after failure.

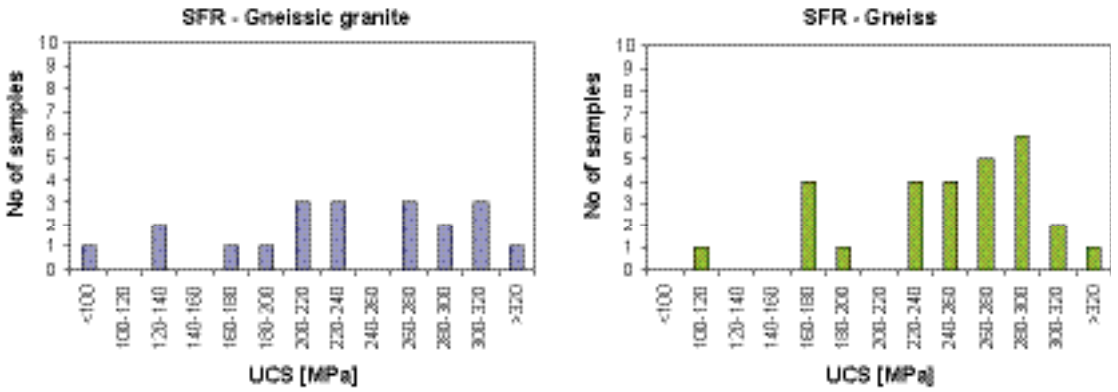

Figure 2-1. *Frequency distributions of the Uniaxial Compressive Strength of similar rock types available at SFR.*

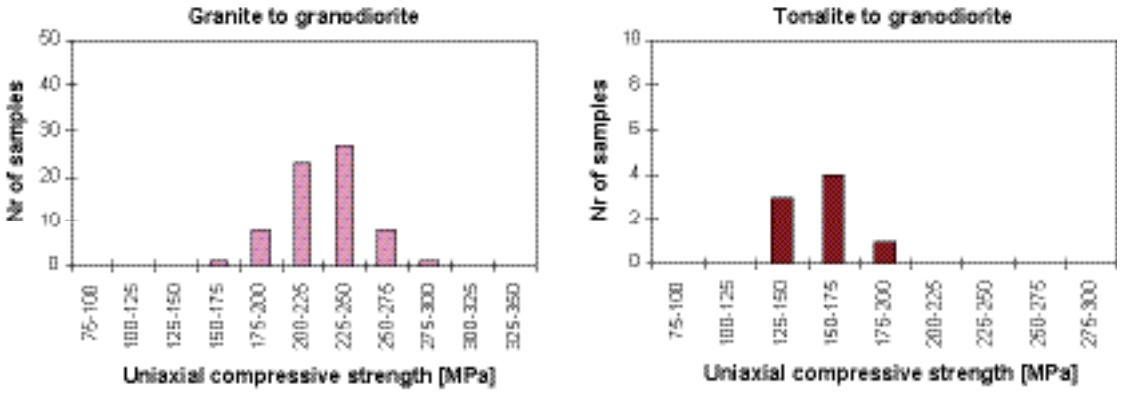

Figure 2-2. *Frequency distributions of the Uniaxial Compressive Strength of similar rock types available for Forsmark modelling stage 2.1.*

2.1.1 Depth dependency

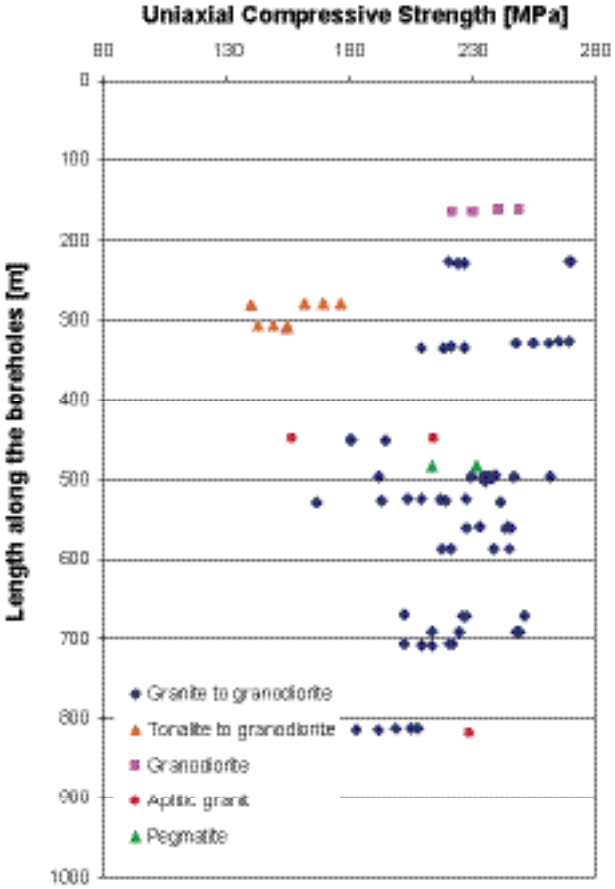

Figure 2-3. *Variation of the uniaxial compressive strength (UCS) of the intact rock with depth based on the data available in modelling stage 2.1 (uniaxial compression tests – boreholes KFM01A, KFM02A, KFM03A, KFM04A, KFM05A and KFM06A). Except for the large difference between granite and granodiorite and tonalite, the tests do not show significant variation of strength with depth for the same rock type.*

2.1.2 Crack initiation stress

Table 2-4. The crack initiation stress σ_{ci} from uniaxial compressive tests performed on intact rock samples from boreholes KFM01A, KFM02A, KFM03A, KFM04A, KFM05A and KFM06A.

Rock type	Number of samples	Minimum σ_{ci} (MPa)	Mean σ_{ci} (MPa)	Frequent σ_{ci} (MPa)	Maximum σ_{ci} (MPa)	σ_{ci}'s Std. dev. (MPa)
Granite to granodiorite	61	60	116	115	187	21
Tonalite to granodiorite	8	69	82	80	95	9
Aplitic granite	7	85	149	160	200	42
Pegmatite	2	110	120	120	130	14

Table 2-5. Comparison of the crack initiation stress from uniaxial compressive tests obtained for Forsmark SDM version 1.2 and modelling stage 2.1.

Rock type	Number of samples	Minimum σ_{ci} (MPa)	Mean σ_{ci} (MPa)	Frequent σ_{ci} (MPa)	Maximum σ_{ci} (MPa)	σ_{ci}'s Std. dev. (MPa)
Granite to granodiorite Forsmark 1.2	45	85	119	117	187	20
Granite to granodiorite Forsmark 2.1	61	60	116	115	187	21

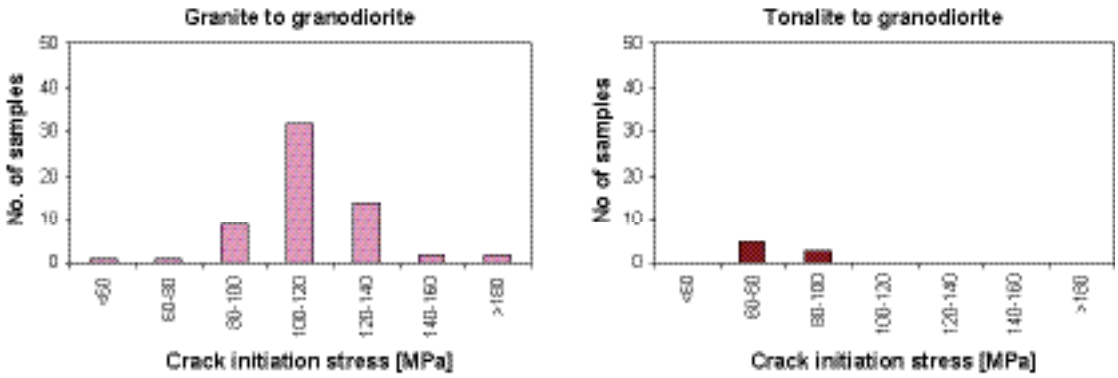

Figure 2-4. *Crack initiation stress for the granite to granodiorite (left) and for the tonalite to granodiorite (right) from the uniaxial compression testing of samples from borehole KFM01A, KFM02A, KFM03A, KFM04A, KFM05A and KFM06A.*

2.2 Triaxial strength

Triaxial tests were carried out on samples from four boreholes /Jacobsson 2004a–d/. For each main rock type (granite to granodiorite, granodiorite, tonalite to granodiorite), the triaxial results were analysed together with the correspondent results of the uniaxial compressive tests. The laboratory results on intact rock samples were interpolated with the Hoek and Brown's Failure Criterion /Hoek et al. 2002/.

$$\sigma'_1 = \sigma'_3 + UCS_T \left(m_i \frac{\sigma'_3}{UCS_T} + 1 \right)^{0.5} \quad (1)$$

where σ'_1 and σ'_3 are the maximum and minimum principal stress and m_i is a strength parameter typical for each rock type. UCS_T is obtained by matching the uniaxial and triaxial test results (Table 2-6).

When analysing the laboratory results, the intact rock parameters in Table 2-6 are obtained. Although obtained in a slightly different way, the results of the UCS are in rather good agreement with the values in obtained on uniaxial tests only (Table 2-2).

The Coulomb's linear approximations of the Hoek and Brown's Criterion were also calculated for a certain stress interval (0 to 15 MPa, Table 2-8).

Table 2-6. Parameters for the Hoek and Brown's Criterion based on the results of uniaxial and triaxial tests performed on intact rock sampled from boreholes KFM01A, KFM02A, KFM03A, KFM04A and KFM05A and KFM06A.

Rock type	Number of samples	Lower limit		Average		Upper limit	
		USC (MPa)	mi	UCS (MPa)	mi	UCS (MPa)	mi
Granite to granodiorite, metamorphic, medium-grained	123	176	30.5	227	28.6	279	27.4
Granodiorite, metamorphic	7[1)]	185	31.6	230	30.6	275	29.9
Tonalite to granodiorite, metamorphic	16[2)]	135	9.6	158	9.4	181	9.2

[1)] Only samples from KFM04A.

[2)] Only samples from KFM03A.

Table 2-7. Comparison of the parameters for the Hoek and Brown's Criterion obtained for Forsmark SDM version 1.2 and modelling stage 2.1.

Rock type	Number of samples	Lower limit		Average		Upper limit	
		USC (MPa)	mi	UCS (MPa)	mi	UCS (MPa)	mi
Granite to granodiorite, Forsmark 1.2	99	178	28.6	227	27.0	275	26.0
Granite to granodiorite, Forsmark 2.1	123	176	30.5	227	28.6	279	27.4

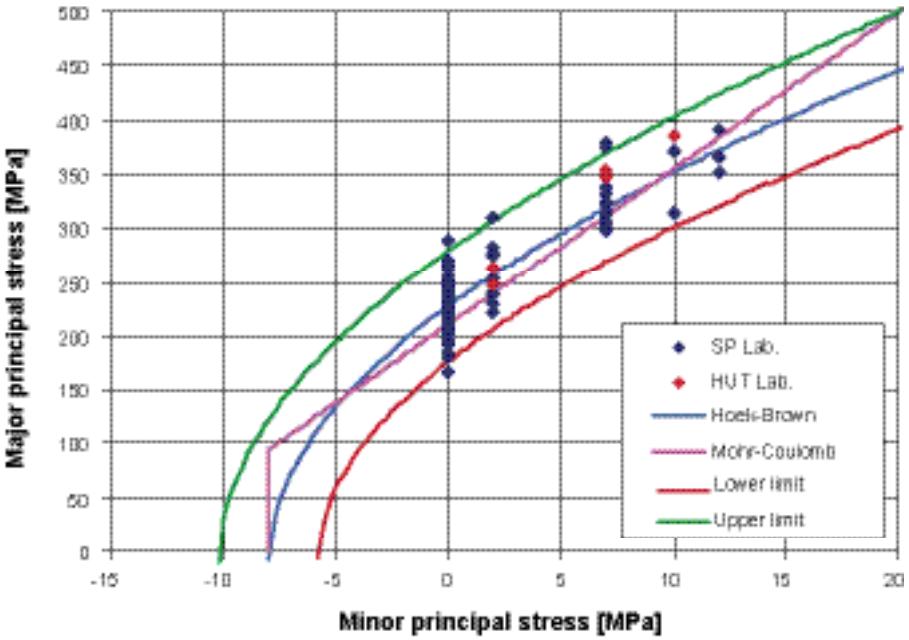

Figure 2-5. *Hoek and Brown's and Coulomb's failure envelopes for the samples of granite to granodiorite from the uniaxial and triaxial tests analysed in modelling stage 2.1 (KFM01A, KFM02A, KFM03A, KFM04A, KFM05A and KFM06A).*

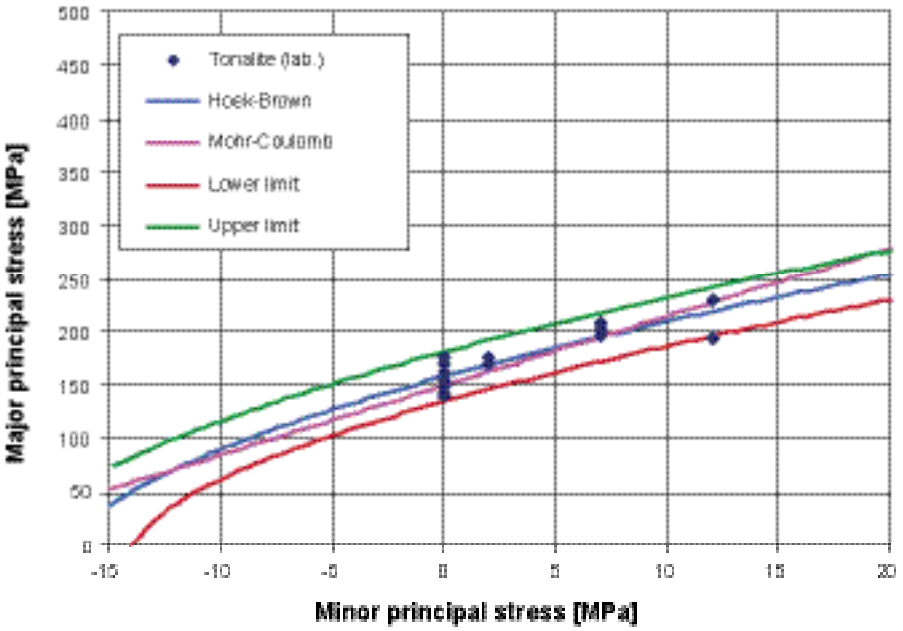

Figure 2-6. *Hoek and Brown's and Coulomb's failure envelopes for the samples of tonalite to granodiorite from the uniaxial and triaxial tests analysed in modelling stage 2.1 (KFM03A, unchanged with respect to version 1.2).*

Table 2-8. Parameters for the Coulomb's Criterion based on the results of uniaxial and triaxial tests performed on intact rock sampled from boreholes KFM01A, KFM02A, KFM03A, KFM04A, KFM05A and KFM06A.

Rock type	Number of samples	Lower limit		Average		Upper limit	
		c'_i (MPa)	ϕ'_i (°)	c'_i (MPa)	ϕ'_i (°)	c'_i (MPa)	ϕ'_i (°)
Granite to granodiorite, metamorphic, medium-grained	123	21.9	59.9	27.6	60.5	33.5	61.0
Granodiorite, metamorphic	7	22.6	60.5	27.3	61.2	32.1	61.7
Tonalite to granodiorite, metamorphic	16	25.2	46.7	29.5	47.0	33.8	47.3

These values of cohesion and friction angle are determined for a confinement stress between 0 and 15 MPa.

Table 2-9. Comparison of the parameters for the Coulomb's Criterion based on the results of uniaxial and triaxial tests performed on intact rock obtained for Forsmark SDM version 1.2 and modelling stage 2.1.

Rock type	Number of samples	Lower limit		Average		Upper limit	
		c'_i (MPa)	ϕ'_i (°)	c'_i (MPa)	ϕ'_i (°)	c'_i (MPa)	ϕ'_i (°)
Granite to granodiorite, Forsmark 1.2	99	22.5	59.4	28.1	60.0	33.7	60.4
Granite to granodiorite, Forsmark 2.1	123	21.9	59.9	27.6	60.5	33.5	61.0

These values of cohesion and friction angle are determined for a confinement stress between 0 and 15 MPa.

Table 2-10. Estimated standard deviation of the cohesion and friction angle of the intact rock from uniaxial and triaxial testing results.

Rock type	Estimated std. dev. of c'_i (MPa)	Estimated std. dev. of ϕ'_i (°)
Granite to granodiorite, metamorphic, medium-grained	3.0	0.3
Granodiorite, metamorphic	2.4	0.3
Tonalite to granodiorite, metamorphic	2.2	0.2

These values of cohesion and friction angle are determined for a confinement stress between 0 and 15 MPa.

2.3 Indirect tensile strength

Table 2-11. Summary of the results of indirect tensile tests performed on intact rock samples from boreholes KFM01A, KFM02A, KFM03A, KFM04A, KFM05A and KFM06A.

Rock type	Number of samples	Minimum TS (MPa)	Mean TS (MPa)	Frequent TS (MPa)	Maximum TS (MPa)	TS Std. dev. (MPa)
Granite to granodiorite, metamorphic, medium-grained	132	9.7	13.5	13.7	17.9	1.7
Granodiorite, metamorphic	11	16.8	18.0	17.8	19.7	1.0
Tonalite to granodiorite, metamorphic	20	13.7	15.6	15.8	17.5	1.1
Pegmatite	5	11.9	14.1	14.2	16.2	1.7

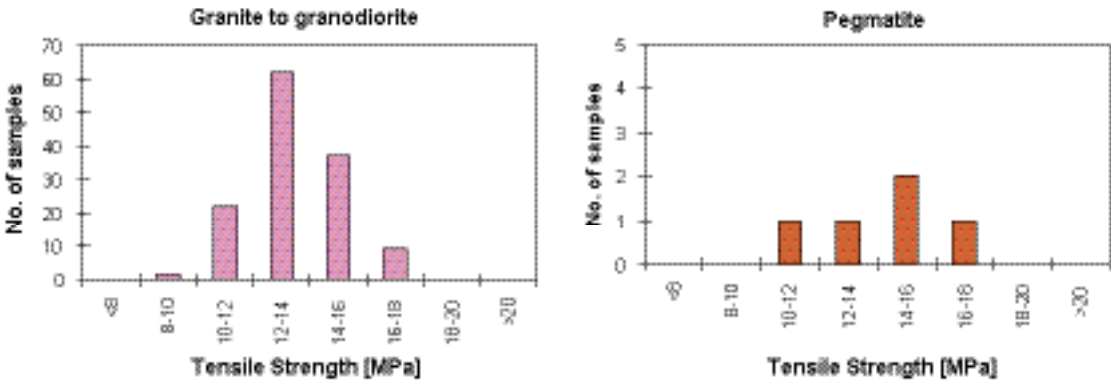

Figure 2-7. *Frequency distribution of all the results from tensile tests on intact rock samples from boreholes KFM01A, KFM02A, KFM03A, KFM04A, KFM05A and KFM06A (all orientations with respect to the foliation).*

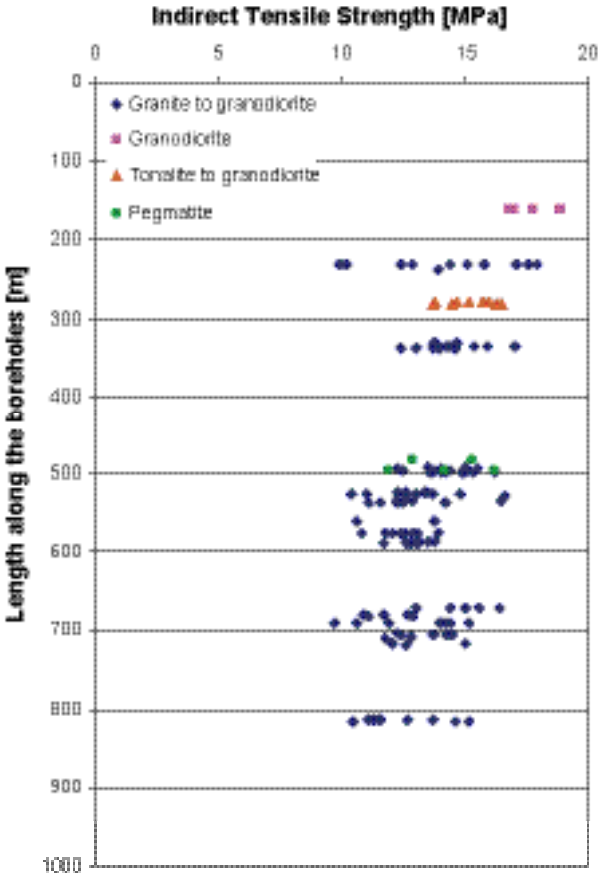

Figure 2-8. *Variation of the indirect tensile strength TS of the intact rock with depth for the data available in modelling stage 2.1 (boreholes KFM01A, KFM02A, KFM03A, KFM04A, KFM05A and KFM06A). For the same rock type, the tests do not show significant variation of strength with depth.*

2.4 Young's modulus

2.4.1 Uniaxial loading

Table 2-12. Summary of the results of Young's modulus E from uniaxial compressive tests performed on intact rock samples from borehole KFM01A, KFM02A, KFM03A, KFM04A, KFM05A and KFM05A.

Rock type	Number of samples	Minimum E (GPa)	Mean E (GPa)	Frequent E (GPa)	Maximum E (GPa)	E's Std. dev. (GPa)
Granite to granodiorite, metamorphic, medium-grained	68	69	76	76	83	3
Granodiorite, metamorphic	4	73	77	77	81	3
Tonalite to granodiorite, metamorphic	8	69	72	71	78	3
Aplitic granite	7	75	81	81	86	4
Pegmatite	2	71	72	72	72	1
Only samples with sealed fractures	5	76	79	79	83	3

Table 2-13. Comparison of the results of Young's modulus E from uniaxial compressive tests performed on intact rock samples for Forsmark SDM version 1.2 and modelling stage 2.1.

Rock type	Number of samples	Minimum E (GPa)	Mean E (GPa)	Frequent E (GPa)	Maximum E (GPa)	E's Std. dev. (GPa)
Granite to granodiorite, Forsmark 1.2	52	69	76	76	82	3
Granite to granodiorite, Forsmark 2.1	68	69	76	76	83	3
Only samples with sealed fractures Forsmark 1.2	4	76	80	80	83	3
Only samples with sealed fractures Forsmark 2.1	5	76	79	79	83	3

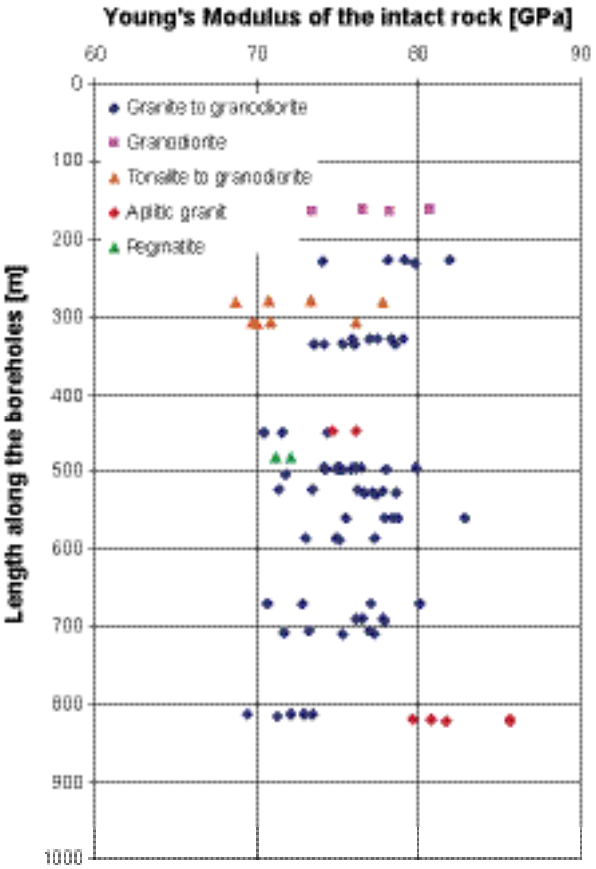

Figure 2-9. *Variation of the Young's modulus of the intact rock with depth for the data available in modelling stage 2.1 (uniaxial compression tests – boreholes KFM01A, KFM02A, KFM03A, KFM04A, KFM05A and KFM06A).*

2.4.2 *Triaxial loading*

Table 2-14. Summary of the results of deformation modulus Et from triaxial compressive tests performed on intact rock samples from borehole KFM01A, KFM02A, KFM03A, KFM04A and KFM05A.

Rock type	Number of samples	Minimum Et (GPa)	Mean Et (GPa)	Frequent Et (GPa)	Maximum Et (GPa)	Et's Std. dev. (GPa)
Granite to granodiorite, metamorphic, medium-grained	55	69	75	75	85	3
Granodiorite, metamorphic	3	71	75	76	78	4
Tonalite to granodiorite, metamorphic	8	65	70	71	75	3

Table 2-15. Comparison of the results of deformation modulus Et from triaxial compressive tests performed on intact rock samples for Forsmark SDM version 1.2 and modelling stage 2.1.

Rock type	Number of samples	Minimum Et (GPa)	Mean Et (GPa)	Frequent Et (GPa)	Maximum Et (GPa)	Et's Std. dev. (GPa)
Granite to granodiorite, Forsmark 1.2	47	69	74	74	81	3
Granite to granodiorite, Forsmark 2.1	55	69	75	75	85	3

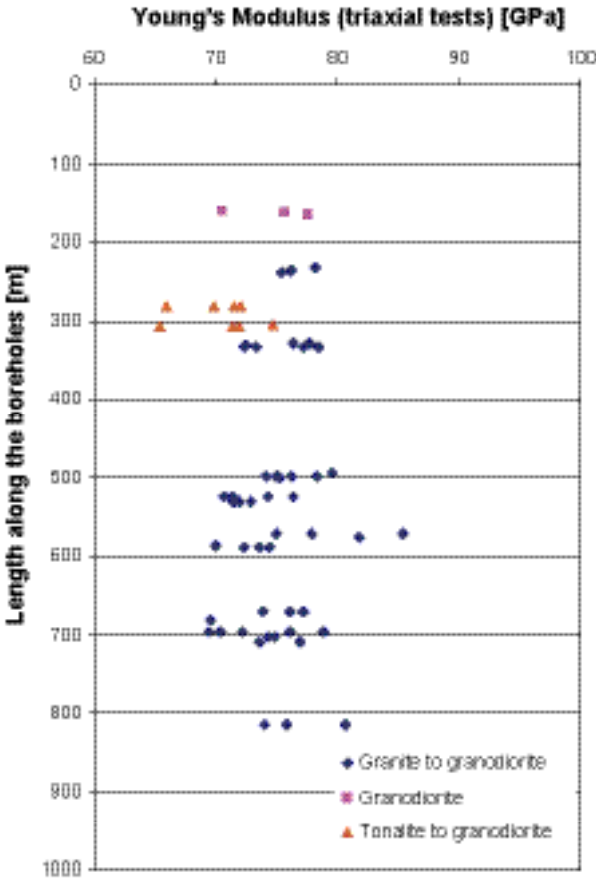

Figure 2-10. *Variation of the Young's modulus of the intact rock with depth for the data available in modelling stage 2.1 (triaxial compression tests – boreholes KFM01A, KFM02A, KFM03A, KFM04 and KFM05A). The tests do not show significant variation of stiffness with depth and with rock type.*

2.5 Poisson's ratio

2.5.1 Uniaxial loading

Table 2-16. Summary of the results of Poisson's ratio ν from uniaxial compressive tests performed on intact rock sampled from borehole KFM01A, KFM02A, KFM03A, KFM04A, KFM05A and KFM06A.

Rock type	Number of samples	Minimum ν (–)	Mean ν (–)	Frequent ν (–)	Maximum ν (–)	ν Std. dev. (–)
Granite to granodiorite, metamorphic, medium-grained	68	0.14	0.24	0.24	0.35	0.04
Granodiorite, metamorphic	4	0.19	0.23	0.24	0.25	0.03
Tonalite to granodiorite, metamorphic	8	0.23	0.27	0.27	0.34	0.04
Aplitic granite	7	0.23	0.26	0.25	0.31	0.03
Pegmatite	2	0.27	0.29	0.29	0.30	0.02
Only samples with sealed fractures	5	0.18	0.23	0.23	0.31	0.05

Table 2-17. Comparison of the results of Poisson's ratio ν from uniaxial compressive tests performed on intact rock sampled for Forsmark SDM version 1.2 and modelling stage 2.1.

Rock type	Number of samples	Minimum ν (–)	Mean ν (–)	Frequent ν (–)	Maximum ν (–)	ν Std. dev. (–)
Granite to granodiorite, Forsmark 1.2	52	0.14	0.24	0.24	0.30	0.04
Granite to granodiorite, Forsmark 2.1	68	0.14	0.24	0.24	0.35	0.04
Only samples with sealed fractures Forsmark 1.2	4	0.18	0.24	0.23	0.31	0.06
Only samples with sealed fractures Forsmark 2.1	5	0.18	0.23	0.23	0.31	0.05

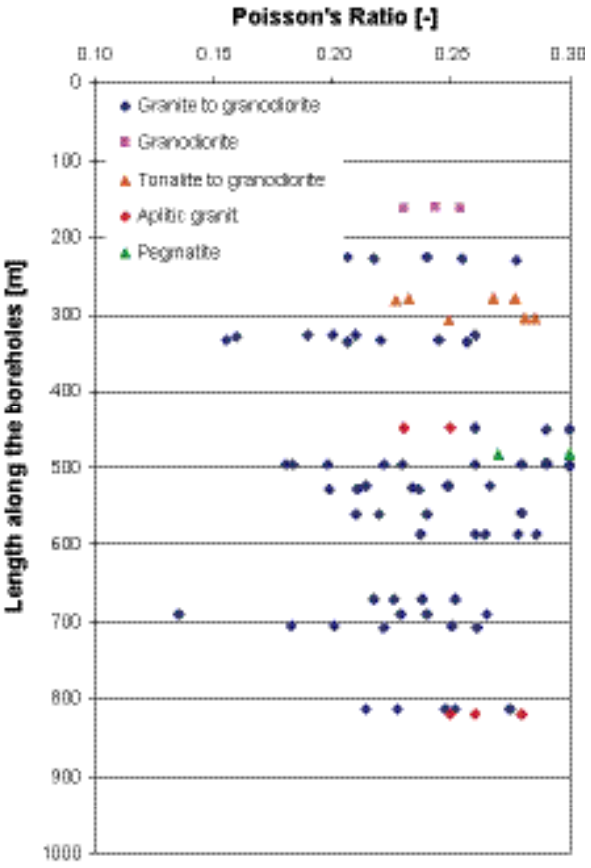

Figure 2-11. *Variation of the Poisson's ratio of the intact rock with depth for the data available in modelling stage 1.2 (uniaxial compression tests – boreholes KFM01A, KFM02A, KFM03A, KFM04A, KFM05A and KFM06A).*

2.5.2 *Triaxial loading*

Table 2-18. Summary of the results of Poisson's ratio νt from triaxial compressive tests performed on intact rock sampled from borehole KFM01A–KFM04A.

Rock type	Number of samples	Minimum νt (–)	Mean νt (–)	Frequent νt (–)	Maximum νt (–)	νt's Std. dev. (–)
Granite to granodiorite, metamorphic, medium-grained	55	0.15	0.20	0.19	0.31	0.04
Granodiorite, metamorphic	3	0.18	0.18	0.18	0.19	0.01
Tonalite to granodiorite, metamorphic	8	0.18	0.20	0.20	0.23	0.02

Table 2-19. Comparison of the results of Poisson's ratio νt from triaxial compressive tests performed on intact rock sampled for Forsmark SDM version 1.2 and modelling stage 2.1.

Rock type	Number of samples	Minimum νt (–)	Mean νt (–)	Frequent νt (–)	Maximum νt (–)	νt's Std. dev. (–)
Granite to granodiorite, Forsmark 1.2	47	0.15	0.20	0.19	0.31	0.04
Granite to granodiorite, Forsmark 2.1	55	0.15	0.20	0.19	0.31	0.04

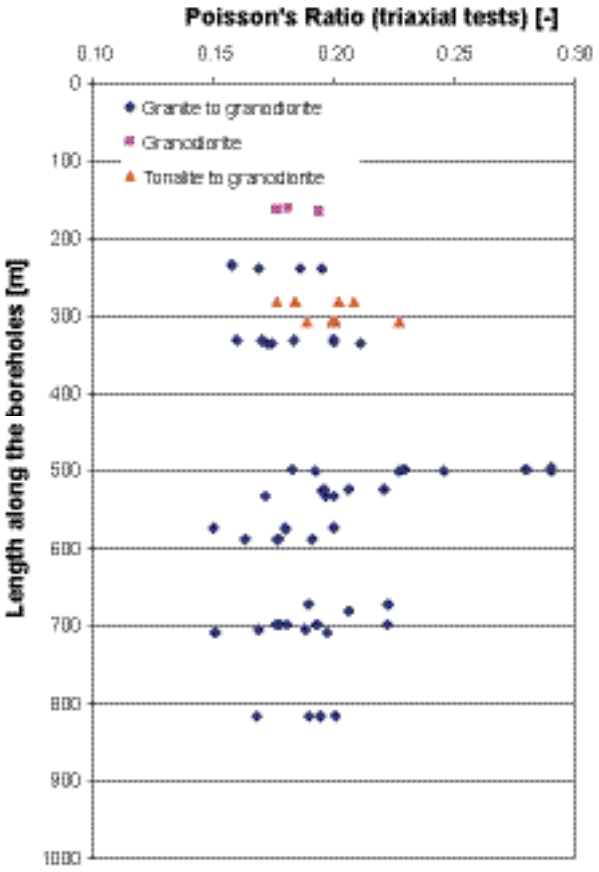

Figure 2-12. *Variation of the Poisson's ratio of the intact rock with depth for the data available in modelling stage 2.1 (triaxial compression tests – boreholes KFM01A, KFM02A, KFM03A, KFM04A, KFM05A and KFM06A).*

2.6 Discussion

The amount of tests available at this stage of the site investigations allows for a deeper analysis of the results with respect to position and elevation (here called “depth”), at least for the predominant rock type (granite to granodiorite – code 101057).

By observing the variation of the mean value and standard deviation of a certain parameter for an increasing number of samples, the representativity of the sample can be estimated. If the samples represent the same population, the mean value and standard deviation should stabilize when the number of samples is large. If this does not occur, then either the number of samples is too small or the samples come from different populations.

For the uniaxial compressive strength, the plot of the mean and standard deviation versus the number of samples show that the mean value is already stable for about 40 samples. The same applies for the standard deviation, except when samples from KFM06A are accounted for. In this last case, the standard deviation still increases for a total amount of test results of 68. This can be explained with the uniaxial compressive strength from borehole KFM06A depending on the position of this borehole.

Comparing different boreholes, the uniaxial compressive strength and the crack initiation stress are largest in KFM01A. Slightly lower mean value than for KFM01A is observed for KFM05A. The lowest mean values belong to borehole KFM02A. The largest variances are found for borehole KFM01A, KFM02A and KFM06A.

When comparing all test results divided according to depth, the mean value of the uniaxial compressive strength and crack initiation stress tend to diminish appreciably beneath 550 m. For these two parameters, the difference between the mean values above and below 550 m is about 10%. Also the standard deviation diminishes with depth.

The mean Young’s modulus of the samples is very stable independently on the number of samples. Its standard deviation, on the other hand, seems to increase almost constantly as the number of samples increases. The standard deviation of the Young’s modulus is largest for test results from borehole KFM03A and KFM06A.

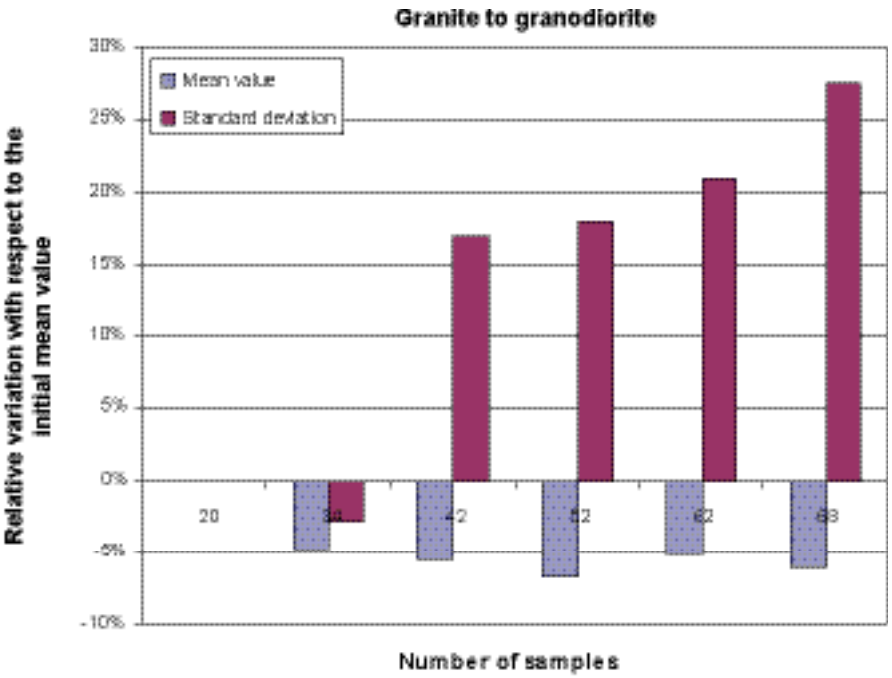

Figure 2-13. *Relative mean value and standard deviation of the uniaxial compressive strength of the intact rock samples of granite to granodiorite collected from a depth between 400 and 550 m – All samples available in modelling stage 2.1. The initial values are calculated on the results for KFM01A.*

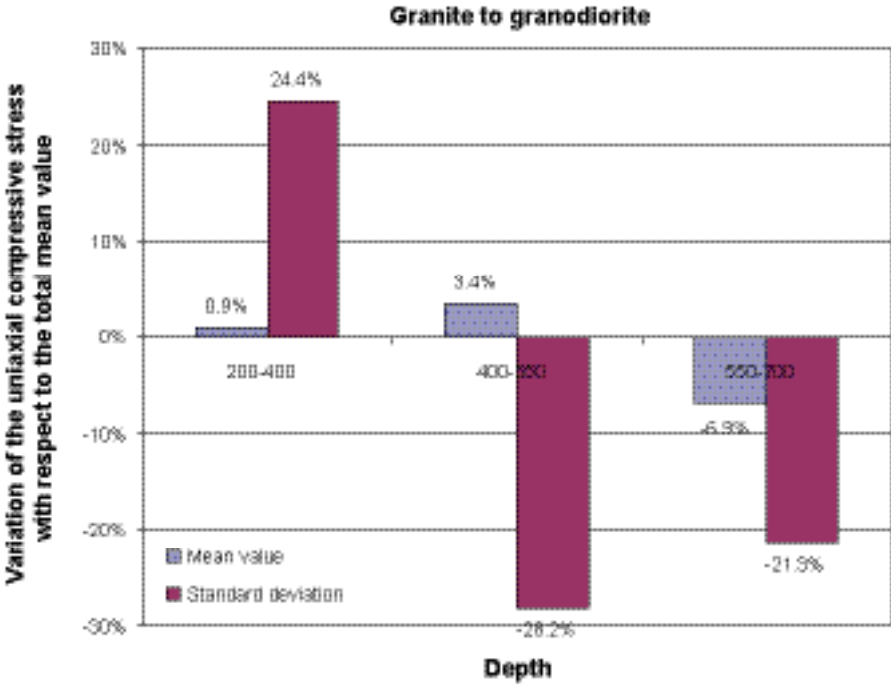

Figure 2-14. *Relative mean value and standard deviation of the uniaxial compressive strength of the intact rock samples of granite to granodiorite collected from a depth between 400 and 550 m in the target area. The reference values are calculated from data at all depths.*

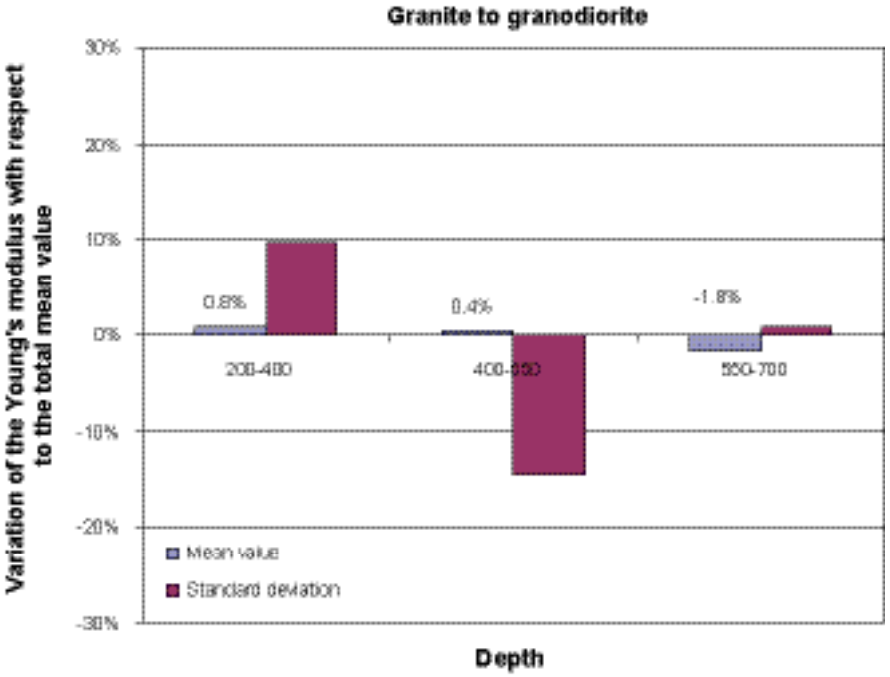

Figure 2-15. *Relative mean value and standard deviation of the Young's modulus of the intact rock samples of granite to granodiorite collected from a depth between 400 and 550 m in the target area. The reference values are calculated from data at all depths.*

The Young's modulus is not as sensitive to depth as the uniaxial compressive strength. The decrease between results above and below 550 m is less than 3%. The standard deviation of the Young's modulus only vary between +10% and –16% for the investigated depths.

The Poisson's ratio of the samples shows a rather different behaviour than the other parameters from uniaxial compression. Grouped for each borehole, the samples give mean Poisson's ratio between 0.21 and 0.25. The samples from KFM06A show much higher mean Poisson's ratio (larger than 0.30). The mean value of the Poisson's ration does not vary more than ± 7% with depth, with the highest value for a depth between 400 and 550 m. For what concerns the standard deviation, this is rather uniform for all boreholes but tends to diminish with depth (–13%).

There seems to be a difference in the strength and the deformability behaviour of the samples from different boreholes. For example:

- KFM01A and KFM05A show the highest uniaxial compressive strength and crack initiation stress of all the boreholes.
- For depths between 400 and 550 m, also KFM04A has high mean strength parameters.
- KFM02A presents among the lowest mean uniaxial compressive strength and crack initiation stress.
- The Young's modulus and Poisson's ratio do not seem to be related to the strength parameters, and all boreholes, except KFM06A, show very good agreement of the results.
- KFM06A represent an exception, showing among the lowest Young's modulus and absolutely the highest Poisson's ratio of all boreholes.

Thus, one hypothesis could be that the intact rock in borehole KFM01A, KFM04A and KFM05A is rather homogeneous. The rock in this area would differ then from the rock in KFM02A, which present lower strength, and from the rock in KFM06A, which show rather different deformability properties. Based on the data available today, the properties of the intact rock in KFM03A seem to resemble to the average properties of the group of boreholes KFM01A, KFM04A and KFM05A.

The mechanical properties of intact rock samples of granite to granodiorite are treated to provide properties of the rock domain RFM029 inside and outside the target area. The following aspects have been considered:

a) Inside the target area, the mechanical properties of the samples from borehole KFM01A, KFM02A, KFM04A, KFM05A and KFM06A have been used.

b) Samples collected from KFM02A at depth between 518 and 520 m were not taken into account because the rock at this depths is classified as potential deformation zone in the "single-hole interpretation" /Carlsten et al. 2004a/.

c) Samples collected from KFM06A show a very large range of uniaxial compressive strength values and unusually high Poisson's ratio that might indicate the influence of frequent intrusions of pegmatite, pegmatitic granite, aplitic granite and amphibolite on the mechanical properties of the samples /Petersson et al. 2005/.

d) Outside the target area, only information from borehole KFM03A is available. Thus, all the boreholes are considered.

The summary of the intact rock properties also shows that the deterioration of the uniaxial compressive strength and crack initiation stress with depth is larger (about 10%) than the deterioration of the Young's modulus and Poisson's ratio (about 3%). This deterioration can be explained with micro-cracking due to high stresses and stress path followed by the core during drilling. However, there is not appreciable difference between the results from vertical boreholes than for inclined boreholes.

Table 2-20. Rock domain RFM029 – target area: Summary of the results of Uniaxial Compressive Strength tests (UCS) performed on intact rock samples of granite to granodiorite from boreholes KFM01A, KFM02A, KFM04A, KFM05A and KFM06A.

Granite to granodiorite, metamorphic, medium-grained	Number of samples	Minimum UCS (MPa)	Mean UCS (MPa)	Frequent UCS (MPa)	Maximum UCS (MPa)	UCS's Std. dev. (MPa)
200–400 m	18	180.4	231.3	225.5	270.1	29.5
400–550 m	24*	192.1	237.0	237.0	288.6	17.0
550–700 m	14	183.1	213.6	211.3	249.1	18.7

* Samples collected at 518–520 m depth along borehole KFM02A are not considered.

Table 2-21. Rock domain RFM029 – target area: Summary of the results of Young's modulus E from uniaxial compressive tests on intact rock samples of granite to granodiorite from boreholes KFM01A, KFM02A, KFM04A, KFM05A and KFM06A.

Granite to granodiorite, metamorphic, medium-grained	Number of samples	Minimum E (GPa)	Mean E (GPa)	Frequent E (GPa)	Maximum E (GPa)	E's Std. dev. (GPa)
200–400 m	18	70.5	76.4	76.5	81.9	3.0
400–550 m	24*	71.8	76.1	75.4	82.9	2.3
550–700 m	14	69.5	74.4	74.4	77.9	2.7

* Samples collected at 518–520 m depth along borehole KFM02A are not considered.

Table 2-22. Rock domain RFM029 – target area: Summary of the results of Poisson's ratio ν from uniaxial compressive tests on intact rock samples of granite to granodiorite from boreholes KFM01A, KFM02A, KFM04A, KFM05A and KFM06A.

Granite to granodiorite, metamorphic, medium-grained	Number of samples	Minimum ν (–)	Mean ν (–)	Frequent ν (–)	Maximum ν (–)	ν's Std. dev. (–)
200–400 m	18	0.16	0.23	0.23	0.30	0.04
400–550 m	24*	0.18	0.26	0.26	0.35	0.04
550–700 m	14	0.14	0.23	0.23	0.28	0.04

* Samples collected 518–520 m depth along borehole KFM02A are not considered.

Table 2-23. Rock domain RFM029 – target area: Summary of the results of crack initiation stress σ_{ci} from uniaxial compressive tests on intact rock samples of granite to granodiorite from boreholes KFM01A, KFM02A, KFM04A, KFM05A and KFM06A.

Granite to granodiorite, metamorphic, medium-grained	Number of samples	Minimum σ_{ci} (MPa)	Mean σ_{ci} (MPa)	Frequent σ_{ci} (MPa)	Maximum σ_{ci} (MPa)	σ_{ci}'s Std. dev. (MPa)
200–400 m	18	60.0	116.2	115.0	187.0	33.6
400–550 m	24*	100.0	121.2	120.0	160.0	13.0
550–700 m	14	95.0	109.9	110.0	130.0	10.1

* Samples collected 518–520 m depth along borehole KFM02A are not considered.

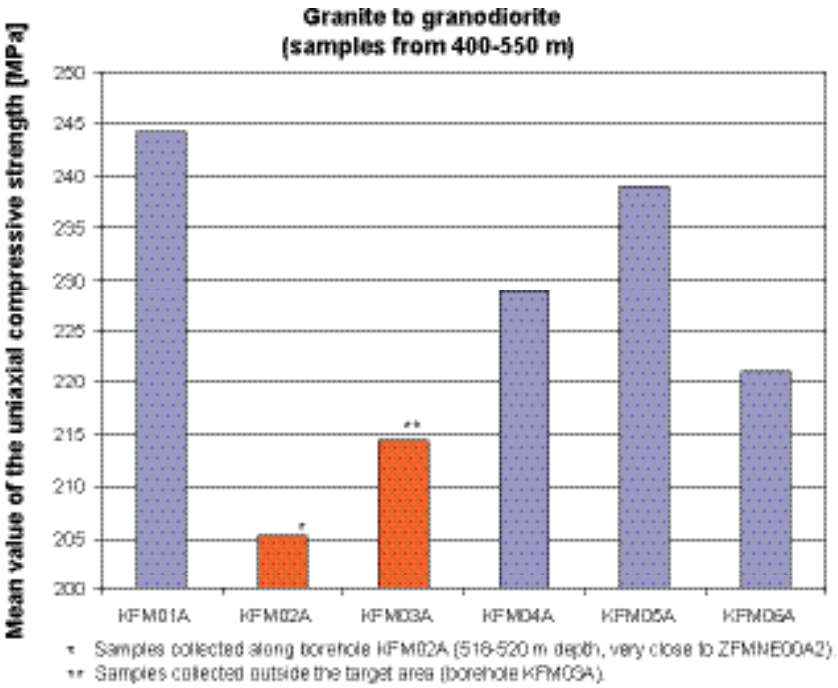

Figure 2-16. Mean value of the uniaxial compressive strength of the samples from intact rock samples of granite to granodiorite collected from a depth between 400 and 550 m. In blue are the boreholes considered for the target area.

Figure 2-17 and Figure 2-18 show the P-wave velocity measured along the borehole in situ and on the borehole core in laboratory for all rock mechanics boreholes at Forsmark, respectively. Some of the boreholes exhibit a reduction of the laboratory values with elevation probably due to the deterioration of the core quality due to microcraking induced by the high in situ stresses.

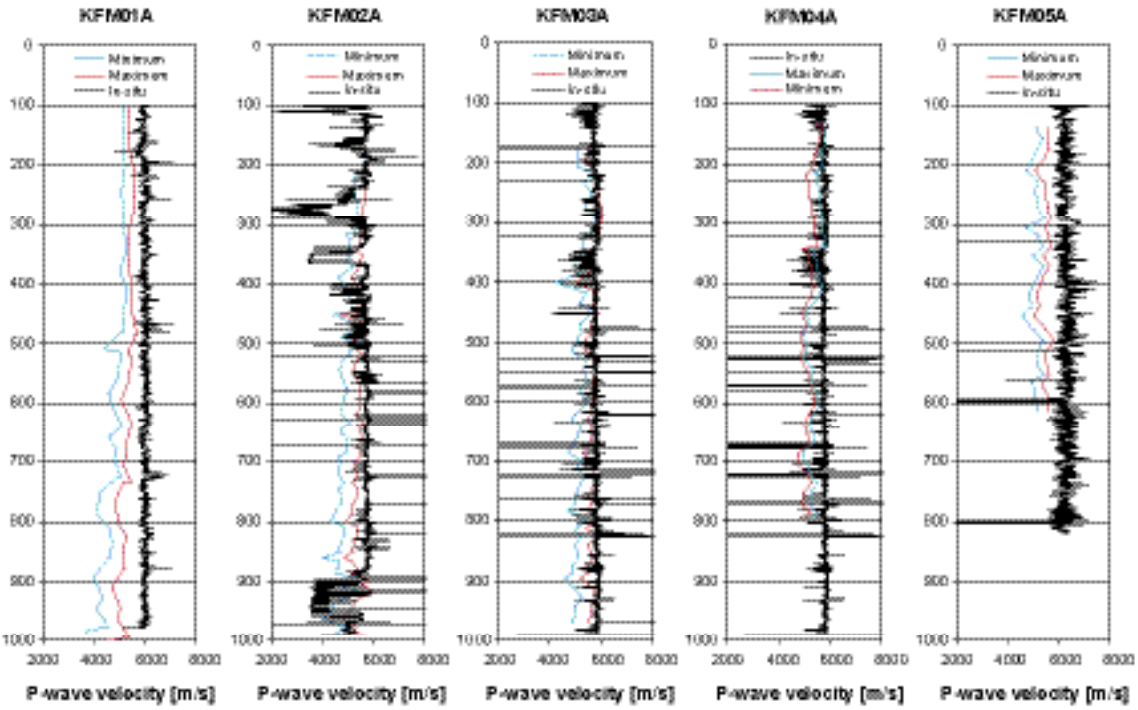

Figure 2-17. *Plot of the P-wave velocity measured in situ and on the borehole cores with depth for all the boreholes included in Forsmark 1.2.*

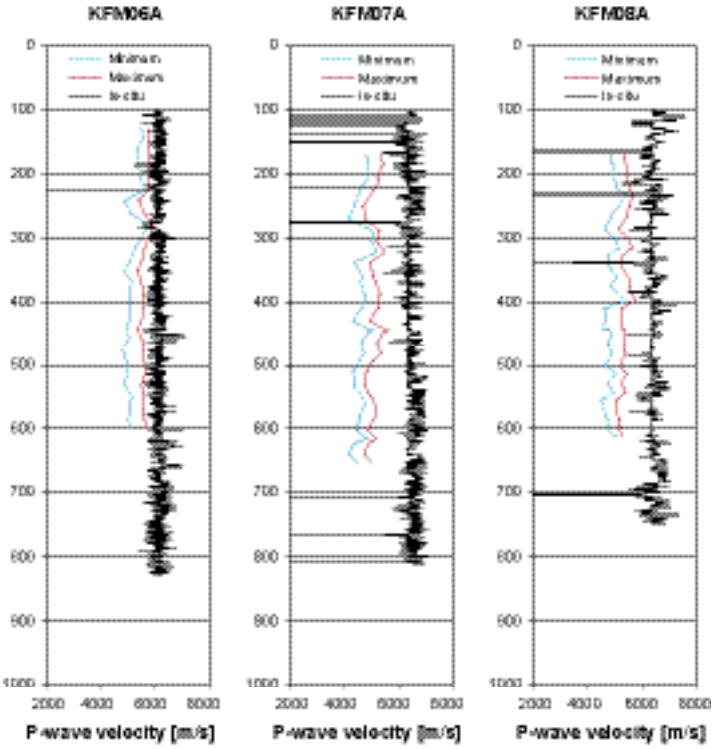

Figure 2-18. *Plot of the P-wave velocity measured in situ and on the borehole cores with depth for the boreholes included in data freeze 2.1.*

3 Mechanical properties of the fractures

Mechanical tests have been performed on rock fractures (Table 3-1):

- Normal loading tests and shear tests in boreholes KFM01A, KFM02A, KFM03A, KFM04A, KFM05A and KFM06A. Peak and residual cohesion and friction angle, dilation angle as well as normal and shear stiffness are calculated from these tests (see Appendix 1 in this report).
- Tilt tests in boreholes KFM01A, KFM02A, KFM03A, KFM04A and KFM05A. The determined parameters are: basic friction angle, JRC, JCS and residual friction angle (see Appendix 1 in this report). The results of these tests are used to evaluate the peak and residual cohesion and friction angle.

The results of the tests have been evaluated and analysed with regards to different aspects such as test method (for peak and residual cohesion and friction angle), fracture orientation sets, depth, and rock unit.

An important issue is the evaluation of the rock fracture properties with respect to the fracture sets and rock unit where the samples are taken. In fact, sometimes, there are uncertainties in the coupling between sampled fractures and mapped fractures in BOREMAP at the same elevation.

3.1 Rock fracture properties from shear tests

The methodology for shear tests have been modified since version 1.2 and the impact of this change on the mechanical properties will first be assessed. The modification was applied as it appeared that the deformation of the mould was affecting the deformation of the sample in the normal direction.

3.1.1 Impact of the modification of the methodology

The modified methodology has been applied on two boreholes only and 10 rock fracture samples (4 from KFM05A and 6 from KFM06A). The only data available for direct comparison are from KFM05A which samples have been tested with both the “old” and the modified methodology. Four rock fracture samples were tested with each methodology.

Table 3-1 illustrates the mechanical properties evaluated, using both methodologies, on rock fracture samples collected in KFM05A. The mechanical properties are evaluated in the interval 0–20 MPa. The impact of the methodology on the normal stiffness is highly significant, up to a factor 3. The values of shear stiffness are still in the same order of magnitude and the values obtained by the modified methodology are included in the range of variation of the values calculated using the “old” methodology. Moreover the properties obtained on samples tested with the modified methodology show a decreased standard deviation and range of values for the same amount of tested samples.

Table 3-2 illustrates that the impact of the modified methodology seems to be higher on the normal stiffness, for which the methodology was modified. In order to complete the study the samples tested with the modified methodology in both KFM05A and KFM06A were combined and the evaluated properties are presented in Table 3-3. These properties are based on 10 rock fractures sampled in two boreholes. Comparing these results with Table 3-2 shows that values obtained in KFM05A with the modified methodology are relatively high. Table 3-3 illustrates the large variation of the normal stiffness for he 10 tested samples.

Table 3-1. Laboratory tests carried out on fractures for the Forsmark site descriptive modelling stage 2.1.

Laboratory test	KFM01A[1)]	KFM02A[1)]	KFM03A[1)]	KFM04A[1)]	KFM05A	KFM06A
Shear tests on fractures	33 (7 samples)	21 (7 samples)	24 (8 samples)	18 (6 samples)	12+12 (4+4 samples)	18 (6 samples)
Tilt tests on fractures	41	40	35	26	9	–

[1)] available for version 1.2.

Table 3-2. Comparison of the rock fracture properties from shear tests using the "old" and the modified methodology, KFM05A.

		Mean	Std. dev.	Min	Max
Normal stiffness, K_n [MPa/mm]	modified	1,304.8	230.8	1,000.8	1,527.6
	"old"	155.7	94.0	68	512.2
Shear stiffness, K_s [MPa/mm]	modified	20.7	5.5	17.8	28.9
	"old"	26.0	15.2	13.9	48.7
Peak cohesion. C_p [MPa]	modified	1.0	0.4	0.4	1.3
	"old"	0.7	0.2	0.7	1.3
Peak friction angle, ϕ_p [°]	modified	33.5	3.6	28.1	36.0
	"old"	36.5	3.0	34.4	40.8
Dilation angle, i [°] at normal stress 0.5 MPa	modified	19.8	6.2	11.0	25.6
	"old"	20.3	4.3	14.0	23.6
Dilation angle, i [°] at normal stress 5 MPa	modified	10.2	4.7	3.2	13.3
	"old"	12.4	3.8	6.8	15.3
Dilation angle, i [°] at normal stress 20 MPa	modified	3.9	2.6	0.04	5.6
	"old"	5.25	2.9	1.1	8.0

Table 3-3. Summary of the results from shear tests applying the modified methodology on KFM05A (4 samples) and KFM06A (6 samples).

	Mean	Std. dev.	Min	Max
Normal stiffness, K_n (MPa/mm)	937.4	462.1	319.1	1,527.6
Shear stiffness, K_s (MPa/mm)	19.9	5.7	9.5	28.9
Peak cohesion. C_p (MPa)	0.8	0.4	0.2	1.3
Peak friction angle, ϕ_p (°)	35.0	2.9	28.1	38.5
Residual cohesion, C_r (MPa)	0.3	0.1	0.1	0.4
Residual friction angle, ϕ_r (°)	33.6	2.2	28.7	36.6
Dilation angle, i (°) at normal stress 0.5 MPa	17.6	6.9	7.7	27.4
Dilation angle, i (°) at normal stress 5 MPa	9.2	3.9	3.2	13.3
Dilation angle, i (°) at normal stress 20 MPa	3.6	2.1	0	6.2

This comparison shows that the results obtained with the "old" and the modified methodology can not be mixed at least for normal stiffness. Therefore the normal stiffness is, in modelling stage 2.1, estimated only on the 10 rock fracture samples that have been tested with the modified methodology. The analysis shows that the other mechanical parameters are slightly influenced by the testing procedure but the values are in the same order of magnitude. Most of the parameters obtained with the modified methodology are in the range of variation defined with the "old" methodology. Hence the other parameters will be estimated by using all samples.

3.1.2 Summary of the fracture mechanical properties in the local model volume

The mechanical properties evaluated in the interval 0–20 MPa from shear tests in all boreholes are summarized in Table 3-4. The normal stiffness is estimated on 10 samples, the other parameters on 41 samples. These values can be compared to the results obtained for version 1.2, see Table 3-5. All parameters are very similar except the normal stiffness and, in minor extent, the shear stiffness. The variation in normal stiffness is explained by the modified methodology. The large standard deviation might be partly explained by the reduced amount of samples tested. However the values obtained on samples from KFM05A only (see Table 3-2) show a smaller standard deviation. This might be explained by a larger heterogeneity of the samples and by the methodology itself.

Table 3-4. Summary of the results of the shear tests in the local model volume version 2.1 performed on rock fractures from boreholes KFM01A, KFM02A, KFM03A, KFM04A, KFM05A and KFM06A.

	Mean	Std. dev.	Min	Max
Normal stiffness, K_n (MPa/mm)[1)]	937.4	462.1	319.1	1,527.6
Shear stiffness, K_s (MPa/mm)	33.0	13.0	9.5	55.1
Peak cohesion. C_p (MPa)	0.7	0.3	0.0	1.3
Peak friction angle, ϕ_p (°)	34.5	2.9	27.3	40.8
Residual cohesion, C_r (MPa)	0.4	0.3	0.0	1.3
Residual friction angle, ϕ_r (°)	31.5	4.7	19.8	39.2
Dilation angle, i (°) at normal stress 0.5 MPa	19.0	6.6	3.9	32.1
Dilation angle, i (°) at normal stress 5 MPa	6.2	4.1	1.1	15.3
Dilation angle, i (°) at normal stress 20 MPa	3.3	2.4	0.0	10.4

[1)] The normal stiffness is estimated from the samples tested with the modified methodology only.

Table 3-5. Comparison of the rock fracture mechanical parameters for Forsmark SDM version 1.2 and modelling stage 2.1.

Parameter	Modelling version/stage	Mean	Std. dev.	Min	Max
Normal stiffness, K_n (MPa/mm)	1.2	128.4	51.6	68.0	288.4
	2.1[1)]	937.4	462.1	319.1	1,527.6
Shear stiffness, K_s (MPa/mm)	1.2	38.8	10.8	11.2	55.1
	2.1	33.0	13.0	9.5	55.1
Peak cohesion. C_p (MPa)	1.2	0.7	0.4	0.0	1.3
	2.1	0.7	0.3	0.0	1.3
Peak friction angle, ϕ_p (°)	1.2	34.3	3.1	27.3	40.8
	2.1	34.5	2.9	27.3	40.8
Residual cohesion, C_r (MPa)	1.2	0.3	0.2	0.0	1.3
	2.1	0.4	0.3	0.0	1.3
Residual friction angle, ϕ_r (°)	1.2	32.0	4.1	19.8	39.2
	2.1	31.5	4.7	19.8	39.2
Dilation angle, i (°) at normal stress 0.5 MPa	1.2	18.9	7.0	3.9	32.1
	2.1	19.0	6.6	3.9	32.1
Dilation angle, i (°) at normal stress 5 MPa	1.2	6.9	4.2	1.1	15.3
	2.1	6.2	4.1	1.1	15.3
Dilation angle, i (°) at normal stress 20 MPa	1.2	3.5	2.4	0.0	10.4
	2.1	3.3	2.4	0.0	10.4

[1)] The normal stiffness is calculated with samples tested with the modified methodology only.

3.2 Fracture mechanical properties from tilt tests

The results of the tilt tests are expressed in terms of joint roughness coefficient, joint compression strength, and basic and residual friction angles. These parameters can be used to estimate the cohesion and friction angle according to Mohr-Coulomb, which can be compared with the values obtained with the shear tests.

The results of the tilt tests (JRC, JCS, basic- and residual friction angle) are inserted in the software Rocdata (Rocscience Inc.). The program draws the best fit curve for c and fi according to Mohr-Coulomb in the given stress for interval and for each rock fracture sample, see Figure 3-1.

The peak and residual cohesion and friction angle have also been determined using the results of the tilt tests conducted on rock fracture samples. The evaluated mechanical properties are presented in Table 3-6. The mechanical properties are evaluated in the interval 0–20 MPa on 151 samples.

These results can be compared with the results obtained from shear tests for the same parameters (see Table 3-4 and Figure 3-2). The values are in the same range of magnitude and the differences obtained by both methods are not highly significant.

The results obtained for peak cohesion and friction angle can be compared to those evaluated in version 1.2 and reported in /Lanaro 2005/, see Table 3-7. The values are quite similar. The different stress intervals and procedures used to evaluate peak cohesion and friction angle might be the source of the discrepancies observed in that table.

Table 3-6. Summary of the results from tilt tests on rock fracture samples from boreholes KFM01A, KFM02A, KFM03A, FKM04A and KFM05A.

	Mean	Std. dev.	Min	Max
Peak cohesion, C_p (MPa)	0.5	0.1	0.2	0.8
Peak friction angle, ϕ_p (°)	33.8	2.0	25.8	37.7
Residual cohesion, C_r (MPa)	0.4	0.1	0.2	0.7
Residual friction angle, ϕ_r (°)	29.4	3.1	20.3	37.9

Table 3-7. Comparison of peak cohesion and friction angle obtained from tilt tests for version 1.2 and modelling stage 2.1.

		Mean		Std. dev.	
Laboratory test method	**Number of samples**	**c_p^{MC} (MPa)**	**ϕ_p^{MC} (°)**	**c_p^{MC} (MPa)**	**ϕ_p^{MC} (°)**
Tilt tests version 1.2[1)]	125	0.3	34	0.1	4
Tilt tests stage 2.1[2)]	151	0.5	33.8	0.1	2

[1)] The values reported here are obtained from the Barton-Bandis' Criterion for normal stresses between 0.5 and 20 MPa.
[2)] The values are obtained from the Coulomb's Criterion for normal stresses between 0 and 20 MPa.

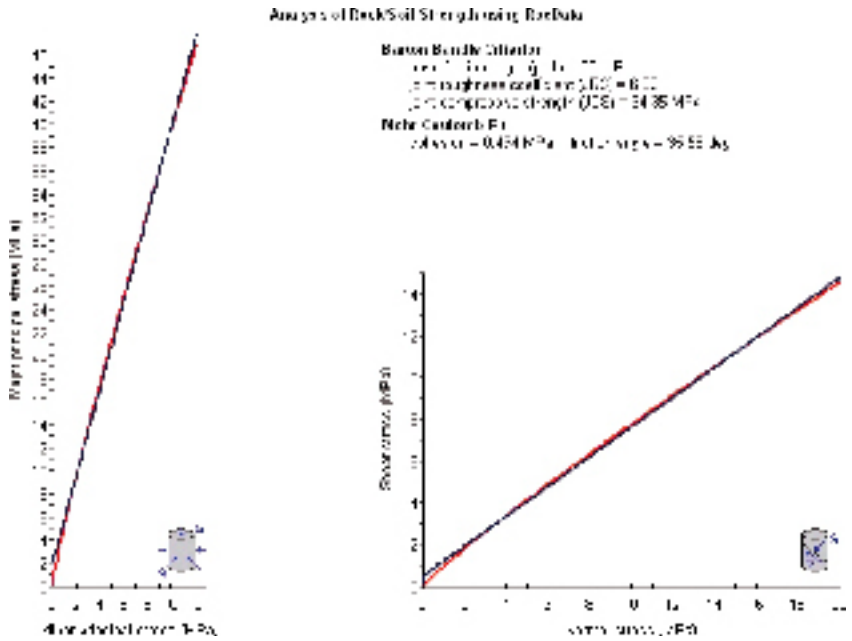

Figure 3-1. *Evaluation of peak- and residual friction angle of rock fracture samples from tilt tests using the software Rocdata (Rocscience Inc.).*

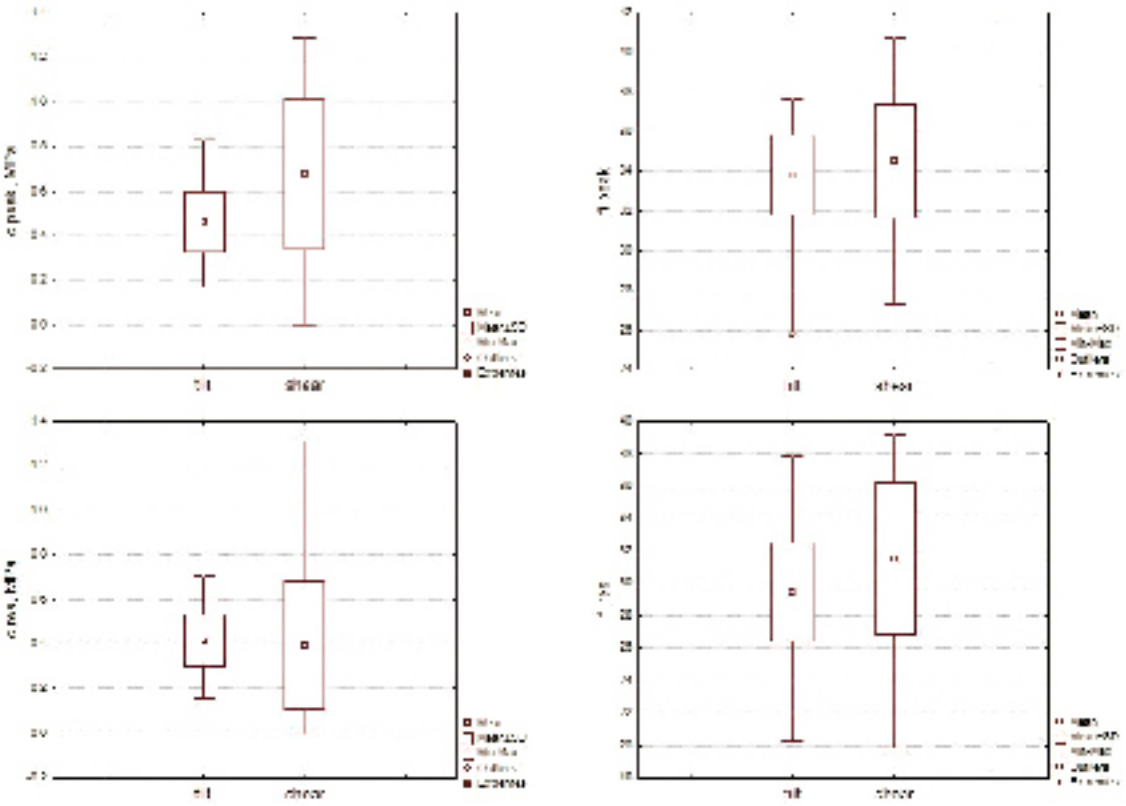

Figure 3-2. *Box plot for peak and residual cohesion and friction angle, for both shear and tilt tests.*

3.3 Influence of orientation sets on mechanical properties

3.3.1 Rock samples from shear tests

In order to determine the potential influence of the fracture orientation on the mechanical properties of rock fractures the tested fractures were coupled to the BOREMAP characteristics such as orientation and mineral filling. There is in some cases a quite high uncertainty pending onto this process, see Section 3.6.

Nevertheless the coupling BOREMAP/tested fractures have been conducted for all samples, and the orientation of tested fracture could be obtained. Figure 3-3 illustrates the plot of fracture poles for all the tested fractures with their confidence.

Based on the DFN definition in Forsmark /SKB 2005/, the tested fractures can be organised according to the different fracture orientation sets.

The distribution of the fracture samples in the different orientation sets is strongly biased, see Table 3-8, and statistic relevance cannot be calculated on samples from the NS, EW and HZ sets. For the NE and NW sets the amount of tested fractures is larger and the statistical variation might be relevant.

Only the NS, NW and NE sets are represented in the rock fractures tested with the modified methodology, and the amount of samples is then not statistically representative. In order to be able to compare between the different orientation of the fracture sets only the results obtained with the "old" methodology are used for the determination of the normal stiffness. Table 3-8 summarizes the mechanical properties evaluated from shear tests for the different fracture orientation sets.

Figure 3-5 and Figure 3-6 illustrate the mean, mean+1 SD and minimum and maximum values for each fracture orientation set. The box plots show differences in the fracture properties for the different sets. Mann-Whitney tests carried out on these data show that the differences between the different of the orientation fracture sets and for the different fracture properties are statistically not significant.

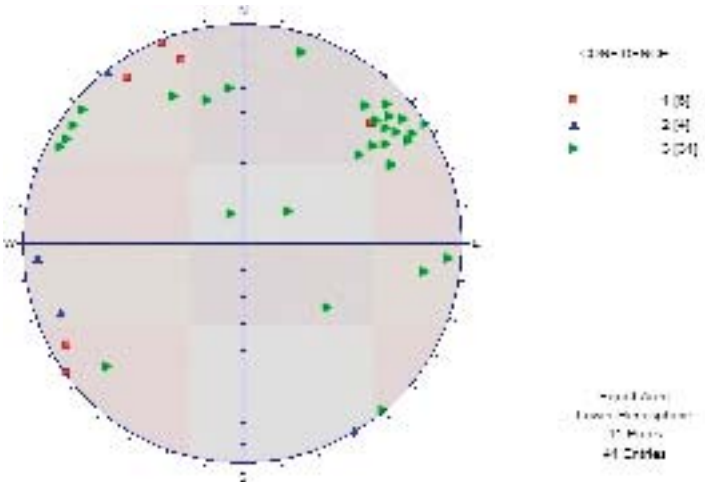

Figure 3-3. Plot of fracture poles. Samples from KFM01A, KFM02A, FKM03A, KFM04A, KFM05A and KFM06A. Confidence from 1: low to 3: high.

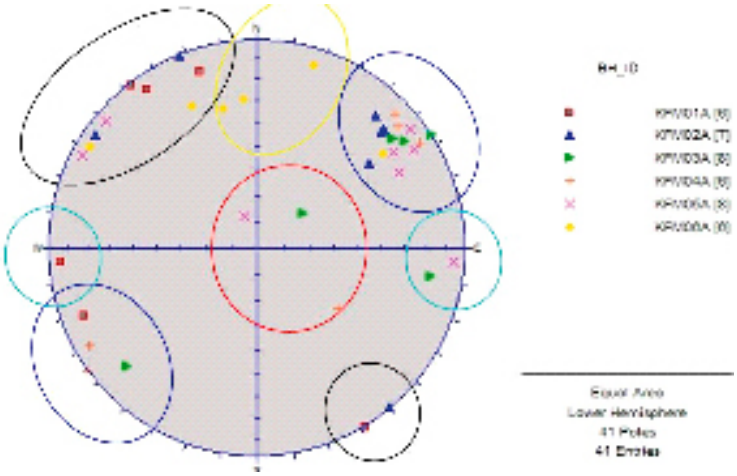

Figure 3-4. Plot of fracture poles with identification of the fracture sets.

Table 3-8. Summary of the mechanical properties of rock fractures for the different orientation of the fracture sets at Forsmark.

		NS	NE	NW	EW	HZ	All sets
No. of samples[1)]		3 (2)	11 (9)	21 (19)	3 (–)	3	41 (31)
K_n	Mean	128.1	98.2	177.1	–	172.6	155.7
	Std. dev.	74.8	9.9	108.4	–	81.4	94
	Min–Max	75.2–181	87.9–113.4	68–512.2	–	110.6–264.8	68–512.2
K_s	Mean	39.3	30.6	36.6	19.1	24.5	33
	Std. dev.	19.3	11.7	12.6	2.8	9.6	13
	Min–Max	17.8–55.1	9.5–50.4	11.2–53.3	17–22.4	13.9–32.6	9.5–55.1
Cp	Mean	0.8	0.6	0.7	0.7	0.7	0.7
	Std. dev.	0.5	0.4	0.3	0.4	0.1	0.3
	Min–Max	0.2–1.3	0–1.1	0.2–1.3	0.4–1.1	0.6–0.8	0–1.3
ϕ_p	Mean	35.8	32.5	35.2	36.6	33.9	34.5
	Std. dev.	2.1	2.7	2.1	1.8	3.3	2.9
	Min–Max	33.6–37.9	27.3–37.9	30.5–37.9	34.9–38.5	30.4–36.9	27.3–40.8

[1)] The amount of samples in brackets is the number of samples available for the estimation of K_n based on rock fracture samples tested with the “old” methodology. Other parameters are evaluated on all samples.

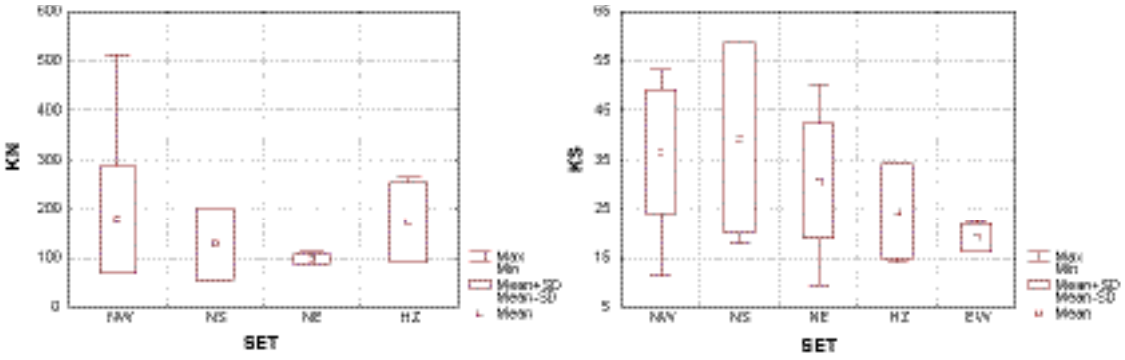

Figure 3-5. *Box plot on the normal stiffness (left) and shear stiffness (right) for the rock fracture samples sorted by fracture orientation sets.*

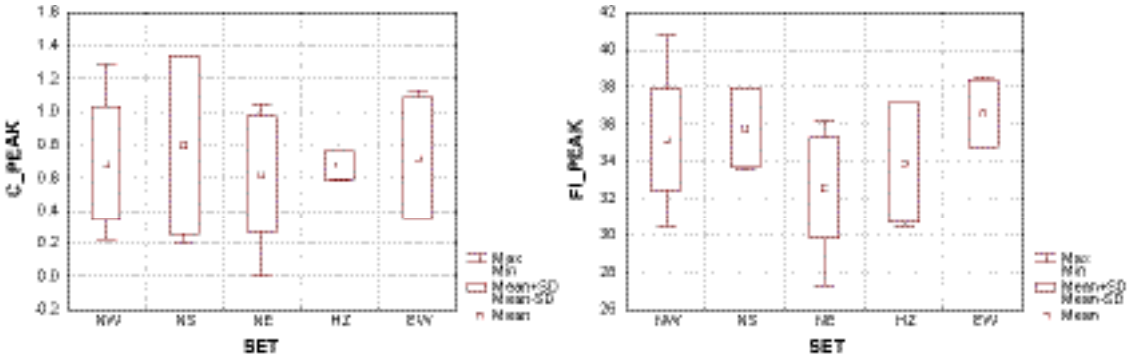

Figure 3-6. *Box plot on the peak cohesion (left) and peak friction angle (right) for the rock fracture samples sorted by fracture orientation sets.*

3.3.2 Tilt test results

The analysis of the influence of fracture sets on mechanical properties has also been studied on the samples for tilt tests. The larger amount of samples increases the significance of the statistical results.

The sampling procedure is similar to the one described for the shear tests and might also lead to some discrepancies. All samples were also coupled to the BOREMAP data as for shear tests samples, and the description of the procedure is presented in Section 3.6. The confidence level was set according to the criteria defined in Section 3.6. The distribution of fracture orientation with respect to their confidence is illustrated in Figure 3-7.

The definition of the fracture sets is taken from the DFN model for Forsmark version 1.2 and the amount of samples in the different sets is presented in Table 3-9. The definition of the limits for fracture sets is the one based on surface fracture data. The sub-horizontal fracture set includes fractures with a dip less than 50°.

Table 3-9. Number of rock samples for the different fracture orientation sets.

Orientation set	Number of samples
NS	17
NE	37
NW	25
EW	5
HZ	67

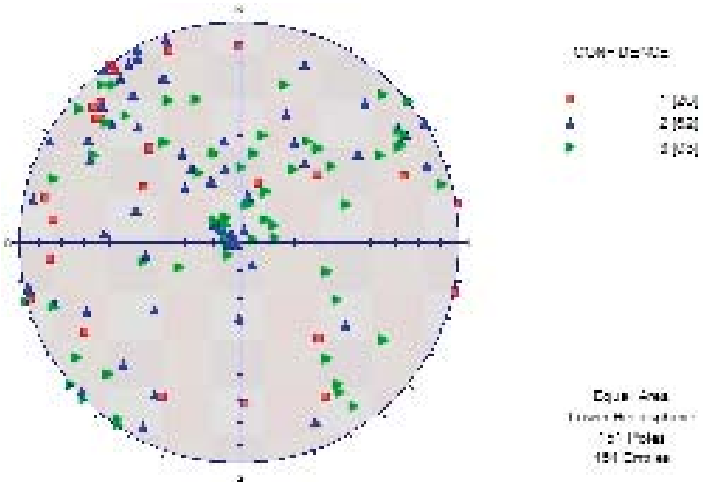

Figure 3-7. *Fracture orientations for the tilt test fracture samples where the confidence of the BOREMAP assignation is indicated.*

The mechanical properties obtained for the different orientation fracture sets are summarized in Table 3-10. Figure 3-8 to Figure 3-9 illustrate the variation of the mechanical parameters between the different fracture sets by means of box plots on mean, standard deviation and min and max values. The probability distribution of the different parameters is illustrated for the different fracture sets in Figure 3-10 to Figure 3-11.

Figure 3-8 and Figure 3-11 illustrate the probability distribution of the different mechanical properties evaluated from tilt tests for the different fracture orientation sets.

Non-parametric analyses (Mann-Whitney tests) conducted on the rock fracture properties for the different groups of orientation sets show that the discrepancies observed between the different sub-vertical sets are not significant. However the discrepancy between the sub-horizontal set and the NE, NW and NS sets are found in some cases statistically significant.

Table 3-10. Summary of the results from tilt tests on rock fractures for the different orientation sets.

		NS	NE	NW	EW	HZ	All sets
No. of samples		17	37	25	5	67	151
C_p (MPa)	Mean	0.5	0.5	0.5	0.4	0.4	0.5
	Std. dev.	0.1	0.1	0.2	0.1	0.1	0.1
	Min–Max	0.3–0.8	0.3–0.7	0.2–0.7	0.3–0.6	0.2–0.8	0.2–0.8
ϕ_p (°)	Mean	34.7	33.8	34.2	33.7	33.4	33.8
	Std. dev.	2	1.9	2.4	0.9	1.8	2
	Min–Max	28.6–37.1	28.9–36.4	25.8–37.2	32.5–35	28.5–37.6	25.8–37.6
C_r (MPa)	Mean	0.4	0.5	0.4	0.4	0.4	0.4
	Std. dev.	0.1	0.12	0.1	0.1	0.1	0.1
	Min–Max	0.2–0.7	0.2–0.6	0.2–0.6	0.3–0.5	0.2–0.7	0.2–0.7
ϕ_r (°)	Mean	30.7	29.6	29.4	29.6	29	29.4
	Std. dev.	2	2.9	3.3	2.1	3.3	3.1
	Min–Max	24.7–33.5	21.5–35.3	20.3–37.2	27.5–33	22.6–37.9	20.3–37.9

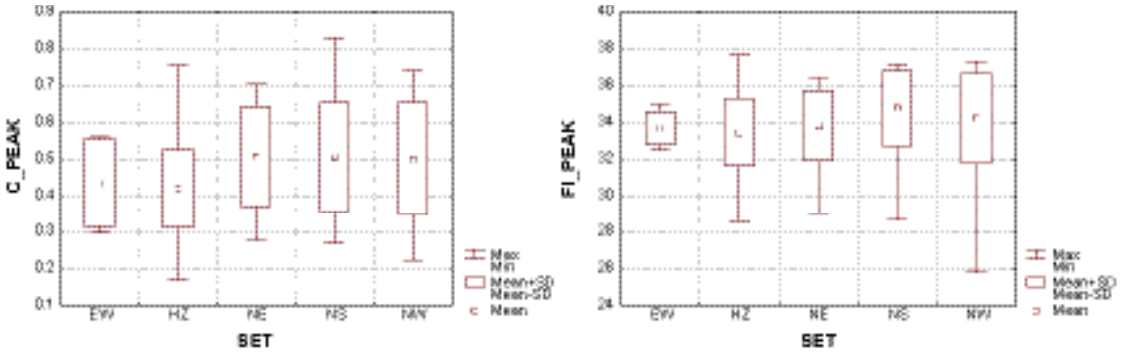

Figure 3-8. *Box plot on peak cohesion (left) and peak friction angle (right) for the rock samples from tilt tests sorted by fracture orientation sets.*

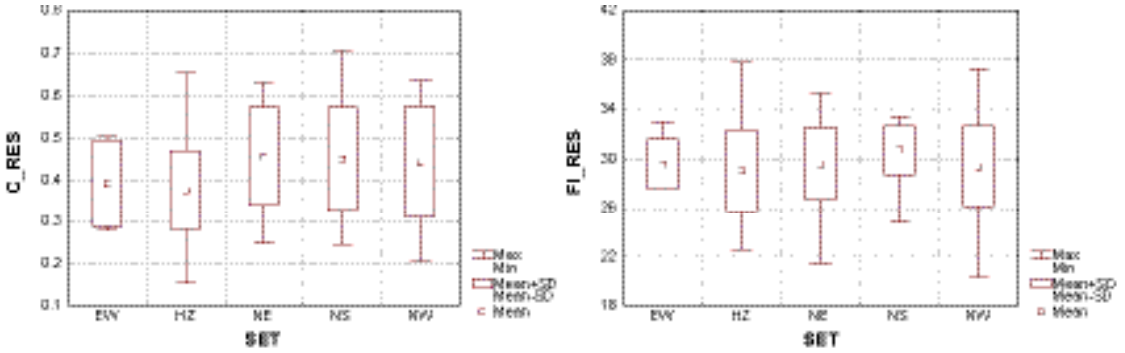

Figure 3-9. *Box plot on residual cohesion (left) and residual friction angle (right) for the rock samples from tilt tests sorted by fracture orientation sets.*

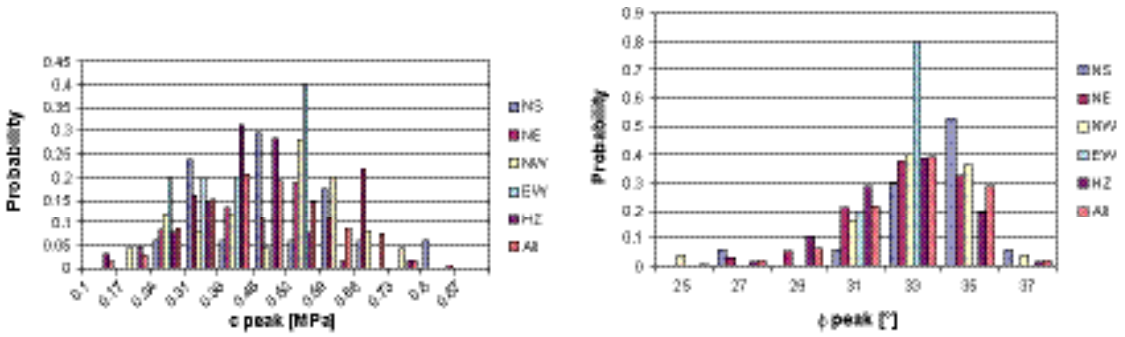

Figure 3-10. *Probability distribution of the peak cohesion (left) and peak friction angle (right) from tilt tests according to fracture orientation sets.*

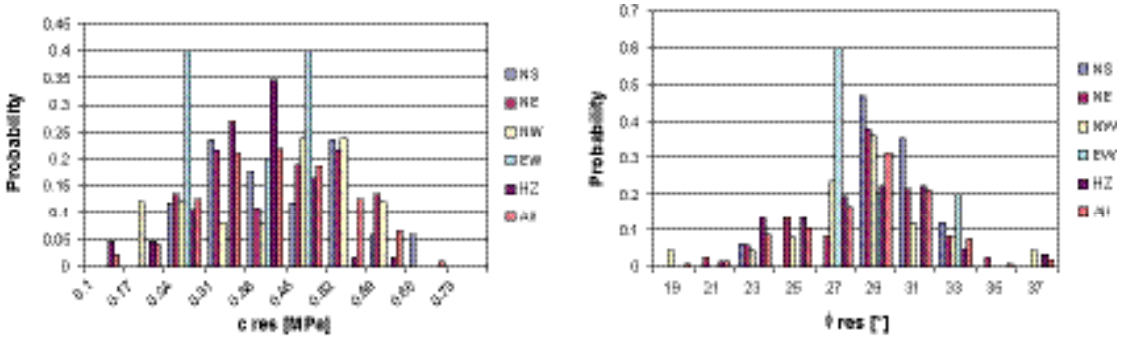

Figure 3-11. *Probability distribution of the residual cohesion (left) residual friction angle (right) from tilt tests according to fracture orientation sets.*

3.4 Analysis of the mechanical properties of the fractures with depth

The same depth intervals as defined in Appendix 3, Section 2, are used, and two complementary intervals were defined to cover the range of depth intervals of the rock fractures. The results for tilt tests are summarized in Table 3-11 and Figure 3-12, and the results for shear tests in Table 3-12 and Figure 3-13. The plots show that the differences are not highly significant. The normal stiffness is evaluated only on fracture samples tested with the "old" methodology, and the samples tested with the "modified" methodology have been removed from the data sets, this to allow comparison between samples at different depths. The other parameters have been evaluated on all tested rock fracture samples.

There is no large variation with depth in rock fracture parameters for tilt tests. The variation between different depth classes is somewhat larger for shear test samples, but no trend can be highlighted.

The variability of parameters for the same depth interval is generally larger for shear tests than for tilt tests (see Figure 3-12 and Figure 3-13). This could be explained by the fact that there are fewer samples for shear tests than for tilt tests, but the plots show that the highest standard deviation cannot be directly coupled to the number of samples. There is no direct correlation with the depth of the samples. Large standard deviation can occur in all of the depth intervals.

Table 3-11. Summary of the frcture mechanical properties with depth evaluated from tilt tests on rock samples from all boreholes.

	Above 200	200–400	400–550	550–700	Below 700
Amount of samples	8	40	44	35	24
Cp (MPa)	0.5/0.1	0.5/0.1	0.5/0.1	0.4/0.1	0.4/0.1
ϕp (°)	31.1/3	33.9/2.2	33.9/1.7	33.9/1.9	34.2/1.3
cr (MPa)	0.4/0.1	0.44/0.1	0.4/0.1	0.4/0.1	0.4/0.1
ϕr (°)	26.3/3.6	28.9/3.4	29.9/2.5	30/3.1	29.7/2.4

Table 3-12. Summary of the fracture mechanical properties with depth evaluated from shear tests on rock samples from all boreholes.

	Above 200	200–400	400–550	550–700	Below 700
No. of samples[1)]	4 (4)	21 (14)	7 (4)	5 (5)	4 (4)
K_n (MPa/mm)	131.9/43.6	169.1/120.8	180.8/89.6	129.8/32.2	139.9/99.5
K_s (MPa/mm)	33.2/17.9	32.1/14.2	31.7/13	37.8/10.2	34.2/8.3
C_p (MPa)	0.6/0.2	0.7/0.4	0.8/0.3	0.6/0.3	0.7/0.2
ϕ_p (°)	32/2	35.4/2.1	33.6/3.5	35.6/2.8	32.8/4.5
c_r (MPa)	0.3/0.3	0.4/0.3	0.4/0.2	0.4/0.2	0.5/0.3
ϕ_r (°)	31.2/0.9	32/5.6	30.7/2.5	32.4/4.4	29.8/6.3
Dilation angle, i (°) at normal stress 0.5 MPa	15.4/8.4	18.3/6.3	20.7/6.3	20.2/7.8	22.3/6.4
Dilation angle, i (°) at normal stress 5 MPa	3.6/1.8	6.6/4.4	6.9/5.6	4.4/2.4	7.4/2.8
Dilation angle, i (°) at normal stress 20 MPa	3/1.3	3.4/2.3	2.9/2.5	3.3/4	3.5/1.9

[1)] K_n is evaluated with fracture samples tested with the "old" methodology as too few samples are available for the "modified" methodology. The amount of samples in brackets is the number of samples available for the estimation of K_n.

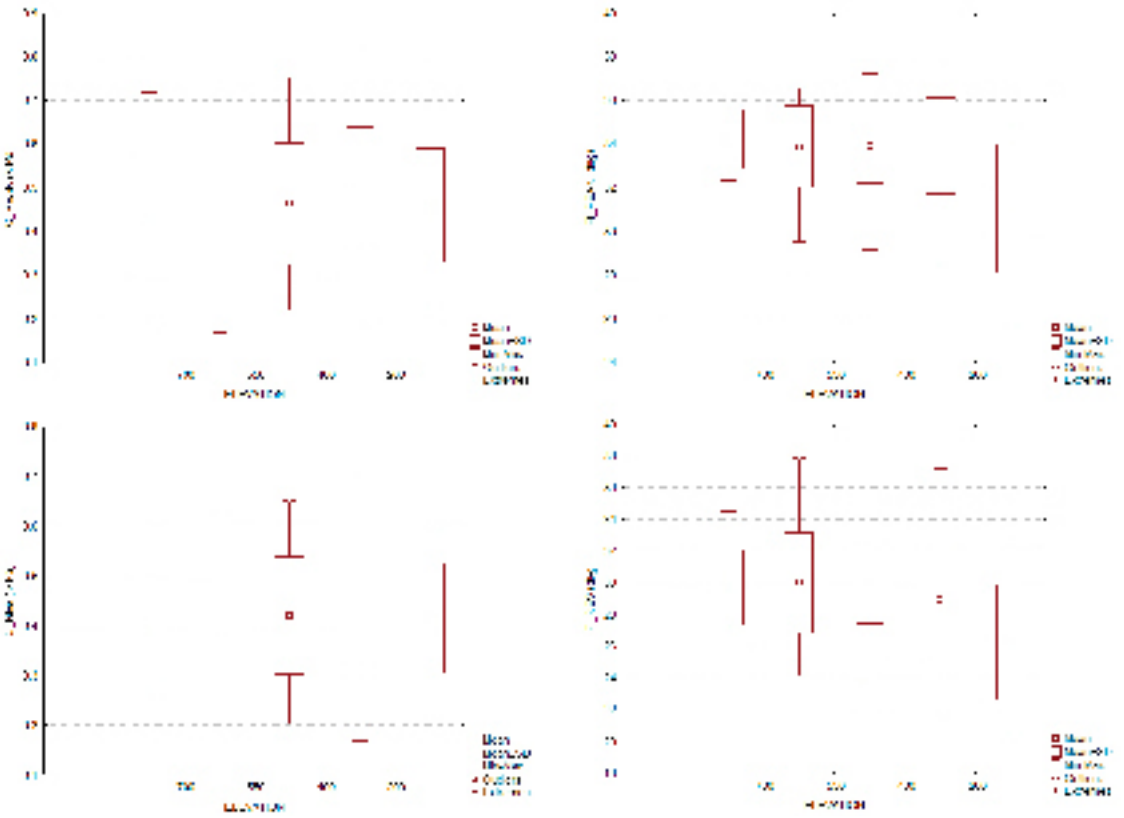

Figure 3-12. *Box plots of peak and residual cohesion and friction angle for fractures at different depth intervals (tilt tests).*

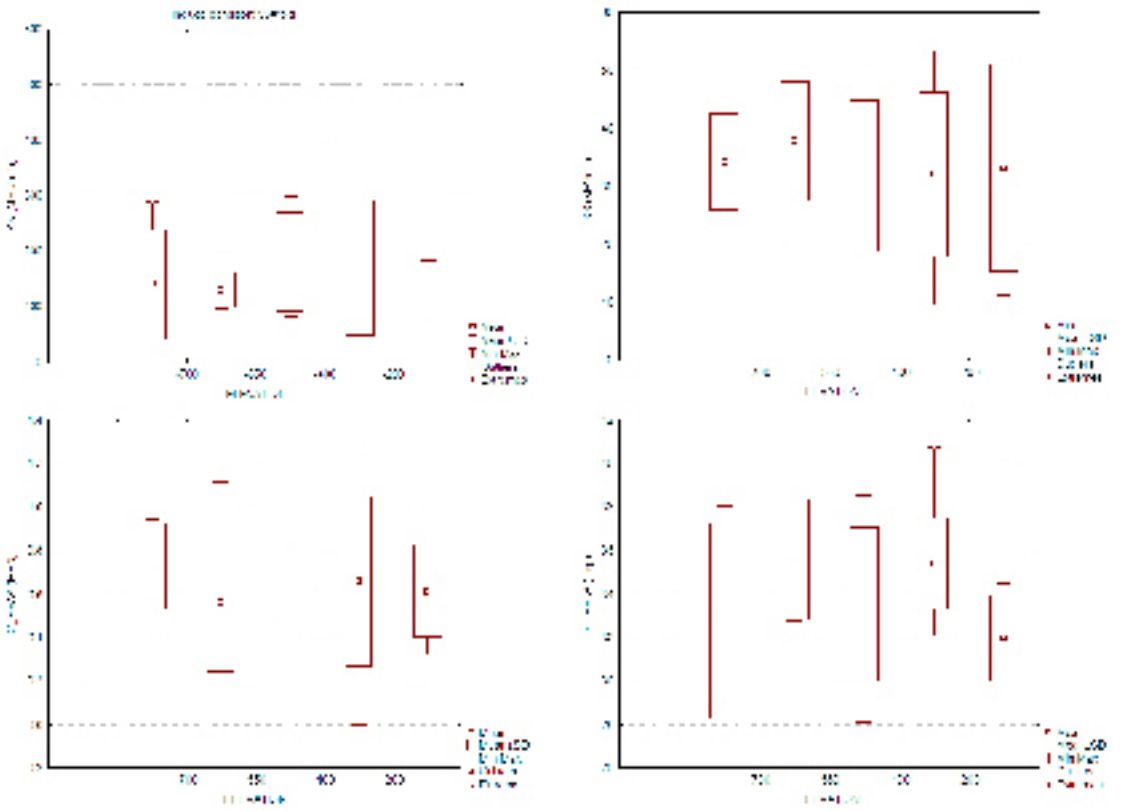

Figure 3-13. *Box plots of normal and shear stiffness, peak cohesion and friction angle for fractures at different depth levels (shear tests).*

3.5 Analysis of the fracture mechanical properties in the deformation zones

36 of the rock fractures samples for tilt tests were collected in the sections of the boreholes that were identified as “deformation zone DZ” contra “rock units RU” in the Single Hole interpretation. The occurrence of rock fracture samples in DZ and RU is dependent on the coupling between tested fractures and BOREMAP mapping, see Appendix 3, Section 3.6. All except one (DZ7 in KFM02A) were also modelled as deformation zones in the geological model, see Table 3-13. The confidence is based on the coupling between tested fractures and BOREMAP, and is defined according to the procedure described in Section 3.6.

Table 3-14 and Table 3-15 summarise the mechanical properties evaluated from tilt tests for the different deformation zones (Figure 3-14 and Figure 3-15). Comparing the summary of results for all samples in RU and all samples in DZ illustrates the similarity in the properties of these samples. However there are some significant discrepancies between the different deformation zones. These must be weighted against the low sampling rate of some zones, and again the uncertainty of coupling fractures to BOREMAP. Non-parametric tests (Kruskal-Wallis) on the samples from the different deformation zones can not reject the hypothesis that the samples are from the same parent population. Most of the values evaluated for DZ are still in the range of variation of parameters for samples in RU.

Table 3-13. Identification of the rock fracture samples collected in “deformation zone”.

Borehole	“RU”	Zone modelled	Amount of samples	Confidence of the identification[1)]
KFM01A	DZ2	ZFMNE1192	3	3
	DZ3	ZFMNE061C	5	3
KFM02A	DZ5	ZFMNE1189	1	3
	DZ6	ZFMNE00A2	10	3
	DZ7	Not modelled (called DZ in Table 3-14)	6	3
KFM03A	DZ3	ZFMNE00B1	3	2
	DZ4	ZFMNE00A3	2	3
KFM04A	DZ5	ZFMNE1188	2	3
KFM05A	DZ2	ZFMNE0401	2	3
	DZ3	ZFMNE0103B	2	1

[1)] Low confidence = 1, medium confidence = 2, high confidence = 3.

Table 3-14. Mechanical properties of fractures from tilt tests in “rock unit” (RU) and “deformation zone” (DZ).

	RU	All DZ	ZFMNE1192	Non deterministic DZ	ZFMNE1188	ZFMNE061C
Amount of samples	115	36	3	6	2	5
C_p (MPa)	0.5/0.1	0.5/0.1	0.6/0.2	0.5/0.1	0.5/0	0.4/0.1
ϕ_p (°)	33.9/2	33.4/2.1	32.2/2.5	33.5/2.5	34.9/0.6	33.1/2.2
c_r (MPa)	0.4/0.1	0.4/0.1	0.5/0.2	0.5/0.1	0.5/0	0.4/0.1
ϕ_r (°)	29.5/3	29.3/3.1	26.7/0.2	30/4	30.4/0.3	30/3.8

Table 3-15. Mechanical properties of fractures from tilt tests in “rock unit” and “deformation zone” (continue).

	ZFMNE0401	ZFMNE00B1	ZFMNE0103B	ZFMNE00A3	ZFMNE1189	ZFMNE00A2
Amount of samples	2	3	2	2	1	10
C_p (MPa)	0.4/0	0.4/0.1	0.4/0.1	0.6/0.2	0.5/–	0.5/0.2
ϕ_p (°)	33/2.7	34.8/0.2	33.6/1.5	34.2/1.8	28.9/–	33.5/2
c_r (MPa)	0.4/0	0.4/0.1	0.4/0.1	0.5/0.2	0.4/–	0.4/0.1
ϕ_r (°)	28.1/4.7	31.2/2.8	28.7/1	27.7/2.1	21.5/–	29.9/2.1

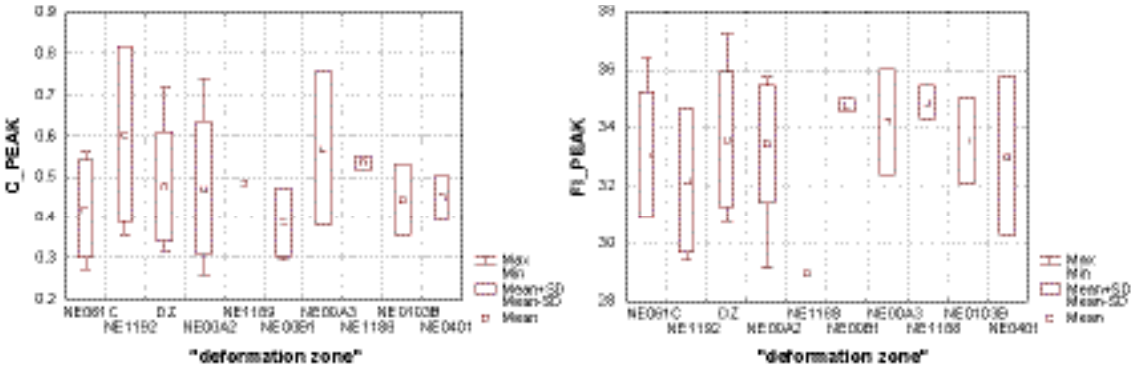

Figure 3-14. *Box plot of peak cohesion (left) and peak friction angle (right) for tilt tests on fracture samples in the different deformation zones.*

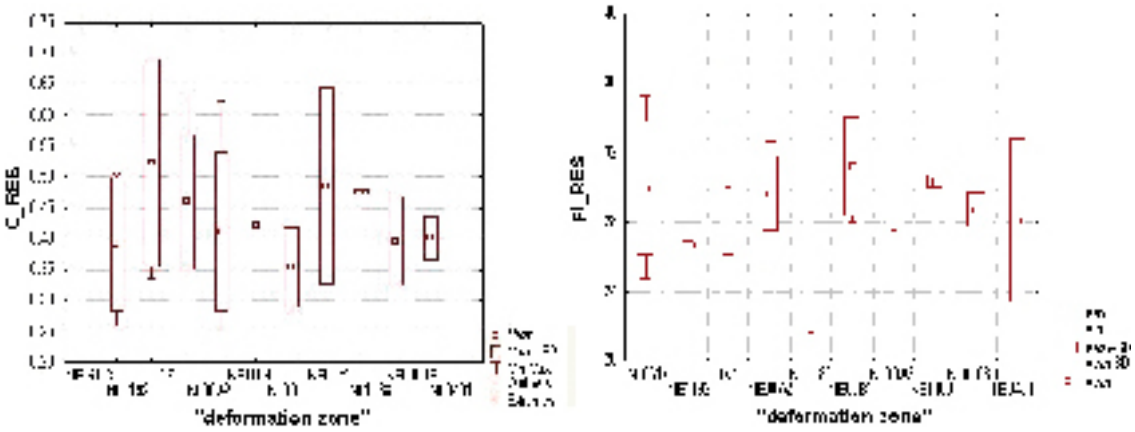

Figure 3-15. *Box plot of residual cohesion (left) and residual friction angle (right) for tilt tests on fracture samples in the different deformation zones.*

For the shear tests only 3 rock fracture samples were coupled to fractures lying in deformation zones sections DZ and all the other samples were associated to rock units RU. Even if the amount of DZ samples is very limited the rock fracture parameters were evaluated for samples associated to RU only. They are presented in Table 3-16. These values are very similar to those obtained for all tested samples (see Table 3-17 for comparison of normal stiffness and Table 3-4 for comparison of other parameters).

One of the DZ samples is associated to DZ2 in KFM01A, which has been modelled as ZFMNE1192 in the geological model. Two samples are associated to DZ7 in KFM02A which has not been modelled as a deformation zone in the geological model. The fracture properties are presented in Table 3-18. Comparing these properties to the one listed in Table 3-4 shows that the properties for the sample associated to ZFMNE1192 are sensibly lower than the mean properties estimated from all samples, but regarding the uncertainty underlying the coupling of rock fracture samples to mapped fractures in BOREMAP the discrepancy is not significant.

Table 3-16. Rock mechanical properties for fracture samples from shear tests and associated to "RU".

	Mean	Std. dev.	Min	Max
Normal stiffness, K_n (MPa/mm)[1)]	159.6	97.5	68	512.2
Shear stiffness, K_s (MPa/mm)	32.4	13.1	9.5	55.1
Peak cohesion. C_p (MPa)	0.7	0.3	0.2	1.3
Peak friction angle, ϕ_p (°)	34.6	27.3	40.7	2.9
Residual cohesion, C_r (MPa)	0.4	0.3	0	1.3
Residual friction angle, ϕ_r (°)	31.7	19.8	39.1	4.8
Dilation angle, i (°) at normal stress 0.5 MPa	19	6.2	3.9	31.9
Dilation angle, i (°) at normal stress 5 MPa	6.4	4.1	1.6	15.3
Dilation angle, i (°) at normal stress 20 MPa	3.4	2.4	0.04	10.4

[1)] K_n is evaluated with fracture samples tested with the "old" methodology as too few samples are available for the "modified" methodology. The amount of samples in brackets is the number of samples available for the estimation of K_n.

Table 3-17. Normal stiffness for shear tests with the "old" methodology.

	Mean	Std. dev.	Min	Max
Normal stiffness, K_n (MPa/mm)	155.7	94	68	512.2

Table 3-18. Fracture properties evaluated from samples collected in "DZ" sections (shear test).

	"RU"	DZ2 i KFM01A	DZ7 i KFM02A
Confidence	2	1	3
Normal stiffness, K_n (MPa/mm)[1)]	159.6	106.9	87.9–163.4
Shear stiffness, K_s (MPa/mm)	32.4	50.4	28–43.6
Peak cohesion. C_p (MPa)	0.7	0	0.95–0.26
Peak friction angle, ϕ_p (°)	34.6	36.2	30.5–32.8
Residual cohesion, C_r (MPa)	0.4	0.2	0.35–0.5
Residual friction angle, ϕ_r (°)	31.7	30.7	26–31.2
Dilation angle, i (°) at normal stress 0.5 MPa	19	7.6	17.2 –32.1
Dilation angle, i (°) at normal stress 5 MPa	6.4	4.2	1.1–3
Dilation angle, i (°) at normal stress 20 MPa	3.4	1.8	0.3–3.2

[1)] Samples tested with the "old" methodology.

3.6 Evaluation of the uncertainties

The confidence on the data depends on the uncertainty and on the spatial variability.

Data uncertainty is related to measuring errors and interpretation errors. Measuring errors are pending directly to the measurement methods, and are not quantified in this report. Interpretation errors concern two steps of the evaluation: 1) the interpretation of the test results (this is not analysed further in this report); 2) the interpretation of the tested fracture which implies a coupling between the reported tested rock fracture samples and the fractures mapped in BOREMAP. This step is further analysed below. Data uncertainty related to measuring and interpretation (step1) errors might be assessed through the P-reports presenting the results of the mechanical tests for each borehole.

The procedure for sampling can be described as follows: the rock fracture samples are collected before the core logging, and the depth of the samples is taken directly from the indication on the core boxes. The location of the samples is marked on the core so that the geologists can then log the sampled intervals with reference to the adjusted length along the hole. This implies that the depth references given in the P-report do often poorly match with the depth given in BOREMAP.

This discrepancy was especially strong for the first holes and leads to severe difficulties in trying to identify the BOREMAP fracture corresponding to the tested fracture.

For the tilt tests samples no such information is available and the coupling procedure is based mostly on the depth parameter. The length given for a tested fracture is coupled to the nearest fracture mapped in BOREMAP. In some cases if the nearest fracture was judged not likely ("unbroken sealed") the next fracture was looked up.

In order to assess the uncertainty in the coupling process we set a confidence level to each sample which is based on the following two criteria:

- the difference in depth between the tested fracture and the mapped fracture in BOREMAP (or the fact that no fractures at all are mapped in the interval given for shear tests),
- the nature of the fracture mapped (variable "fracture_interpret" in Sicada). In fact with consideration to the criteria for choosing rock fracture samples it is very unlikely that "unbroken sealed" fractures were sampled for shear and tilt tests. However some samples are coupled to "unbroken sealed" fractures. The coupling in this case is set to a low confidence.

Three classes of confidence were used, from 1: low confidence to 3: high confidence.

The coupling BOREMAP/tested fractures have been conducted for all samples available in modelling stage 2.1. The results in terms of confidence and interpreted parameters from BOREMAP (nature of mapped fracture and rock unit) are presented in Table 3-19 for shear tests. The same data are available for tilt tests.

Spatial variability is not strictly an uncertainty but it constitutes an indirect source of data uncertainty. In the case of shear tests for example the scarcity of data for some fracture orientation sets or depth sections disables significant statistic analyses of the results. Due to the limited amount of samples it is not always possible to determine if the variability between different fracture sets is larger than the variability within the different fracture sets.

Table 3-19. Confidence level, nature of the mapped fracture and rock unit associated to each sample for shear tests.

Sample ID	Testing procedure	Confidence	Sealed		Open	Rock unit
			Unbroken	Broken		
KFM01A-117-01	"old"	2			X	RU
KFM01A-117-03	"old"	2			X	RU
KFM01A-117-05	"old"	2			X	RU
KFM01A-117-07	"old"	2			X	RU
KFM01A-117-11	"old"	1	X			DZ2
KFM01A-117-12	"old"	1	X			RU
KFM02A-117-01	"old"	3		X		RU
KFM02A-117-02	"old"	1			X	DZ7
KFM02A-117-03	"old"	3		X		DZ7
KFM02A-117-04	"old"	1			X	RU
KFM02A-117-05	"old"	3			X	RU
KFM02A-117-06	"old"	3		X		RU
KFM02A-117-07	"old"	3		X		RU
KFM03A-117-01	"old"	3		X		RU
KFM03A-117-02	"old"	3		X		RU
KFM03A-117-03	"old"	3		X		RU
KFM03A-117-05	"old"	3		X		RU
KFM03A-117-06	"old"	3		X		RU
KFM03A-117-07	"old"	3		X		RU
KFM03A-117-08	"old"	3			X	RU
KFM03A-117-09	"old"	3		X		RU

Sample ID	Testing procedure	Confidence	Sealed		Open	Rock unit
			Unbroken	Broken		
KFM04A-117-01	“old”	3			X	RU
KFM04A-117-02	“old”	3			X	RU
KFM04A-117-03	“old”	3		X		RU
KFM04A-117-04	“old”	3		X		RU
KFM04A-117-06	“old”	1	X			RU
KFM04A-117-08	“old”	1	X			RU
KFM05A-117-01	“old”	3			X	RU
KFM05A-117-03	“old”	3			X	RU
KFM05A-117-04	“old”	3			X	RU
KFM05A-117-06	“old”	3		X		RU
KFM05A-117-02	Modified	3			X	RU
KFM05A-117-05	Modified	3		X		RU
KFM05A-117-07	Modified	3			X	RU
KFM05A-117-08	Modified	3			X	RU
KFM06A-117-01	Modified	3			X	RU
KFM06A-117-02	Modified	3		X		RU
KFM06A-117-04	Modified	3			X	RU
KFM06A-117-05	Modified	3			X	RU
KFM06A-117-07	Modified	3			X	RU
KFM06A-117-08	Modified	3		X		RU

4 Empirical study on the minor deformation zones

4.1 The deformation zone model

The deformation zone model for Forsmark version 1.2 in the local model area contains about 50 deformation zones which position, orientation and size were estimated in /SKB 2005/ and slightly updated in Section 3.1.2. Figure 4-1 shows all the available orientation of the deterministic deformation zones that can be roughly be grouped into three preferential orientations: NE, NW and NE

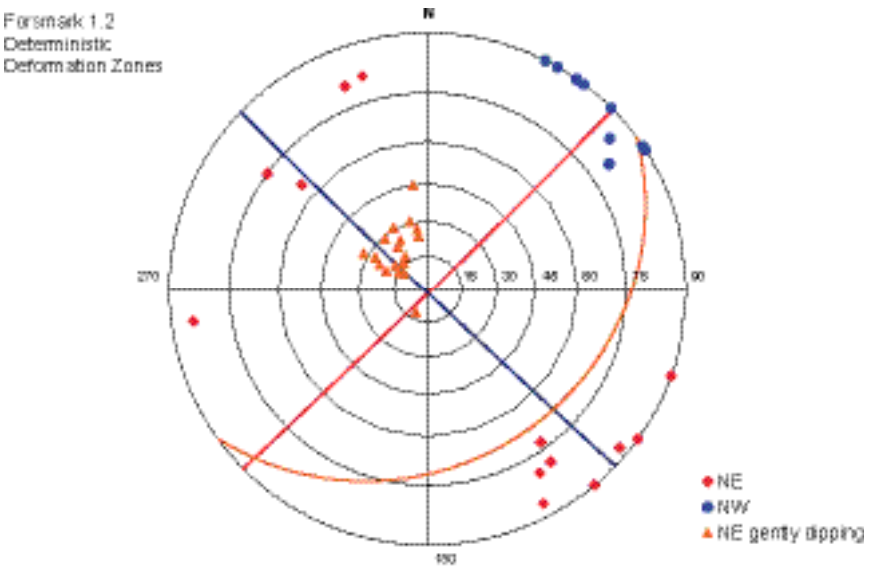

Figure 4-1. *Plot of the orientation of all the deterministic deformation zones given according to Forsmark SDM 1.2 /SKB 2005/. Roughly, three groups can be distinguished. Version 2.1 of the deformation zone model includes only one additional zone (ZFMNE1207).*

gently dipping. Some of these deformation zones intercept borehole KFM01A, KFM02A, KFM03A and KFM04A analysed from a Rock Mechanics point of view. The geometrical information about these zones is summarised in Table 4-1. In the boreholes, additional zones were detected by the "single-hole interpretation" in KFM02 (DZ4), not modelled as deterministic deformation zone, and KFM03 (DZ5) modelled in version 2.1 of the deformation zone model as ZFMNE1207.

Due to time constrains, not all the details of the deformation zone model version 2.1 were available to the studies reported in Appendix 3. However, most of the results of the Forsmark SDM version 1.2 /SKB 2005/ are still valid.

Table 4-1. Deterministic deformation zones in the boreholes in Forsmark SDM 1.2 /SKB 2005/.

Borehole	Characterised length	Deformation zones	Details	% in length
KFM01A	100–1,000 m	ZFMNE00A2	(36–48 m)	9%
		ZFMNE1192	386–412 m	
		ZFMNE0061	639–684 m	
KFM02A	100–1,000 m	ZFMNE0866	(79–91 m)	18%
		ZFMNE00B6	110–122 m	
		ZFMNE00A3	160–184 m	
		ZFMNE1189	303–310 m	
		ZFMNE00A2	415–520 m	
		ZFMNE1195	893–905 m	
		ZFMNE00B4	976–982 m	
KFM03A	100–1,000 m	ZFMNE00A4	356–399 m	8%
		ZFMNE00A7	448–455 m	
		ZFMNE00B1	638–646 m	
		ZFMNE00A3	803–816 m	
KFM04A	105–1,000 m	ZFMNE00A2	169–242 m*	9%
		ZFMNE1188	412–661 m**	

* This zone is discontinuous (169–176, 202–213 and 232–242 m).

** This zone is discontinuous (412–462, 654–661 m).

4.2 Relation between thickness and length

The thickness of the deterministic deformation zones in Table 4-2 represents the width of the transition zone, i.e. the thickness of the volume of rock experiencing a higher fracture frequency than the rest of the rock mass (larger than 4 fractures per metre) and including the core of the deformation zone where the fracture frequency is larger than 9 fractures per metre /Munier and Hökmark 2004/. The plot of the trace length versus the thickness of the deterministic deformation zones in Forsmark 1.2 is shown in Figure 4-2. By fitting the data with a power law of the trace length, the following equation can be obtained (also included in /Follin et al. 2005/):

$$b = 0.0179\ L^{0.8362}\ \text{(m)} \qquad (2)$$

where b is the thickness and L the trace length of the zones.

Assuming that also the minor deformation zones also intercept the boreholes at small angles, the apparent thickness of the zones has to be corrected as follows:

$$b = b' \sin \alpha \qquad (3)$$

where b is the actual thickness, b' is the apparent thickness and is the angle between the zone average plane and the borehole axis.

The importance of this relation is clear when approaching the treatment of shorter deformation zones that intersect the boreholes. By extrapolating the relation between thickness and length to fracture, cross and minor deformation zones, an estimation of their thickness can be obtained. However, a correction should be applied due to the fact that seldom the minor deformation zones cross the boreholes at a right angle.

Table 4-2. Properties of the deformation zones intercepted by the boreholes and considered for rock mechanics purposes in Forsmark SDM 1.2 /SKB 2005/.

Deformation zones	Length	Thickness	Strike/dip	Type of deformation	Comments
ZFMNE00A2	4,874 ± 200 m	65 ± 35 m (20–60 m)	080/24	Brittle	High confidence, three fracture sets, 0–26 fractures/m, oxidized, open and sealed fractures
ZFMNE1192	1,326 ± 50 m	5 m	073/82	Brittle	High confidence, 1–8 fractures/m, oxidized, open and sealed fractures, laumontite
ZFMNE0061	1,727 ± 100 m	15 m	068/81	Brittle	High confidence, oxidized and altered, one fracture set, 1–18 fractures/m mainly sealed, laumontite
ZFMNE0866	2,417 ± 100 m	0–10 m	061/31	Brittle	High confidence, oxidation and chloritization, 1–18 fractures/m, sealed and open fractures, 3 fracture sets
ZFMNE00B6	2,950 ± 200 m	7 ± 4 m	030/32	Brittle	High confidence, strong clay alteration, oxidized bedrock, 1–15 fractures/m, open fractures dominate, clay minerals
ZFMNE00A3	3,889 ± 200 m	13 ± 9 m	055/23	Brittle	High confidence, oxidized bedrock associated with vuggy metagranitoid, 0–15 fractures/m, open and sealed fractures, clay minerals and prehnite
ZFMNE1189	?	4 m	040/65	Brittle	Medium confidence, quartz dissolution and development of vuggy metagranite, albitisation, strong oxidation, 3–8 fractures/m, sealed fractures
ZFMNE1195	1,233 ± 25 m	9 m	080/39	Brittle	High confidence, 0–20 fractures/m, mainly sealed fractures

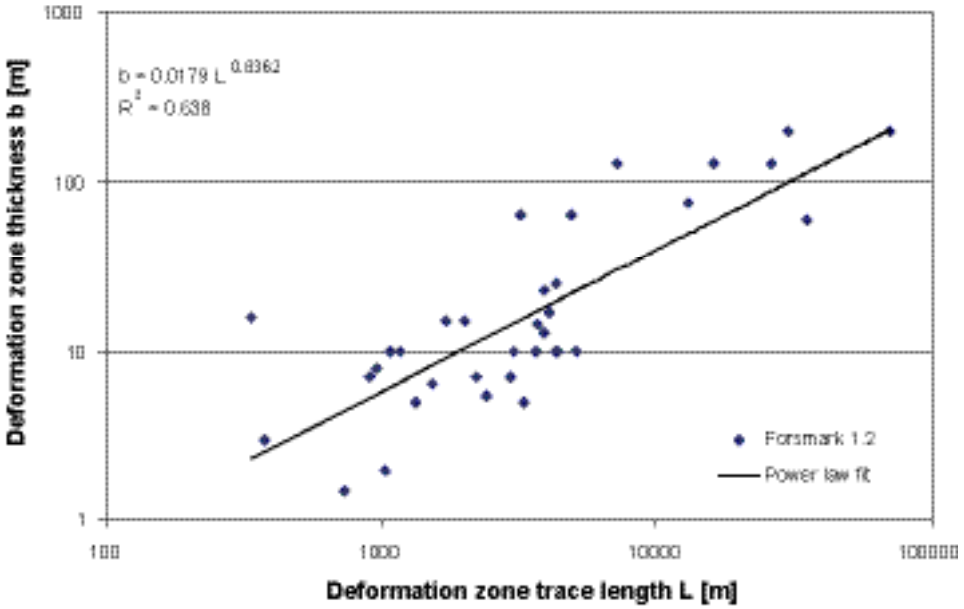

Figure 4-2. Plot of the trace length versus thickness of the deterministic deformation zones identified for Forsmark SDM version 1.2 /Follin et al. 2005/.

Table 4-3. Properties of the deformation zones intercepted by the boreholes and considered for rock mechanics purposes in Forsmark SDM 1.2 /SKB 2005/.

Deformation zones	Length	Thickness	Strike/dip	Type of deformation	Comments
ZFMNE00B4	?	5 m	050/29	Brittle	High confidence, oxidized, 1–11 fractures/m, sealed and open fractures, prehnite
ZFMNE00A4	4,298 ± 200 m	25 ± 13 m	061/25	Brittle	High confidence, oxidized, 0–21 fractures/m, open and sealed fractures, laumontite
ZFMNE00A7	4,090 ± 200 m	17 ± 10	055/23	Brittle	High confidence, oxidized, 0–13 fractures/m, open and sealed fractures, clay minerals, prehnite
ZFMNE00B1	2,208 ± 100 m	7 m	032/27	Brittle	High confidence, oxidized, 1–10 fractures/m, open and sealed fractures, clay minerals, prehnite and laumontite
ZFMNE1188	741 ± 50 m	1–2 m	220/05	Brittle/ductile	High confidence, oxidized, 2–20 fractures/m, mainly sealed fractures, laumontite, prehnite, clay minerals

4.3 Rock mechanics signature of the deformation zones

The deterministic deformation zones are characterised by one or several "cores", often characterised by deformed, altered, migmatised and highly fractured rock mass sometimes with the presence of clay, and a "transition zone" less affected by these phenomena. As provided by the deformation zone model, the thickness of the deterministic zones accounts for both the core and transition zone.

The empirical characterisation of the boreholes in this report can localise the presence of fractured rock mass that affect the average rock mass quality within each 5 m of borehole length. Thus, the value of the empirical ratings such Q and RMR can be used to identify, or confirm, the presence of deformation zones (minor and/or deterministic).

The simplest way to identify of the deformation zones by means of the Q and RMR values is to check the borehole sections where these present the lowest values. According to the Q and RMR system, the limit between the rock mass classes described as "fair rock" and "poor rock" are a Q value of 4 and an RMR value of 40. Considering that the scale of rock quality according to RMR spans from very good crystalline rocks to almost soil-like degradation rocks, the limit between "fair" and "poor" rock does not coincide with that of the Q system, which was designed particularly for better rock classes. Thus, the value of RMR characterising the deformation zones can be assumed to be 60. The occurrence of either a Q value smaller than 4 or a RMR value smaller than 60 is considered as the "signature" identifying the minor and deterministic deformation zones.

Deformation zone signature: $Q < 4$ and/or $RMR < 60$ (4)

At Forsmark, where the rock mass is on average very good, the application of Equation (4) does not detect many zones and, in some cases, not even the deterministic deformation zones. For this reason, other thresholds for Q and RMR were chosen instead:

Deformation zone signature: $Q < 10$ and/or $RMR < 65$ (5)

The application of the thresholds in Equations (2) and (3) gives the results shown in Table 4-4 and are graphically presented in Figure 4-3 and Figure 4-4.

Figure 4-5 shows the results of the application of Equation (5) to the borehole data from zone ZFMNE00A2. The figure also shows that some of the deterministic deformation zones are at the detection limit of Equation (5). Therefore, the recognition of minor deformation zones by this method is interesting because it indicates the presence of rather localized features with poorer rock than some of the deterministic deformation zones.

Table 4-4. Minor deformation zones identified by means of the empirical methods Q and RMR applied to the borehole information.

Borehole	Q < 4 and/or RMR < 60		Q < 10 and/or RMR < 65	
KFM01A			155–175	
			230–235	
KFM02A			115–120	ZFMNE00B6
			235–240	
			260–270	(DZ4)
			305–310	ZFMNE1189 (DZ5)
			420–425	ZFMNE00A2 (DZ6)
			490–495	ZFMNE00A2 (DZ6)
			510–515	ZFMNE00A2 (DZ6)
	890–895	ZFMNE1195 (DZ8)	890–905	ZFMNE1195 (DZ8)
	900–905	ZFMNE1195 (DZ8)		
KFM03A			105–110	–
			370–375	ZFMNE00A4 (DZ1)
			385–390	ZFMNE00A4 (DZ1)
			395–400	ZFMNE00A4 (DZ1)
			440–445	–
	445–450	ZFMNE00A7 (DZ2)	445–450	ZFMNE00A7 (DZ2)
			630–635	–
			640–645	ZFMNE00B1 (DZ3)
	805–810	ZFMNE00A3 (DZ4)	805–810	ZFMNE00A3 (DZ4)
	945–950	ZFMNE1207* (DZ5)	940–950	ZFMNE1207* (DZ5)
KFM04A			140–145	–
			170–175	ZFMNE00A2 (DZ1)

* ZFMNE1207 was identified in version 2.1 of the deformation zone model.

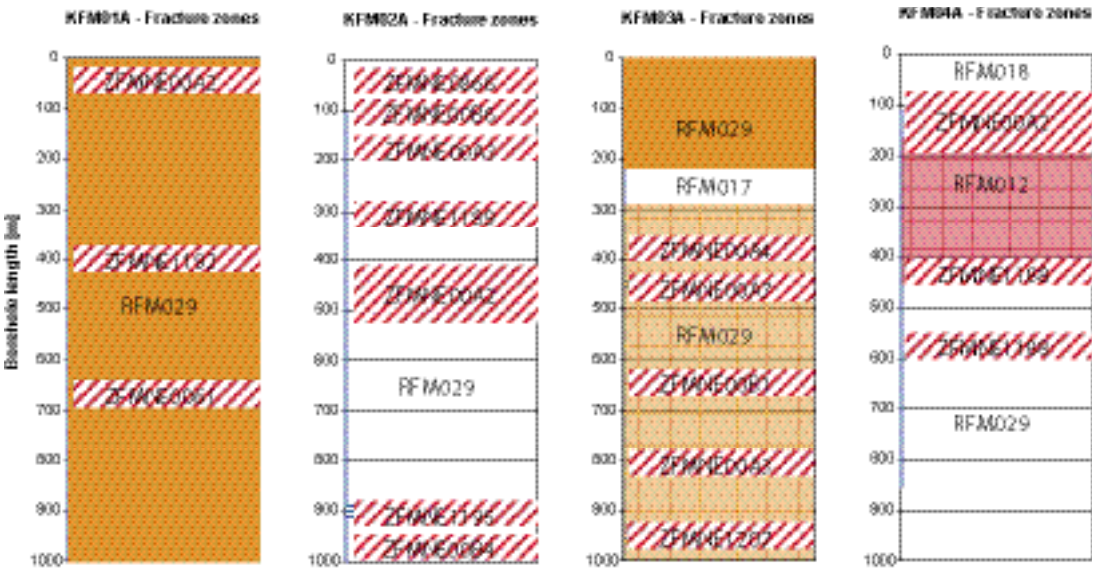

Figure 4-3. Plot of the minor deformation zones identified by means of the empirical methods Q and RMR along the boreholes (Q < 4 and/or RMR < 60). The deterministic deformation zones are given according to version 2.1 of the deformation zone model.

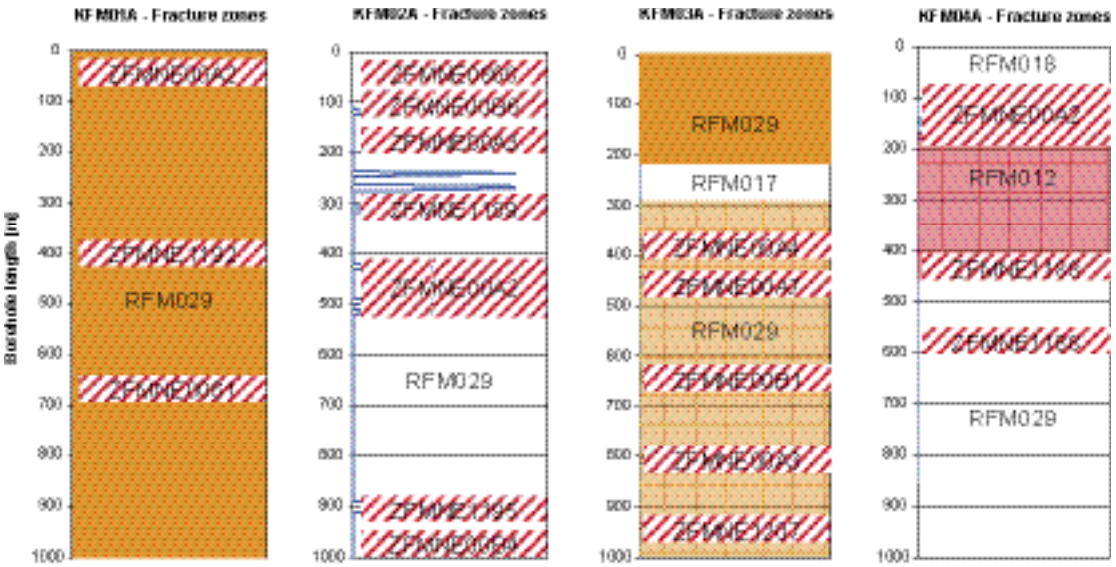

Figure 4-4. *Plot of the minor deformation zones identified by means of the empirical methods Q and RMR along the boreholes (Q < 10 and/or RMR < 65). The deterministic deformation zones are given according to version 1.2 of the deformation zone model.*

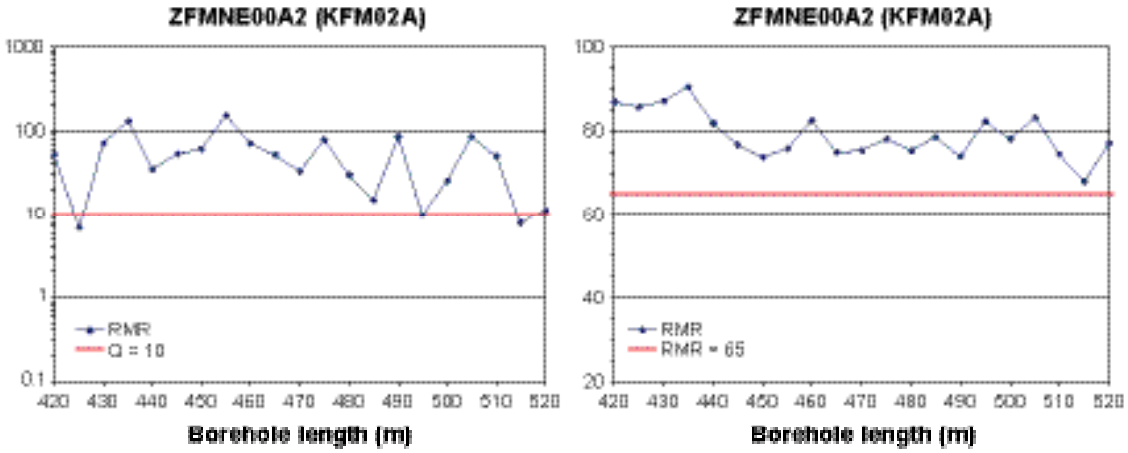

Figure 4-5. *Zone ZFMNE00A2 in borehole KFM02A: mean observed Q (left) and RMR (right) and application of Equation (5).*

4.4 Description of the minor zones

The geology of the borehole sections identified in Table 4-4 was studied more in detail with particular attention to the radar reflectors in the boreholes, the description of the rock fractures and range of variation of the empirical ratings Q and RMR (Table 4-5). From the orientation of the natural open fractures, the possible fracture sets were determined (Figure 4-7). The radar reflectors provide an estimation of the orientation of the zones (Table 4-6) that can be used in Equation (3) to estimate the actual thickness of the zone. From the thickness, the trace length of the zones can also be inferred by means of Equation (2). For this determination, the following assumptions were necessary:

1) The intersection angle between the zones and the borehole axis given by the RAMAC loggings considered accurate within a range of ± 2°. This produces the variation of the estimated thickness.

2) The empirical ratings were calculated for each 5 m section of borehole, thus averaging effects on the worst and best rock mass quality are applied.

3) The thickness of the zones measured along the boreholes overestimates the apparent thickness because it is always a multiple of 5 m. On average, the apparent thickness could be about 25% smaller, but should not be less than 50%. This also contributes to the range of variation of the estimated thickness.

4) The scatter of the plot between the trace length and the thickness of the zones shown in Figure 4-2 is ignored and Equation (2) is used to relate the two parameters.

5) Equation (2) is assumed to be valid for zones with trace length spanning from about 100 m to several kilometres. None of the zones is assumed to be a single rock fracture.

This exercise based on empirical methods shows that the minor deformation zones identified along the four boreholes have estimated traces longer than 200 m. Some of them could even be as long as 1,840 m.

Table 4-5. Detailed information about the minor deformation zones identified by means of the empirical methods Q and RMR: single-hole interpretation, radar measurements and BOREMAP data. The uncertainty on the mean Q and RMR are also given as the interval of possible variation of the mean value.

Borehole	Borehole length	Single-hole interpretation	Crushed rock from BOREMAP	BOREMAP	Q *Uncertainty of the mean*	RMR *Uncertainty of the mean*
KFM01A	155–175 m		No	RQD = 95–97, 3–4 fracture sets, 0–7 open fractures/m, smooth planar fractures, unaltered, laumontite	7.6–9.8 *–30%/+110%*	76–79 *–13%/+10%*
	230–235 m		No	RQD = 92, 4 fracture sets, 3–7 open fractures/m, smooth or undulating and planar, unaltered, laumontite	9.2 *–70%/+200%*	76 *± 20%*
KFM02A	235–240 m		No	RQD = 93–100, 2 fracture sets, 1–5 open fractures/m, planar undulated, fresh to sligtly altered, clay minerals	9.1 *–80%/+650%*	87 *–10%/+6%*
	260–270 m	DZ4: crushed zone and large cavity (> 15 cm) (P-04-117)	266.6–267.2 m (51 cm) 118/36	RQD = 47–100, 2–3 fracture sets, 0–10 open fractures/m, planar and undulating, rough, clay minerals	4.3–7.4 *–80%/+1,500%*	74–76 *± 25%*
KFM03A	105–110 m		No	RQD = 90–100, 2 fracture sets, 0–4 open fractures/m, planar, smooth, fresh, prehnite	9.4 *–60%/+125%*	74 *–15%/+10%*
	940–950 m	ZFMNE1207* (DZ5): Increased frequency of brocken fractures. One aperture of 6 mm. Oxidization and clay mineral coatings (P-04-118)	No	RQD = 87–100, 2 fracture sets, 1–7 fractures/m, planar, rough, sliglty altered, clay minerals	3.0–4.8 *–60%/+2,600%*	76 *–25%/+15%*
KFM04A	140–145 m		No	RQD = 56–99, 2 fracture sets, 7–12 open fractures/m, planar, smooth, sligtly altered, clay minerals	4.7 *–75%/+210%*	79 *–30%/+10%*

* ZFMNE1207 was identified in version 2.1 of the deformation zone model.

Table 4-6. Summary of the geometrical properties of the minor deformation zones identified by means of the empirical methods Q and RMR: fracture sets, zone intersection with the borehole axis, estimated thickness and trace length.

Borehole	Borehole length	Fracture sets	Intersection angle	Estimated thickness	Estimated length
KFM01A (inclination 85°)	155–175 m	145/36 104/02	22°	6 m (4–7 m)	970 m (660–1,225 m)
	230–235 m	013/40 054/11	40°	2.5 m (1.5–3 m)	240 m (160–315 m)
KFM02A (inclination 85°)	235–240 m	344/86 347/14	50°	3 m (2–4 m)	434 m (275–590 m)
	260–270 m	027/18	67°	7 m (4.5–9 m)	1,240 m (775–1,715 m)
KFM03A (inclination 86°)	105–110 m	295/80 040/29	50°	3 m (2–3.5 m)	435 m (275–590 m)
	940–950 m	046/76 031/10	76°	7.5 m (5–9.5 m)	1,320 m (820–1,840 m)
KFM04A (inclination 60°)	140–145 m	141/85 233/74 311/06	40°	2.5 m (1.7–3 m)	350 m (225–471 m)

In Figure 4-6, the orientation of deterministic deformation zones intercepting the four analysed boreholes are shown. Considering that the inclination of the boreholes is prevalently between 60° and 86°, the interception angle between the zones and the borehole axis would roughly be 10°, 40° and 60°. These angles are very close to the intersection angles in Table 4-6, since the boreholes are rather steep. This could confirm that the minor deformation zones belong to the same group as the deterministic deformation zones. Thus, it is reasonable to use the relation between thickness and length in Equation (2) to the minor deformation zones that produces the results in Table 4-6. Figure 4-6 also shows that the boreholes preferentially intersect gently dipping zones rather than steep zones. Among the minor deformation zones, only two could have a dip angle larger than 60°.

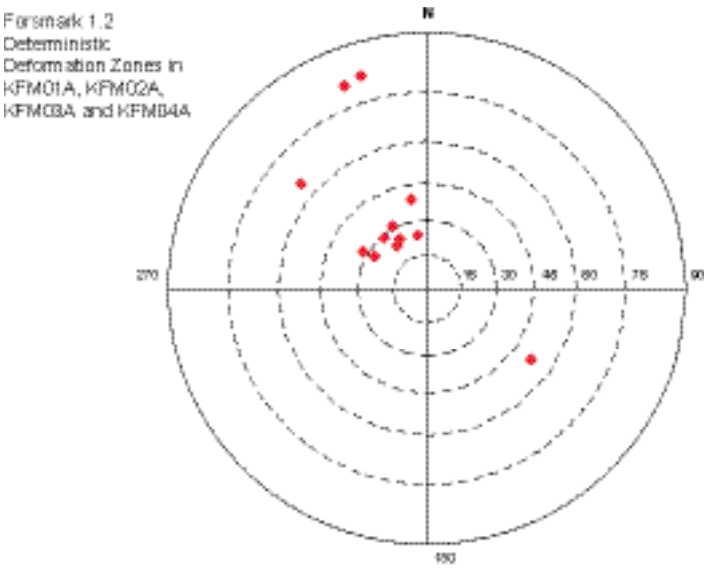

Figure 4-6. *Pole orientation of the deterministic deformation zones in borehole KFM01A, KFM02A, KFM03A and KFM04A (Forsmark SDM version 1.2 /SKB 2005/; compared to version 2.1 of the deformation zone model, only zone ZFMNE1207 is not plotted).*

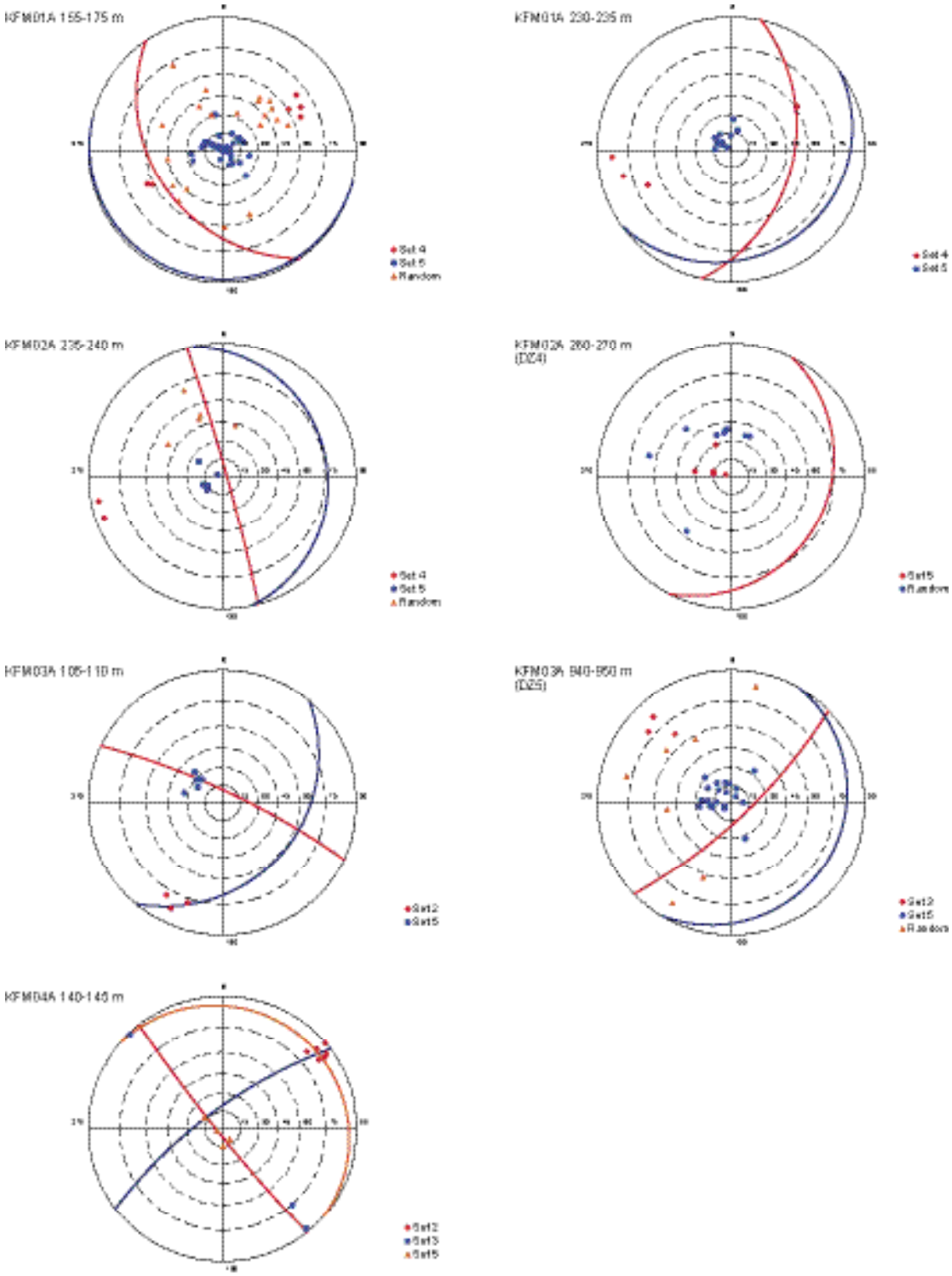

Figure 4-7. *Tentative identification of the fracture sets within each of the minor deformation zones identified by means of the empirical methods Q and RMR along the boreholes (Q < 10 and/or RMR < 65).(Not all the fractures are shown.)*

4.5 Mechanical properties of the deformation zones

By using the empirical characterization results reported in /SKB 2005/, the mechanical properties of the zones identified in Section 4.3 can be calculated and are summarized in Table 4-7. Besides the expected mean values, also gives a quantification of the uncertainty as an interval of possible variation of the mean is given in the table. The intervals tabulated are very wide because there is not much data available about the zones. Moreover, their properties can vary due to several causes:

- Choice of the parameters made by the operator performing the characterization.
- Spatial position where the zones are sampled.

Despite the large uncertainty on the values, the estimated mean values do not vary very much from one zone to another one. Only the zone between 260 and 270 along borehole KFM02A seems to have much worse mechanical properties than the other minor zones. This zone could be related to ZFMNE1189 that occurs in the same borehole between 303 and 310 m. Concerning the other minor zones, if convenient, they could be characterized by means of just one set of parameters. The parameters in Table 4-7 also confirm the values reported in /SKB 2005/ about the minor and short deformation zones (length smaller than 10 km).

Table 4-7. Predicted rock mechanics properties of the rock mass in the minor deformation zones in the Forsmark local model volume. The mean value and the standard deviation of the properties are given with the truncation intervals for the normal distribution. The interval of variation of the mean value due to uncertainties is also given.

Minor deformation zones **Borehole/borehole length**	**KFM01A** **155–175 m**	**KFM01A** **230–235 m**	**KFM02A** **235–240 m**	**KFM02A** **260–270 m**	**KFM03A** **105–110 m**	**KFM03A[6]** **940–950 m**	**KFM04A** **140–145 m**
Properties of the rock mass	**Min–Max** *Uncertainty of the mean*	**Min–Max** *Uncertainty of the mean*	**Min–Max** *Uncertainty of the mean*	**Min–Max** *Uncertainty of the mean*	**Min–Max** *Uncertainty of the mean*	**Min–Max** *Uncertainty of the mean*	**Min–Max** *Uncertainty of the mean*
Uniaxial compressive strength (Coulomb)[1, 4]	104 MPa *–55%/+135%*	100 MPa *–80%/+180%*	132 MPa *± 60%*	62 MPa *–80%/+180%*	96 MPa *–80%/+180%*	99 MPa *–80%/+180%*	108 MPa *–80%/+180%*
Uniaxial compressive strength (Hoek & Brown)[3]	46 MPa *–40%/+60%*	40 MPa *–55%/+80%*	75 MPa *–70%/+100%*	17 MPa *–55%/+80%*	37 MPa *–55%/+80%*	40 MPa *–55%/+80%*	52 MPa *–55%/+80%*
Friction angle[1]	47° *–17%/+10%*	46° *–26%/+16%*	49° *–20%/+10%*	39° *–26%/+16%*	46° *–26%/+16%*	46° *–26%/+16%*	47° *–26%/+16%*
Cohesion[1]	21 MPa *–25%/+40%*	20 MPa *–40%/+50%*	25 MPa *± 40%*	15 MPa *–40%/+50%*	19 MPa *–40%/+50%*	20 MPa *–40%/+50%*	21 MPa *–40%/+50%*
Deformation modulus[2]	51 GPa *± 45%*	45 GPa *–60%/+75%*	75 GPa[7] *–50%/+20%*	44 GPa *–60%/+75%*	41 GPa *–60%/+75%*	45 GPa *–60%/+75%*	54 GPa *–60%/+75%*
Poisson's ratio[2]	0.16 *–30%/+55%*	0.14 *–50%/+90%*	0.24 *± 30%*	0.14 *–50%/+90%*	0.13 *–50%/+90%*	0.15 *–50%/+90%*	0.17 *–50%/+90%*
Tensile strength[4]	0.9 MPa *–55%/+150%*	0.8 MPa *–80%/+200%*	1.8 MPa *± 80%*	0.3 MPa *–80%/+200%*	0.7 MPa *–80%/+200%*	0.8 MPa *–80%/+200%*	1.2 MPa *–80%/+200%*

[1] The apparent uniaxial compressive strength, cohesion and friction angle are obtained from the Coulomb's Strength Criterion between 10 and 30 MPa confinement stress.

[2] The deformation modulus and the Poisson's ratio of the rock mass are given for low stress confinement.

[3] The tensile strength is obtained from the curvilinear Hoek and Brown's Criterion of the rock mass from the RMR-GSI relation.

[4] The uniaxial compressive strength is obtained from the curvilinear Hoek and Brown's Criterion of the rock mass from the RMR-GSI relation.

[5] This value is high, thus no variation with stress is considered for this zone.

[6] Zone ZFMNE1207 in Forsmark deformation zone model version 2.1.

5 Numerical study of two minor deformation zones in KFM03A

The objective of this study is to evaluate the mechanical properties of two sections identified as deformation zones (DZ) by the single-hole interpretation applying the theoretical/numerical Rock Mechanics Site Descriptive Model /Olofsson and Fredriksson 2005/.

The two sections chosen for this study are:

- DZ1 in KFM03A (356–399 m): this section has been modelled as a deformation zone in the geological model version 1.2 (ID: ZFMNE00A4).
- ZFMNE1207 (DZ5) in KFM03A (942–949 m): this section has not been modelled as a deformation zone in the geological model version 1.2. However it has been identified as a potential minor deformation zone with the empirical method which evaluated lower mechanical properties in this DZ section.

This study consists in the first attempt to model and characterise the deformation zones with the numerical mechanical model. It was decided to apply the procedure as it is described in /Olofsson and Fredriksson 2005/, but to update the fracture intensity in accordance to the observations made in each chosen DZ section.

5.1 Geological settings of the zones

The objective was to generate local DFN realizations for the deformation zones DZ1 and ZFMNE1207 (DZ5) in KFM03A. These DFN realizations will serve as input to 3DEC for rock-mechanical simulations. There was no attempt at this stage of the study to analyse specific orientation data of fractures. Therefore orientation and size distributions are taken from the DFN developed for the preliminary site description – version 1.2 /SKB 2005/.

5.2 Scope

The fracture characteristics in the deformation zones DZ1 and ZFMNE1207 (DZ5) in KFM03A deviate from the general characteristics of RFM29. The aim is therefore to adjust the DFN model to the local deformation zone data.

Two approaches are possible:

1) To use bootstrapping to extrapolate local data into DFN realizations (i.e. local statistics of fracture orientation and intensity data are used as the stochastic basis for generating DFNs).
2) To assume that fracture geometry within the deformation zones follow the global set definitions (in terms of orientation and size), but allow for set-specific fracture intensities to vary locally.

The advantage with alternative (1) is that it can account for a potential re-orientation of fracture sets within the deformation zone. However, its drawback is that the data available from the zones are probably too few to provide a reliable parameterization of the local DFN model. In other words, the degree to which the local deformation zone data apply to the entire zone is unknown. Parameters that are particularly difficult to asses from local data are: a) the size distributions for fractures of different orientations, and b) the dispersion in orientation around 'local' fracture sets (Fisher). Over -interpretation of data and unjustified assumptions made in such a 'local DFN model parameterization' can lead to uncertainties or erroneous results (considering the scarcity of deformation zone data in relation to the entire RFM29 data set).

In alternative (2), the size- and orientation parameterization is based on a large data set. This approach was considered to be more reasonable and was therefore selected for the generation of stochastic DFNs. In this approach, fracture intensity (set-specific P_{10} or P_{32}) was treated as the single parameter being influenced by the deformation zone. Thus, the task is to determine set-specific P_{32} by means of numeric calibration to borehole data P_{10}.

5.3 Input data

The fracture borehole data for KFM03A was taken from Sicada. Deformation zone 1 extends for 43 m (356 to 399 m) along the borehole and has a fracture frequency of about 4 fractures/m (contains 178 fractures of which 23 not visible in BIPS; 81 open and partly open, and 97 sealed). Deformation zone 5 extends 5 m (942 to 949 m) along the borehole and has a fracture frequency

of about 8 fractures/m (contains 46 fractures, all visible in BIPS: 6 open and partly open, and 40 sealed).

All DFN parameters (minimum fracture radius, exponent of the size distribution, and orientation), except P32, were taken from Table 9-1 in /LaPointe et al. 2005/.

5.4 Methodology

At the time of this project, it was not decided whether fractures not visible in BIPS should be included or not. For DZ1, P_{32} was therefore calibrated for both cases. Furthermore, fractures of all types (open, partly open, and sealed fractures; without respect to mineral filling) were included in the DFN calibration.

First, all fractures were assigned to their most likely set-of-belonging. This was done by generating large fracture networks to analyze the overall distribution of orientations (on the order of 400,000 fractures). From this analysis, the "hard fracture set sectors" (areas indicated with different colours in Figure 5-1 to Figure 5-3) could be estimated by calculating the dominantly occurring fracture set (i.e. equivalent to the 'expected' fracture set) at any given orientation. From this hard sector division, each fracture could then be assigned to the most likely set based on its orientation.

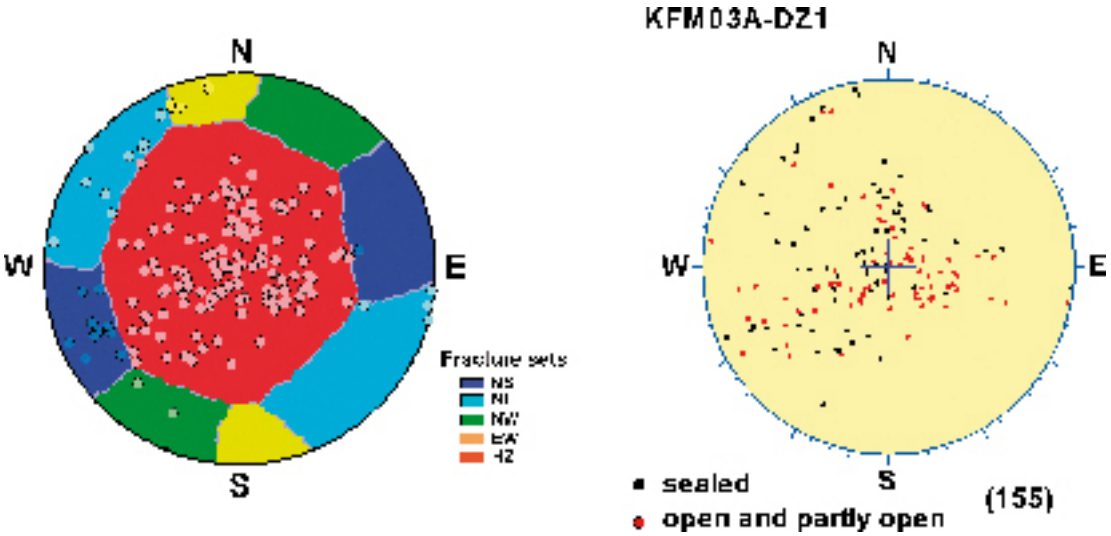

Figure 5-1. *Hard sector division of fractures in DZ1, FKM03A (all fractures).*

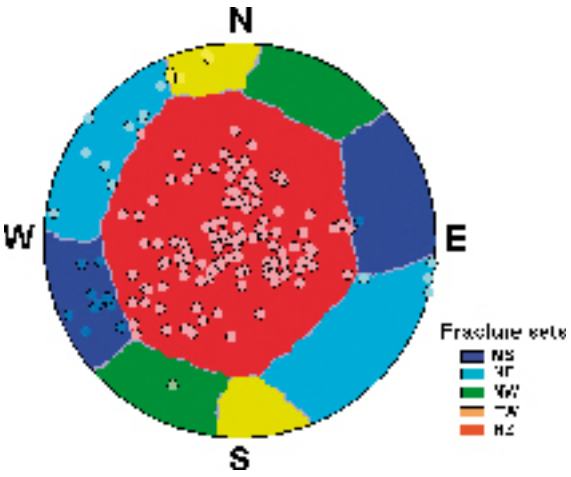

Figure 5-2. *Hard sector division of fractures in DZ1, FKM03A (only fractures visible in BIPS included; fractures removed from sets NW and HZ; Table 1).*

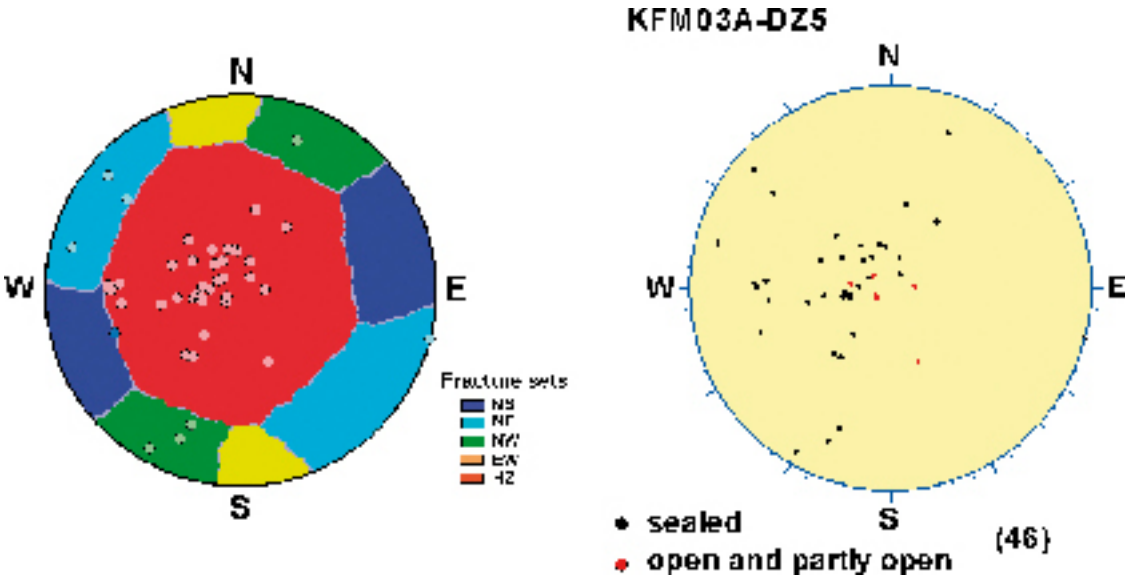

Figure 5-3. *Hard sector division of fractures in ZFMNE1207 (DZ5) in FKM03A .*

Next, set-specific borehole fracture frequency (P_{10}) could be calculated, simply by dividing the number of fractures from a given set, by the borehole length that intersects the deformation zones (Table 5-1 and Table 5-2).

Finally, set-specific fracture intensity (P_{32}) could be calculated for the two deformation zones. Fracture networks with varying fracture intensity were generated (P_{32} = 2, 4, 6, 8, 10, 20 m^2/m^3) and explored by simulated exploration boreholes, to estimate the linear relationship between P_{32} and P_{10} (Figure 5-4 and Figure 5-5). Linear coefficients, C_i (Equation 5–10 in /LaPointe et al. 2005/), were obtained. These coefficients depend only on the borehole geometry (orientation and radius) and on its set-specific fracture orientation distribution. The borehole radius was set to zero, as the data set was assumed only to include fractures that intersect the borehole central axis. From these linear coefficients, the observed set-specific P_{10} data was directly related to P_{32} (Table 5-1 and Table 5-2).

Now, these fracture intensities relate to the minimum truncation radii (Table 9-1 in /LaPointe et al. 2005/), whereas in rock mechanical simulation, fractures shorter than 0.5 m radius are considered to be negligible. Therefore the calibrated P_{32} values need to be rescaled to be valid for such a truncated size distribution. The rescaled fracture intensities, P_{32} (0.5 m ,), were calculated by Equation 5-16 in /LaPointe et al. 2005/; these values are reported in Table 5-3.

Table 5-1. Calibration results for DZ1 (356–399 m) in KFM03A (see Figure 5-4 for the calibration of P_{10} to P_{32}).

	DZ1 (all fractures)			DZ1 (only fractures visible in BIPS)		
Set	**No. fractures**	**P_{10} m^{-1}**	**Match P_{32} (m^2/m^3)**	**No. fractures**	**P_{10} m^{-1}**	**Match P_{32} (m^2/m^3)**
NS	12	0.28	1.60	12	0.28	1.60
NE	13	0.30	2.13	13	0.30	2.13
NW	2	0.05	0.26	1	0.02	0.13
EW	5	0.12	0.71	5	0.12	0.71
HZ	146	3.40	3.98	124	2.88	3.38
Total	178	4.14	8.68	155	3.60	7.95

Table 5-2. Calibration results for ZFMNE1207 (DZ5) (942–949 m) in KFM03A (see Figure 5-5 for the calibration of P_{10} to P_{32}).

	All fractures in ZFMNE1207 (DZ5)		
Set	**No. fractures**	**P_{10} m^{-1}**	**Match P_{32} (m^2/m^3)**
NS	1	0.14	0.83
NE	5	0.71	5.14
NW	4	0.57	3.34
EW	0	0	0
HZ	36	5.14	6.27
Total	46	6.57	15.58

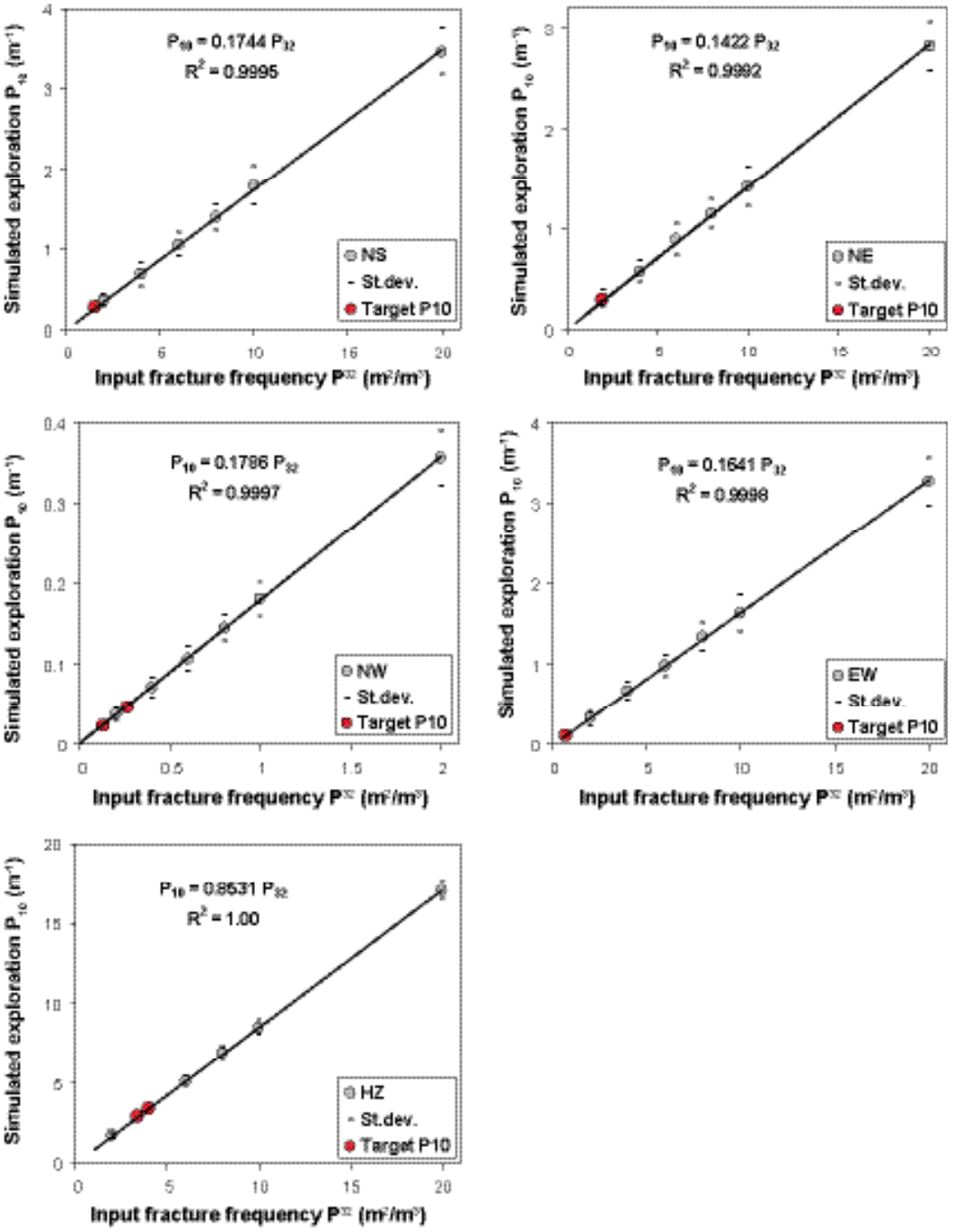

Figure 5-4. *Established relationships between input P_{32} and resulting P_{10} for DZ1 in KFM03A for the different fracture orientation sets.*

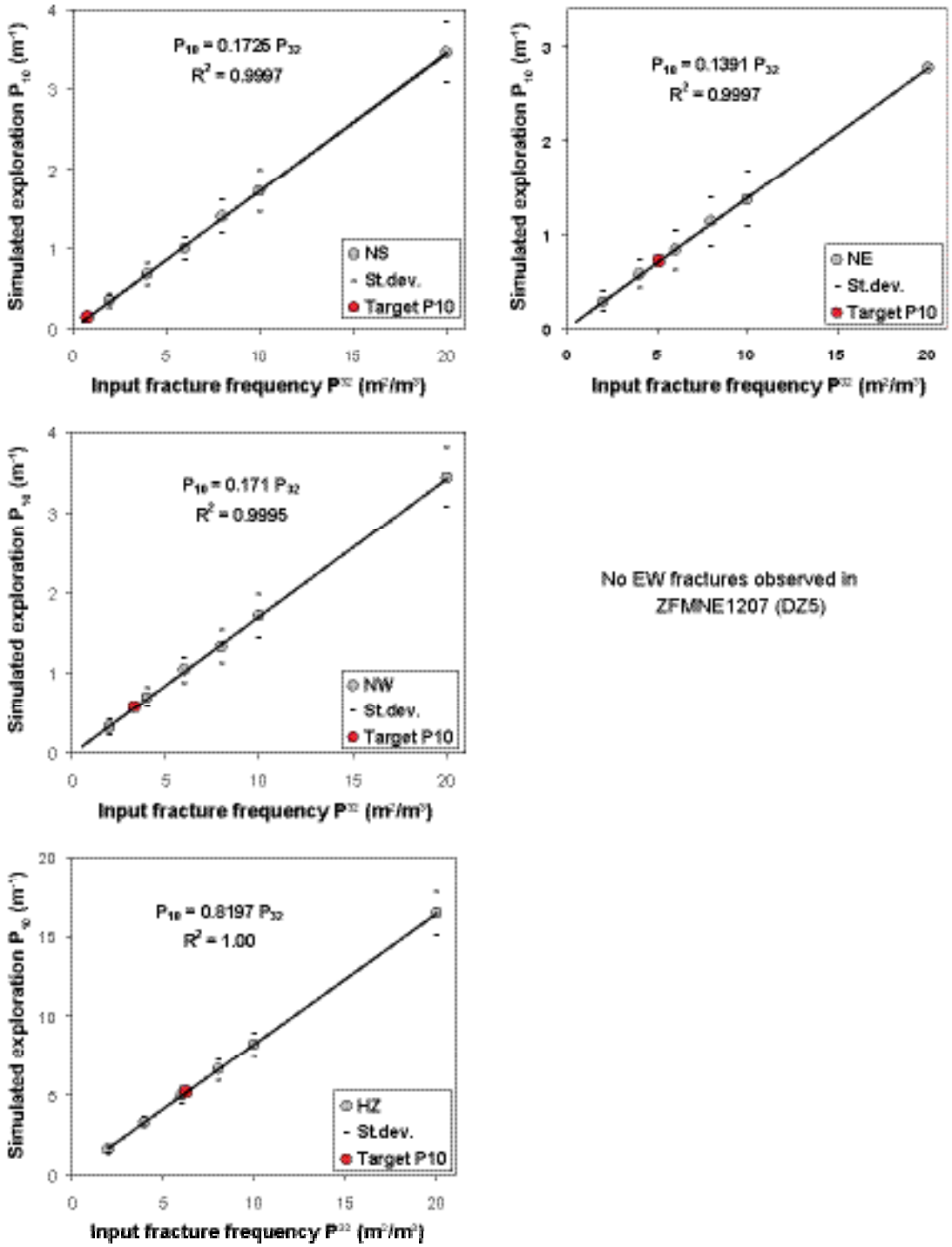

Figure 5-5. *Established relationships between input P_{32} and resulting P_{10} for ZFMNE1207 (DZ5) in KFM03A for the different fracture orientation sets.*

Table 5-3. Calculated P_{32} for truncated size distributions (x_1 = 0.5 m). Untruncated P_{32} (i.e. lower truncation limit x_{r0}) are taken from Table 5-1 and Table 5-2.

	DZ1			ZFMNE1207 (DZ5)		
Set	**Match P_{32} (m^2/m^3)**	**Truncated P_{32} (m^2/m^3)**	**Truncated P_{10} (m^{-1})**	**Match P_{32} (m^2/m^3)**	**Truncated P_{32} (m^2/m^3)**	**Truncated P_{10} (m^{-1})**
NS	1.60	0.95	0.17	0.83	0.49	0.08
NE	2.13	1.04	0.15	5.14	2.52	0.35
NW	0.26 (0.13)[1)]	0.09 (0.05)[1)]	0.02 (0.01)[1)]	3.34	1.18	0.20
EW	0.71	0.22	0.04	0	0	0
HZ	3.98 (3.38)*	2.09 (1.77)*	1.78 (1.51)*	6.27	3.29	2.70
Total	8.68 (7.95)*	4.40 (4.04)*	2.15 (1.87)*	15.58	7.48	3.33

[1)] fractures not visible in BIPS have been removed.

5.5 Numerical simulations

5.5.1 Simulation set-up

The procedure used for the numerical simulation is the same as described in /Olofsson and Fredriksson 2005/, but has in this case been applied to deformation zones. The approach is based on a discrete fracture network (DFN) description of the fractured rock mass system and on the results of mechanical testing of intact rock and on rock fractures. The 3D DFN representative of the site is simulated and fracture trace planes are extracted to be used as input for 3DEC.

In this project only vertical planes parallel to the maximum in situ stress $_1$ have been studied.

To estimate the mechanical properties of the rock mass a load test on a rock block with fractures was simulated with the numerical code 3DEC. Fracture network realisations were first generated with the numerical software FracMan, which were then transferred into the mechanical model. The rock block was loaded in plain strain condition. From the calculated relationship between stresses and deformations the mechanical properties of the rock mass were determined.

The model was loaded at three different confining stress levels, first to give an estimation of the rock mass parameters at different depths, and secondly to interpret the rock mass strength properties according to Hoek & Brown. The parameters are evaluated with the software Rocdata (Rocscience Inc.) using the results of the numerical tests at the three different levels of confining stress. The best fit for the failure envelope is calculated and the Hoek & Brown's parameters of the rock mass for a given uniaxial compressive strength are produced, see Figure 5-6.

The impact of the fracture pattern has been studied in each DZ section by simulating and testing 20 realisations of the same DFN. The influence of the impact of the input mechanical properties has been assessed in some extent by modifying some mechanical properties for DZ1.

The parameters used for the DFN are those published in /SKB 2005/ for orientation and size distribution. The fracture intensity, P_{32}, has been evaluated to fit the observations mapped in the two studied deformation zones, see Section 5.4.

5.5.2 Evaluation of the mechanical properties for DZ1

20 DFN realizations were simulated from the DFN properties of the zone defined in Table 5-33 (orientation sets) and Table 5-34 (size distributions) /SKB 2005/, and Table 5-3 Section 5.4. The aim was to run the different realizations in the numerical mechanical model in order to quantify the influence of the fracture pattern on the rock mass mechanical properties. Seven realizations failed because the fracture pattern was incompatible to the numerical model set-up.

Three different sets of input parameters were applied to the model for all 13 DFN realisations, see Table 5-4. DZ1_1 refers to the mean values of the mechanical properties evaluated for intact rock and fractures in Appendix 3, Sections 2 and 3. For DZ1_2 and DZ1_3, the input properties of the intact rock were not modified but the mechanical properties of the fractures are set to the "worse case". These three cases were studied in order to evaluate the influence of the input parameters on the rock mass properties.

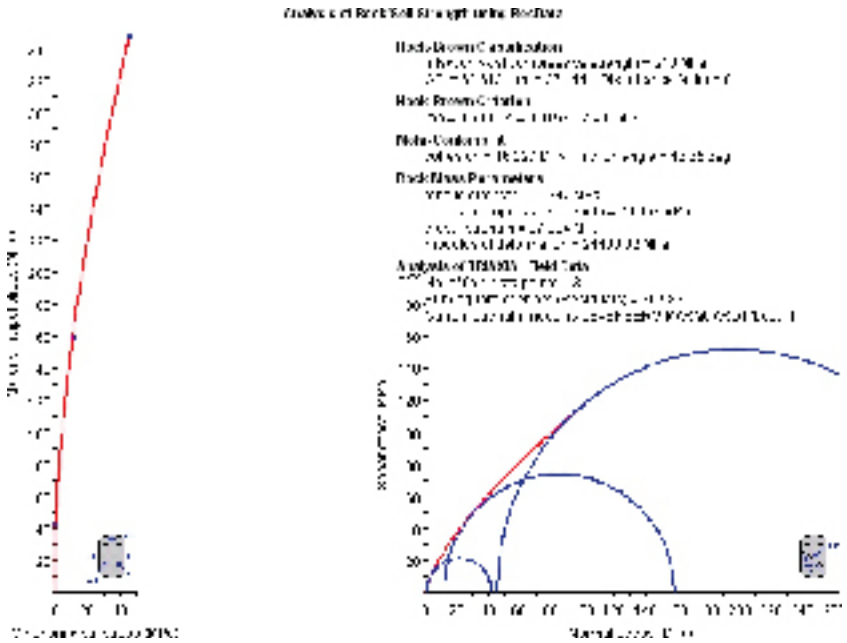

Figure 5-6. *Evaluation of the rock mass parameters according to Hoek & Brown and using the software Rocdata (Rocscience Inc.).*

Table 5-4. Input parameters for intact rock and fracture properties.

		DZ1_1	DZ1_2	DZ1_3
Intact rock	E_i (GPa)	76.0	76.0	76.0
	ν_i	0.23	0.23	0.23
	ϕ_i (°)	60.5	60.5	49.2
	C_i (MPa)	27.66	27.66	19.55
	T_i (MPa)	13.5	13.5	6.75
Fractures	K_n (MPa/mm)	937.4	264.8	264.8
	K_s (MPa/mm)	30.6	13.9	13.9
	ϕ_f (°)	34.3	28.0	28.0
	C_f (MPa)	0.7	0.4	0.4

The 13 DFN realizations were analyzed at three different stress levels: 45 (equivalent to the maximum principal stress $_1$), 11.3 (25% of $_1$) and 0.5 MPa. The mechanical models were loaded with a constant velocity in the vertical direction while the horizontal stresses were constant during the loading test. The deformation modulus, E_m, the Poisson's ratio, $_m$, and the stress of failure, $_{vf}$, were evaluated at the three stress levels to provide an estimation of c_m and ϕ_m. The stress of failure is defined as the maximum vertical stress or the vertical stress at 0.010 vertical strain if the vertical stress-vertical strain curve does not show a marked maximum.

A summary of the obtained distributions for the rock mass deformation parameters, E_m and $_m$ at the three stress levels is given in Table 5-5, Table 5-7 and Table 5-9 for the respective cases DZ1_1, DZ1_2 and DZ1_3. The respective obtained distributions for the rock mass strength properties are presented in Table 5-6, Table 5-8 and Table 5-10. The variability of the parameters for one case account only for the influence of the fracture pattern. The variability of the distributions between the cases accounts for the influence of the mechanical input parameters.

Table 5-5. Rock mass deformation properties of DZ1_1.

	Mean	Std. dev.	Min	Max
$E_{m\ 45\ MPa}$ (GPa)	56.5	5	48.5	64.7
$\nu_{m\ 45\ MPa}$	0.29	0.02	0.25	0.32
$E_{m\ 11.3\ MPa}$ (GPa)	53.6	6	45.6	62.8
$\nu_{m\ 11.3\ MPa}$	0.3	0.02	0.26	0.33
$E_{m\ 0.5\ MPa}$ (GPa)	40.85	13.7	18.3	57.6
$\nu_{m\ 0.5\ MPa}$	0.41	0.09	0.28	0.55

Table 5-6. Rock mass strength properties of DZ1_1 (interval 0.5–45 MPa).

		Mean	Std. dev.	Min	Max
GSI		73.1	9.4	58.9	85.9
m_i		43.3	10.2	16	50
c_m (MPa)	Mohr-Coulomb	14.45	4.5	5.5	20.9
ϕ_m (°)		52.1	3	46.4	55.4
σ_t (MPa)	Hoek & Brown	–0.99	1.14	–4.55	–0.19
σ_c (MPa)		53.2	26.6	21.2	96.1

Table 5-7. Rock mass deformation properties of DZ1_2.

	Mean	Std. dev.	Min	Max
$E_{m\ 45\ MPa}$ (GPa)	44	6.4	34.3	55.2
$\nu_{m\ 45\ MPa}$	0.29	0.02	0.26	0.33
$E_{m\ 11.3\ MPa}$ (GPa)	41.6	6.95	32.2	53.8
$\nu_{m\ 11.3\ MPa}$	0.31	0.03	0.26	0.36
$E_{m\ 0.5\ MPa}$ (GPa)	35.35	10.1	17	49.2
$\nu_{m\ 0.5\ MPa}$	0.38	0.05	0.29	0.46

Table 5-8. Rock mass strength properties of DZ1_2 (interval 0.5–45 MPa).

		Mean	Std. dev.	Min	Max
GSI		60.8	18.8	31.9	85.1
m_i		41.6	9.9	27	50
c_m (MPa)	Mohr-Coulomb	11.5	6.3	3.7	22.3
ϕ_m (°)		48.3	2.9	43.1	53.1
σ_t (MPa)	Hoek & Brown	–0.68	0.77	–2.34	–0.02
σ_c (MPa)		36.5	31.8	4.1	91.5

Table 5-9. Rock mass deformation properties of DZ1_3.

	Mean	Std. dev.	Min	Max
$E_{m\ 45\ MPa}$ (GPa)	43.9	6.3	34.2	55.1
$\nu_{m\ 45\ MPa}$	0.3	0.02	0.26	0.33
$E_{m\ 11.3\ MPa}$ (GPa)	41.5	7	32.1	53.4
$\nu_{m\ 11.3\ MPa}$	0.31	0.03	0.27	0.36
$E_{m\ 0.5\ MPa}$ (GPa)	30.3	10.2	16.15	47.9
$\nu_{m\ 0.5\ MPa}$	0.43	0.06	0.32	0.5

Table 5-10. Rock mass strength properties of DZ1_3 (interval 0.5–45 MPa).

		Mean	Std. dev.	Min	Max
GSI		67.25	15.3	47	97.9
m_i		42.9	9.7	23.7	50
c_m (MPa)	Mohr-Coulomb	8.8	5.3	2.6	23.1
ϕ_m (°)		45.55	2.1	41.8	49.1
σ_t (MPa)	Hoek & Brown	–0.57	1.03	–3.78	–0.04
σ_c (MPa)		24.4	25	5.3	93.5

Influence of the fracture pattern

In order to evaluate the influence of the fracture pattern the fracture intensity P_{10} has been calculated from the DFN realizations. The P_{10} of the DFN realizations is obtained by sampling the P_{10} by 8 vertical boreholes equally distributed in the 7×7 m simulated fracture trace plane, see Figure 5-7.

Figure 5-8 illustrates the variation of the GSI (determined as described in Section 5.5.1) for all realizations in the three cases in relation to the simulated P_{10}. No trend at all could be defined between GSI and P_{10} for DZ1_2 and DZ1_3, and the range of GSI values for closed values of P_{10} for the same case is large. For DZ1_1 the variability of GSI is less and some trend of increasing GSI for increasing P_{10} can be defined ($R^2 = 0.09$).

The larger variability of GSI values for DZ1_2 and DZ1_3 is related to the decreased mechanical properties.

Influence of the input parameters

Figure 5-9 and Figure 5-10 illustrate the variability within a case and the variation between the three different cases for rock mass deformation properties. For the deformation modulus cases DZ1_2 and DZ1_3 are very similar, but the values obtained for DZ1_1 are generally higher. For the Poisson's ratio the values are very similar for the three cases at 11.3 and 45 MPa confining stress, but their variability and range of values is higher for DZ1_1 at 0.5 MPa confining stress.

The variation in rock mass deformation properties accounts for the change in fracture properties, and not at all for the change of intact rock properties (as only the cohesion c_i and friction angle ϕ_i have been reduced in DZ1_3).

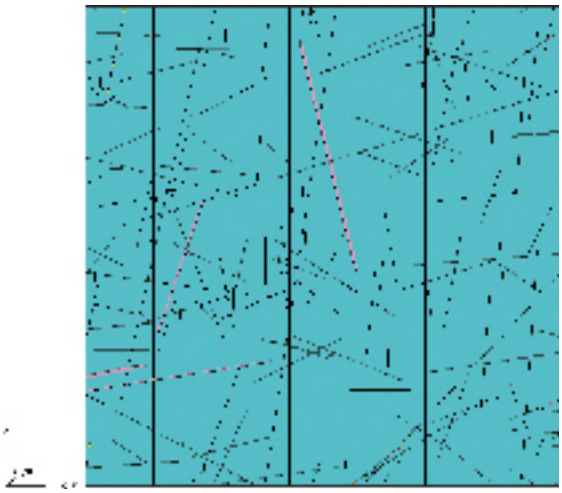

Figure 5-7. *Illustration of the sampled fractures along 8 vertical boreholes in DFN realization 1, DZ1.*

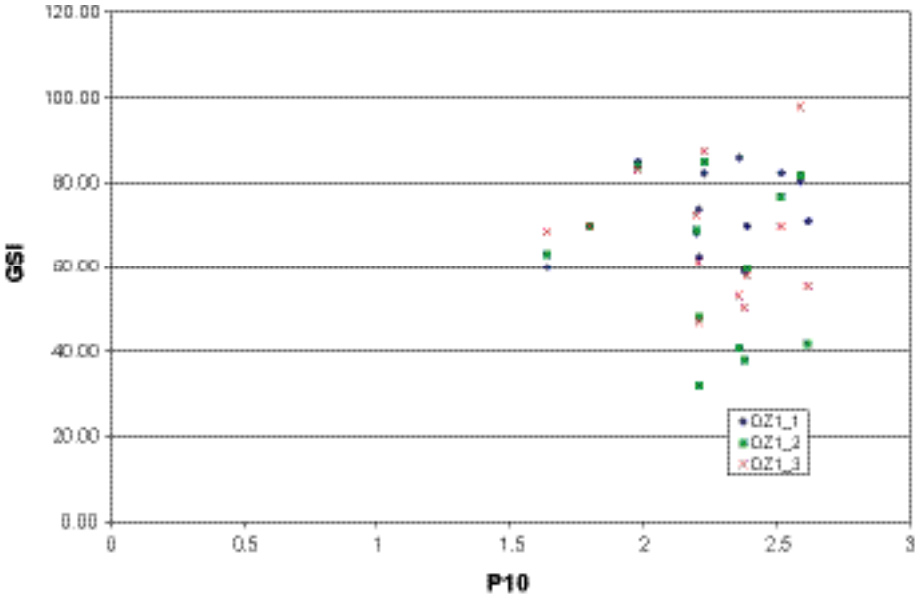

Figure 5-8. *GSI in relation to P_{10} for DZ1_1, DZ1_2 and DZ1_3.*

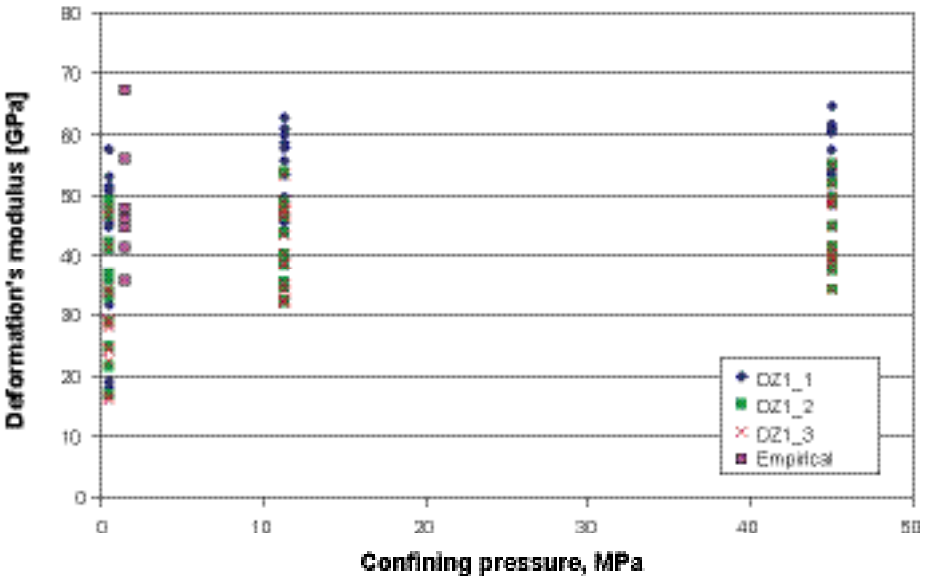

Figure 5-9. *Variation of the deformation modulus E_m with the confining stress for all numerical simulations (in pink the results of the empirical methods in Section 4).*

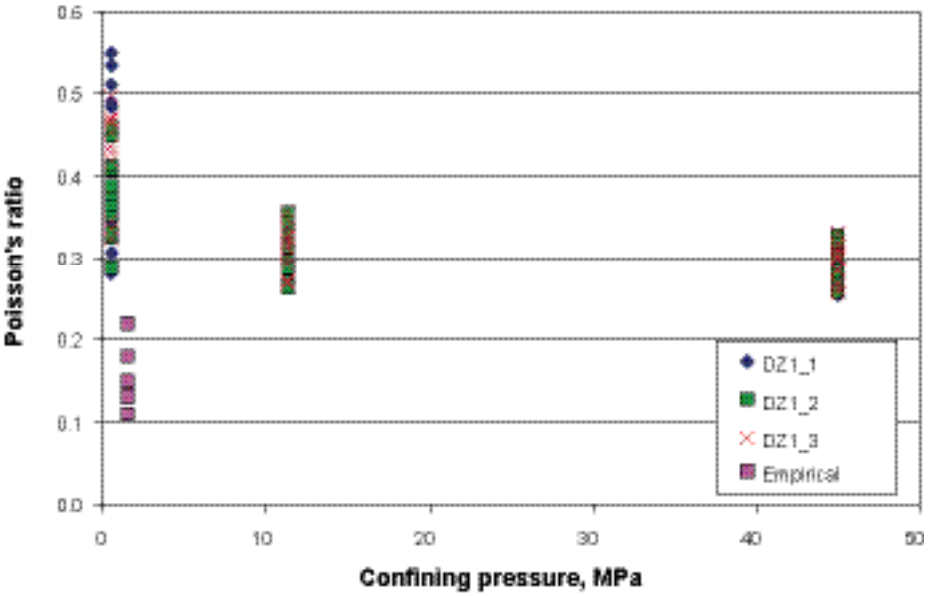

Figure 5-10. *Variation of the Poisson's ratio, $_m$, with confining stress for all numerical simulations (in pink the results of the empirical methods in Section 4).*

The variability of the rock mass strength properties is illustrated in Figure 5-11. These plots show that the variability within the cases is quite similar for DZ1_1, DZ1_2 and DZ1_3. However the variation between the cases DZ1_1 and DZ1_3 is significant (Mann-Whitney tests, $p < 0.05$) and a trend can be defined for all parameters except GSI between the three cases. The cohesion, c_m, friction angle, ϕ_m, and the compressive stress, $_c$, decrease with decreasing fracture and intact rock properties whereas the tensile stress, $_t$, increases slightly.

5.5.3 Evaluation of the mechanical properties for ZFMNE1207 (DZ5)

The same procedure as described in Section 5.5.2 has been applied to deformation zone ZFMNE1207 in KFM03A.

The 20 DFN realizations were simulated from the DFN properties defined for the local model area for orientation and size distributions (Tables 5-33 and 5-34 in /SKB 2005/) and from the adjusted P_{32} of the zone defined in Table 5-3, Section 5.4. Two realizations failed because the fracture pattern was incompatible to the numerical model set-up. The input mechanical parameters were the same as for DZ1_1 in Section 5.5.2, for all the realizations.

The 18 DFN realizations were analyzed at three different stress levels: 45 (equivalent to the maximum principal stress $_1$), 11.3 (25% of $_1$) and 0.5 MPa. The deformation modulus, E_m, the Poisson's ratio, $_m$, and the stress of failure, $_{vf}$, were evaluated at the three stress levels to provide an estimation of c_m and ϕ_m.

A summary of the obtained distributions for the rock mass deformation parameters, E_m and $_m$ at the three stress levels is given in Table 5-11 for the deformation zone ZFMNE1207 (DZ5) in KFM03A. The obtained distributions for the rock mass strength properties are presented in Table 5-12. The distributions of these parameters only account for the influence of the fracture pattern.

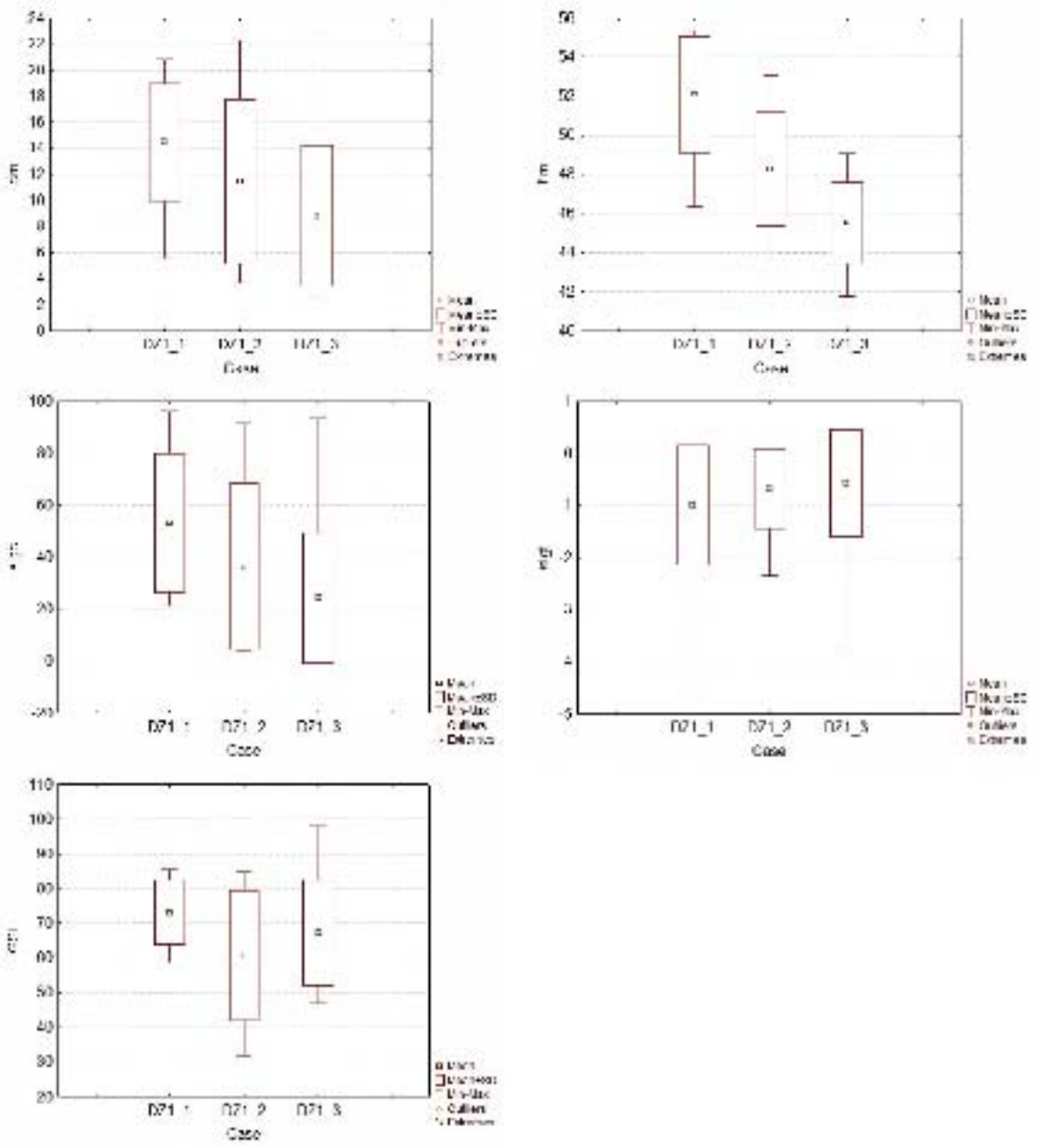

Figure 5-11. *Box plots of the cohesion (cm), friction angle (fim), tensile strength (sigt), compressive strength (sigc) and GSI for the different cases.*

Table 5-11. Rock mass deformation properties of ZFMNE1207 (DZ5).

	Mean	Std. dev.	Min	Max
$E_{m\ 45\ MPa}$ (GPa)	51.7	4	45.6	59.8
$\nu_{m\ 45\ MPa}$	0.30	0.01	0.28	0.32
$E_{m\ 11.3\ MPa}$ (GPa)	48	4.1	38.9	57.3
$\nu_{m\ 11.3\ MPa}$	0.32	0.02	0.29	0.35
$E_{m\ 0.5\ MPa}$ (GPa)	33.1	8.3	20.9	54.8
$\nu_{m\ 0.5\ MPa}$	0.45	0.06	0.33	0.54

Table 5-12. Rock mass strength properties of ZFMNE1207 (DZ5) (interval 0.5–45 MPa).

		Mean	Std. dev.	Min	Max
GSI		69.8	8.3	51.1	86.5
m_i		36.8	9.7	19.2	50
c_m (MPa)	Mohr-Coulomb	12.5	3.36	7.6	20.8
ϕ_m (°)		49.7	2.7	43.3	53.7
σ_t (MPa)	Hoek & Brown	–0.76	0.54	–2.48	–0.11
σ_c (MPa)		43.1	19.8	13.5	99.1

The correlation between c_m and ϕ_m is $c_m = 7.25+0.092\phi_m$.

Figure 5-12 and Figure 5-13 illustrate the variation of the deformation modulus and Poisson's ratio as a function of the confining stress. These figures show that the variability is much higher at 0.5 MPa confining stress.

Figure 5-15 illustrates the variation of GSI (determined as described in Section 5.5.1) for ZFMNE1207 (DZ5) in relation to the simulated P_{10} (see Section 5.5.2 for the sampling method). An example of P_{10} sampling in a simulated trace plane is illustrated in Figure 5-14. As for DZ1 the figure shows that the variability in GSI for similar P_{10} values is very high. Almost no correlation can be observed between back-calculated GSI and input P32 (Figure 5-15).

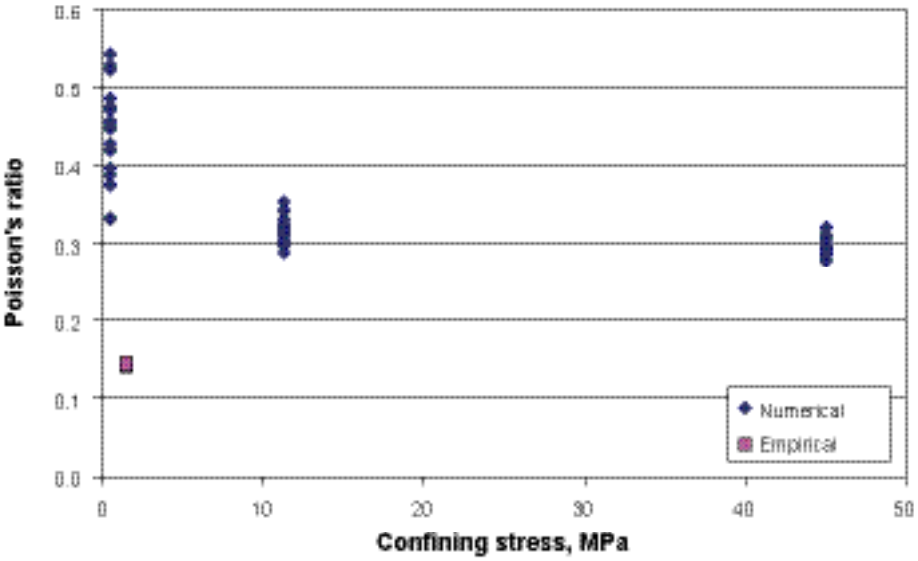

Figure 5-12. *Variation of the deformation modulus, E_m, with confining stress for all numerical simulations (in pink the results of the empirical methods in Section 4).*

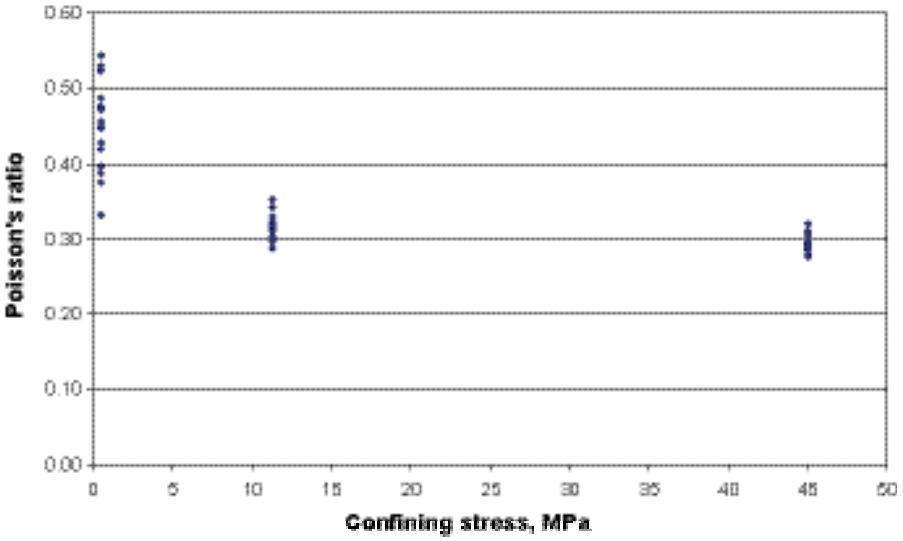

Figure 5-13. *Variation of the Poisson's ratio, $_m$, with confining stress for all simulations.*

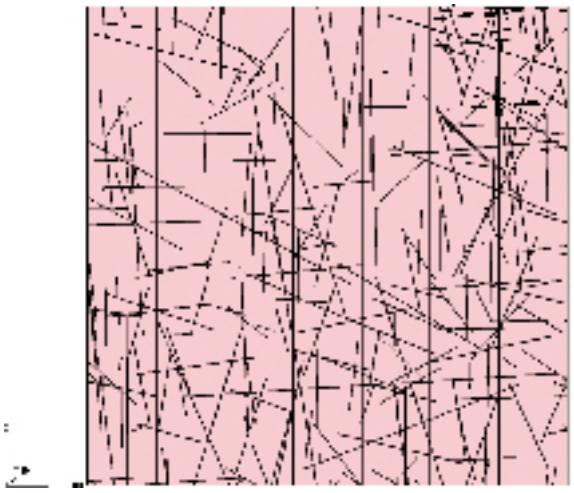

Figure 5-14. *Illustration of the sampled fractures along 8 vertical boreholes in DFN realization 1, ZFMNE1207 (DZ5) in KFM03A.*

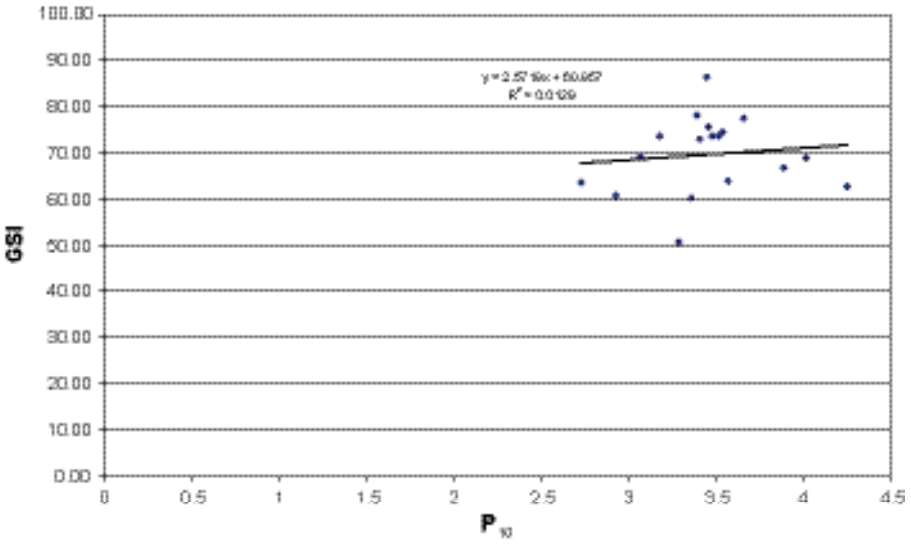

Figure 5-15. *GSI in relation to P_{10} for ZFMNE1207 (DZ5)in KFM03A.*

6 Discussion on the results of the empirical and numerical method applied to the minor deformation zones

6.1 Empirical results

The empirical technique for identification of the minor deformation zones in the boreholes seems to provide relevant results. An estimation of the position, orientation, thickness and apparent trace length can be obtained. Based on the empirical rock mass quality ratings, the mechanical properties of these particular borehole sections are also summarized and compared with the properties of the deterministic deformation zones in the same boreholes.

The uncertainties on the different input parameters (e.g. apparent thickness along the borehole axis, intersection angle) affect the determination of the thickness and length of the zones, together with the necessary assumptions (e.g. Q and RMR thresholds, the power-law fit).

6.2 Numerical results

The aim of the numerical study was to analyse and evaluate the rock mass mechanical properties of two sections identified as deformation zone (DZ) in the single-hole interpretation of the borehole KFM03A. The simulations were carried out following the methodology described in /Olofsson and Fredriksson 2005/. The fracture intensity, P_{32}, of the sections, identified as DZ1 and ZFMNE1207 (DZ5), was adjusted for each section of DZ. The influence of the fracture pattern was studied for both DZ sections. Moreover the impact of the input mechanical properties was studied for DZ1.

- Influence of the input mechanical properties: trends are observed from DZ1_1 to DZ1_3: cohesion, friction angle and compressive strength of the rock mass decrease, whereas the tensile strength increases. The deformation properties of the intact rock were not decreased as to simulate a less competent rock in the deformation zone, which explains why the deformation properties of the three different cases DZ1_1, DZ1_2 and DZ1_3 are so similar. However /Fredriksson and Olofsson 2005/ reviews numerical simulations where the influence of the input mechanical properties were studied. The results show that decreasing the deformation modulus of the intact rock might have a significant impact on the deformation modulus of the rock mass (which will significantly decrease), especially at high stress levels. The impact on cohesion and friction angle of the rock mass is less dramatic.
  A more detailed geological description of the zone (and the rock type and its alteration in the zone) is required to judge which of the simulations is closest to the "real" mechanical properties. DZ1_3 represents an extreme "worst case" as the properties for fractures are set to the worst single fracture tested and might underestimate the mechanical properties in the zone.
- Influence of the fracture pattern: the adjusted fracture intensity is much higher in ZFMNE1207 (DZ5) than in DZ1 (the total truncated P_{32} are respectively 7.38 and 4.39). The influence of the fracture pattern is clearly visible in the rock mass parameters, see Figure 5-11 to Figure 6-1: cohesion, friction angle and compressive strength of the rock mass are lower in ZFMNE1207 (DZ5) compared to DZ1_1, whereas the tensile strength is higher. However the differences are not significant (Mann-Whitney tests, $p < 0.05$) except for the friction angle.
- The values obtained for the two "DZ" sections can be in some extent compared to the rock mass properties evaluated for the rock mass, presented in /Fredriksson and Olofsson 2005/. The mean of the intact rock properties used for the simulations (except for DZ1_3) are very similar to the one reported for the alternative 1 DFN in the preliminary site description – version 1.2. This alternative was chosen as it presents the highest P_{32}. However the normal stiffness of fractures is significantly modified, the shear stiffness is modified but in less extent. The normal stiffness used for the "worse fracture case" simulated in DZ1_2 is comparable to the maximum value reported in version 1.2. In version1.2 the rock mass deformation and strength properties are presented for 40.5 and 11.3 MPa confining stress.

Some of the parameters are presented in Table 6-1 and Table 6-2. They show that the deformation modulus is lower for the DZ sections, and that the Poisson's ratio is higher. The friction angle is quite similar, but the cohesion is also much lower even with the average fracture properties (which are much higher than in version 1.2).

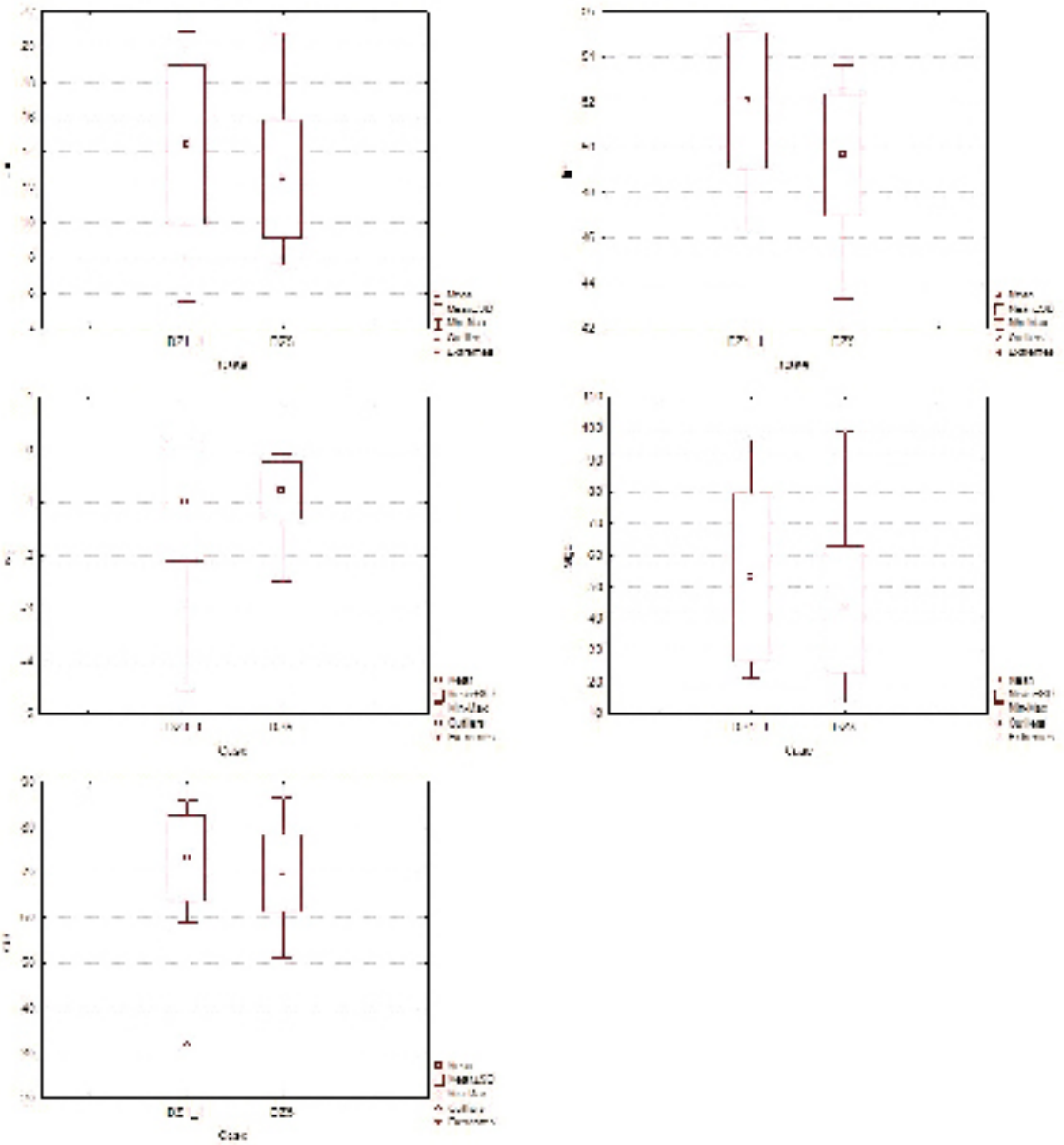

Figure 6-1. *Box plots of the cohesion (cm), friction angle (fim), tensile strength (sigt), compressive strength (sigc) and GSI for DZ1 and ZFMNE1207 (DZ5).*

Table 6-1. Rock mass deformation properties for the rock mass and two DZ at 45 MPa confining stress.

		Rock mass	DZ1_1	DZ1_2	ZFMNE1207 (DZ5)
Deformation modulus	Mean	64.9	56.5	44	51.7
	Std. dev.	4.5	5	6.4	4
	Min	56.1	48.5	34.3	45.6
	Max	73.8	64.7	55.2	59.8
Poisson's ratio	Mean	0.25	0.29	0.29	0.3
	Std. dev.	0.02	0.02	0.02	0.01
	Min	0.21	0.25	0.26	0.28
	Max	0.29	0.32	0.33	0.32

Table 6-2. Rock mass strength properties for the rock mass and two DZ (interval 0.5–45 MPa)[1].

		Rock mass	DZ1_1	DZ1_2	ZFMNE1207 (DZ5)
Friction angle	Mean	48.5	52.1	48.3	49.7
	Std dev.	2.7	3.0	2.9	2.7
	Min	43.3	46.4	43.1	43.3
	Max	53.7	55.4	53.1	53.7
Cohesion	Mean	20.8	14.45	11.5	12.5
	Std dev.	4.0	4.5	6.3	2.7
	Min	12.9	5.5	3.7	7.6
	Max	28.7	20.9	22.3	20.8

[1] The parameters are valid in the interval 11.3–45 MPa for the rock mass.

6.1 Comparison of the empirical and theoretical results

Comparison can be made between the mechanical properties of these two DZ sections evaluated using both the empirical and numerical approach. The parameter used to compare both methodologies is GSI, and it is calculated from RMR by the following equation:

$$GSI = RMR_{89} - 5 \quad (6)$$

Two other parameters calculated from RMR are cohesion and friction angle. RMR is defined for 5 m-sections in the borehole, according to /Hoek and Brown 1997/, and without any consideration for water or tunnel orientation. The minimum, maximum, mean and median values of the sections are evaluated. In order to allow comparison with the approach conducted in this report the RMR values of all sections in respectively DZ1 and ZFMNE1207 (DZ5) were compiled.

The GSI is presented in Table 6-3 for DZ1 and in Table 6-4 for ZFMNE1207 (DZ5). Cohesion and friction angle of the rock mass are presented in Table 6-5 to Table 6-8. However the properties are not directly comparable: the properties calculated with the empirical method are valid in the interval 10–30 MPa of minimum stress. The values presented for the numerical approach are valid in the interval 0.5–45 MPa.

Table 6-3 and Table 6-4 illustrate that the results with both methods present a good agreement. The values are in the same range both for DZ1 and ZFMNE1207 (DZ5).

Considering DZ1 the agreement between both methods is better for DZ1_1 than for DZ1_2 and D1_3 for which the input mechanical properties were reduced. The mean value is lower for these cases, but quite close to the lowest value from the empirical approach. However the variability is much higher than this observed by the empirical approach and also the one observed in case DZ1_1.

The results obtained for the cohesion are much lower with the numerical method (Table 6-5 and Table 6-6). The values presented for the friction angle (Table 6-7 and Table 6-8) are in the same range, and the values with the standard parameters in DZ1 (DZ1_1) are slightly higher than with the empirical method. The variation for all cases is much larger with the empirical method. However the agreement of the Mohr-Coulomb's failure envelopes simulated for both models (mean value for DZ1 and lowest mean value for empirical) are satisfying, see Figure 6-2.

Table 6-3. GSI for DZ1 evaluated with the empirical and the numerical methods.

GSI	Empirical	Numerical		
	DZ1	DZ1_1	DZ1_2	DZ1_3
Mean	71.1–78.1	73.1	60.8	67.25
Std. dev.		9.4	18.8	15.30
Min	55.6	58.9	31.9	47.00
Max	88	85.9	85.1	97.90

Table 6-4. GSI for ZFMNE1207 (DZ5) evaluated with the empirical and the numerical methods.

GSI	Empirical	Numerical
Mean	70.85–71.5	69.8
Std. dev.		8.3
Min	52.25	51.1
Max	84.7	86.5

Table 6-5. Cohesion for DZ1 evaluated with the empirical and the numerical methods.

c_m	Empirical	Numerical		
	DZ1	DZ1_1	DZ1_2	DZ1_3
Mean	19.4–22.4	14.45	11.5	8.8
Std. dev.		4.5	6.3	5.3
Min	12.1	5.5	3.7	2.6
Max	34.6	20.9	22.3	23.1

Table 6-6. Cohesion for ZFMNE1207 (DZ5) evaluated with the empirical and the numerical methods.

c_m	Empirical	Numerical
Mean	19.8–20	12.5
Std. dev.		3.36
Min	11.6	7.6
Max	31.6	20.8

Table 6-7. Friction angle for DZ1 evaluated with the empirical and the numerical methods.

ϕ_m	Empirical	Numerical		
	DZ1	DZ1_1	DZ1_2	DZ1_3
Mean	46–48.2	52.1	48.3	45.55
Std. dev.		3.0	2.9	2.1
Min	34.5	46.4	43.1	41.8
Max	54.5	55.4	53.1	49.1

Table 6-8. Friction angle for ZFMNE1207 (DZ5) evaluated with the empirical and the numerical methods.

ϕ_m	Empirical	Numerical
Mean	46.3–46.5	49.7
Std. dev.		2.7
Min	33.5	43.3
Max	53.9	53.7

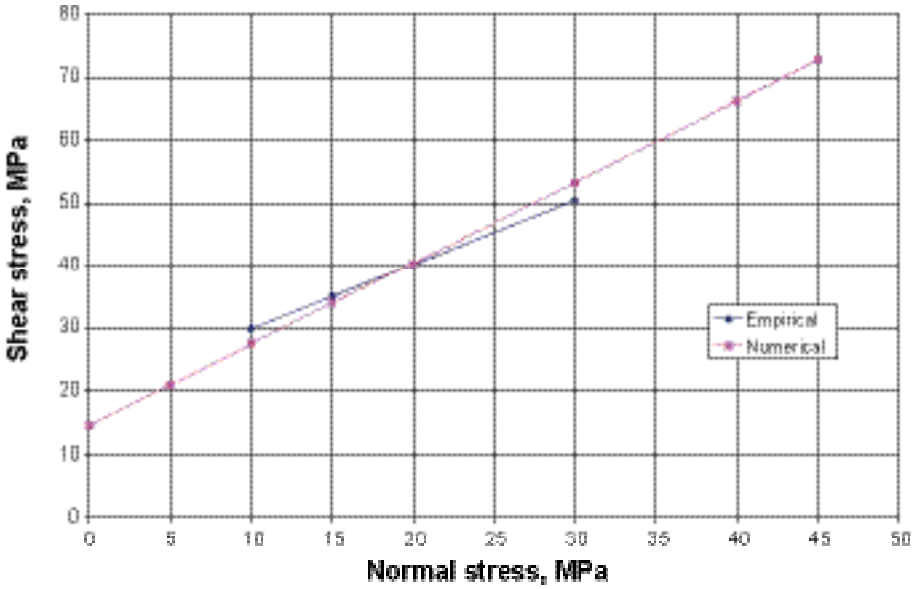

Figure 6-2. *Simulation of the Mohr-Coulomb's failure envelop for the parameters given by the empirical and the numerical models.*

The fact that the match between both methods is better with the average input parameters implies the following:

- Most of the collected DZ samples might be the same fracture population as the samples collected in RU. An explanation might be that there were no attempts to characterise fracture samples from deformation zones. Therefore, "fresh" fracture samples were collected.
- These DZ sections are mostly defined by an increase in open fractures frequency (see also the geological single-hole interpretation /Carlsten et al. 2004b/).

7 Progress of the in situ stress modelling at Forsmark

Based on the status of the structure geological investigations reported in /SKB 2004/ and in parallel with at-the-time ongoing investigations, later reported in /SKB 2005/ a pre-study was carried out, see /Mas Ivars and Hakami 2005/, in which the aim was to investigate how site-specific components like the existence of a central lens (in between Singö fault and Forsmark fault) and/or observed sub-horizontal fracture zone would have influenced the stress field at the site. The work is currently being re-evaluated in order to see which of components included/geometrical layout may enter the new modelling Set-up and which need to be modified.

The current project involves primarily:

- Better understanding/questioning the current state of structure geology of the site, from the rock mechanics standpoint.
- Set up complementary numerical investigations focusing on the influential constituents specifically found at the area, for example the pseudo-layered structure of the uppermost 2–300 m of bedrock.
- Incorporating those constituents, now transformed into numerical entities, in the global stress model of the site.

7.1.1 Tectonic stress phases

A "hook-on point" is the two-dimensional conceptual model presented in /SKB 2005/ (Figure 3-4 to Figure 3-6 in Section 3.2 in this report).

An important aspect that calls for an introductory numerical investigation is to try to find out how the direction of the major principal stress, $_1$, as inferred from the recent in situ stress measurements, would relate to the sense of shearing of the discontinuities as modelled. The outcome would be that an adequately strong relationship exist, otherwise discussions are to be conducted in order to delineate the possible sources for uncertainties.

The depth-wise structure geological model (Figure 3-7, Section 3.2 in this report) is also to be transformed into viable rock mechanical components, entering the numerical simulations.

Numerical modelling may even necessitate including depths beyond 1,000 m. Going deeper down, plausible extrapolations may be needed and this may be done by resorting to the findings from geophysical investigations or, at least, consulting the geological maps of the region.

7.1.2 Regional model

The main purpose of setting up a model at a regional scale pertaining to Forsmark area is to explore the influence of the past major tectonic activities on the current state of in situ stress within rock limits that are considered as candidates for the placement of a repository. Among others, an important consequence of succeeding tectonic activities is the occurrence of a significant change in the direction of the major principal stress.

Based on the reported structure geology presented in Chapter 3 and personal communications made with structure geologists involved, a preliminary geometrical 3D model has been set up by using 3DEC.

Major structures were transformed into planar discontinuities and incorporated into the geometrical 3DEC model. Curved structures were simplified by breaking them into planar segments.

As almost all of major structures have been described qualitatively as steeply dipping or vertical, a crucial step would be – based on existing evidences – to define a general plausible dip, which all faults/fracture zones would be assigned to in the numerical model except those that may be defined more specifically.

Figure 7-1 shows a top view of view of the 3DEC geometrical model. A tentative dip of 80° has been assigned to all structures modelled. Considering the tectonic lenses, with assumingly a higher density than the surrounding rock, found in between Forsmark fault and Singö fault zone, see Figure 1, and visualizations made of the structures in the area, a plausible arrangement for the steeply dipping faults – from a rock mechanical standpoint – would be that faults dipped towards the lenses from both side and not away from them. This assumption was taken into account when incorporating the faults/fracture zones in the 3DEC geometrical model. Figure 7-1 shows four vertical sections showing the arrangement mentioned. The positions where the vertical sections are taken are shown.

On the regional scale considered for this numerical investigation, there is a considerable number of fracture zones that either have not yet been explored or just studied partially. In an attempt to enhance the structure geological model for the purpose of in situ stress modelling, a principle that is widely accepted has been considered: discontinuities tend to have occurred in regular patterns. Having utilised the principle mentioned, some very large volumes of rock could be identified in the most relevant portion of the region. Identification of such blocks helps to study the variation of in situ stresses inside, under geologically subsequent time periods. The idea would then be to investigate if the unexplainable anomalies in current stress measurement could be related to the stress states a chosen block may have been exposed to during geological time spans.

Figure 7-1 shows the fracture zones/faults as modelled in the 3DEC geometrical model. Only relevant parts of the discontinuities enter the numerical calculations and the remaining parts are passive and treated as construction joints. Figure 7-1 also illustrates how the large block could be shaped in between the exiting regional faults/fracture zones.

7.1.3 Preliminary modeling results

The numerical modelling will try to reconstruct the loading phases in geological time and compare them to the evidences of displacements of the modeled deformation zones at the Forsmark Site. In Figure 7-2, an attempt to model the hypothetical stress field at the time of the Svecokarelian orogeny is shown.

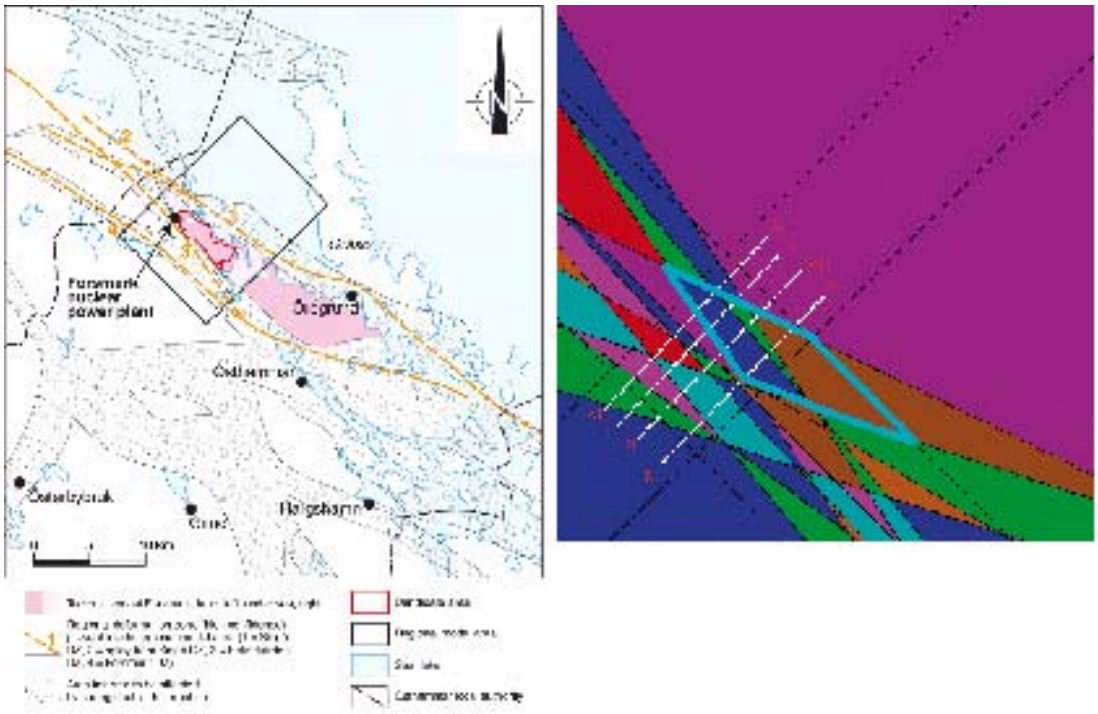

Figure 7-1. *Map of the regional deformation zones (left) and a view of the 3DEC model of the same area seen from above (right).*

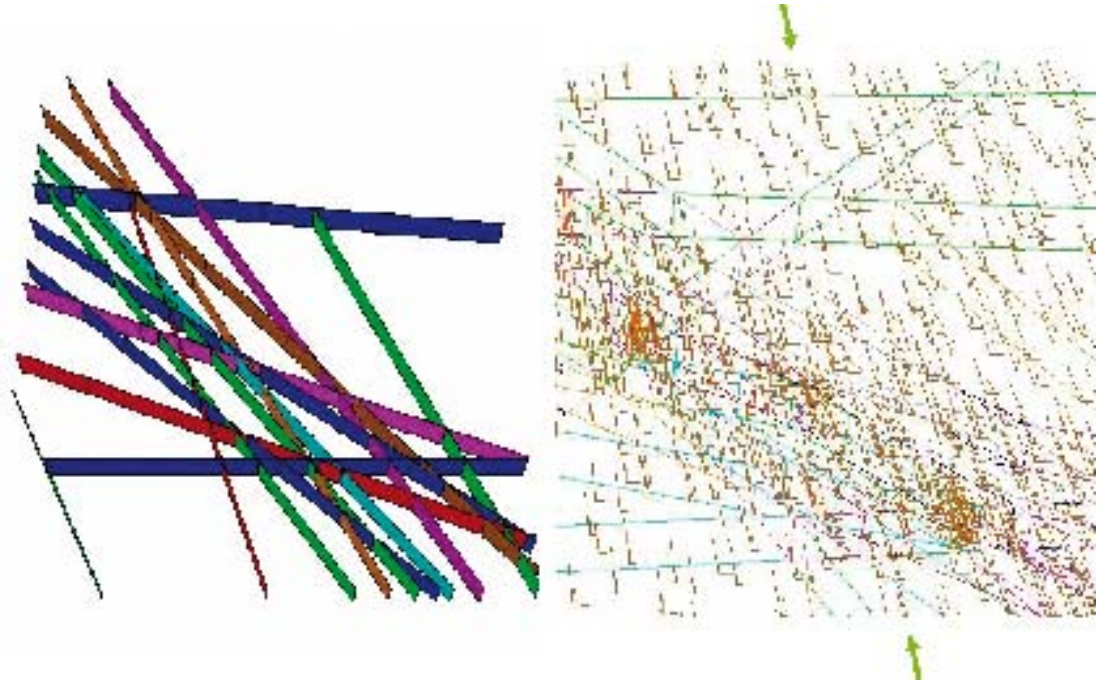

Figure 7-2. *A view of the 3DEC geometrical model with indicated the tectonic lens at Forsmark (left) and a preliminary results of the stress modelling for a loading configuration correspondent to the Svecokarelian orogeny (right).*

8 References

Carlsten S, Petersson J, Stephens M, Mattsson H, Gustafsson J, 2004a. Geological single-hole interpretation of KFM02A and HFM04–05 (DS2). Forsmark site investigation. SKB P-04-117, Svensk Kärnbränslehantering AB.

Carlsten S, Petersson J, Stephens M, Thunehed H, Gustafsson J, 2004b. Geological single-hole interpretation of KFM03B, KFM03A and HFM06–08 (DS3). Forsmark site investigation. P-04-118, Svensk Kärnbränslehantering AB.

Follin S, Stigsson M, Svensson U, 2005. Regional hydrogeological simulations for Forsmark – numerical modelling using Darcy Tools. Preliminary site description Forsmark area – version 1.2. SKB R-05-60, Svensk Kärnbränslehantering AB.

Fredriksson A, Olofsson I, 2005. Rock mechanics site descriptive model – theoretical approach. Preliminary site description Forsmark area – version 1.2, SKB R-05-22, Svensk Kärnbränslehantering AB.

Hoek E, Brown, 1997. Practical estimates of rock mass strength, Int. J. Rock Mech. Min. Sci. Vol. 34, p. 1165–1186.

Hoek E, Carranza-Torres C, Corkum B, 2002. The Hoek-Brown Failure Criterion – 2002 Edition. 5th North American Rock Mechanics Symposium and 17th Tunneling Association of Canada Conference: NARMS-TAC, p. 267-271.

Jacobsson L, 2004a. Borehole KFM01A – Triaxial compression test of intact rock. Forsmark site investigation. SKB P-04-227, Svensk Kärnbränslehantering AB.

Jacobsson L, 2004b. Borehole KFM02A – Triaxial compression test of intact rock. Forsmark site investigation. SKB P-04-228, Svensk Kärnbränslehantering AB.

Jacobsson L, 2004c. Borehole KFM03A – Triaxial compression test of intact rock. Forsmark site investigation. SKB P-04-229, Svensk Kärnbränslehantering AB.

Jacobsson L, 2004d. Borehole KFM04A – Triaxial compression test of intact rock. Forsmark site investigation. SKB P-04-230, Svensk Kärnbränslehantering AB.

Lanaro F, 2005. Rock mechanics model – Summary of primary data – Preliminary site description Forsmark area – version 1.2, SKB R-05-83, Svensk kärnbränslehantering AB.

LaPointe P, Olofsson I, Hermanson J, 2005. Statistical model of fractures and deformation zones for Forsmark. Preliminary site description Forsmark area – version 1.2, SKB R-05-26, Svensk Kärnbränslehantering AB.

Mas Ivars D, Hakami H, 2005. Effect of a sub-horzontal fracture zone and rock mass heterogeneity on the stress field in Forsmark area – A numerical study using 3DEC.. Preliminary site description Forsmark area – version 1.2. SKB R-05-59, Svensk Kärnbränslehantering AB.

Munier R, Hökmark H, 2004. Respect distances. Rationale and means of computation. SKB R-04-17, Svensk Kärnbränslehantering AB.

Olofsson I, Fredriksson A, 2005. Strategy for a numerical Rock Mechanics Site Descriptive Model. Further development of the theoretical/numerical approach. SKB R-05-43, Svensk Kärnbränslehantering AB.

Petersson J, Skogsmo G, Wängnerud A, Stråhle A, 2005. Boremap mapping of telescopic drilled borehole KFM06A and core drilled borehole KFM06B. Forsmark site investigation. SKB P-05-101, Svensk Kärnbränslehantering AB.

SKB, 2004. Preliminary site description. Forsmark area – version 1.2, SKB R-04-15, Svensk Kärnbränslehantering AB.

SKB, 2005. Preliminary site description. Forsmark area – version 1.2, SKB R-05-18, Svensk Kärnbränslehantering AB.

Appendix 4

Hydrogeology

1 Summary of correlation of Posiva Flow Log anomalies to core mapped features in KFM01A through KFM07A

Fracture transmissivity data available for modelling determined with the Posiva Flow Log (PFL-f) exist for boreholes KFM01A–KFM07A. Figure 1-1 shows a BIPS image of a flowing fracture detected by the PFL-f tests.

During the core mapping process each fracture is classified as Broken or Unbroken and the apertures of the Broken fractures are classified as Certain, Probable and Possible. In SICADA each fracture is subsequently classified as Sealed, Open or Partly Open based on this information. Partly Open fractures refers to all fractures that do not cut the core entirely but have (1) altered or weathered fracture planes or are (2) associated with a measurable aperture in the borehole wall using BIPS to indicate an edge of a fracture. Measured PFL-f flow anomalies are classified as Certain or Uncertain. Both the core mapped data and the flow anomalies are rigorously length corrected and it is expected that the positions of objects along the boreholes normally can be correlated to within 0.2–0.3 m.

/Forssman et al. 2004, 2006/ provide a joint interpretation of the PFL-f tests, the fracture data from the core mapping and the single-hole geological interpretations of rock domains and deformation zones. Figure 1-2 through Figure 1-8 show a compilation of their results. The classification of "flow indication Open fractures", or the PFL confidence, is defined as the distance between the anomaly and the interpreted fracture. That is, if the anomaly has a flow indication in Class 1, the interpreted fracture is within 1 dm from the anomaly. In the same way, the anomaly has the flow indication Class 2, if the interpreted fracture is within 2 dm from the anomaly. Four classes have been defined: Class 1: 0–1 dm; Class 2: 1–2 dm; Class 3: 2–3 dm; and Class 4: 3–4 dm.

As a first assumption all Open and Partly Open fractures as well as Crush Zones are assumed to be potential flowing fractures. In most cases, one or several Open fractures were identified within 0.2 m from a given flow anomaly. Only in a few cases could no Open fractures, Partly Open fractures or Crush Zones be linked to within 0.5 m of a flow anomaly, probably indicating that a fracture mapped as Sealed should have been classified as Open. In such cases one could generally find Sealed fractures classified as Probable or Possible and mapped as Broken near the flow anomaly. Table 1-1 shows a compilation of the interpretation by /Forssman et al. 2004, 2006/.

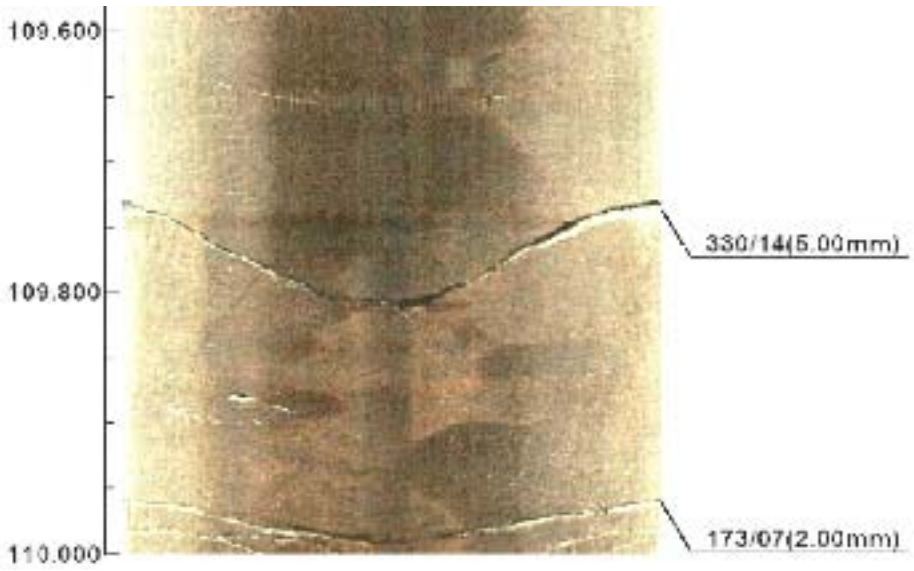

Figure 1-1. *BIPS image showing a borehole section in borehole KFM05A. The fracture in the centre is associated with a flow anomaly determined by the PFL-f tests.*

Table 1-1. Compilation of the results obtained from a joint interpretation between PFL-f tests and Boremap data /Forsman et al. 2004, 2006/.

Object	KFM01A	KFM02A	KFM03A	KFM04A	KFM05A	KFM06A	KFM07A
Total no. of PFL-f anomalies	34	125	52	71	27	99	26
PFL-f anomalies mapped as “Certain”	13	100	34	50	21	70	19
Fractures identified with distance < 0.2 m from PFL-f anomaly	76	185	110	195	80	204	47
Fractures identified with distance 0.2–0.4 m from PFL anomaly	5	7	2	9	0	4	2
Fractures identified with distance 0.4–0.5 m from PFL-f anomaly	0	3	0	1	0	0	0
Fractures identified with distance > 0.5 m from PFL-f anomaly	0	3	2	1	0	0	2
PFL-f anomalies not correlated to Open fractures	0	14	8	1	2	7	0
Sealed fractures (broken/unbroken) within a distance of 0.1 m from PFL-f anomalies not correlated to Open fractures or Crush zones	0/0	29/1	10/2	1/0	4/0	10/0	0/0
Sealed fractures (broken/unbroken) a distance of > 0.1 m from PFL-f anomalies not correlated to Open fractures or Crush zones	N/A	N/A	N/A	N/A	N/A	2/0	0/0

2 References

Forsman I, Zetterlund M, Rhén I, 2004. Correlation of Posiva Flow Log anomalies to core mapped features in Forsmark (KFM01A to KFM05A). SKB R-04-77, Svensk Kärnbränslehantering AB.

Forssman I, Zetterlund M, Forsmark T, Rhén I, 2006. Forsmark site investigation. Correlation of Posiva Flow Log anomalies to core mapped features in KFM06A and KFM07A. SKB P-06-56, Svensk Kärnbränslehantering AB.

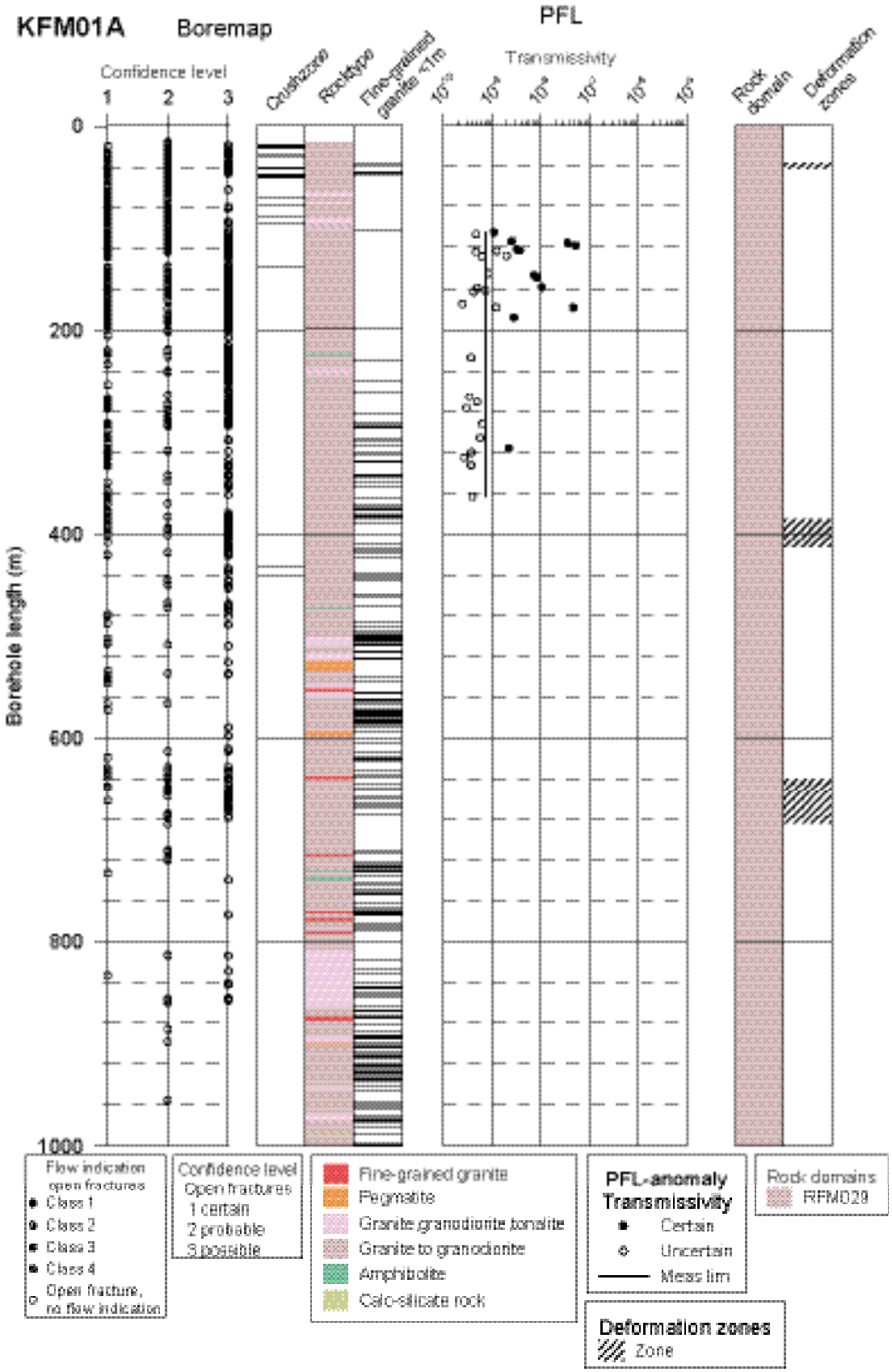

Figure 1-2. *Figure A-2 Correlation of hydraulic fractures in borehole KFM01A based on PFL-f overlapping measurements to mapped Open/Partly Open fractures (all plotted as Open fractures above) or crush zones. Interpreted deformation zones (mainly brittle or ductile) and rock domains shown to the right. Fractures with PFL confidence (flow indication class) > 4 are not plotted /Forssman et al. 2006/.*

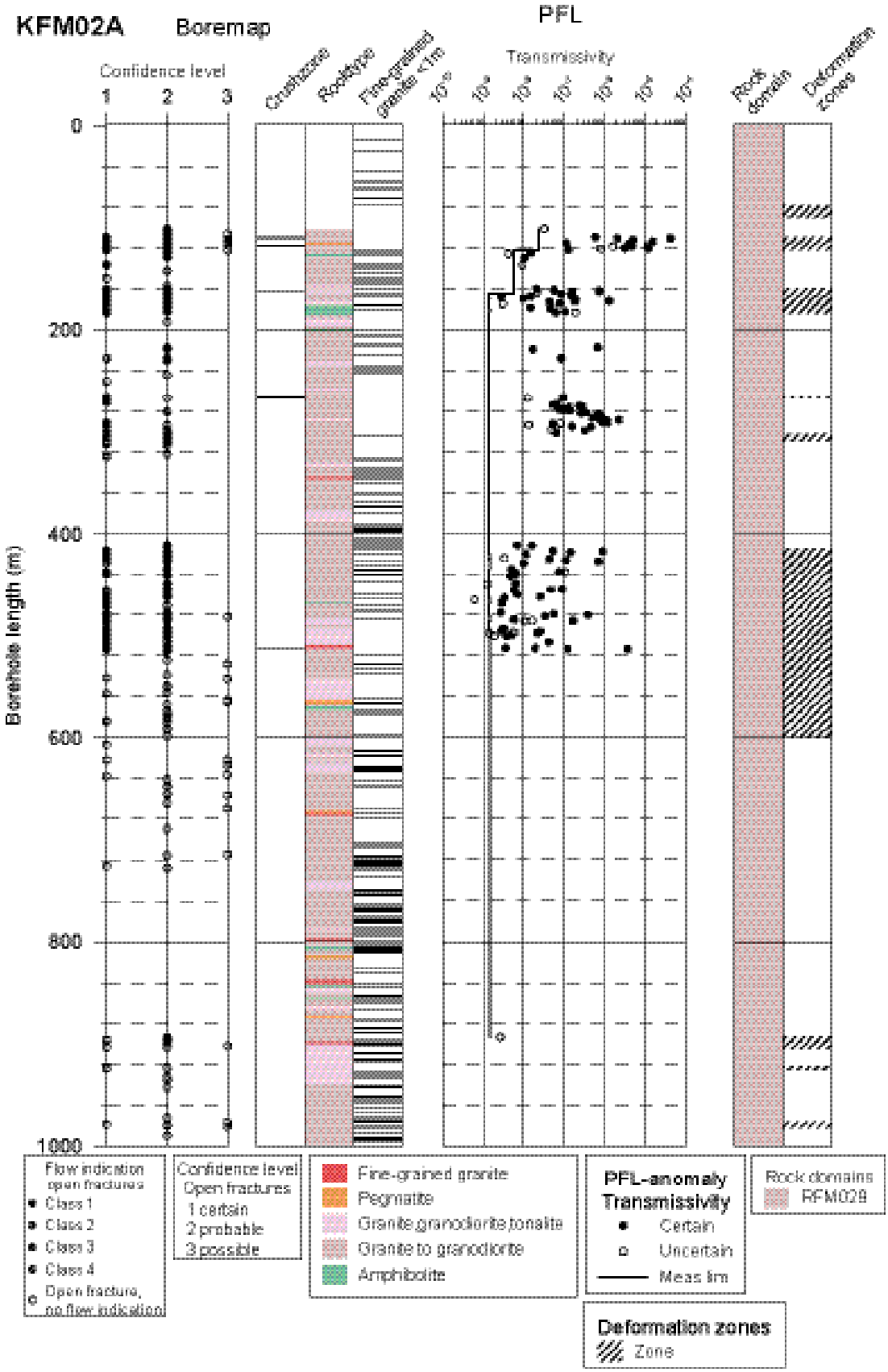

Figure 1-3. *Correlation of hydraulic fractures in borehole KFM02A based on PFL-f overlapping measurements to mapped Open/Partly Open fractures (all plotted as Open fractures above) or crush zones. Interpreted deformation zones (mainly brittle or ductile) and rock domains shown to the right. Fractures with PFL confidence (flow indication class) > 4 are not plotted /Forssman et al. 2006/.*

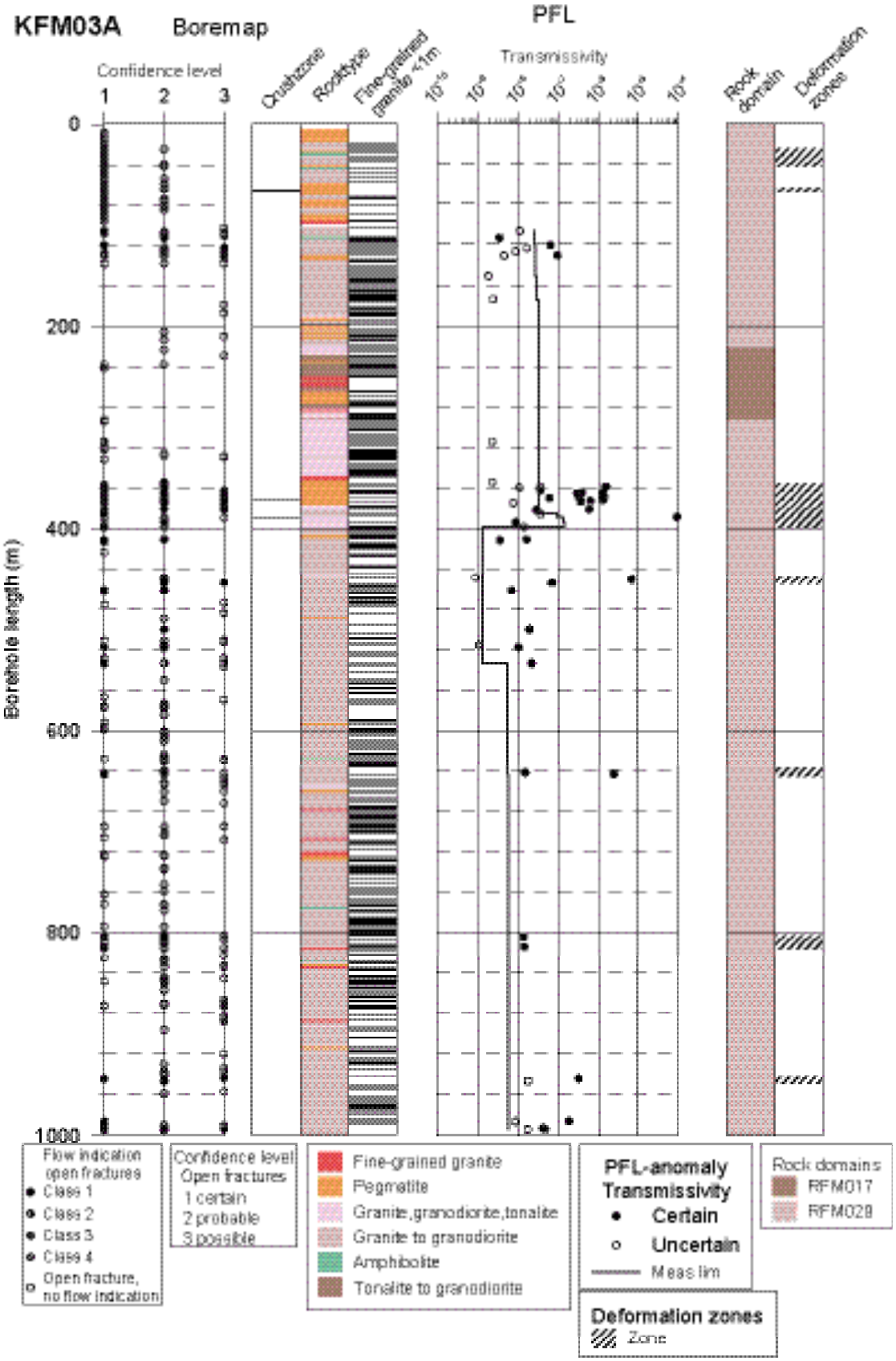

Figure 1-4. *Correlation of hydraulic fractures in borehole KFM03A based on PFL-f overlapping measurements to mapped Open/Partly Open fractures (all plotted as Open fractures above) or crush zones. Interpreted deformation zones (mainly brittle or ductile) and rock domains shown to the right. Fractures with PFL confidence (flow indication class) > 4 are not plotted /Forssman et al. 2006/.*

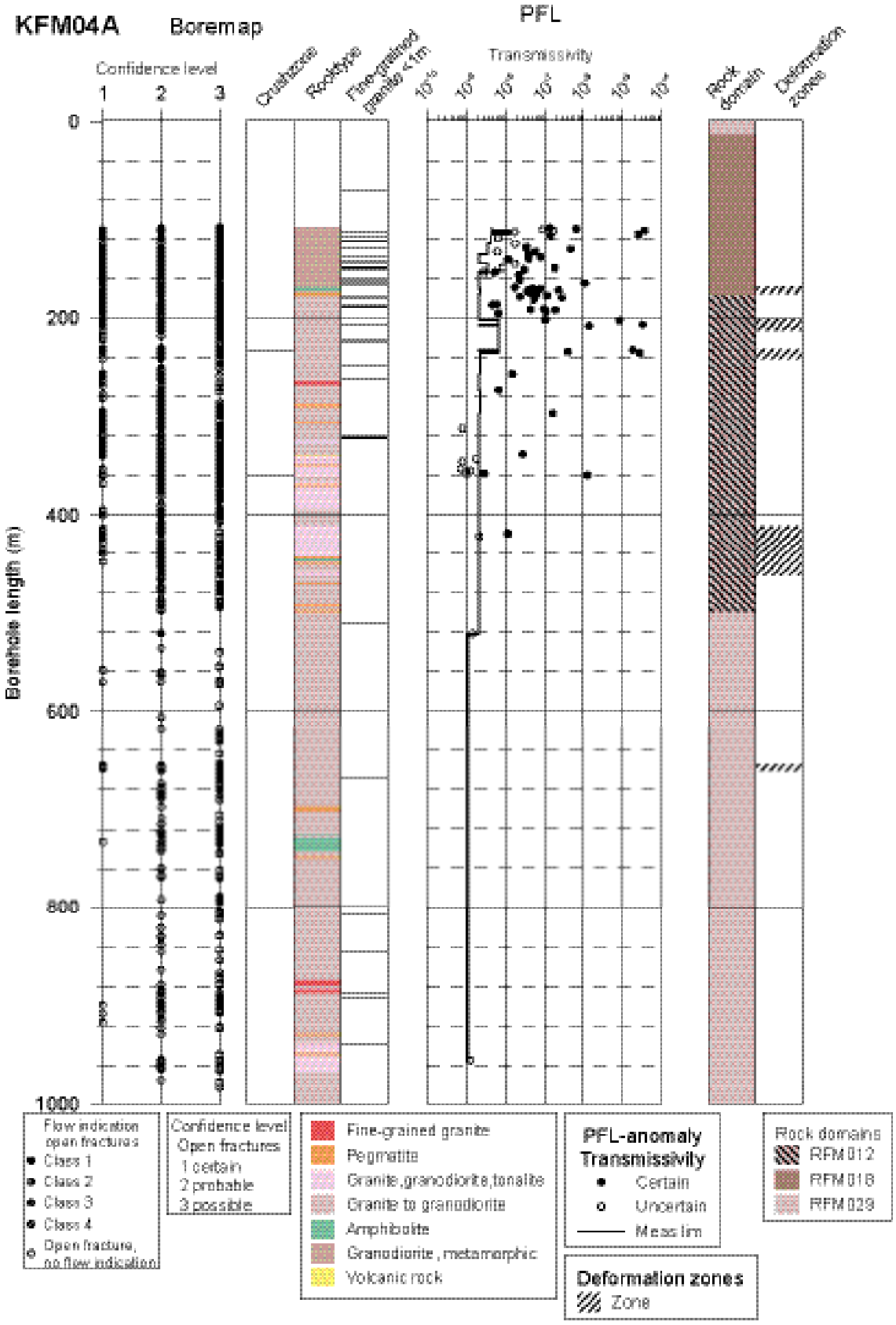

Figure 1-5. *Correlation of hydraulic fractures in borehole KFM04A based on PFL-f overlapping measurements to mapped Open/Partly Open fractures (all plotted as Open fractures above) or crush zones. Interpreted deformation zones (mainly brittle or ductile) and rock domains shown to the right. Fractures with PFL confidence (flow indication class) > 4 are not plotted /Forssman et al. 2006/.*

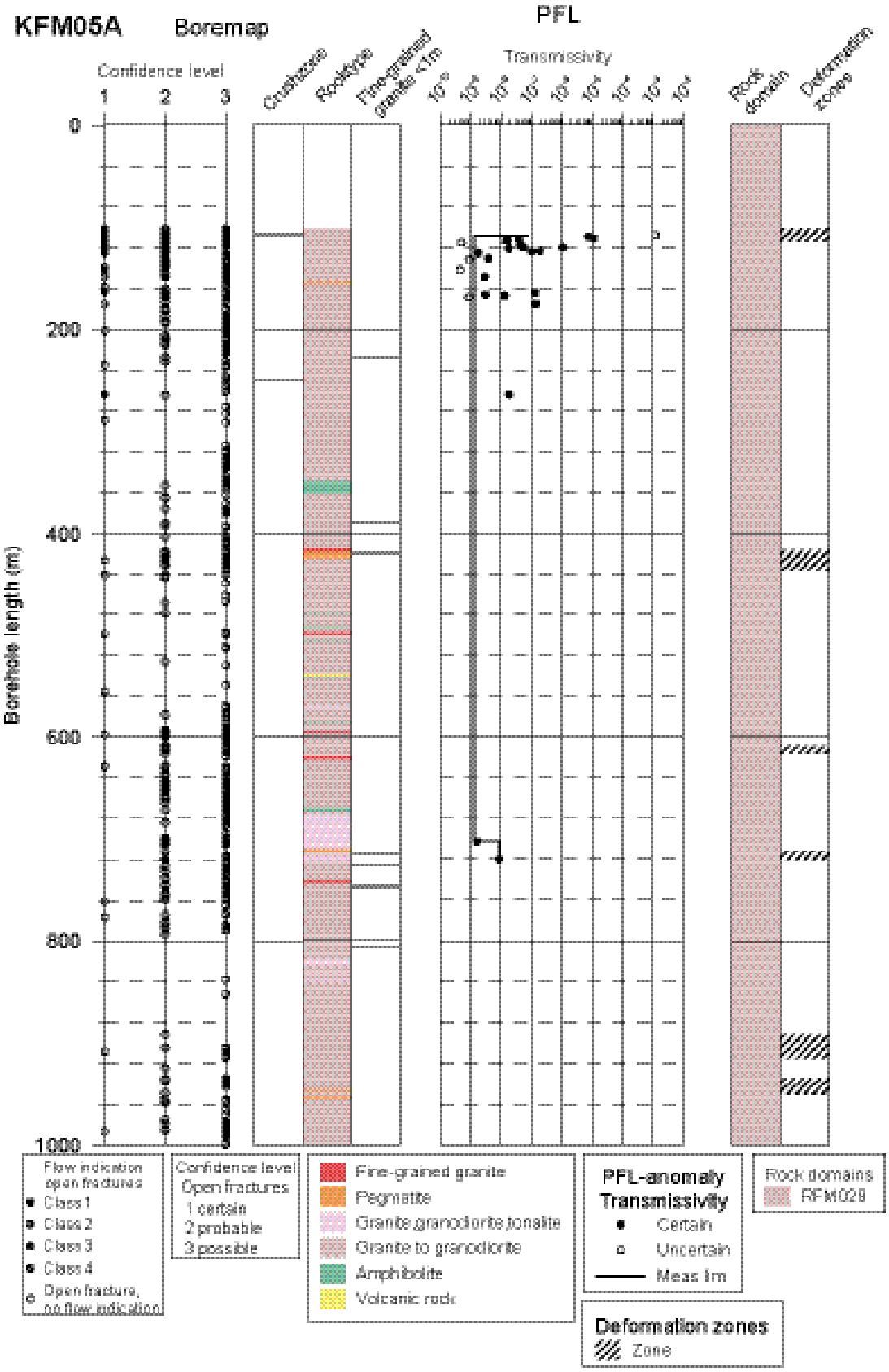

Figure 1-6. *Correlation of hydraulic fractures in borehole KFM05A based on PFL-f overlapping measurements to mapped Open/Partly Open fractures (all plotted as Open fractures above) or crush zones. Interpreted deformation zones (mainly brittle or ductile) and rock domains shown to the right. Fractures with PFL confidence (flow indication class) > 4 are not plotted /Forssman et al. 2006/.*

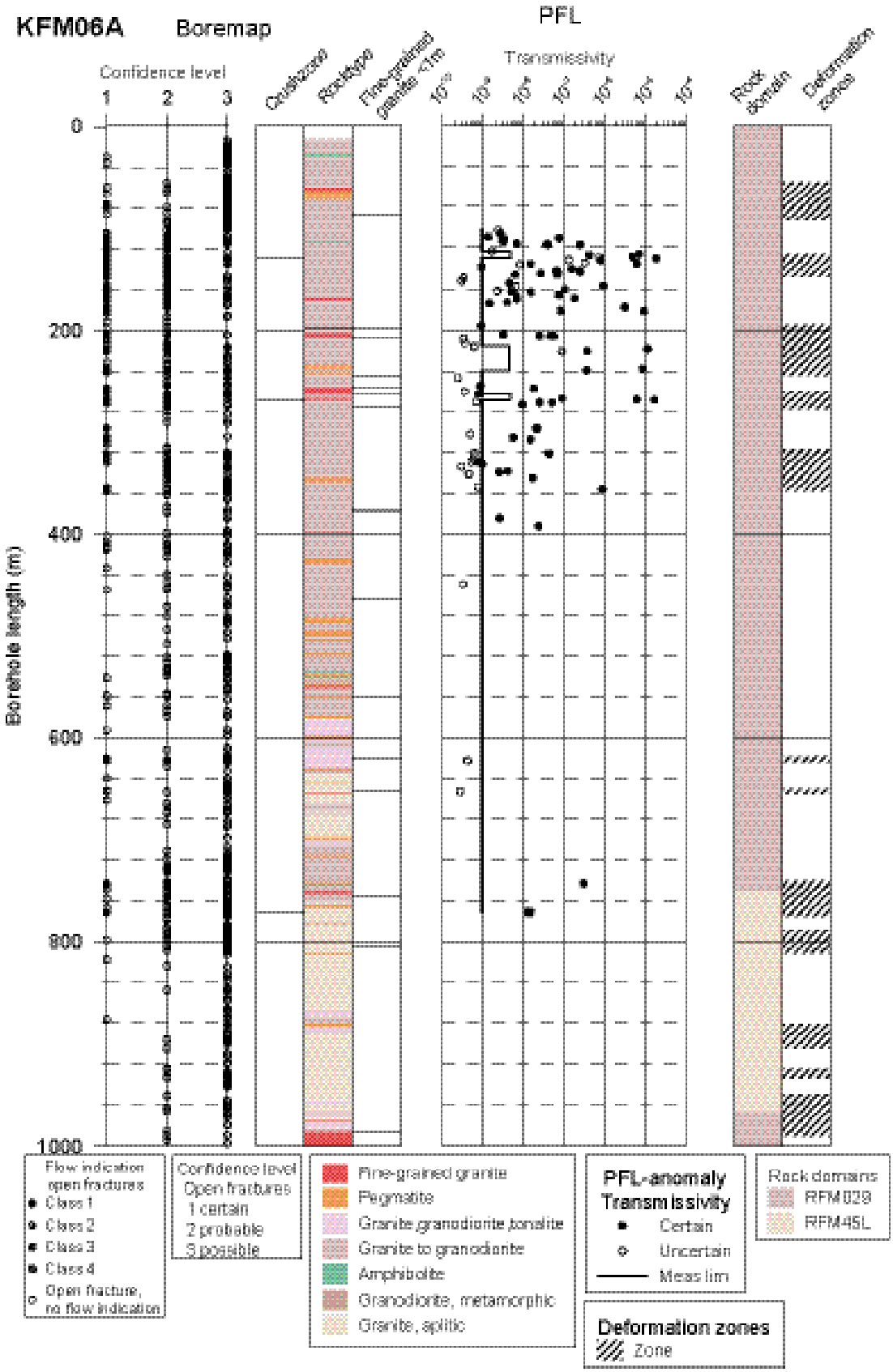

Figure 1-7. *Correlation of hydraulic fractures in borehole KFM06A based on PFL-f overlapping measurements to mapped Open/Partly Open fractures (all plotted as Open fractures above) or crush zones. Interpreted deformation zones (mainly brittle or ductile) and rock domains shown to the right. Fractures with PFL confidence (flow indication class) > 4 are not plotted /Forssman et al. 2006/.*

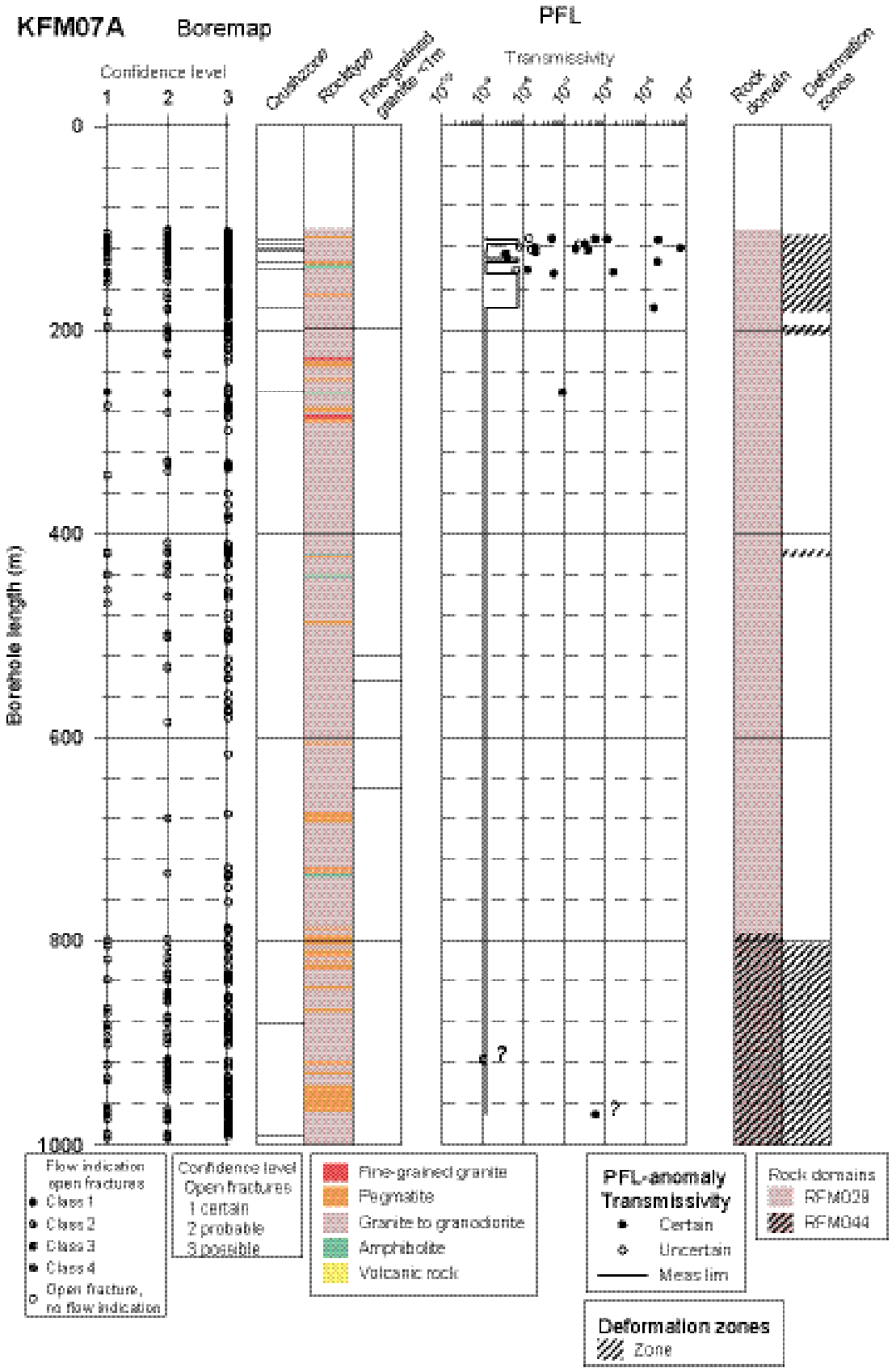

Figure 1-8. *Correlation of hydraulic fractures in borehole KFM07A based on PFL-f overlapping measurements to mapped Open/Partly Open fractures (all plotted as Open fractures above) or crush zones. Interpreted deformation zones (mainly brittle or ductile) and rock domains shown to the right. Fractures with PFL confidence (flow indication class) > 4 are not plotted /Forssman et al. 2006/.*

Appendix 5

Motivation documents for boreholes and investigations

5.1 Study of lineaments in the north-western part of the candidate area − motivation and recommendations for the first phase of investigations, autumn 2005

5.1.1 Background

Lineaments interpreted from both airborne geophysical and topographic data /Isaksson 2003, Isaksson et al. 2004, Isaksson and Keisu 2005/ are one of the components used for the geological modelling of deterministic deformation zones at the Forsmark site /SKB 2002, 2004, 2005a/. They also play an important role in the assessment of the size distribution of fractures in the discrete fracture network (DFN) modelling procedure /e.g. LaPointe et al. 2005/. From a hydrogeological perspective, the modelling of lineaments as deformation zones is a matter of key interest. Nevertheless, the process by which a lineament is identified and transformed into a deformation zone with defined geometric and geological properties is primarily a geological matter. The numerical groundwater flow modelling conducted during model version 1.2 /SKB 2005a/ shows that the occurrence of non-identified deformation zones in the north-western part of the candidate, which has been selected for complete site investigations /SKB 2005b/, is a matter of major concern for the hydrogeological description of recharge and discharge. Furthermore, there are hydraulic observations in existing boreholes that need to be explained geologically in a deterministic fashion in order to reduce the uncertainty concerning the rock mass fracturing (DFN).

Bearing in mind the arguments summarised above, it is critical that the character of lineaments is understood, particularly in the north-western part of the candidate area (Figure 1). On account of safety evaluation considerations, prime attention needs to be placed on the lineaments that are longer than 3,000 m (Figure 2). The terminology used in the description of lineaments is presented in /Triumf 2004, SKB 2005a/.

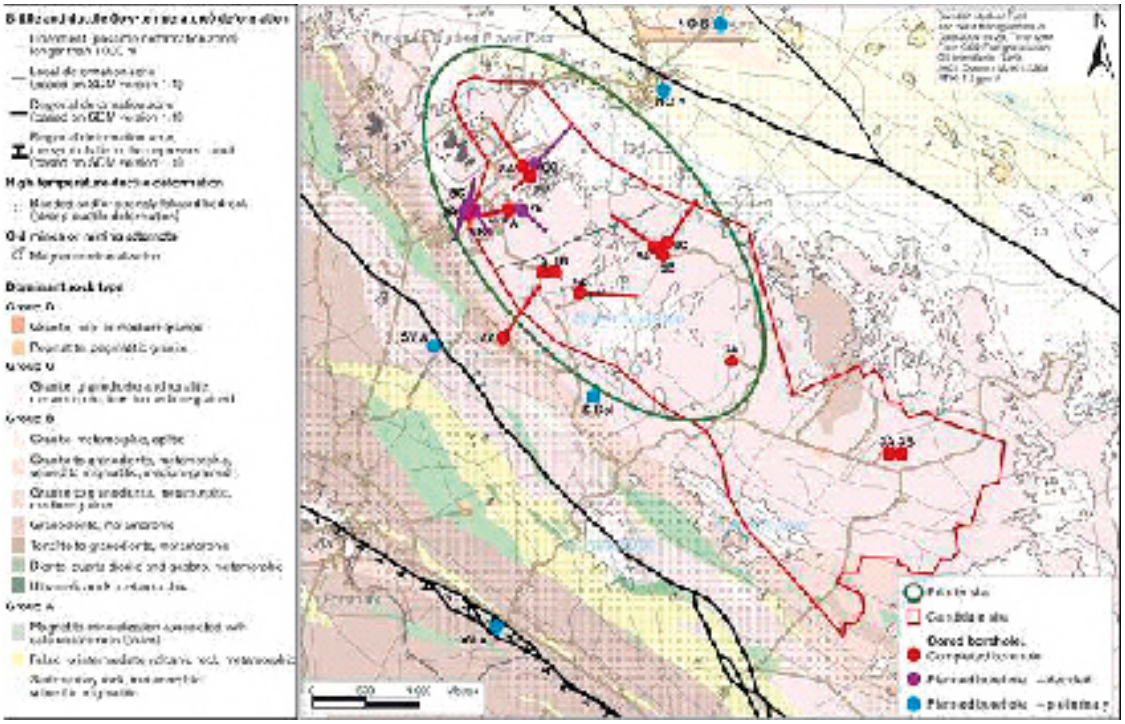

Figure 1. *Geological map of the bedrock (version 1.2) inside and immediately around the candidate area at Forsmark. Completed, planned and possible cored boreholes as well as the priority site are also shown (modified after /SKB 2005b/). The surface projections of gently dipping zones that have been recognised on the basis of seismic reflection and borehole data are not shown on the map.*

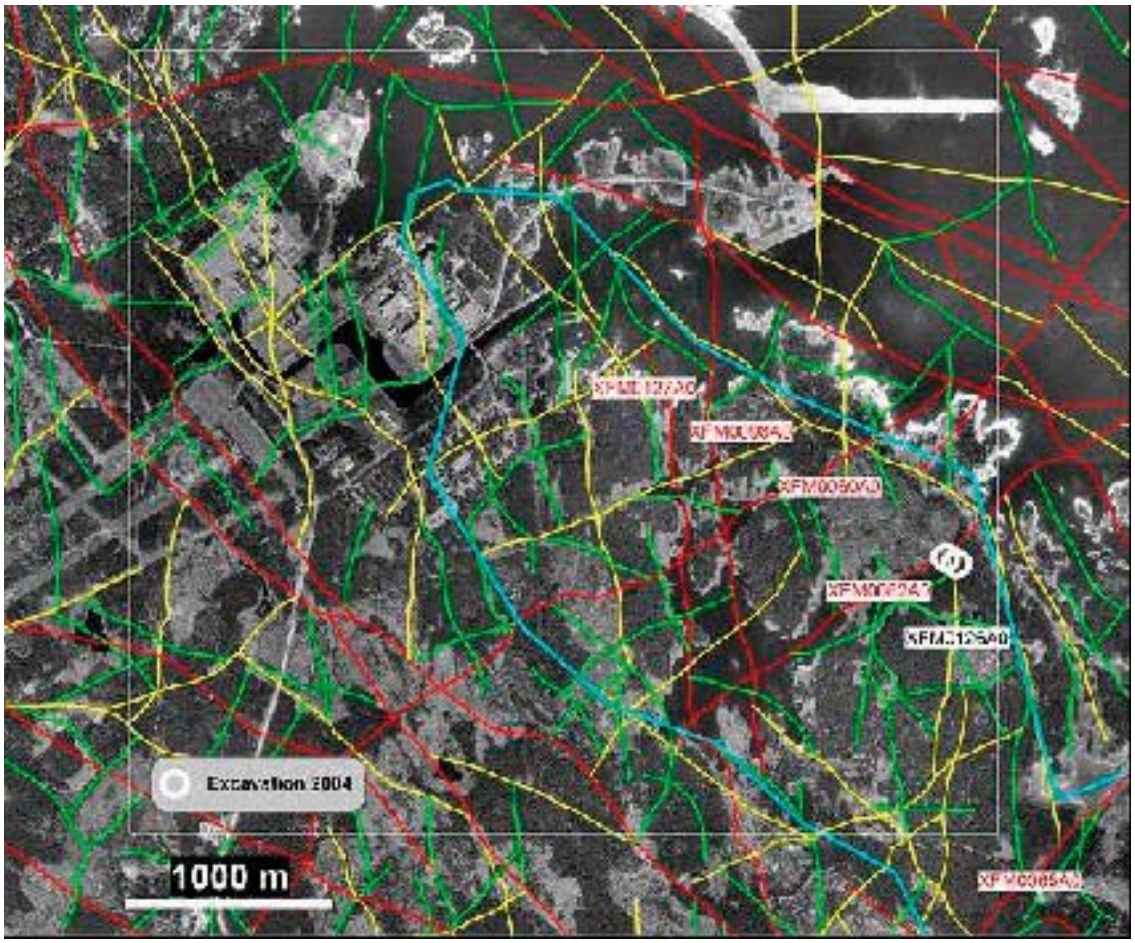

Figure 2. *Linked lineaments with length 500–1,000 m (green), 1,000–3,000 m (yellow) and greater than 3,000 m (red) adopted from /Isaksson and Keisu 2005/. The lineaments that are both longer than 3,000 m and intersect the candidate area as well as lineament XFM0126A0 (see text) are numbered. The Forsmark candidate area is shown as a light blue line. The white rectangle displays the area chosen for assessment of lineaments in the north-western part of the candidate area (meeting at SKB Forsmark, 2004-12-02).*

5.1.2 Previous work

The geological data from especially boreholes KFM01A and KFM05A in the north-western part of the candidate area, which have been used in the site descriptive modelling work /SKB 2004, 2005a/, indicate that several of the lineaments with NE trend that transect this area are minor fault zones with steep dips and a high frequency of sealed fractures. These zones are sandwiched between regional deformation zones that strike WNW and NW, and that show deformation under both ductile and brittle conditions. The regional deformation zones border the candidate area, both to the south-west and to the north-east (Figure 1).

The drilling activity along KFM05A has also shown that steeply dipping fractures with NS strike are common in the Bolundsfjärden area. However, fracture clusters that contain a sufficiently high fracture frequency to merit classification as zones have not been recognised along this borehole /SKB 2005a/. For this reason, there is no evidence to indicate that the predominantly topographic lineaments XFM0098A0 and XFM0127A0 are coupled to brittle deformation zones (fault zones) with a length that exceeds 3,000 m. In this context, it is important to bear in mind that the main ice movement direction occurred from the north /Sohlenius et al. 2004/, more or less parallel to the trend of these lineaments.

Excavation work across two lineaments during 2004 /Cronquist et al. 2005/ illustrates the care that needs to be taken in the geological interpretation of lineaments. One of these excavations exposed the north-western part of a steeply dipping fault zone with NE strike. Excavation work was not

possible in the central part of the zone where the contact between the crystalline bedrock and the Quaternary cover is deepest. This zone is expressed at the surface in the form of a combined magnetic, topographic and electromagnetic lineament (XFM0062A0). The second excavation focused attention on a lineament that trends NS and is low magnetic in character (XFM0126A0). The excavation work showed that this lineament is related to a swarm of low-magnetic, granitic dykes. No direct link to a deformation zone is apparent along this anomaly in the bedrock.

5.1.3 Key questions to be solved with the lineament study

Inside the north-western part of the candidate area, most lineaments trend approximately NE and NS (Figure 2). Lineaments with NW trend are more prominent along the south-western and north-eastern margins of the candidate area (Figure 2). The alternative interpretation of lineaments /Korhonen et al. 2004/ has also revealed a conspicuous lineament (LL0060) through the north-western part of the candidate area that is defined by a magnetic minimum that trends NW (Figure 3).

The lineament study needs to provide the following information:

- The geological character of representative lineaments in the different sets summarised above.
- If it is established that a lineament can be related with confidence to a deformation zone in the bedrock, both the geological and the hydrogeological properties of the zone need to be documented.
- If there are possibilities, the question of lineament length needs to be addressed, particularly for the few lineaments that exceed 3,000 m (Figure 2).

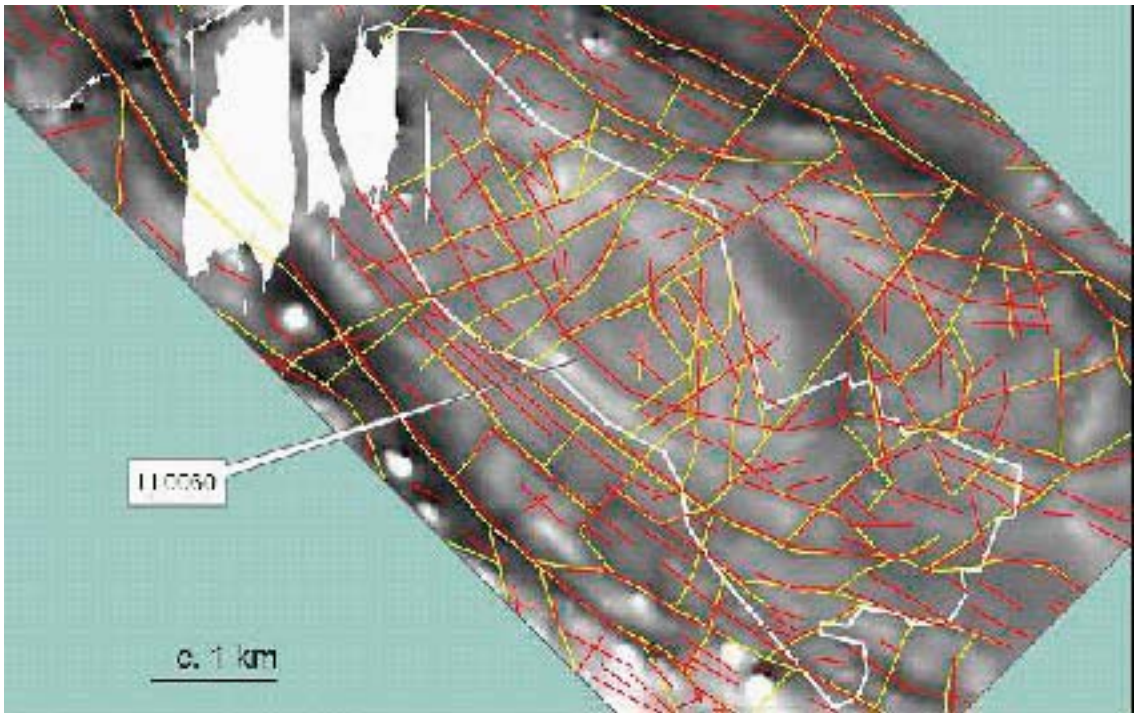

Figure 3. *Comparison of the two interpretations inside the candidate area for the method-specific lineaments based on magnetic minima (north-south survey). The original interpretation /Isaksson et al. 2004/ is shown with yellow lines and the alternative interpretation /Korhonen et al. 2004/ with red lines. The boundary of the candidate area is marked with a white line. The white areas lie close to the nuclear power plant where high-resolution, helicopter-borne geophysical data are lacking. Note the long lineament (LL0060) with north-west trend in the alternative interpretation that passes through the candidate area and is not present in the original interpretation.*

5.1.4 Character of investigations − a generalised view

Excavation work is clearly the most efficient method to assess the geological character of a lineament. This method is direct and avoids all the uncertainties in the modelling work that must be carried out with the use of borehole data. However, the method is sensitive to both nature conservancy and Quaternary cover thickness considerations. Detailed mapping of fractures and rock types in the crystalline bedrock, profile mapping of the Quaternary deposits and, if deemed necessary, complementary ground geophysical measurements need be completed along the excavations.

A second method that can help with the identification and characterisation of brittle deformation zones is a seismic refraction study. Such investigations are in progress at the Forsmark site (Figure 4) and should be completed during Autumn 2005. A systematic integration of the new seismic refraction data with the interpretation of lineaments needs to be completed, in the same manner that older seismic refraction data have been handled /SKB 2005a/.

The properties of deformation zones are best documented with the help of geological and hydrogeological data from cored boreholes. The quality of some geological data from percussion drilling (e.g. fracture frequency, nature of mineral fillings along fractures, character of bedrock) is poor /SKB 2005a/ and the use of this drilling technique severely limits the interpretation of geological data. In the cored boreholes, BIPS, radar and geophysical logging as well as mapping of the drill core should be carried out. Interpretations of the radar and geophysical logs are necessary. All this information will provide a basis for a single hole interpretation and full characterisation of rock units and

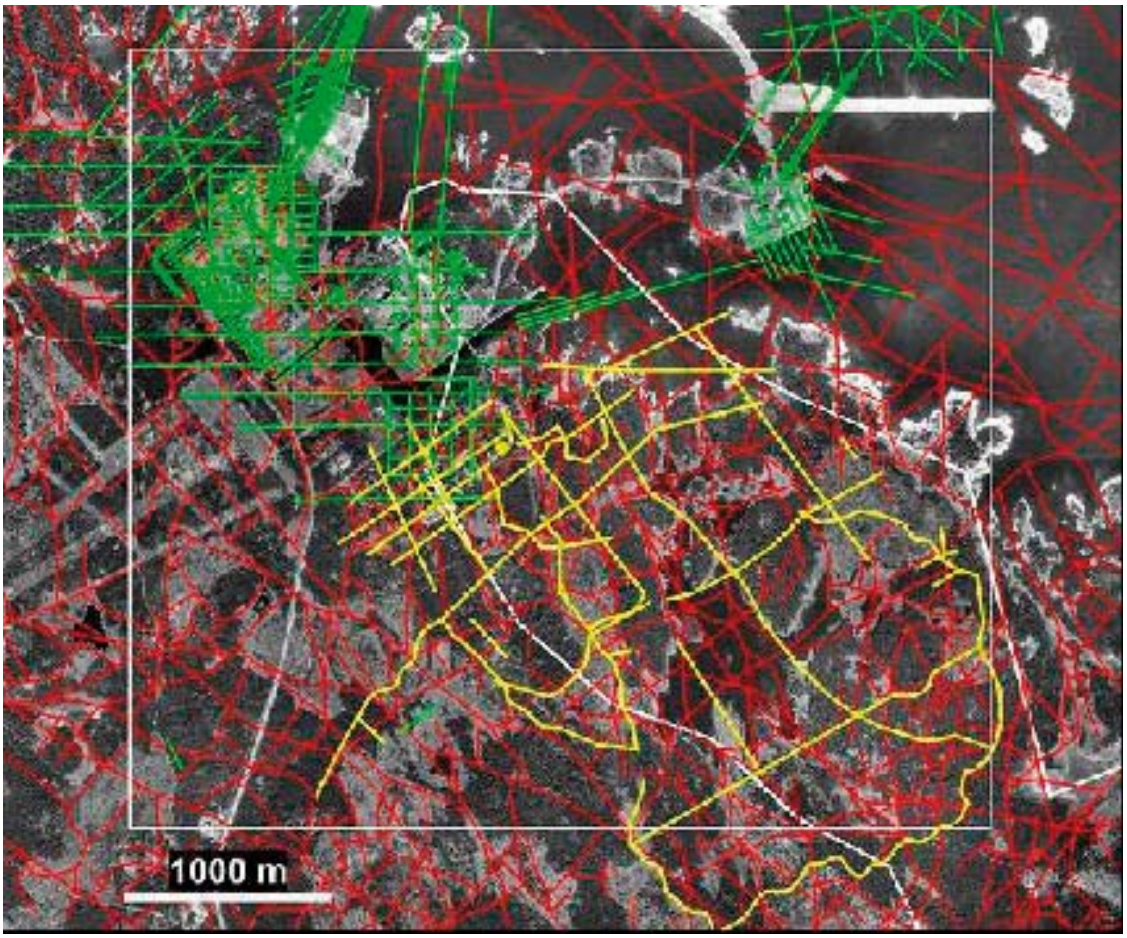

Figure 4. *Profiles for seismic refraction measurements in the north-western part of the candidate area (yellow line) and their relationship to the inferred, linked lineaments (red line). The boundary of the candidate area is shown with a white line. Profiles along which older seismic refraction measurements have been made are shown in green.*

deformation zone intersections. Hydrogeological tests should include measurements with the Posiva Flow Log and/or the Pipe String System. In percussion boreholes, focus should be addressed on the BIPS, radar and geophysical logs with interpretation and the follow-up single hole interpretation. Hydrogeological tests should include pumping tests with the HTHB unit.

The question of lineament length is generally difficult to assess. A comparison study of the two lineament interpretations points out the uncertainty in the establishment of lineament length /Johansson 2005/. However, the confidence in the length of a specific lineament can be judged by assessing the consistency between the different lineament interpretations and by completing detailed ground geophysical measurements in areas where there are questionmarks bearing on the continuity of the lineament. Site specific considerations indicate that only magnetic lineaments at the Forsmark site (e.g. Figure 5) can be confidently related to geological features in the bedrock. For this reason, only ground magnetic measurements are recommended.

5.1.5 Programme − a generalised view

Following the comparison study of the two lineament interpretations /Johansson 2005/, a documentation of what is known about all the lineaments in the north-western part of the candidate area was completed by R. Johansson (Geological Survey of Sweden, SGU) and H. Isaksson (Geovista AB). The results of this work were presented to the geologists at the site (meeting at SGU, 2005-05-24) and a P-report is under preparation. The results provided a sound basis for an ambitious excavation, drilling and ground geophysics programme.

Following a series of follow-up meetings at Forsmark (2005-06-09, 2005-08-18 and 2005-08-25) and at SGU (2005-06-13), which involved geoscientists from the site investigation team and some of the geoscientists from the analysis/modelling team, a somewhat reduced lineament study programme emerged. A radical reduction in the number of excavation sites occurred primarily due to nature conservancy and Quaternary cover thickness considerations. Furthermore, it was decided that the drilling campaign should focus attention on the lineaments (possible deformation zones) that are longer than 3,000 m. It was also decided that all the cored boreholes should be drilled at the already established or planned drill sites. Drilling at new sites should take place by the percussion technique. In order to resolve the question of the length of one of the lineaments that exceeds 3,000 m, a detailed ground magnetic survey should be completed in the area between Bolundsfjärden and the small lake Puttan. All this work should be completed during two time periods, Autumn and the early part of the Winter 2005. The data generated during this programme should be available for model version 2.2.

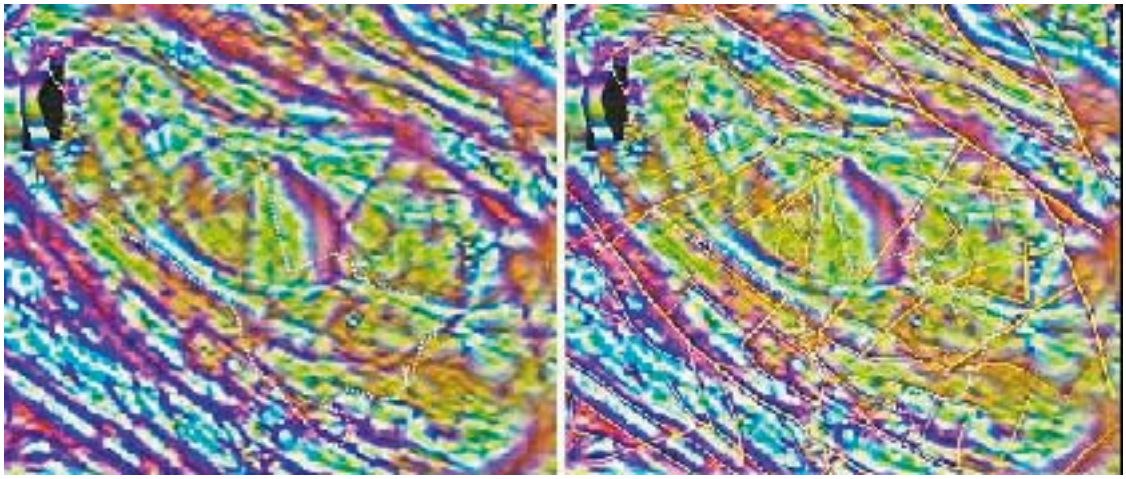

Figure 5. *Contrast enhanced airborne magnetics over the candidate area at Forsmark (north-south survey). The lilac areas indicate low magnetic anomalies and the inferred low magnetic lineaments (method-specific) based on /Isaksson et al. 2004/ are shown in the right hand picture as yellow lines. The thick and thin lines indicate low and high uncertainty lineaments, respectively. The candidate area is marked with a dotted white line.*

The text that follows addresses the excavations, the ground geophysical programme, all the cored boreholes and only the percussion boreholes that will be drilled in the first phase of activities. Since further information is required to recommend the location and orientation for several boreholes in the percussion drilling campaign, a short complementary document that will address these aspects for the second phase of the drilling campaign will be presented later during the Autumn 2005. Possible recommendations for percussion boreholes or other activities that are needed to investigate the low-velocity sections in the seismic refraction study will be included in the second phase.

5.1.6 Selection of lineaments for investigation and recommended type of investigation

Lineaments that have been selected for investigation as well as the locations of recommended excavations, geophysical surveys and percussion and cored boreholes are presented in Figure 6.

Lineament XFM0159A0

Lineament XFM0159A0 is based a combination of magnetic, topographic and electromagnetic data, has a NE trend (mean trend 056°) and is 1,616 m long. The lineament belongs to the group of lineaments with NE trend that transect the candidate area.

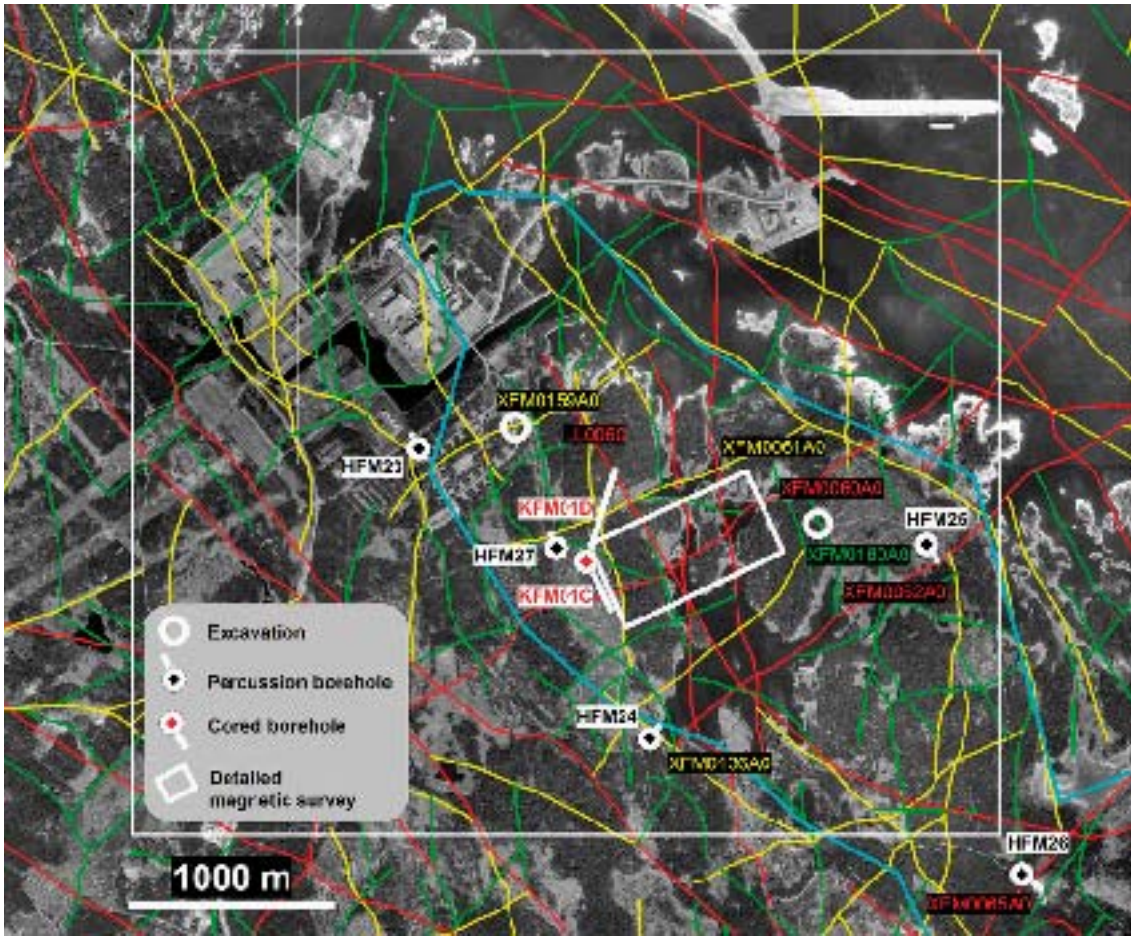

Figure 6. *Recommended sites for excavation work, for the ground magnetic survey close to lineament XFM0060A0, for the percussion boreholes HFM23 to HFM27 and for the cored borehole KFM01C. Linked lineaments with length 500–1,000 m (green), 1,000–3,000 m (yellow) and greater than 3,000 m (red) adopted from /Isaksson and Keisu 2005/. The Forsmark candidate area is shown as a light blue line. The white rectangle displays the area chosen for assessment of lineaments in the north-western part of the candidate area (meeting at SKB Forsmark, 2004-12-02).*

Since nature conservancy and Quaternary cover thickness considerations are favourable for an excavation campaign across lineament XFM0159A0 in the vicinity of drill site 7, it is recommended that such work is carried out at this site.

Lineaments XFM0160A0/LL0018

East of drill site 6, lineament XFM0160A0 /Isaksson et al. 2004, Isaksson and Keisu 2005/ lies immediately to the west of lineament LL0018, which was recognised in the alternative interpretation /Korhonen et al. 2004/. In both interpretations, these two lineaments have been recognised on the basis of a combination of topographic and electromagnetic data. Both show a NS trend (mean trend of XFM0160A0 is 345°) and lineament XFM0160A0 is 663 m long.

Since nature conservancy and Quaternary cover thickness considerations are favourable for an excavation campaign across both XFM0160A0 and LL0018 in the vicinity of drill site 6, it is recommended that short excavations are carried out across both lineaments in this area. This work should provide key information on the character of the group of NS lineaments that transect the north-western part of the candidate area.

Lineament XFM0062A0/Fault zone ZFMNE062A in model version 1.2

The linked lineament XFM0062A0 is defined by a combination of magnetic, topographic and electromagnetic data. The lineament is inferred to be 3,745 m long.

Lineament XFM0062A0 was excavated and studied at the surface during 2004 /Cronquist et al. 2005/. Furthermore, it was modelled with high confidence together with DZ5 in borehole KFM05A, which occurs at a depth of c. 775 m, to generate the steeply dipping fault zone with NE strike referred to as ZFMNE0062A /SKB 2005a/. The strike and dip of this zone, as estimated in the version 1.2 modelling work, is 234°/73° (right-hand-rule method, i.e. N54E/73NW) and its length in the geological model is 3,704 m. The dip estimated from the modelling of ground magnetic data across lineament XFM0062A0 /Pitkänen et al. 2004/ is consistent with the dip estimated by linking this lineament with the deformation zone intersection DZ5 in KFM05A.

It is recommended that the excavation work during 2004 is followed up with percussion drilling in order to confirm the earlier modelling work and to investigate the character of the modelled zone at shallower crustal levels. It is recommended that borehole HFM25 is sited close to the excavation site, north-west of the lineament. The borehole should be inclined to the south-east. In order to confirm that the zone has been fully intersected, a preliminary evaluation of especially the BIPS and geophysical log data from HFM25 should be carried out. If the evaluation shows doubts that the deformation zone has not been fully intersected, it is recommended that a second percussion borehole is drilled from a location close to the first site but south-east of the lineament with an inclination to the north-west.

Lineament XFM0065A0/Fault zone ZFMNE0065 in model version 1.2

The linked lineament XFM0065A0 is defined by a combination of magnetic, topographic and electromagnetic data. The lineament is inferred to be 3,981 m long and forms a conspicuous low magnetic anomaly between drill sites 2 and 3 (Figures 1 and 2).

Lineament XFM0065A0 was modelled with high confidence together with DZ3 in borehole HFM18, which occurs at a depth of c. 115 m, to generate the steeply dipping fault zone with NE strike referred to as ZFMNE0065 /SKB 2005a/. The strike and dip of this zone, as estimated in the version 1.2 modelling work, is 036°/75° (N36E/75SE) and its length in the geological model is 3,895 m. It is important to keep in mind that the gently dipping brittle deformation zone ZFMNE00A7 was also modelled to intersect HFM18 at DZ3. In the version 1.2 modelling work /SKB 2005a/, some gently dipping zones were either truncated (ZFMNE0866) or separated into different segments (ZFMNE0B5A/ZFMNE0B5B) across ZFMNE0065, and it remains possible that several more of the gently dipping zones either terminate or change their orientation across this zone.

In order to test the earlier modelling work and to avoid the complexities of double intersections, it is recommended that a second percussion borehole is drilled through the zone inferred to be related to lineament XFM0065A0. It is recommended that borehole HFM26 is drilled north-west of the lineament and should be inclined to the south-east. In this way, the borehole will complement the borehole HFM18 that was drilled in the opposite direction. On the condition that zone ZFMNE0065 does not dip more gently to the south-east as that indicated in model version 1.2 /SKB 2005a/, then it is anticipated that borehole HFM26 will intersect the zone. The orientation provided in model version 1.2 predicts an intersection at c. 150 m borehole length in HFM26. If zone ZFMNE0065 dips at an angle that is c. 65° to the south-east, as indicated in the ongoing modelling work (version 2.1), then borehole HFM26 will most probably fail to intersect this zone.

Lineament XFM0061A0/Fault zone ZFMNE061A in model version 1.2

The linked lineament XFM0061A0 is defined by a combination of magnetic, topographic and electromagnetic data. The lineament is inferred to be 1,731 m long.

Lineament XFM0061A0 was modelled with high confidence together with DZ3 in borehole KFM01A, which occurs at a depth of c. 650 m, to generate the steeply dipping fault zone with NE strike referred to as ZFMNE0061 /SKB 2004, 2005a/. The strike and dip of this zone, as estimated in the version 1.2 modelling work, is 068°/81° (N68E/81SE) and its length in the geological model is 1,727 m. According to the hydraulic tests conducted with the Posiva Flow Log, the transmissivity (conductivity-thickness product) of ZFMNE0061 lies below the measurement limit. However, the current interpretation of the strike and dip of ZFMNE0061 suggests an intercept with borehole KFM06A, where an interval of a relatively high transmissivity that possibly correlates with ZFMNE0061 has been measured with the Posiva Flow Log as well as the Pipe String System.

In order to confirm the earlier modelling work and to investigate the character of the modelled zone at shallower crustal levels, it is recommended that a percussion borehole is drilled at an environmentally suitable location close to and south-east of the lineament XFM0061A0. The borehole should be inclined to the north-west.

Lineament XFM0060A0/Fault zone ZFMNE060A in model version 1.2

The linked lineament XFM0060A0 is defined by a combination of magnetic, topographic and electromagnetic data. The lineament is inferred to be 4,567 m long. There are significant differences concerning the continuity of the magnetic component of this lineament in the area between Bolundsfjärden and the small lake Puttan. These differences may have important consequences for the size of a deformation zone that is linked to this lineament. In the interpretation of lineaments provided by /Korhonen et al. 2004/, the lineament can be divided into two segments north-east and south-west, respectively, of the critical area between Bolundsfjärden and Puttan.

Lineament XFM0060A0 was modelled with medium confidence to correspond to a minor fault zone similar to ZFMNE0061, -62 and -65 /SKB 2005a/. The strike and dip of this zone, as defined in the version 1.2 modelling work, is 242°/87° (N62E/87NW) and its length in the geological model is 3,012 m. The dip estimated from the modelling of ground magnetic data across lineament XFM0060A0 /Pitkänen et al. 2004/ is consistent with the dip estimated in the modelling work /SKB 2005a/.

Borehole KFM06A was designed to test the characteristics of lineaments with both NS and NE trends that transect the candidate area north of Bolundsfjärden. In particular, the drilling provides information on the north-eastern segment of XFM0060A0. The resulting data were not available for model version 1.2 but are presently under analysis during model version 2.1. In order to improve the confidence level of the inferred deformation zone and to establish its geological characteristics, it is recommended that a cored borehole, referred to as KFM01C, is drilled from site 1 through the zone inferred to be related to the south-western segment of lineament XFM0060A0. Borehole KFM01C will be drilled north-west of the lineament and should be inclined to the south-east. One or more percussion boreholes may also be needed to further study this segment of the lineament and confirm its continuation in a south-westerly direction. However, it is recommended that a preliminary evaluation of especially the BIPS and geophysical log data from KFM01C is carried out prior to the second phase of drilling through lineament XFM0060A0.

In order to assess the continuity of the lineament XFM0060A0 in the critical area between Bolundsfjärden and Puttan, it is recommended that high resolution ground magnetic measurements are carried out in this area.

Percussion boreholes HFM23 and HFM24

The percussion boreholes HFM23 and HFM24 will be drilled with the prime aim to supply the cored boreholes at drill sites 9 and 10 with flush water. For this reason, they are located close to these two drill sites. However, the orientation of these two boreholes has been chosen to maximize the possibilities to intersect the possible continuation at depth of two structures that are represented by lineaments at the surface, XFM0428A0 and XFM0136A0. Lineament XFM0428A0 is based entirely on topographic data, has a NE trend (mean trend 054°) and is only c. 300 m long (not marked in Figure 6). Lineament XFM0136A0 is based on a combination of magnetic and topographic data, trends in a NW direction (mean trend 305 °) and is c. 1,250 m long. The magnetic component is visible along its entire length.

5.1.7 Location of excavations and ground magnetic survey, and the location and orientation of boreholes

The recommended sites for excavation work, for the ground magnetic survey close to lineament XFM0060A0, for the percussion boreholes HFM23 to HFM27 and for the cored boreholes KFM01C and KFM10B are shown in Figure 6. The recommended coordinates, inclination, direction and length of all the boreholes are also listed in Table 1.

5.1.8 Cored borehole KFM01D

Following interactive discussions at the Forsmark site between some members of the modelling group and personnel responsible for the site investigations, in particular during a meeting at Forsmark on 2005-08-18, the need for a long cored borehole to be drilled from drill site 1 into the bedrock volume that includes the central part of the proposed repository area was recognised. The preliminary aims for this borehole are:

1. To obtain base geological, rock mechanical and hydrogeological information in the central volume.
2. To intersect ZFMNE0061 at approximately repository depth.
3. To intersect several other potential zones related to lineaments at the surface, including a conspicuous lineament with NW trend (LL0060) that was recognised solely in the alternative interpretation work /Korhonen et al. 2004/. No deformation zone related to this lineament was detected in KFM05A.

This borehole received the name KFM01D and was initially planned to be drilled at the end of the 2.2 drilling campaign with a motivation in the memorandum from the modelling group in November.

Table 1. Position, inclination, direction and borehole length of the recommended cored and percussion boreholes.

Borehole	Drill site	Northing in RT 90, 2.5 gon V (m)	Easting in RT 90, 2.5 gon V (m)	Inclination (°)	Direction (°)	Borehole length (m)
HFM23	New	6700076	1630585	60	335	150
HFM24	New	6698663	1631717	60	045	150
HFM25	New	6699611	1633046	60	140	180
HFM26	New	6698011	1633507	55	125	200
HFM27	New	6699594	1631252	70	335	180
KFM01C	1	6699530	1631397	50	165	400 (max)

Following the meeting on 2005-08-18, considerable pressure has been raised from personnel at the Forsmark site to place this borehole earlier in the programme and to build the new foundation for the borehole as quickly as possible. In order to meet these wishes, two members of the modelling team (Stephens and Simeonov) have studied both the version 1.2 geological models for the site and the preliminary layout for the repository, and estimated a preliminary orientation for this borehole to be 030°/55°. The borehole with this orientation was placed at the coordinates 1631397/6699530 and was estimated to be 800 m long. These recommendations were released to the Forsmark site on 2005-09-06 without a thorough review by all members of the modelling group.

The exact position, orientation and borehole length of KFM01D (Figure 6), as provided above, are preliminary in character and may be modified when all members of the modelling group have completed their version 2.1 activities during the Autumn and reported their recommendations to the site in November. At this stage, it cannot be excluded that the foundation now being constructed may need to be abandoned and a new foundation completed to match a revised borehole orientation.

5.1.9 References

Cronquist T, Forssberg O, Hansen L M, Jonsson A, Koyi S, Leiner P, Vestgård J, Petersson J, Skogsmo G, 2005. Forsmark site investigation. Detailed fracture mapping of two trenches at Forsmark. SKB P-04-88, Svensk Kärnbränslehantering AB.

Isaksson H, 2003. Forsmark site investigation. Interpretation of topographic lineaments 2002. SKB P-03-40, Svensk Kärnbränslehantering AB.

Isaksson H, Thunehed H, Mattsson H, Keisu M, 2004. Interpretation of airborne geophysics and integration with topography. Stage 1 (2002). SKB P-04-29, Svensk Kärnbränslehantering AB.

Isaksson H, Keisu M, 2005. Forsmark site investigation. Interpretation of airborne geophysics and integration with topography. Stage 2 (2002–2004). SKB P-04-282, Svensk Kärnbränslehantering AB.

Johansson R, 2005. A comparison of two independent interpretations of lineaments from geophysical and topographic data at the Forsmark site. Preliminary site description. Forsmark area – version 1.2. SKB R-05-23, Svensk Kärnbränslehantering AB.

Korhonen K, Paananen M, Paulamäki S, 2004. Forsmark site investigation. Interpretation of lineaments from airborne geophysical and topographic data. An alternative model within version 1.2 of the Forsmark modelling project. SKB P-04-241, Svensk Kärnbränslehantering AB.

LaPointe P R, Olofsson I, Hermanson J, 2005. Statistical model of fractures and deformation zones for Forsmark. Preliminary site description. Forsmark area – version 1.2. SKB R-05-26, Svensk Kärnbränslehantering AB.

Pitkänen T, Thunehed H, Isaksson H, 2004. A ground geophysical survey prior to the siting of borehole KFM05A and KFM06A and control of the character of two SW-NE oriented lineaments. Forsmark site investigation. SKB P-03-104, Svensk Kärnbränslehantering AB.

SKB, 2002. Forsmark – site descriptive model version 0. SKB R-02-32, Svensk Kärnbränslehantering AB.

SKB, 2004. Preliminary site description. Forsmark area – version 1.1. SKB R-04-15, Svensk Kärnbränslehantering AB.

SKB, 2005a. Preliminary site description. Forsmark area – version 1.2. SKB R-05-18, Svensk Kärnbränslehantering AB.

SKB, 2005b. Forsmark site investigation. Programme for further investigations of geosphere and biosphere. SKB R-05-14, Svensk Kärnbränslehantering AB

Sohlenius G, Hedenström A, Rudmark L, 2004. Forsmark site investigation. Mapping of unconsolidated Quaternary deposits 2002–2003. Map description. SKB R-04-39, Svensk Kärnbränslehantering AB.

Triumf C-A, 2004. Oskarshamn site investigation. Joint interpretation of lineaments. SKB P-04-49, Svensk Kärnbränslehantering AB.

M B Stephens, Geological Survey of Sweden
S Follin, SF GeoLogic AB
A Simeonov, Svensk Kärnbränslehantering AB

Uppsala, 2005-10-27

5.2 Lineaments and seismic reflectors in the north-western part of the candidate area − motivation and recommendations for the stage II investigations, winter 2005

5.2.1 Background

The argumentation for a study of lineaments in the north-western part of the candidate area at Forsmark, as well as a general outline of the character of these investigations and a detailed programme for stage I of the study, has recently been presented in a motivation report. This report formed the basis for a decision document (ID code 1045795) that concerned the work to be carried out during stage I. Surface excavations, a ground geophysical programme, and several percussion and cored boreholes were recommended. The locations of the different investigations as well as the orientation of boreholes were specified in the report. Since it was recognised that further information was required in order to recommend the location and orientation for some boreholes in the percussion drilling campaign, it was foreseen that a short complementary document would be required to address the motivation for stage II in the investigations.

5.2.2 Character of stage II investigations

The present report provides a motivation for four new percussion boreholes, HFM29 to HFM32, during stage II of the investigations. Two of these boreholes (HFM29 and HFM30) aim to test the possible existence of deformation zones beneath two lineaments that strike WNW and are longer than 3,000 m. Both lineaments occur along the south-western marginal part of the candidate area. One percussion borehole (HFM31) addresses the character of a seismic reflector that has been recognised during the stage 2 seismic reflection work at Forsmark /Juhlin and Palm 2005/. The fourth percussion borehole (HFM32) addresses the question of groundwater flow in the bedrock volume beneath Bolundsfjärden that is situated above the gently dipping deformation zone ZFMNE00A2.

BIPS, radar and geophysical logging should be carried out in all four boreholes and all these data need to be interpreted according to standard procedures. If deemed necessary, the fine rock fragments that are generated during the drilling procedure can be studied. All this information will provide a basis for single hole interpretations that aim to provide a characterisation of rock units and deformation zone intersections in the boreholes. Hydrogeological tests along boreholes HFM29, HFM30 and HFM31 should include pumping tests with the HTHB unit. The hydrogeological work to be completed along HFM32 is specified below (see section entitled “Groundwater flow above ZFMNE00A2 beneath Bolundsfjärden”).

Lineament XFM0017A0

Lineament XFM0017A0 is based on a combination of magnetic, topographic and electromagnetic data, has a WNW trend (mean trend 308°) and is c. 6,900 m long. The lineament belongs to the group of lineaments with WNW and NW trend that are situated along the south-western margin of the candidate area. Ground geophysical data /Pitkänen and Isaksson 2003/ provide some support that lineament XFM0017A0 represents a deformation zone. Furthermore, in model version 1.2, several gently dipping deformation zones have been truncated against the deformation zone that has been inferred, with medium confidence, to be represented at the surface by this lineament /SKB 2005/.

On the basis of the observations summarised above, it is recommended that percussion borehole HFM29 is drilled in order to investigate the character of the bedrock beneath this lineament. Since modelling work indicates that the zones with NW strike along the south-western margin of the candidate area dip steeply (c. 85°) to the south-west, it is recommended that borehole HFM29 is sited to the south-west of the lineament and is inclined to the north-east.

North-westerly continuation of lineament XFM0123A0

Lineament XFM0123A0 is based on a combination of magnetic and topographic data, has a WNW trend (mean trend 285°) and is 3,070 m long. The lineament also belongs to the group of lineaments with WNW and NW trend that lie along the south-western margin of the candidate area. Lineament XFM0123A0 connects in a north-westerly direction with lineament XFM0136A0 via a short magnetic lineament. Bearing in mind this interpretation, it is apparent that a modified lineament 123 is considerably longer than 3,000 m. Furthermore, ongoing version 2.1 modelling work suggests that several gently dipping deformation zones truncate to the west against lineament 123.

Bearing in mind the considerations above, it is recommended that a percussion borehole (HFM30) is drilled in order to assess the character of the bedrock beneath the magnetic lineament that connects XFM0123A0 and XFM0136A0. It is recommended that borehole HFM30 is also sited to the south-west of the lineament and is inclined to the north-east. The results of this drilling complement those of HFM24 (see earlier document for stage I investigations) that aims to intersect the possible continuation at depth of lineament XFM0136A0.

Seismic reflector B8

Along seismic profile lines 11, 12 and 13 /Juhlin and Palm 2005/, north-west of the candidate area close to the reactor 3 site, a seismic reflector is apparent at depth (Figure 1). Ongoing version 2.1 modelling work suggests that this reflector corresponds to the gently dipping, brittle deformation zone that was intersected in KFK001 (DBT1) at c. 320 m depth /Carlsson and Christiansson 1987/.

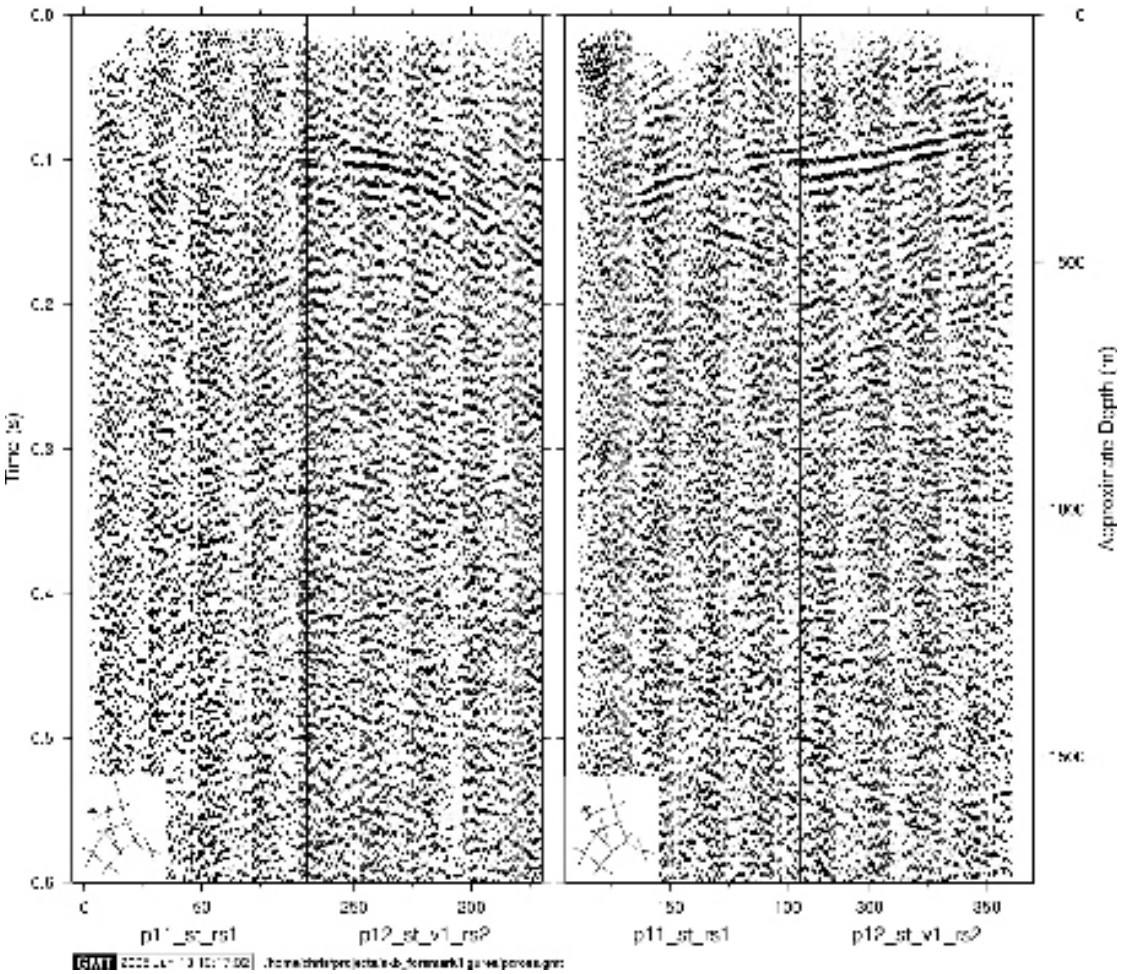

Figure 1. *Seismic reflector B8 in the upper parts of profiles 11 and especially 12 (after /Juhlin and Palm 2005/).*

It is recommended that a percussion borehole (HFM31) is drilled in order to confirm this interpretation. The location and orientation of this borehole has taken into consideration the results of the version 2.1 modelling work. An intersection of the deformation zone that corresponds to seismic reflector B8 is predicted at c. 115 m borehole length along HFM31.

Groundwater flow above ZFMNE00A2 beneath Bolundsfjärden

Monitoring of the lake water level and the groundwater level in the till below and in the immediate vicinity of Lake Bolundsfjärden shows that the lake is a discharge area during the dominating part of the year, i.e. the groundwater flow has an upward gradient. However, during very dry conditions, as during the summer of 2003, the groundwater gradients are such that prerequisites exist for a flow of water from the lake to the till aquifer, i.e. the lake acts as a recharge area. Water analyses for the observation well in till below the lake (SFM0023) also show a "Littorina signature" which can be explained by a continuous upward flow of old groundwater or by a more or less stagnant groundwater below the lake.

In order to better understand the groundwater flows in the prioritized north-western part of the candidate are, it is recommended that a vertical percussion borehole is drilled in the central part of Lake Bolundsfjärden. If technically possible, the borehole should aim to reach zone ZFMNE00A2. Measurements of groundwater levels in sections separated by packers should make it possible to see if a continuous upward gradient exists from the bottom of the borehole to the surface, i.e. if the central part of the lake is a discharge area all the way from the depth of the borehole to the surface. The packers should be placed so that important water-bearing fractures are separated. From water sampling in the separated sections of the borehole the existence of water with a "Littorina signature" could be checked. Percussion drilling should be combined with the installation of an additional groundwater observation well in till below the lake and a tip for pore pressure measurements in the gyttja. This will provide possibilities to carry out a pumping test in the percussion-drilled borehole in order to estimate the hydraulic properties of the sediments decisive for the hydraulic contact between the lake and the groundwater beneath the lake. Resting groundwater level should be measured twice during the drilling. It should be noted that this borehole also serves to investigate the bedrock beneath lineament LL0060 (see Figure 2).

The drilling should be executed from the small island in Lake Bolundsfjärden and a prerequisite is that the drilling rig can be transported over the ice. Measures to strengthen the bearing capacity of the ice should be taken (removal of snow and pumping of water) along a planned transport road. The time for the drilling depends on weather and environmental considerations but the drilling should be carried out as soon as the ice can carry the drilling rig. Permission to drill until mid-February should be applied for at the Regional County Board.

5.2.3 Location and orientation of percussion boreholes HFM29 to HFM32

The recommended sites for the percussion boreholes HFM29 to HFM32 are shown in Figure 2. The recommended co-ordinates, inclination, direction and length of the four boreholes are presented in Table 1.

Table 1. Position, inclination, direction and borehole length of the recommended percussion boreholes HFM29−HFM32.

Borehole	Drill site	Northing in RT 90, 2.5 gon V (m)	Easting in RT 90, 2.5 gon V (m)	Inclination (°)	Direction (°)	Borehole length (m)
HFM29	New	6698004	1632506	60	030	200
HFM30	New	6697916	1631825	60	030	200
HFM31	New	6700866	1629199	70	300	200
HFM32	New	6699025	1632135	85	270	Preferably should intersect ZFMNE00A2. Maximum borehole length 300 m

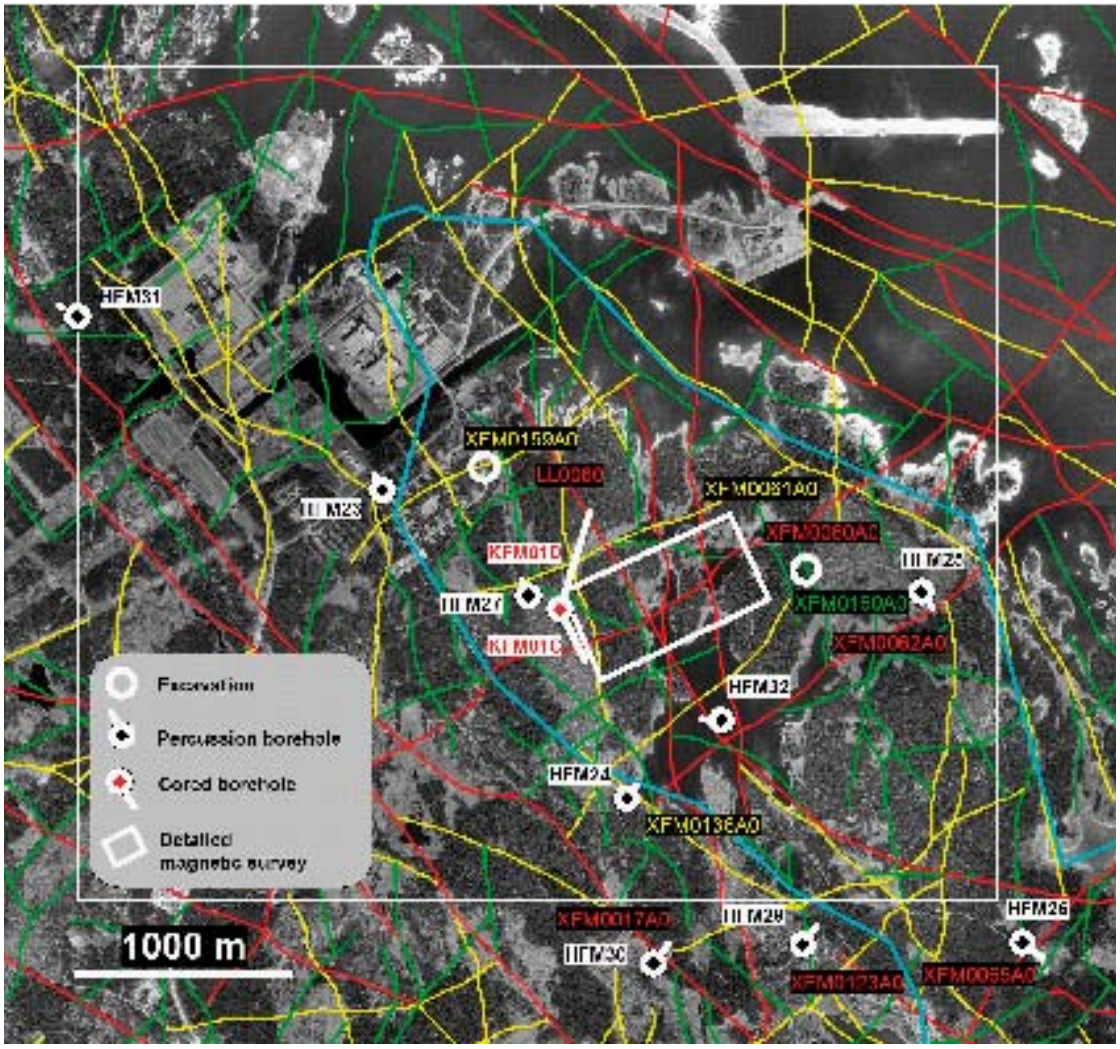

Figure 2. *Recommended sites for percussion boreholes HFM29 to HFM32 during the stage II investigations. The recommended sites for excavation work, for the ground magnetic survey close to lineament XFM0060A0, for the percussion boreholes HFM23 to HFM27 and for the cored borehole KFM01C, in connection with the stage I investigations, are also shown. Linked lineaments with length 500–1,000 m (green), 1,000–3,000 m (yellow) and greater than 3,000 m (red) adopted from /Isaksson and Keisu 2005/. The Forsmark candidate area is shown as a light blue line. The white rectangle displays the area chosen for assessment of lineaments in the north-western part of the candidate area (meeting at SKB Forsmark, 2004-12-02).*

5.2.4 References

Carlsson A, Christiansson R, 1987. Geology and tectonics at Forsmark, Sweden. SKB SFR-87-04, Svensk Kärnbränslehantering AB.

Isaksson H, Keisu M, 2005. Forsmark site investigation. Interpretation of airborne geophysics and integration with topography. Stage 2 (2002–2004). SKB P-04-282, Svensk Kärnbränslehantering AB.

Juhlin C, Palm H, 2005. Forsmark site investigation. Reflection seismic studies in the Forsmark area, 2004: Stage 2. SKB R-05-42, Svensk Kärnbränslehantering AB.

Pitkänen T, Isaksson H, 2003. Forsmark site investigation. A ground geophysical survey prior to the siting of borehole KFM04A. SKB P-03-55, Svensk Kärnbränslehantering AB.

SKB, 2005. Preliminary site description. Forsmark area – version 1.2. SKB R-05-18, Svensk Kärnbränslehantering AB.

M B Stephens, Geological Survey of Sweden
P-O Johansson, Artesia
A Simeonov, Svensk Kärnbränslehantering AB

Uppsala, 2005-11-28

5.3 Motivation for and orientation of telescope borehole KFM01D, with special focus on the procedures for the sampling of rocks to be used in the characterisation of pore space fluids

5.3.1 Background

In accordance with the results of the initial site investigation (ISI) at Forsmark, including the site descriptive model (SDM) version 1.2 /SKB 2005a/, a decision was taken by SKB to focus the complementary site investigation (CSI) to a target area in the north-western part of the candidate area /SKB 2005b/.

In a series of decision and motivation documents, an extensive core drilling programme at five separate sites (DS1, DS6, DS7, DS8 and DS9) was planned in the target area (see /SKB documents 1024611, 1038014, 1038090, 1039868 and 1045795). At the time of writing of the present document, all boreholes except KFM08C and KFM09C have been or are being drilled (Figure 1). These boreholes complement the telescope and cored boreholes KFM01A/KFM01B, KFM02A, KFM04A, KFM05A and KFM06A/KFM06B, which are also situated wholly or partly inside the target volume and which were drilled during the ISI. Three drilling sites (7, 8 and 9) are located in the area north-west of the steeply dipping deformation zone ZFMNE0061 (Figure 1) and the gently dipping zone ZFMNE00A2.

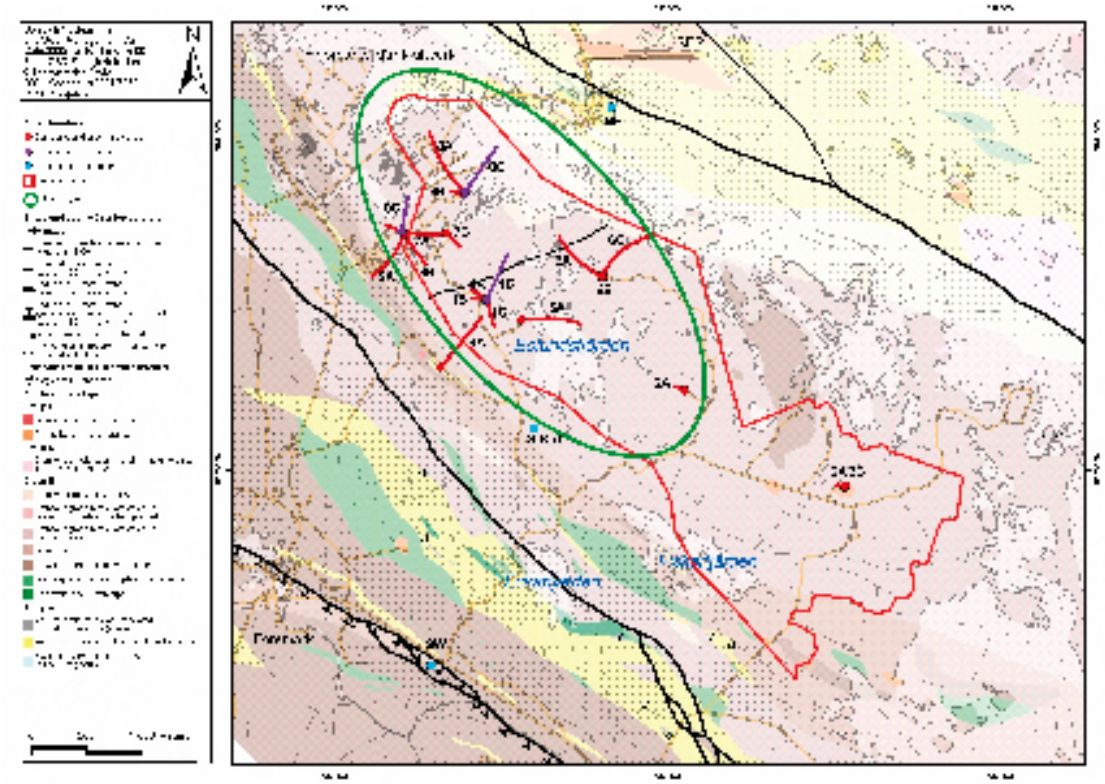

Figure 1. *Geological map of the bedrock inside and immediately around the candidate area at Forsmark (map version 1.2). Completed and ongoing, planned and possible telescope and cored boreholes as well as the target area, which is referred to as the priority site in /SKB 2005b/, are also shown (modified after /SKB 2005b/). Telescope borehole KFM01D, which is addressed in this report, is included with the planned boreholes.*

Following interactive discussions at the Forsmark site between the modelling group and personnel responsible for the site investigations, there crystallised a need for particularly more geological, hydrogeological and hydrogeochemical data in the central part of the proposed repository area that lies within the target area. As is apparent in Figure 2, such data are lacking. The present document provides a brief motivation for an inclined telescope borehole that will penetrate this area. It also provides a recommendation for the activities to be carried out during and immediately after the drilling work. Special focus is made on the sample selection, preservation and laboratory procedures to be implemented in the hydrogeochemical studies (Appendix 1).

The choice of site and the orientation of the new borehole, which is referred to as KFM01D (Figures 1 and 2), are also recommended in this document. It is anticipated that this drilling activity will help to validate our understanding of the bedrock characteristics in the target area that was presented in /SKB 2005a/ and that has been developed further during model version 2.1.

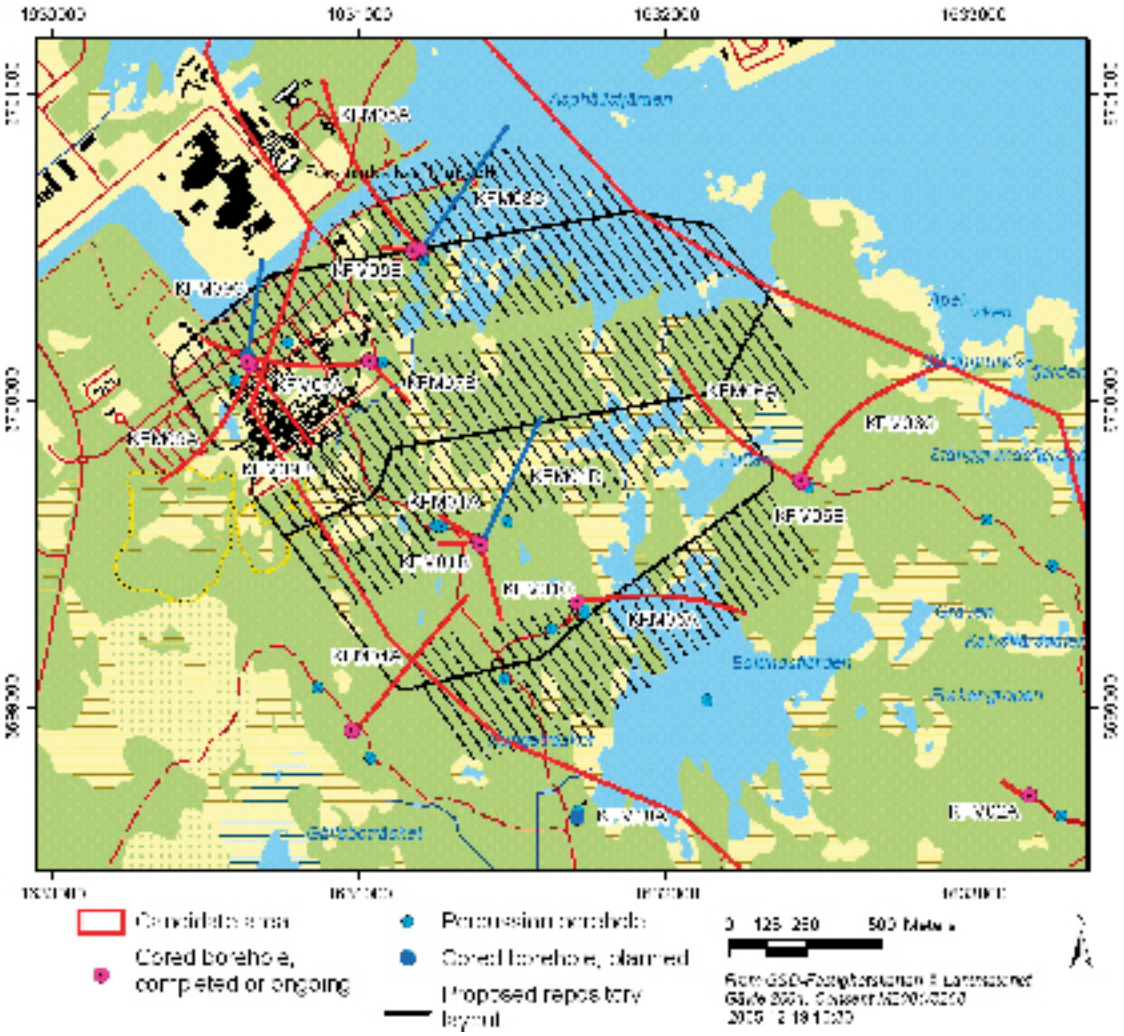

Figure 2. *Possible repository layout at 400 m depth in the target area. This design is based on the results of SDM, version 1.2. Boreholes, including KFM01D that is addressed in this report, are also shown.*

5.3.2 What are the key questions to be solved with the drilling

Bedrock geology

From a geological perspective, the prime aim of borehole KFM01D is to provide base geological information bearing on the character of the bedrock in the central part of the proposed repository area. Secondly, if a suitable borehole site and orientation are selected (see below), it will be possible to confirm the presence of two deformation zones in the north-western part of the candidate area and to test key working hypotheses on the character of some of the lineaments in this area.

Analysis of data and modelling work during SDM version 2.1 have confirmed the interpretation from KFM01A that the linked lineament XFM0061A0 is the surface expression of a minor brittle deformation zone (ZFMNE0061) with a high frequency of sealed fractures, i.e. a cohesive deformation product. However, it appears that zone ZFMNE0061 is composed of several segments that, at depth, splay from and merge together with each other in a complex network. All the segments strike NE and dip steeply. One of the aims of the drilling of KFM01D is to intersect zone ZFMNE0061 in order to document the character of this zone close to repository depth. Earlier modelling work also suggests that the gently dipping zone ZFMNE00A2 will be intersected in the upper part of borehole KFM01D.

The lineament LL0060 with NW trend that is defined by a magnetic minimum /Korhonen et al. 2004/ is a long (> 3 km) structural feature at the surface in the north-western part of the candidate area (Figure 3). Bearing in mind the results from previous drilling activities as well as excavation work, only lineaments defined by magnetic minima have been utilised in the modelling of deformation zones during SDM version 2.1 (Figure 4). This re-evaluation has also recognised the occurrence of a lineament defined by a magnetic minimum (MFM1190) that corresponds in part to lineament LL0060 (cf. Figures 3 and 4).

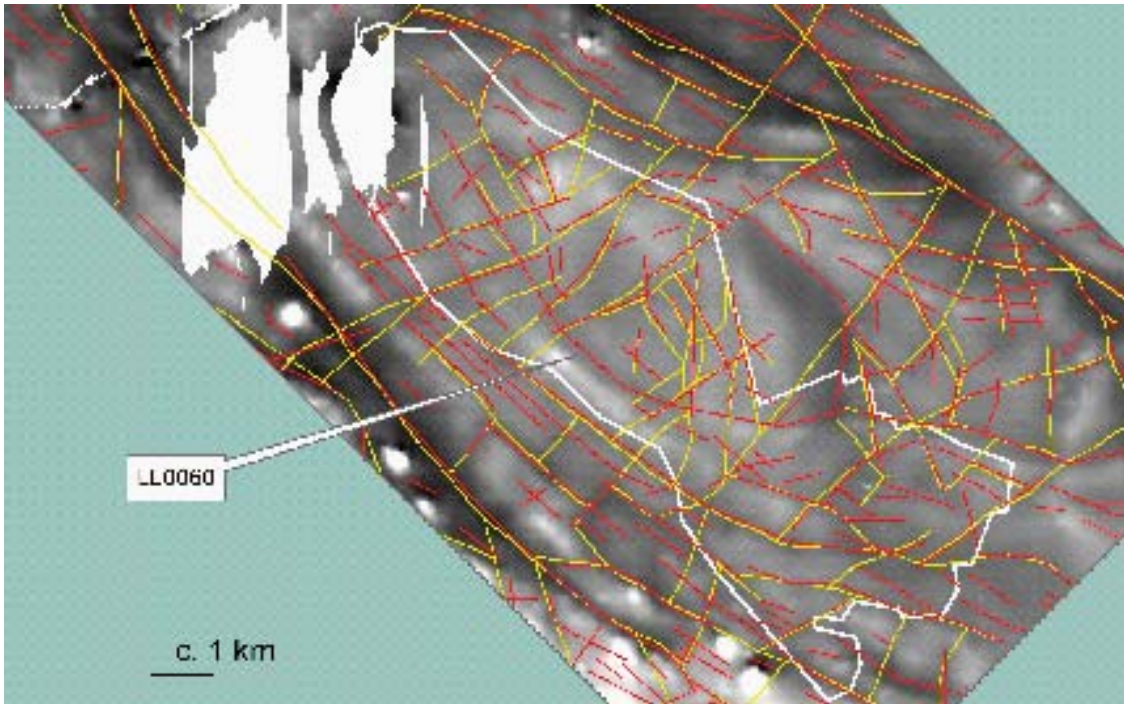

Figure 3. *Comparison of the two interpretations inside the candidate area for the method-specific lineaments based on magnetic minima (north-south survey). The original interpretation /Isaksson et al. 2004/ is shown with yellow lines and the alternative interpretation /Korhonen et al. 2004/ with red lines. The boundary of the candidate area is marked with a white line. The white areas lie close to the nuclear power plant where high-resolution, helicopter-borne geophysical data are lacking. Note the long lineament (LL0060) with north-west trend in the alternative interpretation that passes through the candidate area and is not present in the original interpretation.*

The analysis of the data from borehole KFM05A showed that it was not possible to link lineament LL0060 with any of the deformation zone intersections in this borehole /SKB 2005a/. For this reason, the working hypothesis that the lineament is related in some way to the primary variation in magnetite content in the bedrock has been adopted. Furthermore, the data from this borehole indicate that the topographic lineaments with NNW trend in the north-western part of the candidate area are not related to significant deformation zones /SKB 2005a/. Instead, it is inferred that these conspicuous topographic lineaments poorly reflect geological features in the bedrock since they are parallel to the principal ice movement direction.

It is judged necessary that more geological data are acquired in order to test the working hypotheses for LL0060 and the NNW topographic lineaments. In particular, the character of the representative, NNW topographic lineament XFM0099A0 /Isaksson et al. 2004/ at depth can be assessed with the help of cored borehole data and compared with the data of poorer quality from the percussion borehole HFM19.

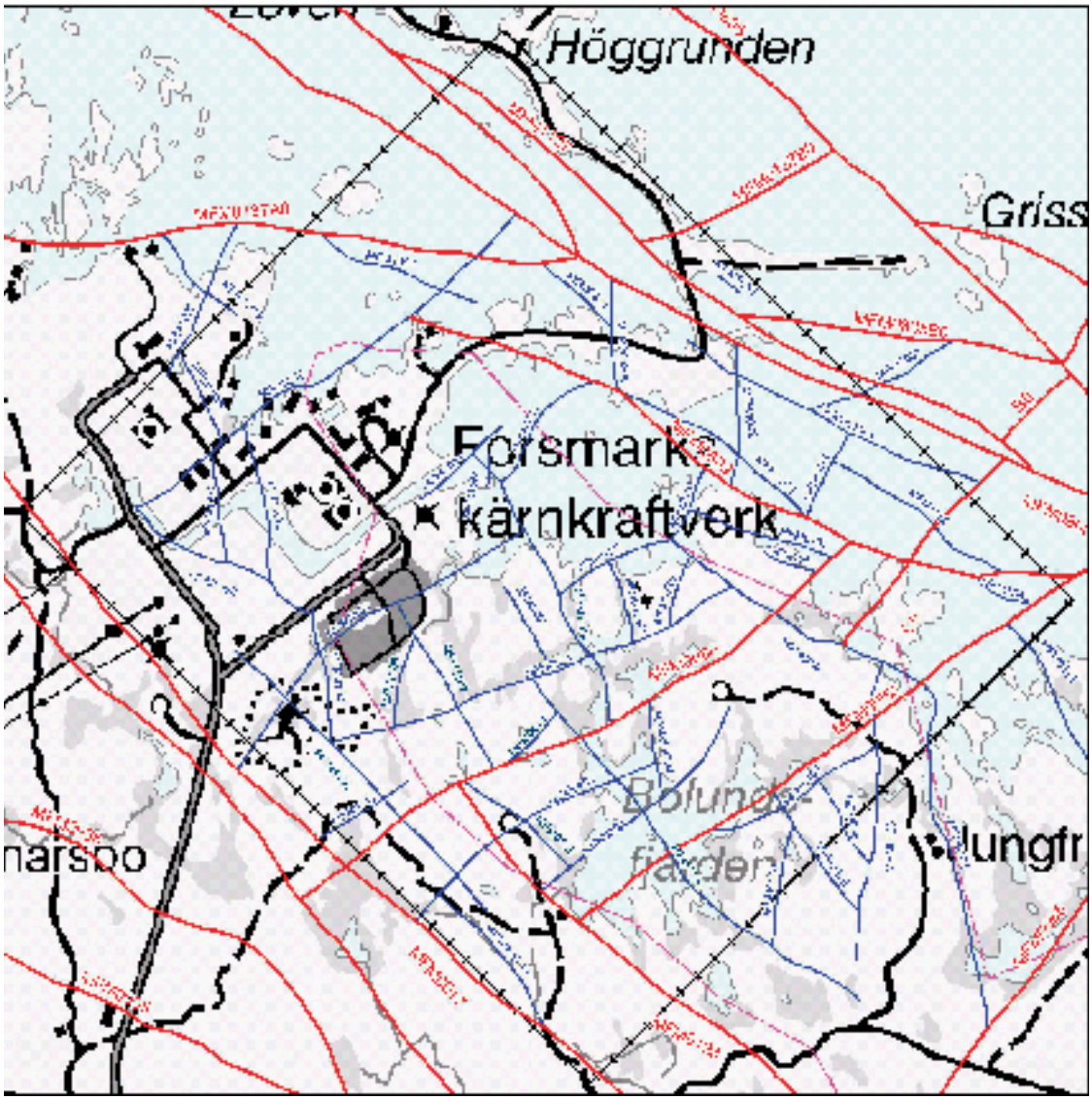

Figure 4. *Lineaments defined by magnetic minima inside the local model area, version 2.1. The lineaments marked in red are longer than 3 km. The lineaments marked in blue are shorter than 3 km. The boundaries of the local model area are marked with a black line. The lineament with NW trend through Bolundsfjärden (MFM1190) corresponds to a part of lineament LL0060 /Korhonen et al. 2004/.*

Hydrogeology

The key questions for the hydrogeology at the Forsmark site to be solved by the drilling and investigations along the new telescope borehole KFM01D are:

- To confirm whether the expected high transmissive structure in the superficial rock exists or not during the initial percussion drilling of the KFM01D borehole.
- To attain detailed hydraulic characterisation of the rock mass fractures as well as possible deformation zones penetrated by the subsequent core drilling of KFM01D, in particular in the central part of the repository area.

Hydrogeochemistry

Hydrogeochemical studies planned for borehole KFM01D include normal routine groundwater sampling and complete chemical characterisation from water-conducting deformation zones, possible sampling from low-conductive deformation zones, and the sampling and chemical characterisation of pore waters from the rock matrix.

In crystalline rocks, the pore water resides in the low-permeable rock matrix between principal water-conducting deformation zones related to regional or local deformation networks. Depending on the residence time of groundwater in these hydraulically-active deformation zones, interaction with water present in the pore space of the low-permeable rock matrix volume might become significant. In addition, the interconnected pore water present in the low-permeable rock matrix will be the first to interact with any artificial construction made in such rock volumes (i.e. the repository). For safety assessment considerations, it is therefore important to know the composition of such pore water and its evolution over the last thousands to hundreds of thousands of years. The latter can be assessed by combining the information gained from pore water profiles determined through a low-permeable rock matrix volume, with the chemical and isotopic data of groundwater circulating in the deformation zones.

The information obtained from sampling and characterising pore waters from borehole KFM01D should help to:

- Support the pore water chemical and isotopic trends already indicated from borehole KFM06A /Waber and Smellie 2005/, and obtain greater insight into the spatial distribution of pore water chemistry at the Forsmark site.
- Obtain important information from repository level, which may provide useful input to safety assessment calculations.
- Supplement information derived from normal routine hydrogeochemical characterisation and the characterisation of low-conductive deformation zones. Knowledge of these three hydrogeochemical components will make it possible for the first time to show the variation (or lack of variation) in groundwater chemistry in the same rock mass across the range of permeability from $> 10^{-9}$ m^2s^{-1} (normal routine sampling), c. 10^{-10}–10^{-9} m^2s^{-1} (sampling low-conductive zones) and 10^{-14}–10^{-10} m^2s^{-1} (pore water sampling).

A further long-time objective of pore water studies has been to analyse a continuous rock profile from a well defined, water-conducting deformation zone out into a homogeneous and low transmissive bedrock volume. By supplementing the normal parameters measured for pore water studies with helium and/or U-decay series analysis, it may be possible to detect in the bedrock surrounding the hydraulically-active deformation zone: a) the presence and extent of diffusion profile(s), and b) pore waters with a signature of residual Littorina Sea and/or cold climate recharge glacial melt water. For example, the extent of a diffusion profile (i.e. distance), together with a Littorina Sea signature (i.e. known time constraint), would provide a good estimate of solute diffusion rates over the past few thousands of years under undisturbed hydraulic and hydrogeochemical conditions. Diffusion profiles restricted to the U-decay-series will extend the time constraints to tens of thousands to hundreds of thousands of years.

Based on the reasoning above, it is recommended that, if a well defined, water-conducting deformation zone is intercepted during drilling, the opportunity should be taken to sample drillcore material along an approximately 15 m profile perpendicular to the zone and out into the adjacent rock matrix.

This distance of 15 m is based on conservative scoping diffusion calculations for a duration of up to 10 ka. An obvious difficulty is knowing when a suitable deformation zone has been located. This may be facilitated by integrating the known geology and structures in the adjacent boreholes KFM01A and KFM01B, which have already been characterised. Such an exercise may lead to a predicted depth of intersection with one or more important deformation zones in the immediate area. However, it should be noted that the bedrock below c. 350 m is hydraulically sterile in KFM01A and KFM01B and, for this reason, there is a possibility that sampling from a low conductive deformation zone may not be able to be carried out in KFM01D.

5.3.3 Activities to be completed during and after the drilling

Bedrock geology

A standard geological programme should be carried out following the drilling of KFM01D. This programme includes:

- Documentation of the character of the wall of the borehole using the Borehole Image Processing System (BIPS).
- Radar logging.
- Geophysical logging.
- Detailed geological mapping of rock types and both ductile and brittle structures.

Follow-up analytical work that characterise the mineralogical, geochemical, physical and rock mechanical properties of the bedrock along the borehole should be carried out after the geological mapping has been completed and after an assessment of the need for complementary data has been made.

Hydrogeology

Prior to the drilling of KFM01D, it is necessary to assure that the pressure monitoring in nearby boreholes is functioning up to the standards of a good interference test set-up. If high flow rates are encountered during the core drilling procedure, a few hours of flushing and water sampling should be allowed before proceeding with the drilling.

After the core drilling is completed, measurements with the Posiva Flow Log should be conducted allowing for high resolution (1 m/0.1 m) in/out-flow rate measurements and EC measurements. As soon as the hydrogeochemical programme is completed (see below), single-hole hydraulic testing with the Pipe String System equipment should be carried out using a telescoping measurement strategy (100 m, 20 m and 5 m).

Hydrogeochemistry

A special focus during the KFM01D drilling activity concerns the sample selection, sample preservation and laboratory procedures to be implemented in the hydrogeochemical work. The activities to be followed during and after drilling are described in detail in Appendix 1.

5.3.4 Choice of site and borehole orientation

In order to provide the necessary data described above, it is recommended that a new telescope borehole is drilled from drill site 1 and is identified as KFM01D (see Figures 1 and 2). The recommended co-ordinates, inclination, direction and length of KFM01D are listed in Table 1.

Table 1. Position, inclination, direction and borehole length of the recommended telescope borehole KFM01D.

Borehole	Drill site	Northing in RT 90, 2.5 gon V (m)	Easting in RT 90, 2.5 gon V (m)	Inclination (°)	Direction (°)	Borehole length (m)
KFM01D	1	6699530	1631397	55	035	800

It is anticipated that KFM01D will intersect zone ZFMNE00A2 close to the surface in the upper 100 m. It should also intersect different segments of zone ZFMNE0061 in the borehole interval c. 490–560 m (c. 400–460 m depth). If lineaments LL0060 and XFM0099A0 are related to deformation zones that are vertical, then these structures will be intersected at c. 630 m (c. 515 m depth) and c. 230 m (c. 190 m depth) borehole lengths, respectively.

5.3.5 References

Isaksson H, Thunehed H, Mattsson H, Keisu M, 2004. Interpretation of airborne geophysics and integration with topography. Stage 1 (2002). SKB P-04-29, Svensk Kärnbränslehantering AB.

Korhonen K, Paananen M, Paulamäki S, 2004. Forsmark site investigation. Interpretation of lineaments from airborne geophysical and topographic data. An alternative model within version 1.2 of the Forsmark modelling project. SKB P-04-241, Svensk Kärnbränslehantering AB.

SKB, 2005a. Preliminary site description. Forsmark area – version 1.2. SKB R-05-18, Svensk Kärnbränslehantering AB.

SKB, 2005b. Forsmark site investigation. Programme for further investigations of geosphere and biosphere. SKB R-05-14, Svensk Kärnbränslehantering AB.

Waber H N, Smellie J, 2003. Oskarshamn site investigation. Pore space groundwaters in low permeable crystalline rock in borehole KSH02 (Feasibility Study). SKB P-04-249, Svensk Kärnbränslehantering AB.

Waber H N, Smellie J, 2005. Forsmark site investiagtion. Borehole KFM06: Characterisation of pore water. Part I: Diffusion experiments. SKB P-05-196, Svensk Kärnbränslehantering AB.

Michael Stephens, Geological Survey of Sweden

John Smellie, Conterra AB

Sven Follin, SF GeoLogic AB

Marcus Laaksoharju, Geopoint AB

Uppsala, 2005-12-14

Appendix 1 – Procedures for the sampling, preservation and laboratory studies of rocks to be used in the characterisation of pore space fluids along borehole KFM01D

Sample selection and preservation

Sampling and selection requirements to characterise the pore space fluids or waters are basically quite simple but speed and care are necessary to prevent any potential evaporation of these fluids when the drillcore is first exposed to the atmosphere at the surface. Selection and preservation should be carried out within a maximum of 30–40 minutes following exposure. One obvious difficulty is ensuring that correct samples have been selected prior to knowing the geology and hydrology of the bedrock being drilled. Sampling and final selection will therefore be conducted in two stages:

- Sampling and preservation, and
- evaluation and final selection.

Two categories of sampling will be carried out, if conditions are favourable:

- Sampling of low permeable rock matrix at regular intervals along the borehole length, and
- sampling of rock material along a profile perpendicular from an established hydraulically-active deformation zone into the adjacent rock matrix, for a distance of approximately 15 m.

Category 1 sampling: Along the borehole length

In common with KFM06A, 40 cm samples will be collected approximately every 50 m along the full length of the borehole (i.e. approximately 800 m, see below). From this total of around 20 samples (normally more are sampled than required), a maximum of 16 will be selected for full analysis. The selection of these final samples will be based on the overall homogeneity of the bedrock and the absence of hydraulically-active deformation zones close to the selected samples. Experience from earlier studies will be implemented and final selection emphasis will be put on samples representing repository depths (400–600 m).

Stage 1. Sampling and preservation

This stage, by necessity, will be based on: a) an initial impression of the drillcore during drilling, and b) prior knowledge of the geology from other completed near-vicinity boreholes (e.g. KFM01A and KFM01B).

Sampling and selection should be carried out as follows:

- Core lengths (approximately 40 cm, with at least one of minimum 12 cm length) representative of the major lithological units, should be selected from macroscopically tight, homogeneous (if possible) and fracture-free portions of the rock matrix at least 15 m away from any water-conducting deformation zones. If a deformation zone occurs within 15 m from the collected sample (i.e. if the drillcore is particularly fractured and heterogeneous and this criterion can not be achieved) it should be documented.
- Samples should be selected from approximately every 50 m along the borehole although in practice this will vary based on the lithology and structures encountered; this may mean up to 20 samples for the total length of the borehole since it is better to take too many than too few. Selected samples sent to the University of Bern will be subject to an iterative process of judgment during drilling, i.e. if earlier selected samples are found to be unsuitable following continued drilling they will be withdrawn.
- The decision to withdraw any sample will be made by the field coordinator, Kenneth Åkerström, together with the assignment manager and the activity leader. The decision must be relayed to the project leader, Niklaus Waber, as soon as possible.

When a suitable rock matrix locality has been identified:

- The 40 cm core length should be removed quickly; if a 40 cm length is not available, smaller lengths may suffice, but not less than 12 cm.
- The core length should be gently wiped with a clean dry towel.
- No labelling should be made directly on the drillcore surface.
- Photographing the drillcore is optional providing it can be carried out rapidly at the site (within five minutes).
- The sample should be placed in a heavy-duty PVC plastic bag (about 0.5 mm thick).
- The plastic bag should be heat sealed leaving an opening for the flushing of nitrogen and the evaporation tube. If possible a rubber stopper can be attached to the tubes if the initial opening is too wide.
- The PVC bag is flushed with nitrogen gas to remove the air.
- The PVC bag should then be evacuated using a small rotary electrical pump to remove all the nitrogen gas. The evacuated bag should also be squeezed by hand to help remove any residual pockets of gas (the plastic bag must be tightly in contact with the core sample).
- The PVC bag should be permanently heat sealed (double or treble sealed as an extra precaution). This can be done when the evacuation tube still is in place to avoid oxygen entering the bag, i.e. by sealing the plastic bag below the inserted tube. Sealing of the drillcore sample should be completed within one hour of exposure.

- The packed sample should be placed inside an additional PVC bag and the evacuation and sealing procedure repeated.
- At this juncture a final check to the suitability of the sample can be made by the responsible geologist if sample selection has been made by personnel other than himself or herself.
- The sealed PVC plastic bag should be placed finally in a PVC plastic bag lined with aluminium foil.
- This outer aluminium foil plastic bag should be flushed with nitrogen, evacuated and heat sealed in a similar fashion as carried out for the previous two PVC plastic bags.
- Following each packing/sealing stage, the bags should be tightly taped around the preserved core.
- Each specimen package should be marked with a SKB number and also the length/depth interval sampled.
- The preserved drillcore length should be packed securely in a suitable portable box/tube and air freighted (pre-paid) as soon as possible to the laboratory at the University of Bern (ideally within 24 hours).
- When received at the University of Bern, the drillcore length will be prepared immediately for the diffusion experiment. If this is not possible, the sample will be stored under refrigeration (+1–5°C).
- The empty box/tube should then be returned by air freight for re-use.

Great care is required to avoid puncturing the plastic bag during preservation and transport. Since the drillcore portion will be selected from a homogeneous and fracture-free part of the rock matrix, its absence should not interfere with the subsequent drillcore mapping. Anything unusual about the removed core can be noted by the field personnel.

The required field equipment is listed below:

- Clean dry towel.
- Camera (optional).
- Thick heavy-duty PVC plastic bags (about 0.5 mm thick).
- Nitrogen gas.
- Small rotary electrical pump.
- Equipment for heat sealing.
- PVC plastic bags lined with aluminium foil.
- Re-usable case for reliable transport.

Stage 2. Evaluation and final selection

When drilling is completed and details of the core mapping, BIPS imaging and differential flow meter measurements become available, the final suitability of the selected drillcore samples undergoing diffusion leaching can be reassessed. The most suitable samples will continue being leached whilst those considered unsuitable will be removed and freighted back to Sweden where they will be returned to the core box.

The samples that are finally chosen for matrix water analysis should, by preference, represent the major lithological units as well as homogeneous and fracture-free parts of the drillcore.

Category 2 sampling: Along a rock profile perpendicular from a hydraulically-active deformation zone into the adjacent rock matrix

This will require detailed sampling of drillcore material along a rock profile perpendicular from an established hydraulically-active deformation zone into the adjacent rock matrix, for a distance of approximately 15 m. The extent of the profile to be sampled (i.e. 15 m) is based on conservative

diffusion scoping calculations assuming a period of 1–30 ka duration in rock matrix and using the pore diffusion coefficient derived from one of the KFM06A samples (/Waber and Smellie 2005/: $Dp = 1.3E^{-10}$ m^2s^{-1} at 20°C, $De = 3.9E^{-13}$ m^2s^{-1} at 20°C).

An obvious difficulty is knowing when a suitable deformation zone has been located. This may be facilitated by integrating the known geology and structures of the Forsmark site based on mapping, and interpolation and extrapolation of data from nearby boreholes already drilled and characterised (e.g. KFM01A and KFM01B). When the frequency of water-conducting deformation zones is high, there should be a minimum of 20–25 m separating, for example, two water-conducting deformation zones, thus allowing a 15 m profile to be selected into the rock matrix from one zone which is beyond the influence of the second zone.

Because of the potential difficulties that may be encountered, the following approaches are recommended:

- Since the upper 200–300 m of the bedrock close to drill site 1 has a high frequency of fractures, is affected by the gently dipping zone ZFMNE00A2 and possibly some minor deformation zones, and is hydraulically dynamic, there may be the problem of locating a hydraulically-active deformation zone sufficiently isolated within a low-permeable rock matrix unit. It is therefore suggested to concentrate at repository depths (300–600 m) in order to increase the probability of a more suitable location and to produce data more relevant to safety assessment issues. However, we are aware that the experience from KFM01A and KFM01B indicates that the bedrock at these depths is hydraulically sterile.
- An additional approach is to aim at the sampling of important deformation zones which are known to exist and are expected to be intercepted by the KFM01D drilling programme. The approximate depth of interception may be extrapolated from the on-going site interpretation (see below).
- When a suitable deformation zone is located, sampling should commence at some centimetres from the zone face (e.g. 3–5 cm) in order to preserve fracture filling material and the immediate rock matrix for mineralogical, petrographical and geochemical studies carried out elsewhere. It is envisaged that the total 15 m profile will be sampled and immediately prepared for packing and dispatch to Bern.
- On arrival at Bern, 20 cm lengths (i.e. minimum of 12 cm for the laboratory diffusion experiments and the remaining c. 8 cm for porosity determinations and general mineralogy) will be selected from a continuous 1.5 m profile close to the fracture (approximately 8 samples), followed by 20 cm lengths at regular distances to the end of the c. 15 m profile (i.e. additional 14 samples at one metre intervals). See Figure 5.
- The “Sampling and preservation” stage described for the Category 1 sampling above also applies to the rock profile samples.

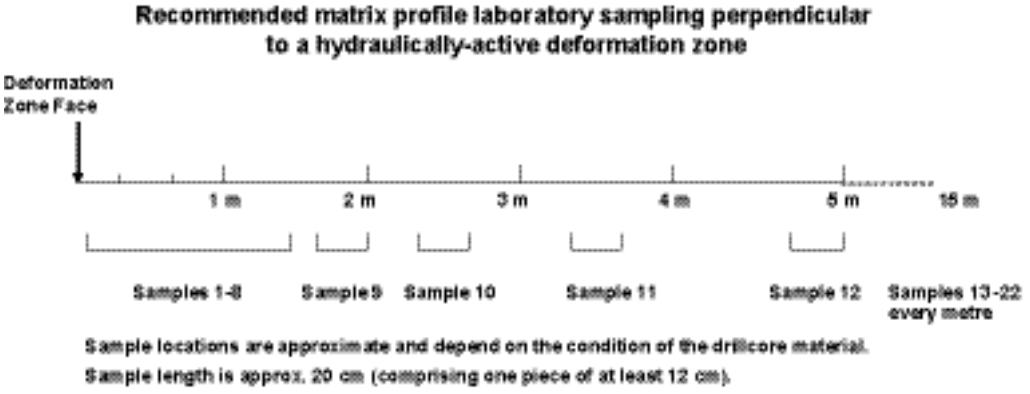

Figure 5. *Recommended laboratory sampling of matrix profile oriented perpendicular to a hydraulically-active deformation zone.*

Laboratory studies

Laboratory studies will be conducted at the University of Bern as follows:

- Out-diffusion laboratory studies will be carried out on all initially selected core samples representing both Category 1 and 2 sampling programmes. As indicated above, the number of samples will be reduced eventually to meet budgetry requirements based on additional information such as: a) the out-diffusion experiments themselves, b) drillcore mapping, c) BIPS-imaging, and d) differential flow meter measurements.
- In order to fully understand the nature of the matrix porewaters in the drillcore, knowledge of the relative volumes and the chemistry of the accessible and inaccessible fluids are important. Since the major lithological units of the Forsmark site have already been characterised in previous studies (cf. /Waber and Smellie 2005/), complete mineralogy, geochemistry and fluid inclusion studies of such material will not be required unless drilling reveals a hitherto unknown lithological unit not previously described and characterised.
- If a suitable hydraulically-active deformation zone profile is sampled, some additional basic mineralogy will be necessary to provide a background for interpretation of the matrix porewaters.
- Since the diffusion studies are non-destructive, all rock material eventually will be returned intact to the core boxes on completion of the laboratory investigations.

Mineralogy

Mostly completed from earlier studies although it may be necessary to provide additional data for the deformation zone profile studies. These data will comprise mainly petrographic and bulk/grain density studies of 3–5 core samples chosen from the total number of samples collected.

Inaccessible fluid volume (fluid inclusions)

Not included in this present programme as they have been already covered in previous investigations.

Total fluid volume

Not included in this present programme as they have been already covered in previous investigations.

Diffusion leaching experiments

Laboratory diffusion leaching experiments will be conducted on all drillcore samples to extract only the accessible, interconnected pore space fluids. Full details of the experimental procedures are given in /Waber and Smellie 2003/.

John Smellie, Conterra AB

Stockholm, 2005-12-13

5.4 Motivation for and orientation of telescope borehole KFM10A

5.4.1 Background

In accordance with the results of the initial site investigation (ISI) at Forsmark, including the site descriptive model (SDM) version 1.2 /SKB 2005a/, a decision was taken by SKB to focus the complete site investigation (CSI) to a target area (Figure 1) in the north-western part of the candidate area /SKB 2005b/.

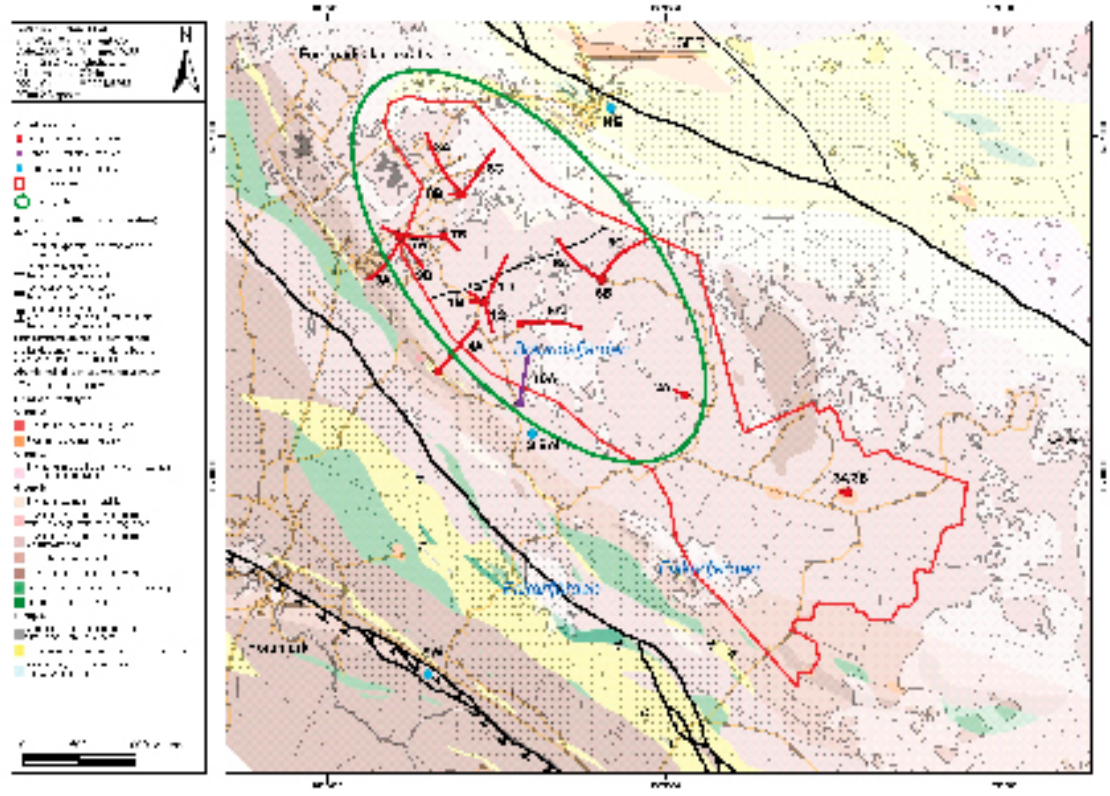

Figure 1. *Geological map of the bedrock inside and immediately around the candidate area at Forsmark (map version 1.2). Completed, ongoing, planned and possible telescope and cored boreholes as well as the target area, which is referred to as the priority site in /SKB 2005b/, are shown (modified after /SKB 2005b/). Telescope borehole KFM10A, which is addressed in this report, is included as a planned borehole.*

In a series of decision and motivation documents, an extensive core drilling programme at five separate sites (DS1, DS6, DS7, DS8 and DS9) was planned in the target area (see SKB documents 1024611, 1038014, 1038090, 1039868, 1045795 and 1048162). At the time of writing of the present document, all boreholes have been or are being drilled (Figure 1). These boreholes complement the telescope and cored boreholes KFM01A/KFM01B (DS1), KFM02A (DS2), KFM04A (DS4), KFM05A (DS5) and KFM06A/KFM06B (DS6), which are also situated wholly or partly inside the target volume and which were drilled during the ISI.

5.4.2 KFM10A − general motivation and choice of drill site

Following interactive discussions at the Forsmark site between the modelling group and personnel responsible for the site investigations, there has crystallised a need for better control on the geological and hydrogeological conditions along the major fracture zone ZFMNE00A2. The first indications of this water-bearing zone emerged in connection with the stage 1 seismic reflection work at Forsmark /Juhlin et al. 2002/, and its geometry and character were documented during the SDM version 1.2 work. Selection of a drill site to investigate zone ZFMNE00A2 should also take into account the generation of new, subsurface data, in order to improve our understanding of the character of lineaments. A focus on any lineament that is longer than 3,000 m needs to be prioritised.

Several cored and percussion boreholes confirm that zone ZFMNE00A2 intersects the surface close to DS1, DS5 and DS6, and is present at a depth of c. 500 m along borehole KFM02A (DZ6 in the single hole interpretation, /Carlsten et al. 2004a/). It has also been inferred to intersect borehole KFM04A at a depth of c. 180 m (DZ1, DZ2 and DZ3 in the single hole interpretation, /Carlsten et al. 2004b/). Interference tests confirm a hydrogeological contact along zone ZFMNE00A2 between the bedrock close to the surface at DS1 and DS6, and the bedrock at c. 500 m depth along KFM02A /Rouhiainen and Sokolnicki 2005, Gokall-Norman and Ludvigson 2005, Gokall-Norman et al.

2005a/. However, hydrogeological contact appears to be absent along ZFMNE00A2 between the boreholes close to DS1 and borehole KFM04A at DS4 /Gokall-Norman et al. 2005b /. The possibility that one or more steeply dipping zones situated between these two sites accounts for the change in the hydrogeological character of zone ZFMNE00A2 must be considered.

On the basis of the seismic reflection and borehole data, it can be inferred that zone ZFMNE00A2 dips gently (24°) towards the south (170°). The occurrence of this zone along a vertical cross-section in a NW-SE direction, inside the target volume, is shown in Figure 2. Zone ZFMNE00A2 effectively forms a roof to the preliminary repository layout that has been placed at 400 m depth inside the target volume. The location of the south-eastern limit of the repository layout is defined by a combination of the gently dipping zone ZFMNE00A2 and the steeply dipping fracture zone ZFMNE0062A (Figure 3).

Bearing in mind the above considerations, it is recommended that a cored borehole is drilled at a site that is situated either directly to the south-west or south-east of Bolundsfjärden, in the south-eastern part of the target area. Since both drilling and excavation work has been carried out in connection with the investigation of zone ZFMNE0062A, a drill site to the south-west of Bolundsfjärden that can permit an investigation of one or more of the lineaments in this area is preferred. Choice of a drill site to the south-west of Bolundfjärden is also favoured from environmental and infrastructural considerations.

5.4.3 What are the key questions to be solved with the drilling

Bedrock geology

From a geological perspective, the prime aim of borehole KFM10A is to provide base geological information bearing on the character of zone ZFMNE00A2 at a depth close to that preliminarily envisaged for the repository. These new data will complement the geological information at both shallower and deeper crustal levels along the zone and, thereby, shed more light on the questions concerning heterogeneity in properties along important deformation zones, in particular zone ZFMNE00A2.

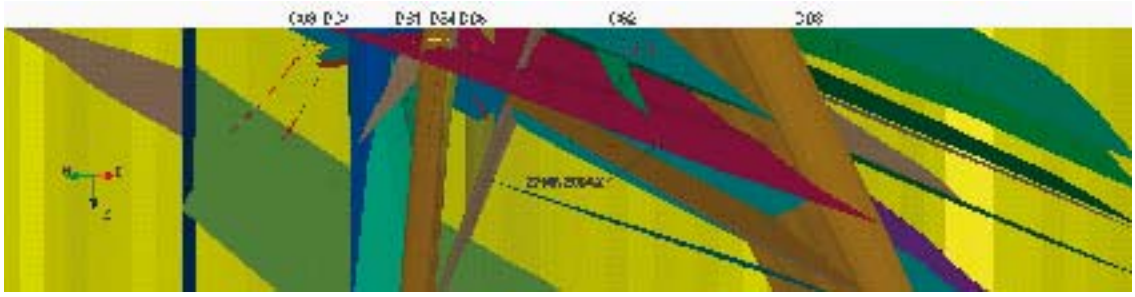

Figure 2. *View to the north-east of the three-dimensional deformation zone model, version 2.1. The figure shows a selected number of gently and steeply dipping fracture zones that strike ENE and NE, and transect the candidate volume. The gently dipping zone ZFMNE00A2 is marked. The complex Singö deformation zone (ZFMNW0001), with both ductile and brittle deformation, is present in the background (yellow shade).*

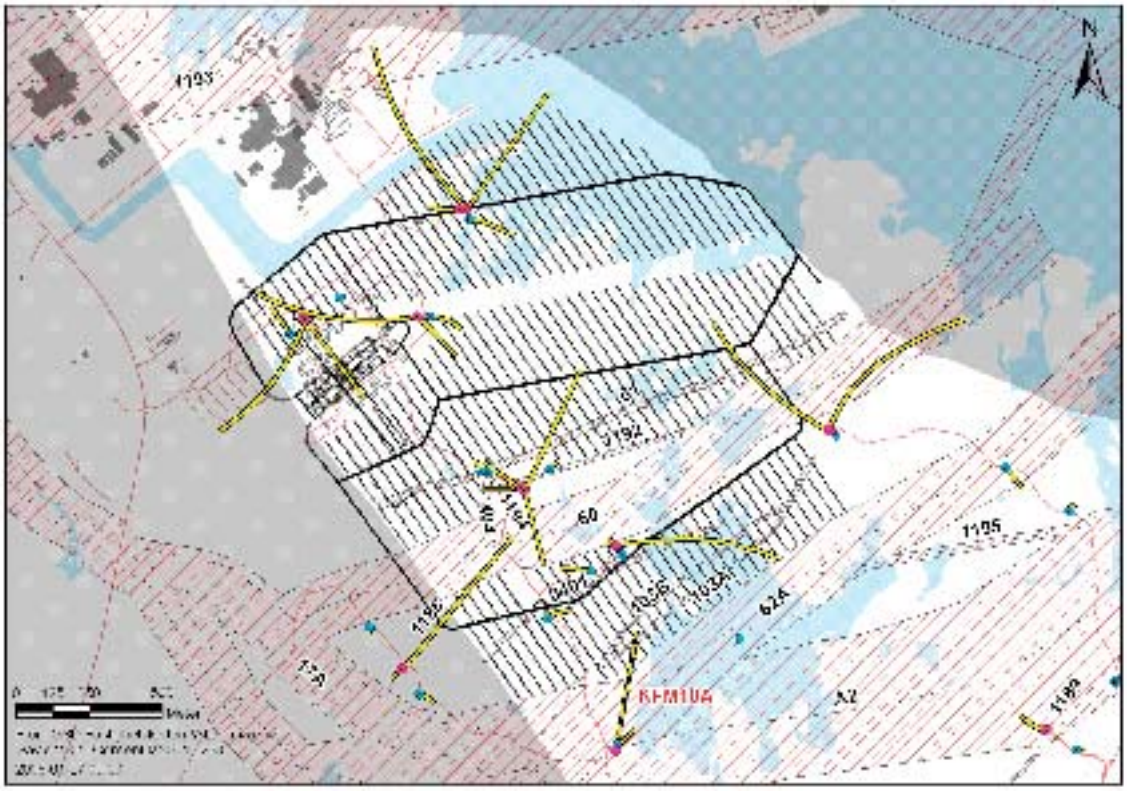

Figure 3. *Possible repository layout at 400 m depth inside the target volume. The intersection of the various deformation zones (A2, 62A etc), and the respective safety intervals for the zones longer than 3,000 m, are also shown at this depth. The repository layout is based on the results of SDM, version 1.2. Note how the south-eastern limit of the repository layout is dictated by the projection of the fracture zones ZFMNE00A2 and ZFMNE0062A at 400 m depth. All boreholes, including KFM10A that is addressed in this report, are shown. The boreholes are projected up to the ground surface.*

Bearing in mind the results from previous drilling activities as well as excavation work, only lineaments defined by magnetic minima have been utilised in the modelling of deformation zones during SDM version 2.1 (Figure 4). A borehole sited immediately to the south-west of Bolundsfjärden can be oriented so as to test the character of some of the lineaments in this area.

Lineament MFM0123 with a north-westerly trend occurs within but close to the south-western margin of the target area (Figure 4). It is longer than 3,000 m. It has been modelled as a deformation zone and is inferred to intersect borehole KFM04A at DZ5, as recognised in the single hole interpretation /Carlsten et al. 2004b/. The shorter lineaments MFM0133 and MFM0103 with north-westerly and north-easterly trends, respectively (Figure 4), have also been modelled as minor deformation zones, ZFMNW0133 and ZFMNE0103A, respectively, in model version 2.1. Zone ZFMNW0133 is inferred to intersect borehole KFM04A along the interval 980–984 m, while different segments of zone ZFMNE103 (segments A and B) are interpreted to intersect borehole KFM05A along intervals 685–720 m and 590–616 m, respectively. These highly fractured and altered sections occur along DZ3, as recognised in the single hole interpretation /Carlsten et al. 2004c/.

The planned borehole KFM10A serves to verify the modelling of, at least, deformation zone ZFMNW0123 (see below) that is expressed at the surface as a magnetic lineament. The borehole may also provide an assessment of how much the character of this zone varies along its strike. With the version 2.1 model in mind, borehole KFM10A fails to intersect the minor zones ZFMNE0103A and ZFMNW0133.

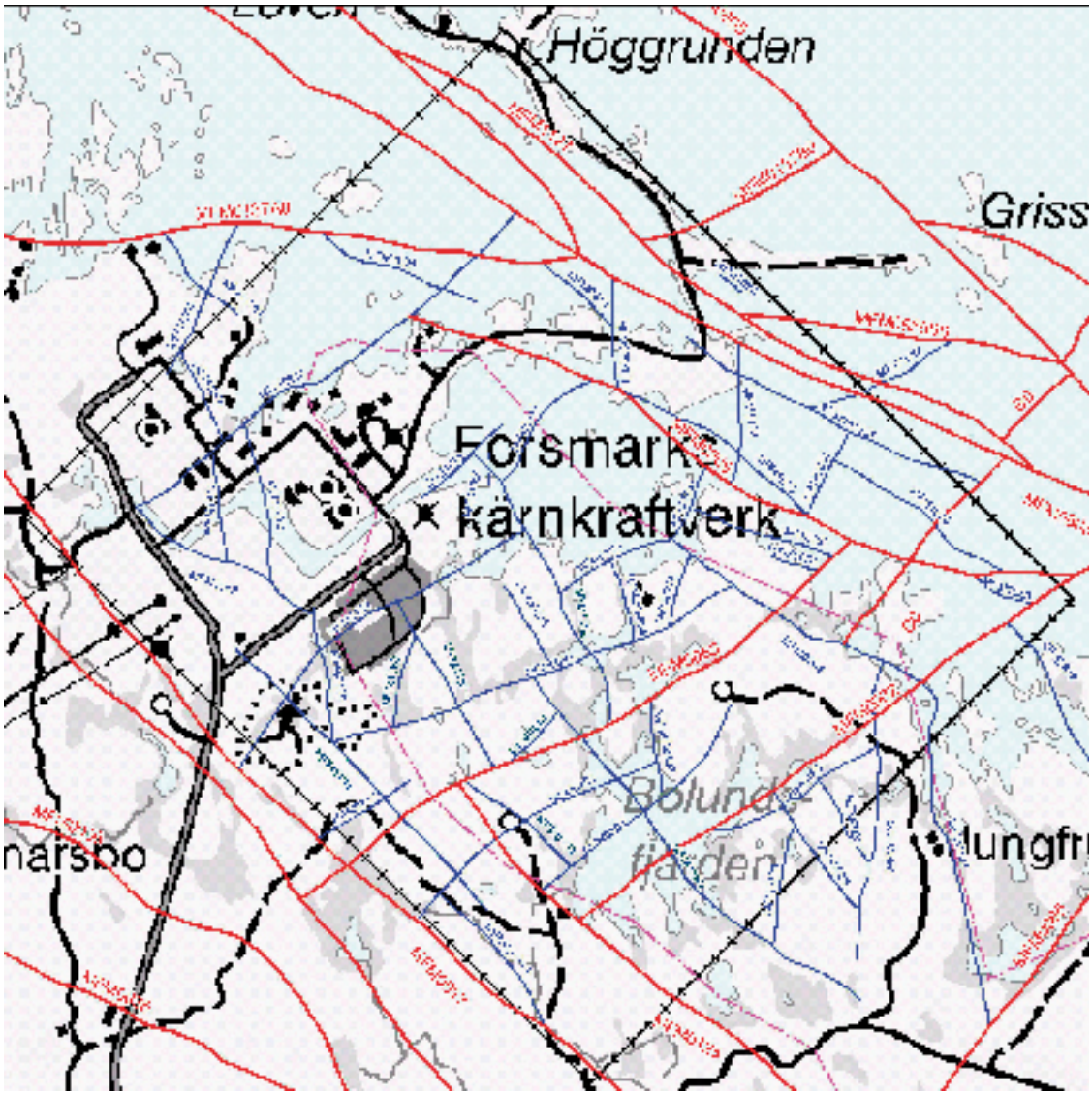

Figure 4. *Lineaments defined by magnetic minima inside the local model area, version 2.1. The lineaments marked in red are longer than 3,000 m. The lineaments marked in blue are shorter than 3,000 m. The boundaries of the local model area are marked with a black line. Note the occurrence of lineaments MFM0123, MFM0133 and MFM0103 close to the minor road south-west of Bolundsfjärden.*

Hydrogeology

The key questions for the hydrogeology at the Forsmark site to be solved by the drilling and investigations along the new telescope borehole KFM10A are:

- To confirm whether highly transmissive structures in the superficial rock exist or not during the initial percussion drilling of the KFM10A borehole.
- To attain detailed hydraulic characterisation of the rock mass fractures as well as possible deformation zones penetrated by the subsequent core drilling of KFM10A. Of particular interest are the geological, geometrical and hydraulic properties of zone ZFMNE00A2 with regard to the experiences gained in the KFM02A borehole.

5.4.4 Activities to be completed during and after the drilling

Bedrock geology

A standard geological/geophysical programme for the study of the bedrock in boreholes should be carried out, following the drilling of KFM10A. This programme includes:

- Documentation of the character of the wall of the borehole using the Borehole Image Processing System (BIPS).
- Radar logging.
- Geophysical logging.
- Detailed geological mapping of rock types and both ductile and brittle structures.

Follow-up analytical work that characterise the mineralogical, geochemical, physical and rock mechanical properties of the bedrock along the borehole should be carried out, after the geological mapping has been completed and after an assessment of the need for complementary data has been made. It is recommended that, after the single hole interpretation has been completed, attention is focused in follow-up work on the character of all the deformation zones intersected during the drilling, in particular zone ZFMNE00A2. This should include an assessment of the style of deformation along a zone, a description of the character of any fault rocks, a kinematic study, and a detailed assessment of the mineral fillings along different orientation sets of fractures within a zone. If deemed appropriate, mineral samples should be separated for geochronological work with the aim to gain some constraints on the timing of movement along zone ZFMNE00A2.

Hydrogeology

Prior to the core drilling of the KFM10A borehole, it is necessary to assure that the pressure monitoring in nearby boreholes is functioning up to the standards of a good interference test set-up, in particular the KFM02A borehole. If high flow rates are encountered during the core drilling procedure, a few hours of flushing and water sampling should be allowed before proceeding with the drilling.

After the core drilling is completed, measurements with the Posiva Flow Log (PFL) should be conducted allowing for high resolution (1 m/0.1 m) in/out-flow rate measurements and EC measurements. If a hydrogeochemical programme is decided to be carried out based on the drilling and PFL results, single-hole hydraulic testing with the Pipe String System equipment should be carried out as soon as the hydrogeochemical programme is completed using a telescoping measurement strategy (100 m, 20 m and 5 m).

5.4.5 Choice of site and borehole orientation

In order to provide the necessary data described above, it is recommended that a new telescope borehole is drilled from drill site 10 and is identified as KFM10A (see Figures 1 and 3). The recommended co-ordinates, inclination, direction and length of KFM10A are listed in Table 1.

It is anticipated that KFM10A will intersect zone ZFMNE00A2 at c. 340−410 m borehole length and zone ZFMNW0123 at c. 90−100 m borehole length.

Table 1. Position, inclination, direction and borehole length of the recommended telescope borehole KFM10A.

Borehole	Drill site	Northing in RT 90, 2.5 gon V (m)	Easting in RT 90, 2.5 gon V (m)	Inclination (°)	Direction (°)	Borehole length (m)
KFM10A	10	6698641	1631710	50	010	c. 650

5.4.6 References

Carlsten S, Petersson J, Stephens M B, Mattsson H, Gustafsson J, 2004a. Geological single-hole interpretation of KFM02A and HFM04–5 (DS2). SKB P-04-117, Svensk Kärnbränslehantering AB.

Carlsten S, Petersson J, Stephens M B, Mattsson H, Gustafsson J, 2004b. Geological single-hole interpretation of KFM04A and HFM09–10 (DS4). SKB P-04-119, Svensk Kärnbränslehantering AB.

Carlsten S, Petersson J, Stephens M B, Thunehed H, Gustafsson J, 2004c. Geological single-hole interpretation of KFM05A, HFM14–15 and HFM19 (DS5). SKB P-04-296, Svensk Kärnbränslehantering AB.

Gokall-Norman K, Ludvigsson J-E, 2005. Hydraulic interference tests. Boreholes HFM16, HFM19 and KFM02A. Forsmark site investigation. SKB P-05-78, Svensk Kärnbränslehantering AB.

Gokall-Norman K, Ludvigsson J-E, Jönsson S, 2005a. Hydraulic interference test in borehole HFM01. Forsmark site investigation. Manuscript submitted, SKB P-05-XX, Svensk Kärnbränslehantering AB.

Gokall-Norman K, Ludvigsson J-E, Jönsson S, 2005b. Hydraulic interference test. Boreholes KFM04A, HFM10, HFM13, HFM19 and HFM252. Forsmark site investigation. Manuscript submitted, SKB P-05-186, Svensk Kärnbränslehantering AB.

Juhlin C, Bergman B, Palm H, 2002. Reflection seismic studies in the Forsmark area – stage 1. SKB R-02-43, Svensk Kärnbränslehantering AB.

Rouhiainen P, Sokolnicki M, 2005. Difference flow logging in borehole KFM02A during pumping in HFM16. Forsmark site investigation. SKB P-05-37, Svensk Kärnbränslehantering AB.

SKB 2005a. Preliminary site description. Forsmark area – version 1.2. SKB R-05-18, Svensk Kärnbränslehantering AB.

SKB 2005b. Forsmark site investigation. Programme for further investigations of geosphere and biosphere. SKB R-05-14, Svensk Kärnbränslehantering AB.

Michael Stephens, Geological Survey of Sweden

Sven Follin, SF GeoLogic AB

Assen Simeonov, Svensk Kärnbränslehantering AB

Uppsala, 2006-01-26

5.5 Motivation for and orientation of telescope borehole KFM02B

5.5.1 Background

In accordance with the results of the initial site investigation (ISI) at Forsmark, including the site descriptive model (SDM) version 1.2 /SKB 2005a/, a decision was taken by SKB to focus the complete site investigation (CSI) to a target area (Figure 1) in the north-western part of the candidate area /SKB 2005b/.

One of the key issues addressed in the CSI programme is the need to deepen our understanding of the state of stress at the Forsmark site. A key issue concerns the possible influence of larger deformation zones on the state of stress. It has been indicated by scooping modelling that the gently dipping deformation zone ZFMNE00A2 may have a significant influence on the concentration of stress in the bedrock (Figure 2). It is suggested that this gently dipping zone influences the in situ stresses, such that below the zone there is a stress concentration and a significant influence of stress release as the surface is approached (see also Figure 3). The present stress measurement results do not provide sufficient resolution to support the possibility to have differences in stress magnitudes on each side of deformation zone ZFMNE00A2. Thus, it was concluded in the CSI programme that an additional borehole that could provide stress measurements with both overcoring and hydraulic methods

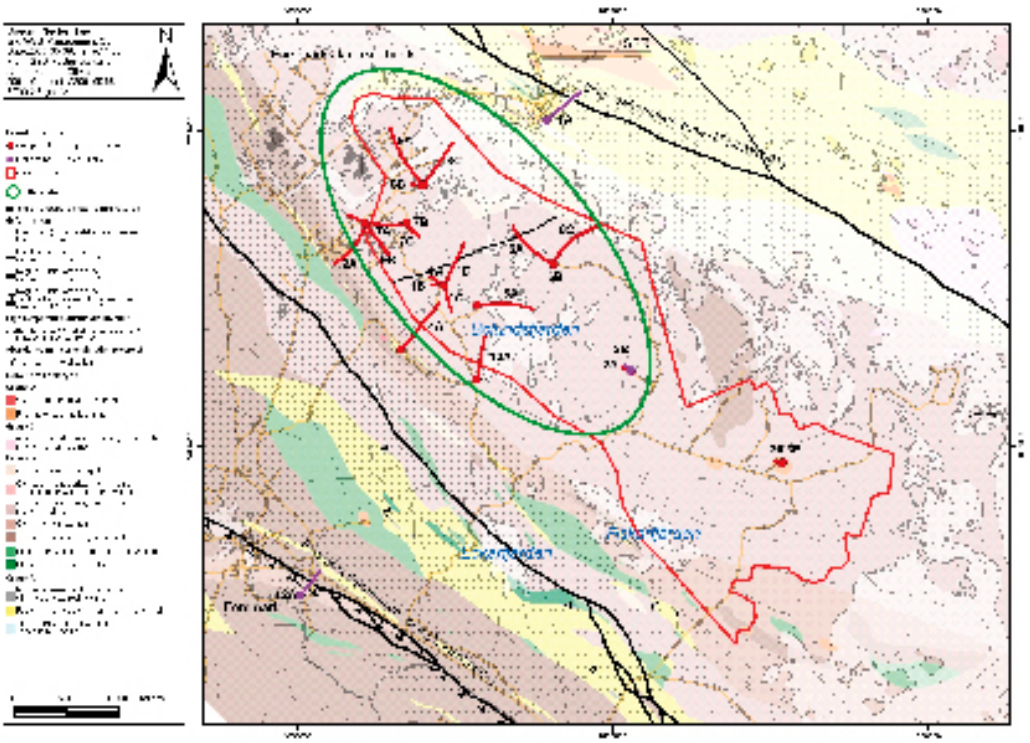

Figure 1. *Geological map of the bedrock inside and immediately around the candidate area at Forsmark (map version 1.2). Completed and ongoing telescope and cored boreholes as well as the target area in /SKB, 2005a/ are also shown. The planned borehole KFM02B, which is addressed in this document, is included on the map.*

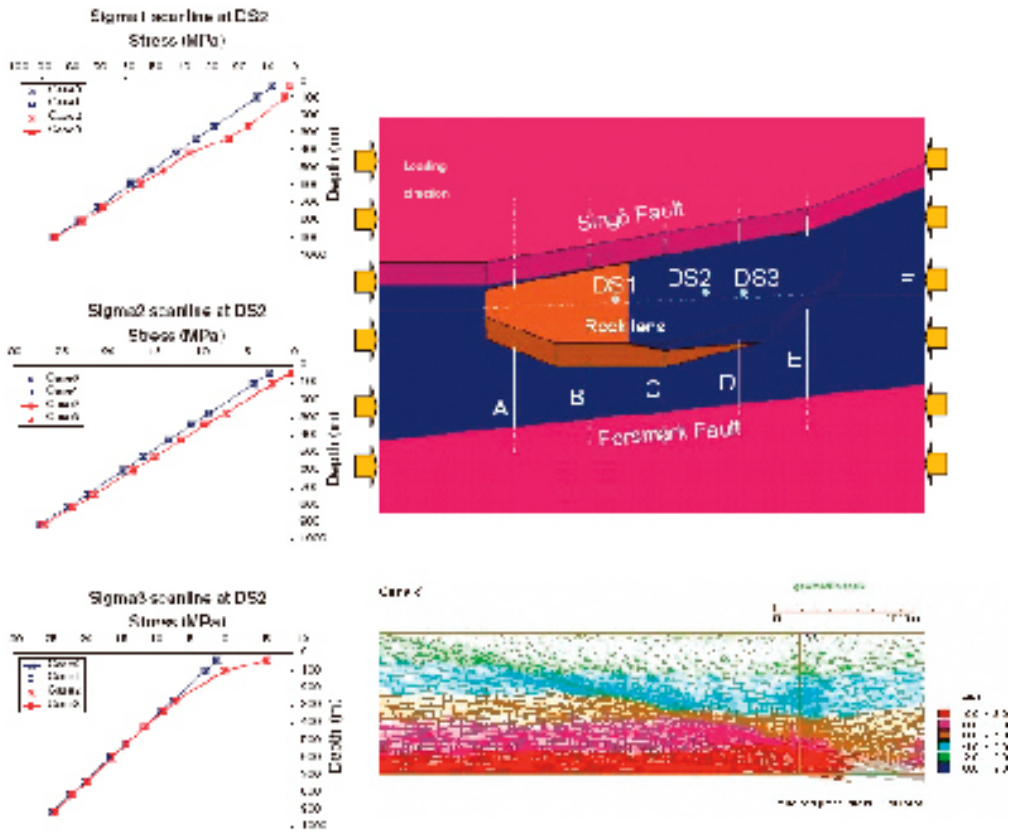

Figure 2. *Summary of the 3DEC modelling for the simplified geometry of the Forsmark regional area (top). The principal stresses along the scan line DS 2 are shown on the left. At the bottom, a plot of the stress directions on a vertical cross section along scan line F is shown. Please note that the picture refers to slightly different cases (see Figure 6-18 in /SKB 2005a/).*

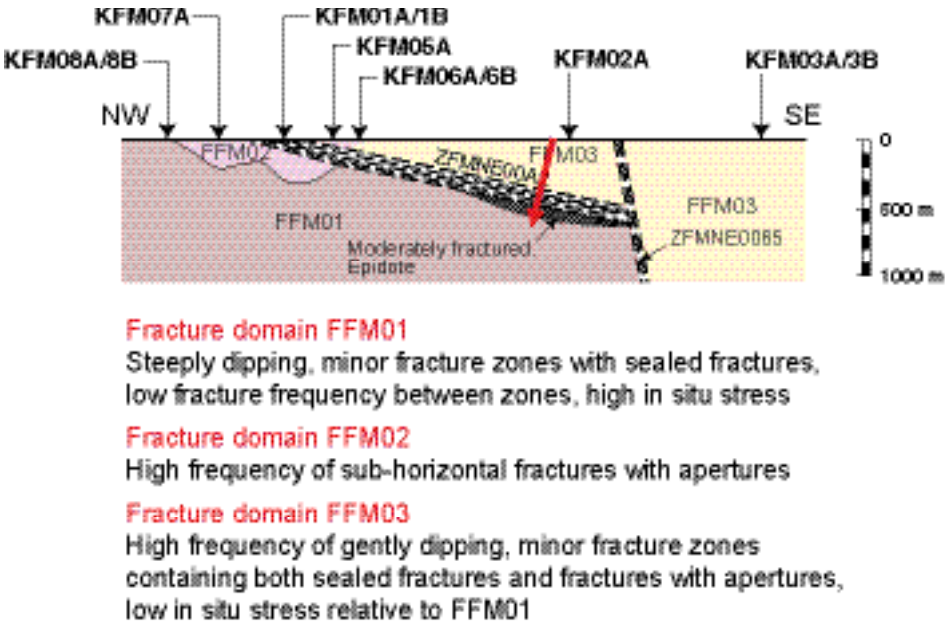

Figure 3. *Approximate location of borehole KFM2B (red arrow).*

above deformation zone ZFMNE00A2 would be valuable. This would then permit a comparison to be made with the data in the focused area for a tentative repository that is situated beneath zone ZFMNE00A2.

5.5.2 General motivation, key questions and choice of drill site

Stress measurements

Investigations in the north-western target area at Forsmark have shown that the uppermost part of the bedrock, down to c. 100−200 m depth, contains a high concentration of sub-horizontal and gently dipping fractures with large apertures. It is considered necessary to carry out stress measurements at the new drill site beneath such a superficial rock mass. The possible limitation for the overcoring method may be between 400 and 500 m, if the stresses are not too high. A siting of the borehole such that it penetrates the deformation zone ZFMNE00A2 around 400–500 m depth would allow for the possibility to perform stress measurements by overcoring below the superficial rock mass and down to the gentle dipping zone ZFMNE00A2, such that both stress magnitudes and gradients can be determined. The results should be directly comparable with previous results from overcoring in KFM01B and the ongoing measurements in borehole KFM07C.

The original plan was to carry out measurements in borehole KFM10A, but this was abandoned due to various reasons, for example, the need for hydrogeological monitoring in this borehole. The choice of drill site 2 was considered as a better alternative, not only due to logistics in the field work, but also due to the previous stress measurement results with hydraulic methods in borehole KFM02A and the fact that drill site 2 is located closer to the centre of the tectonic lens. Overcoring results would permit a direct comparison with the results from hydraulic methods. In addition, if further stress measurements with hydraulic methods are completed at a later stage, a larger HTPF inversion could be carried out, using data from both boreholes. The choice of drill site 2 also reduces uncertainty in the location of deformation zone ZFMNE00A2, which is known to intersect KFM02A at c. 400–500 m depth.

Bedrock geology

From a geological point of view, choice of a borehole close to KFM02A will provide a possibility to understand better the geometry of the vuggy metagranite body that was observed along the borehole intervals 171–180 m and 247–302 m in KFM02A /Möller et al. 2004/. The geometry of this geological phenomenon at the Forsmark site remains poorly understood.

A standard geological/geophysical programme for the study of the bedrock in boreholes should be carried out, following the drilling of borehole KFM02B. This programme should include:

- a documentation of the character of the wall of the borehole using the Borehole Image Processing System (BIPS),
- radar logging,
- geophysical logging,
- detailed geological mapping of rock types and both ductile and brittle structures.

Follow-up analytical work that characterise the mineralogical, geochemical, physical and rock mechanical properties of the bedrock along each borehole should be carried out, after the geological mapping has been completed and after an assessment of the need for complementary data has been made.

Hydrogeology

From a hydrogeological point of view, the position of the KFM02B borehole is interesting because of its proximity to the KFM02A borehole. The KFM02A borehole was investigated hydraulically with the PFL method as well as with the PSS method during the ISI stage. The knowledge acquired from these investigations has resulted in a multipacker installation, which has been used for interference tests as well as dilution tests during the CSI stage. By the drilling and hydraulic testing of the KFM02B borehole, it will be possible to make geometrical (structural) and hydraulic comparisons with the findings reported from the investigations in the KFM02A borehole. It is absolutely essential that the multipacker installation in the KFM02A borehole is operating throughout the drilling and testing of the KFM02B borehole.

In the preliminary plans for the KFM02B borehole a wider diameter will be used in the uppermost part (telescope drilling). This will allow for a multipacker installation as soon as all other investigations have been completed. A wider diameter also allows for hydraulic testing with the PFL method. However, due to the limited time frame allocated for detailed investigations in Forsmark prior to the 2.3 data freeze, hydraulic measurements with the PFL method are not planned to be conducted in the KFM02B borehole. All hydraulic testing during the remaining part of the CSI stage will be made with the PSS method.

Of particular interest, though not explicitly planned to be a part of the CSI stage, is the possibility to conduct cross-hole interference tests at "repository depth" between the two boreholes. The expectations are to intersect the ZFMNE00A2 deformation zone also in the KFM02B borehole depth. This zone occurs between c. 400–500 m depth in the KFM02A borehole. Another potential use of the multipacker installation is dilution measurements in borehole KFM02A while drilling borehole KFM02B.

Hydrogeochemistry

Borehole KFM02B is primarily for rock mechanic studies but will also be available for porewater sampling and sampling from fractures of low hydraulic conductivity (lower limit of 10^{-9} ms^{-1}); groundwater characterisation has already been carried out in borehole KFM02A which is located in the near-vicinity of the planned KFM02B borehole, although not exactly in parallel. Drilling of the borehole is scheduled for August/September, 2006.

The borehole is planned to drill through the gently dipping deformation zone ZFMNE00A2 and to extend into the underlying low-transmissive bedrock for a further 100–200 m. Porewater samples will be collected intermittently above and through the c. 100 m wide zone ZFMNE00A2. When the termination of zone ZFMNE00A2 is close (approximated position extrapolated from nearby borehole geological data), core samples will be taken continuously until some 30 m into the underlying low-transmissive bedrock mass. The extent of the profile to be sampled (i.e. 30 m) is based on chloride diffusion calculations carried out for durations of 1 ka, 5 ka, 10 ka and 30 ka in rock matrix using the pore diffusion coefficient derived from a KFM06A matrix sample (Dp = $1.3E^{-10}$ m^2/s at 20°C, De = $3.9E^{-13}$ m^2/s at 20°C; /Waber and Smellie 2005/).

The individual samples collected and the continuous core length sampled will be preserved immediately during drilling and placed under refrigeration at a temperature of +1° to +5°C. Following completion of the borehole a decision will be taken based on differential flow meter logging as to which samples are most suitable for analysis. These will be sent to Bern.

At this juncture, it is not possible to estimate the number of samples required for analysis because of the unknown dimensions and complexity of zone ZFMNE00A2 and the nature of the bedrock underlining the zone. One of many uncertainties is the effect of an inferred lens of moderately fractured bedrock with epidote-filled fractures immediately under zone ZFMNE00A2 at the chosen location of the borehole (Figure 3).

As mentioned above, borehole KFM02B is intended for rock mechanic measurements where in situ rock stress is inferred to be lower above zone ZFMNE00A2 than below it. This variation in stress field, especially at depth below this zone, may have an important influence on the porewater chemistry. Rock core stress-release during and immediately following drilling may result in: a) some ingress of drilling water into the outer margin of the core sample, b) an enhanced measured porosity value, and c) a calculated dilution of the porewater due to using an erroneously high porosity value. At the moment these potential repercussions are not known with certainty.

To try and test for these uncertainties, triaxial measurements will be carried out on the extracted rock core material to determine the volumetric extension of core samples immediately following drilling. In addition, it is hoped that core sample splits will be measured for connected porosity at two independent laboratories (Bern and Borås) as soon as possible following extraction. The measurement will be repeated at regular intervals for some weeks to check if there is any change in porosity with time that may reflect gradual changes in rock stress-release. Lastly, the drilling water will be spiked with tracers to test for direct contamination of the porewater during drilling (see below).

Spiked drilling water

Based on the experiment carried out at the Äspö HRL (TD AP F47-05-010), some drilling water (spiked with uranine, iodide and bromide) was shown to have penetrated into the outer margins of the studied drill cores, but this was restricted to the width of the outer grain-size layer. The larger the rock minerals, the greater the expected effect. Even so, the total effect in terms of the volume of contaminating fluid was very small. However, this experiment was run under conditions of low rock stress and low drilling water pressure where marked effects might not be expected. To follow through with this type of study under realistic in situ conditions, it is proposed to drill borehole KFM2B using spiked drilling water. Uranine is routinely used although unfortunately the concentration used is normally too small (0.2 mg/L) to detect in the extracted porewater. Even if the concentration is increased to 5 mg/L it is still to low. Of iodide and bromide, bromide is not recommended as it is naturally present in sizeable quantities in the medium to deep Forsmark groundwaters. Iodide (as sodium iodide) is therefore recommended but concentration levels need to be around 1,000 mg/L. Furthermore, it is advisable not to use the tracer at shallow depths where increased transmissivities will probably dilute the drilling water. It is best to restrict its usage from around 300–600 m vertical depth.

Borehole location, orientation and length

In order to carry out stress measurements using hydraulic methods, drilling of a steeply inclined borehole is favoured. It is also considered desirable that the borehole is drilled in a direction close to the estimated trend of the principal horizontal stress (NW–SE). Drilling in a NW direction will provide a favourable intersection angle to the deformation zone ZFMNE00A2 that dips gently to the SSE /SKB 2005a/. It was decided to carry out the drilling down to approximately 650 m depth, to allow for stress measurements with hydraulic methods both above and below zone ZFMNE00A2. It is also considered important to allow for a safety distance of at least c. 5 m as the minimum distance between the boreholes, so that hydraulic fracturing would not cause hydraulic connection to borehole KFM02A. These considerations have motivated the location, orientation and length of borehole KFM02B at drill site 2 (Table 1).

Table 1. Position, inclination, direction and borehole length of telescope borehole KFM02B.

Borehole	Drill site	Northing in RT 90, 2.5 gon V (m)	Easting in RT 90, 2.5 gon V (m)	Inclination (°)	Direction (°)	Borehole length (m)
KFM02B	2	6698728	1633178	80	312	650

5.5.3 References

Möller C, Snäll S, Stephens M B, 2004. Dissolution of quartz, vug formation and new grain growth associated with post-metamorhic hydrothermal alteration in KFM02A. Forsmark site investigation. SKB P-03-77, Svensk Kärnbränslehantering AB.

SKB, 2005a. Preliminary site description Forsmark area – version 1.2. SKB R-05-18, Svensk Kärnbränslehantering AB.

SKB, 2005b. Programme for further investigations of geosphere and biosphere. Forsmark site investigation. SKB R-05-14, Svensk Kärnbränslehantering AB.

Waber N, Smellie J, 2005. SKB Site Investigations Forsmark. Borehole KFM06: Characterisation of pore water. Part I: Diffusion experiments. SKB P-05-196, Svensk Kärnbränslehantering AB.

Rolf Christiansson, Svensk Kärnbränslehantering AB

Sven Follin, SF GeoLogic AB

Marcus Laaksoharju, Geopoint

John Smellie, Conterra AB

Michael Stephens, Geological Survey of Sweden

Stockholm 2006-05-09

5.6 Motivation for and orientation of two deep telescope boreholes KFM11A and KFM12A

5.6.1 Background

The Singö and Forsmark deformation zones constitute the two most important geological discontinuities in the crystalline bedrock at Forsmark. Furthermore, the Forsmark deformation zone corresponds to a marked topographic break along which a disturbance in the sub-Cambrian peneplain is apparent /SKB 2002/. Figure 1 shows the location of the Singö and Forsmark deformation zones with regard to the target area for the ongoing complementary site investigations (CSI) in the northwestern part of the candidate area.

The Singö and Forsmark deformation zones do not intersect the candidate area and were not investigated geologically and hydrogeologically by means of boreholes and subsequent hydraulic tests during the 0, 1.1 and 1.2 modelling stages /SKB 2002, 2004, 2005b/. Pending the results of such investigations, the description of the structural and hydraulic properties in the 1.1 and 1.2 modelling stages have only been treated provisionally in the Preliminary Site Description /e.g. SKB 2005b/.

Following interactive discussions between the Forsmark modelling group and personnel responsible for the site investigations at Forsmark, see e.g. /SKB 2005c/, there crystallised a need for an improved description of the structural and hydraulic properties within and adjacent to the Singö and Forsmark deformation zones. This is in accordance with earlier plans to investigate the boundary conditions around the candidate area at Forsmark /SKB 2001, 2005a/.

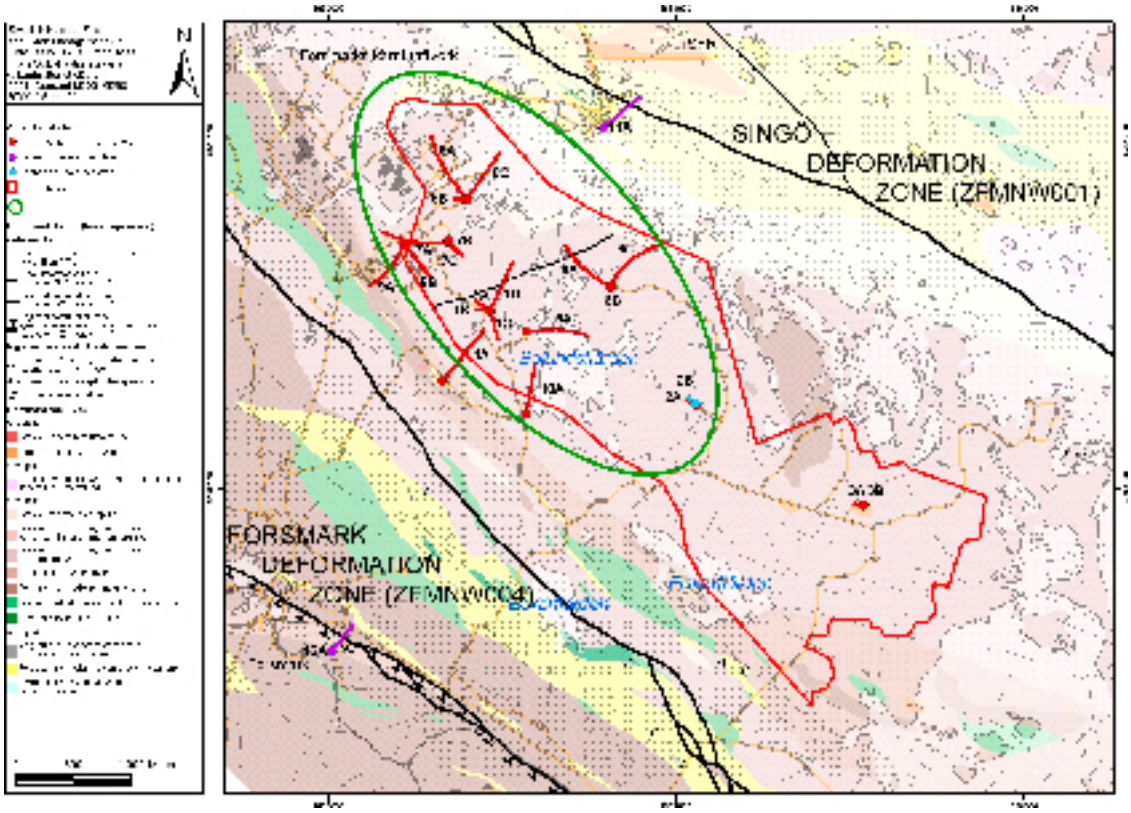

Figure 1. *Geological map of the bedrock inside and immediately around the candidate area at Forsmark (model version 1.2). Completed and ongoing telescope and cored boreholes as well as the target area in /SKB 2005a/ are also shown. Telescope boreholes KFM11A and KFM12A, which are addressed in this document, are included on the map.*

5.6.2 What are the questions to be resolved with the drilling?

Bedrock geology

From a geological perspective, the prime aim of boreholes KFM11A and KFM12A is to provide base geological information bearing on the character of zones ZFMNW0001 (Singö deformation zone) and ZFMNW0004 (Forsmark deformation zone), respectively. Key properties that need to be determined along both zones are the orientation, thickness, fracture orientation and fracture mineralogy of each zone. The relative importance of ductile and brittle deformation along each zone also needs to be addressed. Geological data at shallower levels along the Singö deformation zone are available from earlier construction work. However, data from deeper crustal levels along the Singö deformation zone as well as data from the Forsmark zone are lacking. Choice of sites for complementary percussion drilling at the two sites should take into consideration the occurrence of other lower confidence deformation zones as well as lineaments in the vicinity of the sites, in order to improve our understanding of the geological significance of these structures.

Hydrogeology and hydrogeochemistry

The issues of concern for the hydrogeological-hydrogeochemical description to be resolved by the drilling and investigations along the new telescope borehole KFM11A are:

- hydraulic characterisation of the Singö deformation zone parallel and orthogonal to its expected strike,
- examine the hydraulic responses in nearby boreholes as well as at the SFR facility during the drilling operations and the subsequent hydraulic tests, and
- chemical characterisation of the groundwater in the rock mass on both sides of the Singö deformation zone as well as of the groundwater within the zone.

The issues of concern for the hydrogeological-hydrogeochemical description to be resolved by the drilling and investigations along the new telescope borehole KFM12A are:

- hydraulic characterisation of the Forsmark deformation zone along the borehole trajectory, and,
- chemical characterisation of the groundwater in the Forsmark deformation zone along the borehole trajectory.

Hydrogeochemical sampling is recommended at every opportunity in these boreholes since these regional deformation zones are probably the main conductors towards depth.

5.6.3 Activities to be completed prior to, during and after the drilling

Bedrock geology

A standard geological/geophysical programme for the study of the bedrock in boreholes should be carried out, following the drilling of boreholes KFM11A and KFM12A. This programme should include:

- a documentation of the character of the wall of the borehole using the Borehole Image Processing System (BIPS),
- radar logging,
- geophysical logging,
- detailed geological mapping of rock types and both ductile and brittle structures.

Follow-up analytical work that characterises the mineralogical, geochemical, physical and rock mechanical properties of the bedrock along each borehole should be carried out, after the geological mapping has been completed and after an assessment of the need for complementary data has been made. Following stage 1 in the single hole interpretation, attention needs to be focused in follow-up work, during stage 2, on a more detailed characterisation of the deformation zones that are intersected in the boreholes. This should include:

- an assessment of the style of deformation along each zone, ductile, brittle or composite,
- a description of the position and character of rocks that were formed in connection with strong deformation (e.g. mylonite, cataclasite, breccia) along each zone,
- a kinematic study of each zone.

If deemed appropriate, mineral samples should be separated for geochronological work with the aim to gain some constraints on the timing of movement along the zones.

Hydrogeology and hydrogeochemistry

Prior to the core drilling of the KFM11A borehole, it is necessary to assure that the selected pressure monitoring in the SFR facility is functioning up to the standards of a good interference test setup. Further, the percussion drilled boreholes associated with the investigation programme of the Singö deformation zone should be hydraulically tested with the HTHB method prior to the core drilling of the KFM11A borehole. The positions of the percussion-drilled boreholes are shown in Figure 2. Two of the three percussion boreholes penetrate the Singö deformation zone. The objective of the third borehole is to act as flush water well during the core drilling.

During the core drilling of the KFM11A borehole, the two percussion drilled boreholes penetrating the Singö deformation zone should be monitored to track pressure changes.

After the completion of the KFM11A borehole high resolution measurements with the Posiva Flow Log (PFL-f) should be conducted allowing for detailed fracture flow measurements and fracture EC[2] measurements. Subsequent hydrogeochemical measurements should be carried out based on the drilling responses and the PFL-f results acquired. Depending on the results of the aforementioned

[2] If measurements with the Posiva Flow Log (PFL-f) cannot be conducted, PSS measurements should be carried out using the standard telescopic measurement strategy (100 m, 20 m and 5 m).

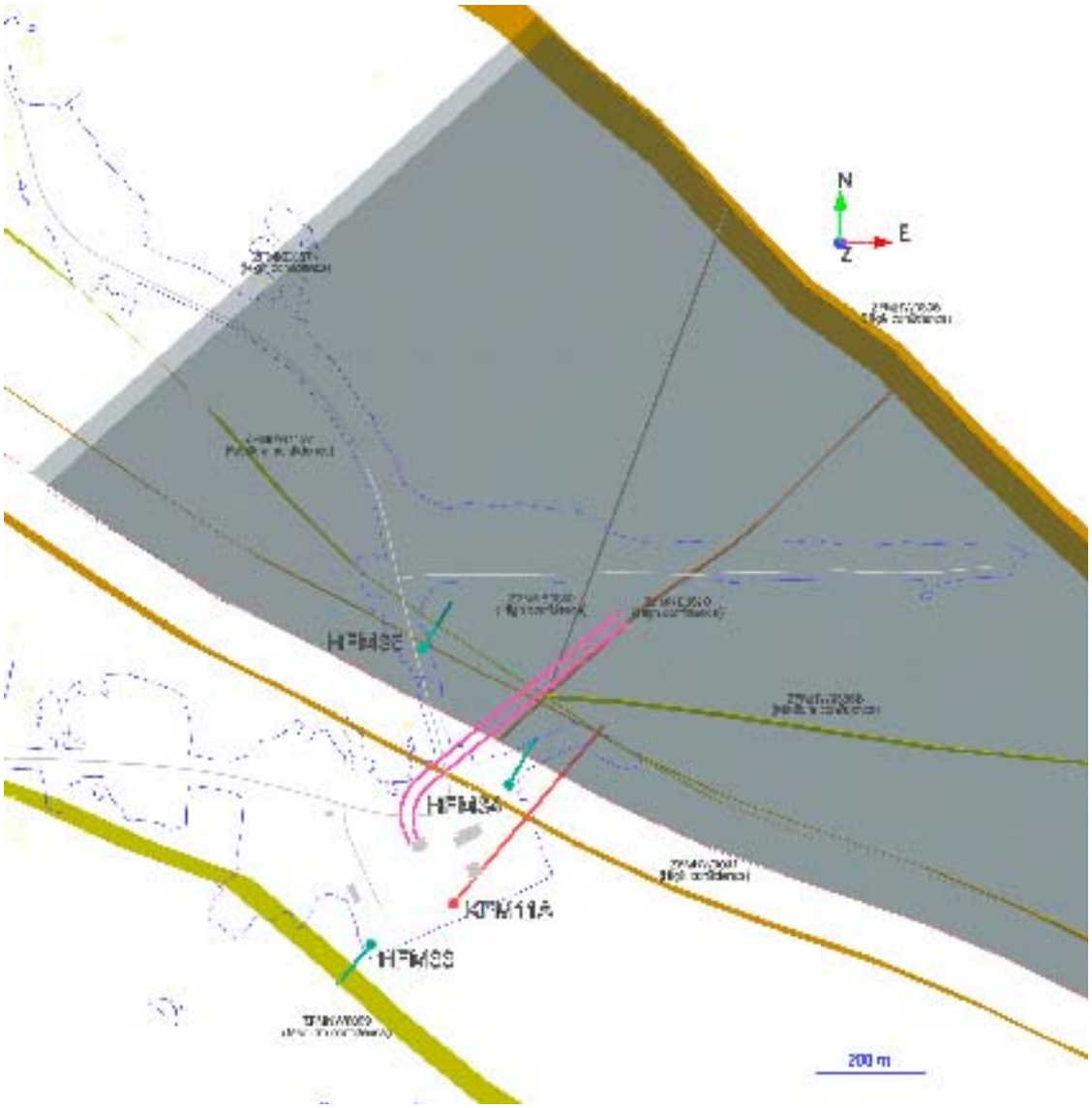

Figure 2. *Map showing positions of boreholes at drill site 11 associated with the investigation programme of the Singö deformation zone (ZFMNW0001). Excerpt from deformation zone model 2.1.*

activities, the hydrogeological characterisation programme may also require a supplementary hydraulic interference test at the end investigation programme to resolve possible uncertainties in the previous data acquisition. The information acquired from such a test will benefit if the KFM11A borehole is first equipped with a multipacker installation and connected to the HMS.

The hydraulic and chemical activities prior to, during and after the drilling of the KFM12A borehole should follow the standard programme for the study of the bedrock by telescopic boreholes. Potential observation wells in the proximity of drill site 12 should be surveyed prior to the drillings. Figure 3 shows the borehole settings of drill site 12.

5.6.4 Choice of borehole co-ordinates and orientation

The locations of the boreholes in relation to the inferred deformation zones at the two sites (SDM version 2.1) are shown in Figures 2 and 3. It should be noted that the choice of drill site 11 has been steered after careful assessment of the results from the SDM version 2.1 modelling work. The choice of site 12 has also taken into consideration the vicinity of the chosen site to a low velocity anomaly in older seismic refraction data (profile line W0577). The recommended co-ordinates, inclination, direction and length of the different boreholes addressed in this document are listed in Table 1.

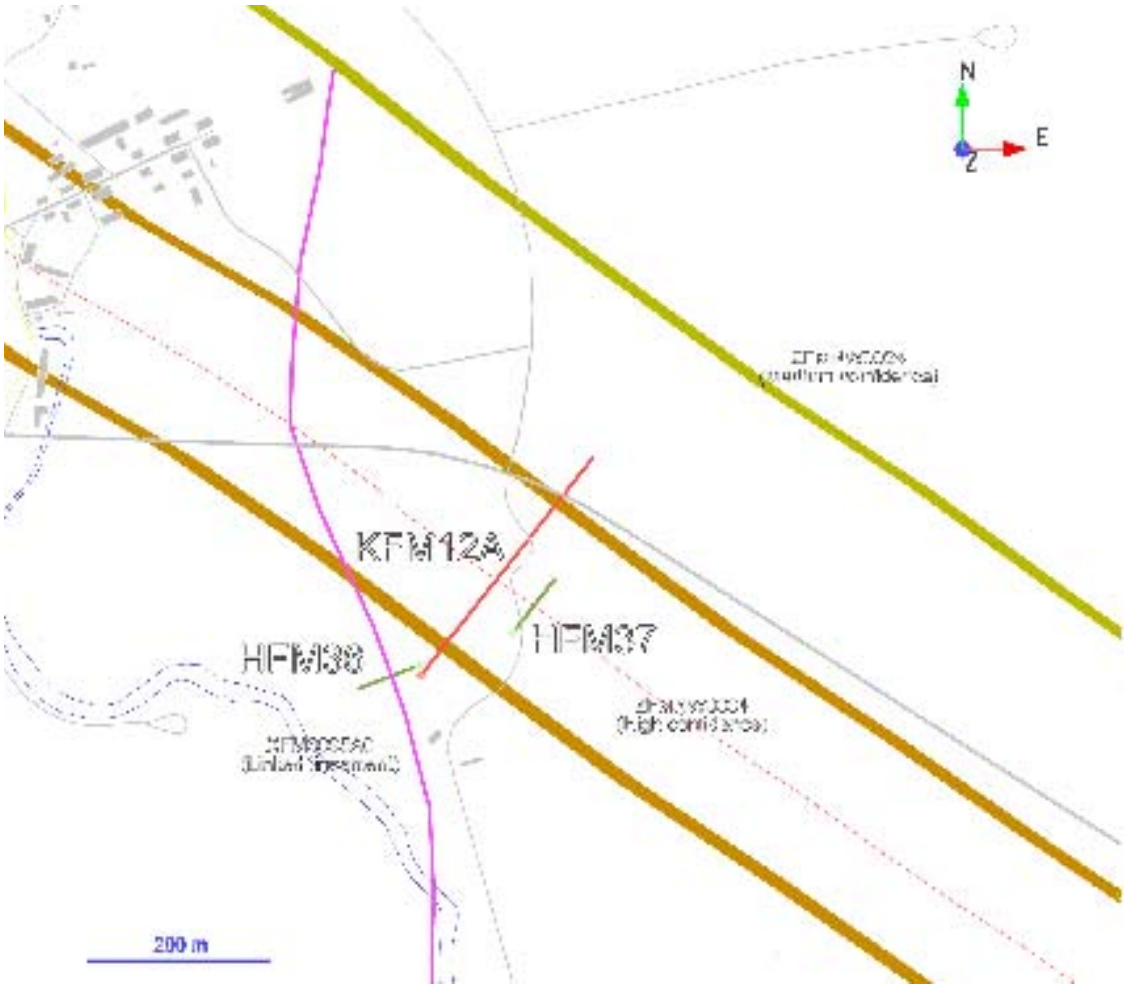

Figure 3. Map showing positions of boreholes at drill site 12 associated with the investigation programme of the Forsmark deformation zone (ZFMNW0004). Excerpt from deformation zone model 2.1.

Table 1. Position, inclination, direction and borehole length of all boreholes at drill sites 11 and 12.

Borehole	Drill site	Northing in RT 90, 2.5 gon V (m)	Easting in RT 90, 2.5 gon V (m)	Inclination (°)	Direction (°)	Borehole length (m)
KFM11A	11	6701109	1632371	60	040	850
HFM33	11	6701035	1632221	60	220	200
HFM34	11	6701325	1634716	60	030	200
HFM35	11	6701572	1632316	60	030	200
KFM12A	12	6696588	1630032	60	037	600
HFM36	12	6696600	1630032	60	250	150
HFM37	12	6696635	1630132	60	037	150

5.6.5 References

SKB 2001. Program för platsundersökning vid Forsmark, SKB R-01-42, Svensk Kärnbränslehantering AB.

SKB 2002. Forsmark – site descriptive model version 0. SKB R-02-32, Svensk Kärnbränslehantering AB.

SKB 2004. Preliminary site description. Forsmark area – version 1.1. SKB R-04-15, Svensk Kärnbränslehantering AB.

SKB 2005a. Forsmark site investigation. Programme for further investigations of geosphere and biosphere. SKB R-05-14, Svensk Kärnbränslehantering AB.

SKB 2005b. Preliminary site description. Forsmark area – version 1.2. SKB R-05-18, Svensk Kärnbränslehantering AB.

SKB 2005c. Anteckningar från planeringsmöte nr 7 – fortsatta undersökningar i Forsmark, SKB Doc-ID1043379, Svensk Kärnbränslehantering AB.

Sven Follin, SF GeoLogic

Michael Stephens, Geological Survey of Sweden

Lennart Ekman, Assen Simeonov, Svensk Kärnbränslehantering AB

Marcus Laaksoharju, Geopoint

Stockholm, 2006-04-24

5.7 Motivation for drill site 9 and cored boreholes KFM09A, KFM09B and KFM09C

5.7.1 Background

The strategy for the remainder of the site investigation at Forsmark was outlined in a program report issued in January this year (CSI-program /SKB 2005a/). A key-component in this strategy is to focus the complementary investigations on the north-western part of the candidate area. Arguments for this are as follows:

- Investigations so far indicate that bedrock conditions in the north-western part of the original candidate area meet requirements for a repository, and compare favourably to conditions in the south-eastern part.
- Preliminary layout work suggests that the north-western part of the candidate area provides sufficient space for a repository.
- Proximity to the existing industrial facilities at Forsmark would offer environmental and operational advantages for a repository.

Based on the chosen strategy and prevailing data needs, the program for core drilling and other investigations was outlined. Major objectives of the core drilling is to determine how far the volume of potentially suitable bedrock for a repository extends to the west and north, and to provide key lithological, structural, hydrogeological, hydrogeochemical and geomechanical data from parts of the area where such information is not available from earlier investigations.

In compliance with the program, a series of decisions have been taken detailing locations, orientations and programmes for to-date seven cored boreholes, all drilled from sites within the prioritized area (see Figure 1):

- KFM06B and KFM06C at drill site 6 /2005b/.
- KFM07A and KFM07B at drill site 7 /SKB 2005b/.
- KFM08A, KFM08B and KFM08C at drill site 8 /SKB 2005bcd/.

On the basis of the priority decision and the results of version 1.2 modelling work, an update of the preliminary layout for a repository at a depth of 400 m has been presented, see Figure 2. This version of the layout is input to the ongoing, preliminary safety assessment work.

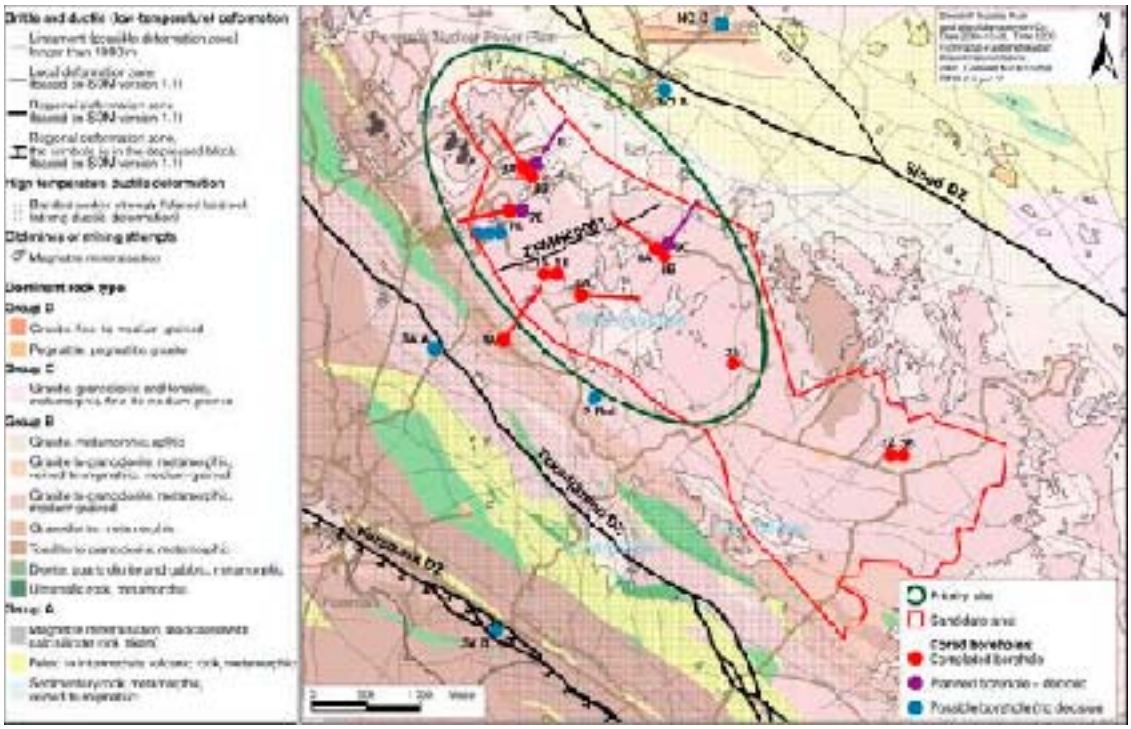

Figure 1. *Geological map of the bedrock inside and immediately around the candidate area at Forsmark. Completed, planned and possible cored boreholes as well as the priority site are also shown (modified after /SKB 2005a/).*

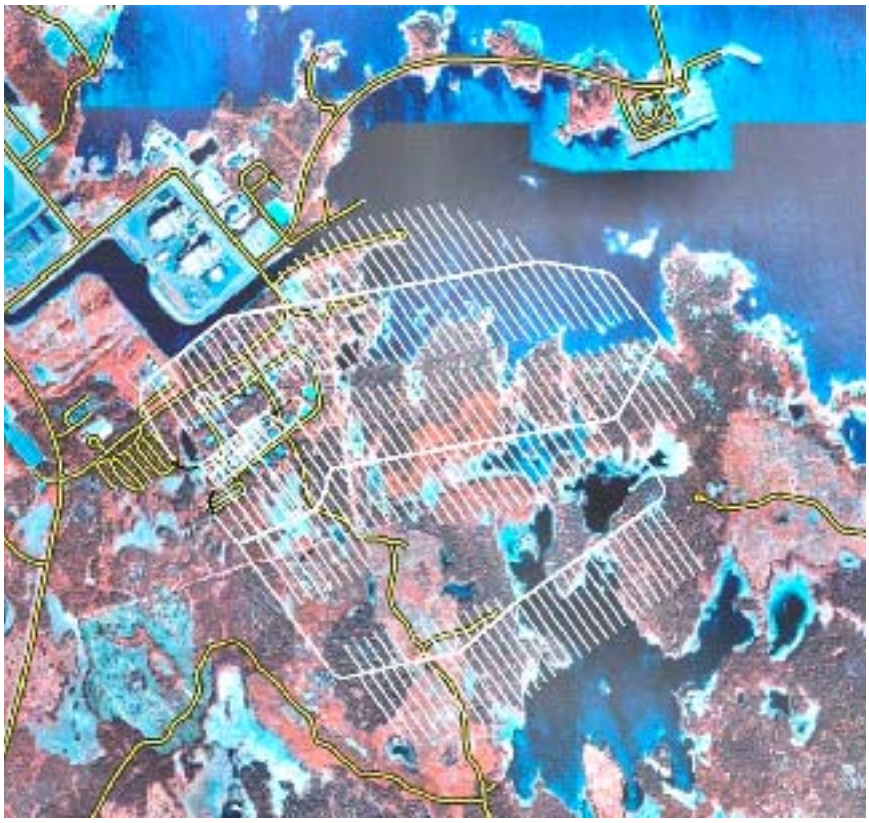

Figure 2. *Preliminary layout (February 2005) for a repository at 400 m depth at Forsmark.*

The CSI-program also includes investigations to support the design of access facilities from surface, i.e. an access ramp and four vertical shafts (according to current design premises), and the common facility area at repository level. The program tentatively dedicates two or three medium-deep (to or beyond repository depth) cored boreholes for this purpose, without specifying any details as regards locations or orientations. To this should be added more shallow percussion- or core drilling and surface investigations (refraction seismics, soil mechanics survey etc). The sections below provide a motivated recommendation for a new drilling site and three cored boreholes.

5.7.2 Preliminary layout of access routes and common facility area

Figure 3 shows the preliminary layout of the access routes and common facility area, as presented in February this year and produced primarily to guide further investigations. The geological input for the layout corresponds to SDM version 1.2, supplemented with preliminary information from borehole KFM07A. The facilities are located more or less below the present barrack area. For a repository depth set to 400 m (highest point of the entire facility), the deepest excavations will reach c. 480 m. It should be kept in mind that the layout is preliminary and will to all probability be subject to changes, both revisions prompted by functional requirements and adjustments of location prompted by geological information and/or requirements of shaft locations etc at the surface.

5.7.3 Objectives for drilling in the barrack area

Key objectives for the recommended drilling campaign are:

1) To constrain the geometry and characteristics of the geological units bordering the tectonic lens.
2) To determine rock engineering characteristics at locations suggested for the common facility area and access routes.
3) To resolve uncertainties regarding possible deformation zones within the rock volume of interest for these facilities.

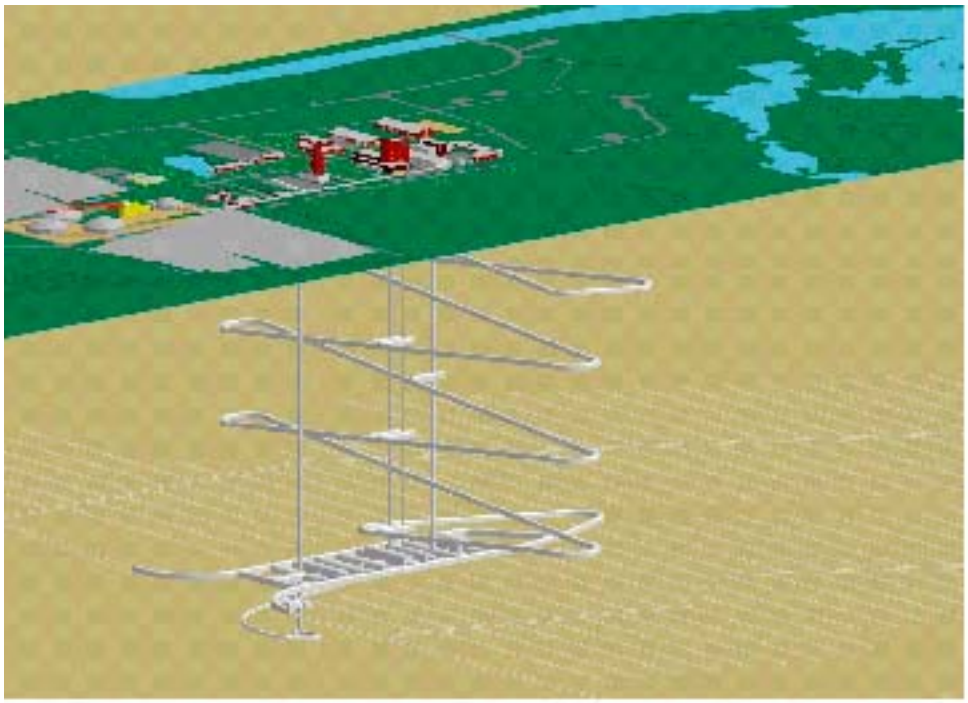

Figure 3. *Preliminary layout (February 2005) of access tunnel, shafts and common facilities at repository level.*

1) Constrain geometry and characteristics of rock units bordering the tectonic lens.

Figure 4 shows the present interpretation of the border of the tectonic lens, i.e. the transition from rock domain 29 (RD 29), to RD 12 and further into RD 18, in a section through the common facility area. The interpretation relies mainly on information from KFM04A, some 800 m to the southwest, and data from the detailed bedrock mapping. Knowledge of the geometry and engineering characteristics of the sequence from RD 29 and into RD 18, within the section of interest and at repository level, is essential for the next step of design work. According to the present layout, the southwesternmost excavations within the common facility area enter into RD 12. The two connecting transport tunnels, heading northwest and southeast respectively, are for the most part located outside RD 29, i.e. within RD 12 and RD 18, in order to save space for the repository itself. Whether such a solution, or in fact any interference between the common facilities and the rock domains outside RD 29, is appropriate depends on the characteristics of RD's 12 and 18.

2) Determine rock engineering characteristics at the locations for the common facility area and access routes.

Key parameters for design are:

- Rock mass quality.
- State of stress.
- Hydraulic conductivity.

Rock mass quality is a function of the state of fracturing as well as strength and deformation properties. Existing information suggests rather high ratings for the rock mass quality within the volume of interest, especially at depths exceeding some 200 m. Drilling is however required to verify this.

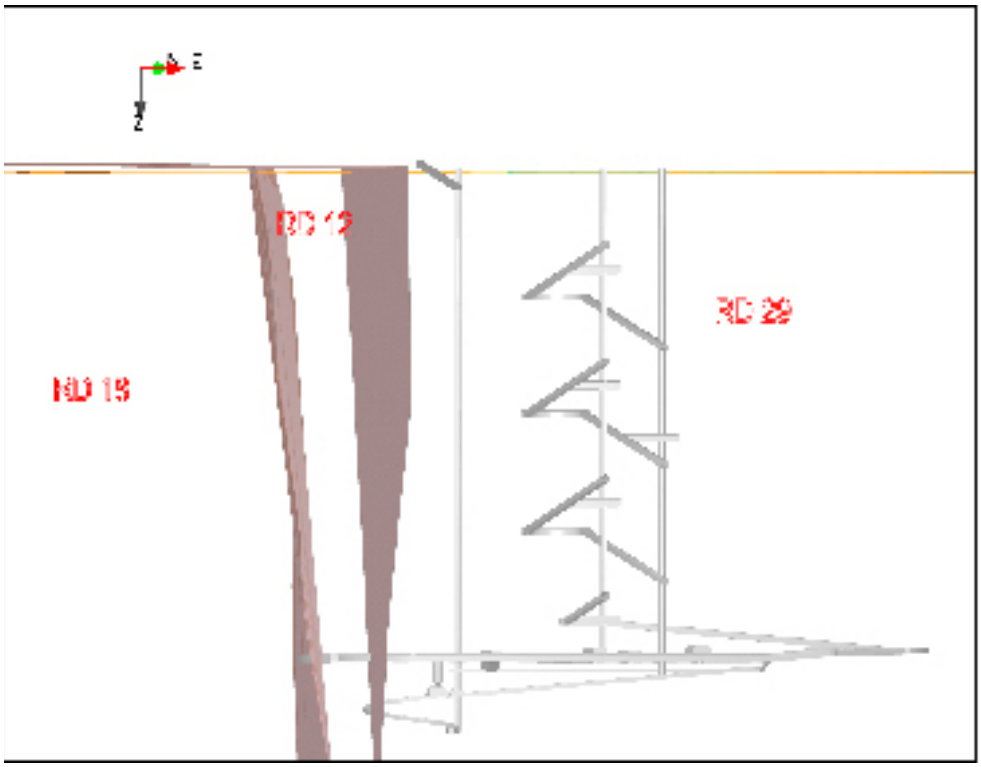

Figure 4. *Vertical NE-SW section showing the present interpretation of the boundaries between RD 29, RD 12 and RD 18 in relation to the common facility area.*

The state of stress is a key parameter at Forsmark, because of the potential for stress-driven instability in excavations at depth. Comprehensive stress measurements are planned in borehole KFM07B, to be drilled some 250 m northeast of the common facility area. Results from these tests will determine whether additional measurements in any of the boreholes to be drilled at drill site 9 are motivated.

Judging from data from KFM07A and other information, few if any water-bearing structures would be expected at depths from 200 m and downwards, but this must be verified by drilling. At more shallow depths, the prediction is to encounter a few, distinct and highly water conductive structures of large lateral extension. These features are important for the design of the shafts and the access tunnel. The core drilling campaign can contribute information in this respect, but complementary investigations with other methods will also be required.

3) Resolve uncertainties regarding possible deformation zones.

Current interpretation of borehole and seismic data suggests that no major deformation zone intersects the volume enveloping the access and common area facilities, but surprises in this respect cannot be excluded. Furthermore, uncertainty remains regarding the interpretation of a number of lineaments. Drilling should be planned to resolve as far as possible these uncertainties.

5.7.4 Drill site

Several options have been considered as regards locations and orientations of boreholes required to meet the objectives listed above. The conclusion is that a new drilling site (DS9) should be established at the north-western side of the barrack area, as shown in Figure 5. More precisely, the location is about 30 m southwest of the car-wash building, at approximate coordinates 6700114/1630646. Arguments for a drilling site at this location are:

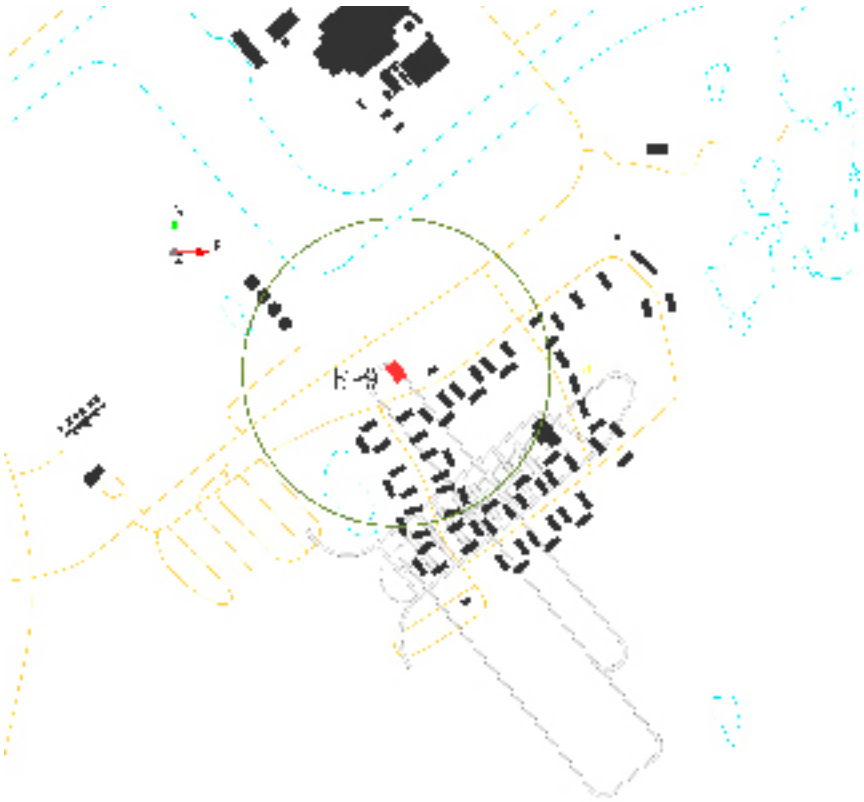

Figure 5. *Location of drill site 9 (red symbol) in the barrack area. The circle indicates horizontal reach at 400 m depth of boreholes drilled at 60° dip.*

- The margin of RD29 to the southwest can be reached and penetrated at repository depth by inclined drilling.
- Part of the common facility area to the southeast can also be reached by inclined drilling.
- The rock volume hosting the access ramp can be efficiently penetrated.
- There is a potential to intersect three lineaments longer than 1,000 m and two lineaments shorter than 1,000 m.
- A significant rock volume to the northwest, north and northeast can be reached with inclined drill holes.
- At the surface, space is available for a drill site and the necessary infrastructure can be arranged.
- Despite the proximity to some of the barracks, interference with other activities in the area can be kept at acceptable level, provided that precautions are taken to limit drilling noise.

5.7.5 Boreholes

It is recommended to drill three cored boreholes from drill site 9. Table 1 summarizes the orientations and lengths of these boreholes. Figure 6 shows orientations projected on a surface map that also illustrates interpreted lineaments. Figure 7 shows the borehole array in relation to rock domains and planned facilities.

Boreholes KFM09A and KFM09B are primarily motivated by the objectives presented above. KFM09C is primarily motivated by the fact that the repository layout, cf. Figure 2, extends some 200 m to the northwest from the drill site into bedrock that has so far not been investigated by core drilling at repository depth (borehole KFM07A penetrates part of this volume, but at considerably larger depth).

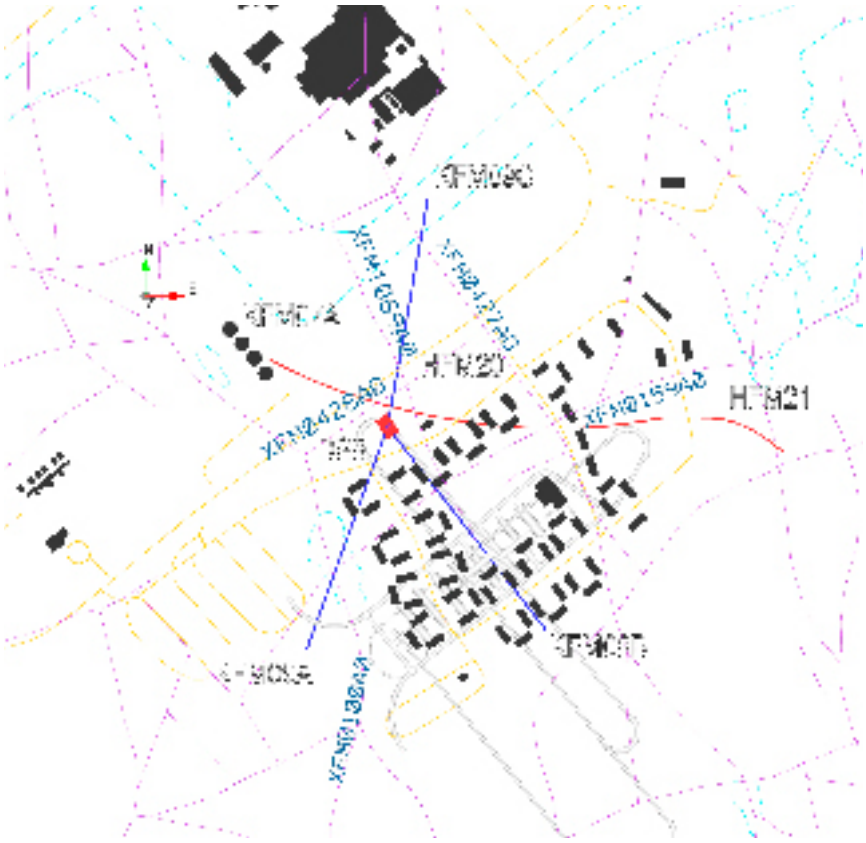

Figure 6. *Orientations of planned boreholes at drill site 9 (DS 9).*

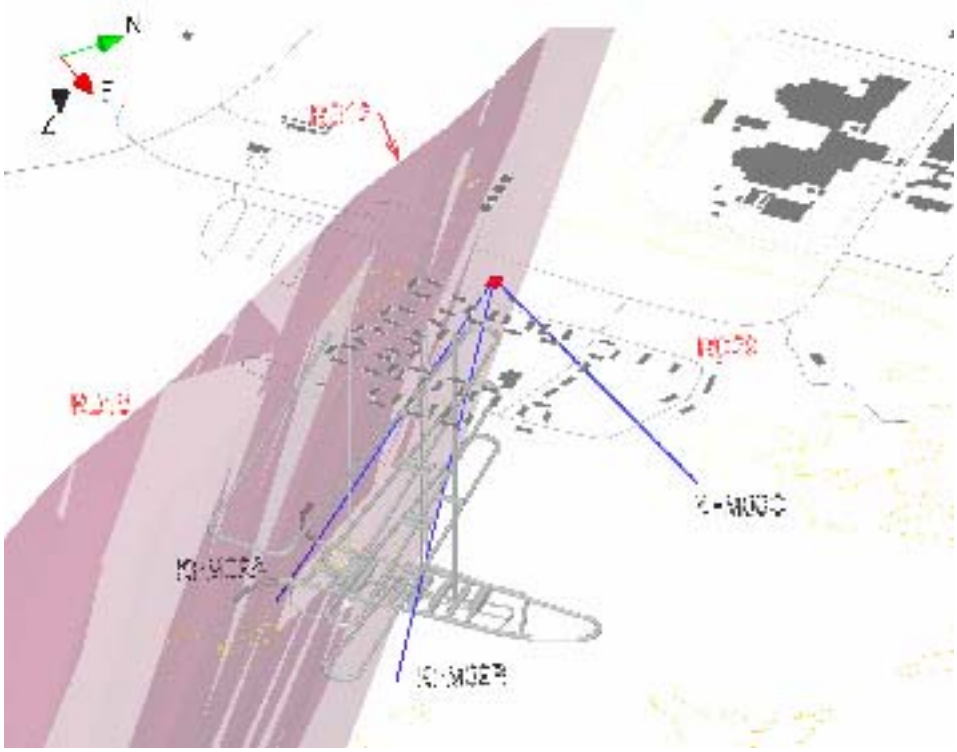

Figure 7. *Boreholes KFM09A, KFM09B and KFM09C in relation to rock domains and the preliminary layout of excavations. The shaded brownish object represents the volume of rock domain 12 (RD 12).*

Table 1. Orientation, length and vertical depth of planned boreholes at drill site 9.

Borehole	Dip (°)	Direction (°)	Borehole length (m)	Vertical depth (m)
KFM09A	60	200	650	550
KFM09B	55	140	615	500
KFM09C	55	010	550	450

As can be seen in Figure 6, the barrack area is transacted by a NE-SW trending lineament referred to as XFM0159A0. Furthermore, the vertical projection of four additional minor lineaments (XFM0100A0, XFM0427A0, XFM0428A0 and XFM1069A0) are intersected by the planned drill holes.

All three boreholes will be core drilled according to standard procedures and without any telescopic parts. Test programmes for the individual boreholes will be detailed separately and are not discussed here.

It should be noted that the borehole array reflects a compromise between interests that are to some extent conflicting: On the one hand, data needs call for boreholes through and below the rock volume where excavations (descends, common facilities) are actually planned to be located. On the other hand, boreholes running through (or very close to) excavations should be avoided /SKB 2005e/. Given uncertainties in both drilling precision and, more importantly, the location and design of excavations, these requirements are not entirely compatible. To really eliminate the risk of interference between boreholes and excavations within the common facility area, drilling directed towards this area must be terminated before reaching excavation depth. This is however considered unacceptable with respect to data needs for design. The compromise adopted is a borehole geometry that 1) can be defended with respect to investigation requirements; 2) does not conflict with excavations as per the present, preliminary layout. This implies that later layout changes and/or borehole deviations may require either adjustment of tunnel positions to avoid boreholes, or borehole sealing measures such that borehole-tunnel intersections can be accepted.

Borehole KFM09A. The purpose with this borehole is to meet objective 1) above, i.e. to constrain and characterize the border of RD 29 and to enter RD 18 at the depth and position of the common facility area. It is expected to reach the boundary between RD 29 and RD 12 at c. 460 m borehole length (depth 400 m) and to enter RD 18 at c. 595 m borehole length (depth 490 m). Drilling should continue well into RD 18. Final borehole length is estimated to c. 650 m, but must be decided on the basis of preliminary core logging on site.

Borehole KFM09B. The primary purpose of this borehole is to meet objective 2) above, i.e. to determine rock engineering characteristics at locations for the common facility area and access routes. In addition, it will provide information that can resolve whether the interpreted lineament XFM0159A0 (see Figure 6) represents a deformation zone, which is an important question from a rock engineering point of view. The borehole will penetrate downwards and across the shaft/ramp tunnel volume above the common facility area. The dip has been chosen to pass just southeast of the excavations (see Figure 7) in order to avoid unnecessary conflict with excavations. Drilling should continue well below the maximum depth of the floor level of the excavations, which is about 430 m. Vertical borehole depth is therefore set to 500 m, corresponding to a borehole length of c. 615 m. Orientation is preliminary, pending data from KFM09A and other input that may change the layout. The possibility to deepen the hole in a later stage should be maintained.

Borehole KFM09C. As mentioned, the main purpose of this borehole is to characterize the rock volume hosting the north-eastern “corner” of the repository according to the current layout. In addition, it will potentially shed some light on the character of a number of lineaments; XFM0428A0, XFM1069A0 and XFM0428A0 (see Figure 6).

5.7.6 References

SKB, 2005a. Forsmark site investigation. Programme for further investigations of geosphere and biosphere. SKB R-05-14, Svensk Kärnbränslehantering AB.

SKB, 2005b. Internal document 1024611. Decision regarding location and orientation of cored boreholes KFM07A, KFM07B, KFM08A, KFM08B, KFM06B, KFM06C and percussion boreholes HFM20, HFM21 and HFM22.

SKB, 2005c. Internal document 1038014. Revised decision regarding length and orientation of cored borehole KFM08B.

SKB, 2005d. Internal document 1038406. Decision regarding location and orientation of cored borehole KFM08C.

SKB, 2005e. Internal document 1028049. Respektavstånd från borrhål till deponeringshål.

Bengt Leijon

Assen Simeonov

20050519